

**Invention and Development of the Controlled Ring-Opening  
Polymerisation of 2,5-Diketopiperazines to Produce  
Poly(amino acids)**

Patrick Anthony Wall

Supervised by Dr Paul Thornton

Co-Supervisors: Dr Thomas Chamberlain and Dr  
David Harbottle

Submitted in accordance with the requirements for the  
degree of Doctor of Philosophy

School of Chemistry, University of Leeds

October 2023



The candidate confirms that the work submitted is his own and that appropriate credit has been given within the thesis where reference has been made to the work of others.

This copy has been supplied on the understanding that it is copyright material and that no quotation from the thesis may be published without proper acknowledgement.

The right of Patrick Wall to be identified as Author of this work has been asserted by Patrick Wall in accordance with the Copyright, Designs and Patents Act 1988.

© 2023 the University of Leeds and Patrick Wall

## **Acknowledgements**

First and foremost, the author would like to express his sincere gratitude to Dr Paul Thornton for his continued supervision, wise council and relentless support. The author would like to extend his thanks to the School of Chemistry at the University of Leeds for the award of the Lund Stephenson Clarke Scholarship which has funded the research presented in this thesis. The author would also like to extend thanks to the Leeds Institute of Textiles and Colour for additional funding towards an electrospinning project which resulted in the work reported in Chapter 7.

The author would like to thank Algy Kazlauciusas for his extensive assistance with SEM and DSC. The author would also like to thank Jeanine Williams for her support with all things chromatography. The author would also like to express thanks to Dr Thomas Chamberlain for his training and advice on MALDI-TOF. The author would like to express gratitude and appreciation to the Thornton group, as well as the other groups working in lab 3.14, for their advice, support and company.

The author would like to express thanks to his mother and father, Louise and Tony Wall, for their continuous support and reassurance since 1995. Finally, the author would like to express gratitude to and for Ellice Price; for her patience, her resolute support and her continued supply of high quality flat whites; no barista can make them better.



## Abstract

Polymers are versatile materials, boasting wide-ranging physicochemical properties and, as such, are utilised across a plethora of applications within multiple sectors. A particular group of polymers, poly(amino acids), are naturally derived, biomimetic, biodegradable and, depending on the specific amino acid units within the polymer, can have a host of different physicochemical properties. There are several established synthetic routes for the production of poly(amino acids), such as direct polycondensation of amino acids, solid-state peptide synthesis, and N-carboxyanhydride (NCA) ring-opening polymerisation (ROP). The latter two methods have much greater control with respect to targeting polymer length and minimising dispersity. However, each has significant drawbacks such as compromised yields when targeting longer polymers and, in particular for NCA ROP, requires the use of harsh and extremely toxic reagents such as phosgene. These issues render the production of narrow dispersity poly(amino acids) at industrial scale at best undesirable and, at worst, unfeasible. As such, an alternative route to poly(amino acids) that does not rely on extremely toxic reagents, is efficient, straightforward, and environmentally sustainable, is in demand. The ROP of 2,5-diketopiperazines (DKPs) potentially provides this alternative; DKP synthesis is simplistic and essentially without chemical hazard. As a cyclic dipeptide, the ROP of DKPs propagates by the attachment of a dipeptide unit, which opens up an avenue to new poly(amino acids) and ensures that the polymerisation boasts excellent atom economy.

The synthesis of a library of DKPs is reported, including the DKPs of several canonical amino acids as well as sarcosine DKP and an asymmetric DKP of sarcosine-phenylalanine. Most of the DKPs reported have not been synthesised via the reported route previously. The controlled ROP of DKPs is demonstrated for the first time to produce a collection of poly(amino acids). Homopolymers of glycine, alanine, phenylalanine, lysine, sarcosine, proline, methionine, and arginine are reported. A circular lifecycle is demonstrated for polyalanine, comprised of the polymer degradation by elastase to alanine, followed by cyclisation to alanine DKP and polymerisation to polyalanine. Application of the polymers produced is demonstrated. The production of poly(ethylene glycol) based block co-polymers boasting narrow dispersity and amphiphilic properties are also reported; these polymers self-assemble in aqueous solution to form discrete nanoparticles with the capacity to encapsulate an anticancer therapeutic. Drug release is achieved in acidic conditions, suggesting potential material applicability as chemotherapeutic delivery devices. Polysarcosine-based copolymers are reported, including polysarcosine-*b*-polyalanine which underwent self-assembly, therapeutic encapsulation, and controlled drug release upon elastase incubation. Finally, the production of nanofibres of

polyalanine and polysarcosine, each with polycaprolactone, by electrospinning is reported. The nanofibres possessed enhanced toughness and, particularly for polysarcosine/polycaprolactone, enhanced water uptake compared to polycaprolactone fibres. Notably, the polyalanine/polycaprolactone fibres degrade upon incubation with elastase; this provides scope for incubation of a therapeutic and subsequent release at a chronic wound, a site of elastase overexpression. This thesis reports the ease in creating poly(amino acids) from DKPs, and applying the polymers produced in a range of applications. The work reported in this thesis has also resulted in a patent application, as well as the submission of a manuscript for review and publication.

## **Table of Contents**

Acknowledgements	ii
Abstract	iii
Table of Contents	v
List of Figures	xii
List of Tables	xvi
List of Schemes	xviii
List of Abbreviations	xx
<b>Chapter 1 – Introduction</b>	<b>1</b>
1.1. Polymerisation	1
1.2. Monomers	1
1.2.1. Amino Acids	1
1.2.2. N-carboxyanhydrides (NCAs)	4
1.2.3. 2,5-Diketopiperazines (DKPs)	8
1.3. Polymerisation to Form Poly(amino acids)	11
1.3.1. Polycondensation of Amino Acids	11
1.3.2. Solid-Phase Peptide Synthesis	12
1.3.3. NCA Ring-Opening Polymerisation (NCA ROP)	13
1.3.4. 2,5-Diketopiperazine Ring-Opening Polymerisation (DKP ROP)	16
1.4. Drug Delivery Vehicles	18
1.4.1. Block Copolymers	19
1.4.2. Amphiphilic Polymer Self-Assembly	20
1.4.3. Optimisation of Nanoparticles	21
1.5. Enzyme-Responsive Materials	22
1.5.1. Enzymes and Their Action	22
1.5.2. Using Enzymes as Stimuli for Material Manipulation	24
1.5.3. Enzyme Sensitive Functionalities	24
1.5.4. Translation of Enzymatic Action into Material Response	25

1.5.5. Types of Enzyme-Responsive Systems and Their Applications	25
1.6. Wound Healing Devices	27
1.6.1. Mechanism of Wound Healing	27
1.6.2. Traditional Approach to Expedite Wound Healing	29
1.6.3. Modern and Responsive Healing Devices	30
1.6.4. Electrospinning of Polymer Nanofibres	32
1.7. Renewability and Environmental Impact of Polymer Synthesis	34
1.8. Research Aims and Thesis Outline	36
1.9. References	39
<b>Chapter 2 – Instrumentations, General Methods and Materials</b>	<b>57</b>
2.1. Nuclear Magnetic Resonance (NMR) Spectroscopy	57
2.2. Fourier-Transform Infrared (FTIR) Spectroscopy	57
2.3. Centrifugation, Sample-Drying and Lyophilisation	57
2.4. Liquid Chromatography – Mass Spectrometry (LC-MS)	57
2.5. Ultra Violet – Visible (UV-Vis) Spectrophotometry	58
2.6. Preparation of Phosphate Buffered Saline (PBS) and Sodium Acetate Buffer Solutions	58
2.7. Preparation of Nanoparticles and Loaded Nanoparticles (Nanoprecipitation)	58
2.8. Dynamic Light Scattering (DLS) and Zeta Potential Studies	58
2.9. High Performance Liquid Chromatography (HPLC)	59
2.10. Advanced Polymer Chromatography (APC)	60
2.11. Matrix-Assisted Laser Desorption/Ionisation – Time of Flight Mass Spectrometry (MALDI-TOF MS)	60
2.12. Scanning Electron Microscopy (SEM)	60
2.13. Drug Encapsulation Efficiency and Drug Loading Content	60
2.14. Electrospinning of Polymer Solutions	61
2.15. Tensile Testing	61
2.16. Differential Scanning Calorimetry (DSC)	61
2.17. Materials Inventory	61

2.18. References	63
<b>Chapter 3 – Synthesis of DKPs</b>	<b>64</b>
3.1. Synthetic Routes to DKPs	64
3.1.1. Peptide Coupling and Cyclisation	64
3.1.2. Ugi Synthesis	64
3.1.3. Cyclisation via Haloacetamides	65
3.1.4. Diels-Alder Reaction	66
3.1.5. Enolate Acylation	66
3.1.6. Direct Amino Acid Condensation	67
3.2. Experimental Details	67
3.2.1. General DKP Synthesis	67
3.2.2. Synthesis of Glycine DKP	68
3.2.3. Synthesis of Alanine DKP	69
3.2.4. Synthesis of Phenylalanine DKP	69
3.2.5. Synthesis of Lysine(Cbz) DKP	70
3.2.6. Synthesis of Valine DKP	71
3.2.7. Synthesis of Tyrosine DKP	72
3.2.8. Synthesis of Methionine DKP	73
3.2.9. Synthesis of Tryptophan DKP	73
3.2.10. Synthesis of Arginine(Pbf) DKP	74
3.2.11. Synthesis of Sarcosine DKP	75
3.2.12. Synthesis of Proline DKP	76
3.2.13. Synthesis of Sarcosine-Phenylalanine DKP	77
3.3. References	79
<b>Chapter 4 – The Ring-Opening Polymerisation of 2,5-Diketopiperazines to Create Poly(amino acids)</b>	<b>81</b>
Abstract	81
4.1. Introduction	81

4.2. Experimental Details	83
4.2.1. Synthesis of DKPs	83
4.2.2. Synthesis of Poly(amino acid) Homo-polymers	84
4.2.3. Deprotection of Polylysine(Cbz)	85
4.2.4. Enzymatic Degradation of Polyalanine	86
4.3. Results and Discussion	86
4.3.1. Synthesis of DKPs	86
4.3.2. Synthesis of Poly(amino acid) Homo-polymers	87
4.3.3. Deprotection of Polylysine(Cbz)	92
4.3.4. Enzymatic Degradation of Polyalanine	94
4.4. Conclusion	95
4.5. References	97
<b>Chapter 5 – Exploiting DKPs to Afford Nanoparticles for Acid-Mediated Drug Release</b>	<b>100</b>
Abstract	100
5.1. Introduction	100
5.2. Experimental Section	103
5.2.1. Synthesis of 2,5-Diketopiperazines	103
5.2.2. Synthesis of PEG- <i>b</i> -Poly(amino acid) Copolymers	103
5.2.3. Preparation of PEG- <i>b</i> -Poly(amino acid) Copolymer Nanoparticles	104
5.2.4. Preparation of Doxorubicin (Dox) Free-Base	105
5.2.5. Preparation of Dox-loaded Nanoparticles	105
5.2.6. pH-Mediated Release of Doxorubicin from Dox-Loaded Nanoparticles	105
5.3. Results and Discussion	105
5.3.1. Synthesis of 2,5-Diketopiperazines	105
5.3.2. Synthesis of PEG- <i>b</i> -Poly(amino acid) Copolymers	106
5.3.3. Formation of PEG- <i>b</i> -Poly(amino acid) Nanoparticles	112
5.3.4. Drug Release Studies from PEG- <i>b</i> -Poly(amino acid) Nanoparticle Dispersions	115
5.4. Conclusions	117

5.5. References	118
<b>Chapter 6 – Ring-Opening Polymerisation of Sarcosine-DKP as a Route to Polysarcosine-Based Enzyme-Sensitive Vehicles and Polysarcolation</b>	<b>121</b>
Abstract	121
6.1. Introduction	121
6.2. Experimental Section	124
6.2.1. Synthesis of 2,5-Diketopiperazines	124
6.2.2. Synthesis of Polysarcosine	124
6.2.4. Synthesis of Polysarcosine- <i>b</i> -Polyalanine Copolymers	125
6.2.5. Synthesis of Polysarcosine- <i>ran</i> -Polyalanine Copolymer	126
6.2.6. Synthesis of Camptothecin-Polysarcosine	126
6.2.7. Synthesis of Polysarcosine- <i>alt</i> -Polyphenylalanine	127
6.2.8. Enzyme Degradation of Polysarcosine- <i>alt</i> -Polyphenylalanine	127
6.2.9. Preparation of PSar- <i>ran</i> -PAla Copolymer Gels	128
6.2.10. Preparation of PSar- <i>b</i> -PAla Copolymer Nanoparticles	128
6.2.11. Preparation of Dox-loaded Nanoparticles	128
6.2.12. Enzyme-Mediated Release of Doxorubicin from Dox-Loaded Nanoparticles	128
6.3. Results and Discussion	129
6.3.1. Synthesis of 2,5-Diketopiperazines	129
6.3.2. Synthesis of Polysarcosine	129
6.3.3. Synthesis of Polysarcosine- <i>b</i> -Polyalanine	132
6.3.4. Synthesis of Polysarcosine- <i>ran</i> -Polyalanine	134
6.3.5. Synthesis of Polysarcosine- <i>alt</i> -Polyphenylalanine	136
6.3.6. Polysarcolation of Camptothecin	139
6.3.7. Polysarcosine- <i>b</i> -Polyalanine Nanoparticles	142
6.3.8. Enzyme-Mediated Release of Doxorubicin from Dox-Loaded Nanoparticles	144
6.4. Conclusion	146
6.5. References	147

<b>Chapter 7 – Electrospinning of Polyalanine-based, Elastase-Responsive Nanofibres as Potential Materials for the Treatment of Chronic Wounds</b>	<b>151</b>
Abstract	151
7.1. Introduction	151
7.2. Experimental Details	155
7.2.1. Synthesis of Diketopiperazines	155
7.2.2. ROP of Diketopiperazines	155
7.2.3. Preparation of Polymer Solutions	155
7.2.4. Electrospinning of Polymer Solutions	155
7.2.5. Water Uptake Testing of Nanofibre Samples	157
7.2.6. Tensile Testing of Nanofibre Samples	157
7.2.7. Enzyme Degradation Study of PCL/PAla Nanofibre Samples	157
7.3. Results and Discussion	157
7.3.1. Synthesis of Diketopiperazines	157
7.3.2. ROP of Diketopiperazines	158
7.3.3. Electrospinning of PCL, PCL/PAla and PCL/PSar Nanofibres	158
7.3.4. Water Uptake Testing of Nanofibre Mats	163
7.3.5. Tensile Testing of Nanofibre Mats	164
7.3.6. Enzyme Degradation Study of PCL/PAla Nanofibre Samples	166
7.4. Conclusion	170
7.5. References	172
<b>Chapter 8 – Expansion of Poly(amino acid) Library and ROP Conditions</b>	<b>177</b>
Abstract	177
8.1. Introduction	177
8.2. Experimental Details	179
8.2.1. Synthesis of DKPs	179
8.2.2. Synthesis of Polyproline	179
8.2.3. Synthesis of Polymethionine	180



8.2.4. Synthesis of Polyarginine(Pbf)	181
8.2.5. eROP of Alanine DKP	181
8.3. Results and Discussion	182
8.3.1. ROP of DKPs	182
8.3.2. Synthesis of Polyproline	183
8.3.3. Synthesis of Polymethionine	186
8.3.4. Synthesis of Polyarginine(Pbf)	187
8.3.5. eROP of Alanine DKP from CALB	188
8.4. Conclusions	190
8.5. References	191
<b>Conclusions and Future Work</b>	<b>193</b>
<b>List of Publications</b>	<b>196</b>
<b>Appendices</b>	<b>197</b>
Appendix I – FTIR Spectroscopy	197
Appendix II – <sup>1</sup> H NMR Spectroscopy	224
Appendix III – Liquid Chromatography-Mass Spectrometry (LC-MS)	235
Appendix IV – High-Performance Liquid Chromatography (HPLC)	240
Appendix V – UV-visible (UV-vis) Spectrophotometry	241
Appendix VI – Calibration Curves	247
Appendix VII – MALDI-TOF Mass Spectrometry	248

## List of Figures

Figure 1.1. – General structure of an $\alpha$ -amino acid.	1
Figure 1.2. – General structure of an amino acid N-carboxyanhydride.	4
Figure 1.3. – Structure of phosgene (left) and triphosgene (right).	5
Figure 1.4. – Structure of propylphosphonic anhydride (T3P).	7
Figure 1.5. – General structure of a 2,5-diketopiperazine (DKP).	9
Figure 1.6. – General structures of 2,5-diketopiperazines (left), glycolides (centre) and 2,5-morpholinediones (right).	16
Figure 1.7. – Structure of tin(II) 2-ethylhexanoate (Sn(Oct) <sub>2</sub> ).	17
Figure 1.8. – Structure of poly(ethylene glycol).	19
Figure 1.9. – Structure of polysarcosine.	20
Figure 1.10. – Diagram of a typical electrospinning setup.	33
Figure 3.1. - Glycine DKP structure.	68
Figure 3.2. - Alanine DKP structure.	69
Figure 3.3. - Phenylalanine DKP structure.	69
Figure 3.4. - Lysine(Cbz) DKP structure.	70
Figure 3.5. - Valine DKP structure.	71
Figure 3.6. - Tyrosine DKP structure.	72
Figure 3.7. - Methionine DKP structure.	73
Figure 3.8. - Tryptophan DKP structure.	73
Figure 3.9. - Arginine(Pbf) DKP, where Pbf signifies a 2,2,4,6,7-Pentamethyldihydrobenzofuran-5-sulfonyl protecting group.	74
Figure 3.10. - Sarcosine DKP structure.	75
Figure 3.11. - Proline DKP structure.	76
Figure 3.12. - Sar-Phe DKP structure.	77
Figure 4.1. - <sup>1</sup> H NMR spectra of polymer 1, PGly <sub>54</sub> (brown, CDCl <sub>3</sub> , 500 MHz), polymer 2, PAla <sub>65</sub> (blue, DMSO-d <sub>6</sub> , 500 MHz), polymer 3, PPhe <sub>37</sub> (green, DMSO-d <sub>6</sub> , 500 MHz) and polymer 4, PLys(Cbz) <sub>55</sub> (purple, DMSO-d <sub>6</sub> , 500 MHz).	88
Figure 4.2. – MALDI-TOF spectra of: a) polymer 1, PGly <sub>54</sub> , b) polymer 2, PAla <sub>68</sub> , c) polymer 3, PPhe <sub>37</sub> , and d) PLys(Cbz) <sub>47</sub> .	89
Figure 4.3. – MALDI-TOF spectra of: a) polymer 5, PGly <sub>48</sub> , b) polymer 6, PAla <sub>45</sub> , c) polymer 7, PPhe <sub>18</sub> , and d) polymer 8, PLys(Cbz) <sub>15</sub> .	90
Figure 4.4. - <sup>1</sup> H NMR spectra (DMSO-d <sub>6</sub> , 500 MHz) of polymer 5, PGly <sub>52</sub> (brown), polymer 6, PAla <sub>51</sub> (blue), polymer 7, PPhe <sub>19</sub> (green) and polymer 8, PLys(Cbz) <sub>18</sub> (purple).	91

Figure 4.5. - $^1\text{H}$ NMR spectra (DMSO- $d_6$ , 500 MHz) of polymer 8, (PLys(Cbz) $_{18}$ ) (brown) and deprotected polymer 8, (PLys $_{18}$ ) (blue).	93
Figure 4.6. - UV-vis spectrum of polymer 8, PLys(Cbz) $_{18}$ , suspended in deionised water at 1.3 mg mL $^{-1}$ (red) and deprotected polymer 8, PLys $_{18}$ , in deionised water at 12 mg mL $^{-1}$ (blue).	93
Figure 4.7. - $^1\text{H}$ NMR spectrum (DMSO- $d_6$ , 500 MHz) of polymer 9, PAla $_{45}$ , synthesised from alanine DKP that was produced from the degradation products of PAla $_{65}$ .	94
Figure 4.8. - MALDI-TOF spectrum of polymer 9, PAla $_{45}$ , synthesised from alanine DKP that was produced from the degradation products of PAla $_{65}$ .	95
Figure 5.1. - $^1\text{H}$ NMR (CDCl $_3$ , 400 MHz) spectra of PEG methyl ether (Average $M_w$ = 5000 gmol $^{-1}$ ) (black), polymer 1, PEG $_{5000}$ - <i>b</i> -PGly $_{31}$ (green), polymer 2, PEG $_{5000}$ - <i>b</i> -PGly $_{14}$ (blue) and polymer 3, PEG $_{5000}$ - <i>b</i> -PGly $_{20}$ (red).	108
Figure 5.2. - APC chromatograms of PEG $_{5000}$ -OH (black, dashed), polymer 1, PEG $_{5000}$ - <i>b</i> -PGly $_{31}$ (green), polymer 2, PEG $_{5000}$ - <i>b</i> -PGly $_{14}$ (blue) and polymer 3, PEG $_{5000}$ - <i>b</i> -PGly $_{20}$ (red).	108
Figure 5.3. - $^1\text{H}$ NMR spectra of PEG methyl ether (Average $M_w$ = 5000 gmol $^{-1}$ ) (black, CDCl $_3$ , 500 MHz), polymer 4, PEG $_{5000}$ - <i>b</i> -PAla $_6$ (blue, D $_2$ O, 500 MHz) and polymer 5, PEG $_{5000}$ - <i>b</i> -PAla $_{14}$ (green, D $_2$ O, 500 MHz).	109
Figure 5.4. - APC chromatogram of PEG $_{5000}$ -OH (black, dashed), polymer 4, PEG $_{5000}$ - <i>b</i> -PAla $_6$ (blue) and polymer 5, PEG $_{5000}$ - <i>b</i> -PAla $_{14}$ (green).	110
Figure 5.5. - $^1\text{H}$ NMR of PEG methyl ether (Average $M_w$ = 5000 gmol $^{-1}$ ) (black, CDCl $_3$ , 400 MHz) and polymer 6, PEG $_{5000}$ - <i>b</i> -PPhe $_{25}$ (red, DMSO- $d_6$ , 400 MHz).	111
Figure 5.6. - APC chromatogram of PEG $_{5000}$ -OH (black, dashed) and polymer 6, PEG $_{5000}$ - <i>b</i> -PPhe $_{25}$ (red).	111
Figure 5.7. - DLS traces, taken in triplicate, of nanoparticle dispersions of a) polymer 1, PEG- <i>b</i> -PGly $_{31}$ , b) polymer 2, PEG- <i>b</i> -PGly $_{14}$ , c) polymer 3, PEG- <i>b</i> -PGly $_{20}$ , d) polymer 4, PEG- <i>b</i> -PAla $_6$ , e) polymer 5, PEG- <i>b</i> -PAla $_{14}$ and f) polymer 6, PEG- <i>b</i> -PPhe $_{25}$ .	113
Figure 5.8. - SEM images representative of nanoparticle dispersions of a) polymer 1, PEG- <i>b</i> -PGly $_{31}$ with 1 $\mu\text{m}$ scale bar, b) polymer 2, PEG- <i>b</i> -PGly $_{14}$ with 1 $\mu\text{m}$ scale bar, c) polymer 3, PEG- <i>b</i> -PGly $_{20}$ with 5 $\mu\text{m}$ scale bar, d) polymer 4, PEG- <i>b</i> -PAla $_6$ with 1 $\mu\text{m}$ scale bar, e) polymer 5, PEG- <i>b</i> -PAla $_{14}$ with 1 $\mu\text{m}$ scale bar and f) polymer 6, PEG- <i>b</i> -PPhe $_{25}$ with 1 $\mu\text{m}$ scale bar.	113
Figure 5.9. - Release of doxorubicin from nanoparticles of a) polymer 2, PEG $_{112}$ - <i>b</i> -PGly $_{14}$ , b) polymer 3, PEG $_{112}$ - <i>b</i> -PGly $_{20}$ , c) polymer 4, PEG $_{112}$ - <i>b</i> -PAla $_6$ and d) polymer 5, PEG $_{112}$ - <i>b</i> -PAla $_{14}$ , in response to incubation in acetate buffer at pH 5.0 (red) and PBS buffer at pH 7.4 (black).	116
Figure 6.1. - $^1\text{H}$ NMR spectrum (D $_2$ O, 500 MHz) of polymer 1, polysarcosine $_{77}$ .	130
Figure 6.2. - MALDI-TOF spectrum of polymer 1, polysarcosine $_{77}$ .	131
Figure 6.3. - $^1\text{H}$ NMR spectrum (CDCl $_3$ , 500 MHz) of polymer 6, PSar $_{77}$ - <i>b</i> -PAla $_9$ .	133

Figure 6.4. – MALDI-TOF spectra of polymer 1, polysarcosine <sub>77</sub> (blue) and polymer 6, polysarcosine <sub>77</sub> - <i>b</i> -polyalanine <sub>9</sub> (yellow).	133
Figure 6.5. – <sup>1</sup> H NMR spectrum (CDCl <sub>3</sub> , 500 MHz) of polymer 10, polysarcosine <sub>70</sub> - <i>ran</i> -polyalanine <sub>8</sub> .	135
Figure 6.6. – MALDI-TOF spectrum of polymer 10, polysarcosine <sub>70</sub> - <i>ran</i> -polyalanine <sub>8</sub> .	135
Figure 6.7. – <sup>1</sup> H NMR spectrum (DMSO- <i>d</i> <sub>6</sub> , 500 MHz) of polymer 11, polysarcosine <sub>35</sub> - <i>alt</i> -polyphenylalanine <sub>35</sub> .	137
Figure 6.8. – MALDI-TOF spectrum of polymer 11, polysarcosine <sub>35</sub> - <i>alt</i> -polyphenylalanine <sub>35</sub> .	138
Figure 6.9. – MALDI-TOF spectrum of the degradation products of polymer 11 after incubation with thermolysin at 37 °C for one week.	139
Figure 6.10. – <sup>1</sup> H NMR spectrum (CDCl <sub>3</sub> , 500 MHz) of camptothecin-polysarcosine <sub>14</sub> .	140
Figure 6.11. – MALDI-TOF spectrum of camptothecin-polysarcosine <sub>14</sub> .	140
Figure 6.12. - UV-vis spectrum of camptothecin suspended in deionised water (1 mg mL <sup>-1</sup> ) (red) and camptothecin-polysarcosine <sub>14</sub> dissolved in deionised water (7 mg mL <sup>-1</sup> ) (blue).	141
Figure 6.13. – DLS traces of nanoparticle dispersions of: a) polymer 6, b) polymer 7, c) polymer 8 and d) polymer 9.	142
Figure 6.14. – SEM images of nanoparticles of: a) polymer 6 (1 μm scale bar), b) polymer 7 (1 μm scale bar), c) polymer 8 (1 μm scale bar) and d) polymer 9 (10 μm scale bar).	143
Figure 6.15. – Percentage drug release over time from nanoparticles of polymer 6 when incubated with: ■) No enzyme, ▼) 20U chymotrypsin, ●) 8U elastase and ▲) 20U elastase.	145
Figure 7.1. – Representative SEM images of PCL fibres produced in A) spin 1, and B) spin 2 with scale bars of 10 μm.	160
Figure 7.2. – Representative SEM images of PCL/PAla nanofibres produced in A) spin 3, and B) spin 4 with scale bars of 10 μm.	160
Figure 7.3. – Representative SEM images of PCL/PAla nanofibres produced in A) spin 5, and B) spin 6 with scale bars of 10 μm.	161
Figure 7.4. - Representative SEM image of PCL/PAla nanofibres produced in spin 7, with a scale bar of 10 μm.	162
Figure 7.5. - Representative SEM image of PCL/PSar nanofibres produced in spin 8, with a scale bar of 10 μm.	162
Figure 7.6. – Stress-strain curves of PCL nanofibres produced in spin 2 (black), PCL/PAla nanofibres produced in spin 7 (red) and PCL/PSar nanofibres produced in spin 8 (blue).	165
Figure 7.7. – FTIR spectra of PCL/PAla nanofibre samples produced in spin 7 before (black) and after incubation with neutrophil elastase for 30 minutes (red), one hour (blue), 1.5 hours (green) and 2 hours (purple).	168

Figure 7.8. – SEM image of PCL/PAla nanofibres produced in spin 7 A) 0 minutes, B) 30 minutes, C) 60 minutes, D) 90 minutes and E) 120 minutes of incubation with 8U elastase.	169
Figure 7.9. – Stress-strain curves of PCL nanofibres (brown), PCL/PAla nanofibres before (black) and after incubation with elastase for 30 minutes (red), 1 hour (blue), 1.5 hours (green) and 2 hours (purple).	170
Figure 8.1. – $^1\text{H}$ NMR ( $\text{D}_2\text{O}$ , 500 MHz) spectrum of polymer 13, PPro <sub>59</sub> .	184
Figure 8.2. – MALDI-TOF spectrum of polymer 13, PPro <sub>59</sub> .	184
Figure 8.3. – $^1\text{H}$ NMR ( $\text{D}_2\text{O}$ , 500 MHz) spectrum of PPro <sub>106</sub> .	185
Figure 8.4. – MALDI-TOF spectrum of PPro <sub>103</sub> .	185
Figure 8.5. – $^1\text{H}$ NMR ( $\text{DMSO-d}_6$ , 500 MHz) spectrum of polymethionine <sub>21</sub> .	186
Figure 8.6. – $^1\text{H}$ NMR ( $\text{DMSO-d}_6$ , 500 MHz) spectrum of polyarginine(Pbf) <sub>24</sub> .	188
Figure 8.7. – $^1\text{H}$ NMR ( $\text{CDCl}_3$ , 500 MHz) spectrum of polyalanine produced via enzyme-catalysed ROP of alanine DKP.	189
Figure 8.8. – UV-vis spectrum of alanine DKP (red) dissolved in deionised water ( $5 \text{ mg mL}^{-1}$ ) and polyalanine (blue) suspended in deionised water ( $2.5 \text{ mg mL}^{-1}$ ).	190


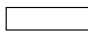

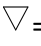
## List of Tables

Table 1.1. - Canonical, naturally occurring amino acid R groups.	3
Table 1.2. – Approximate particle size range for drug deposition in various body organs via different dosage forms and routes of administration.	22
Table 1.3. – Parameters of electrospinning and the effect of increasing or decreasing each parameter.	34
Table 1.4. – GSK Solvent Sustainability Guide <sup>205</sup> .	36
Table 2.1. – Chemicals used within the research conducted.	62
Table 4.1. - Mass and mole values of reagents and targeted number of repeat units of poly(amino acid) homopolymers.	84
Table 4.2. – Targeted and observed number of repeat units of poly(amino acid) homopolymers and polymeric formula of the resultant polymers.	85
Table 5.1. - Mass and mole values of reagents, and targeted number of repeat units of PEG- <i>b</i> -poly(amino acids).	104
Table 5.2. – Targeted and observed number of repeat units by <sup>1</sup> H NMR spectroscopy and APC of PEG- <i>b</i> -poly(amino acids).	104
Table 5.3. - Mean particle size and polydispersity values of polymers 4-9. Values obtained by DLS and SEM analyses.	114
Table 6.1. - Reagents, conditions, amounts and results of polymerisations of sarcosine DKP and block co-polymerisations of alanine DKP from polysarcosine.	125
Table 6.2. – Targeted number of repeat units and observed number of repeat units of homo polysarcosine (polymers 1-5), by NMR and MALDI analyses.	131
Table 6.3. - Targeted number of repeat units and observed number of repeat units of polysarcosine- <i>block</i> -polyalanine (polymers 6-9), by NMR and MALDI analyses.	134
Table 6.4. – Average particle diameter and polydispersity of nanoparticle solutions of polymers 6-9, determined by DLS and SEM analyses.	144
Table 7.1. – Parameters of electrospinning PCL, PCL/PAla and PCL/PSar nanofibres including solvent selection, weight percentage of polymer in solution, ratio of polymer solutions, potential difference applied during electrospinning, flow rate of solution, and time of electrospinning.	156
Table 7.2. - Percentage beading by area, average nanofibre diameter with standard deviation and average pore diameter with standard deviation of the 8 electrospun samples.	156
Table 7.3. – Weights of nanofibre samples before and after immersion in deionised water and their % water uptake and results from tensile testing including maximum stress and strain, elastic moduli and toughness of PCL, PCL/PAla and PCL/PSar nanofibre samples taken from spin 2, spin 7 and spin 8 respectively.	164

Table 7.4. – % mass loss, % beading, average fibre diameter, average pore diameter, and carbonyl intensities in FTIR spectra of PCL/PAla nanofibre samples that had been incubated with neutrophil elastase for 0, 0.5, 1, 1.5 and 2 hours. 166

Table 7.5. - Maximum strain, maximum stress, elastic moduli and toughness of PCL/PAla nanofibre samples that had been incubated with neutrophil elastase for 0, 0.5, 1, 1.5 and 2 hours. 167

## List of Schemes

Scheme 1.1. – Mechanism for the synthesis of an NCA via Leuchs’s method.	4
Scheme 1.2. – NCA synthesis via the Fuchs-Farthing method.	5
Scheme 1.3. – Phosgene-free synthesis of an NCA <sup>21</sup> .	6
Scheme 1.4. – Mechanism of NCA synthesis from Boc-protected amino acid and T3P, with heat or base catalysis <sup>22</sup> .	8
Scheme 1.5. - Dipeptide formation and cyclisation to form a 2,5-diketopiperazine <sup>23</sup> .	9
Scheme 1.6. - Direct amino acid condensation to form a 2,5-diketopiperazine <sup>23</sup> .	10
Scheme 1.7. – Reaction scheme of solid-phase peptide synthesis, where  = anchoring resin,  = linker,  = N-protecting group and  = side-chain protecting group, X,Y & Z = various amino acid side-chain functional groups.	12
Scheme 1.8. – General mechanism of NCA ROP via the normal amine mechanism <sup>38</sup> .	14
Scheme 1.9. - General mechanism of NCA ROP via the activated monomer mechanism, adapted from <sup>40,41</sup> .	15
Scheme 1.10. – Complexation of alcohol bearing initiators to Sn(Oct) <sub>2</sub> . <sup>71</sup>	17
Scheme 1.11. – Mechanism of ROP of lactide with Sn(Oct) <sub>2</sub> . <sup>71</sup> .	18
Scheme 3.1. – Ugi synthesis <sup>1</sup> .	65
Scheme 3.2. – Cyclisation of chloroacetamides to form a symmetric, 1,4-disubstituted DKP, where R <sub>1</sub> is aryl or alkyl <sup>1</sup> .	65
Scheme 3.3. – [4+2] Diels-Alder Cycloaddition to form DKP ring <sup>1</sup> .	66
Scheme 3.4. – Intramolecular cyclisation of an enolate onto a carbonyl to form a DKP ring <sup>1</sup> .	67
Scheme 4.1. - ROP of a DKP, initiated by benzylamine when R = benzyl and hexylamine when R = hexyl, and catalysed using tin(II) 2-ethylhexanoate.	84
Scheme 4.2. - Deprotection of Polylysine(Cbz) via hydrogenation with HBr/acetic acid.	85
Scheme 4.3. - Enzymatic degradation of polyalanine via incubation with elastase at 37 °C.	86
Scheme 5.1. - ROP of a DKP, initiated by PEG methyl ether (Average M <sub>w</sub> = 5000 g mol <sup>-1</sup> ) and catalysed using tin(II) 2-ethylhexanoate.	103
Scheme 6.1. - ROP of sarcosine DKP, initiated by benzylamine and catalysed initially by methanesulfonic acid (MSA) and followed by DIPEA catalysis, at 110 °C.	124
Scheme 6.2. - ROP of alanine DKP, initiated by polysarcosine and catalysed using tin(II) 2-ethylhexanoate (Sn(Oct) <sub>2</sub> ).	125
Scheme 6.3. - One-pot ROP of a sarcosine DKP and alanine DKP, initiated by benzylamine to produce polysarcosine- <i>ran</i> -polyalanine. The polymerisation is initially catalysed using MSA, followed by DIPEA, all of which at 110 °C.	126



Scheme 6.4. - ROP of sarcosine DKP from camptothecin, catalysed initially by MSA, followed by DIPEA, all of which at 110 °C.	126
Scheme 6.5. - ROP of sarcosine-L-phenylalanine DKP, initiated by benzylamine and catalysed initially by MSA and followed by the catalysis of DIPEA, at 110 °C.	127
Scheme 7.1. – Amino acid to nanofibres; via DKP synthesis, DKP ROP and electrospinning with PCL.	158
Scheme 8.1. - Reaction scheme of ROP of proline DKP, initiated with benzylamine and catalysed using MSA initially, followed by neutralisation and base catalysis with DIPEA, at 110 °C.	179
Scheme 8.2. – Ring-opening polymerisation of methionine DKP at 130 °C in anhydrous DMF, initiated from benzylamine and catalysed by tin(II) 2-ethylhexanoate.	180
Scheme 8.3. – ROP of arginine(Pbf) DKP from benzylamine in DMF at 110 °C, catalysed by N,N-diisopropylethylamine.	181
Scheme 8.4. – Enzyme-catalysed ring-opening polymerisation of alanine DKP in deionised water at 65 °C, catalysed by Candida Antarctica Lipase B.	181

## List of Abbreviations

Đ - Dispersity	3D - Three dimensional
AC - Alternating current	Ala - Alanine
APC - Advanced Polymer Chromatography	APD - Avalanche Photodiode
API - Active pharmaceutical ingredient	Arg - Arginine
Asn - Asparagine	Asp - Aspartic acid
ATP - Adenosine Triphosphate	Boc - Tert-butyloxycarbonyl
CAC - Critical aggregate concentration	CALB - Candida Antarctica Lipase B
Cbz - Benzyloxycarbonyl	Cys - Cysteine
DC - Direct current	DCC - N,N'-Dicyclohexylcarbodiimide
DCM - Dichloromethane	DIPEA - N,N-Diisopropylethylamine
DKP - 2,5-Diketopiperazine	DLS - Dynamic Light Scattering
DMAP - Dimethylaminopyridine	DMF - N,N-Dimethylformamide
DMSO - Dimethyl sulfoxide	Dox - Doxorubicin
DPC - Diphenyl carbonate	DSC - Differential Scanning Calorimetry
ECM - Extracellular matrix	EDC - 1-ethyl-3-(3-dimethylaminopropyl)carbodiimide
EE% - encapsulation efficiency %	eROP - enzyme-catalysed ring-opening polymerisation
Fmoc - Fluorenylmethoxycarbonyl	FTIR - Fourier-Transform Infrared
Gln - Glutamine	Glu - Glutamic acid
Gly - Glycine	GSK - GlaxoSmithKline
HBTU - Hexafluorophosphate Benzotriazole Tetramethyl Uronium	HFIP - Hexafluoroisopropanol
His - Histidine	HPLC - High-Performance Liquid Chromatography
Ile - Isoleucine	IRI - Ice-recrystallisation inhibition

LC% - Loading Content %	LC-MS - Liquid Chromatography - Mass Spectrometry
Leu - Leucine	Lys - Lysine
M.W.C.O. - Molecular weight cut-off	MALDI-TOF - Matrix-Assisted Laser Desorption/Ionisation - Time of Flight
Met - Methionine	MMP-1 - Metalloprotease 1
Mn - Number averaged molecular weight	MPS - Mononuclear phagocyte system
Mw - Weight averaged molecular weight	NCA - N-carboxyanhydride
NIOSH - National Institute for Occupational Safety and Health	NMR - Nuclear Magnetic Resonance
EDC - 1-ethyl-3-(3-dimethylaminopropyl)carbodiimide	NP - Nanoparticle
OCA - O-carboxyanhydride	P (when preceding amino acid abbreviation) - Poly
PAla - Polyalanine	Pbf - 2,2,4,6,7-Pentamethyldihydrobenzofuran-5-sulfonyl
PBS - Phosphate-buffered saline	PCL - Polycaprolactone
PEG - Poly(ethylene glycol)	PHBV - poly(hydroxy-co-hydroxyvalerate)
Phe - Phenylalanine	Pro - Proline
RI - Refractive Index	ROP - Ring-Opening Polymerisation
ROPISA - Ring-Opening Polymerisation-Induced Self-Assembly	Sar - Sarcosine
SEM - Scanning Electron Microscopy	Ser - Serine
Sn(Oct) <sub>2</sub> - Tin(II) 2-ethylhexanoate	SSPS - Solid-state peptide synthesis
T3P - Propylphosphonic anhydride	TFA - Trifluoroacetic acid
THF - Tetrahydrofuran	Thr - Threonine
Trp - Tryptophan	Tyr - Tyrosine
UV-vis - Ultra violet - visible	Val - Valine



## Chapter 1 – Introduction

### 1.1. Polymerisation

Polymerisation is a chemical process in which a polymer is formed via the chemical bonding of repeating monomer units<sup>1</sup>. There are two umbrella classifications of polymerisation; chain-growth polymerisation and step-growth polymerisation.

Chain-growth polymerisation involves monomers freely binding to an active-chain end via transfer of activity from an initiator to a monomer. As the monomer binds to the initiator, the active-chain end migrates to the monomer, which then transfers to another monomer and the polymerisation propagates until the radical is terminated. These polymerisations can also be driven by ion transfer, coordination or the opening of a ring. In this mechanism, higher molecular weight polymers are produced rapidly due to the free binding of monomers to the active chain-end<sup>2,3</sup>.

Step-growth polymerisation involves monomers binding to form dimers, followed by dimers forming tetramers, which form octamers and so on. This process takes a greater amount of time to form longer polymer chains. However, with particular monomers, and by utilising catalysts and initiators, step-growth polymerisation can be a rapid and controlled method to producing long-chained polymers with a narrow dispersity ( $\mathcal{D}$ ) and active chain ends<sup>2,3</sup>.

### 1.2. Monomers

#### 1.2.1. Amino Acids

$\alpha$ -Amino acids (Figure 1.1.) comprise of an amine group at one terminus and a carboxylic group at the other, along with an R group attached at the  $\alpha$ -carbon that varies dependent on the amino acid in question. In naturally occurring amino acids, the R group adopts the L configuration, alternatively expressed as the S configuration using the Cahn-Ingold-Prelog rules.

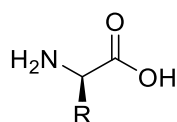


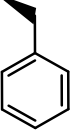
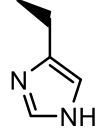
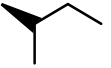
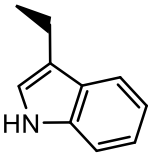
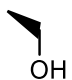
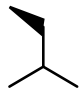
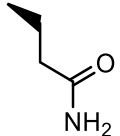

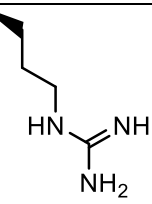
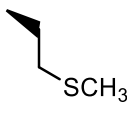
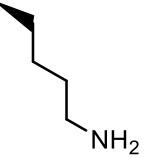
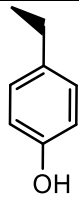
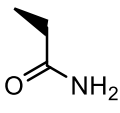

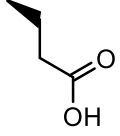
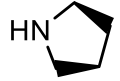
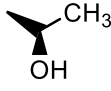
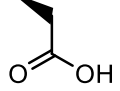
Figure 1.1. – General structure of an  $\alpha$ -amino acid.

Amino acids may be polymerised in polycondensation reactions to form poly(amino acids) via step-growth polymerisation. These reactions occur naturally in the formation of proteins and peptides in living organisms<sup>4</sup>. Over 250 amino acids exist, however, only 20 of these occur

naturally (Table 1.1.). The R groups of these amino acids have a wide variety of functional groups which significantly influence chemical and physical properties, of both the amino acid itself and its corresponding polymer<sup>5</sup>. The R groups can be distinguished as aliphatic hydrophobic, aromatic hydrophobic, hydrophilic, polar neutral, non-polar neutral, acidic, and basic side chains.

Amino acids are attractive building blocks for polymers; they are naturally occurring, biocompatible and the variety of R groups present in different amino acids provides versatility of function of resultant polymers<sup>5</sup>.

Table 1.1. - Canonical, naturally occurring amino acid R groups<sup>6</sup>.

Name	Abbreviation	R Group Structure	Name	Abbreviation	R Group Structure
Phenylalanine	Phe		Histidine	His	
Isoleucine	Ile		Glycine	Gly	H
Tryptophan	Trp		Serine	Ser	
Leucine	Leu		Glutamine	Gln	
Valine	Val		Arginine	Arg	
Methionine	Met		Lysine	Lys	
Tyrosine	Tyr		Asparagine	Asn	
Cysteine	Cys		Glutamic Acid	Glu	
Alanine	Ala	CH <sub>3</sub>	Proline	Pro	
Threonine	Thr		Aspartic Acid	Asp	

### 1.2.2. N-carboxyanhydrides (NCAs)

Amino acid polycondensation to produce poly(amino acids) offers little control with respect to molecular weight and  $\bar{D}$ . A well-documented alternative is to use amino acids to synthesise amino acid based cyclic molecules such as amino acid N-carboxyanhydrides (NCAs) (Figure 1.2.)<sup>8</sup>. Such molecules, when polymerised from an initiator, produce polymers much closer to the targeted molecular weight and with a much narrower  $\bar{D}$  compared to poly(amino acids) produced by step-growth polymerisation.

NCAs are heterocyclic five membered rings containing an anhydride group as well as an R group matching that of the respective amino acid.

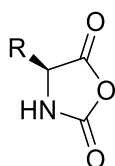
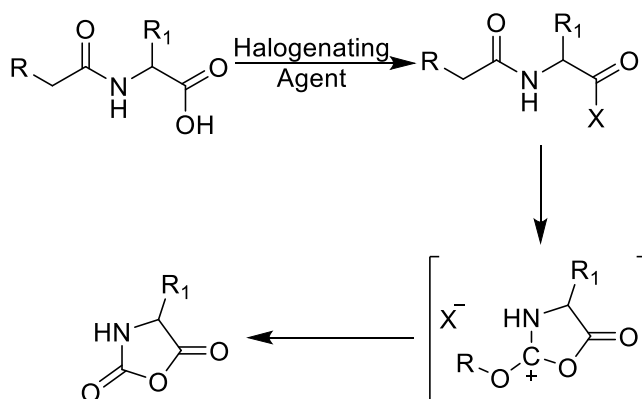


Figure 1.2. – General structure of an amino acid N-carboxyanhydride.

NCAs are well documented as a desirable monomer for the synthesis of poly(amino acids) due to the controllability and facility of their polymerisation. They were first synthesised accidentally by Leuchs when attempting to distil N-alkoxycarbonyl amino acid chlorides<sup>9,10</sup>. The following Leuchs's method involved heating N-alkoxycarbonyl amino acids in the presence of a halogenating agent under vacuum and at 60 °C (Scheme 1.).

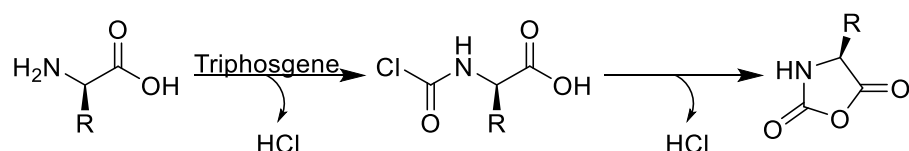


Scheme 1.1. – Mechanism for the synthesis of an NCA via Leuchs's method.



However, NCAs are delicate and very susceptible to ring-opening. The heat required in this method results in the degradation of the NCA, resulting in lower and less pure yields.

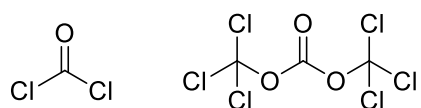
A notable improvement, and the most common method used for NCA synthesis today, is the Fuchs-Farthing method which utilises phosgene gas in order to directly phosgenate a free  $\alpha$ -amino acid (Scheme 1.2.). The N-chloroformyl amino acid intermediate is formed upon ejection of a molecule of HCl and, subsequently, a second HCl molecule is lost resulting in cyclisation to form the NCA.



*Scheme 1.2.* – NCA synthesis via the Fuchs-Farthing method.

This method is desirable as it involves a one-step synthesis and results in high percentage yields with little side product or waste<sup>11</sup>. However, the use of phosgene poses a significant problem, especially when scaling up to an industrial level. Phosgene is extremely poisonous; its use in World War I as a chemical weapon resulted in approximately 85,000 deaths<sup>12</sup>. The National Institute for Occupational Safety and Health (NIOSH) determined that the Immediately Dangerous to Life or Health concentration of phosgene is only 2 ppm<sup>13</sup>. Due to phosgene being gaseous at room temperature and pressure, it is difficult to control and, in the case of a leak, difficult to contain. As such, it poses a significant hazard which is exacerbated further when scaling up.

The trimer of phosgene, triphosgene, exists as a solid crystal structure at room temperature and pressure (Figure 1.3.). Under reflux conditions, triphosgene can be broken down to release phosgene molecules *in situ*, reducing the significance of the hazard posed<sup>14,15,16</sup>.

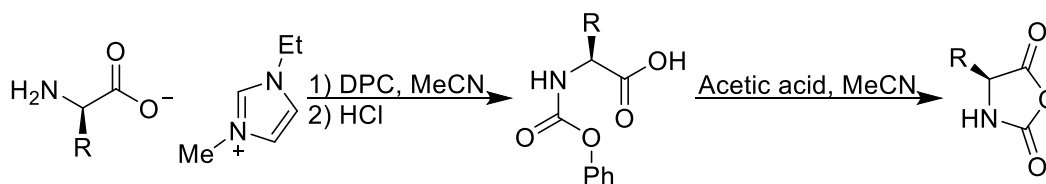


*Figure 1.3.* – Structure of phosgene (left) and triphosgene (right).

When scaling up, there is an increased preponderance for the NCA to react with HCl to form an  $\alpha$ -amino acid chloride, compromising the yield and quality of NCA product<sup>17,18</sup>. There are multiple approaches to combat this issue; the most common of which is to utilise an HCl scavenger such as  $\alpha$ -pinene or limonene during NCA synthesis to remove the HCl<sup>19</sup>. Other strategies, such as including activated charcoal or the continuous addition of strong base, are also employed<sup>20</sup>.

Despite these improvements, NCAs produced via the Fuchs-Farthing method require time consuming purification steps to remove unwanted impurities and reactants that remain. High purity of NCAs is essential for their successful application, particularly in poly(amino acid) synthesis as electrophilic impurities such as HCl and HCl salts of unreacted amino acids can act as chain transfer agents in ring-opening polymerisation (ROP) of the NCA, disrupting the polymerisation and detrimentally affecting  $\bar{M}_n$  of the resultant polymer. Recrystallisation under anhydrous conditions is a commonly practiced method that results in moderately pure products. However, thermal recrystallisation is unsuitable when handling NCAs with extended functionality and lower melting points; multi-solvent recrystallisation/precipitation is much more effective.

The combined drawbacks of HCl generation, the hazardous nature of phosgene use and the compromised purity of the Fuchs-Farthing method, all of which are exacerbated when scaled up, have driven the development of phosgene-free alternatives of NCA synthesis. Koga *et al.*<sup>21</sup> report a three-step phosgene-free synthesis of NCAs in which an amino acid is firstly converted to the corresponding imidazolium salt, then reacted with diphenyl carbonate (DPC) forming the urethane derivative which is finally heated with acetic acid to trigger cyclisation to form the NCA<sup>21</sup>.



Scheme 1.3. – Phosgene-free synthesis of an NCA<sup>21</sup>.

DPC is much less toxic than phosgene, relatively inexpensive and produced in a completely phosgene-free synthesis. However, DPC is also less electrophilic than phosgene, as such the zwitterions of  $\alpha$ -amino acids are not sufficiently nucleophilic enough to react. Additionally, several  $\alpha$ -amino acids have significantly poor solubility in many organic solvents, in this case

acetonitrile. As such, conversion of the  $\alpha$ -amino acid to the imidazolium salt was required to increase solubility and stimulate reactivity with DPC<sup>21</sup>.

Successful conversion of imidazolium salts to the corresponding urethanes was achieved via a rapid reaction with DPC, resulting in high yields and maintaining stereochemistry with very limited racemisation. Cyclisation of urethanes to the respective NCAs was acid catalysed, producing phenol as the only side product. Addition of activated charcoal to the NCA/phenol solution was effective in removing the phenol, yielding the highly pure NCA. This procedure requires a minimum of four days to complete all three synthetic steps, not including the final purification step required to remove phenol. Considering this, as well as the lower yield compared to that of the Fuchs-Farthing method, it is apparent that synthesising NCAs phosgene-free comes with compromises. However, despite the drawbacks, this synthesis can serve as a suitable foundation for further development of phosgene-free syntheses of NCAs<sup>21</sup>.

A recently proposed route to NCA synthesis, in the absence of phosgene, is by the conversion of a tert-butyloxycarbonyl-protected (Boc)  $\alpha$ -amino acid using propylphosphonic anhydride (T3P)<sup>22</sup> (Figure 1.4.). The reaction is activated by the opening of T3P using heat or basic conditions (Scheme 1.4.). The linear T3P esterifies the exposed carboxylic acid of the amino acid, providing an excellent leaving group. After cleavage of the Boc and T3P groups, the exposed amino acid can cyclise, yielding the desired NCA and a collection of side products. This route promises to be a facile method to produce NCAs on small or large scale. However, it is in early stages of development, requires Boc-protection of the amine group of the amino acid and currently requires substantial purification to remove the side products.<sup>22</sup>

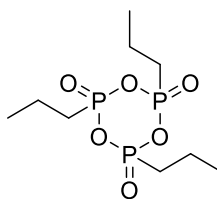
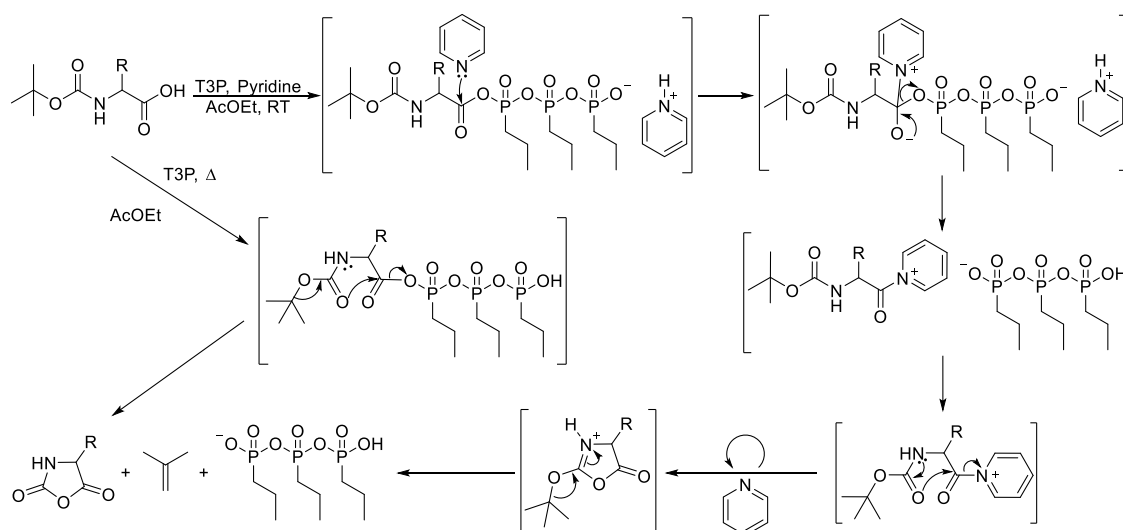


Figure 1.4. – Structure of propylphosphonic anhydride (T3P).



*Scheme 1.4.* – Mechanism of NCA synthesis from Boc-protected amino acid and T3P, with heat or base catalysis<sup>22</sup>.

NCA use is limited by their instability and poor resistance to nucleophilic attack, requiring storage under anhydrous conditions and extremely thorough purification to prevent premature polymerisation. Furthermore, there are other amino acid based monomers that have greater stability than NCAs, as well as more mild and facile syntheses.

### 1.2.3. 2,5-Diketopiperazines (DKPs)

The nomenclature of 2,5-diketopiperazines is rather convoluted. Depending on the source, 2,5-diketopiperazine is named as piperazine-2,5-dione, glycine anhydride and cyclo(Gly-Gly). All of the names are accurate descriptors, however, herein they will be referred to as 2,5-diketopiperazines and abbreviated to “DKP”(s) as no other diketopiperazines (such as 2,3-diketopiperazines or 2,6-diketopiperazines) are used or referenced within the research. DKPs are found in reasonable abundance in nature, produced often as the degradation products of polypeptides but also as a subunit of larger, more complex structures<sup>23</sup>. A DKP is a conformationally constrained, six membered heterocyclic ring, consisting of two amide linkages with cis-amide bonds such that the nitrogen atoms and carbonyl groups occupy opposite sides of the ring from each other<sup>23</sup> (Figure 1.5.). As such, they contain two H-bond acceptor sites and two H-bond donor sites<sup>23</sup>. Attached to the carbons between the amide linkages are the R groups determined by the amino acid used to synthesise the DKP.

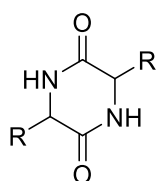
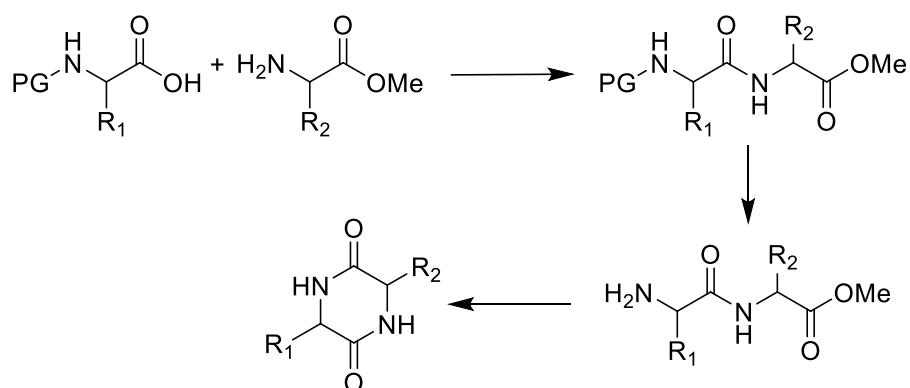


Figure 1.5. – General structure of a 2,5-diketopiperazine (DKP).

Over the past century, many synthetic routes have been developed to produce DKPs. Reviewers such as Borthwick<sup>23</sup>, Fischer<sup>24</sup> and Dinsmore and Beshore<sup>25</sup> have succinctly summarised these different methods.

There are four general mechanisms via which DKPs are formed, each of which can be achieved through a number of synthetic routes. These are: amide bond formation, N-alkylation, tandem cyclisation and C-acylation<sup>23,24,25</sup>.

The most common method used to synthesise DKPs is dipeptide formation and cyclisation<sup>23</sup> (Scheme 1.5.). Dipeptides, when esterified at the carboxylic terminus and substituted at the amine terminus, can spontaneously cyclise upon deprotection of the amine group across a range of pH. In order to limit racemisation, reagents must be carefully selected<sup>23</sup>.



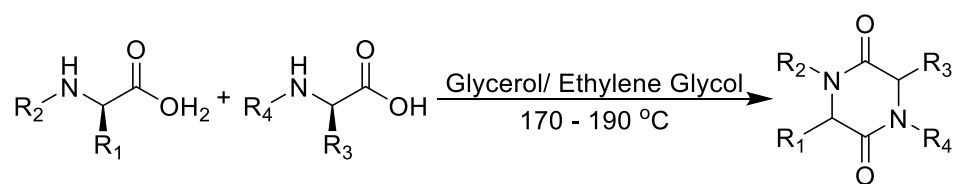
Scheme 1.5. - Dipeptide formation and cyclisation to form a 2,5-diketopiperazine<sup>23</sup>.

A dipeptide can be formed via the coupling of an N-protected amino acid and an  $\alpha$ -amino acid ester<sup>23,24,25</sup>. Many coupling reagents are appropriate. For example, a combination of 4-dimethylaminopyridine (DMAP) and N,N'-dicyclohexylcarbodiimide (DCC), with a similar procedure to Steglich esterification<sup>26</sup>, can be utilised. After cleaving the N-protecting group utilising standard deprotection procedures, the amino dipeptide ester can cyclise *in situ* to form

the DKP. Cyclisation requires a cis-orientation of the amide bond. As such, restriction of the cis-orientation by steric or electronic hindrance is detrimental to cyclisation and reduces the rate of reaction significantly. However, heating the amino peptide ester under acidic conditions can force ring closure<sup>27</sup>. Basic conditions may also be utilised, however this can result in greater racemization<sup>27</sup>.

This synthetic route retains the stereo chemistry of the R group as well as allowing for the combination of two different amino acids, forming asymmetric DKPs<sup>23</sup>. However, unless amino acids are purchased bearing protecting groups and as amino acid esters, the synthesis can become arduous, involving five steps; N-protection of amino acid, esterification of amino acid, coupling to form protected dipeptide ester, deprotection of dipeptide ester and subsequent cyclisation. At each step, yields are moderate. As such, the final yield can be small compared to that of the starting materials of the first step.

A simpler alternative to dipeptide synthesis and cyclisation is direct condensation of two amino acids<sup>23</sup> (Scheme 1.6.).



*Scheme 1.6.* - Direct amino acid condensation to form a DKP<sup>23</sup>.

This can be achieved by dissolving the amino acids in glycerol or ethylene glycol and heating at 170 – 190 °C<sup>28</sup>. Despite its ease, this method is not frequently utilised due to poor reported yields<sup>23</sup>. A common improvement is to activate the amino acid with phosgene, or a similar halogenating agent, and subsequently adding the second amino acid<sup>23</sup>. However, as mentioned previously regarding the synthesis of NCAs, the use of phosgene has many significant issues, making it unsuitable for industrial scale application.

Santagada *et al.*<sup>29</sup> report an improvement to amino acid condensation, involving the use of microwave radiation as well as amide bond-coupling agents (HBTU/DMAP). With 400 W of microwave radiation in DMF, very high yields of pure DKPs can be achieved with very short reaction times. This reaction method has since been developed further. By adding small amounts of ionic liquid to the microwave catalysed reaction, symmetrical and unsymmetrical DKPs can be stereoselectively prepared in the absence of protecting groups<sup>30</sup>. Jainta *et al.*<sup>30</sup> and Nonappa *et al.*<sup>31</sup> have achieved similarly high yields with high purity of DKPs utilising microwave

radiation, synthesising a plethora of DKPs including N-substituted DKPs and asymmetric DKPs<sup>30,31</sup>. However, scaling up reactions involving microwave radiation poses significant problems. Most of the chemical industry does not have microwave reactors and incorporating a microwave reactor into established systems would incur considerable expense<sup>32</sup>. Therefore, other methods must be considered as a starting point for the development of an industrially reproducible, facile synthesis of DKPs.

### **1.3. Polymerisation to Form Poly(amino acids)**

#### **1.3.1. Polycondensation of Amino Acids**

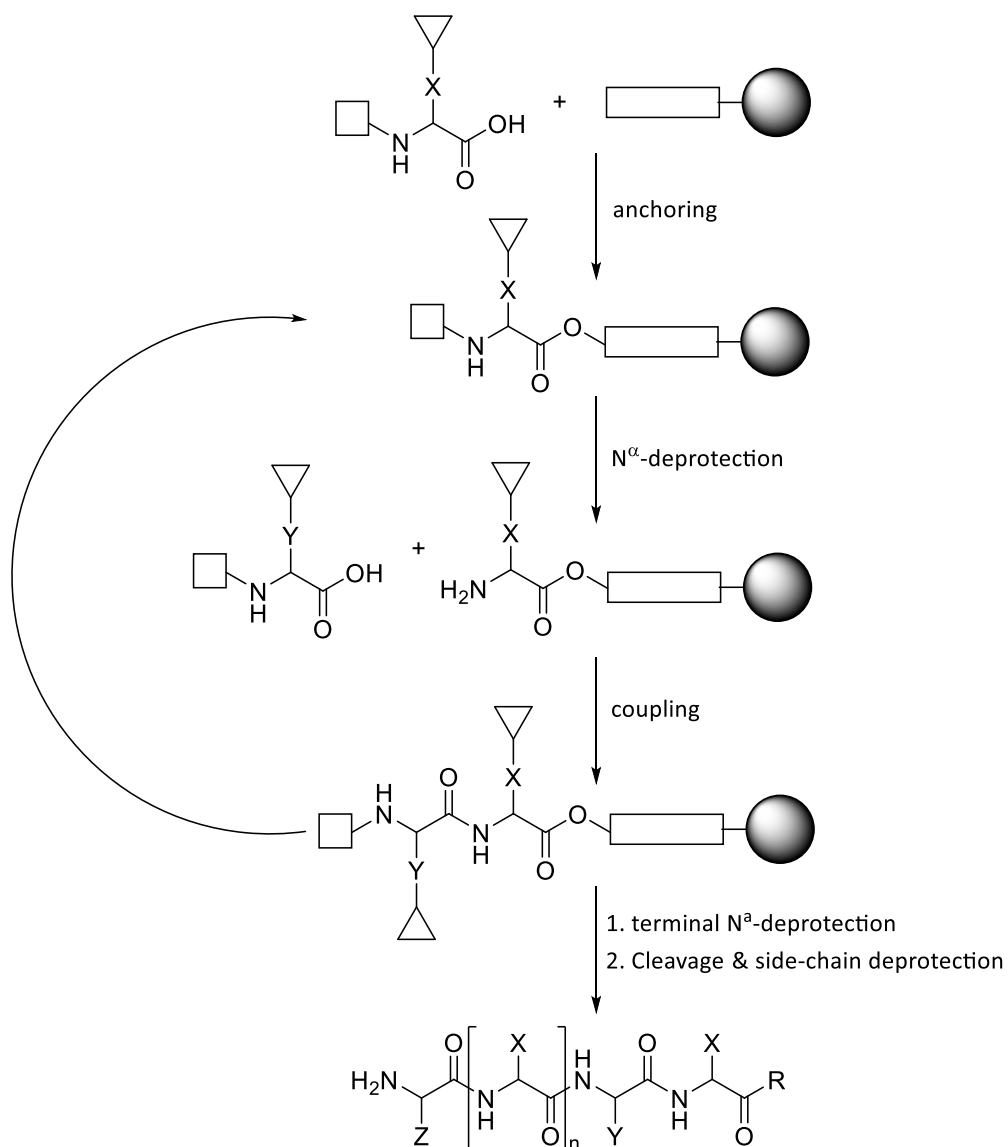
The simplest route to producing a poly(amino acid) is the direct polycondensation of amino acids. Typically, this is achieved by melting the amino acid(s), causing polymerisation to occur. Due to their zwitterionic properties and a resultant ionic attraction between zwitterions, amino acids have very high melting points. As a consequence, very high temperatures are required to melt the amino acids and induce polymerisation.

Early works by Frankel and Katchalski<sup>33,34</sup> included the successful polymerisation of methyl and ethyl esters of both glycine and alanine. Both methyl and ethyl esters of glycine and alanine are liquid at room temperature, removing the requirement for high temperature reactions. For glycine, the methyl ester resulted in polymers with 110 repeat units, whereas that of the ethyl ester reached 42 repeat units. However, alanine ethyl ester showed limited polymerisation, resulting in a maximum of 16 repeat units. Room temperature polymerisations of alanine ethyl ester were demonstrated, albeit with only four repeat units. Polymerisations of alanine from a 14 repeat unit polyalanine (PAla) macro initiator were attempted at 150 °C in order to achieve higher molecular weight polymers. However, the maximum number of repeat units of polyalanine were 23, short enough to be soluble in water. This polymerisation route offers little control with respect to targeting number of repeat units and minimising Đ, as well as producing a substantial amount of side-product such as 2,5-diketopiperazine of the respective amino acid.<sup>33,34</sup>

Subsequently, Harada and Fox<sup>7</sup> produced linear random copolymers by direct thermal polycondensation of glycine and glutamic acid, observing a greater degree of polymerisation at their highest temperature, 190 °C. Whilst high molecular weight polymers were produced, approximately 20 kDa, Đ of the obtained polymers was very high and the synthetic route offers little control with respect to targeting number of repeat units.<sup>7</sup>

### 1.3.2. Solid-Phase Peptide Synthesis

Another common route to poly(amino acids) is by solid phase peptide synthesis (SSPS)<sup>35</sup>, involving the construction of a peptide by the coupling of one amino acid at a time<sup>36</sup>.



*Scheme 1.7.* – Reaction scheme of solid-phase peptide synthesis, where  $\bullet$  = anchoring resin,  $\square$  = linker,  $\square$  = N-protecting group and  $\nabla$  = side-chain protecting group, X, Y & Z = various amino acid side-chain functional groups.

The amino acid coupling is achieved by anchoring an N-protected and side-chain protected amino acid to a resin by a linker. Following anchoring, the amino acid is N-deprotected and a second side-chain and N-protected amino acid is coupled<sup>36</sup>. This deprotection and coupling cycle can be repeated to grow the peptide to the desired length. Once the targeted polymer is



produced, it is obtained by terminal N-deprotection, cleavage from the anchoring resin and side-chain deprotection<sup>36</sup>.

SSPS offers very precise control over the length and composition of a poly(amino acid), allowing for the production of complex and nuanced peptide structures with specific amino acid sequences<sup>36</sup>. However, it suffers from poor atom economy owing to requisite protecting groups of both the amine group of the amino acid and the side-chain group, as well as coupling reagents and a resin support. Whilst each amino acid coupling can achieve high yields, the required repetition of the reaction guarantees exponentially suffering yields as longer polymers are targeted<sup>37</sup>. As such, this method is limited in achievable polymer length, scalability and sustainability.

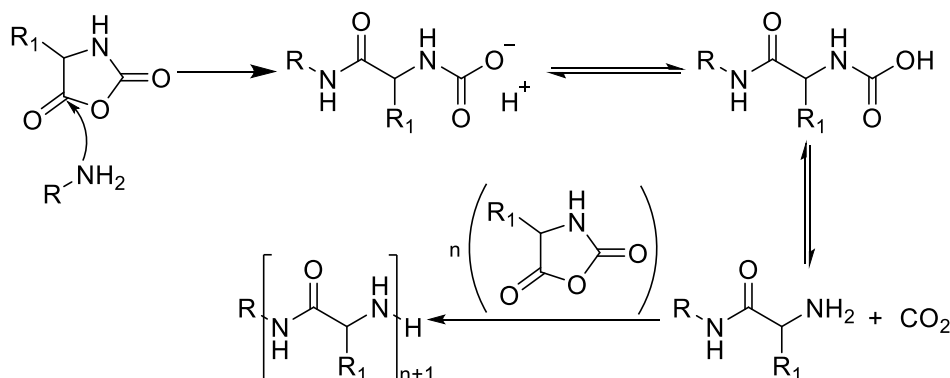
### **1.3.3. NCA Ring-Opening Polymerisation (NCA ROP)**

Ring-opening polymerisation (ROP) involves the attack of an initiator/initiator-catalyst system on cyclic monomers to form a polymer, the terminus of which becomes a reactive centre that can continue to attack cyclic monomers to propagate the polymerisation. ROP can be radical, anionic or cationic in mechanism. Cyclic molecules, such as glycolides, NCAs, DKPs and 2.5-morpholinediones, as well as other lactones and lactams, are suitable monomers for ROP. This is a form of chain-growth polymerisation that begins from a functional initiator, which offers control over the number of repeat units, i.e. the molecular weight of the polymer. ROP is usually driven by relief of bond-angle strain, however the rate can be increased by using a catalyst. This research will place a focus on developing ROP of DKPs as a viable synthetic route to poly(amino acids). Utilising this method may provide access to poly(amino acids) previously thought to be unobtainable.

NCA ROP offers a simplistic and versatile method of preparation of poly(amino acids), be that of high molecular weight or low molecular weight. Recent developments of NCA ROP, in concert with the wide variety of amino acids that are commercially available, has allowed for the synthesis of polymers with a variety of physicochemical properties, defined molecular weights and narrow Đ.

There are two mechanisms via which an NCA ROP can proceed; the normal amine mechanism (Scheme 1.8.) and the activated monomer mechanism<sup>38</sup> (Scheme 1.9.). The mechanism by which the ROP proceeds is determined by the type of initiator used.

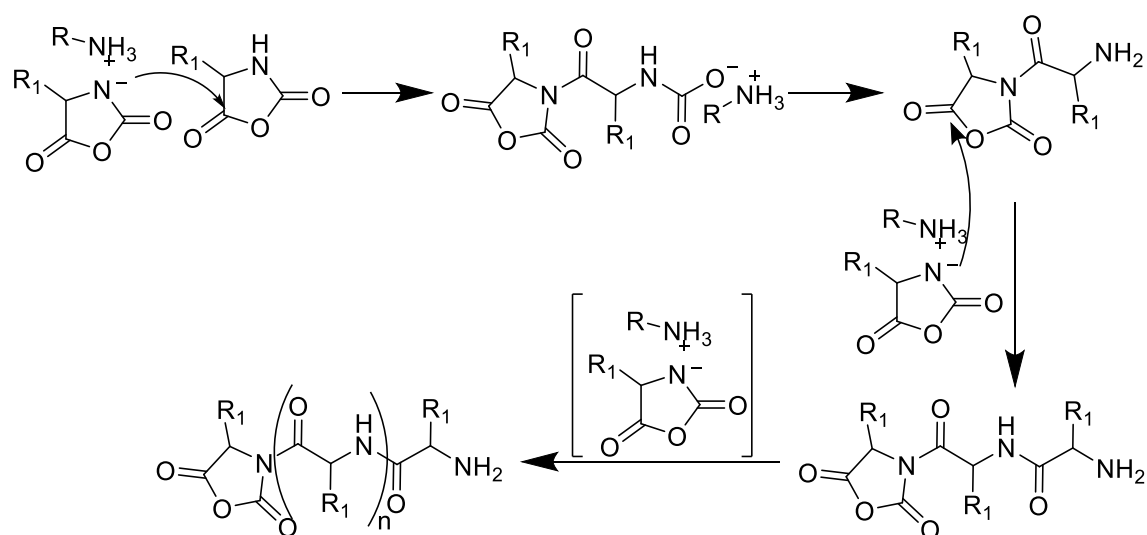
NCA ROP via the normal amine mechanism can be initiated by molecules bearing nucleophilic groups, particularly molecules that are non-ionic and bear a mobile proton<sup>39</sup>, examples of which are primary and secondary amines, alcohols and water.



*Scheme 1.8.* – General mechanism of NCA ROP via the normal amine mechanism<sup>38</sup>.

The nucleophilic initiator attacks the NCA at the most electrophilic carbonyl, this being the carbonyl that is on the opposite side of the ring from the nitrogen atom. This attack triggers the NCA to open and following a proton migration, forms an unstable carbamic acid. Upon ejection of a carbon dioxide molecule a terminal amine group is exposed and able to attack another NCA ring in the same fashion, propagating the polymerisation. The final polymer length can be controlled by the monomer:initiator molar ratio. As this mechanism is initiated by a nucleophilic group, the extent to which the initiator is nucleophilic dictates the efficacy of the initiator and therefore the rate of initiation<sup>40</sup>. Most initiators utilised in the normal amine mechanism of NCA ROP are very nucleophilic, to the extent that rate of initiation exceeds rate of propagation, restricting the maximum molecular weight achievable for polymers generated. Measures can be implemented to slow the rate of initiation such as reducing reaction temperature. However, depending on the targeted molecular weight, this may not be necessary and could compromise the Đ of the polymer.

NCA ROP via the activated monomer mechanism is initiated by bases; particularly tertiary amines. However, in this case, it is more accurate to describe the tertiary amine as a catalyst rather than an initiator<sup>40,41,42</sup> (Scheme 1.9.).



*Scheme 1.9.* - General mechanism of NCA ROP via the activated monomer mechanism, adapted from<sup>40,41</sup>.

As a base, the tertiary amine does not bind to the NCA, it instead activates an NCA by deprotonating the nitrogen in the ring and increasing its nucleophilicity. The activated NCA is able to nucleophilically attack a non-activated NCA, causing ring-opening and ejection of a carbon dioxide molecule in a way that is similar to the initiator in the normal amine mechanism. Another activated NCA can then attack the unopened ring and propagate the polymerisation. N-substituted NCAs are not able to be ring-opening polymerised via the activated monomer mechanism as deprotonation of the nitrogen is required. Tertiary amine groups are not very reactive, as such the rate of initiation is considerably slower than the rate of propagation. This results in polymers with high molecular weights but broad  $\bar{D}$ <sup>38,39,43</sup>.

The facility of and the interest in products generated by NCA ROP have driven procedural optimisation in order to minimise chain transfer and termination, reducing  $\bar{D}$  and obtaining polymers that have average molecular weight values closer to the targeted value. Optimisations include utilising high vacuum systems<sup>42</sup>, low temperatures<sup>41,44</sup> and a plethora of catalysts. The latter is of limited use to this research as any catalyst that compromises polymer biocompatibility would render the product unusable for a drug delivery vehicle or, at best, require substantial purification to remove the catalyst from the products.

High vacuum systems are a facile method to extract impurities, such as carbon dioxide and carbamic species, from the reaction mixture<sup>41,45</sup>. This minimises the extent to which impurities can promote side reactions or otherwise terminate the polymerisation<sup>41,45</sup>. As such, a living polymerisation can be sustained, resulting in 100% yields and very narrow  $\bar{D}$  of polymers<sup>46,47</sup>.

Temperature has been found to have a significant effect on NCA ROP, influencing the  $\bar{M}_n$  and molecular weight of yielded polymers<sup>48</sup>. The literature indicates that degree of polymerisation decreases as the temperature of the reaction is increased<sup>49</sup>, suggesting that rate of chain transfer and termination are dominant at higher temperatures whereas rate of propagation is dominant at lower temperatures. Low temperatures (0 °C), in concert with high vacuum systems, have been used successfully with a range of NCAs to produce polymers and block copolymers with low  $\bar{M}_n$ <sup>38</sup>.

#### 1.3.4. 2,5-Diketopiperazine Ring-Opening Polymerisation (DKP ROP)

It is clear from literature surrounding DKPs, as well as literature surrounding ROP, that ROP of DKPs has not been explored previously. However, polymerisation of the oxygen-bearing analogues, glycolides and 2,5-morpholinediones, is well established.

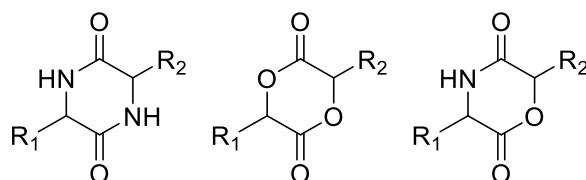


Figure 1.6. – General structures of 2,5-diketopiperazines (left), glycolides (centre) and 2,5-morpholinediones (right).

There are significant structural similarities between DKPs, glycolides and 2,5-morpholinediones (Figure 1.6.). Therefore, techniques used to polymerise glycolides and 2,5-morpholinediones may serve as a suitable starting point for the polymerisation of DKPs.

For both glycolides and 2,5-morpholinediones, ROP is conducted in a very similar fashion. The monomer(s), along with an initiator and catalyst, are heated under nitrogen beyond the melting point of the monomer and the polymerisation proceeds in bulk<sup>50,51,52,53,54,55,56,57,58</sup>. Commonly, the ROP is catalysed by FDA approved, food grade tin(II) 2-ethylhexanoate ( $\text{Sn}(\text{Oct})_2$ )<sup>59</sup> (Figure 1.7.), which aids in the production of stereo-regular polymers with high molecular weights<sup>50-58</sup>. Similar to NCA ROP, ROP utilising  $\text{Sn}(\text{Oct})_2$  allows for copolymerisation of more than one type of monomer, be it statistical or block co-polymerisation<sup>50,51,53,54,57</sup>. ROP with  $\text{Sn}(\text{Oct})_2$  can be fairly slow; increasing the rate of polymerisation is desirable for economic and commercial benefit<sup>60</sup>. This can be achieved by the addition of an equimolar amount of triphenyl phosphine, which additionally reduces the occurrence of back-biting reactions<sup>60,61</sup>.

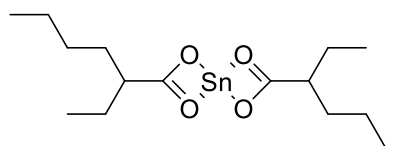
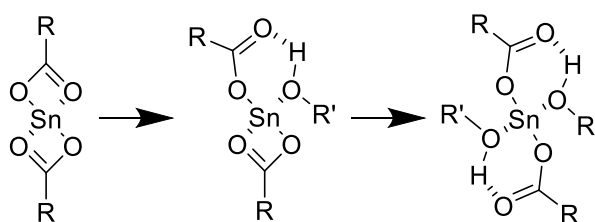


Figure 1.7. – Structure of tin(II) 2-ethylhexanoate (Sn(Oct)<sub>2</sub>).

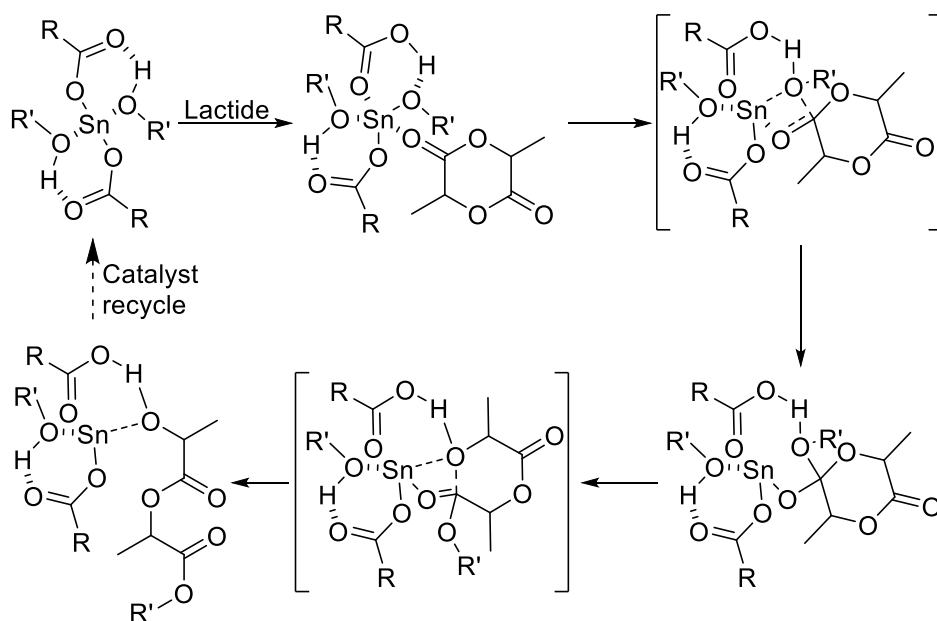
The literature indicates two ROP mechanisms using Sn(Oct)<sub>2</sub>: the activated monomer mechanism<sup>62,63</sup> and the coordination-insertion mechanism<sup>64,65,66,67,68</sup>. Both mechanisms are thought to be initiated by a hydroxyl group<sup>63,64</sup>, due to a dependence of polymer molecular weight to monomer:alcohol initiator ratio<sup>69,70</sup>.

The activated monomer mechanism involves Sn(Oct)<sub>2</sub> forming a complex with the monomer, activating the carbonyl centre for nucleophilic attack. A hydroxyl initiator attacks the carbonyl group (of the ester group in 2,5-morpholinediones, either ester group in a glycolide) and triggers ring opening. Alternatively, the coordination-insertion mechanism involves the formation of an initiator- Sn(Oct)<sub>2</sub> complex which then initiates the polymerisation<sup>71</sup> (Scheme 1.10.).



Scheme 1.10. – Complexation of alcohol bearing initiators to Sn(Oct)<sub>2</sub>.<sup>71</sup>

Initiation begins by the monomer complexing to the initiator/catalyst complex, stimulating a proton migration from the hydroxyl group of the initiator to an octanoate ligand. This allows the deprotonated alkoxy group of the initiator to nucleophilically attack the carbonyl of the monomer, forming a transition state that resolves via the dissociation of the oxygen of the alkoxy initiator from the tin(II) centre. The former carbonyl oxygen coordinates with the tin centre, which allows for rotation around the C-O axis. This enables ring opening and results in the dissociation of the inactive terminus of the polymer. The central tin cation then becomes able to complex to another monomer and propagate the polymerisation. The energy of the final transition state is dependent upon the R groups of the monomer and the ring strain of the six membered ring<sup>71</sup> (Scheme 1.11.).



Scheme 1.11. – Mechanism of ROP of lactide with  $\text{Sn}(\text{Oct})_2$ <sup>71</sup>.

Morpholine-2,5-diones can be regarded as a six-membered lactone and as a six-membered lactam as they contain both groups within their ring. The manner of the ROP of morpholine-2,5-diones can be used as an indication of the relative facility of lactone and lactam ROP. An investigation by in't Veld *et al.*<sup>55</sup> determined that morpholine-2,5-diones are exclusively ring-opening polymerised at the ester carbonyl, demonstrating that the energy required to ring-opening polymerise lactones is lower than that for lactams<sup>55</sup>.

However, lactams have been successfully ring-opening polymerised utilising the  $\text{Sn}(\text{Oct})_2$  catalyst system<sup>72</sup>. Lee and Yang<sup>72</sup> copolymerised trans-4-hydroxy-N-benzyloxycarbonyl-L-proline with  $\epsilon$ -caprolactam, achieving fairly high yields and high monomer conversion<sup>72</sup>. As such,  $\text{Sn}(\text{Oct})_2$  catalysis, in concert with a primary alcohol-bearing initiator, appears to be a usable foundation to develop reproducible and industrially scalable ROP of DKPs in order to produce poly(amino acids) with narrow  $\bar{D}$ .

#### 1.4. Drug Delivery Vehicles

Successful drug delivery vehicles must be biodegradable, biocompatible, have the capacity to encapsulate a payload, protect the payload from degradation and have sensitivity to a target stimulus present at the target site in order to trigger release of the payload. There are several models of drug delivery vehicle established in the literature, including prodrug systems<sup>73</sup>, micelle/nanoparticle formation<sup>74</sup>, stimuli responsive hydrogels<sup>75</sup>, and polymeric drugs<sup>76</sup>.

Poly(amino acids) boast many of the criteria outlined above and, as such, present as a useful material to produce a drug delivery vehicle.

#### 1.4.1. Block Copolymers

If a single kind of monomer is used in a polymerisation, then the homo-polymer will be uniform in its physicochemical properties from head to tail. For example, if styrene was polymerised, then polystyrene would be the product. However, if two or more monomers are utilised, then the properties of the polymer can be much more complex and dependent on the manner in which the two or more monomer types were introduced. For example, if ethylene glycol were polymerised to form poly(ethylene glycol) (PEG), and subsequently styrene were added to the mixture, the product would be PEG-*block*-polystyrene. This is termed a block copolymer. Poly(amino acid)-based block copolymers can be synthesised via the sequential polymerisation of NCAs and/or DKPs following methods outlined in sections 1.3.3. and 1.3.4. respectively. This can be achieved by allowing the polymerisation of the first monomer to proceed to completion, followed by the addition of a second monomer. Block copolymers are not limited to two blocks, in theory there is no limit to the number of discrete blocks in a single polymer. Block copolymers are not restricted to a single class of monomer. For example, a poly(amino acid) can be copolymerised with a polyester or any other polymer that polymerises via polycondensation. These polymers are defined as hybrid block copolymers and combine properties of each polymer type into one<sup>77</sup>.

PEG is widely utilised in the synthesis of hybrid block copolymers suitable for biomedical applications. It is a commercially viable polymer that boasts many desirable features including high biocompatibility, hydrophilicity, protein resistance and good pharmacokinetics<sup>41,78,79</sup>. Due to the wide variety of end functionalisation of PEG, it can be utilised as a macro-initiator in the synthesis of poly(amino acid)-based materials via DKP ROP.

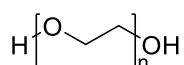


Figure 1.8. – Structure of poly(ethylene glycol).

However, the human body is not able to biodegrade ether bonds and as such, cannot degrade PEG blocks<sup>80</sup>. As a consequence, excretion of PEG macromolecules is not possible and these structures gather in the liver, spleen and kidneys. This issue is of particular significance with larger molecular weights. Additionally, the human body can produce anti-PEG immunoglobulins

in response to PEG-bearing therapeutics. This further limits the efficacy and therefore biomedical applicability of PEG-based macrostructures<sup>81,82</sup>.

A potential replacement to PEG as the hydrophilic block in an amphiphilic block copolymer is polysarcosine (Figure 1.9.).

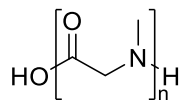


Figure 1.9. – Structure of polysarcosine.

Polysarcosine is a biodegradable and biocompatible polymer that is peptidomimetic<sup>83,84</sup>. It is hydrophilic, has no known side effects<sup>85,86</sup> and can be synthesised via ROP of sarcosine NCA or SSPS using Boc-protected sarcosine.

Yu *et al.*<sup>87</sup> utilise polysarcosine as the hydrophilic block of an amphiphilic block copolymer capable of self-assembly<sup>87</sup>. The nanoparticles produced were applicable for targeted drug release, showing thermo-sensitivity via the release of doxorubicin<sup>87</sup>.

#### 1.4.2. Amphiphilic Polymer Self-Assembly

Block copolymers comprised of a hydrophobic block and a hydrophilic block are able to self-assemble in an aqueous medium to form nanoparticles such as micelles, vesicles and aggregates. Micelles are spherical or cylindrical aggregates, arranged such that the hydrophobic blocks occupy the core of the nanoparticle and the hydrophilic blocks occupy the surface, minimising negative interactions between hydrophobic blocks with the aqueous medium and maximising positive interactions between hydrophilic blocks and the aqueous medium. Vesicles differ to micelles in their arrangement by forming a bilayer where hydrophilic blocks are exposed to the aqueous medium and hydrophobic blocks are isolated within the bilayer, resulting in a membrane surrounding a hollow core<sup>88</sup>. The concentration at which a particular block copolymer aggregates is termed the critical aggregation concentration (CAC). At concentrations below the CAC, amphiphilic polymers will gather at the surface of the aqueous medium to minimise negative interactions between hydrophobic blocks and the aqueous medium.

Other intermolecular interactions, such as hydrogen bonding,  $\pi$ - $\pi$  stacking and Van der Waals interactions influence self-assembly. Poly(amino acids) are capable of substantial hydrogen bonding. As such, when block co-polymerised with a hydrophilic polymer block, poly(amino acid)-based materials can self-assemble to form stable nanoparticles suitable for drug delivery.



In practice, there are several methods to form nanoparticles, the most common of which is nanoprecipitation via co-solvation.

### 1.4.3. Optimisation of Nanoparticles

The efficacy of nanoparticles as a controlled release vehicle can be improved by fine-tuning properties of the polymers that make up the nanoparticle, as well as fine-tuning the method of nanoparticle formulation. Features such as solubility of the polymer, number of repeat units and interactions between repeat units determine the properties of the resultant nanoparticles.

Increasing the maximum drug loading of nanoparticles is desirable as lower number of particles are needed to deliver an equivalent dose of the active pharmaceutical ingredient (API), which therefore reduces the amount of resources and cost needed to manufacture the therapeutic<sup>89</sup>. However, lower drug loaded nanoparticles can have a more favourable pharmacokinetic profile than that of higher drug loaded nanoparticles<sup>89</sup>. When studying the effects of varying the percentage loading of the chemotherapeutic, Docetaxel, in nanoparticles, Chu *et al*<sup>89</sup> observed an increase in therapeutic efficacy in recipients of the lower drug loaded nanoparticles. Mice that received the 9% Docetaxel-NP formulation had less docetaxel exposure in the organs of the mononuclear phagocyte system (MPS) and an increase plasma and tumour docetaxel exposure than those that received the 20% docetaxel-NP formulation, resulting in an increase in therapeutic efficacy<sup>89</sup>.

Stability of nanoparticles in the absence of the payload release stimuli is crucial to the quality of drug delivery. Particularly in large-scale synthesis, physical instability of nanoparticles can lead to aggregation, this increases the  $\Delta$  and results in a loss of particle homogeneity and nanoscale properties. Increased stability of the nanoparticles can combat this issue<sup>90</sup>.

Sensitivity to a particular stimulus is vital to ensuring the targeted delivery of the therapeutic within the nanoparticles. Selected stimuli can be temperature, the presence of a particular enzyme and environmental pH change. The latter two are of interest to this research as the pH within cancerous cells can approach pH 5.0, which is significantly more acidic than normal bodily pH<sup>91</sup>. As such, pH responsive nanoparticles can be utilised as drug delivery vehicles for applications such as chemotherapy. Sensitivity to pH can be ensured by including ester linkages within the backbone of the polymer chain. Ester linkages can be cleaved under acidic conditions, this would cause the polymers to breakdown and therefore disassembly of the nanoparticles.

Size can be a restrictive feature on the applicability of nanoparticles. Diffusion across biological barriers is a necessity for nanoparticles to reach their target site. As such, nanoparticles must be

below a particular size threshold in order to cross such barriers. For example, nanoparticles must be under 100 nm in diameter to cross the blood-brain barrier<sup>92</sup>. A summary of possible routes of nanoparticle-therapeutic administration for nanoparticles within different size ranges is included in Table 1.2.

*Table 1.2.* – Approximate particle size range for drug deposition in various body organs via different dosage forms and routes of administration<sup>93</sup>.

Route of Administration/Dosage Form	Particle Size Range
Lymphatic (Reticuloendothelial system)	10-50 nm
Long-circulating carriers (brain, tumour)	5-200 nm
Transdermal	10-600 nm
Intravenous/ intramuscular	200-2000 nm
Ocular	100-3000 nm
Aerosol	1-10 $\mu\text{m}$
Nasal	8-20 $\mu\text{m}$

## 1.5. Enzyme-Responsive Materials

Responsive materials are a collection of materials that are able to change form and/or function in the presence of a stimulus such as pH, temperature, light, electric field or enzyme<sup>94,95,96,97</sup>. Therefore, enzyme-responsive materials are a class of material that change their functionality as a result of the action of an enzyme on the material. Such changes can be to the macroscopic structure, microscopic structure and includes materials that display different interactions with their environment after enzymatic exposure<sup>98</sup>. Enzyme-responsive materials are well explored in the literature; concise reviews such as those written by Zelzer *et al.*<sup>98</sup> and Li *et al.*<sup>99</sup> provide excellent summaries of recent developments.

### 1.5.1. Enzymes and Their Action

Enzymes are proteins that act upon specific molecules, the molecules that they are able to bind with and act upon are called substrates. Enzymes decrease the activation energy required for a chemical reaction to occur by lowering the energy of the transition state between the starting molecule and the product of the reaction. The enzyme does this by binding to the substrate at its active site, forming an enzyme-substrate complex. This catalysis allows reactions to occur at physiologically significant rates and under mild aqueous conditions. An enzyme is comprised of

a specific sequence of amino acids, as is the area of it that can bind to substrates which is called the active site. This specificity in amino acid sequence results in a unique physicochemical structure, which informs the specificity of enzyme selection, the reactions that they are able to catalyse and the substrate(s) they are able to complex with.<sup>100</sup>

There are six main categories of enzymes: hydrolases, isomerases, ligases, lyases, oxidoreductases and transferases. Each category of enzyme carries out a specific reaction type, with each enzyme within a category targeting a specific substrate for that reaction. Hydrolases catalyse the hydrolysis of a substrate: examples of this in the human body include digestive enzymes such as amylase, maltase and lactase, as well as elastase which is involved in the regulation of elastin in the skin<sup>101</sup>. Isomerases catalyse the isomerisation of molecules, that is, they catalyse the structural rearrangement of a molecule without adding or subtracting any groups. An example present in the human body is glucose isomerase, which reversibly isomerizes D-glucose to D-fructose and D-xylose to D-xylulose and plays a critical role in the metabolism of sugar<sup>102</sup>. Ligases are a class of enzyme that catalyse the joining of two molecules together. An example of a ligase present in the human body is DNA ligase which facilitates the joining of two DNA strands by the formation of a phosphodiester bond<sup>103</sup>. Lyases are a class of enzyme that catalyse the removal or addition of elements of ammonia, carbon dioxide or water from a substrate via processes other than hydrolysis. An example of a lyase present in the human body is histidine decarboxylase which removes the carboxylic acid group from the amino acid histidine to form histamine<sup>104</sup>. Oxidoreductases are a class of enzymes that catalyse redox reactions of a substrate, an example of this in the human body is the enzyme xanthine oxidoreductase that catalyses the oxidative hydroxylation of hypoxanthine to xanthine and of xanthine to uric acid<sup>105</sup>. Over-activity of xanthine oxidoreductase in the body can lead to hyperuricemia along with an increased production of reactive oxygen species, which increases the risk of developing a collection of medical conditions such as gout, cardiovascular disease or hypertension<sup>105</sup>. Transferases are enzymes that catalyse the transfer of a functional group from one molecule to another, an example of this in the human body is choline acetyltransferase which catalyses the transfer of an acetyl group from an acetyl compound to choline in order to produce the neurotransmitter acetylcholine<sup>106</sup>. Despite the specificity of enzymes to their substrate and reaction type, there are a wide variety of accessible reactions and target substrates using enzymes.

### **1.5.2. Using Enzymes as Stimuli for Material Manipulation**

The inclusion of a substrate within a given material allows for an enzyme sensitive functionality. To be enzyme-responsive, the change made by the enzyme to the enzyme-sensitive component, or substrate, must be translated to the rest of the material and that translation must cause a change in the overall properties of the material<sup>98</sup>. The specificity and selectivity of enzymes for their respective substrate allows for the use of enzymes as stimuli in targeted and nuanced ways. The selection of a substrate, the manner in which it is incorporated into a material and the transformation that the enzyme catalyses all affect the way in which the material may respond to enzyme stimulation. For these reasons, as well as the innate biocompatibility of enzymes, enzyme-responsive materials are particularly suitable for use in biological applications. The natural occurrence of enzymes within the body provides further advantage over alternative stimuli such as light, electric or magnetic fields and temperature. Furthermore, imbalances in the activity or expression of enzymes often occur in disease states, this provides a marker for the location of the disease within the body and a stimulus required to release a therapeutic payload from the enzyme-responsive material. For this reason, selection of the substrate to be included in the enzyme-responsive material is critical to the targeted application and can be selected to match an overexpressed enzyme or an enzyme that is secreted from a particular location in the body.<sup>98</sup>

### **1.5.3. Enzyme Sensitive Functionalities**

As highlighted in section 1.5.1., despite the extensive number of enzyme-substrate pairs, there are only a few reaction types that enzymes are able to catalyse, namely bond formation and cleavage, redox and isomerisation reactions. So far, proposed enzyme-responsive materials have relied on bond formation and cleavage or redox reactions that will not reverse unless the system or enzymes change. This is in opposition to alternative smart materials where the stimulus affects equilibrium states and the smart material will often revert to its original state once the stimulus is removed. Utilising the formation of new bonds in enzyme-responsive materials by enzymatic catalysis has been achieved through the condensation of amino acids or oligopeptides<sup>107</sup>, as well as the cross-linking of side chains of amino acids<sup>108</sup> and the phosphorylation of amino acids<sup>109</sup>. Using bond cleavage as the enzyme sensitive functionality in enzyme responsive materials is also well explored, typically involving peptide<sup>110</sup> and amino acid ester<sup>111</sup> cleavage, as well as ester bonds between polymers and small molecules<sup>112</sup>. It is common that peptides are utilised as the enzyme sensitive functionality within an enzyme-responsive material; many substrates are comprised of amino acid sequences. This is inclusive of a wide variety of peptides such as amphiphiles for self-assembling materials<sup>107</sup>, cross-linkers in

polymeric hydrogels<sup>113,114</sup> and surface<sup>115</sup> and particle<sup>116</sup> decoration. Whilst under one set of conditions, an enzyme will bind with a substrate to produce one product, under another set of conditions, the reverse process is possible. An example of this is the phosphatase/kinase system that allows dephosphorylation of alcohols in the presence of adenosine triphosphate (ATP), which demonstrates the possibility of reversible/dynamic enzyme responsive materials<sup>117,118</sup>.

#### **1.5.4. Translation of Enzymatic Action into Material Response**

Whilst current enzyme-responsive materials mainly utilise two types of enzyme-catalysed reaction, this being bond formation and cleavage or redox, there are a plethora of consequential effects to the substrate. These include: hydrophilicity change<sup>119</sup>, charge removal or addition<sup>120,121</sup>, change in lengths of polymer chains<sup>122</sup>, change in steric effects<sup>123</sup>, addition<sup>124</sup> or revealing<sup>125</sup> of functional groups or bond rearrangement<sup>126</sup>.

Translation of the enzyme sensitive functionality into a material response is the central challenge in the design of enzyme responsive materials, and is largely dependent on the manner in which the substrate, or enzyme-sensitive component, is incorporated into the smart material. This can be achieved via a collection of methods which are selected based upon the bulk material, the enzyme-substrate pair, the targeted application and the type of smart material. The enzyme sensitive functionality can be covalently bonded to the bulk material where the response involves a change in functional group, charge or hydrophilicity, as has been achieved when attaching oligopeptides to surfaces and particles through amide formation<sup>127</sup> or thiol-metal bonding<sup>128</sup>. However, should the enzymatic change involve molecular or intramolecular structural rearrangement, covalent attachment of the substrate to the bulk material is not sufficient and more nuanced methods of incorporation are required.

#### **1.5.5. Types of Enzyme-Responsive Systems and Their Applications**

A broad selection of systems that incorporate enzyme responsivity have been proposed and developed, such as polymer hydrogels, particles, self-immolative materials, supramolecular materials and surfaces as well as others. Whilst all of these systems are well-explored and effective in their utilisation of enzyme sensitivity, only the former two are of relevance to this research.

Polymer hydrogels are three-dimensional networks with high porosity, surface area and are capable of uptake of large amounts of water relative to their mass. They are comprised of hydrophilic polymers with extensive covalent cross-linking, resulting in hydrophilicity yet

insolubility in aqueous solution, leading to their impressive water uptake<sup>129</sup>. Hydrogels usually find applicability as agents to fill vacant pockets, therapeutic delivery vehicles and tissue engineering scaffolds, all of which due to their extensive porosity and capacity for high volume uptake and retention of aqueous solution. Enzyme responsivity in hydrogels is typically in their formation and/or degradation via the use of cross-links that can be formed and cleaved enzymatically.

Hydrogels that utilise enzyme-triggered cross-linking are applicable as injectable scaffolds<sup>130</sup> and drug delivery systems<sup>110,131,132</sup> where the hydrogel can be formed *in situ* using mild conditions. An example of this is the transglutaminase catalysed crosslinking of gelatin<sup>133,134</sup>. Hydrogels that can be degraded enzymatically find application as synthetic extracellular matrix mimics or as vehicles for controlled release of therapeutics<sup>98</sup>. In this application, either the polymer chains or the cross-linkers can be degraded enzymatically, as is exemplified by the degradation of dextran fibres by dextranase<sup>135</sup> and a PEG-polypeptide system designed by West and Hubbell<sup>136</sup> respectively. The cross-linkers of the PEG-polypeptide system could be degraded by matrix metalloprotease 1 (MMP-1) or plasmin.

Reversible polymer hydrogels can be formed and degraded via the enzyme catalysed formation and degradation of cross-linkers. Lutolf and co-workers<sup>137</sup> report a dual population of multi-armed PEG polymers, one of which ends with a glutamic acid containing sequence and the other with a lysine containing peptide sequence. The system may form cross-links between the glutamic acid and the lysine groups on addition of transglutaminase. The peptide sequences also contained a substrate of MMP-1, which may degrade on addition of MMP-1 causing breakdown of the hydrogel.<sup>137</sup>

Additionally, changes to hydrogel morphology, such as pore size change or sol-gel transitions, can be triggered by enzyme stimulation. Thornton *et al.*<sup>127</sup> propose poly(ethylene glycol acrylamide) functionalised with charged oligopeptide sequences. When subjected to the respective enzyme, part of the charged peptide sequence is cleaved, altering the overall charge of the hydrogel and its swelling characteristics<sup>138,139</sup>.

There are several types of particles: polymer particles, metal particles, mesoporous silica particles, quantum dot conjugates and many others. Enzyme-sensitive particles typically target applications such as enzyme detection and drug delivery, both of which can utilise a wide variety of enzymes. Whilst all the aforementioned types of particles are all effective, this research is concerned only with polymer particles and does not explore the others.

As summarised in sections 1.4.1. and 1.4.2., polymer nanoparticles are typically comprised of amphiphilic block copolymers that are able to self-assemble in aqueous conditions. They can be designed to self-assemble to form micellar spheres or worms, as well as other structures. Crucially, the unoccupied, hydrophobic centre of the particles can be used to encapsulate a payload which, upon exposure to a stimulus, can be released. With respect to enzyme response, exposure to a particular enzyme can be utilised to induce self-assembly or to degrade the polymer based nanoparticles. For both aforementioned applications, the use of enzyme degradation is more typical and therefore the inclusion of peptide components within the amphiphilic polymer that can be cleaved by a corresponding enzyme is common. In the case of enzyme detection, the particles may be loaded with fluorescent or coloured indicator. On exposure to a particular enzyme, the nanoparticle may break down and release the indicator, demonstrating that the enzyme is present. Therefore, the peptide included within the amphiphilic block copolymer can be selected according to the enzyme that needs to be detected. Applying particles for drug delivery follows a similar mechanism. A therapeutic may be encapsulated within the particle and, on exposure to the respective enzyme which is produced at the target site, the therapeutic may be released over a prolonged period to maintain an active dose. An example of enzyme-responsive particles that utilise the enzymatic breakdown of peptide-based polymers has been proposed by Habraken *et al.*<sup>140</sup> involving block copolymers of poly(*n*-butyl acrylate) and poly(glutamic acid-*co*-alanine). Upon exposure to elastase, the alanine sections were cleaved causing particle degradation and aggregation.

## **1.6. Wound Healing Devices**

A wound can be defined as a break or discontinuity in the epithelial lining of the skin or mucosa due to physical, thermal or chemical damage<sup>141</sup>. Depending on the size and condition of the wound, physiological healing processes may not be capable of healing the wound within an acceptable amount of time, if at all. Wound healing devices are comprised of materials used to expedite the healing of a wound in as short a time frame as possible. Such materials must be biocompatible, have the capability of being processed to form porous structures, and, ideally, biodegradable. Consequently, poly(amino acids) offer great potential for use in wound healing devices, particularly if they can be produced in a safe and cost-effective manner.

### **1.6.1. Mechanism of Wound Healing**

Skin is a critical barrier between internal tissues of the body and an often hostile environment; rapid closure of a wound and regeneration of the damaged skin is vital to minimise internal

damage and infection<sup>142</sup>. Wound healing is achieved through four precise and overlapping phases of healing: haemostasis, inflammation, proliferation and remodelling<sup>142</sup>. Should all four phases occur successfully, haemostasis should conclude within 24 hours, inflammation should conclude after three days, proliferation should conclude within three weeks and remodelling can conclude anywhere between three weeks and one year<sup>143</sup>. However, depending on the properties of the wound and its location on the body, one or more of the phases may not be able to reach completion.

Haemostasis, the first phase of healing, begins immediately through vascular constriction and fibrin clot formation. The newly formed clot, as well as the wound tissue that surrounds the clot, release a collection of cytokines and growth factors which stimulates the chemotaxis of inflammatory cells and leading into the second phase of healing.<sup>144</sup>

The chemotaxis of inflammatory cells into the wound site promotes the sequential influx of neutrophils, macrophages and lymphocytes, each of which play important roles<sup>145,146,147</sup>.

Neutrophils play a dual role; removing foreign microbes and cellular debris whilst also releasing proteases and reactive oxygen species<sup>144</sup>. Whilst this is vital to the maintenance of a clean wound environment, it can also cause additional bystander damage and, if deregulated, can result in wound healing inhibition<sup>144</sup>. Macrophages also carry out multiple functions in wound healing. In the inflammation stage, macrophages release cytokines which feedback into the inflammatory response by recruiting and activating additional leukocytes. They also induce apoptosis in cells and clear the apoptotic cells in order to bring the inflammation stage to a close. As apoptotic cells are cleared, macrophages undergo a phenotypic transition and stimulate fibroblasts, keratinocytes and angiogenesis to begin tissue regeneration, thus transitioning into the proliferation stage.<sup>144,148,149</sup>

T-lymphocytes enter the wound site following inflammatory cells and macrophages; their concentration peaks towards the end of the proliferative stage and into the remodelling stage<sup>144</sup>. Whilst their role is not fully understood, it is an area garnering thorough research and there are many studies that propose how T-lymphocytes affect the wound healing process. Several of such studies suggest that a delay in T-cell access to the wound and lower T-cell concentration has an associated impairment of wound healing<sup>150</sup>, whilst other studies report that T-helper cells (CD4+ cells) promote wound healing whilst T-suppressor-cytotoxic cells (CD8+ cells) act to inhibit wound healing<sup>151</sup>.

Proliferation follows the inflammation stage, typically with some overlap. It involves epithelial proliferation and migration over the provisional matrix of the wound. In the site of repair,



fibroblasts and endothelial cells are of highest concentration and promote capillary growth, collagen formation as well as the formation of granulation tissue within the wound. In the wound bed, fibroblasts produce the major components of the extracellular matrix (ECM) which are collagen, glycosaminoglycans and proteoglycans. As proliferation draws to a close with the formation of ECM, the wound enters the final stage of healing (remodelling). This involves the recession of many of the new capillaries that formed during the proliferation stage, returning vascular density to a normal level. Granulation tissue remodels to a structure resembling more typical tissue; this process can continue for a number of years.<sup>144,145, 147</sup>

For most wounds, healing follows the aforementioned sequence of stages. However, there are circumstances in which this is not the case. Haemostasis can be disrupted by many sets of conditions, examples of which include: the wound being too large and too deep<sup>152</sup>, wounds that involve venous or arterial bleeding<sup>153</sup>, patients taking anticoagulant<sup>154</sup> or anti-platelet medication<sup>155</sup>, patients with haemophilia<sup>156</sup>, as well as many others. The inflammation stage is a complex system and balances between maintaining a clean wound environment and destroying newly formed tissue. Healing can also stall in the inflammation stage for various reasons: significant infection and poor microbial clearance<sup>144</sup>, poor blood supply and oxygenation<sup>157,158</sup>, overexpression of neutrophils and macrophages and destruction of newly formed ECM<sup>159</sup>, as well as a collection of systemic factors such as chronic diseases<sup>144</sup>. For these reasons, as well as others, treatment is often required in order for a wound to heal.

### **1.6.2. Traditional Approach to Expedite Wound Healing**

In general, treating wounds via traditional methods involves the maintenance of a dry wound environment, low humidity and allowing wound exposure to air in order to allow oxygen present to participate in reproductive repair<sup>160</sup>. The overall objective of a traditional dressing is to: decrease pain, apply compression to facilitate haemostasis, protect the wound from the environment and from soiling with exudate or waste, to immobilize the injured body part and to ultimately promote wound healing<sup>141</sup>. Traditional wound dressings have been used extensively to achieve this collection of objectives due to their easy application, low cost and simple manufacturing<sup>161</sup>. They are capable of protecting a wound from external infections, as well as physical damage<sup>161</sup>. However, within this approach there is a collection of different dressings each of which having particular features most suited to a specific wound type<sup>161</sup>. Dressings such as gauze, bandages, plasters, lint and many others fall under this category<sup>161</sup>.

In many cases where wounds require treatment, a traditional approach is sufficient in order to facilitate healing. However, most wounds that stall in the inflammation stage, whether due to

infection or non-healing, require more elaborate and modern treatments to allow healing to commence.

### **1.6.3. Modern and Responsive Healing Devices**

Modern dressings, as well as smart or responsive dressings, have emerged in the past few decades as a consequence of a shift in approach to wound treatment, with a particular focus on how to treat non-healing or chronic wounds. Chronic wounds are defined as wounds that fail to proceed through the normal phases of wound healing in an orderly and timely manner<sup>159</sup>. It is common that chronic wounds stall in the inflammation stage of healing as a consequence of both local and systemic factors outlined in section 1.6.2.; a collection of modern dressings have been developed in response to the demand for new treatments for such wounds.

Semi-permeable film dressings are transparent polyurethane-based films with a desensitized medical adhesive<sup>161</sup>. They are porous and therefore permeable to oxygen, CO<sub>2</sub> and water vapour. Despite this, bacteria are not able to penetrate into its structure<sup>161</sup>. These dressings have several advantages, due to their transparency, they allow for direct monitoring of the progression of the wound without the need to remove the dressing<sup>161</sup>. Furthermore, they are flexible and elastic and do not require tape, this minimises the risk of secondary damage to the wound on removal of the dressing<sup>161</sup>. However, these dressings are not sterile and therefore not suitable for deep wounds, wounds with heavy exudate or wounds with fragile peri-wound skin<sup>161</sup>. They find application as treatment for burns, skin defects, catheterization, fixation of stoma, and prevention of pressure ulcers<sup>161</sup>. Current semi-permeable film dressings on the market are Opsite<sup>162</sup>, Tegaderm<sup>163</sup> and Bioclusive<sup>164</sup>.

Foam dressings are comprised of a hydrophobic external layer that protects from bacterial infection and a hydrophilic internal layer that absorbs a moderate amount of wound exudate<sup>161</sup>. They are made of polyurethane or poly(vinyl alcohol foams) and, due to their high porosity, allow for gaseous exchange of CO<sub>2</sub> and oxygen<sup>161</sup>. Additionally, they have the capacity to act as a carrier for therapeutic molecules such as anti-inflammatory agents or analgesics<sup>165</sup>. They are malleable, elastomeric, lightweight, have low-surface tension, and have the capacity to absorb 10 times their weight in aqueous solution<sup>166</sup>. As a consequence of these properties, as well as their compatibility with wound shape, foam dressings are applicable for wounds with moderate to large amounts of exudate. However, they are not suitable for dry wounds, they demand frequent changing due to their high absorption<sup>167</sup> and they can inhibit proliferation of granulation tissue when used with an elastic bandage<sup>168</sup>. Foam dressings that are currently commercially available are Lyofoam<sup>169</sup> and Allveyn<sup>170</sup>.

Hydrogels have been defined and explained in detail in section 1.5.5., particularly within the context of enzyme-responsivity. They are a soft, hydrophilic material with a three-dimensional structure similar to natural ECM<sup>171</sup>. As dressings, hydrogels can be water or glycerin based and their main polymeric components are typically poly(ethylene glycol), polyacrylamide or poly(vinyl pyrrolidone)<sup>172</sup>. A substantial benefit of the use of hydrogel dressings is that they facilitate autogenous debridement which involves the breakdown of necrotic tissue by collagen degrading enzymes from the wound's own exudate in a moist environment<sup>161</sup>. Additionally, hydrogels can be used to fill empty spaces within the wound bed and do not adhere to the wound, therefore minimizing the risk of secondary damage on application or removal<sup>161</sup>. There are two categories of hydrogels – amorphous or sheet. Amorphous hydrogels contain small amounts of natural polymers with very high molecular weights such as collagen, alginate or carbohydrate<sup>161</sup>, whereas sheet hydrogels have a three-dimensional structure produced by the cross-linking of hydrophilic polymers<sup>173</sup>. Gokoo *et al.*<sup>174</sup> demonstrated that the use of hydrogel dressings resulted in faster wound closure and re-epithelialization than hydrocolloid dressings<sup>174</sup>. They are elastic, capable of rehydrating dry wounds and are simple to apply and remove<sup>161</sup>. However, when used on wounds with large amounts of exudate, excessive water content of the hydrogel may lead to wound maceration and bacterial infiltration<sup>161</sup>. As a consequence of these features, hydrogel dressings are applicable for wounds that require debridement of necrotic tissue, burn wounds, trauma wounds, ulcerations and bedsores<sup>161</sup>. Current hydrogel dressings available on the market are Nu-gel<sup>175</sup>, Aquaform polymers<sup>176</sup> and Purilon<sup>177</sup>.

Hydrocolloid dressings are opaque medical dressings composed of hydrocolloid molecules with strong water absorption capability, a rubber base with adhesive properties and a protective film with semi-permeability<sup>178</sup>. The rubber substrate provides adhesion to the wound site, this promotes a closed and moist wound environment<sup>161</sup>. As the hydrocolloid component absorbs moisture, the adhesion of the dressing to the wound site reduces, allowing for straightforward removal of a used dressing and minimising the risk of secondary damage to the wound<sup>179</sup>. The water absorption capacity of hydrocolloid dressings are not high, and their rate of water uptake is relatively low<sup>180</sup>. As a consequence, these dressings are not suitable for highly exuding wounds and, instead, find applicability for wounds such as burns, stomas, pressure sores and trauma wounds<sup>161</sup>. Hydrocolloid dressings that are currently commercially available include Granuflex<sup>181</sup>, Comfeel<sup>182</sup> and Tegaserb<sup>183</sup>.

Alginate dressings are the most effective dressings with respect to exudate absorption; they are able to absorb 20 times their own weight in fluids<sup>184</sup>. They are primarily composed of sodium methyl carbonate cellulose or calcium alginate and can control exudation excellently, prolonging

the usage of a single dressing<sup>161</sup>. On contact with the wound surface, alginate dressings will form a gel like substance, minimizing debridement. As a consequence of the calcium ions present within the dressing, they are able to promote haemostasis and produce a defensive film within the wound<sup>161</sup>. Despite this, they can be removed easily with saline irrigation and without causing secondary damage<sup>161</sup>. As such, alginate dressings are suitable for wounds with heavy exudate such as pressure ulcers<sup>161</sup>. Currently available alginate dressings on the market are Sorbsan<sup>185</sup>, Kaltostat<sup>186</sup> and Algisite<sup>187</sup>.

Bioactive dressings are composed of naturally occurring, high molecular weight biopolymers such as collagen<sup>188</sup>, hyaluronic acid<sup>189</sup>, chitosan<sup>190</sup>, alginate and elastin. The biopolymer component can be sourced from both artificial synthesis and natural sources; sources of which include thin-film elastomeric rubber, nylon, porcine skin, amniotic membrane, animal skin and tissue derivatives of animals<sup>191</sup>. Consequently, these dressings are biocompatible, biodegradable, non-toxic and have adjustable permeability<sup>161</sup>. However, due to the costly nature of sourcing the required materials, bioactive dressings are expensive to produce and highly demanding for storage and transportation<sup>192</sup>.

Nanofibrous dressings are polymeric nanostructures composed of fibres with nanoscale diameter. Networks containing fibres with these physical dimensions have a physical structure that can function as a mimic of human ECM<sup>160</sup>. Additionally, they have high porosity and a large specific surface area, which is effective in absorbing wound exudate as well as promoting nutrient transfer and gas exchange<sup>193,194</sup>. Furthermore, the high porosity allows for the loading of therapeutics as part of the fibres themselves or within the network macrostructure<sup>195,196</sup>. The functional properties of the nanofibre dressings facilitates better tissue regeneration, cell migration and proliferation<sup>197</sup>. Nanofibres of polymers can be produced by electrospinning of a polymer melt or solution; this allows for tunable nano-patterning and adjustability of not only the composition of the fibres, but also their arrangement and morphology of the macrostructure of the nanofibre network<sup>160</sup>. However, electrospinning as a process currently faces challenges with respect to reproducibility of nanofibres, as well as scaling up to industrial level<sup>198</sup>.

#### **1.6.4. Electrospinning of Polymer Nanofibres**

Electrospinning is a process through which fibres with diameters in the nanometer scale are able to be produced<sup>199</sup>. Depending on the flow rate, concentration of the polymer solution and amount of time, nanofibre mats with very small thicknesses can be produced. The resultant mats are highly porous and can have highly tunable nanostructures depending on the parameters of the electrospinning setup. Such nanostructures may be usable as, or as part of, a wound healing

device. As such, poly(amino acids) are suitable candidates for this application and, as of yet, their use in electrospun materials is relatively unexplored.

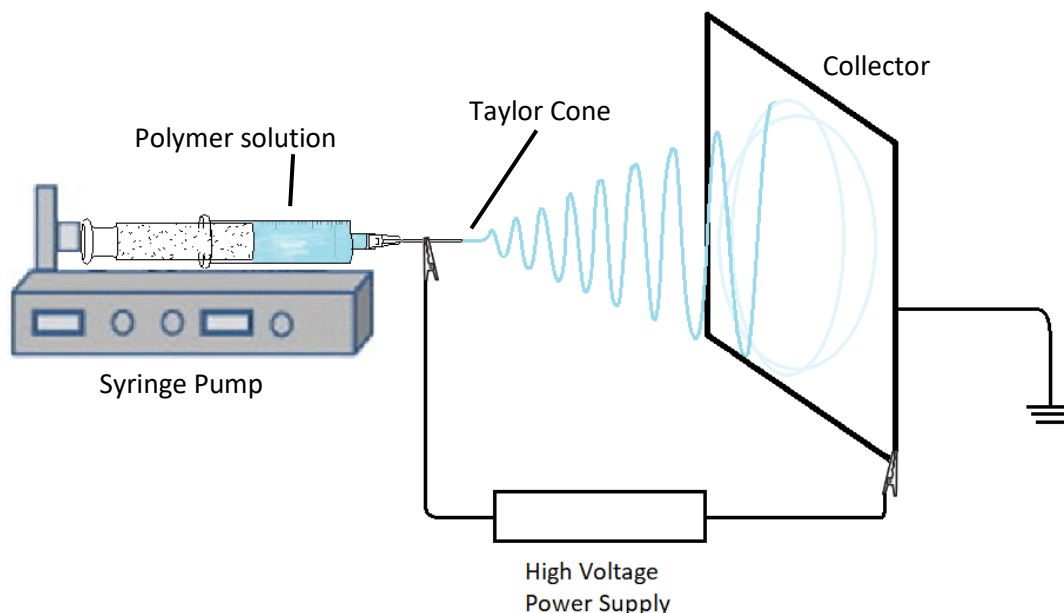


Figure 1.10. – Diagram of a typical electrospinning setup.

Electrospinning is an electrohydrodynamic process involving the electrification of a liquid droplet to form a jet of polymer solution, followed by its stretching and elongation to form a very thin fibre<sup>199</sup>. The components required to electrospin are a high-voltage power supply (DC or AC), a syringe pump, a spinneret and an electrically-conductive collector<sup>199</sup>. The polymer melt or solution is extruded from a spinneret to produce a droplet which, upon electrification, is deformed into a Taylor cone by the potential difference between the spinneret and the collector<sup>200</sup>. The potential difference causes positively and negatively charged ions within the solution to separate where ions of the same charge as the spinneret migrate toward the surface of the droplet<sup>199</sup>. As the potential difference is increased, the density of charge at the surface of the droplet increases until the electrostatic repulsion of the charges overcomes the surface tension of the droplet and a Taylor cone forms<sup>200</sup>. At the apex of the Taylor cone, a jet of electrically charged solution is ejected and extended in the direction of the electric field<sup>201</sup>. The jet then undergoes a vigorous whipping motion due to bending instabilities. As the jet stretches finer, it solidifies more quickly which results in the deposition of solid fibres on the grounded collector<sup>202</sup>. Whilst reproducibility is a significant challenge for electrospinning<sup>198</sup>, the tunability

of nanofibres as a result of varying the electrospinning parameters make it an attractive method for the production of polymer nanofibres. The parameters of electrospinning to be varied are: polymer molecular weight, polymer concentration in solution, solvent selection (evaporation rate, viscosity and conductivity), spinning voltage, flow rate, working distance (tip to collector) and the type of collector. The alteration of each of these parameters has a substantial effect on the resultant fibres, as well as, the fibre mat macrostructure as a whole. Included in Table 1.3. are the effects of increasing or decreasing each parameter on nanofibre morphology.

*Table 1.3.* – Parameters of electrospinning and the effect of increasing or decreasing each parameter.

<b>Parameter</b>	<b>Effect of Increasing Parameter</b>	<b>Effect of Decreasing Parameter</b>
Polymer molecular weight	Increased fibre diameter	Decreased fibre diameter
Solvent evaporation rate	Increased fibre diameter Increased fibre porosity Increased specific surface area	Decreased fibre diameter Decreased fibre porosity Decreased specific surface area More difficult to remove solvent residue
Spinning solution viscosity	Increased fibre diameter Increased risk of blocking spinneret	Decreased fibre diameter If too low, results in electrospray
Conductivity of solution	Decreased fibre diameter	Increased fibre diameter If too low, results in beading
Spinning Voltage	Decreased fibre diameter If too high, spinning becomes unstable	Increased fibre diameter If too low, results in droplets
Flow Rate	Increased fibre diameter If too high, results in droplets	Decreased fibre diameter If too low, increases chance of interrupting spinning
Working Distance	Decreased fibre diameter Increases diameter of deposition of fibres	Increased fibre diameter, increased risk of not allowing full solvent evaporation

### 1.7. Renewability and Environmental Impact of Polymer Synthesis

The focus on environmental and social impact within the chemical and materials industries has become more central in recent years<sup>203</sup>. Since the introduction of green chemistry, and its 12 associated principles by Anastas and Warner<sup>204</sup>, the development of processes with greater

sustainability has become a high priority<sup>203</sup>. This can be achieved by utilising starting materials sourced from a renewable feedstock rather than oil-derived materials. Examples typically include materials from biomass or waste products from pre-existing processes<sup>203</sup>. Atom economy must also be considered when evaluating a new prospective synthetic route. The minimisation of waste production, particularly waste of a hazardous nature, is of critical importance to prevent detrimental environmental effects<sup>203</sup>. The process of NCA synthesis via the Fuchs-Farthing method and subsequent polymerisation has relatively poor atom economy, producing a collection of by-products including hydrochloric acid, a protonated proton scavenger and carbon dioxide<sup>15</sup>. Alternative, phosgene-free syntheses of NCAs have a similar amount of by-products<sup>21</sup>. Despite these concessions in atom economy, the production of poly(amino acids) from NCA synthesis and polymerisation compares favourably to oil-derived hydrocarbon polymers due to the renewable feedstock of amino acids and the efficiency of NCA polymerisation.

Solvent selection has a significant impact on the sustainability and environmental impact of a chemical process. Whilst it is common practice to minimise the volume of solvent use, selecting solvents based upon their 'greenness' is still relatively new. The greenness of solvents can be broken down to their environmental impact and the health and safety hazards associated with their use<sup>205</sup>. A reliable and widely used solvent sustainability guide has been produced by GlaxoSmithKline (GSK), which scores each solvent upon their disposal capacity, environmental impact, impact on human health, safety, and life cycle<sup>205</sup>.

Table 1.4. – GSK Solvent Sustainability Guide<sup>205</sup>.

Classification	Solvent Name	CAS Number	Composite Colour	Boiling Point (°C)	Incineration	Recycling	Bioremediation	VOC Emissions	Aquatic Impact	Air Impact	Health Hazard	Exposure potential	Flammability & Explosion	Reactivity & Stability	Life Cycle Analysis*
Water & Acids	Water	7732-18-5	Green	100	4	2	4	6	10	8	10	9	8	10	10
	Acetic Acid	64-19-7	Yellow	118	3	5	4	7	8	4	7	5	8	6	8
	Trifluoroacetic acid*	76-05-1	Red	72	3	5	4	7	8	4	4	4	7	6	8
Alcohols	1-Heptanol	111-70-6	Yellow	173	5	8	10	9	8	4	10	7	9	10	9
	Ethylene glycol	107-21-1	Green	197	4	5	5	10	10	8	7	10	10	10	9
	1-Octanol	111-87-5	Yellow	196	9	7	8	10	5	4	7	10	9	10	9
	1-Butanol	71-36-3	Green	118	6	7	5	8	9	1	7	7	8	9	5
	1-Propanol	71-23-8	Green	97	5	3	4	6	10	4	10	7	8	10	7
	Ethanol	64-17-5	Green	78	5	5	3	4	9	5	10	8	6	10	10
	2-Propanol	67-63-0	Green	82	5	5	3	5	8	7	10	6	6	8	4
	t-Butanol	75-65-0	Yellow	82	5	5	3	5	9	7	7	5	6	10	8
	IMS (ethanol, denatured)	64-17-5	Yellow	78	5	5	3	5	9	5	4	7	6	10	10
	Methanol	67-56-1	Yellow	65	4	7	7	10	7	4	6	5	10	10	9
Esters	Glycerol diacetate	111-55-7	Yellow	184	5	6	6	10	6	8	10	8	10	10	9
	Isobutyl acetate	110-19-0	Yellow	116	7	9	8	6	9	6	10	6	8	10	9
	Isoamyl acetate	123-92-2	Yellow	142	9	9	8	8	4	6	7	8	8	10	10
	Isopropyl acetate	108-21-4	Yellow	89	6	7	5	5	9	5	10	6	6	10	7
	Ethyl acetate	141-78-6	Green	77	5	6	5	4	9	5	10	7	5	10	6
Carbonates	Propylene carbonate*	108-32-7	Yellow	242	4	5	6	10	10	10	10	10	10	10	10
	Diethyl carbonate*	105-58-8	Yellow	126	7	9	9	7	9	8	4	5	8	10	10
	Dimethyl carbonate	616-38-6	Yellow	91	4	3	5	5	9	7	10	6	6	10	8
Ketones	Cyclopentanone	120-92-3	Yellow	155	8	9	6	7	10	5	7	6	8	10	6
	Methylisobutyl ketone	108-10-1	Yellow	117	7	8	5	7	9	8	7	6	7	9	3
	Methylethyl ketone	78-93-3	Yellow	80	5	5	3	4	8	4	10	6	5	9	8
	Acetone	67-64-1	Yellow	56	5	6	2	10	6	10	6	4	9	7	7
Aromatics	Anisole	100-66-3	Yellow	154	8	8	8	8	7	6	7	8	7	9	5
	p-Xylene	106-42-3	Yellow	138	10	9	6	7	5	2	7	7	5	10	7
	p-Cymene*	99-87-6	Yellow	177	10	8	7	9	4	2	10	6	6	9	9
	Toluene	108-88-3	Yellow	111	10	7	6	7	7	2	7	6	5	10	7
	Trifluorotoluene	98-08-8	Yellow	102	4	4	5	6	3	8	10	4	4	10	10
	Pyridine	110-86-1	Yellow	115	3	6	2	7	7	1	4	4	8	9	2
Hydrocarbons	Benzene	71-43-2	Red	80	9	6	6	4	7	5	2	3	1	10	7
	Isocetane	540-84-1	Yellow	99	10	4	5	6	2	5	10	7	3	10	7
	Heptane	142-82-5	Yellow	98	10	4	5	6	1	5	10	6	3	10	7
	Cyclohexane	110-82-7	Yellow	81	10	6	5	4	1	5	10	6	2	10	7
	Hexane	110-54-3	Yellow	69	10	8	4	1	3	5	7	4	2	10	7
	Petroleum spirits	8032-32-4	Yellow	55	8	9	4	7	5	5	1	6	2	10	7
	Diethyl isosorbide*	5306-85-4	Yellow	236	4	4	5	10	9	6	4	9	9	8	9
Ethers	Cyclopentyl methyl ether	5614-37-9	Yellow	106	8	4	5	6	4	1	4	4	6	9	4
	2-Methyltetrahydrofuran*	96-47-9	Yellow	78	6	5	3	4	7	4	4	3	4	6	4
	t-Butylmethyl ether	1634-04-4	Yellow	55	7	8	4	2	7	5	7	4	3	9	8
	Diisopropyl ether	108-20-3	Yellow	68	9	7	6	3	5	4	10	6	4	8	9
	Tetrahydrofuran	109-99-9	Yellow	65	5	5	3	3	9	3	7	5	4	6	4
	1,4-Dioxane	123-91-1	Yellow	102	4	3	1	6	8	4	4	4	4	6	6
	Diethyl ether	60-29-7	Yellow	35	7	7	3	1	5	3	10	4	2	6	6
	1,2-Dimethoxyethane	110-71-4	Yellow	85	4	4	4	5	8	7	1	4	4	6	7
Dipolar Aprotics	Dimethyl sulphoxide	67-68-5	Yellow	189	3	4	4	9	8	6	7	9	9	5	6
	Acetonitrile	75-05-8	Yellow	82	3	5	1	4	10	8	7	5	6	10	4
	N-Methyl pyrrolidone	872-50-4	Yellow	202	3	4	3	10	10	6	1	9	9	9	4
	N,N-Dimethyl acetamide	127-19-5	Yellow	185	3	6	3	9	10	6	1	7	9	9	2
	N,N-Dimethyl formamide	68-12-2	Yellow	153	3	6	3	8	10	4	1	6	9	9	7
Chlorinated	Dichloromethane	75-09-2	Red	40	3	10	4	1	8	6	7	4	4	10	7
	1,2-Dichloroethane	107-06-2	Red	84	2	7	5	5	9	7	4	2	5	10	7
	Chloroform	67-66-3	Red	61	3	9	5	8	7	5	4	1	5	10	6
	Carbon tetrachloride	56-23-5	Red	77	3	7	5	4	4	3	4	1	4	10	7



Column Headings Colour Key

Orange	Waste
Green	Environment
Blue	Human Health
Purple	Safety

Composite Colour Key

Light Green	Few Known Issues
Yellow	Some Known Issues
Red	Major Known Issues

\*The scoring assessment for this solvent includes 4 or more data gaps, therefore there is a lower level of confidence in the solvent's placement on this guide.

\*A blank value for Life Cycle Analysis (LCA) indicates that this data is currently not available.

\*The composite colour represents an overall categorization of the holistic sustainability of a solvent, taking all category scores into consideration.

Estimates of the amount of plastic waste in surface water range between tens of thousands to hundreds of thousands of tonnes<sup>206</sup>. Despite this, the global production of plastic waste reached 460 million tonnes in 2019, approximately 230 times greater than that of 1950<sup>206</sup>. As such, the demand for biodegradable alternatives, that are renewably sourced, for the production of single use plastics has never been greater.

### 1.8. Research Aims and Thesis Outline

This research is focused on the creation, development and optimisation of the ring-opening polymerisation of 2,5-diketopiperazines to produce poly(amino acids). This route to poly(amino acid) synthesis has not been reported previously. The primary goal was to establish facile and repeatable methods for the ROP of a selection of DKPs in the absence of toxic and costly reagents or solvents. Such a synthetic route should produce poly(amino acids) with narrow Đ and comparable monomer conversions to NCA ROP. As such, refinement of a controlled poly(amino acid) synthesis to be more environmentally friendly, more efficient and more



directly applicable in industry was a central objective. The capacity to produce a variety of poly(amino acids) via DKP ROP was also an integral target, including polymers that have already been synthesised via NCA ROP and those that were previously inaccessible. The polymers should possess a plethora of physical and chemical properties applicable for a wide range of applications within the biomedical sector and beyond.

The original inspiration behind this project is the hazardous nature of the route to poly(amino acids) with narrow dispersity via NCA ROP, particularly NCA synthesis which requires the use of phosgene. As such, establishing a green, reliable and straightforward method to produce DKPs from their respective amino acid(s) and in the absence of phosgene was central to this research. This development, as well as the production of a library of DKPs, is reported in Chapter 3.

Chapter 4 includes the creation of poly(amino acid) homopolymers from DKPs, which is reported for the first time. The DKPs that were successfully polymerised were glycine DKP, alanine DKP, phenylalanine DKP and lysine(benzyloxycarbonyl) (lysine(Cbz)) DKP. The polymerisations were repeated using an alternative catalyst and a greener solvent. All polymers were fully characterised and the monomer conversions of each polymerisation was quantified. Polylysine(Cbz) was deprotected by acid-mediated cleavage using trifluoroacetic acid (TFA) and hydrogen bromide (HBr), yielding polylysine that boasted greater water solubility and the potential for further functionalisation. To demonstrate the biodegradability of these polymers, one of the polyalanine samples was incubated with elastase resulting in the complete breakdown to alanine. The yielded alanine was again used to synthesise alanine DKP which in turn ROP to produce polyalanine, demonstrating the potential for an entirely circular economy.

Chapter 5 includes the ROP of glycine DKP, alanine DKP and phenylalanine DKP from PEG to afford amphiphilic block copolymers. The polymers were fully characterised and assessed for their capacity to self-assemble in aqueous conditions using dynamic light scattering and scanning electron microscopy. Drug release studies were conducted using the nanoparticles with the most narrow  $\mathcal{D}$ , in which doxorubicin was encapsulated within the nanoparticles and subsequently released in response to incubation in an acidic medium. The encapsulation efficiency, drug loading content, percentage release and release profile was assessed, demonstrating the potential for applicability as anti-cancer therapeutic delivery vehicles.

Reported in Chapter 6 is the novel, repeatable and phosgene-free synthesis of polysarcosine via the ring-opening polymerisation of sarcosine DKP. Reaction conditions capable of opening the stable tertiary lactam bond were identified, and ROP of DKPs was exploited for its dipeptide repeat unit, opening access to a host of materials with tunable enzyme sensitivity. Polysarcosine-*b*-polyalanine and polysarcosine-*random*-polyalanine were synthesised, and utilised to produce

elastase-sensitive nanoparticles and gels respectively. Polysarcosine-*b*-polyalanine was used to encapsulate doxorubicin and assessed for its capacity to release it in a controlled manner in response to elastase incubation. Additionally, polysarcosine-*alt*-polyphenylalanine was produced from the ROP of a single monomer, the asymmetric sarcosine-phenylalanine DKP. The polymer was assessed for its sensitivity to breakdown by various enzymes. Furthermore, a pro-drug system of camptothecin-polysarcosine was produced via ROP of sarcosine-DKP from camptothecin, demonstrating the versatility of DKP synthesis and polymerisation, particularly that of sarcosine DKP.

Reported in Chapter 7 is the electrospinning of polyalanine and polysarcosine with polycaprolactone as a carrier. The electrospinning of the copolymer solutions is reported for the first time and, additionally, as are the electrospinning parameters required to produce nanofibres that replicate the physical structure and characteristics of human extracellular matrix. The produced nanofibre mats were assessed by FTIR spectroscopy and SEM to determine polymer content and the morphology of the resultant fibres. They were also assessed for their tensile strength and sensitivity to degradation by elastase, demonstrating their potential applicability as dressings to facilitate healing in chronic wounds.

To further investigate the value of DKP ROP as a synthetic route to poly(amino acids), alternative conditions and reagents were also explored. Chapter 8 includes the expansion of the library of poly(amino acids) accessible via ROP of DKPs, including polyproline, polyarginine and polymethionine. Plausible alternative for solvents, catalysts and reaction conditions for DKP ROP were also identified.

## 1.9. References

---

- 1) Engineer Student. *Polymerisation*. [Online]. 2019. [Accessed 24/02/21]. Available from: <http://www.engineerstudent.co.uk/polymerisation.php>
- 2) Polymer Properties Database. *Chain-Growth Versus Step-Growth Polymerization*. [Online]. 2015. [Accessed 28/04/19]. Available from: <https://polymerdatabase.com/polymer%20chemistry/Chain%20versus%20Step%20Growth.html>
- 3) Department of Materials Science and Engineering, University of Illinois. *Scientific Principles*. [Online]. 2019. [Accessed 28/04/19]. Available from: <http://matse1.matse.illinois.edu/polymers/prin.html>
- 4) de la Rica, R. and Matsui, H. Applications of peptide and protein-based materials in bionanotechnology. *Chemical Society Reviews*. 2010, **39**(9), 3499-3509.
- 5) Chow, D., Nunalee, M. L., Lim, D. W., Simnick, A. J. and Chilkoti, A. Peptide-based Biopolymers in Biomedicine and Biotechnology. *Materials and Science Engineering: R: Reports*. 2008, **62**(4), 125-155.
- 6) Merck Millipore. *Amino acid reference charts*. [Online]. 2021. [22/02/21]. Available from: <https://www.sigmaaldrich.com/life-science/metabolomics/learning-center/amino-acid-reference-chart.html>
- 7) Harada, K. and Fox, S. W. The Thermal Condensation of Glutamic Acid and Glycine to Linear Peptides. *Journal of the American Chemical Society*. 1958, **80**(11), 2694-2697.
- 8) Kricheldorf, H. R. Polypeptides and 100 years of chemistry of alpha-amino acid N-carboxyanhydrides. *Angewandte Chemie (International ed. in English)*. 2006, **45**(35), 5752-5784.
- 9) Leuchs, H. Ueber die Glycin-carbonsäure. *Berichte der deutschen chemischen Gesellschaft*. 1906, **39**(1), 857-861
- 10) Deming, T. Synthetic polypeptides for biomedical applications. *Progress in Polymer Science*. 2007, **32**, 858-875.
- 11) Robin, Y.  $\alpha$ -Amino acid N-Carboxy Anhydrides in pharmaceutical innovations: try them to capture new value. *Chemistry Today*. 2015, **33**(4), 27-31.
- 12) Fitzgerald, G. J. Chemical Warfare and Medical Response During World War I. *American Journal of Public Health*. 2008, **98**(4), 611-625.

- 
- 13) Centers for Disease Control and Prevention. *The National Institute for Occupational Safety and Health: Phosgene – Immediately Dangerous to Life or Health Concentrations*. [Online]. 1994. [20/02/21]. Available from: <https://www.cdc.gov/niosh/idlh/75445.html#:~:text=An%20IDLH%20of%20%20ppm,prevent%20irreversible%20adverse%20health%20effects>.
- 14) Kralingen, L. V. *Controlled Polymerization of Amino acid Derivatives*. PhD thesis, Stellenbosch University, 2008.
- 15) Farthing, A. C. Synthetic polypeptides. Part I. *Journal of the Chemical Society*. 1950, **0**, 3213-3217.
- 16) Wilder, R. and Mobashery, S. The use of triphosgene in preparation of N-carboxy- $\alpha$ -amino acid anhydrides. *Journal of Organic Chemistry*. 1992, **57**(9), 2755-2756.
- 17) Smeets, N. M. B, Van der Weide, P. L. J., Meuldijk, J., Vekemans, J. A. J. M. and Hulshof, L. A. A Scalable Synthesis of L-Leucine-N-carboxyanhydride. *Organic Process Research & Development*. 2005, **9**(6), 757-763.
- 18) Robin, Y. Production process of  $\alpha$ -Amino acid N-Carboxyanhydrides: Batch process development, scale-up concerns and industrial solution. *Organic Process Research & Development*. Conference and Exhibition, Lisbon, 9th – 11th September 2009
- 19) Dmitrovic, V., Habraken, G. J. M., Hendrix, M. M. R. M., Habraken, W. J. E. M., Heise, A., de With, G. and Sommerdijk, N. A. J. M. Random Poly(Amino Acid)s Synthesised by Ring Opening Polymerization as Additives in the Biomimetic Mineralization of  $\text{CaCO}_3$ . *Polymers*. 2012, **4**(2), 1195-1210.
- 20) Chen, X., Lai, H., Xiao, C., Tian, H., Chen, X., Tao, Y. and Wang, X. New bio-renewable polyester with rich side amino groups from L-lysine via controlled ring-opening polymerization. *Polymer Chemistry*. 2014, **5**(22), 6495-6502.
- 21) Koga, K., Sudo, A. and Endo, T. Revolutionary Phosgene-Free Synthesis of  $\alpha$ -Amino Acid N-Carboxyanhydrides Using Diphenyl Carbonate Based on Activation of  $\alpha$ -Amino Acids by Converting into Imidazolium Salts. *Journal of Polymer Science: Part A: Polymer Chemistry*. 2010, **48**, 4351-4355.
- 22) Laconde, G., Amblard, M. and Martinez, J. Synthesis of  $\alpha$ -Amino Acid N-Carboxyanhydrides. *Organic Letters*. 2021, **23**, 6412-6416.

- 
- 23) Borthwick, A. D. 2,5-Diketopiperazines: Synthesis, Reactions, Medicinal Chemistry, and Bioactive Natural Products. *Chemical Reviews*. 2012, **112**(7), 3641-3716.
- 24) Fischer, P. M. Diketopiperazines in Peptide and Combinatorial Chemistry. *Journal of Peptide Science*. 2003, **9**, 9-35.
- 25) Dinsmore, C. J. and Beshore, D. C. Recent Advances in the synthesis of diketopiperazines. *Tetrahedron*. 2002, **58**(17), 3297-3312.
- 26) Rowley, J. V., Wall, P., Yu, H., Tronci, G., Devine, D. A., Vernon, J. J. and Thornton, P. D. Antimicrobial Dye-Conjugated Polyglobalide-Based Organogels. *ACS Applied Polymer Materials*. 2020, **2**(7), 2927-2933.
- 27) Depew, K. M., Marsden, S. P., Zatorska, D., Zatorski, A., Bornmann, W. G. and Danishefsky, S. J. Total Synthesis of 5-N-Acetylardeemin and Amauromine: Practical Routes to Potential MDR Reversal Agents. *Journal of the American Chemical Society*. 1999, **121**(51), 11953-11963.
- 28) Pokorna, A., Bobal, P., Oravec, M., Rarova, L., Bobalova, J. and Jampilek, J. Investigation of Permeation of Theophylline through Skin Using Selected Piperazine-2,5-Diones. *Molecules*. 2019, **24**(3), 566-579.
- 29) Santagada, V., Fiorino, F., Perissutti, E., Severino, B., Terracciano, S., Cirino, G. and Caliendo, G. A convenient strategy of dimerization by microwave heating and using 2,5-diketopiperazine as scaffold. *Tetrahedron Letters*. 2003, **44**(6), 1145-1148.
- 30) Jainta, M., Nieger, M. and Bräse, S. Microwave-Assisted Stereoselective One-Pot Synthesis of Symmetrical and Unsymmetrical 2,5-Diketopiperazines from Unprotected Amino Acids. *European Journal of Organic Chemistry*. 2008, **2008**(32), 5418-5424.
- 31) Nonappa, K. A., Lahtinen, M. and Kolehmainen, E. Cyclic dipeptides: catalyst/promoter-free, rapid and environmentally benign cyclization of free amino acids. *Green Chemistry*. 2011, **13**, 1203-1209.
- 32) Prielcel, P. and Lopez-Sanchez, J. A. Advantages and Limitations of Microwave Reactors: From Chemical Synthesis to the Catalytic Valorization of Biobased Chemicals. *ACS Sustainable Chemistry and Engineering*. 2019, **7**(1), 3-21.
- 33) Frankel, M. and Katchalski, E. Poly-condensation of  $\alpha$ -Amino Acid Esters. I. Poly-condensation of Glycine Esters. *Journal of the American Chemical Society*. 1942, **64**(10), 2264-2268.

- 
- 34) Frankel, M. and Katchalski, E. Poly-condensation of  $\alpha$ -Amino Acid Esters. II. Poly-condensation of Alanine Ethyl Ester. *Journal of the American Chemical Society*. 1942, **64**(10), 2268-2271.
- 35) Palomo, J.M. Solid-phase peptide synthesis: an overview focused on the preparation of biologically relevant peptides. *RSC Advances*. 2014, **4**(62), 32658-32672.
- 36) Fields, G. B. Introduction to Peptide Synthesis. *Current Protocols in Protein Science*. 2002, **26**(1), 18.1.1-18.1.9.
- 37) GYROS PROTEIN Technologies. Solid-phase peptide synthesis (SPPS) in research & biopharmaceutical development. [Online]. 2023. [18/09/2023]. Available from: <https://www.gyrosproteintechnologies.com/peptides/spps-applications>
- 38) Habraken, G. J., Wilsens, K. H., Koning, C. E. and Heise, A. Optimization of N-carboxyanhydride (NCA) polymerization by variation of reaction temperature and pressure. *Polymer Chemistry*. 2011, **2**(6), 1322-1330.
- 39) Huang, J. and Heise, A. Stimuli responsive synthetic polypeptides derived from N-carboxyanhydride (NCA) polymerisation. *Chemical Society Reviews*. 2013, **42**(17), 7373-7390.
- 40) Deming, T. J. Living polymerization of  $\alpha$ -amino acid-N-carboxyanhydrides. *Journal of Polymer Science Part A: Polymer Chemistry*. 2000, **38**(17), 3011-3018.
- 41) Cheng, J. and Deming, T. Synthesis of Polypeptides by Ring-Opening Polymerization of  $\alpha$ -Amino Acid N-Carboxyanhydrides. *Top Current Chemistry*. 2012, **310**, 1-26.
- 42) Hadjichristidis, N., Iatrou, H., Pitsikalis, M. and Sakellariou, G. Synthesis of Well-Defined Polypeptide-Based Materials via the Ring-Opening Polymerization of  $\alpha$ -Amino Acid N-Carboxyanhydrides. *Chemical Reviews*. 2009, **109**(11), 5528-5578.
- 43) Johnson, R. P., John, J. V. and Kim, I. Recent developments in polymer-*block*-polypeptide and protein-polymer bioconjugate hybrid materials. *European Polymer Journal*. 2013, **49**(10), 2925-2948.
- 44) Vayaboury, W., Giani, O., Cottet, H., Deratani, A. and Schué, F. Living Polymerization of  $\alpha$ -Amino Acid N-Carboxyanhydrides (NCA) upon Decreasing the Reaction Temperature. *Macromolecular Rapid Communications*. 2004, **25**(13), 1221-1224.
- 45) Habraken, G. J. M., Heise, A. and Thornton, P. D. Block Copolypeptides Prepared by N-Carboxyanhydride Ring-Opening Polymerization. *Macromolecular Rapid Communications*. 2012, **33**(4), 272-286.

- 
- 46) Karatzas, A., Iatrou, H., Hadjichristidis, N., Inoue, K., Sugiyama, K. and Hirao, A. Complex Macromolecular Chimeras. *Biomacromolecules*. 2008, **9**(7), 2072-2080.
- 47) Robson Marsden, H. and Kros, A. Polymer-Peptide Block Copolymers – An Overview and Assessment of Synthesis Methods. *Macromolecular Bioscience*. 2009, **9**(10), 939-951.
- 48) Odian, G. *Principles of polymerization*. John Wiley & Sons, 2004.
- 49) Wang, L-L., Wu, Y-X., Xu, R-W., Wu, G-Y. and Yang, W-T. Synthesis and Characterization of poly(L-glutamic acid-co-L-aspartic acid). *Chinese Journal of Polymer Science*. 2008, **26**(4), 381-391.
- 50) in't Veld, P. J. A, Wei-ping, Y., Klap, R., Dijkstra, P. J. and Feijen, J. Copolymerisation of  $\epsilon$ -caprolactone and morpholine-2,5-dione derivatives. *Die Makromolekulare Chemie*. 1992, **193**(8), 1927-1942.
- 51) Kricheldorf, H. R. and Hauser, K. Homo- and Copolymerizations of 3-Methylmorpholine-2,5-dione Initiated With a Cyclic Tin Alkoxide. *Macromolecular Chemistry and Physics*. 2001, **202**, 1219-1226.
- 52) Jörres, V., Keul, H. and Höcker, H. Polymerisation of (3S,6S)-3-isopropyl-6-methyl-2,5-morpholinedione with tin octoate and tin acetylacetonate. *Macromolecular Chemistry and Physics*. 1998, **199**, 835-843.
- 53) Sun, H., Meng, F., Dias, A. A., Hendriks, M., Feijen, J. and Zhong, Z.  $\alpha$ -Amino Acid Containing Degradable Polymers as Functional Biomaterials: Rational Design, Synthetic Pathway, and Biomedical Applications. *Biomacromolecules*. 2011, **12**, 1937-1955.
- 54) in't Veld, P. J. A., Dijkstra, P. J. and Feijen, J. Synthesis of biodegradable polyesteramides with pendant functional groups. 1992, **193**, 2713-2730.
- 55) in't Veld, P. J. A., Dijkstra, P. J., van Lochem, J. H. and Feijen, J. Synthesis of alternating polydepsipeptides by ring-opening polymerization of morpholine-2,5-dione derivatives. *Die Makromolekulare Chemie*. 1990, **191**, 1813-1825.
- 56) Ouchi, T., Nozaki, T., Okamoto, Y., Shiratani, M. and Ohya, Y. Synthesis and enzymatic hydrolysis of polydepsipeptides with functionalized pendant groups. *Macromolecular Chemistry and Physics*. 1996, **197**, 1823-1833.
- 57) Feng, Y., Klee, D. and Höcker, H. Synthesis of Poly[(lactic acid)-*alt*- or *co*-((S)-aspartic acid)] from (3S,6R,S)-3-[(Benzyloxycarbonyl)methyl]-6-methylmorpholine-2,5-dione. *Macromolecular Chemistry and Physics*. 2002, **203**, 819-824.

- 
- 58) Sobczak, M. Ring-opening polymerization of cyclic esters in the presence of choline/SnOct<sub>2</sub> catalytic system. *Polymer Bulletin*. 2012, **68**, 2219-2228.
- 59) U.S. Food and Drug Administration. CFR – Code of Federal Regulations Title 21. [Online]. 2020. [25/02/21]. Available from: <https://www.accessdata.fda.gov/scripts/cdrh/cfdocs/cfCFR/CFRSearch.cfm?fr=175.300>
- 60) Stridsberg, K. M. *Controlled Ring-Opening Polymerization: Polymers with designed Macromolecular Architecture*. Ph.D. thesis, Royal Institute of Technology, Stockholm, Sweden, 2000.
- 61) Degée, Ph., Dubois, Ph., Jacobsen, S., Fritz, H-G. and Jérôme, R. Beneficial effect of triphenylphosphine on the bulk polymerization of L,L-lactide promoted by 2-ethylhexanoic acid tin(II) salt. *Journal of Polymer Science Part A: Polymer Chemistry*. 2000, **37**(14), 2413-2420.
- 62) in't Veld, P. J. A., Velner, E. M., van de Witte, P., Hamhuis, J., Dijkstra, P. J. and Feijen, J. Melt Block copolymerization of  $\epsilon$ -caprolactone and L-Lactide. *Journal of Polymer Science Part A: Polymer Chemistry*. 1997, **35**(2), 219-226.
- 63) Du, Y. J., Lemstra, P. J., Nijenhuis, A. J., van Aert, H. A. M. and Bastiaansen, C. ABA Type Copolymers of Lactide with Poly(ethylene glycol). Kinetic, Mechanistic, and Model Studies. *Macromolecules*. 1995, **28**(7), 2124-2132.
- 64) Kowalski, A., Duda, A. and Penczek, S. Kinetics and mechanism of cyclic esters polymerization initiated with tin(II) octoate, 1. Polymerization of  $\epsilon$ -caprolactone. *Macromolecular Rapid Communications*. 1998, **19**(11), 567-572.
- 65) Kricheldorf, H. R., Kreiser-Saunders, I. and Boettcher, C. Polylactones: 31. Sn(II)octoate-initiated polymerization of L-lactide: a mechanistic study. *Polymer*. 1995, **36**(6), 1253-1259.
- 66) Zhang, X., Macdonald, D. A., Goosen, M. F. A. and McAuley, K. B. Mechanism of lactide polymerization in the presence of stannous octoate: The effect of hydroxyl and carboxylic acid substances. *Journal of Polymer Science Part A: Polymer Chemistry*. 1994, **32**(15), 2965-2970.
- 67) Kricheldorf, H. R., Stricker, A. Polymers of carbonic acid, 28. SnOct<sub>2</sub>-initiated polymerizations of trimethylene carbonate (TMC, 1,3-dioxanone-2). *Macromolecular Chemistry and Physics*. 2000, **201**(17), 2557-2567.
- 68) Kowalski, A., Duda, A. and Penczek, S. Kinetics and Mechanism of Cyclic Esters Polymerization Initiated with Tin(II) Octoate. Polymerisation of Dilactide. *Macromolecules*. 2000, **33**(20), 7359-7370.



- 
- 69) Kowalski, A., Duda, A. and Penczek, S. Mechanism of Cyclic Ester Polymerization Initiated with Tin(II) Octoate. Macromolecules Fitted with Tin(II) Alkoxide Species Observed Directly in MALDI-TOF Spectra. *Macromolecules*. 2000, **33**(3), 689-695.
- 70) Duda, A., Penczek, S., Kowalski, A. and Libiszowski, J. Polymerizations of  $\epsilon$ -caprolactone and L,L-dilactide initiated with stannous octoate and stannous butoxide- a comparison. *Macromolecular Symposia*. 2000, **153**(1), 41-53.
- 71) Ryner, M., Stridsberg, K. and Albertsson, A-C. Mechanism of Ring-Opening Polymerisation of 1,5-Dioxepan-2-one and L-Lactide with Stannous 2-Ethylhexanoate. A Theoretical Study. *Macromolecules*. 2001, **34**, 3877-3881.
- 72) Lee, R-S. and Yang, J-M. Synthesis and Characterization of Degradable Copoly(ester-amide)s: Poly(*trans*-4-hydroxy-L-proline-co- $\epsilon$ -caprolactam). *Journal of Applied Polymer Science*. 2002, **86**, 1615-1621.
- 73) Delahousse, J., Skarbek, C. and Paci, A. Prodrugs as drug delivery system in oncology. *Cancer Chemotherapy and Pharmacology*. 2019, **84**, 937-958.
- 74) Yadav, S., Sharma, A. K. and Kumar, P. Nanoscale Self-Assembly for Therapeutic Delivery. *Frontiers in Bioengineering and Biotechnology*. 2020, **8**(127), 1-24.
- 75) Sood, N., Bhardwaj, A., Mehta, S. and Mehta, A. Stimuli-responsive hydrogels in drug delivery and tissue engineering. *Drug Delivery*. 2016, **23**(3), 758-780.
- 76) Li, J., Yu, F., Chen, Y. and Oupicky, D. Polymeric drugs: Advances in the development of pharmacologically active polymers. *Journal of Controlled Release*. 2015, **219**, 369-382.
- 77) Murphy, R., Borase, T., Payne, C., O'Dwyer, J., Cryan, S.A. and Heise, A. Hydrogels from amphiphilic star block copolypeptides. *RSC Advances*. 2016, **6**(28), 23370-23376.
- 78) Li, Y., Shen, Y., Wang, S., Zhu, D., Du, B. and Jiang, J. Disulfide cross-linked cholic-acid modified PEG-poly(amino acid) block copolymer micelles for controlled drug delivery of doxorubicin. *RSC Advances*. 2015, **5**(38), 30380-30388.
- 79) Iatrou, H., Frielinghaus, H., Hanski, S., Ferderigos, N., Ruokolainen, J., Ikkala, O., Richter, D., Mays, J. and Hadjichristidis, N. Architecturally Induced Multiresponsive Vesicles from Well-Defined Polypeptides. Formation of Gene Vehicles. *Biomacromolecules*. 2007, **8**(7), 2173-2181.
- 80) Larson, N. and Ghandehari, H. Polymeric conjugates for drug delivery. *Chemistry of materials: a publication of the American Chemical Society*. 2012, **24**(5), 840-853.

- 
- 81) Harris, J. M. and Chess, R. B. Effect of pegylation on pharmaceuticals. *Nature Reviews. Drug Discovery*. 2003, **2**(3), 214-221.
- 82) Knop, K., Hoogenboom, R., Fischer, D. and Schubert, U. S. Poly(ethylene glycol) in drug delivery: pros and cons as well as potential alternatives. *Angewandte Chemie-International Edition*. 2010, **49**(36), 6288-6308.
- 83) Culf, A. S. and Ouellette, R. J. Solid-Phase Synthesis of N-Substituted Glycine Oligomers ( $\alpha$ -Peptoids) and Derivatives. *Molecules*. 2010, **15**(8), 5282-5335.
- 84) Schneider, M., Fetsch, C., Amin, I., Jordan, R. and Luxenhofer, R. Polypeptoid brushes by surface-initiated polymerization of N-substituted glycine N-carboxyanhydrides. *Langmuir: the ACS Journal of Surfaces and Colloids*. 2013, **29**(23), 6983-6988.
- 85) Birke, A., Huesmann, D., Kelsch, A., Weillbacher, M., Xie, J., Bros, M., Bopp, T., Becker, C., Landfester, K. and Barz, M. Polypeptoid-*block*-polypeptide Copolymers: Synthesis, Characterization, and Application of Amphiphilic Block Copolypept(o)ides in Drug Formulations and Miniemulsion Techniques. *Biomacromolecules*. 2014, **15**(2), 548-557.
- 86) Kwon, Y-U. and Kodadek, T. Quantitative Evaluation of the Relative Cell Permeability of Peptoids and Peptides. *Journal of the American Chemical Society*. 2007, **129**(6), 1508-1509.
- 87) Yu, H., Ingram, N., Rowley, J. V., Parkinson, S., Green, D. C., Warren, N. J. and Thornton, P. D. Thermoresponsive polysarcosine-based nanoparticles. *Journal of Materials Chemistry B*. 2019, **7**(26), 4217-4223.
- 88) Li, M.-H. and Keller, P. Stimuli-responsive polymer vesicles. *Soft Matter*. 2009, **5**, 927-937.
- 89) Chu, K. S., Schorzman, A. N., Finniss, M. C., Bowerman, C. J., Peng, L., Luft, C. J., Madden, A., Wang, A. Z., Zamboni, W. C. and DeSimone, J. M. Nanoparticle Drug Loading as a Design Parameter to Improve Docetaxel Pharmacokinetics and Efficacy. *Biomaterials*. 2013, **34**(33), 8424-8429.
- 90) Sultana, S., Alzahrani, N., Alzahrani, R., Alshamrani, W., Aloufi, W., Ali, A., Najib, S. and Siddiqui, N. A. Stability issues and approaches to stabilised nanoparticles based drug delivery system. *Journal of Drug Targeting*. 2020, **28**(5), 468-486.
- 91) Liu, Y., Wang, W., Yang, J., Zhou, C. and Sun, J. pH-sensitive polymeric micelles triggered drug release for extracellular and intracellular drug targeting deliver. *Asian Journal of Pharmaceutical Sciences*. 2013, **8**(3), 159-167.

- 
- 92) Schubert, S., Delaney, J. J. T. and Schubert, U. S. Nanoprecipitation and nanoformulation of polymers: from history to powerful possibilities beyond poly(lactic acid). *Soft Matter*. 2011, **7**, 1581-1588.
- 93) Danaei, M., Dehghankhold, M., Ataei, S., Davarani, F. H., Javanmard, R., Dokhani, A., Khorasani, S. and Mozafari, M. R. Impact of Particle Size and Polydispersity Index on the Clinical Applications of Lipidic Nanocarrier Systems. *Pharmaceutics*. 2018, **10**, 57-73.
- 94) Hoffman, A. S. and Stayton, P. S. Applications of “Smart Polymers” as Biomaterials. In: Wagner, W. R., Sakiyama-Elbert, S. E., Zhang, G. and Yaszemski, M. J. *Biomaterials Science*. [Online] Fourth Edition. Elsevier Academic Press, 2020, 191-203.
- 95) Kopecek, J. Smart and genetically engineered biomaterials and drug delivery systems. *European Journal of Pharmaceutical Sciences*. 2003, **20**(1), 1-16.
- 96) Mano, J. F. Stimuli-Responsive Polymeric Systems for Biomedical Applications. *Advanced Engineering Materials*. 2008, **10**(6), 515-527.
- 97) Schmaljohann, D. Thermo- and pH-responsive polymers in drug delivery. *Advanced Drug Delivery Reviews*. 2006, **58**(15), 1655-1670.
- 98) Zelzer, M., Todd, S. J., Hirst, A. R., McDonald, T. O. and Ulijn, R. V. Enzyme responsive materials: design strategies and future developments. *Biomaterials Science*. 2013, **1**, 11-39.
- 99) Li, M., Zhao, G., Su, W-K. and Shuai, Q. Enzyme-Responsive Nanoparticles for Anti-tumor Drug Delivery. *Frontiers in Chemistry*. 2020, **8**, 647.
- 100) Lewis, T. and Stone, W. L. Biochemistry, Proteins Enzymes. *Stat Pearls*. 2023, Available from: <https://www.ncbi.nlm.nih.gov/books/NBK554481/>
- 101) Heinz, A. Elastases and elastokines: elastin degradation and its significance in health and disease. *Critical reviews in biochemistry and molecular biology*. 2020, **55**(3), 252-273.
- 102) Nam, K. H. Glucose Isomerase: Functions, Structures, and Applications. *Applied Science*. 2022, **12**(1), 428-439.
- 103) Howes, T. R. L. and Tomkinson, A. E. DNA ligase I, the replicative DNA ligase. *Subcell Biochemistry*. 2012, **62**, 327-341.
- 104) Moriguchi, T. and Takai, J. Histamine and histidine decarboxylase: Immunomodulatory functions and regulatory mechanisms. *Gene Cells*. 2020, **25**(7), 443-449.

- 
- 105) Rullo, R., Cerchia, C., Nasso, R., Romanelli, V., De Vendittis, E., Masullo, M. and Lavecchia, A. Novel Reversible Inhibitors of Xanthine Oxidase Targeting the Active Site of the Enzyme. *Antioxidants*. 2023, **12**(4), 825-837.
- 106) Oda, Y. Choline acetyltransferase: the structure, distribution and pathologic changes in the central nervous system. *Pathology International*. 1999, **49**(11), 921-937.
- 107) Toledano, S., Williams, R. J., Jayawarna, V. and Ulijn, R. V. Enzyme-Triggered Self-Assembly of Peptide Hydrogels via Reversed Hydrolysis. *Journal of the American Chemical Society*. 2006, **128**(4), 1070-1071.
- 108) Sperinde, J. J. and Griffith, L. G. Synthesis and Characterization of Enzymatically-Cross-Linked Poly(ethylene glycol) Hydrogels. *Macromolecules*. 1997, **30**(18), 5255–5264.
- 109) Yang, Z., Gu, H., Fu, D., Gao, P., Lam, J. K. and Xu, B. Enzymatic Formation of Supramolecular Hydrogels. *Advanced Materials*. 2004, **16**(16), 1440-1444.
- 110) Thornton, P. D., Mart, R. J. and Ulijn, R. V. Enzyme-Responsive Polymer Hydrogel Particles for Controlled Release. *Advanced Materials*. 2007, **19**(9), 1252–1256.
- 111) Das, A. K., Collins, R. and Ulijn, R. V. Exploiting enzymatic (reversed) hydrolysis in directed self-assembly of peptide nanostructures. *Small*. 2008, **4**(2), 279-287.
- 112) Wang, M., Gu, X., Zhang, G., Zhang, D. and Zhu, D. Continuous Colorimetric Assay for Acetylcholinesterase and Inhibitor Screening with Gold Nanoparticles. *Langmuir*. 2009, **25**(4), 2504-2507.
- 113) Lutolf, M. P. and Hubbell, J. A. Synthesis and Physicochemical Characterization of End-Linked Poly(ethylene glycol)-*co*-peptide Hydrogels Formed by Michael-Type Addition. *Biomacromolecules*. 2003, **4**(3), 713-722.
- 114) Mann, B. K., Gobin, A. S., Tsai, A. T., Schmedlen, R. H. and West, J. L. Smooth muscle cell growth in photopolymerized hydrogels with cell adhesive and proteolytically degradable domains: synthetic ECM analogs for tissue engineering. *Biomaterials*. 2001, **22**(22), 3045-3051.
- 115) Todd, S. J., Farrar, D., Gough, J. E. and Ulijn, R. V. Enzyme-triggered cell attachment to hydrogel surfaces. *Soft Matter*. 2007, **3**(5), 547-550.
- 116) Shi, L., De Paoli, V., Rosenzweig, N. and Rosenzweig, Z. Synthesis and Application of Quantum Dots FRET-Based Protease Sensors. *Journal of the American Chemical Society*. 2006, **128**(32), 10378-10379.

- 
- 117) Webber, M. J., Newcomb, C. J., Bitton, R. and Stupp, S. I. Switching of self-assembly in a peptide nanostructure with a specific enzyme. *Soft Matter*. 2011, **7**(20), 9665-9672.
- 118) Yang, Z., Liang, G., Wang, L. and Xu, B. Using a kinase/phosphatase switch to regulate a supramolecular hydrogel and forming the supramolecular hydrogel in vivo. *Journal of the American Chemical Society*. 2006, **128**(9), 3038-3043.
- 119) Wang, C., Chen, Q., Wang, Z. and Zhang, X. An enzyme-responsive polymeric superamphiphile. *Angewandte Chemie (International ed. in English)*. 2010, **49**(46), 8612-8615.
- 120) Choi, Y., Ho, N-H. and Tung, C-H. Sensing Phosphatase Activity by Using Gold Nanoparticles. *Angewandte Chemie International Edition*. 2007, **46**(5), 707-709.
- 121) Xu, X., Liu, X., Nie, Z., Pan, Y., Guo, M. and Yao, S. Labile-Free Fluorescent Detection of Protein Kinase Activity Based on the Aggregation Behavior of Unmodified Quantum Dots. *Analytical Chemistry*. 2011, **83**(1), 52-59.
- 122) Morimoto, N., Ogino, N., Narita, T., Kitamura, S. and Akiyoshi, K. Enzyme-Responsive Molecular Assembly System with Amylose-Primer Surfactants. *Journal of the American Chemical Society*. 2007, **129**(3), 458-459.
- 123) Patel, K., Angelos, S., Dichtel, W. R., Coskun, A., Yang, Y-W., Zink, J. I. and Stoddart, J. F. Enzyme-responsive snap-top covered silica nanocontainers. *Journal of the American Chemical Society*. 2008, **130**(8), 2382-2383.
- 124) Wang, Z., Levy, R., Fernig, D. G. and Brust, M. Kinase-Catalyzed Modification of Gold Nanoparticles: A New Approach to Colorimetric Kinase Activity Screening. *Journal of the American Chemical Society*. 2006, **128**(7), 2214-2215.
- 125) Yeo, W-S. and Mrksich, M. Self-Assembled Monolayers That Transduce Enzymatic Activities to Electrical Signals. *Angewandte Chemie*. 2003, **42**, 3121-3124.
- 126) Dos Santos, S., Chandravarkar, A., Mandal, B., Mimna, R., Murat, K., Saucède, L., Tella, P., Tuchscherer, G. and Mutter, M. Switch-Peptides: Controlling Self-Assembly of Amyloid  $\beta$ -Derived Peptides in vitro by Consecutive Triggering of Acyl Migrations. *Journal of American Chemical Society*. 2005, **127**(34), 11888-11889.
- 127) Thornton, P. D., McConnell, G. and Ulijn, R. V. Enzyme responsive polymer hydrogel beads. *Chemical Communications*. 2005, (47), 5913-5915.

- 
- 128) Laromaine, A., Koh, L., Murugesan, M., Ulijn, R. V. and Stevens, M. M. Protease-Triggered Dispersion of Nanoparticle Assemblies. *Journal of the American Chemical Society*. 2007, **129**(14), 4156-4157.
- 129) Wichterle, O. and Lím, D. Hydrophilic Gels for Biological Use. *Nature*. 1960, **185**, 117-118.
- 130) Jin, R., Moreira Teixeira, L. S., Dijkstra, P. J., van Blitterswijk, C. A., Karperien, M. and Feijen, J. Enzymatically-crosslinked injectable hydrogels based on biomimetic dextran-hyaluronic acid conjugates for cartilage tissue engineering. *Biomaterials*. 2010, **31**(11), 3103-3113.
- 131) Aimetti, A. A., Tibbitt, M. W. and Anseth, K. S. Human Neutrophil Elastase Responsive Delivery from Poly(ethylene glycol) Hydrogels. *Biomacromolecules*. 2009, **10**(6), 1484-1489.
- 132) Garripelli, V. K., Kim, J-K., Son, S., Kim, W. J., Repka, M. A. and Jo, S. Matrix Metalloproteinase-Sensitive Thermogelling Polymer For Bioresponsive Local Drug Delivery. *Acta Biomaterialia*. 2011, **7**(5), 1984-1992.
- 133) Folk, J. E. and Finlayson, J. S. The epsilon-(gamma-glutamyl)lysine crosslink and the catalytic role of transglutaminases. *Advances in Protein Chemistry*. 1977, **31**, 1-133.
- 134) Fuchsbaauer, H. L., Gerber, U., Engelmann, J., Seeger, T., Sinks, C. and Hecht, T. Influence of gelatin matrices cross-linked with transglutaminase on the properties of an enclosed bioactive material using  $\beta$ -galactosidase as model system. *Biomaterials*. 1996, **17**(15), 1481-1488.
- 135) Hovgaard, L. and Brøndsted, H. Dextran hydrogels for colon-specific drug delivery. *Journal of Controlled Release*. 1995, **36**(1-2), 159-166.
- 136) West, J. L. and Hubbell, J. A. Polymeric Biomaterials with Degradation Sites for Proteases Involved in Cell Migration. *Macromolecules*. 1999, **32**(1), 241-244.
- 137) Ehrbar M., Rizzi, S. C., Schoenmakers, R. G., San Miguel, B., Hubbell, J. A., Weber, F. E. and Lutolf, M. P. Biomolecular hydrogels formed and degraded via site-specific enzymatic reactions. *Biomacromolecules*. 2007, **8**(10), 3000-3007.
- 138) McDonald, T. O., Qu, H., Saunders, B. R. and Ulijn, R. V. Branched peptide actuators for enzyme responsive hydrogel particles. *Soft Matter*. 2009, **5**(8), 1728–1734.
- 139) Thornton, P. D., Mart, R. J., Webb, S. J. and Ulijn, R. V. Enzyme-responsive hydrogel particles for the controlled release of proteins: designing peptide actuators to match payload. *Soft Matter*. 2008, **4**(4), 821-827.

- 
- 140) Habraken, G. J. M., Peeters, M., Thornton, P. D., Koning, C. E. and Heise, A. M. Selective enzymatic degradation of self-assembled particles from amphiphilic block copolymers obtained by the combination of N-carboxyanhydride and nitroxide-mediated polymerization. *Biomacromolecules*. 2011, **12**(10), 3761-3769.
- 141) Britto, E. J., Nezwek, T. A., Popowicz, P. and Robins, M. Wound Dressings. *StatPearls*. 2023. Available from: <https://www.ncbi.nlm.nih.gov/books/NBK470199/>
- 142) Landen, N. X., Li, D. and Stähle, M. Transition from inflammation to proliferation: a critical step during wound healing. *Cellular and Molecular Life Sciences*. 2016, **73**(20), 3861-3885.
- 143) Reinke, J. M. and Sorg, H. Wound repair and regeneration. *European Surgical Research*. 2012, **49**(1), 35-43.
- 144) Guo, S. and DiPietro, L. A. Factors Affecting Wound Healing. *Journal of Dental Research*. 2010, **89**(3), 219-229.
- 145) Gosain, A. and DiPietro, L. A. Aging and wound healing. *World Journal of Surgery*. 2004, **28**(3), 321-326.
- 146) Broughton 2<sup>nd</sup>, G., Janis, J. E. and Attinger, C. E. The basic science of wound healing. *Plastic and Reconstructive Surgery*. 2006, **117**(7 Suppl), 12S-34S.
- 147) Campos, A. C. L., Groth, A. K. and Branco, A. B. Assessment and nutritional aspects of wound healing. *Current opinion in clinical nutrition and metabolic care*. 2008, **11**(3), 281-288.
- 148) Meszaros, A. J., Reichner, J. S. and Albina, J. E. Macrophage-induced neutrophil apoptosis. *Journal of Immunology*. 2000, **165**(1), 435-441.
- 149) Mosser, D. M. and Edwards, J. P. Exploring the full spectrum of macrophage activation. *Nature Reviews. Immunology*. 2008, **8**(12), 958-969.
- 150) Swift, M. E., Burns, A. L., Gray, K. L. and DiPietro, L. A. Age-related alterations in the inflammatory response to dermal injury. *The Journal of Investigative Dermatology*. 2001, **117**(5), 1027-1035.
- 151) Park, J. E. and Barbul, A. Understanding the role of immune regulation in wound healing. *American Journal of Surgery*. 2004, **187**(5A), 11-16.
- 152) NHS. *Does my cut need stitches?*. [Online] 2020. [26/08/2023]. Available from: <https://www.nhs.uk/common-health-questions/accidents-first-aid-and-treatments/does-my-cut-need-stitches/>

- 
- 153) Hoogenboom, B. J. and Smith, D. Management of Bleeding and Open Wounds in Athletes. *International Journal of Sports Physical Therapy*. 2012, **7**(3), 350-355.
- 154) NHS. *Side Effects – Anticoagulant Medicines*. [Online] 2021. [26/08/2023]. Available from: <https://www.nhs.uk/conditions/anticoagulants/side-effects/#:~:text=A%20possible%20side%20effect%20of,also%20experience%20other%20side%20effects.>
- 155) Godier, A., Albaladejo, P. and the French Working Group on Perioperative Haemostasis (GIHP). *Journal of Clinical Medicine*. 2020, **9**(7), 2318-2328.
- 156) NHS. *Overview – Haemophilia*. [Online] 2020. [26/08/2023]. Available from: <https://www.nhs.uk/conditions/haemophilia/>
- 157) Bishop, A. Role of oxygen in wound healing. *Journal of Wound Care*. 2008, **17**(9), 399-402.
- 158) Rodriguez, P. G., Felix, F. N., Woodley, D. T. and Shim, E. K. The role of oxygen in wound healing: a review of the literature. *Dermatologic Surgery: official publication of American Society for Dermatologic Surgery [et al.]*. 2008, **34**(9), 1159-1169.
- 159) Frykberg, R. G. and Banks, J. Challenges in the Treatment of Chronic Wounds. *Advances in Wound Care (New Rochelle)*. 2015, **4**(9), 560-582.
- 160) Ji, Y., Song, W., Xu, L., Yu, D-G. and Bligh, S. W. A. A Review on Electrospun Poly(amino acid) Nanofibres and Their Applications of Hemostasis and Wound Healing. *Biomolecules*. 2022, **12**, 794-820.
- 161) Ghomi, E. R., Niazi, M. and Ramakrishna, S. The evolution of wound dressings: From traditional to smart dressings. *Polymer Advanced Technologies*. 2023, **34**, 520-530.
- 162) Smith+Nephew. *OPSITE POST-OP VISIBLE Dressings*. [Online]. 2023 [31/08/2023]. Available from: <https://www.smith-nephew.com/en-au/health-care-professionals/products/advanced-wound-management/opsite-post-op-visible>
- 163) 3M. *Tegaderm Bandages & Dressings*. [Online]. 2023. [31/08/2023]. Available from: [https://www.3m.co.uk/3M/en\\_GB/p/c/medical/bandages-dressings/b/tegaderm/#](https://www.3m.co.uk/3M/en_GB/p/c/medical/bandages-dressings/b/tegaderm/#)
- 164) 3M+KCI. *BIOCLUSIVE Plus Transparent Film Dressing*. [Online]. 2020. [31/08/2023]. Available from: <https://www.acelity.com/healthcare-professionals/global-product-catalog/catalog/bioclusive-plus-dressing>



- 
- 165) Kalowes, P., Messina, V. and Li, M. Five-Layered Soft Silicone Foam Dressing to Prevent Pressure Ulcers in the Intensive Care Unit. *American Journal of Critical Care: an official publication, American Association of Critical-Care Nurses*. 2016, **25**(6), e108-e119.
- 166) Banks, V., Bale, S., Harding, K. and Harding, E. F. Evaluation of a new polyurethane foam dressing. *Journal of Wound Care*. 1997, **6**(6), 266-269.
- 167) Adzick, N. S. The Molecular and Cellular Biology of Wound Repair, 2<sup>nd</sup> Edition. *Annals of Surgery*. 1997, **225**(2), 236.
- 168) Gamage McEvoy, J. and Zhang, Z. Antimicrobial and photocatalytic disinfection mechanisms in silver-modified photocatalysts under dark and light conditions. *Journal of Photochemistry & Photobiology, C: Photochemistry Reviews*. 2014, **19**, 62-75.
- 169) MEDICAL DRESSINGS. *Lyof foam Max Foam Dressing*. [Online]. 2023. [31/08/2023]. Available from: <https://medicaldressings.co.uk/lyof foam-max-foam-dressing/>
- 170) Smith+Nephew. *ALLEVYN Wound Dressings*. [Online]. 2023. [31/08/2023]. Available from: <https://www.smith-nephew.com/en/health-care-professionals/products/advanced-wound-management/allevyn-foam-dressings-new#product-family>
- 171) Weller, C. Interactive dressings and their role in moist wound management. In: Rajendran, S. ed. *Advanced Textiles for Wound Care*. 2<sup>nd</sup> Edition. United Kingdom: Woodhead Publishing, 2009, 105-134.
- 172) Wang, H., Xu, Z., Zhao, M., Liu, G. and Wu, J. Advances of hydrogel dressings in diabetic wounds. *Biomaterials Science*. 2021, **9**(5), 1530-1546.
- 173) Tavakoli, S. and Klar, A. S. Advanced Hydrogels as Wound Dressings. *Biomolecules*. 2020, **10**(8), 1169-1188.
- 174) Gokoo, C. and Burhop, K. A comparative study of wound dressings on full-thickness wounds in micropigs. *Decubitus*. 1993, **6**(5), 42-43, 46, 48, *passim*.
- 175) 3M. *3M Nu-Gel Hydrogel with Alginate*. [Online]. 2023. [31/08/2023]. Available from: [https://www.3m.co.uk/3M/en\\_GB/p/d/b5005265144/](https://www.3m.co.uk/3M/en_GB/p/d/b5005265144/)
- 176) CooperVision. *Aquaform Technology*. [Online]. 2023. [31/08/2023]. Available from: <https://coopervision.com/practitioner/our-products/contact-lens-technology/aquaform-technology>

- 
- 177) Coloplast. *Purilon – Purilon Gel*. [Online]. 2023. [31/08/2023]. Available from: <https://products.coloplast.co.uk/coloplast/wound-care/purilon-gel/>
- 178) Kamińska, M. S., Cybulska, A. M., Skonieczna-Żydecka, K., Augustyniuk, K., Grochans, E. and Karakiewicz, B. Effectiveness of Hydrocolloid Dressings for Treating Pressure Ulcers in Adult Patients: A Systematic Review and Meta-Analysis. *International Journal of Environmental Research and Public Health*. 2020, **17**(21), 7881-7899.
- 179) Kong, D., Zhang, Q., You, J., Cheng, Y., Hong, C., Chen, Z., Jiang, T. and Hao, T. Adhesion loss mechanism based on carboxymethyl cellulose-filled hydrocolloid dressings in physiological wounds environment. *Carbohydrate Polymers*. 2020, **235**, 115953-115959.
- 180) Abraham, S., Harsha, G. G. S., Desai, K., Furtado, S. and Srinivasan, B. Nano Calcium Oxide Incorporated Hydrocolloid Dressings for Wound Care. *Journal of Pharmaceutical Innovation*. 2022, **17**, 215-226.
- 181) Convatec. *DuoDERM / Granuflex*. [Online]. 2023. [31/08/2023]. Available from: <https://www.convatec.com/en-gb/products/advanced-wound-care/brand-names/pc-wound-duoderm-granuluflex/granuluflex-bordered-dressing/>
- 182) Coloplast. *Comfeel Plus Transparent*. [Online]. 2023. [31/08/2023]. Available from: <https://www.coloplast.co.uk/wound/wound-/comfeel-plus/>
- 183) Williams, C. 3M Tegaserb Thin: a hydrocolloid dressing for chronic wounds. *British Journal of Nursing*. 2000, **9**(11), 720-723.
- 184) Aderibigbe, B. A. and Buyana, B. Alginate in Wound Dressings. *Pharmaceutics*. 2018, **10**(2), 42-60.
- 185) SORBSAN. *SORBSAN – Sterile Calcium Alginate Wound Dressings*. [Online]. 2023. [31/08/2023]. Available from: <https://sorbsan.co.uk/>
- 186) Convatec. *Kaltostat*. [Online]. 2023. [31/08/2023]. Available from: <https://www.convatec.com/en-gb/products/advanced-wound-care/brand-names/pc-wound-kaltostat/>
- 187) Smith+Nephew. *ALGISITE M – Calcium Alginate Dressing*. [Online]. 2023. [31/08/2023]. Available from: <https://www.smith-nephew.com/en/health-care-professionals/products/advanced-wound-management/algisite-ppl>
- 188) Ramshaw, J. A. M., Peng, Y. Y., Glattauer, V. and Werkmeister, J. A. Collagens as biomaterials. *Journal of Materials Science. Materials in Medicine*. 2009, **20**, S3-S8.

- 
- 189) Vigani, B., Rossi, S., Sandri, G., Bonferoni, M. C., Caramella, C. M. and Ferrari, F. Hyaluronic acid and chitosan-based nanosystems: a new dressing generation for wound care. *Expert Opinion on Drug Delivery*. 2019, **16**(7), 715-740.
- 190) Ishihara, M., Nakanishi, K., Ono, K., Sato, M., Kikuchi, M., Saito, Y., Yura, H., Matsui, T., Hattori, H., Uenoyama, M. and Kurita, A. Photocrosslinkable chitosan as a dressing for wound occlusion and accelerator in healing process. *Biomaterials*. 2002, **23**(3), 833-840.
- 191) Shakiba, M., Rezvani Ghomi, E., Khosravi, F., Jouybar, S., Bigham, A., Zare, M., Abdouss, M., Moaref, R. and Ramakrishna, S. Nylon—A material introduction and overview for biomedical applications. *Polymers for Advanced Technologies*. 2021, **32**(9), 3368-3383.
- 192) Pruitt Jr, B. A. and Levine, N. S. Characteristics and uses of biologic dressings and skin substitutes. *Archives of Surgery*. 1984, **119**(3), 312-322.
- 193) Luraghi, A., Peri, F. and Moroni, L. Electrospinning for drug delivery applications: A review. *Journal of Controlled Release*. 2021, **334**, 463-484.
- 194) Liu, R., Hou, L., Yue, G., Li, H., Zhang, J., Liu, J., Miao, B., Wang, N., Bai, J., Cui, Z., Liu, T. and Zhao, Y. Progress of Fabrication and Applications of Electrospun Hierarchically Porous Nanofibres. *Advanced Fibre Materials*. 2022, **4**, 604-630.
- 195) Varshosaz, J., Choopannejad, Z., Minaiyan, M. and Kharazi, A.Z. Rapid hemostasis by nanofibers of polyhydroxyethyl methacrylate/polyglycerol sebacic acid: An in vitro/in vivo study. *Journal of Applied Polymer Science*. 2021, **138**(5), 49785-49800.
- 196) Adeli, H., Khorasani, M. T. and Parvazinia, M. Wound dressing based on electrospun PVA/chitosan/starch nanofibrous mats: Fabrication, antibacterial and cytocompatibility evaluation and in vitro healing assay. *International Journal of Biological Macromolecules*. 2019, **122**, 238–254.
- 197) Gao, Z., Su, C., Wang, C., Zhang, Y., Wang, C., Yan, H. and Hou, G. Antibacterial and hemostatic bilayered electrospun nanofibrous wound dressings based on quaternized silicone and quaternized chitosan for wound healing. *European Polymer Journal*. 2021, **159**, 110733-110746.
- 198) Rezvani Ghomi, E., Khosravi, F., Neisiany, R. E., Shakiba, M., Zare, M., Lakshminarayanan, R., Chellappan, V., Abdouss, M. and Ramakrishna, S. Advances in electrospinning of aligned nanofiber scaffolds used for wound dressings. *Current Opinion in Biomedical Engineering*. 2022, **22**, 100393-100400.

- 
- 199) Xue, J., Wu, T., Dai, Y. and Xia, Y. Electrospinning and Electrospun Nanofibers: Methods, Materials, and Applications. *Chemical Reviews*. 2019, **119**(8), 5298-5415.
- 200) Taylor, G. I. Disintegration of Water Drops in an Electric Field. *Proceedings of the Royal Society A*. 1964, **280**(1382), 383–397.
- 201) Collins, R. T., Jones, J. J., Harris, M. T. and Basaran, O. A. Electrohydrodynamic Tip Streaming and Emission of Charged Drops from Liquid Cones. *Nature Physics*. 2008, **4**, 149–154.
- 202) Reneker, D. H. and Yarin, A. L. Electrospinning Jets and Polymer Nanofibers. *Polymer*. 2008, **49**(10), 2387–2425.
- 203) Llevot, A. and Meier, M. A. R. Renewability – a principle of utmost importance! *Green Chemistry*. 2016, **16**(18), 4800-4803.
- 204) Anastas, P. T. and Warner, J. C. *Green chemistry: Theory and practice*. Warner, Oxford University Press, 1998.
- 205) Alder, C. M., Hayler, J. D., Henderson, R. K., Redman, A. M., Shukla, L., Shuster, L. E. and Sneddon, H. F. Updating and further expanding GSK's solvent sustainability guide. *Green Chemistry*. 2016, **18**(13), 3879-3890.
- 206) Our World in Data. *Plastic Pollution*. [Online]. 2022. [31/08/2023]. Available from: <https://ourworldindata.org/plastic-pollution>

## **Chapter 2 – Instrumentations, General Methods and Materials**

### **2.1. Nuclear Magnetic Resonance (NMR) Spectroscopy**

$^1\text{H}$  and  $^{13}\text{C}$  NMR spectra were recorded on a Bruker AV-NEO 500 MHz NMR spectrometer equipped with a 5 mm DCH cryoprobe and a Bruker AV3HD 400 MHz NMR spectrometer equipped with a 5 mm BBO Probe for polymers and small molecules respectively. Chemical shifts (in ppm) were referenced to a trimethylsilane (TMS) standard whose chemical shift is 0 ppm. Norell® XR-55 NMR tubes and WILMAD 528-PP NMR tubes were used for the 400 MHz and 500 MHz spectrometers respectively. NMR spectra were analysed using MestreNova® Research Lab software. The following abbreviations are used in  $^1\text{H}$  NMR analyses: s = singlet, d = doublet, t = triplet, q = quartet, m = multiplet, dd = doublet of doublets,  $J$  = coupling constants (in Hertz).

### **2.2. Fourier-Transform Infrared (FTIR) Spectroscopy**

Samples were dried in a vacuum oven (50 °C) for a minimum of 24 hours prior to infrared spectroscopic analysis. Spectra were recorded for solid samples using a Perkin Elmer Spectrum One equipped with Bruker OPUS 7.0 software and a Specac Golden Gate Attenuated Total Reflection (ATR) diamond top plate, accumulating 100 scans. Vibrational frequencies are expressed in  $\text{cm}^{-1}$ .

### **2.3. Centrifugation, Sample-Drying and Lyophilisation**

Samples were centrifuged using a HERMLE Z 326 K centrifuge unit, maintained at 0 °C (0 – 4500 rpm). Samples were dried for a minimum of 24 hours in a Fistreem vacuum oven, equipped with a variable temperature control unit (0 °C – 200 °C) and a pressure gauge (0 mbar – 1020 mbar). Samples were lyophilised using a Thermo-electric Heto Powerdry LLI500 freeze-dryer, equipped with an Edwards two stage vacuum pump. Samples were lyophilised in deionised water in 50 mL polypropylene centrifuge tubes.

### **2.4. Liquid Chromatography – Mass Spectrometry (LC-MS)**

LC-MS analysis was performed using a Thermo Scientific Ultimate 3000 HPLC system (Thermo Fisher Scientific, Waltham, MA, USA), interfaced with a mass spectrometer equipped with an electrospray-ionization source operated in the positive mode (Bruker amaZon Speed, Bruker Daltonik GmbH, Billerica, MA, United States). Chromatographic separations were performed using a Kinetex C18 (2.1×50 mm i.d., 2.6  $\mu\text{m}$  particle size; Phenomenex, Torrance, CA, USA) at a

column temperature of 40 °C. The mobile phases were (A) 0.1% Formic acid in water and (B) 0.1% Formic acid in acetonitrile. A gradient was used starting at 98% of A and 2% of B over 1.2 minutes, ending with 2% A and 98% B at a flow rate of 1.3 mL/min.

### **2.5. Ultra Violet – Visible (UV-Vis) Spectrophotometry**

Absorbance readings (200 – 800 nm) were performed on a dual beam Varian Cary 50 UV0902M112 UV-vis spectrophotometer (Agilent Technologies), equipped with a xenon pulse lamp and Varian Cary WinUV 3.0 software. Samples were analysed in UV micro quartz cuvettes (10 mm, 700 µL and 1700 µL, black-walled). ‘Simple-reads’ at fixed wavelengths were carried out using a Jenway 6305 spectrophotometer (Cole-Parmer Ltd). All of the readings were taken in triplicate.

### **2.6. Preparation of Phosphate Buffered Saline (PBS) and Sodium Acetate Buffer Solutions**

One PBS tablet was dissolved in deionised water (200 mL) under vigorous stirring to obtain a PBS buffer solution (pH 7.4). A sodium acetate buffer solution (pH 5.0) was prepared by homogeneously mixing 0.1M acetic acid glacial solution (357mL) with 0.1M sodium acetate tri-hydrate solution (643mL).

### **2.7. Preparation of Nanoparticles and Loaded Nanoparticles (Nanoprecipitation)**

Nanoparticles of self-assembling amphiphilic polymers were formed by nanoprecipitation via the dropping-in (co-solvent) method<sup>1</sup>. The sample polymer was dissolved in the minimum amount of organic solvent (e.g. chloroform, tetrahydrofuran (THF), acetonitrile) and added dropwise to the aqueous medium, under vigorous stirring. The resultant suspension was stirred until the organic solvent had completely evaporated. For nanoparticles containing a payload, the sample polymer and payload were dissolved separately in minimum amount of organic solvent and added simultaneously in a dropwise fashion to the aqueous medium, under vigorous stirring. Again, the suspension was stirred until the organic solvent had completely evaporated.

### **2.8. Dynamic Light Scattering (DLS) and Zeta Potential Studies**

DLS analyses were conducted using a Malvern Zetasizer Nano ZSP instrument equipped with a 4 mW He-Ne laser, operating at a wavelength of 633 nm, and an avalanche photodiode (APD)

detector. The non-invasive back-scatter-optic arrangement was used to collect the light scattered, at an angle of 173.25 °C. Samples were equilibrated for two minutes and then analysed at 37 °C in disposable 12 mm poly(styrene) cuvettes. Data were processed by cumulative analysis of the experimental correlation function. The diameter of particles was computed from the diffusion coefficients, using Stokes-Einstein's equation. Measurements were carried out in triplicate. Analysis of the results was carried out using the Malvern Zetasizer Software. Zeta potential studies were carried out using a Malvern Zetasizer Nano ZSP instrument, at pH 7.4 and 37 °C. Background electrolytes were not added. A viscosity of 0.891 mPa.s, dielectric constant of 78.6 and Henry function of 1.5 were used in the zeta potential computations.

### **2.9. High Performance Liquid Chromatography (HPLC)**

HPLC analysis was performed using an Agilent 1290 Infinity II HPLC system (Agilent, Santa Clara, CA, United States), with a diode array and fluorescence detectors. Chromatographic separations were performed using an InfinityLab Poroshell 120 EC-C18 (2.1×50 mm i.d., 1.9 µm particle size; Agilent, Santa Clara, CA, United States) at a column temperature of 40 °C. The mobile phase used was 40 mM Na<sub>2</sub>HPO<sub>4</sub> pH 7.8 (A) and acetonitrile:methanol:water (45:45:10 v/v/v) with the gradient starting at 2% B; holding it at 2% for 1 minute, and then increasing to 98% B after 7 minutes at a flow rate of 0.5 mL/min. The DAD recorded the chromatogram at a wavelength of 338 nm. The excitation wavelength was set at 345 nm and the emission wavelength was set at 450 nm on the fluorescence detector. The sample was derivatised with OPA using an injector program on the autosampler. A 2µL aliquot of borate buffer (0.4 M in water, pH 10.2) was drawn and mixed with 1µL of the sample. After a 0.2 min wait, 3µL of the OPA reagent (10 mg/mL in 0.4M borate buffer) was added and mixed with the sample in borate buffer. Thereafter 5µL of the injector diluent (mobile phase A acidified with H<sub>3</sub>PO<sub>4</sub>) was drawn and mixed with the derivatised mixture and waiting for 1 minute. The whole mixture (10µL) was injected onto the column. This method was based upon the following application note: Henderson Jr J.W., Brooks A (2010). Improved Amino Acid Methods using Agilent ZORBAX Eclipse Plus C18 Columns for a Variety of Agilent LC Instrumentation and Separation Goals (Application Report 5990-4547EN). Retrieved from Agilent Technologies website: <https://www.agilent.com/Library/applications/5990-4547EN.pdf>

### 2.10. Advanced Polymer Chromatography (APC)

APC analyses (DMF solution phase, 1 g/L LiBr) were carried out using an ACQUITY APC AQ (200Å, 2.5 µm) column packed with bridged poly(ethylene) hybrid particles, on a Waters ACQUITY APC system, equipped with an ACQUITY refractive index (ACQ-RI) detector. The column temperature was maintained at 40 °C and the flow rate was 0.5 mL/minute. System calibration was carried out using PEG standards and data were processed using Empower 3 software to provide polymer  $\bar{M}_w$  values.

### 2.11. Matrix-Assisted Laser Desorption/Ionisation – Time of Flight Mass Spectrometry (MALDI-TOF MS)

Matrix-Assisted Laser Desorption/Ionisation Time-Of-Flight (MALDI-TOF) Spectroscopy Mass Spectrometry was carried out using a MALDI-TOF spectrometer (Shimadzu AXIMA performance) in positive mode. An  $\alpha$ -Cyano-4-hydroxycinnamic acid matrix was used with NaI salt as a cationisation reagent and chloroform used as the solvent.

### 2.12. Scanning Electron Microscopy (SEM)

Scanning Electron Microscopy (SEM) samples were prepared on conductive tape and sputter-coated with a thin layer of gold (30 nm thickness) in a Quorum Q150RS sputter-coater. Images were then collected using a Jeol JSM-6610LV instrument with the following conditions: accelerating voltage = 15 kV, electron beam spot size = 40, and sample working distance = 10-11 mm. Resultant secondary electron micrographs were analysed on ImageJ.

### 2.13. Drug Encapsulation Efficiency and Drug Loading Content

The drug encapsulation efficiency (EE%) of nanoparticles and the drug loading content (LC%) in the nanoparticles was determined using the following equations;

$$EE\% = \frac{W_0 - W_n}{W_0} \times 100$$

$$LC\% = \frac{W_0 - W_n}{W_{np}} \times 100$$

Where:  $W_0$  = total mass of payload administered during nanoprecipitation,  $W_n$  = total mass of drug not encapsulated within the nanoparticles,  $W_{np}$  = mass of drug-loaded nanoparticles.



#### **2.14. Electrospinning of Polymer Solutions**

Nanofibre samples were prepared by dissolving fully in a high vapour pressure solvent and electrospun as follows. Each solution was fed from a 1 mL capacity syringe to a 21 gauge needle. The volume feed rate was digitally controlled by a KD Scientific Model 200 Series positive displacement microprocessor syringe pump. The needle was connected to one electrode of a Glassman EH60P1.5 high voltage direct current (DC) power supply. The processing parameters used during electrospinning were: 5-25 kV applied voltage, 1-2.5 ml/h flow rate, and 12 cm tip-to-collector distance. An 8 x 8 cm sheet of aluminium foil was used as a collector and the second electrode was connected to it.

#### **2.15. Tensile Testing**

Samples of electrospun fibres were prepared to a minimum size of 2 x 4 cm. Tensile strength of the samples was tested using an Instron 3365 using a 500 N load cell. The length, width and depth of the samples were measured using callipers. The samples were loaded into the clamps, ensuring there were no obvious rips or deformations. The fixture separation was recorded and the clamps drawn apart at a strain rate of 5 mm min<sup>-1</sup>.

#### **2.16. Differential Scanning Calorimetry (DSC)**

Samples were weighed accurately using the Sartorius 4503 micro-balance. Differential scanning calorimetry (DSC) analyses were carried out using a DSC Q20 instrument, acquired from TA Instruments. The instrument was calibrated with indium. Aluminium pans were used to contain the samples that were heated at rates varying between 5 °C and 10 °C/ per minute, under an inert nitrogen atmosphere (40 mL/min). The sample purge was maintained at 10 mL per minute.

#### **2.17. Materials Inventory**

All of the chemicals (Table 2.1.) were used as received from suppliers unless otherwise specified.

Table 2.1. – Chemicals used within the research conducted.

Chemical	Supplier	Chemical	Supplier
Acetic acid Glacial (≥99.9%)	Sigma-Aldrich	Activated charcoal	ACROS
Alpha Chymotrypsin Crystallized	Worthington-Biochem	Benzylamine 99%	Sigma-Aldrich
Camptothecin	Sigma-Aldrich	<i>Candida Antarctica</i> Lipase B (CALB)	Sigma-Aldrich
Chloroform	Sigma-Aldrich	d-chloroform	Sigma-Aldrich
DMSO-d6	Euristop	Diethyl ether (≥99%)	Fluorochem
Dimethylformamide (dry)	ACROS	Doxorubicin hydrochloride (≥95%)	Sigma-Aldrich
Ethylene glycol 99%	Alfa Aesar	Glycerol	Fisher Scientific
Glycine 98.5%	Alfa Aesar	HBr/Acetic Acid (33 wt.%)	Sigma-Aldrich
Hexafluoroisopropanol	Sigma-Aldrich	Hexylamine 99%	Alfa Aesar
L-alanine	Alfa Aesar	L-arginine(Pbf)	Sigma-Aldrich
L-lysine(Cbz)	Sigma-Aldrich	L-methionine	Sigma-Aldrich
L-phenylalanine	Fluorochem	L-proline	Sigma-Aldrich
L-tryptophan	Sigma-Aldrich	L-tyrosine	Sigma-Aldrich
L-valine (≥99.8%)	Alfa Aesar	Magnesium sulfate	Sigma-Aldrich
Methanesulfonic acid	Sigma-Aldrich	Methanol (99.8%)	Sigma-Aldrich
N,N-diisopropylethylamine	Alfa Aesar	Neutrophil elastase	Sigma-Aldrich
PBS tablets	Sigma-Aldrich	PEG methyl ether (Average Mw = 5000 g mol <sup>-1</sup> )	Sigma-Aldrich
Polycaprolactone (Average Mw 70 kDa)	Sigma-Aldrich	Sarcosine 98%	Alfa Aesar
Sodium acetate trihydrate (≥99%)	Sigma-Aldrich	Tetrahydrofuran (dry)	ACROS
Thermolysin from <i>Geobacillus Stearothermophilus</i>	Sigma-Aldrich	Tin (II) 2-ethylhexanoate	Sigma-Aldrich
Triethylamine (anhydrous)	Fluorochem	Trifluoroacetic acid	Sigma-Aldrich

## 2.18. References

---

- 1) Khuphe, M, Ingram, N and Thornton, P, D. Exploiting poly( $\alpha$ -hydroxy acids) for the acid-mediated release of doxorubicin and reversible inside-out nanoparticle self-assembly. *Nanoscale*. 2018, **10**(29), 14201-14206.

## Chapter 3 – Synthesis of DKPs

As highlighted in section 1.2.3., DKPs are a family of conformationally constrained 6-membered rings containing two amide bonds<sup>1</sup>. As a consequence, it is plausible that DKPs can undergo ring-opening at one of the amide bonds, revealing an active chain end of a primary amine that is able to propagate and form a poly(amino acid). The exploration of this possibility is the central objective of this project and, if successful, will allow comparison of the ROP of DKPs to alternative syntheses of poly(amino acids). As such, the selection and development of a green, efficient, and cost-effective method to synthesise DKPs is critical to the success of the project. There are several plausible syntheses of DKPs that require critical evaluation in order to select the most appropriate method.

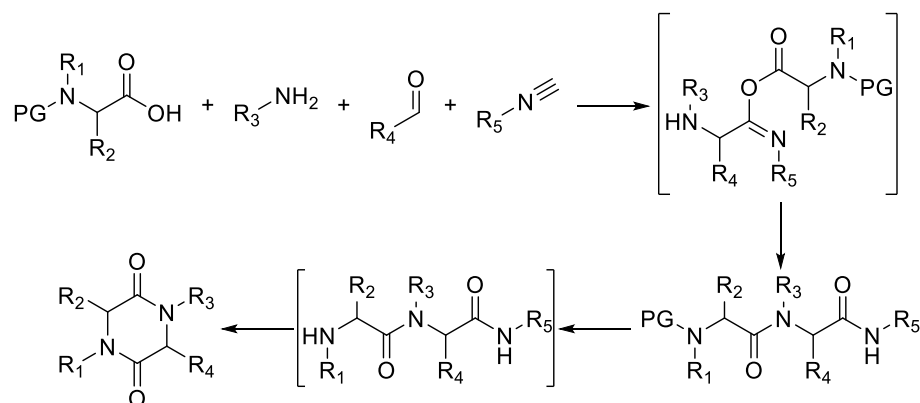
### 3.1. Synthetic Routes to DKPs

#### 3.1.1. Peptide Coupling and Cyclisation

As highlighted in section 1.2.3., dipeptide cyclisation involves the coupling of an amino acid ester and an N-protected amino acid to form a dipeptide with end capped protection<sup>1</sup>. Whilst this route allows for the retention of stereochemistry in the R groups of the amino acids, and allows for precise synthesis of asymmetric DKPs, it requires four synthetic steps: esterification of an amino acid, N-protection of another amino acid using a protecting group such as Boc or fluorenylmethoxycarbonyl (Fmoc), coupling the amino acid ester and the N-protected amino acid together, and removal of the N-protecting group to allow cyclisation<sup>1</sup>. The requirement of four synthetic steps renders this route unattractive; it requires more time and investment to carry out all four steps, there is risk of yield loss at each step, the product of each step requires purification and analysis, and it has poor overall atom economy due to the use and loss of protecting groups. As such, in terms of efficiency, this route compares poorly with NCA synthesis and its applicability to industrial level is limited.

#### 3.1.2. Ugi Synthesis

The Ugi synthesis, so named after Ivar Ugi<sup>2</sup>, involves an N-protected amino acid, an amine, an aldehyde, and an isonitrile to form an end capped dipeptide<sup>1</sup>.

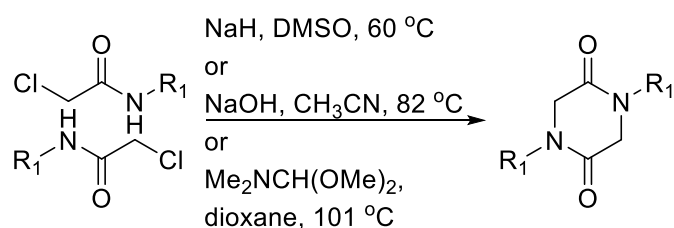


Scheme 3.1. – Ugi synthesis<sup>1</sup>.

The Ugi synthesis can produce a dipeptide with high yield<sup>3</sup>, similarly to the previously described dipeptide synthesis. However, whilst the peptide coupling route requires access to respective homochiral amino acids, the Ugi synthesis requires reagents that are more commonly used and readily available<sup>1</sup>. Additionally, the Ugi synthesis involves only two steps: formation of the dipeptide and N-deprotection to allow cyclisation<sup>1</sup>. As such, it compares favourably to peptide coupling. However, the dipeptide formed in the first step of the Ugi synthesis has a C-terminal amide, which is more difficult to cyclise than the typical ester<sup>1</sup>. As a consequence, the use of an activated isocyanide such as an N-acyliminium<sup>4</sup>, an indolamide<sup>5</sup> or a resin bound isocyanide<sup>6</sup> is required to ensure that the resultant amide is able to cyclise to the DKP.

### 3.1.3. Cyclisation via Haloacetamides

A common alternative to amide bond formation is bis-N-alkylation, primarily exemplified by the ring closure of  $\alpha$ -haloacetamides in a one-pot synthesis with moderate heating and base catalysis<sup>1</sup>.

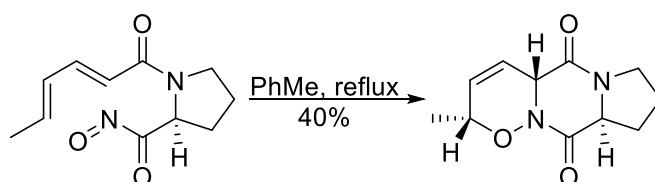


Scheme 3.2. – Cyclisation of chloroacetamides to form a symmetric, 1,4-disubstituted DKP, where  $R_1$  is aryl or alkyl<sup>1</sup>.

This route can afford high yields of a plethora of DKPs, including those with alkyl, aryl, and bulky N-substituents that may sterically hinder the reaction<sup>7</sup>. However, this reaction performs poorly when the N-substituent contains an aryl ring bearing electron-withdrawing groups such as a *meta*-nitro group or a *para*-ester group<sup>8</sup>. Additionally, the reaction requires strong base catalysis and very hazardous solvents such as dioxane or dimethyl sulfoxide (DMSO)<sup>1</sup>. Furthermore, haloacetamides are considerably more expensive than the corresponding amino acids and, as such, this route lacks the cost-effectiveness and greenness of alternative syntheses.

### 3.1.4. Diels-Alder Reaction

Synthesis of DKPs is achievable by the stereospecific intramolecular Diels-Alder reaction<sup>1</sup>. Sheradsky and Silcoff<sup>9</sup> prepared an asymmetric proline derivative DKP by the reflux of an acylnitroso derivation of N-sorbyl-L-proline in toluene as an intermediate product in a multi-step synthesis to (2R,5R)-2-amino-5-hydroxyhexanoic acid<sup>9</sup>.

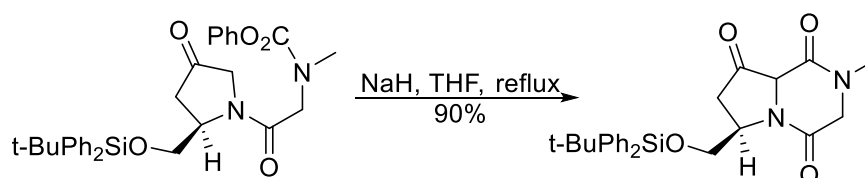


Scheme 3.3. – [4+2] Diels-Alder Cycloaddition to form DKP ring<sup>1</sup>.

Whilst this step is appropriate in the context set out by Sheradsky and Silcoff (to utilise an amino acid as a temporary tether to control stereo and regiochemistry of a cycloaddition reaction)<sup>9</sup>, the starting material has a very niche chemical structure and the process is not commercially viable. Furthermore, only a 40% yield was achieved<sup>9</sup> in the reaction step and, therefore, it is not a cost-effective route for the purposes of general DKP synthesis.

### 3.1.5. Enolate Acylation

Acylation of the C2 carbon is also a viable method to DKP synthesis<sup>1</sup>. Peng and Clive<sup>10</sup> report the formation of a multi-substituted DKP by intramolecular cyclisation of an enolate onto the carbonyl of a phenyl carbamate. The reaction involved refluxing with sodium hydride in THF and achieved a 90% yield<sup>10</sup>.



*Scheme 3.4.* – Intramolecular cyclisation of an enolate onto a carbonyl to form a DKP ring<sup>1</sup>.

Whilst the reaction achieved a high yield of 90%<sup>10</sup>, the requirement of elaborate and niche starting materials, as well as heating under reflux with a strong base, raises similar concerns to the cyclisation by haloacetamides and, therefore, may be unsuitable for industrial scale synthesis of DKPs.

### 3.1.6. Direct Amino Acid Condensation

As highlighted in section 1.2.3., DKPs can be synthesised via the facile, direct condensation of amino acids by heating in a high-boiling solvent such as glycerol or ethylene glycol (Scheme 1.6.)<sup>1</sup>. Whilst this synthetic route is compromised by poorer yields as a consequence of the occurrence of side reactions<sup>11</sup>, its simplicity, cost-effectiveness and low environmental impact makes it a strong candidate for scale up to industrial level. When compared to the starting materials and reagents required for syntheses highlighted above, direct amino acid condensation is considerably more affordable, requiring only the respective amino acid(s) of the desired DKP and a high boiling solvent such as glycerol. Additionally, glycerol has no known hazards and can be renewably sourced from the degradation products of animal fats and oils<sup>12</sup>. Furthermore, this reaction pathway boasts excellent atom economy; the only atomic loss from the reaction are two molecules of water per DKP formed. As a consequence of its excellent environmental and economic credentials, this method was utilised as the primary route to produce DKPs. The synthesis of glycine DKP<sup>13,14</sup>, phenylalanine DKP<sup>15</sup>, valine DKP<sup>16</sup> and tyrosine DKP<sup>15</sup> have previously been reported via this route. The remaining DKP syntheses via amino acid condensation, listed below, are reported for the first time.

## 3.2. Experimental Details

### 3.2.1. General DKP Synthesis

The general procedure for preparation of the following DKPs is based upon previously established methods<sup>13-17</sup>. Briefly, the amino acid (1 weight equivalent) was added to an oven-

dried vessel and flushed with N<sub>2(g)</sub>. The solid was then suspended in ethylene glycol/glycerol (7 weight equivalents) and stirred at 170-190°C under constant flow of N<sub>2(g)</sub>. The reaction mixture was then allowed to cool to room temperature and collected according to the following, DKP specific procedures. All accompanying spectra for each DKP are included in the appendices (FTIR spectroscopy – appendix I, <sup>1</sup>H NMR spectroscopy – appendix II, LC-MS – appendix III).

### 3.2.2. Synthesis of Glycine DKP

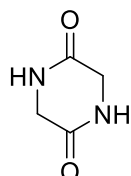


Figure 3.1. - Glycine DKP structure.

Glycine DKP was prepared according to the general procedure described above from glycine (5 g, 66.6 mmol) in glycerol (36 mL) at 175 °C for 3 hours. Upon cooling to room temperature, brown crystals precipitated out of solution. The mixture was cooled in an ice bath for one hour, after which it was filtered by vacuum and washed at the filter with ice-cold methanol (40 mL). The brown crystals were recrystallised from boiling deionised water (30 mL). The resultant crystals were collected by vacuum filtration and decolourised by stirring with activated charcoal (0.4 g) in hot deionised water (40 mL) for 3 minutes. The charcoal was removed by hot filtration and the solution allowed to cool to room temperature. The off-white crystals were collected by vacuum filtration and dried *in vacuo*.

Yield: 2.81 g, 74% (off-white crystals).

<sup>1</sup>H NMR (400 MHz, DMSO-d<sub>6</sub>, δ, ppm): 8.00 (s, 2H, 2 x NH); 3.71 (d, J = 3.7 Hz, 4H, 2 x CH<sub>2</sub>).

<sup>13</sup>C NMR (400 MHz, DMSO-d<sub>6</sub>, δ, ppm): 166.1 (2 x C=O amide); 44.3 (2 x NH-CH<sub>2</sub>-C=O).

LC-MS: for C<sub>4</sub>H<sub>6</sub>N<sub>2</sub>O<sub>2</sub> calculated [M + H]<sup>+</sup> 115.05 m/z; found 114.65 m/z.

FTIR (solid, cm<sup>-1</sup>): 3160m (N-H stretch, H-bonded), 3039m, 2984m (C-H stretch), 2913m (C-H stretch), 2873m, 1664s (C=O δ-lactam), 1466s (-CH<sub>2</sub>- deformation, H-bonded), 1438s, 1338m, 1073m, 911m, 831m, 804s (br.).



### 3.2.3. Synthesis of Alanine DKP

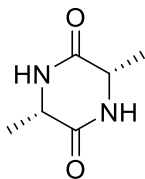


Figure 3.2. - Alanine DKP structure.

Alanine DKP was prepared according to the general procedure described above from L-alanine (8 g, 89.20 mmol) in ethylene glycol (56 mL) at 185 °C for 24 hours. The reaction mixture was allowed to cool to room temperature and the precipitate was collected by vacuum filtration and washed at the filter with ice-cold methanol (30 mL). The precipitate were collected by vacuum filtration and dried *in vacuo*.

Yield: 4.87 g, 76% (off-white crystals).

$^1\text{H}$  NMR (400 MHz, DMSO- $d_6$ ,  $\delta$ , ppm): 8.07 (s, 2H, 2 x NH); 3.92-3.83 (m, 2H, 2 x CH); 1.25 (d, 6H, 2 x CH $_3$ ).

$^{13}\text{C}$  NMR (400 MHz, DMSO- $d_6$ ,  $\delta$ , ppm): 169.5 (2 x C=O amide); 50.53 (2 x NH-CH(CH $_3$ )-C=O); 19.0 (2 x CH $_3$ ).

LC-MS: for C $_6$ H $_{10}$ N $_2$ O $_2$  calculated [M + H] $^+$  143.08 m/z, found 142.86 m/z.

FTIR (solid, cm $^{-1}$ ): 3189m (N-H stretch, H-bonded), 3049m, 2983m (C-H stretch), 2941m (C-H stretch), 2887m (C-H stretch), 1667s (C=O  $\delta$ -lactam), 1432m (C-CH $_3$  deformation), 1374s (C-CH $_3$  deformation), 1319s, 1298m, 1135m, 1115m, 959w, 812s, 769s, 676w.

### 3.2.4. Synthesis of Phenylalanine DKP

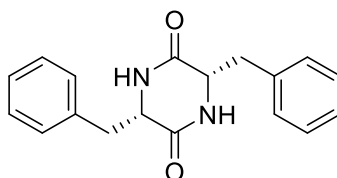


Figure 3.3. - Phenylalanine DKP structure.

Phenylalanine DKP (5 g, 30.27 mmol) was prepared according to the general procedure described above from L-phenylalanine in ethylene glycol (40 mL) at 190 °C for 24 hours. After cooling to room temperature, the precipitate was collected by vacuum filtration and washed at the filter with deionised water (100 mL), followed by ice-cold methanol (30 mL). The precipitate was then dried *in vacuo*.

Yield: 3.10 g, 70% (off-white fine crystals).

<sup>1</sup>H NMR (400 MHz, DMSO-d<sub>6</sub>, δ, ppm): 8.05 (s, 2H, 2 x NH); 7.24 (m, 6H, 6 x CH aromatic); 7.14 (d, J = 7.4 Hz, 4H, 4 x CH aromatic); 3.39 (m, 2H, 2 x CH); 3.03-2.99 (dd, J = 16, 4 Hz, 4H, 2 x CH<sub>2</sub>); 2.75-2.71 (dd, J = 16, 4 Hz, 4H, 2 x CH<sub>2</sub>).

<sup>13</sup>C NMR (400 MHz, DMSO-d<sub>6</sub>, δ, ppm): 167.4 (2C, 2 x C=O amide); 136.4 (2C, 2 x C *ipso* arom.); 130.6 (4C, 2 x 2 *ortho* arom. C); 128.5 (4C, 2 x 2 *meta* arom. C); 127.1 (2C, 2 x *para* arom. C); 55.1 (2C, 2 x NH-CH(CH<sub>2</sub>)-C=O); 38.2 (2C, 2 x CH-CH<sub>2</sub>-Ph).

LC-MS: for C<sub>18</sub>H<sub>18</sub>N<sub>2</sub>O<sub>2</sub> calculated [M + H]<sup>+</sup> 295.15 m/z, found 294.96 m/z.

FTIR (solid, cm<sup>-1</sup>): 3188m (N-H stretch, H-bonded), 3034m (C-H stretch aromatic), 2959m (C-H stretch), 2928m (C-H stretch), 2896m (C-H stretch), 1667s (C=O δ lactam), 1602m (C=C stretch), 1495m (C=C stretch), 1460m (-CH<sub>2</sub>- deformation), 1323m, 1242w, 1192w, 1094m, 1018m, 922m, 850m, 811m, 754s (C-H deformation aromatic), 721s, 697s (C-H deformation aromatic), 652m, 579m.

### 3.2.5. Synthesis of Lysine(Cbz) DKP

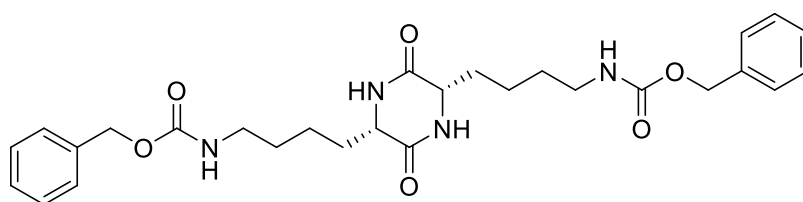


Figure 3.4. - Lysine(Cbz) DKP structure.

Lysine(Cbz) DKP was prepared according to the general procedure described above from L-lysine(Cbz) (5 g, 24.0 mmol) in glycerol (30 mL) at 175 °C for 24 hours. After cooling to room temperature, the solids were collected by vacuum filtration and washed at the filter with ice-cold methanol (30 mL). The solids were then recrystallised in hot methanol (5 mL), collected by vacuum filtration and dried *in vacuo*.

Yield: 3.06 g, 66% (fine, off-white crystals).

$^1\text{H}$  NMR (400 MHz, DMSO- $d_6$ ,  $\delta$ , ppm): 8.10 (*s*, 2H, 2 x NH); 7.42-7.32 (*m*, 10H, 10 x aromatic CH); 5.03 (*s*, 4H, 2 x O-CH<sub>2</sub>-C); 3.85 (*t*, 2H, 2 x NH-CH-C=O); 3.03 (*t*, 4H, 2 x CH<sub>2</sub>-CH<sub>2</sub>-NH); 1.76 (*q*, 4H, 2 x CH<sub>2</sub>); 1.68 (*s*, 2H, 2 x NH); 1.46 (*m*, 4H, 2 x CH<sub>2</sub>); 1.33 (*m*, 4H, 2 x CH<sub>2</sub>).

$^{13}\text{C}$  NMR (400 MHz, DMSO- $d_6$ ,  $\delta$ , ppm): 168.5 (2C, 2 x C=O amide); 156.5 (2C, 2 x NH-(C=O)-O); 137.7 (2C, 2 x *i*-aromatic); 128.8-127.8 (10C, 10 x aromatic); 65.6 (2C, 2 x O-CH<sub>2</sub>-C); 54.3 (2C, 2 x NH-CH(CH<sub>2</sub>)-C=O); 33.15 (2C, 2 x CH<sub>2</sub>-CH<sub>2</sub>-NH); 32.7 (2C, 2 x CH-CH<sub>2</sub>-CH<sub>2</sub>); 29.6 (2C, 2 x CH<sub>2</sub>-CH<sub>2</sub>-NH); 21.8 (2C, 2 x CH<sub>2</sub>-CH<sub>2</sub>-CH<sub>2</sub>).

LC-MS: for C<sub>28</sub>H<sub>36</sub>N<sub>4</sub>O<sub>6</sub> calculated [M + H]<sup>+</sup> 525.27 m/z, found 525.12 m/z.

FTIR (solid, cm<sup>-1</sup>): 3320*m* (N-H  $\delta$ -lactam), 3050*m* (C-H aromatic stretch), 2940*m* (C-H stretch), 2880*m* (C-H stretch), 1680*s* (C=O amide), 1240*m* (C-O stretch), 1150*m* (C-N stretch).

### 3.2.6. Synthesis of Valine DKP

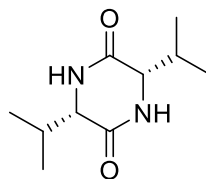


Figure 3.5. - Valine DKP structure.

Valine DKP was synthesised as described in the general procedure above from L-valine (5 g, 42.7 mmol) in ethylene glycol (36 mL) at reflux for 48 hours. After cooling to room temperature, the precipitate was collected by vacuum filtration, washed at the filter with ice-cold methanol (50 mL) and dried *in vacuo*.

Yield: 2.33 g, 55% (fine, bright white crystals).

$^1\text{H}$  NMR (400 MHz, DMSO- $d_6$ ,  $\delta$ , ppm): 8.02-7.95 (*d*, 2H, 2 x N-H); 3.70-3.66 (*d*, 2H, 2 x NH-CH-C=O); 2.22-2.17 (*m*, 2H, 2 x CH<sub>3</sub>-CH-CH<sub>3</sub>); 0.97-0.94 (*t*, 6H, 2 x CH-CH<sub>3</sub>); 0.85-0.83 (*d*, 6H, 2 x CH-CH<sub>3</sub>).

$^{13}\text{C}$  NMR (400 MHz, DMSO- $d_6$ ,  $\delta$ , ppm): 168.17 (2C, 2 x C=O amide); 59.58 (2C, 2 x NH-CH-C=O); 32.12 (2C, 2 x CH<sub>3</sub>-CH-CH<sub>3</sub>); 18.66 (2C, 2 x CH<sub>3</sub>-CH-CH<sub>3</sub>); 17.18 (2C, 2 x CH<sub>3</sub>-CH-CH<sub>3</sub>).

LC-MS: for C<sub>10</sub>H<sub>18</sub>N<sub>2</sub>O<sub>2</sub> calculated [M + H]<sup>+</sup> 199.11 m/z, found 198.39 m/z.

FTIR (solid,  $\text{cm}^{-1}$ ): 3187 $m$  (H-bonded N-H stretch  $\delta$ -lactam), 3089 $m$ , 3055 $m$ , 2965 $s$  (C-H stretch), 2938 $m$  (C-H stretch), 2876 $m$  (C-H stretch), 1657 $s$  (C=O  $\delta$ -lactam), 1446 $s$  (C-CH<sub>3</sub> deformation), 1392 $m$ , 1374 $m$  (C-CH<sub>3</sub> deformation), 1349 $s$ , 1290 $s$ , 1267 $m$ , 1181 $m$ , 1139 $m$ , 1111 $m$ , 1046 $m$ , 1003 $m$ , 911 $w$ , 845 $s$ , 810 $s$ , 678 $w$ , 657 $w$ , 637 $w$ .

### 3.2.7. Synthesis of Tyrosine DKP

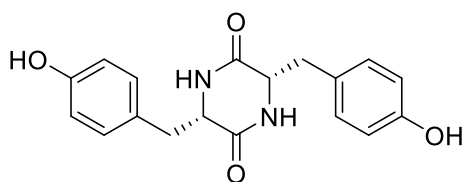


Figure 3.6. - Tyrosine DKP structure.

Tyrosine DKP was prepared according to the general procedure outlined above from L-tyrosine (3 g, 9.17 mmol) in ethylene glycol (36 mL) at reflux for 24 hours. Upon cooling to room temperature, the precipitate was collected by vacuum filtration and washed at the filter with ice-cold methanol (30 mL). The solids were then recrystallised in hot methanol (5 mL), collected by vacuum filtration and dried *in vacuo*.

Yield: 1.42 g, 53% (fine, white crystals).

<sup>1</sup>H NMR (400 MHz, DMSO- $d_6$ ,  $\delta$ , ppm): 9.32 (*s*, 2H, 2 x N-H); 7.92 (*s*, 2H, 2 x O-H); 6.91 (*d*, 4H, 4 x  $\text{CH-C-OH}$ ); 6.63 (*d*, 4H, 4 x  $\text{CH-C-CH}_2$ ); 4.44 (*m*, 2H, 2 x NH- $\text{CH-C=O}$ ); 2.91-2.55 (*dd*, 4H, 2 x  $\text{CH-CH}_2\text{-C}$ ).

<sup>13</sup>C NMR (400 MHz, DMSO- $d_6$ ,  $\delta$ , ppm): 167.52 (2C, 2 x C=O amide); 156.54 (2C, 2 x aromatic  $\text{C-OH}$ ); 131.55 (4C, 3 x *m*-aromatic); 126.31 (2C, 2 x *p*-aromatic); 115.27 (4C, 4 x *o*-aromatic); 55.3 (2C, 2 x NH- $\text{CH-C=O}$ ), 37.46 (2C, 2 x  $\text{CH-CH}_2\text{-C}$ ).

LC-MS: for C<sub>18</sub>H<sub>18</sub>N<sub>2</sub>O<sub>4</sub> calculated [M + H]<sup>+</sup> 326.13 m/z, found 326.58 m/z.

FTIR (solid,  $\text{cm}^{-1}$ ): 3210 $m$  (br., H-bonded O-H stretch), 2950 $m$  (C-H stretch), 2910 $m$  (C-H stretch), 2830 $m$ , 1640 $s$  (C=O  $\delta$ -lactam), 1595 $m$  (C=C aromatic stretch), 1504 $m$  (C=C aromatic stretch), 1432 $m$ , 1358 $w$ , 1318 $s$  (phenol C-O stretch and O-H deformation), 1213 $s$  1318 $s$  (phenol C-O stretch and O-H deformation), 1156 $m$ , 1085 $w$ , 1044 $w$ , 1018 $m$ , 905 $w$ , 887 $w$ , 801 $s$  (*p*-disubstituted aromatic C-H deformation), 721 $m$ , 674 $m$ .

### 3.2.8. Synthesis of Methionine DKP

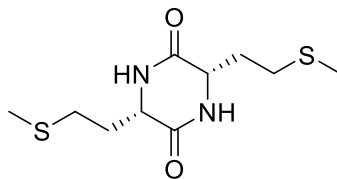


Figure 3.7. - Methionine DKP structure.

Methionine DKP was prepared according to the general procedure described above from L-methionine (4 g, mmol) in ethylene glycol (30 mL) at 180 °C for 24 hours. After cooling to room temperature, the precipitate was collected by vacuum-filtration, washed at the filter with ice-cold deionised water (50 mL) and dried *in vacuo* overnight.

Yield: 2.06 g, 59% (Off white crystalline powder).

<sup>1</sup>H NMR (500 MHz, CDCl<sub>3</sub>, δ, ppm): 6.40-6.36 (s, 2H, 2 x NH δ-lactam); 4.14-4.11 (m, 2H, 2 x CH); 2.63-2.58 (m, 2H, 2 x CH<sub>2</sub>-S); 2.06 (s, 2H, 2 x S-CH<sub>3</sub>); 2.26-1.95 (m, 2H, 2 x CH<sub>2</sub>).

<sup>13</sup>C NMR (500 MHz, CDCl<sub>3</sub>, δ, ppm): 167.8 (2C, 2 x C=O amide); 54.2 (2C, 2 x O=C-CH(CH<sub>2</sub>)-NH); 32.7 (2C, 2 x CH-CH<sub>2</sub>-CH<sub>2</sub>); 30.1 (2C, 2 x CH<sub>2</sub>-CH<sub>2</sub>-S); 15.4 (2C, 2 x S-CH<sub>3</sub>).

LC-MS: for C<sub>10</sub>H<sub>18</sub>N<sub>2</sub>O<sub>2</sub>S<sub>2</sub> calculated [M + H]<sup>+</sup> 262.08 m/z, found 262.41 m/z.

FTIR (solid, cm<sup>-1</sup>): 3312w (H-bonded N-H stretch δ-lactam), 3190m, 3092m, 3051m, 2965m (C-H alkyl stretch), 2912m (C-H alkyl stretch), 2863m (C-H alkyl stretch), 1666s (C=O stretch secondary δ-lactam), 1446s (CH<sub>2</sub> alkyl deformation), 1426s, 1333s, 1288s, 1273s, 1226w, 1161m, 1096m, 1033w, 961m, 931m, 873w, 799s (C-S thioether stretch), 689m.

### 3.2.9. Synthesis of Tryptophan DKP

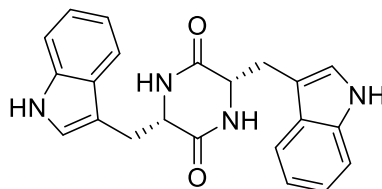


Figure 3.8. - Tryptophan DKP structure.

Tryptophan DKP was prepared as described by the general procedure above from L-tryptophan (3 g, 14.7 mmol) in ethylene glycol (25 mL) at 190 °C for 24 hours. After cooling to room temperature, deionised water (80 mL) was added. The resultant precipitate was collected by vacuum filtration and washed at the filter with further deionised water (40 mL). The solids were dried *in vacuo*.

Yield: 1.66 g, 61% (fine yellow crystals).

<sup>1</sup>H NMR (500 MHz, DMSO-d<sub>6</sub>, δ, ppm): 10.86 (s, 2H, 2 x N-H indole); 7.84-7.73 (dd, 2H, 2 x alkyl NH); 7.54-7.36 (d, *J* = 8.0 Hz, 2H, 2 x aromatic CH); 7.32-7.29 (m, 2H, 2 x aromatic CH); 7.07-7.03 (m, 2H, 2 x aromatic CH); 6.97-6.92 (m, 2H, 2 x aromatic CH); 6.99-6.61 (d, *J* = 2.3 Hz, 2H, 2 x indole CH); 3.89-3.43 (dt, 2H, 2 x alkyl CH); 3.14-2.85 (dd, *J* = 14.6, 4.3 Hz, 2H, 2 x alkyl CH); 2.74-2.18 (dd, *J* = 14.3, 5.4 Hz, 2H, 2 x alkyl CH).

<sup>13</sup>C NMR (500 MHz, DMSO-d<sub>6</sub>, δ, ppm): 168.1 (2C, 2 x C=O amide); 136.5 (2C, 2 x NH-C-CH); 128.1 (2C, 2 x C-C-CH); 124.9 (2C, 2 x C-CH-NH); 121.3 (2C, 2 x aromatic CH); 119.4 (2C, 2 x aromatic CH); 118.8 (2C, 2 x aromatic CH); 111.7 (2C, 2 x aromatic CH); 109.2 (2C, 2 x CH<sub>2</sub>-C-CH); 55.8 (2C, 2 x O=C-CH(CH<sub>2</sub>)-NH); 30.5 (2C, 2 x CH-CH<sub>2</sub>-C).

LC-MS: for C<sub>22</sub>H<sub>20</sub>N<sub>4</sub>O<sub>2</sub> calculated [M + H]<sup>+</sup> 372.16 m/z, found 372.58 m/z.

FTIR (solid, cm<sup>-1</sup>): 3586w (N-H indole stretch), 3399m, 3343m (H-bonded N-H stretch δ-lactam), 3055m (C-H aromatic stretch), 2922m (C-H alkyl stretch), 1659s (C=O stretch secondary δ-lactam), 1549w, 1492s (C=C aromatic stretch), 1456m (CH<sub>2</sub> alkyl deformation), 1434w, 1361w, 1324s, 1256m, 1231m, 1091s, 1011s, 921w, 738s (C-H aromatic deformation).

### 3.2.10. Synthesis of Arginine(Pbf) DKP

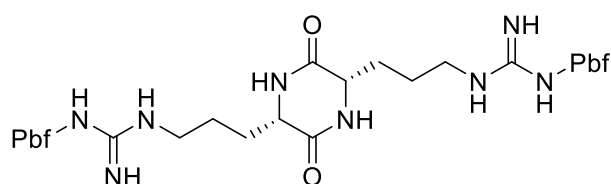


Figure 3.9. - Arginine(Pbf) DKP, where Pbf signifies a 2,2,4,6,7-Pentamethyldihydrobenzofuran-5-sulfonyl protecting group.

Arginine(Pbf) DKP was prepared according to the general procedure described above from L-arginine(Pbf) (3 g, 7.03 mmol) in ethylene glycol (24 mL) at 175 °C for 21 hours. After cooling to

room temperature, ice-cold deionised water (100 mL) was added, causing the product to precipitate. The solids were collected by vacuum filtration and washed at the filter with additional ice-cold deionised water (50 mL) and minimal ice-cold methanol (10 mL). The product was left to dry on the vacuum filter and subsequently dried *in vacuo*.

Yield: 1.81 g, 63% (Brown clustered solid).

$^1\text{H}$  NMR (500 MHz, DMSO- $d_6$ ,  $\delta$ , ppm): 7.03 (s, 2H, 2 x NH  $\delta$ -lactam); 6.40 (s, 2H, 2 x NH guanidinium); 4.47 (s, 4H, 4 x NH guanidinium); 2.85 (s, 4H, 2 x  $\text{CH}_2$  Pbf group); 2.47-2.48 (m, 2H, 2 x CH); 2.45-2.47 (m, 4H, 2 x  $\text{CH}_2$ -NH); 2.43-2.45 (m, 4H, 2 x  $\text{CH}_2$ -CH); 2.40-2.41 (m, 4H, 2 x  $\text{CH}_2$ ); 2.10 (s, 6H, 2 x  $\text{CH}_3$  Pbf); 2.07 (s, 6H, 2 x  $\text{CH}_3$  Pbf); 1.95 (s, 6H, 2 x  $\text{CH}_3$  Pbf); 1.38 (s, 12H, 2 x 2 x  $\text{CH}_3$ ).

$^{13}\text{C}$  NMR (500 MHz, DMSO- $d_6$ ,  $\delta$ , ppm): 158.0 (2C, 2 x C=O  $\delta$ -lactam); 156.8 (2C, 2 x HN-C(NH)=NH guanidinium); 137.4 (2C, 2 x aromatic C-O); 135.6 (2C, 2 x aromatic C- $\text{CH}_3$ ); 133.3 (2C, 2 x C-S(O) $_2$ -NH); 130.6 (2C, 2 x aromatic C- $\text{CH}_3$ ); 122.1 (2C, 2 x aromatic C( $\text{CH}_3$ )C- $\text{CH}_2$ ); 114.1 (2C, 2 x aromatic C- $\text{CH}_3$ ); 85.7 (2C, 2 x O-C( $\text{CH}_3$ ) $_2$ - $\text{CH}_2$ ); 62.9 (2C, 2 x C(O)-CH-NH); 42.5 (2C, 2 x  $\text{CH}_2$ -NH); 41.6 (2C, 2 x O-C( $\text{CH}_3$ ) $_2$ - $\text{CH}_2$ ); 28.4 (4C, 4 x  $\text{CH}_3$ ); 19.0 (2C, 2 x C(O)-CH- $\text{CH}_2$ ); 18.3 (2C, 2 x CH- $\text{CH}_2$ - $\text{CH}_2$ ); 17.7 (2C, 2 x aromatic C- $\text{CH}_3$ ); 12.3 (2C, 2 x aromatic C- $\text{CH}_3$ ); 11.5 (2C, 2 x aromatic C- $\text{CH}_3$ ).

LC-MS: for  $\text{C}_{38}\text{H}_{56}\text{N}_8\text{O}_8\text{S}_2$  calculated  $[\text{M} + \text{H}]^+$  817.37 m/z, found 817.66 m/z.

FTIR (solid,  $\text{cm}^{-1}$ ): 3427m (N-H guanidinium stretch), 3339w (N-H guanidinium stretch), 3262m (H-bonded N-H stretch  $\delta$ -lactam), 2973m (C-H alkyl stretch), 2931m (C-H alkyl stretch), 2868m (C-H alkyl stretch), 1708m, 1626m (C=O stretch secondary  $\delta$ -lactam), 1575m (C=C aromatic stretch), 1547m (N-H deformation), 1454m (C=C aromatic stretch), 1408m, 1368s (S=O sulfonamide stretch), 1312s, 1284s (C-O aryl ether), 1262m, 1157s (S=O sulfonamide stretch), 1086s, 1032m, 996m, 955m, 898m, 853m, 839m, 780s, 646s, 571s.

### 3.2.11. Synthesis of Sarcosine DKP

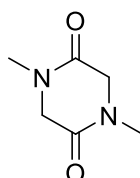


Figure 3.10. - Sarcosine DKP structure.

Sarcosine DKP was prepared according to the general procedure described above from sarcosine (10 g, 112.2 mmol) in glycerol (56 mL). Upon cooling to room temperature, deionised water (50 mL) was added to the reaction mixture, from which the product was extracted with chloroform (5 x 25 mL). The chloroform layers were combined and reduced to dryness by rotary evaporation. The solids were then recrystallised in hot methanol (5 mL) and the crystals collected by vacuum filtration and dried *in vacuo*.

Yield: 6.17 g, 77% (off-white needle crystals).

$^1\text{H}$  NMR (400 MHz,  $\text{CDCl}_3$ ,  $\delta$ , ppm): 3.95 (s, 4H, 2 x  $\text{CH}_2$ ); 2.96 (s, 6H, 2 x  $\text{CH}_3$ ).

$^{13}\text{C}$  NMR (400 MHz,  $\text{CDCl}_3$ ,  $\delta$ , ppm): 163.1 (2C, 2 x C=O amide); 55.7 (2C, 2 x N- $\text{CH}_2$ -C=O); 33.3 (2C, 2 x N- $\text{CH}_3$ ).

LC-MS: for  $\text{C}_6\text{H}_{10}\text{N}_2\text{O}_2$  calculated  $[\text{M} + \text{H}]^+$  143.08 m/z, found 142.86 m/z.

IR (solid,  $\text{cm}^{-1}$ ): 3026w, 2969w (C-H stretch), 2927m (C-H stretch), 2872w (C-H stretch), 2785w, 1645s (C=O tertiary  $\delta$  lactam), 1497s, 1445s ( $-\text{CH}_2-$  deformation), 1396s, 1337s, 1251s, 1164m, 1132m, 1015s, 991m, 839m, 737s, 603s.

### 3.2.12. Synthesis of Proline DKP

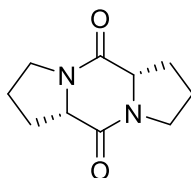


Figure 3.11. - Proline DKP structure.

Proline DKP was prepared according to the general procedure described above from L-proline (10 g) in glycerol (72 mL) at 175°C for 24 hours. After cooling to room temperature, deionised water (50 mL) was added and the product was extracted with chloroform (5 x 25 mL). The chloroform layers were collected and evaporated to dryness. The solids were then recrystallised in hot methanol (8 mL) and the resultant crystals were collected by vacuum filtration and dried *in vacuo*.

Yield: 5.85 g, 69% (fine, off-white crystals).



$^1\text{H}$  NMR (400 MHz,  $\text{CDCl}_3$ ,  $\delta$ , ppm): 4.17-4.13 (*t*, 2H, 2 x N-CH-C=O); 3.53-3.49 (*td*, 4H, 2 x N-CH<sub>2</sub>-CH<sub>2</sub>); 2.33-2.11 (*m*, 4H, 2 x CH-CH<sub>2</sub>-CH<sub>2</sub>); 2.05-1.83 (*m*, 4H, 2 x CH<sub>2</sub>-CH<sub>2</sub>-CH<sub>2</sub>).

$^{13}\text{C}$  NMR (400 MHz,  $\text{CDCl}_3$ ,  $\delta$ , ppm): 166.5 (2C, 2 x C=O amide); 60.6 (2C, 2 x N-CH-C=O); 45.3 (2C, N-CH<sub>2</sub>-CH<sub>2</sub>); 27.8 (2C, 2 x CH-CH<sub>2</sub>-CH<sub>2</sub>); 23.4 (2C, 2 x CH<sub>2</sub>-CH<sub>2</sub>-CH<sub>2</sub>).

LC-MS: for  $\text{C}_{10}\text{H}_{14}\text{N}_2\text{O}_2$  calculated  $[\text{M} + \text{H}]^+$  195.11 m/z, found 194.51 m/z.

FTIR (solid,  $\text{cm}^{-1}$ ): 2993*m* (C-H stretch), 2960*m* (C-H stretch), 2867*m* (C-H stretch), 1644*s* (C=O tertiary  $\delta$  lactam), 1428*s* (-CH<sub>2</sub>- deformation), 1332*m*, 1295*m*, 1272*m*, 1229*m*, 1201*m*, 1152*m*, 1071*w*, 1006*w*, 967*w*, 923*w*, 876*w*, 788*w*, 766*w*, 630*s*, 597*m*.

### 3.2.13. Synthesis of Sarcosine-Phenylalanine DKP

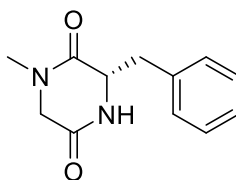


Figure 3.12. - Sar-Phe DKP structure.

L-phenylalanine (3.25 g, 19.67 mmol) and sarcosine (1.75 g, 19.67 mmol) were added to an oven-dried vessel, sealed and flushed with  $\text{N}_{2(\text{g})}$ . Glycerol (36 mL) was added and the mixture was stirred at 185 °C for 24 hours. The reaction mixture was allowed to cool to room temperature, which allowed the Phe-DKP to precipitate. This precipitate was collected by filtration, washed at the filter with ice-cold deionised water (85 mL). The remaining products were extracted from the reaction mixture with chloroform (5 x 25 mL). The chloroform layers were evaporated to dryness and mixed with ice-cold methanol (10 mL). The undissolved solid, Sar-Phe-DKP, was collected by vacuum filtration and washed at the filter with further ice-cold methanol (20 mL). What dissolved in the ice-cold methanol, Sar-DKP, was evaporated to dryness. All three products were recrystallised separately in hot methanol (8 mL).

Sar-Phe-DKP yield: 1.13 g, 26% (cream flakes). Sar-DKP yield: 0.93 g, 21% (off-white needle crystals) Phe-DKP yield: 0.91 g, 20% (off-white fine powder).

For Sar-Phe-DKP:

$^1\text{H}$  NMR (400 MHz,  $\text{CDCl}_3$ ,  $\delta$ , ppm): 7.28-7.20 (*m*, 3H, aromatic); 7.13-7.10 (*m*, 2H, aromatic); 6.94 (*s*, 1H, N-H); 4.23 (*m*, 1H, NH- $\underline{\text{C}}\text{H}$ -C=O); 3.48-3.44 (*d*,  $J = 17.5$  Hz, 2H, CH- $\underline{\text{C}}\text{H}_2$ -C); 2.86-2.82 (*d*,  $J = 17.5$  Hz, 2H, CH- $\underline{\text{C}}\text{H}_2$ -C); 3.15-3.01 (*qd*,  $J = 19.6, 4.9$  Hz, 2H,  $\text{H}_3\text{CN-}\underline{\text{C}}\text{H}_2$ -C=O); 2.76 (*s*, 3H, N- $\underline{\text{C}}\text{H}_3$ ).

$^{13}\text{C}$  NMR (400 MHz,  $\text{CDCl}_3$ ,  $\delta$ , ppm): 166.0 (1C, C=O 3°  $\delta$ -lactam); 165.4 (1C, C=O 2°  $\delta$ -lactam); 135.0 (1C, *i*-aromatic); 130.0 (2C, *o*-aromatic); 128.8 (2C, *m*-aromatic); 127.6 (1C, *p*-aromatic); 56.5 (1C, NH- $\underline{\text{C}}\text{H}$ -C=O); 50.9 (1C,  $\text{H}_3\text{C-N-}\underline{\text{C}}\text{H}_2$ -C=O); 40.9 (1C,  $\underline{\text{C}}\text{H-CH}_2$ -C); 33.6 (1C, N- $\underline{\text{C}}\text{H}_3$ ).

LC-MS: for  $\text{C}_{12}\text{H}_{14}\text{N}_2\text{O}_2$  calculated  $[\text{M} + \text{H}]^+$  219.11  $m/z$ , found 218.38  $m/z$ .

FTIR (solid,  $\text{cm}^{-1}$ ): 3275*m* (br., H-bonded N-H stretch  $\delta$ -lactam), 3034*w* (C-H aromatic stretch), 2962*w* (C-H stretch), 2935*w* (C-H stretch), 2889*w* (C-H stretch), 1674*s* (C=O stretch secondary  $\delta$ -lactam), 1646*s* (C=O stretch tertiary  $\delta$ -lactam), 1581*w* (C=C aromatic stretch), 1523*w* (C=C aromatic stretch), 1467*m* (- $\text{CH}_2$ - deformation), 1455*m* (- $\text{CH}_3$  deformation), 1434*m*, 1404*m*, 1336*m*, 1320*s*, 1299*m*, 1265*m*, 1233*w*, 1204*m*, 1158*w*, 1101*m*, 1026*m*, 981*m*, 948*m*, 924*m*, 874*m*, 780*s*, 750*s* (mono-substituted aromatic C-H deformation), 701*s* (mono-substituted aromatic C-H deformation), 589*s*.

### 3.3. References

---

- 1) Borthwick, A. D. 2,5-Diketopiperazines: Synthesis, Reactions, Medicinal Chemistry, and Bioactive Natural Products. *Chemical Reviews*. 2012, **112**(7), 3641-3716.
- 2) Ugi, I. The  $\alpha$ -Addition of Immonium Ions and Anions to Isonitriles Accompanied by Secondary Reactions. *Angewandte Chemie International Edition in English*. 1962, **1**(1), 8-21.
- 3) Armstrong, R. W., Combs, A. P., Tempest, P. A., Brown, D. and Keating, T. A. Multiple-Component Condensation Strategies for Combinatorial Library Synthesis. *Accounts of Chemical Research*. 1996, **29**, 123-131.
- 4) Hulme, C., Morrissette, M. M., Volz, F. A. and Burns, C. J. The solution phase synthesis of diketopiperazines libraries via the Ugi reaction: Novel application of Armstrong's convertible isonitrile. *Tetrahedron Letters*. 1998, **39**(10), 1113-1116.
- 5) Rhoden, C. R. B. Rivera, D. G., Kreye, O., Bauer, A. K., Westermann, B. and Wessjohann, L. A. Rapid access to N-substituted diketopiperazines by one-pot Ugi-4CR/deprotection+activation/cyclization (UDAC). *Journal of Combinatorial Chemistry*. 2009, **11**(6), 1078-1082.
- 6) Hulme, C., Peng, J., Morton, G., Salvino, J. M., Herpin, T. and Labaudiniere, R. Novel safety-catch linker and its application with a Ugi/De-BOC/Cyclization (UDC) strategy to access carboxylic acids, 1,4-benzodiazepines, diketopiperazines, ketopiperazines and dihydroquinoxalinones. *Tetrahedron Letters*. 1998, **39**(40), 7227-7230.
- 7) Hazra, A., Paira, P., Palit, P., Banerjee, S., Mondal, N. B. and Sahu, N. P. Synthesis of Symmetrically 1,4-disubstituted piperazine-2,5-diones: A New Class of Antileishmanial Agents. *Journal of Chemical Research*. 2007, **7**, 381-383.
- 8) Cho, S-D., Song, S-Y., Kim, K-H., Zhao, B-X., Ahn, C., Joo, W-H., Yoon, Y-J., Falck, J. R. and Shin, D-S. One-pot Synthesis of Symmetrical 1,4-Disubstituted Piperazine-2,5-diones. *Bulletin of the Korean Chemical Society*. 2004, **25**(3), 415-416.
- 9) Sheradsky, T. and Silcoff, E. R. Synthesis of (2R,5R)-2-Amino-5-Hydroxyhexanoic Acid by Intramolecular Cycloaddition. *Molecules*. 1995, **3**(3), 80-87.
- 10) Peng, J. and Clive, D. L. J. Asymmetric Synthesis of the ABC-Ring System of the Antitumor Antibiotic MPC1001. *The Journal of Organic Chemistry*. 2009, **74**(2), 513-519.

- 
- 11) Falorni, M., Giacomelli, G., Porcheddu, A. and Taddei, M. Solution-Phase Synthesis of Mixed Amide Libraries by Simultaneous Addition of Functionalities (SPSAF) to a Diketopiperazine Tetracarboxylic Acid Scaffold Monitored by GC Analysis of Isobutyl Alcohol. *European Journal of Organic Chemistry*. 2000, **2000**(8), 1669-1675.
- 12) Bagnato, G., Iulianelli, A., Sanna, A. and Basile, A. Glycerol Production and Transformation: A Critical Review with Particular Emphasis on Glycerol Reforming Reaction for Producing Hydrogen in Conventional and Membrane Reactors. *Membranes (Basel)*. 2017, **7**(2), 17-47.
- 13) Xiao, G., Xu, S., Xie, C., Zi, G., Ye, W., Zhou, Z., Hou, G. and Zhang, Z. Enantioselective Synthesis of Chiral Substituted 2,4-Diketoimidazolidines and 2,5-Diketopiperazines via Asymmetric Hydrogenation. *Organic Letters*. 2021, **23**(15), 5734-5738.
- 14) Pokorna, A., Bobal, P., Oravec, M., Rarova, L., Bobalova, J. and Jampilek, J. Investigation of Permeation of Theophylline through Skin Using Selected Piperazine-2,5-Diones. *Molecules*. 2019, **24**(3), 566-579.
- 15) Manchineella, S., Voshavar, C. and Govindaraju, T. Radical-Scavenging Antioxidant Cyclic Dipeptides and Silk Fibroin Biomaterials. *European Journal of Organic Chemistry*. 2017, **30**, 4363-4369.
- 16) Kelly, S., Goddard, R. and Guiry, P. J. The Preparation and Resolution of Novel Axially Chiral Pyrazine-Containing P, N Ligands for Asymmetric Catalysis and Their Application in Palladium-Catalysed Allylic Substitution. *Helvetica Chimica Acta*. 2021, **105**(1), e202100205.
- 17) Basiuk, V.A., Gromovoy, T.Y., Chuiko, A.A., Soloshonok, V.A. and Kukhar, V.P. A Novel Approach to the Synthesis of Symmetric Optically Active 2,5-Dioxopiperazines. *Synthesis*. 1992, **5**, 449-451.

## Chapter 4 – The Ring-Opening Polymerisation of 2,5-Diketopiperazines to Create Poly(amino acids)

### Abstract

Poly(amino acids) are a collection of versatile materials, boasting a range of chemical functionalities and resultant physical properties. As a consequence of their inherent biodegradability, biocompatibility and renewable feedstock source, poly(amino acids) have vast potential across a plethora of applications within a multitude of sectors. At present, commercial poly(amino acid) utilisation is limited due to the hazardous and costly synthetic route required for their production with narrow  $\Delta$ , involving the synthesis and ROP of NCAs using triphosgene. A possible, unreported alternative that may relieve this difficulty is the ROP of DKPs. DKPs are natural molecules that may be derived from biological sources and boast unique structural and biological properties. They demonstrate antimicrobial, anticancer, anti-inflammatory, and antioxidant properties and have been employed as carriers for the controlled delivery of therapeutic and fragrant molecules. DKPs can be synthesised via a number of possible routes; the method boasting the most efficient and green credentials is the direct condensation of amino acids by heating in glycerol. This procedure is essentially without chemical hazard; all chemicals involved are relatively inexpensive and can be renewably sourced. As such, the use of DKPs as cyclic monomers in an original route to controlled poly(amino acid) synthesis is reported. DKP creation is performed in the absence of phosgene and hazardous organic solvents, consequently rendering poly(amino acid) synthesis safe and cost-effective. The creation of polyalanine, as well as three other polymers, from a DKP feedstock is demonstrated for the first time, in addition to enzymatic polyalanine degradation and re-polymerisation of recovered alanine following DKP synthesis. The synthesis and ROP of DKPs may facilitate poly(amino acid) use in both everyday and high-value products.

### 4.1. Introduction

DKPs are naturally abundant cyclic dipeptides in the form of conformationally constrained six membered heterocyclic ring molecules. They may be naturally occurring and bio-derived, and have found application as effective materials in numerous applications including antimicrobial<sup>1</sup>, anticancer<sup>2</sup>, anti-inflammatory<sup>3</sup>, anti-fouling agents<sup>4</sup>, and as carriers for controlled payload release<sup>5</sup>. The potential of DKPs, owing to their unique and adaptable chemical properties and environmental credentials, is enormous.

The diamide containing structure of DKPs also suggests that they are good candidates for ring-opening polymerisation to yield poly(amino acids). Such polymers are produced from a renewable feedstock (amino acids) and are inherently biodegradable by hydrolysis<sup>6</sup>. As summarised in Chapter 1, poly(amino acids) are polyamides that boast an extensive range of possible chemical functionalities and physical properties based simply on the amino acid(s) that is/are polymerised. This versatility in polymer design is uncommon in the creation of biodegradable commodity polymers and allows a range of polymers with different polarities, electrostatic charges, and pendant functional groups, including thiol, amine, carboxylic acid, and alcohol, to be created. As homopolypeptides, extensive polymer-polymer interactions may form via hydrogen bonding, allowing the formation of a secondary structure that facilitates the creation of polymers of high strength, and potentially with the capacity to self-assemble to form very stable (nano)structures such as organogels<sup>7</sup>, hydrogels<sup>8</sup> and, as part of block copolymer nanoparticles<sup>9</sup>. Poly(amino acids) are therefore of enormous potential value, both as commodity polymers and as intricate components of biomaterials<sup>10</sup>. However, a safe and cost-effective route to poly(amino acids) must be found if their enormous potential is to be fully realised.

Although solid phase peptide synthesis enables the creation of poly(amino acids)<sup>11</sup>, ring-opening polymerisation is the most common method of polymer creation owing to efficiency. In particular, N-carboxyanhydride ring-opening polymerisation (NCA ROP) is commonly used for poly(amino acid) creation<sup>12</sup>. Commercially, the use of poly(amino acids) is limited owing to the economic and environmental cost of polymer synthesis. Triphosgene is commonly used in NCA synthesis as the precursor to the highly toxic gas phosgene; a cyclisation agent which forms *in situ* and forms the NCA upon reaction with the amino acid<sup>13</sup>. Although this route to poly(amino acid) synthesis is used commercially in the production of the billion-dollar immunomodulator medication Glatiramer Acetate<sup>14</sup>, phosgene is lethal by inhalation and so its use should be avoided. The recognised need for poly(amino acids) and the effectiveness of ROP over solid-phase peptide-synthesis and polycondensation reactions has driven great interest into the development of phosgene-free synthetic routes to NCAs.

Koga *et al.*<sup>15</sup> reported the non-halogenated and much less toxic analogue of phosgene, diphenyl carbonate, to convert the imidazolium salt of an amino acid to the corresponding urethane which can then be cyclised in the presence of an acid catalyst. The final cyclisation step produces phenol as a side product, requiring purification for removal from the monomer product. Despite avoiding the use of phosgene, this procedure requires the use of the imidazolium salt rather than the free amino acid, as well as a minimum of four days to complete three synthetic steps and a fourth purification step, resulting in a lower yield when compared to the one pot Fuchs-

Farthing method of NCA synthesis<sup>16</sup>. More recent attempts utilise similar synthetic steps and bring comparable drawbacks<sup>17</sup>, ensuring that the creation of poly(amino acids) from NCAs via the use of phosgene remains extremely common for poly(amino acid) synthesis.

Instead of augmenting NCA synthesis by producing and refining a phosgene-free method, creating poly(amino acids) by DKP ROP may serve as a preferable alternative. DKPs may be produced synthetically through the condensation of two  $\alpha$ -amino acids in ethylene glycol or glycerol.<sup>18</sup> This straightforward and relatively green process involves one simple reaction step, minimal purification, and excludes both toxic organic solvents and cyclising agents such as phosgene-producing chemicals. If DKPs can undergo ROP, they offer a viable alternative to NCAs for producing poly(amino acids) in a route that boasts far superior economic and environmental credentials.

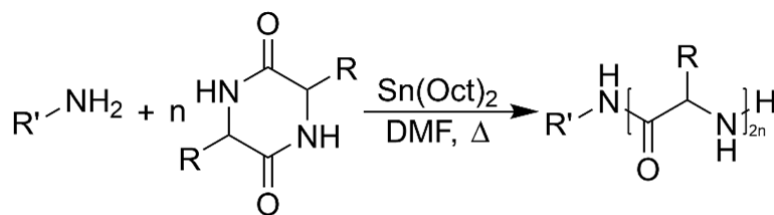
Herein, the creation of poly(amino acid) homopolymers formed from DKPs are reported for the first time. This method of poly(amino acid) synthesis avoids the use of costly cyclising agents in monomer creation, potentially offering a plausible method of economically-viable poly(amino acid) synthesis that will enable their widespread use beyond the pharmaceutical industry. Both monomer and polymer syntheses are straightforward, enabling the creation of biodegradable polymers that may boast a range of functionalities and chemical properties to be created. Polymerisations in DMF, a commonly used solvent in poly(amino acid) production, were conducted, as well as an alternative system in deionised water. Furthermore, the enzymatic degradation of polyalanine, the collection of the degradation products, cyclisation and polymerisation of those degradation products is also reported, demonstrating the circularity of poly(amino acids).

## **4.2. Experimental Details**

### **4.2.1. Synthesis of DKPs**

The general procedure for preparation of DKPs is based upon previously established methods<sup>3, 19, 20</sup>. The DKPs of glycine, alanine, phenylalanine and lysine(Cbz) were synthesised as described in Chapter 3, sections 3.2.1 – 3.2.5.

#### 4.2.2. Synthesis of Poly(amino acid) Homo-polymers



*Scheme 4.1.* - ROP of a DKP, initiated by benzylamine when R = benzyl and hexylamine when R = hexyl, and catalysed using tin(II) 2-ethylhexanoate.

The respective DKP (Table 4.1.) and benzylamine/hexylamine (Table 4.1.) were added to an oven-dried vessel and flushed with  $N_{2(g)}$ . For polymers 1 to 4, tin(II) 2-ethylhexanoate (Table 4.1.) was used as the catalyst and the mixture was suspended in anhydrous DMF (Table 4.1.) and stirred at 130 °C under constant flow of  $N_{2(g)}$ . After 167 hours, the reaction mixture was allowed to cool to room temperature and filtered by gravity. The filtrate was precipitated in ice-cold diethyl ether (90 mL) and collected by centrifuge (4500 rpm, 0°C, 3 min). The solids were washed further with additional ice-cold diethyl ether (3 x 30mL) and dried in a vacuum oven (50°C) overnight.

For polymers 5 to 9, N,N-diisopropylethylamine (DIPEA) (Table 4.1.) was included as an organic catalyst and the mixture was suspended in deionised water (Table 4.1.) and stirred at 80 °C under constant flow of  $N_{2(g)}$ . After 167 hours, the mixture was allowed to cool, after which the dispersion was dialysed (M.W.C.O. 2000 Da) against deionised water for two days. The remaining contents within the dialysis tubing were frozen using liquid nitrogen and lyophilised.

*Table 4.1.* - Mass and mole values of reagents and targeted number of repeat units of poly(amino acid) homopolymers.

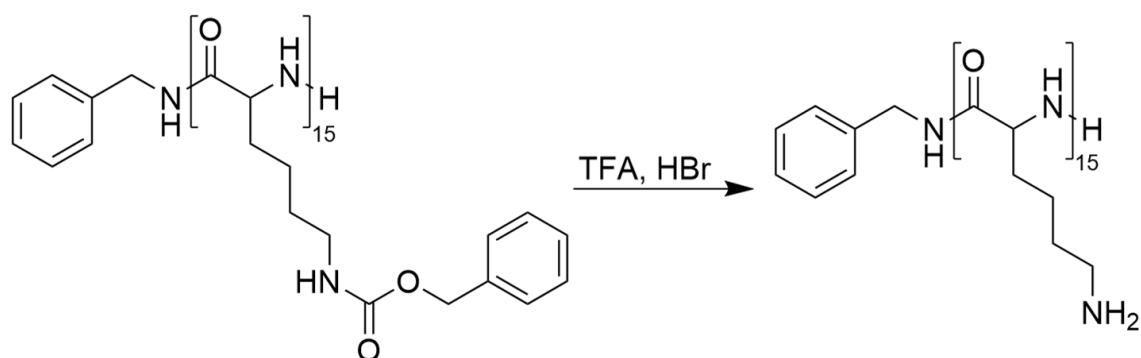
Polymer	Initiator		Monomer		Catalyst Mols (mmol)	Solvent Vol. (mL)	Reaction Time (hrs)	Targeted Repeat Units
	Name	Mols (mmol)	Name	Mols (mmol)				
1	Benzylamine	0.24	Gly-DKP	9.65	0.12	20	167	80
2	Benzylamine	0.089	Ala-DKP	3.52	0.045	20	167	80
3	Hexylamine	0.043	Phe-DKP	1.62	0.022	20	167	80
4	Benzylamine	0.033	Lys(Cbz)-DKP	0.53	0.017	10	167	80
5	Benzylamine	0.132	Gly-DKP	5.26	0.789	10	167	80
6	Benzylamine	0.106	Ala-DKP	4.22	0.633	10	167	80
7	Benzylamine	0.051	Phe-DKP	2.04	0.306	10	167	80
8	Benzylamine	0.018	Lys(Cbz)-DKP	0.73	0.11	10	167	80
9	Benzylamine	0.014	Ala-DKP	0.7	0.07	10	167	50



Table 4.2. – Targeted and observed number of repeat units of poly(amino acid) homopolymers and polymeric formula of the resultant polymers.

Polymer	Poly(amino acid) repeat units			Polymeric Formula
	Target	Observed (NMR)	Observed (MALDI)	
1	80	61	54	PGly <sub>54</sub>
2	80	65	68	PAla <sub>68</sub>
3	80	40	37	PPhe <sub>37</sub>
4	80	55	47	PLys(Cbz) <sub>47</sub>
5	80	52	48	PGly <sub>48</sub>
6	80	51	45	PAla <sub>45</sub>
7	80	19	18	PPhe <sub>18</sub>
8	80	18	15	PLys(Cbz) <sub>15</sub>
9	50	45	39	PAla <sub>39</sub>

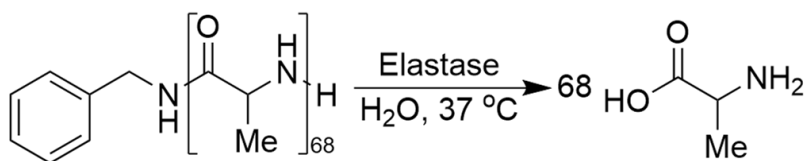
#### 4.2.3. Deprotection of Polylysine(Cbz)



Scheme 4.2. - Deprotection of Polylysine(Cbz) via hydrogenation with HBr/acetic acid.

PLys(Cbz) (polymer 8) (280 mg, 0.072 mmol) was added to an oven-dried vessel and dissolved in trifluoroacetic acid (TFA) (12.57 mL). The vessel was sealed and acetic HBr/acetic acid solution (1.57 mL) was added dropwise via syringe. A N<sub>2(g)</sub> inlet, fitted with a bubbler, was added as an overpressure safety feature and the reaction was stirred at room temperature for 22 hours. The reaction mixture was precipitated in ice-cold diethyl ether (65 mL) and collected via centrifugation (4500 rpm, 0 °C, 30 seconds). The solids were dissolved in deionised water (5 mL) and dialysed (M.W.C.O. 2000 Da) against deionised water for two days. The remaining contents within the dialysis tubing were frozen using liquid nitrogen and lyophilised.

#### 4.2.4. Enzymatic Degradation of Polyalanine



Scheme 4.3. - Enzymatic degradation of polyalanine *via* incubation with elastase at 37 °C.

Polyalanine (polymer 2) (300 mg, 0.057 mmol) was suspended in deionised water (10 mL). Elastase was added (8.28 units) and the mixture was stirred at 37 °C for one week, after which the mixture was dialysed (2000 Da M.W.C.O) against deionised water (100 mL) for a further three days. The dialysate was frozen in liquid nitrogen and lyophilised.

### 4.3. Results and Discussion

#### 4.3.1. Synthesis of DKPs

The DKPs of glycine, L-alanine, L-phenylalanine and L-lysine(Cbz) were synthesised by heating the respective amino acid in glycerol or ethylene glycol as reported in section 3.1. to 3.5. They were obtained as off-white crystals and their successful syntheses were confirmed by FTIR spectroscopy, <sup>1</sup>H NMR spectroscopy, and LC-MS (appendices I, II and III). Although the yields of DKP syntheses are limited due to the occurrence of side reactions, such as the formation of oligomers, DKP formation is a facile and straightforward method to generate a wide-range of monomers for the creation of degradable polymers that boast a plethora of functionalities. Notably, such monomers are produced in the absence of other reagents; this compares extremely favourably to NCA synthesis, which relies on the use of an HCl scavenger in addition to the cyclisation agent. These DKPs were selected in particular due to their reported sensitivity to enzymatic breakdown. The peptide bonds between Ala-Ala, Phe-Phe and Lys-Lys dipeptide units are selectively degraded by elastase<sup>21</sup>, chymotrypsin<sup>22</sup>, and trypsin<sup>23</sup> respectively. The respective polymers of these DKPs have additional, favourable properties as homopolymers that further contributed to their selection. Polyalanine has extensive intramolecular hydrogen bonding, resulting in excellent physical properties such as high mechanical strength<sup>24</sup>. Polylysine, once deprotected, is a cationic polymer bearing free primary amine groups that allow for substantial post-polymerisation functionalisation such as covalent conjugation to (bio)molecules, the formation of branched structures via subsequent polymerisation, and both covalent and physical cross-linking. Additionally, α-polylysine has been reported to have anti-microbial properties<sup>25</sup>.

### 4.3.2. Synthesis of Poly(amino acid) Homo-polymers

Determining the feasibility of DKP ROP is central to this research. As six-membered rings, DKPs do not bear the ring-strain present in NCAs that facilitates ring-opening, and resultantly polymerisation. For this reason, DKP ROP may be less likely to proceed without the use of catalysis to overcome a requisite activation energy. Despite this, the successful ROP of  $\delta$ -valerolactam to form nylon-5 has been reported<sup>26</sup>, supporting the plausibility of DKP ROP.

For the polymerisations resulting in polymers 1-4, the four monomers (glycine DKP, alanine DKP, phenylalanine DKP and  $\alpha$ -lysine(Cbz) DKP) (Table 4.1.) were polymerised from benzylamine or hexylamine, using tin(II) 2-ethylhexanoate as an FDA-approved catalyst<sup>27</sup>. The rate of ROP using tin(II) 2-ethylhexanoate as a catalyst is maximised at 130°C<sup>28</sup>. As such, these polymerisations were all conducted at 130°C. The polymers (Table 4.1., entries 1-4) were characterised using FTIR spectroscopy (appendix I), <sup>1</sup>H NMR spectroscopy (Figure 4.1.) and MALDI-TOF spectrometry (Figure 4.2.) All four polymers, aside from polymer 3, were synthesised using benzylamine as the initiator, the five phenyl protons of which come to resonance between 7.14-7.26 ppm. As such, integrals of peaks ascribed to the poly(amino acid) were normalised to these peaks which allowed for the determination of number of repeat units of the polymer.

Polymer 1 (Table 4.1.), PGly, showed a peak in the <sup>1</sup>H NMR spectrum (Figure 4.1.) at 3.94 ppm corresponding to the CH<sub>2</sub> of the polyglycine repeat unit. The integrals of the spectrum were normalised as described above which gave the CH<sub>2</sub> peak an integration of 122, signifying 61 repeat units and 72.25% monomer conversion. Analysis by MALDI-TOF spectrometry (Figure 4.2., spectrum a) gave a distribution with number averaged molecular weight ( $M_n$ ) = 2929 g mol<sup>-1</sup> and weight averaged molecular weight ( $M_w$ ) = 3105 g mol<sup>-1</sup>, signifying 54 repeat units and a narrow  $\mathcal{D}$  of 1.060. This showed moderate agreement with that determined by <sup>1</sup>H NMR spectroscopic analysis.

Polymer 2 (Table 4.1.), PAla, showed three peaks in the <sup>1</sup>H NMR spectrum (Figure 4.1.); one at 1.26 ppm corresponding to the CH<sub>3</sub>, the second at 3.84-3.93 ppm corresponding to the CH and the third at 8.08 ppm corresponding to the NH of the polyalanine repeat unit. The integrals of the spectrum were normalised as described above which gave integrals that signified 65 repeat units and 81.25% monomer conversion. Analysis by MALDI-TOF (Figure 4.2., spectrum b) gave a distribution with  $M_n$  = 4923 g mol<sup>-1</sup> and  $M_w$  = 5278 g mol<sup>-1</sup>, signifying 71 repeat units and a narrow  $\mathcal{D}$  of 1.072. This shows reasonable agreement with that determined by <sup>1</sup>H NMR spectroscopic analysis. Such a narrow dispersity suggests that, although the polymerisation duration is

relatively long, DKP ROP combines the benefits of solid-state peptide synthesis (narrow dispersity) and NCA ROP (efficient and straightforward synthesis) to create poly(amino acids).

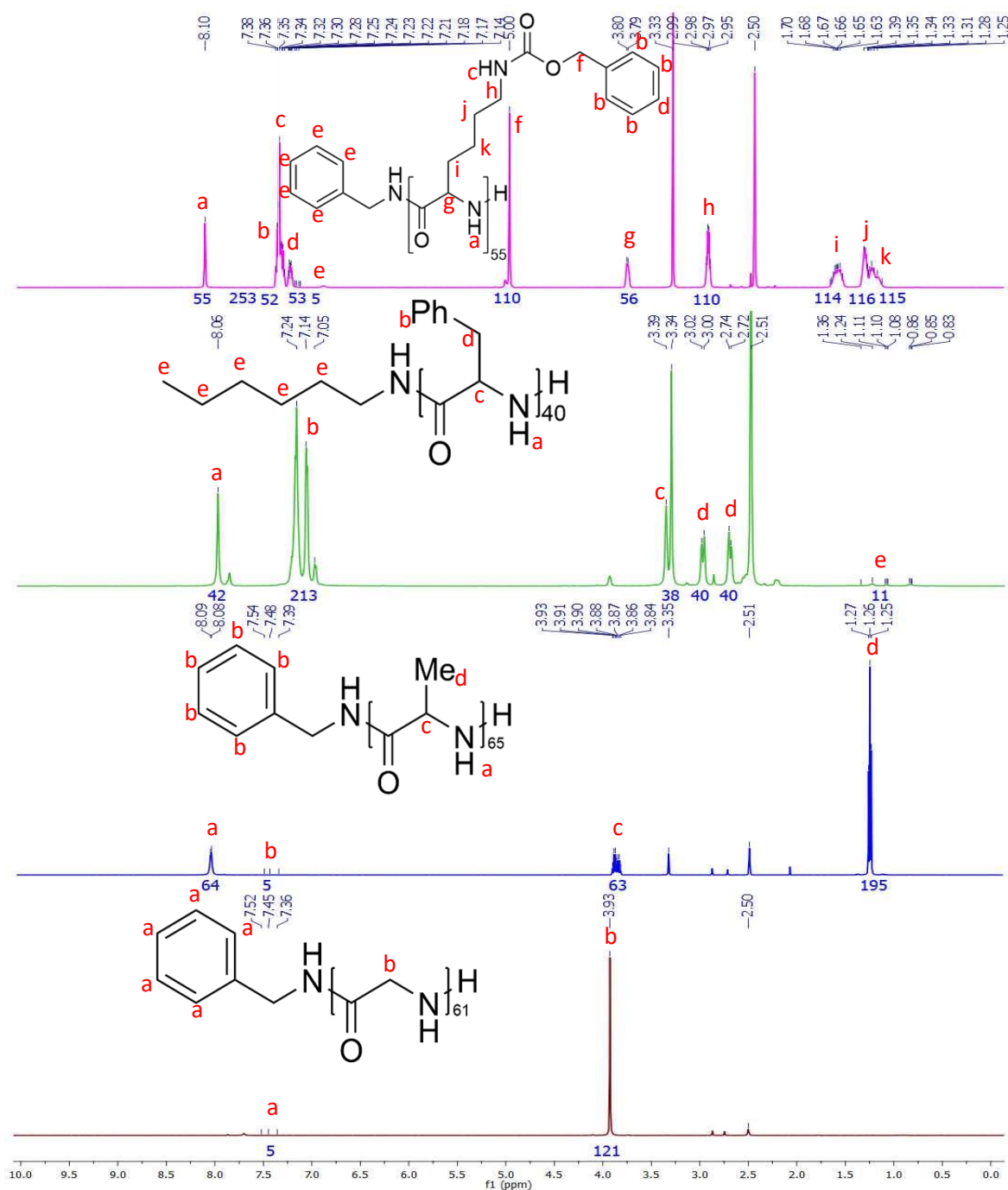


Figure 4.1. <sup>1</sup>H NMR spectra of polymer 1, PGly<sub>54</sub> (brown, CDCl<sub>3</sub>, 500 MHz), polymer 2, PALa<sub>65</sub> (blue, DMSO-d<sub>6</sub>, 500 MHz), polymer 3, PPhe<sub>37</sub> (green, DMSO-d<sub>6</sub>, 500 MHz) and polymer 4, PLys(Cbz)<sub>55</sub> (purple, DMSO-d<sub>6</sub>, 500 MHz).

Polymer 3 (Table 4.1.), PPhe, was synthesised via the ROP of phenylalanine DKP with hexylamine as the initiator. The terminal CH<sub>3</sub>, as well as the subsequent four CH<sub>2</sub> come to resonance between 0.83-1.86 ppm in the <sup>1</sup>H NMR spectrum (Figure 4.1.). As such, the integrals of the spectrum were normalised to these peaks. The peaks at 8.06 ppm, 7.05-7.24 ppm, 3.39 ppm and 2.72-3.02 ppm corresponded to the NH, the five phenyl CH's, the CH of the α carbon and the CH<sub>2</sub> of the R group of the phenylalanine repeat unit. The integrals of these peaks signified 40 repeat units and 50% monomer conversion. Analysis by MALDI-TOF spectrophotometry (Figure 4.2., spectrum c) gave a distribution with M<sub>n</sub> = 5105 g mol<sup>-1</sup> and M<sub>w</sub> = 5542 g mol<sup>-1</sup>, signifying 38 repeat units and a narrow Đ of 1.086. This shows good agreement with that of the <sup>1</sup>H NMR spectrum.

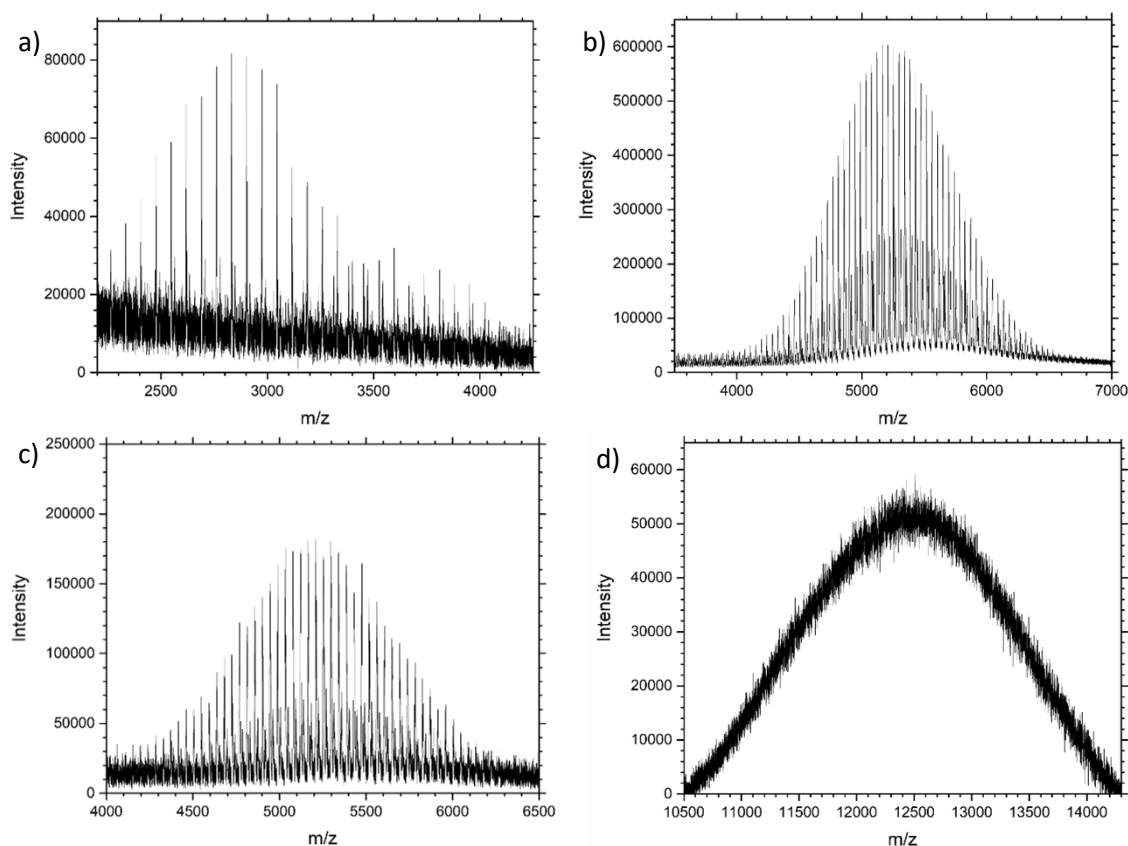


Figure 4.2. – MALDI-TOF spectra of: a) polymer 1, PGLy<sub>54</sub>, b) polymer 2, PAla<sub>68</sub>, c) polymer 3, PPhe<sub>37</sub>, and d) PLys(Cbz)<sub>47</sub>.

Polymer 4 (Table 4.1.), PLys(Cbz), was synthesised via the ROP of lysine(Cbz) DKP with benzylamine as the initiator. As such, the integrals of the <sup>1</sup>H NMR spectrum were normalised as described for polymers 1 and 2. The peaks in the spectrum (Figure 4.1.) corresponded as follows: 8.10 ppm (α N-H), 7.34 ppm (ε N-H), 7.28-7.38 ppm (*ipso* and *meta* aromatic 4 x C-H of protecting group), 7.21-7.25 ppm (*para* aromatic C-H of protecting group), 5.00 ppm (CH<sub>2</sub> of protecting group), 3.79 ppm (α C-H), 2.95-2.99 ppm (ε CH<sub>2</sub>), 1.60-1.70 ppm (β CH<sub>2</sub>), 1.31-1.39 ppm (δ CH<sub>2</sub>)

and 1.25-1.28 ppm ( $\gamma$  CH<sub>2</sub>). The integrals of the listed peaks resulted in 55 repeat units. Analysis by MALDI-TOF spectrophotometry (Figure 4.2., spectrum d) gave a distribution with  $M_n = 11847$  g mol<sup>-1</sup> and  $M_w = 12568$  g mol<sup>-1</sup>, signifying 47 repeat units and a narrow  $\mathcal{D}$  of 1.061. As a consequence of the poor ionisation of polymer 4 due to its large molecular weight, the use of the linear mode and higher intensity laser was required, resulting in lower resolution. Despite this, the spectrum shows reasonable agreement with that of the <sup>1</sup>H NMR spectra.

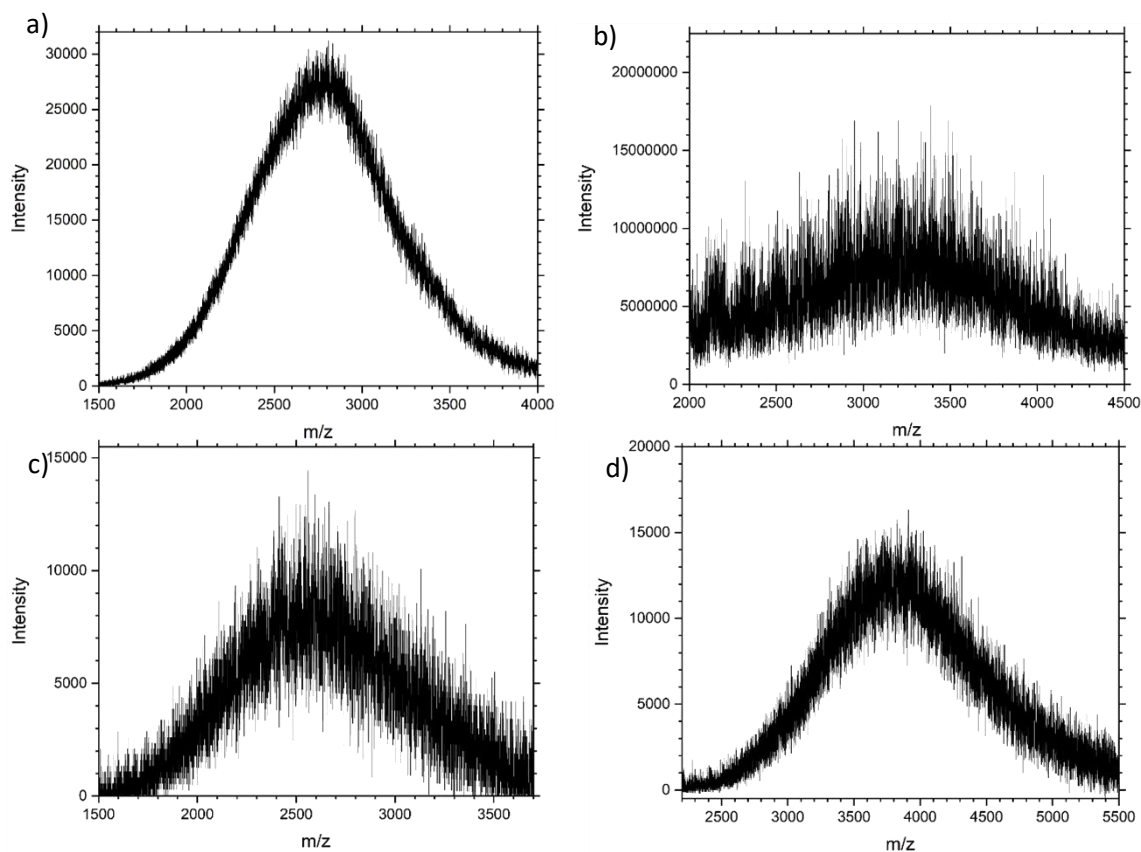


Figure 4.3. – MALDI-TOF spectra of: a) polymer 5, PGly<sub>48</sub>, b) polymer 6, PAla<sub>45</sub>, c) polymer 7, PPhen<sub>18</sub>, and d) polymer 8, PLys(Cbz)<sub>15</sub>.

A substantial advantage of DKPs over NCAs for ROP is the greater water solubility of some DKPs. DKPs are also more resistant to hydrolysis compared to NCAs, and so premature/unwanted polymerisation that is initiated by water molecules, as opposed to the initiator, is less likely. Correspondingly, DKP ROP may feasibly be achieved in water that does not contain buffer salts which are typically used to inhibit NCA hydrolysis during NCA ring-opening polymerisation-induced self-assembly (ROPISA) in aqueous solution.<sup>29,30</sup> As such, a controlled polymerisation of DKPs may be achieved in water, further minimising the environmental impact of the route to the respective polymer. The polymerisation of polymers 5 through 8 were conducted in water

using benzylamine as an initiator. The initial four polymerisations utilised tin(II) 2-ethylhexanoate as a Lewis acid and coordination catalyst in order to activate the monomer, whereas the subsequent set of polymerisations were performed in water and utilised DIPEA as a base catalyst. In water, the amine group of benzylamine and the terminal amine of the propagating poly(amino acid) chain are readily protonated in water to form their respective ammonium cation, resulting in a decrease in nucleophilicity. DIPEA deprotonates these ammonium groups to form the free amines in order to reduce their impact on polymerisation rate. Polymers 5 through 8 (Table 4.1.) were analysed as described for polymers 1 to 4, the  $^1\text{H}$  NMR spectra of which are shown below (Figure 4.4.) and the MALDI-TOF spectra are shown above (Figure 4.3.). The results of such analyses are summarised in (Table 4.1.).

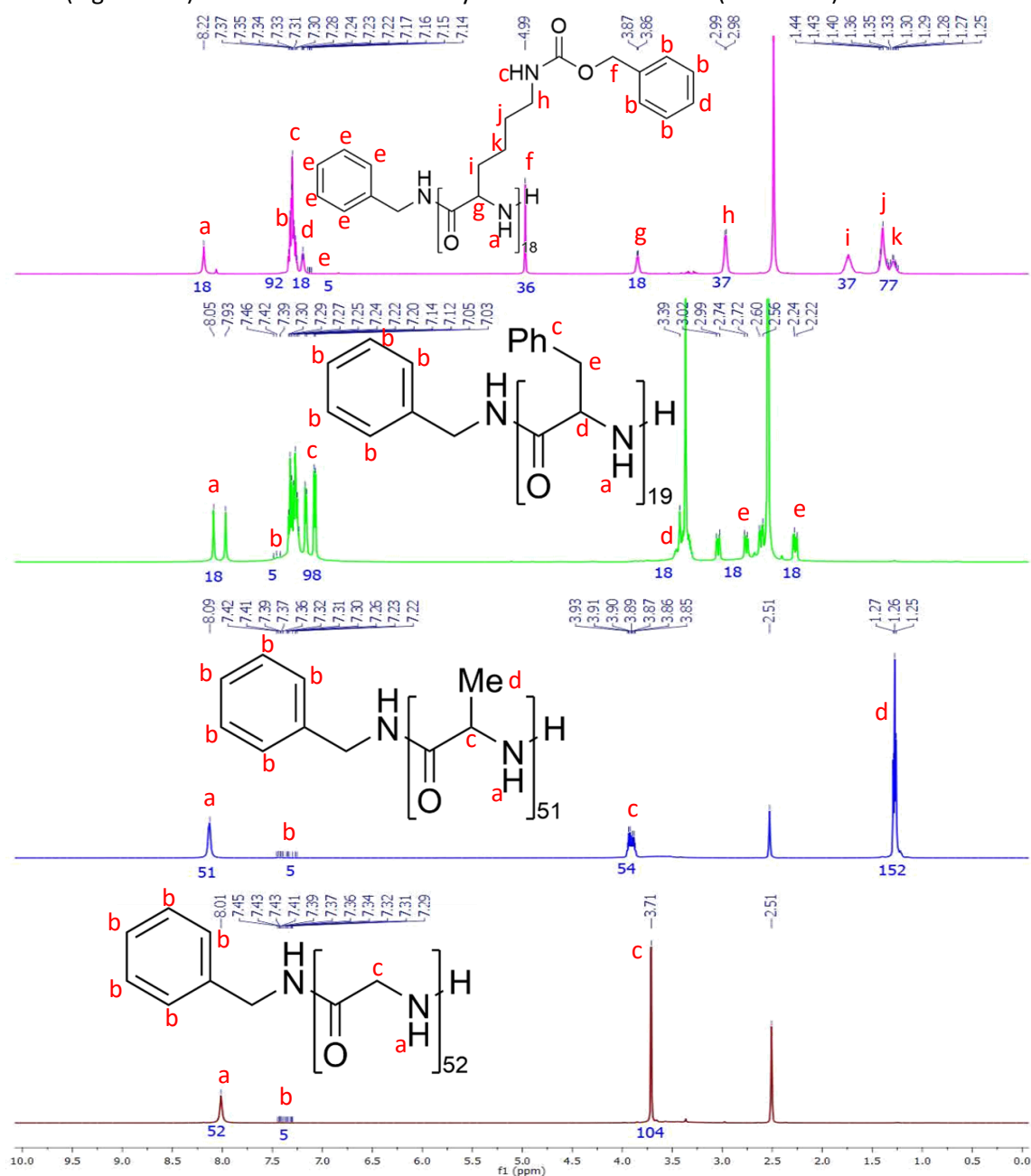


Figure 4.4. -  $^1\text{H}$  NMR spectra (DMSO- $d_6$ , 500 MHz) of polymer 5, PGly<sub>52</sub> (brown), polymer 6, PALa<sub>51</sub> (blue), polymer 7, PPhe<sub>19</sub> (green) and polymer 8, PLys(Cbz)<sub>18</sub> (purple).

In general, polymerisations performed in deionised water were not able to reach as a high a % monomer conversion as polymerisations conducted in DMF. Perhaps this is due to greater interaction between the water molecules and the propagating active chain of the polymer compared to the respective interactions with DMF. Additionally, the propagating polymer chains are more likely to have enhanced solubility in DMF compared to water, enabling homogenous polymerisation in solution. Polymers 7 and 8 particularly suffered from poor monomer conversion due to poor solubility of the polymers and monomers in water, resulting in heterogeneous propagation and associated slower reaction rates. Aggregation of the hydrophobic polymers occurs, restricting access to the active centre of the propagating chain to unreacted DKP monomers.

#### 4.3.3. Deprotection of Polylysine(Cbz)

To produce polylysine, a hydrophilic polymer capable of post-polymerisation functionalisation, polylysine(Cbz) was deprotected by acidolysis using TFA as a solvent and hydrogen bromide as the acid. The reaction mixture was dialysed after the deprotection to remove the cleaved protecting group and residual TFA and HBr. The success of the deprotection was quantified by  $^1\text{H}$  NMR spectroscopy (Figure 4.5.) and solubility studies in water quantified by UV-vis spectrophotometry (Figure 4.6.). Shown in Figure 4.5., the peaks that correspond to the protons of the Cbz protecting group, 7.24-7.37 ppm and 4.99 ppm labelled b, d and f in the brown spectrum, have entirely disappeared following deprotection (aside from those corresponding to the benzylamine initiator). The peak at 7.83 ppm in the blue, labelled b, has doubled in integration, confirming the conversion of the  $\epsilon$ -amine from secondary to primary due to the successful deprotection. Additionally, the deprotected polylysine showed considerably greater water-solubility than polylysine(Cbz) (Figure 4.6.). PLys(Cbz)<sub>15</sub> was insoluble in deionised water at a low concentration of 1.3 mg mL<sup>-1</sup>; this is illustrated by the high absorbance in the UV-vis spectrum at 650 nm, Whereas PLys<sub>15</sub> dissolved well in deionised water at a significantly higher concentration of 12 mg mL<sup>-1</sup>. The greater absorbance of PLys(Cbz)<sub>15</sub> illustrates the poor solubility and opacity of the suspension, whilst the low absorbance of the PLys<sub>15</sub> solution illustrates its transparency and therefore increased solubility of PLys<sub>15</sub>. This further confirms the successful deprotection of polylysine(Cbz). Access to deprotected polylysine, a polymer capable of post-polymerisation functionalisation, via DKP ROP provides a mild and green synthetic route to biodegradable cross-linked networks, such as gels, as well as pro-drugs and other biomaterials with nuanced functionality.



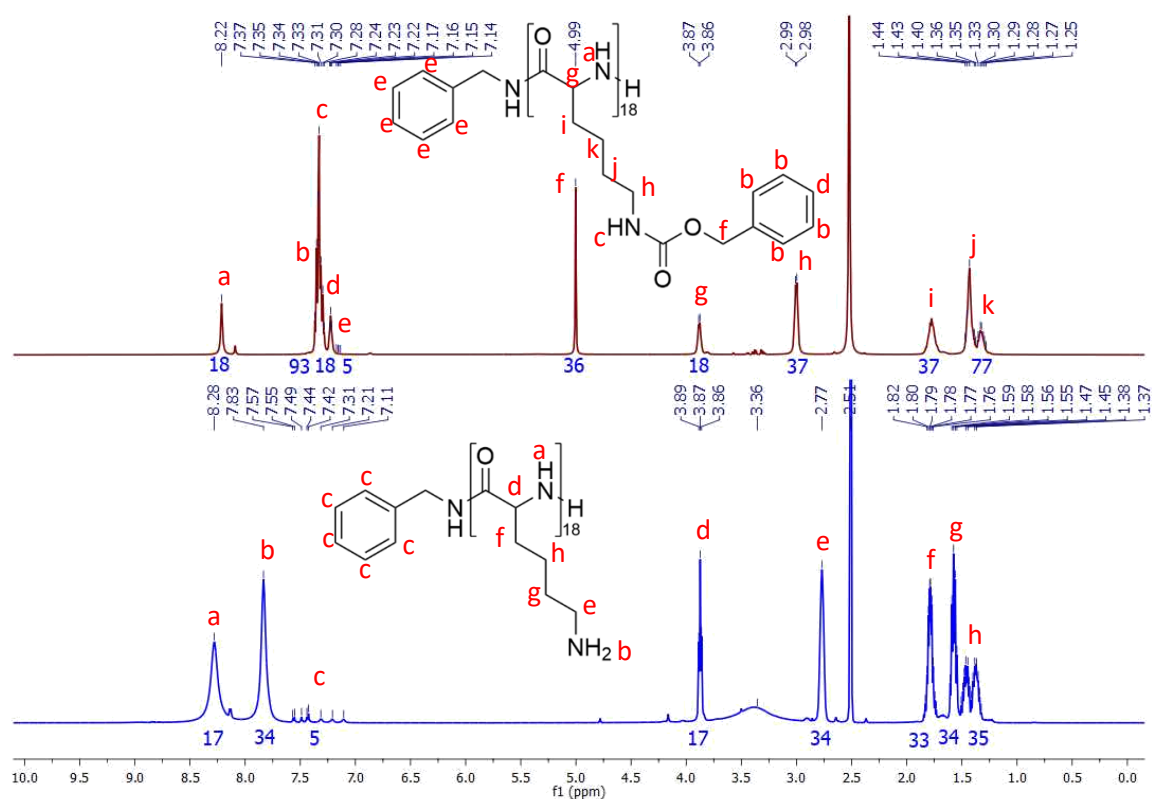


Figure 4.5. -  $^1\text{H}$  NMR spectra (DMSO- $d_6$ , 500 MHz) of polymer 8, PLys(Cbz) $_{18}$  (brown) and deprotected polymer 8, PLys $_{18}$  (blue).

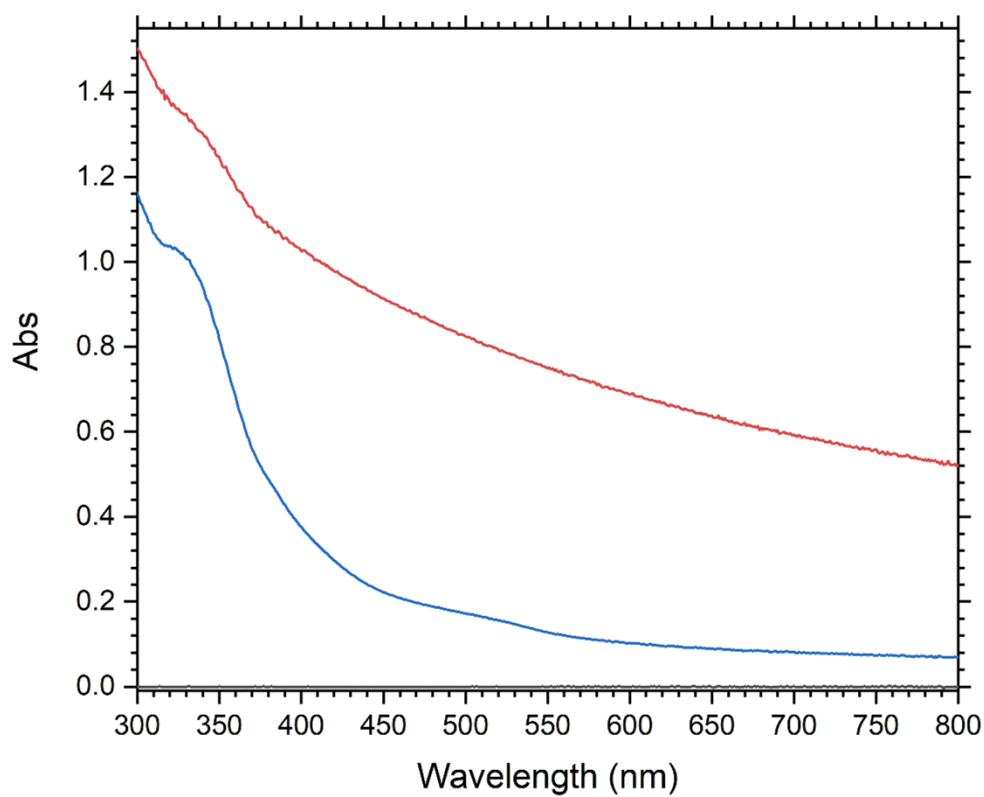


Figure 4.6. - UV-vis spectrum of polymer 8, PLys(Cbz) $_{18}$ , suspended in deionised water at 1.3 mg mL $^{-1}$  (red) and deprotected polymer 8, PLys $_{18}$ , in deionised water at 12 mg mL $^{-1}$  (blue).

#### 4.3.4. Enzymatic Degradation of Polyalanine

To confirm the biodegradability of polyalanine, as well as its potential for circularity of its lifespan, polymer 2 was incubated with 8 units elastase at 37 °C for one week. The degradation products were analysed by FTIR spectroscopy (appendix I),  $^1\text{H}$  NMR spectroscopy (appendix II) and HPLC (appendix IV). All methods of analysis showed the complete degradation to the amino acid alanine. From 300mg of polymer 2,  $\text{PALa}_{68}$ , 240 mg of alanine was obtained.

After confirmation of complete degradation, this sample of alanine was cyclised to alanine DKP according to the procedure described in section 3.2.3., yielding 113 mg of alanine DKP which was characterised by  $^1\text{H}$  NMR spectroscopy (appendix II), FTIR spectroscopy (appendix I) and LC-MS (appendix III). The obtained alanine DKP was utilised to produce polymer 9,  $\text{PALa}_{39}$ , using DIPEA as a catalyst and deionised water as a solvent. Polymer 9 was characterised by  $^1\text{H}$  NMR spectroscopy (Figure 4.7.), MALDI-TOF (Figure 4.8.) and FTIR spectroscopy (appendix I) as described above for polymers 2 and 6.

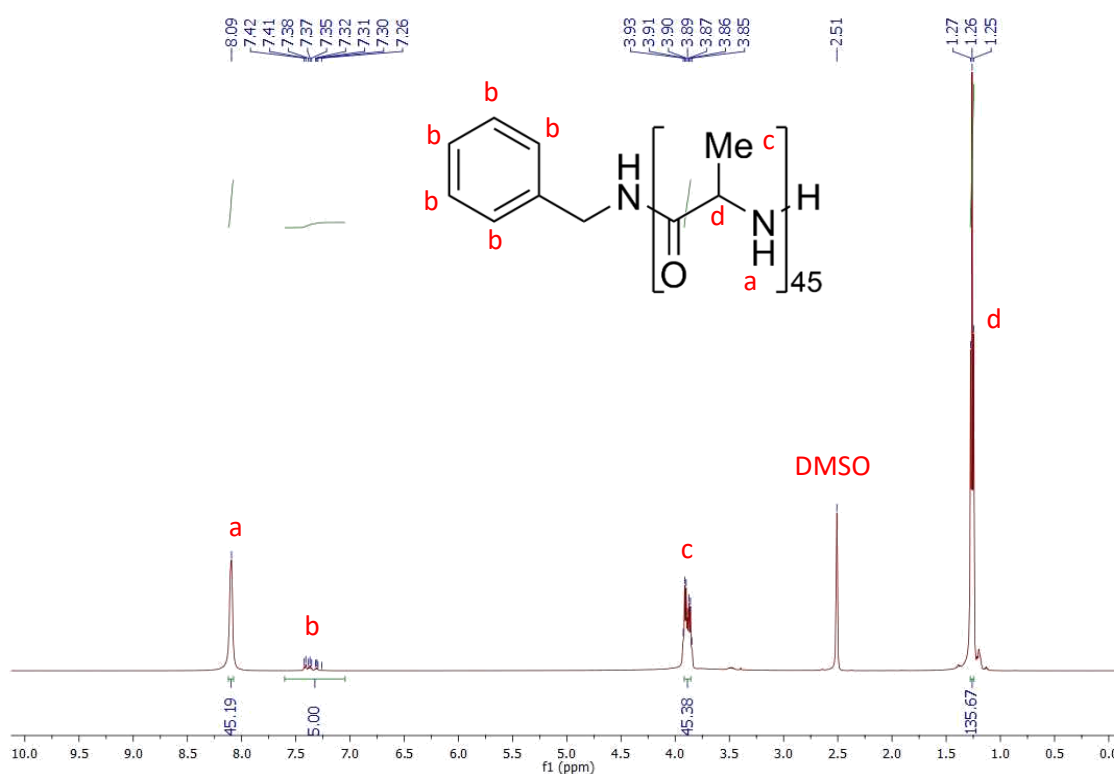


Figure 4.7. –  $^1\text{H}$  NMR spectrum (DMSO- $d_6$ , 500 MHz) of polymer 9,  $\text{PALa}_{45}$ , synthesised from alanine DKP that was produced from the degradation products of  $\text{PALa}_{65}$ .

The successful formation of polymer 9 from the degradation products of polymer 2 demonstrates the recyclability of this process and the potential for a circular economy.

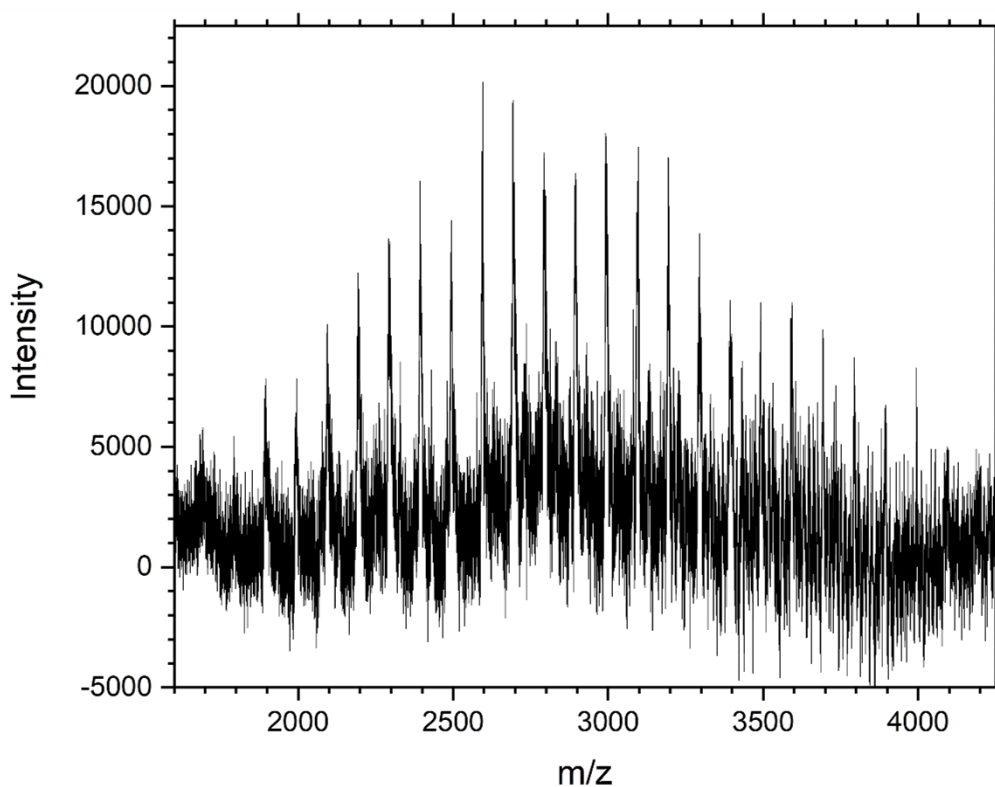


Figure 4.8. – MALDI-TOF spectrum of polymer 9, PALa<sub>45</sub>, synthesised from alanine DKP that was produced from the degradation products of PALa<sub>65</sub>.

#### 4.4. Conclusion

The synthesis and ROP of DKPs to produce poly(amino acids) via a controlled and environmentally benign route is reported for the first time. Poly(amino acids) have enormous potential as commodity and high-value polymers owing to their environmental credentials, including their biocompatibility, bio-renewability, and biodegradability. Additionally, poly(amino acids) boast unparalleled chemical properties amongst common biodegradable polymers due to the wide-range of functional groups that they may possess dependent on the starting amino acid(s) selected. Poly(amino acid) creation from DKPs offers a controlled route to poly(amino acid) creation that bypasses the common issues that have plagued the widespread use of poly(amino acids); safety, environmental, and economic issues in NCA synthesis. The versatility of the process of creating poly(amino acids) from DKPs is demonstrated in the reporting of four different poly(amino acids), and the circularity of polymer synthesis owing to the biodegradability of poly(amino acids) shown. Polymer synthesis was also achieved using deionised water as the solvent, as well as via Lewis acid/coordination catalysis and base catalysis. Successful deprotection of polylysine(Cbz) was also achieved, yielding a polymer

bearing free, primary amines allowing for post polymerisation functionalisation. It is anticipated that this route to poly(amino acid) synthesis will allow their widespread use in applications ranging from everyday materials to advanced healthcare devices.

#### 4.5. References

---

- 1) Labriere, C., Kondori, N., Caous, J. S., Boomgaren, M., Sandholm, K., Ekdahl, K. N., Hansen, J. H. and Svenson, J. Development and evaluation of cationic amphiphilic antimicrobial 2,5-diketopiperazines. *Journal of Peptide Science*. 2018, **24**(7), e3090.
- 2) Mollica, A, Costante, R., Fiorito, S., Genovese, S., Stefanucci, A., Mathieu, V., Kiss, R. and Epifano, F. Synthesis and anti-cancer activity of naturally occurring 2,5-diketopiperazines. *Fitoterapia*. 2014, **98**, 91-97.
- 3) Manchineella, S., Voshavar, C. and Govindaraju, T. Radical-Scavenging Antioxidant Cyclic Dipeptides and Silk Fibroin Biomaterials. *European Journal of Organic Chemistry*. 2017, **30**, 4363-4369.
- 4) Grant, T. M., Rennison, D., Arabshahi, H. J., Brimble, M. A., Cahill, P. and Svenson, J. Effect of regio- and stereoisomerism on antifouling 2,5-diketopiperazines. *Organic & Biomolecular Chemistry*. 2022, **20**(47), 9431-9446.
- 5) Manchineella, S., Murugan, N. A. and Govindaraju, T. Cyclic Dipeptide-Based Ambidextrous Supergelators: Minimalistic Rational Design, Structure-Gelation Studies, and *In Situ* Hydrogelation. *Biomacromolecules*. 2017, **18**(11). 3581-3590.
- 6) Obst, M. and Steinbüchel. Microbial degradation of poly(amino acid)s. *Biomacromolecules*. 2004, **5**(4), 1166-1176.
- 7) Aktas, N., Alpaslan, D. and Dudu, T.E. Polymeric Organo-Hydrogels: Novel Biomaterials for Medical, Pharmaceutical, and Drug Delivery Platforms. *Frontiers in Materials*. 2022, **9**, 845700-845709.
- 8) Zanna, N. and Tomasini, C. Peptide-Based Physical Gels Endowed with Thixotropic Behaviour. *Gels*. 2017, **3**(4), 39-56.
- 9) Rao, J., Luo, Z., Ge, Z., Liu, H. and Liu, S. "Schizophrenic" Micellization Associated with Coil-to-Helix Transitions Based on Polypeptide Hybrid Double Hydrophilic Rod-Coil Diblock Copolymer. *Biomacromolecules*. 2007, **8**(12), 3871-3878.
- 10) Zhou, M., Hou, T., Li, J., Yu, S., Xu, Z., Yin, M., Wang, J. and Wang, X. Self-Propelled and Targeted Drug Delivery of Poly(aspartic acid)/Iron-Zinc Microrocket in the Stomach. *ACS Nano*. 2019, **13**(2), 1324-1332.

- 
- 11) Palomo, J.M. Solid-phase peptide synthesis: an overview focused on the preparation of biologically relevant peptides. *RSC Advances*. 2014, **4**(62), 32658-32672.
- 12) Cheng, J. and Deming, T. Synthesis of Polypeptides by Ring-Opening Polymerization of  $\alpha$ -Amino Acid N-Carboxyanhydrides. *Top Current Chemistry*. 2012, **310**, 1-26.
- 13) Otake, Y., Nakamura, H. and Fuse, S. Rapid and Mild Synthesis of Amino Acid N-Carboxy Anhydrides: Basic-to-Acidic Flash Switching in a Microflow Reactor. *Angewandte Chemie*. 2018. **130**(35), 11559-11563.
- 14) Cohen, R, Habbah, S and Safadi, M. *Process for manufacturing glatiramer acetate product*. 9,763,993. 2017.
- 15) Koga, K., Sudo, A. and Endo, T. Revolutionary Phosgene-Free Synthesis of  $\alpha$ -Amino Acid N-Carboxyanhydrides Using Diphenyl Carbonate Based on Activation of  $\alpha$ -Amino Acids by Converting into Imidazolium Salts. *Journal of Polymer Science: Part A: Polymer Chemistry*. 2010, **48**, 4351-4355.
- 16) Khuphe, M. and Thornton, P.D. Poly(hydroxy acid) Nanoparticles for the Encapsulation and Controlled Release of Doxorubicin. *Macromolecular Chemistry and Physics*. **219**(23), 1800352-1800356.
- 17) Endo, T and Sudo, A. Well-defined environment-friendly synthesis of polypeptides based on phosgene-free transformation of amino acids into urethane derivatives and their applications. *Polymer International*. 2020, **69**(3), 219-227.
- 18) Borthwick, A.D. 2,5-Diketopiperazines: Synthesis, Reactions, Medicinal Chemistry, and Bioactive Natural Products. *Chemical Reviews*. 2012, **112**(7), 3641-3716.
- 19) Pokorna, A., Bobal, P., Oravec, M., Rarova, L., Bobalova, J. and Jampilek, J. Investigation of Permeation of Theophylline through Skin Using Selected Piperazine-2,5-Diones. *Molecules*. 2019, **24**(3), 566-579.
- 20) Basiuk, V.A., Gromovoy, T.Y., Chuiko, A.A., Soloshonok, V.A. and Kukhar, V.P. A Novel Approach to the Synthesis of Symmetric Optically Active 2,5-Dioxopiperazines. *Synthesis*. 1992, **5**, 449-451.
- 21) Oh, H. J., Joo, M. K., Sohn, Y. S. and Jeong, B. Secondary Structure Effect of Polypeptide on Reverse Thermal Gelation and Degradation of l/dl-Poly(alanine)-Polyoxamer-l/dl-Poly(alanine) Copolymers. *Macromolecules*. 2008, **41**(21), 8204-8209.

- 
- 22) Kim, C-J., Park, J-e., Hu, X., Albert, S. K. and Park, S-J. Peptide-Driven Shape Control of Low-Dimensional DNA Nanostructures. *ACS Nano*. 2020, **14**(2), 2276-2284.
- 23) Zou, J., Zhou, M., Ji, Z., Xiao, X., Wu, Y., Cui, R., Deng, S. and Liu, R. Controlled copolymerization of  $\alpha$ -NCAs and  $\alpha$ -NNTAs for preparing peptide/peptoid hybrid polymers with adjustable proteolysis. *Polymer Chemistry*. 2022, **13**(3), 388-394.
- 24) Zhao, S., Ye, X., Wu, M., Ruan, J., Wang, X., Tang, X. and Zhong, B. Recombinant Silk Proteins with Additional Polyalanine Have Excellent Mechanical Properties. *International Journal of Molecular Sciences*. 2021, **22**(4), 1513-1526.
- 25) Pranantyo, D., Xu, L. Q., Hou, Z., Kang, E-T. and Chan-Park, M. B. Increasing bacterial affinity and cytocompatibility with four-arm star glycopolymers and antimicrobial  $\alpha$ -polylysine. *Polymer Chemistry*. 2017, **8**(21), 3364-3373.
- 26) von Tiedemann, P., Anwar, S., Kemmer-Jonas, U., Asadi, K. and Frey, H. Synthesis and Solution Processing of Nylon-5 Ferroelectric Thin Films: The Renaissance of Odd-Nylons? *Macromolecular Chemistry and Physics*. 2020, **221**(5), 1900468-1900474.
- 27) U.S. Food and Drug Administration. CFR – Code of Federal Regulations Title 21. [Online]. 2020. [25/02/21]. Available from: <https://www.accessdata.fda.gov/scripts/cdrh/cfdocs/cfCFR/CFRSearch.cfm?fr=175.300>
- 28) Ryner, M., Stridsberg, K. and Albertsson, A-C. Mechanism of Ring-Opening Polymerisation of 1,5-Dioxepan-2-one and L-Lactide with Stannous 2-Ethylhexanoate. A Theoretical Study. *Macromolecules*. 2001, **34**, 3877-3881.
- 29) Grazon, C., Salas-Ambrosio, P., Ibarboue, E., Buol, A., Garanger, E., Grinstaff, M. W., Lecommandoux, S. and Bonduelle, C. Aqueous Ring-Opening Polymerization-Induced Self-Assembly (ROPISA) of N-Carboxyanhydrides. *Angewandte Chemie International Edition*. 2019, **59**(2), 622-626.
- 30) Grazon, C., Salas-Ambrosio, P., Antoine, S., Ibarboue, E. Sandre, O., Clulow, A. J., Boyd, B. J., Grinstaff, M. W., Lecommandoux, S. and Bonduelle, C. Aqueous ROPISA of  $\alpha$ -amino acid N-carboxyanhydrides: polypeptide block secondary structure controls nanoparticle shape anisotropy. 2021, **12**(43), 6242-6251.

## Chapter 5 – Exploiting DKPs to Afford Nanoparticles for Acid-Mediated Drug Release

### Abstract

Interest in degradable polymer particles has grown to match the increasing recognition of the detrimental impact of non-degradable polymer particles on the environment. Most commonly, the focus of such research is on biodegradable polyesters, however, poly(amino acids) should play an essential role in the quest to create useful products from biodegradable and biorenewable polymers. Due to extensive hydrogen bonding, poly(amino acids) have the capacity to form stable secondary structures and, when polymerised in a controlled manner as part of an amphiphilic polymer structure, such materials are capable of self-assembly in aqueous solution to form nanostructures. DKPs can be utilised as cyclic monomers in an original route to controlled poly(amino acid) synthesis. The resultant polymers boast a narrow  $\bar{M}_w/\bar{M}_n$  and, if initiated from a hydrophilic macroinitiator, may form an amphiphilic block copolymer capable of self-assembly. DKP creation is performed in the absence of cyclising agents such as phosgene and hazardous organic solvents, therefore rendering poly(amino acid) synthesis safe and cost-effective, potentially allowing the wide-range use of poly(amino acid) block copolymers across numerous commercial, industrial and medical sectors. Consequently, the creation of polymer nanoparticles sensitive to acidic-mediated disassembly is reported. Doxorubicin encapsulation and release from such nanoparticles was achieved confirming the suitability poly(amino acid) block copolymers created from DKPs as potential materials for triggered drug delivery applications.

### 5.1. Introduction

Increased recognition and understanding of the environmental impact of non-degradable polymer particles in the ecosystem has led to widespread research into the development of biodegradable analogues<sup>1</sup>. Most commonly, polyesters such as poly(lactic acid)<sup>2</sup>, poly(glycolic acid)<sup>3</sup>, and polycaprolactone<sup>4</sup> have been the focus of such research. However, such polymers lack functionality to enhance their effectiveness, for instance by drug or dye conjugation, and hydrogen bond intermolecular interactions to ensure the stability of nanoparticles formed.

As a consequence of extensive hydrogen bonding, poly(amino acids) appear as optimum candidates for self-assembly and nanostructure formation. Indeed, longevity of poly(amino acid)-based nanoparticles in aqueous solution makes them extremely appropriate for use as drug delivery vehicles<sup>5</sup>. The use of poly(amino acids) to produce very stable nanoparticles is of



great significance for the encapsulation and prolonged discharge of active molecules including exfoliating, fragrant, therapeutic, and antimicrobial molecules that form part of both everyday and high-value formulations<sup>6</sup>.

In the context of oncology, encapsulating cytotoxic chemotherapeutic molecules within polymer nanoparticles improves the pharmacokinetic profile of the therapeutic. This is due to a reduced premature drug metabolism and drug release to non-target cells, therefore enabling an increased drug concentration to reach the target site. This has attractive consequences such as the reduction in the development or intensity of side-effects<sup>7</sup>, as well as a steady release of the therapeutic, maintaining a prolonged active concentration<sup>8</sup>. Elegant drug delivery systems have been reported for the release of anti-cancer drugs in response to acidic conditions<sup>9</sup> and temperature change<sup>10</sup> as well as more specific stimuli such as enzyme concentration<sup>11</sup>. Poly(amino acids) offer great potential in the quest to produce highly stable, biodegradable nanoparticles that may boast chemical functionality for nanoparticle modification (i.e. cell targeting groups) capable of payload release in a controlled manner, if their synthesis is amiable to industrial needs.

Poly(amino acids) have been utilised successfully as part of nanoparticle formulations and drug delivery vehicles. Price *et al.*<sup>12</sup> produce a set of poly(serine)-graft-poly(phenylalanine hydroxyl acid) graft copolymers with precise lengths via NCA and O-carboxyanhydride (OCA) ROP that are capable of self-assembly in aqueous solution. Despite the short length of polymer chains, all polymers self-assembled to produce particles of around 100 nm in diameter with very low nanoparticle polydispersity (<0.2) that are suitable for industrial use<sup>13</sup>. The most promising candidate, poly(Ser)<sub>19.6</sub>-*graft*-poly(Phe  $\alpha$ -hydroxyacid)<sub>6</sub> was selected for drug release studies and demonstrated a reasonable encapsulation efficiency of 52.3% $\pm$ 6.2%. The nanoparticles demonstrated excellent stability at pH 7.4, showing minimal leakage of therapeutic. Unsurprisingly, the nanoparticles also demonstrated sensitivity to acidic conditions due to the presence of acid-labile ester bonds between the polyserine chain and poly(Phe  $\alpha$ -hydroxyacid) branches, as well as between the repeat units of poly(Phe  $\alpha$ -hydroxyacid). This is relevant in the context of anti-cancer treatments as cancerous endosomal pH ranges between 5.0 and 6.0, whilst cancerous lysosomal pH ranges between 4.0 and 5.0<sup>14</sup>. As such, nanoparticles able to degrade in acidic conditions are capable of releasing an encapsulated anti-cancer therapeutic at the cancer site in a targeted manner. The study concluded with a final release of 95.4% of encapsulated dox after six days of incubation, demonstrating suitability as an acid-sensitive drug delivery vehicle.<sup>12</sup>

Kataoka *et al.*<sup>15</sup> produced PEG-*b*-poly( $\beta$ -benzyl-L-aspartate) via NCA ROP. After self-assembly, the resultant micelles boasted a very narrow polydispersity of <0.04 and average particle diameters of 67 nm and 45 nm. These sizes of nanoparticles are suitable for the encapsulation and delivery of therapeutics via several administrative methods<sup>13</sup>. The micelles demonstrated to have reasonable loading content of 17.3% and 20.1% and a subsequent release study that demonstrated a preferential release to acidic conditions (pH 5.0) to the pH of physiological fluid (pH 7.4). However, the final release of dox after 70 hours when incubated at pH 7.4 was not trivial, releasing 70% as much dox as that released at pH 5.0. Despite this, *in vivo* anti-tumour studies of the dox loaded particles revealed a greater reduction volume than that of free dox, demonstrating the efficacy of such a system.<sup>15</sup>

As is the case for both homo-poly(amino acids) and their copolymers, the typical synthetic route is ROP of NCAs. Whilst NCA ROP can afford poly(amino acids) with narrow  $\bar{M}_w/\bar{M}_n$ <sup>12,15</sup>, the synthesis of NCAs has a collection of problems which are explored in more detail in sections 4.1. and 1.2.2. However, DKPs can be synthesised by a one-step reaction that is both green and economically viable. It requires minimal purification and is without the use of both harsh solvents and coupling reagents. As reported in Chapter 4, the polymerisation of glycine DKP, alanine DKP and phenylalanine DKP afforded hydrophobic polymers with reasonable monomer conversions and very low  $\bar{M}_w/\bar{M}_n$ . If the ROP of these DKPs were initiated from a hydrophilic polymer bearing a nucleophilic end group, such as poly(ethylene glycol) methyl ether, the resultant polymer may be amphiphilic and capable of self-assembly. To the best of the authors knowledge, ROP of DKPs from a macro-initiator to afford amphiphilic block copolymers, as well as the use of such block copolymers to create nanoparticles capable of therapeutic encapsulation and targeted release is, as of yet, unexplored.

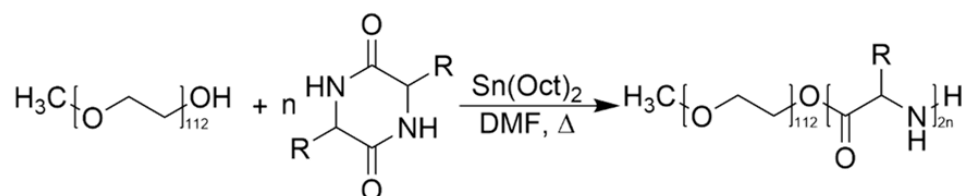
The creation of poly(amino acid)-based amphiphilic block copolymers via DKP ROP is reported for the first time as a cost-effective and facile method. The amphiphilic block copolymers produced were assessed for their capacity to self-assemble in aqueous solution and formed stable nanoparticles, offering a simple, environmentally-benign and cost-effective route to poly(amino acid)-based nanoparticles. The effectiveness of the nanoparticles as potential drug delivery vehicles was demonstrated by the controlled release of doxorubicin to acidic solution only. This method of poly(amino acid) synthesis reported enables genuine opportunity to commercially exploit a class of polymer that possess biodegradability, biocompatibility, excellent self-assembly capability, and tunable mechanical and responsive properties, as a component of a drug delivery vehicle.

## 5.2. Experimental Section

### 5.2.1. Synthesis of 2,5-Diketopiperazines

The general procedure for preparation of 2,5-diketopiperazines is based upon previously established methods<sup>16, 17, 18</sup>. The DKPs of glycine, alanine and phenylalanine were synthesised as described in Chapter 3, sections 3.2.1 – 3.2.4.

### 5.2.2. Synthesis of PEG-*b*-Poly(amino acid) Copolymers



*Scheme 5.1.* - ROP of a DKP, initiated by PEG methyl ether (Average  $M_w = 5000 \text{ g mol}^{-1}$ ) and catalysed using tin(II) 2-ethylhexanoate.

The respective DKP (Table 5.1.), poly(ethylene glycol) methyl ether (Average  $M_w = 5000 \text{ g mol}^{-1}$ ) and tin(II) 2-ethylhexanoate were added to an oven-dried vessel and flushed with  $\text{N}_{2(\text{g})}$ . The mixture was suspended in anhydrous DMF and stirred at  $130^\circ\text{C}$  under constant flow of  $\text{N}_{2(\text{g})}$ . After an allotted period of time (Table 5.1.), the reaction mixture was allowed to cool to room temperature and filtered by gravity. The filtrate was precipitated by ice-cold diethyl ether (150 mL) and the solids collected by centrifuge (4500 rpm,  $0^\circ\text{C}$ , 3 min).

For polymerisations of glycine DKP and alanine DKP (where  $\text{R} = \text{H}$  and  $-\text{CH}_3$  respectively), the solids were re-dissolved in minimal THF and the mixture centrifuged (4500 rpm,  $0^\circ\text{C}$ , 3 min) to separate unreacted DKP which remained undissolved. The supernatant was then precipitated in ice-cold diethyl ether (3 x 30 mL) and dried in a vacuum oven ( $50^\circ\text{C}$ ) overnight.

For polymerisations of phenylalanine DKP (where  $\text{R} = \text{Benzyl}$ ), the solids were suspended in toluene (30 mL) to dissolve unreacted phenylalanine DKP. The suspension was then centrifuged (4500 rpm,  $0^\circ\text{C}$ , 3 min) and the supernatant decanted. The remaining solid was washed with ice-cold diethyl ether (3 x 30 mL) and dried in a vacuum oven ( $50^\circ\text{C}$ ) overnight.

Table 5.1. - Mass and mole values of reagents, and targeted number of repeat units of PEG-*b*-poly(amino acids).

Polymer	Initiator		Monomer		Catalyst Mols (mmol)	Solvent Vol. (mL)	Reaction Time (hrs)	Targeted Repeat Units
	Name	Mols (mmol)	Name	Mols (mmol)				
1	PEG-OH <sub>5000</sub>	0.053	Glycine-DKP	2.63	0.46	40	162	100
2	PEG-OH <sub>5000</sub>	0.1	Glycine-DKP	0.7	0.46	20	239	14
3	PEG-OH <sub>5000</sub>	0.08	Glycine-DKP	0.8	0.04	20	132	20
4	PEG-OH <sub>5000</sub>	0.035	Alanine-DKP	2.11	0.018	10	118	20
5	PEG-OH <sub>5000</sub>	0.053	Alanine-DKP	2.11	0.027	10	118	80
6	PEG-OH <sub>5000</sub>	0.08	Phenylalanine-DKP	1.2	0.04	40	120	30

Table 5.2. – Targeted and observed number of repeat units by <sup>1</sup>H NMR spectroscopy and APC of PEG-*b*-poly(amino acids).

Polymer	Poly(amino acid) repeat units			Polymeric Formula
	Target	Observed (NMR)	Observed (APC)	
1	100	31	29	PEG <sub>112</sub> - <i>b</i> -PGly <sub>30</sub>
2	14	14	13	PEG <sub>112</sub> - <i>b</i> -PGly <sub>14</sub>
3	20	20	19	PEG <sub>112</sub> - <i>b</i> -PGly <sub>20</sub>
4	20	6	6	PEG <sub>112</sub> - <i>b</i> -PAla <sub>6</sub>
5	80	14	11	PEG <sub>112</sub> - <i>b</i> -PAla <sub>12</sub>
6	30	25	24	PEG <sub>112</sub> - <i>b</i> -PPhe <sub>25</sub>

### 5.2.3. Preparation of PEG-*b*-Poly(amino acid) Copolymer Nanoparticles

PEG-*b*-poly(amino acid) copolymer nanoparticles were prepared based upon a previously established nanoprecipitation method<sup>9</sup>. Each polymer (10 mg) was dissolved in chloroform (1 mL) and the solution added dropwise to deionised water (10 mL) under vigorous stirring. The dispersions were stirred overnight and examined to ensure there was no visible organic phase. All nanoparticle dispersions were made at a concentration of 1 mgmL<sup>-1</sup>.

#### **5.2.4. Preparation of Doxorubicin (Dox) Free-Base**

Dox hydrochloride (2.00 mg, 3.67  $\mu\text{mol}$ ) was added to a solution of triethylamine (20  $\mu\text{L}$ , 55  $\mu\text{mol}$ ) in anhydrous chloroform (3 mL). The solution was isolated from light and stirred at room temperature for 4 hours.

#### **5.2.5. Preparation of Dox-loaded Nanoparticles**

Polymers 2, 3, 4 and 5 (10 mg) were each dissolved in chloroform (1 mL). Doxorubicin was then encapsulated within the nanoparticles of each respective polymer as follows: the respective polymer solutions and dox-free base solution (2 mg  $\text{mL}^{-1}$ , 3.67  $\mu\text{mol}$ ) were added simultaneously, in a dropwise fashion, to vigorously stirring PBS buffer solution (pH 7.4, 10 mL). The nanoparticles were dialysed (2000 Da M.W.C.O.) for one week to remove excess, free doxorubicin.

#### **5.2.6. pH-Mediated Release of Doxorubicin from Dox-Loaded Nanoparticles**

The dox-loaded nanoparticle solutions were split into two equal portions by volume and decanted into fresh dialysis tubing (2000 Da M.W.C.O.). One dox-loaded nanoparticle dispersion was then dialysed (M.W.C.O. 2000 Da) against an acetate buffer (pH 5.0) solution, whilst the other was dialysed (M.W.C.O. 2000 Da) against fresh PBS buffer solution (pH 7.4). The vessels were incubated in the dark under constant agitation at 37°C. At predetermined intervals, 1 mL aliquots were removed from the dialysate and analysed by UV-vis spectrophotometry. The amount of dox released at each time point was quantified by UV-vis spectrophotometry using a prepared standard calibration curve (appendix VI). The release from the nanoparticles was studied over the course of 194 hours.

### **5.3. Results and Discussion**

#### **5.3.1. Synthesis of 2,5-Diketopiperazines**

The DKPs of glycine, L-alanine and L-phenylalanine were synthesised by heating the respective amino acid in glycerol or ethylene glycol as reported in section 3.1. to 3.4. They were obtained as off-white crystals and their successful syntheses were confirmed by FTIR spectroscopy (appendix I),  $^1\text{H}$  NMR spectroscopy (appendix II), and LC-MS (appendix III). These DKPs were selected based upon their successful polymerisation to form homopolymers reported in Chapter

4. Additionally, the respective polymers of these DKPs are hydrophobic and, as such, would function well as the hydrophobic block of an amphiphilic block copolymer.

### 5.3.2. Synthesis of PEG-*b*-Poly(amino acid) Copolymers

PEG is a hydrophilic and charge-neutral polymer that is ubiquitous within the commercial and biomedical industries, and beyond. It is a polyether comprised of ethylene oxide repeat units and its use in formulations is effective in increasing half-life, reducing immunogenicity and improving stability of biological molecules and therapeutics<sup>19</sup>. Due to its common use, PEG can be purchased at several molecular weights and with a variety of end-group functionality. However, larger PEG chains ( $>10,000 \text{ g mol}^{-1}$ ) are poorly metabolised within the body and build up in the kidneys.<sup>20</sup> PEG has been reliably used as a macroinitiator for the ROP of a collection of cyclic monomers<sup>21</sup> and, for these reasons, PEG methyl ether (Average  $M_w = 5000 \text{ g mol}^{-1}$ ) was selected as the macroinitiator for this research.

To determine the extent to which the ROP of DKPs is controlled and able to produce polymer blocks with narrow  $\bar{D}$  from a macroinitiator, as well as to quantify the capability of such polymers to self-assemble to form discrete structures, each monomer was polymerised from PEG methyl ether (Average  $M_w = 5000 \text{ g mol}^{-1}$ ) using tin(II) 2-ethylhexanoate as an FDA-approved catalyst<sup>22</sup>. The rate of ROP using tin(II) 2-ethylhexanoate as a catalyst is maximised at  $130^\circ\text{C}$ <sup>23</sup>. As such, these polymerisations were all conducted at  $130^\circ\text{C}$ . Polymer blocks of alanine<sup>24</sup> and phenylalanine<sup>25</sup> have been utilised successfully as the hydrophobic component of an amphiphilic block copolymer due to their hydrophobicity and capacity to hydrogen bond intermolecularly. As such, the resultant PEG-*b*-poly(amino acid) polymers of glycine, alanine and phenylalanine should have sufficient amphiphilicity and hydrogen bonding to self-assemble to form nanostructures in aqueous solution.

A key target application of these materials is their self-assembly into nanoparticles that are capable of encapsulating and then releasing of chemotherapeutic molecules in response to an acidic stimulus. Using PEG that bears a terminal alcohol group as a macro-initiator results in the two blocks formed to be bound by an acid-sensitive ester linkage, designed to act as an actuator for acid-induced nanoparticle disassembly and payload release.

Polymers 1, 2 and 3 (Table 5.1.) were characterised using FTIR spectroscopy (appendix I) and  $^1\text{H}$  NMR spectroscopy (Figure 5.1.). Both the  $\text{CH}_2$  of polyglycine and the  $\text{CH}_2$  of PEG come to resonance at  $\sim 3.65 \text{ ppm}$  in the  $^1\text{H}$  NMR spectrum. By comparing the integration of this peak in the  $^1\text{H}$  NMR spectrum of unreacted PEG to that of the peak in the product polymer spectra, the

integration of the CH<sub>2</sub> peak in the PGly block of the product and consequently, the number of repeat units of the PGly block as well as the percentage monomer conversion of the polymerisation can be obtained.

The terminal methyl group of PEG methyl ether comes to resonance at 3.37 ppm; this was used as the reference peak with an integral of 3 in the <sup>1</sup>H NMR spectra of PEG and PEG-*b*-poly(amino acid) copolymers to obtain accurate integrals. After calibrating the integrals of the peaks in the spectrum to the reference peak, the main peak of PEG at ~3.6 ppm has an integral of 450. This agrees with the number of protons expected in 112 repeat units of PEG with an average molecular weight of 5000 g mol<sup>-1</sup>. Using this methodology, the integration of the peak corresponding to the PGly block of polymer 1 was found to be 62, signifying 31 repeat units and 31% monomer conversion. Advanced polymer chromatography (APC), a form of size exclusion chromatography, was utilised (Figure 5.2.) to reveal a distribution M<sub>n</sub> of polymer 1 as 6524 g mol<sup>-1</sup> and M<sub>w</sub> as 6794 g mol<sup>-1</sup>, resulting in a narrow Đ of 1.041 and shows good agreement with the <sup>1</sup>H NMR spectrum. Polymers 2 and 3 (Table 5.1.) were characterised in the same fashion, showing 14 and 20 repeat units of the PGly block for polymers 2 and 3 respectively. Therefore, both of these polymerisations had 100% monomer conversion. APC was utilised to obtain molecular weight values that showed good agreement with those determined by NMR spectroscopy, giving M<sub>n</sub> of 5626 g mol<sup>-1</sup> and M<sub>w</sub> of 5832 g mol<sup>-1</sup> with a narrow Đ of 1.037 for polymer 2 and M<sub>n</sub> of 6085 g mol<sup>-1</sup> and M<sub>w</sub> of 6231 g mol<sup>-1</sup> with a narrow Đ of 1.024 for polymer 3.

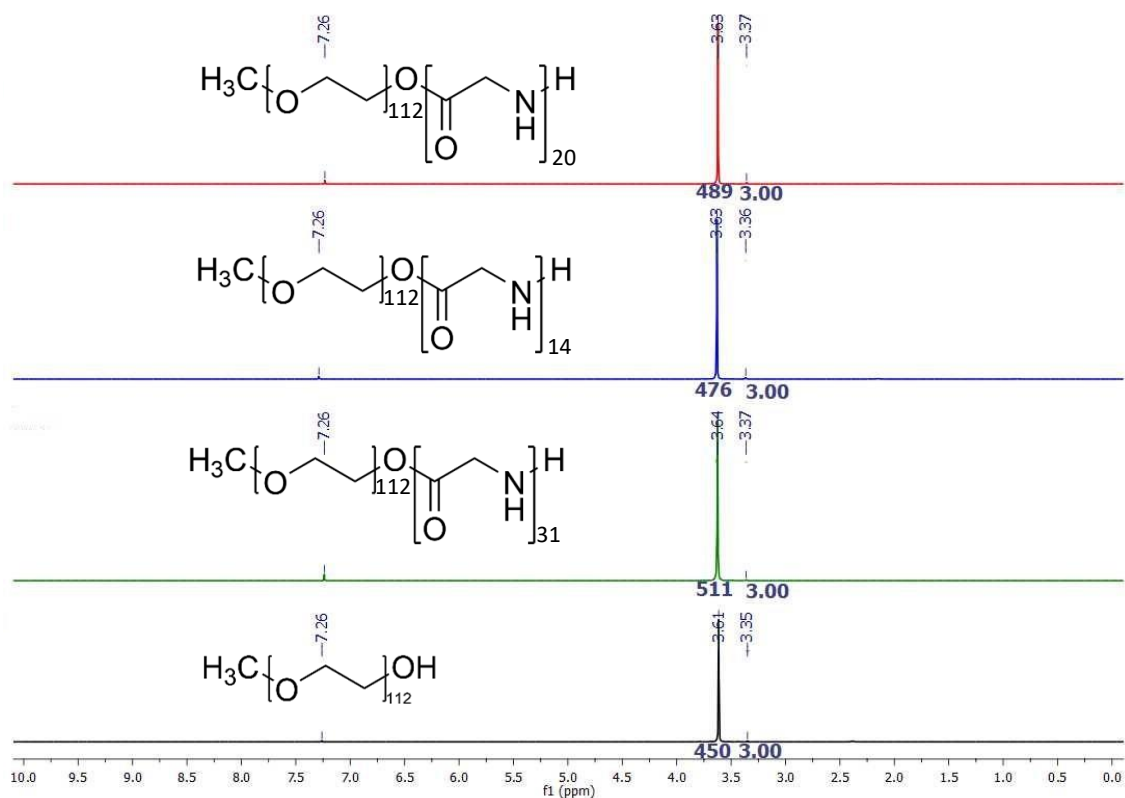


Figure 5.1.  $^1\text{H}$  NMR ( $\text{CDCl}_3$ , 400 MHz) spectra of PEG methyl ether (Average  $M_w = 5000 \text{ g mol}^{-1}$ ) (black), polymer 1, PEG<sub>5000</sub>-*b*-PGly<sub>31</sub> (green), polymer 2, PEG<sub>5000</sub>-*b*-PGly<sub>14</sub> (blue) and polymer 3, PEG<sub>5000</sub>-*b*-PGly<sub>20</sub> (red).

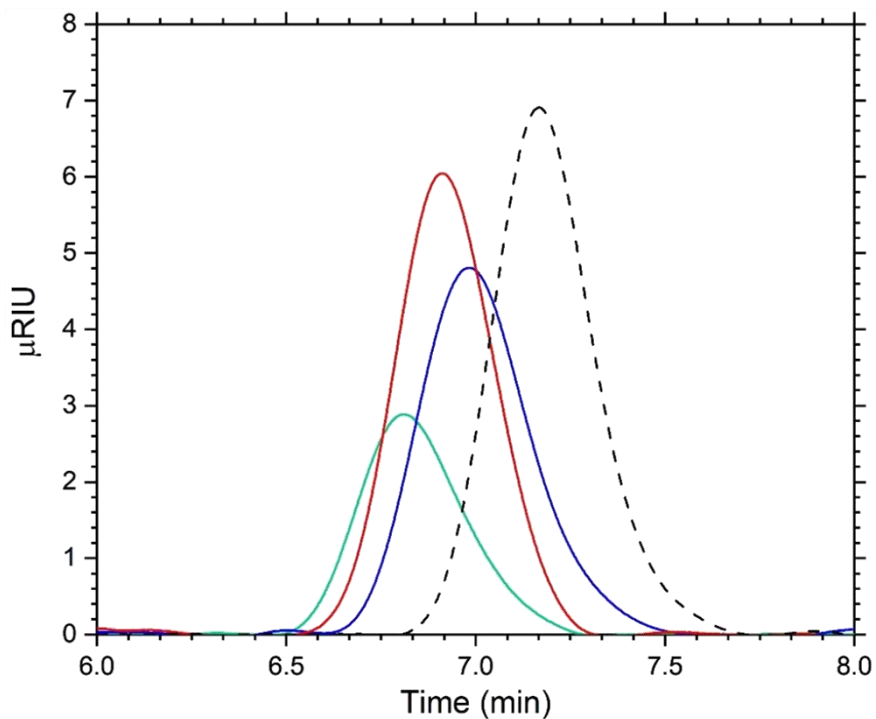


Figure 5.2. – APC chromatograms of PEG<sub>5000</sub>-OH (black, dashed), polymer 1, PEG<sub>5000</sub>-*b*-PGly<sub>31</sub> (green), polymer 2, PEG<sub>5000</sub>-*b*-PGly<sub>14</sub> (blue) and polymer 3, PEG<sub>5000</sub>-*b*-PGly<sub>20</sub> (red).



Polymers 4 and 5 (Table 5.1.) were synthesised via the ROP of alanine DKP from PEG methyl ether (Average  $M_w = 5000 \text{ g mol}^{-1}$ ), forming PEG-*b*-polyalanine. Polymers 4 and 5 were characterised using FTIR spectroscopy (appendix I),  $^1\text{H}$  NMR spectroscopy (Figure 5.3.) and APC (Figure 5.4.). The  $\text{CH}_3$  of polyalanine comes to resonance in a  $^1\text{H}$  NMR spectrum at  $\sim 1.9 \text{ ppm}$ , whereas the  $\text{CH}$  of polyalanine comes to resonance at 4.14 - 4.23 ppm. Accurate integrals of these peaks can be obtained by comparison to that of the reference peak (terminal  $\text{CH}_3$  of PEG) at  $\sim 3.33 \text{ ppm}$ . Integrals of the peaks at 1.45 – 1.50 ppm and 4.14 - 4.23 ppm revealed that the number of repeat units of the polyalanine block for polymers 4 and 5 as 6 and 14 repeat units respectively. Therefore, the polymerisations had percentage monomer conversions of 30% and 17.5% respectively. MALDI-TOF was utilised to obtain molecular weight values of polymers 4 and 5. For polymer 4,  $M_n = 5229 \text{ g mol}^{-1}$  and  $M_w = 5286 \text{ g mol}^{-1}$  with a narrow  $\text{Đ}$  of 1.011. For polymer 5,  $M_n = 5297 \text{ g mol}^{-1}$  and  $M_w = 5400 \text{ g mol}^{-1}$  with a narrow  $\text{Đ}$  of 1.020. Whilst the % monomer conversions of these polymerisations are poor, a low number of alanine repeat units has been demonstrated to provide sufficient non-covalent interactions to drive self-assembly in aqueous solution<sup>26</sup> and the extremely low  $\text{Đ}$  further increases the probability of self-assembly.

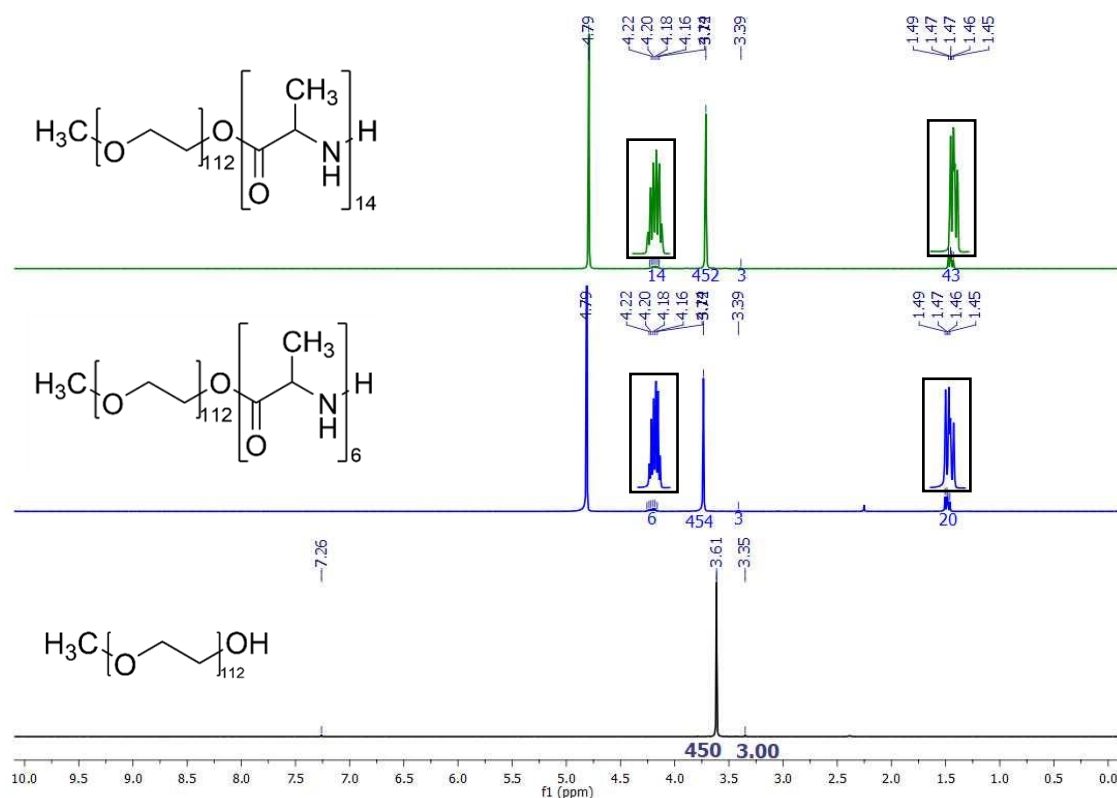


Figure 5.3. -  $^1\text{H}$  NMR spectra of PEG methyl ether (Average  $M_w = 5000 \text{ g mol}^{-1}$ ) (black,  $\text{CDCl}_3$ , 500 MHz), polymer 4, PEG<sub>5000</sub>-*b*-PAla<sub>6</sub> (blue,  $\text{D}_2\text{O}$ , 500 MHz) and polymer 5, PEG<sub>5000</sub>-*b*-PAla<sub>14</sub> (green,  $\text{D}_2\text{O}$ , 500 MHz).

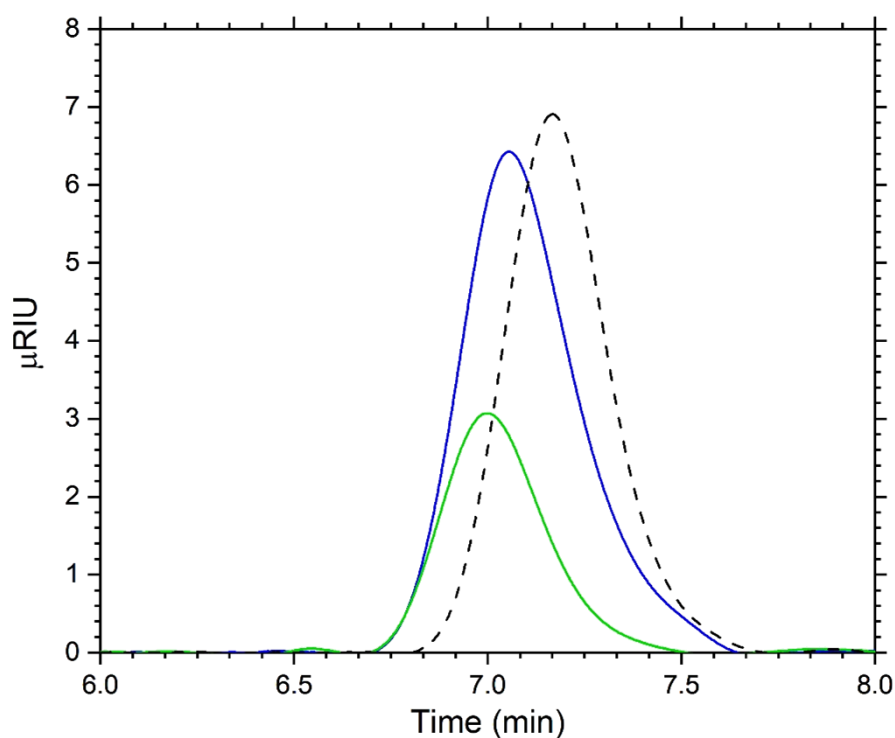


Figure 5.4. – APC chromatogram of PEG<sub>5000</sub>-OH (black, dashed), polymer 4, PEG<sub>5000</sub>-*b*-PAla<sub>6</sub> (blue) and polymer 5, PEG<sub>5000</sub>-*b*-PAla<sub>14</sub> (green).

Polymer 6 (Table 5.1.) was synthesised via the ROP of phenylalanine DKP initiated by PEG methyl ether (Average  $M_w = 5000 \text{ g mol}^{-1}$ ), and characterised using FTIR spectroscopy (appendix I),  $^1\text{H}$  NMR spectroscopy (Figure 5.5.) and APC (Figure 5.6.). Polyphenylalanine is very hydrophobic and, additional to extensive hydrogen bonding, boasts intermolecular  $\pi$ - $\pi$  interactions that further facilitate self-assembly when part of an amphiphilic block copolymer. Due to the phenyl R group of phenylalanine, there are several chemical environments of the PPhe block observable in the  $^1\text{H}$  NMR spectrum that can be used to quantify the number of repeat units. The five aromatic CH environments come to resonance between 7.29 – 7.03 ppm, as well as the  $\text{CH}_2$  environment that comes to resonance at 3.00 ppm and 2.71 ppm. By calibrating the integrals of the peaks in the  $^1\text{H}$  NMR spectrum to the terminal methyl peak of PEG, the number of repeat units of the PPhe block was revealed to be 25. Therefore, the polymerisation had 83.3% monomer conversion. APC was utilised to obtain  $M_n$  as  $8253 \text{ g mol}^{-1}$  and  $M_w$  as  $8634 \text{ g mol}^{-1}$  with a narrow  $\mathcal{D}$  of 1.046 for polymer 6, which shows good agreement with the values determined by NMR spectroscopy.

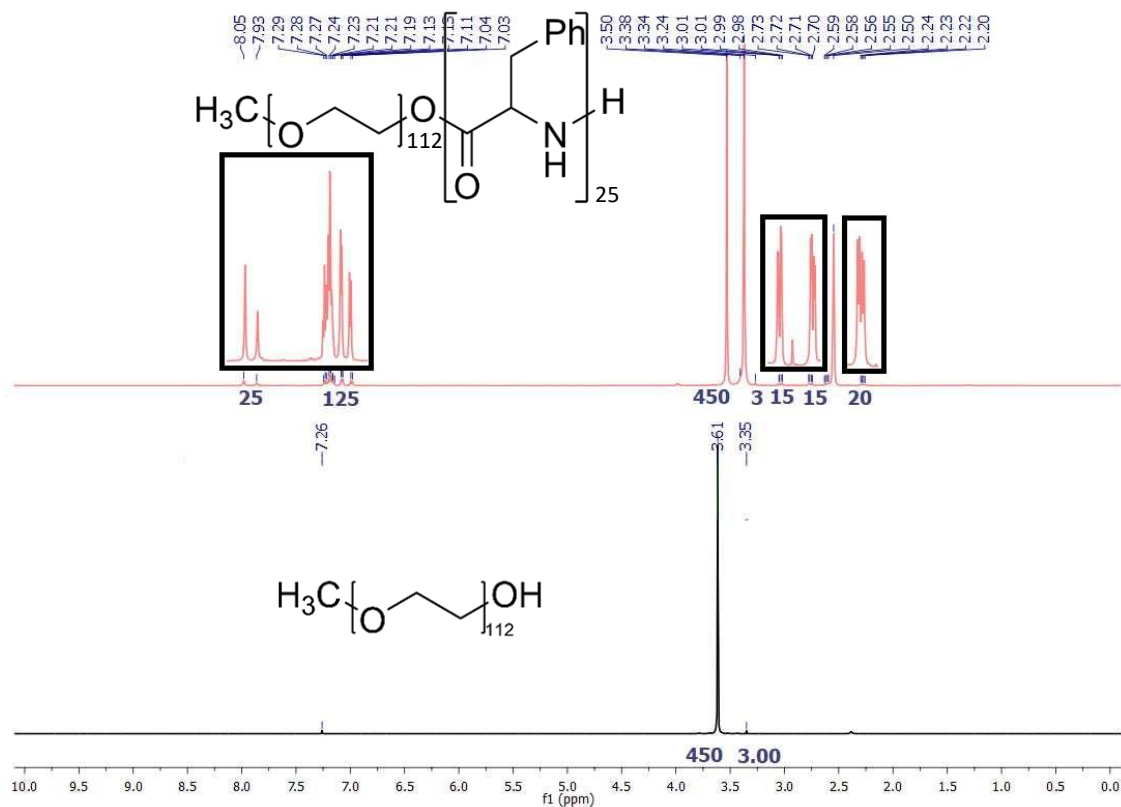


Figure 5.5. -  $^1\text{H}$  NMR of PEG methyl ether (Average  $M_w = 5000 \text{ g mol}^{-1}$ ) (black,  $\text{CDCl}_3$ , 400 MHz) and polymer 6,  $\text{PEG}_{5000}\text{-}b\text{-PPhe}_{25}$  (red,  $\text{DMSO-d}_6$ , 400 MHz).

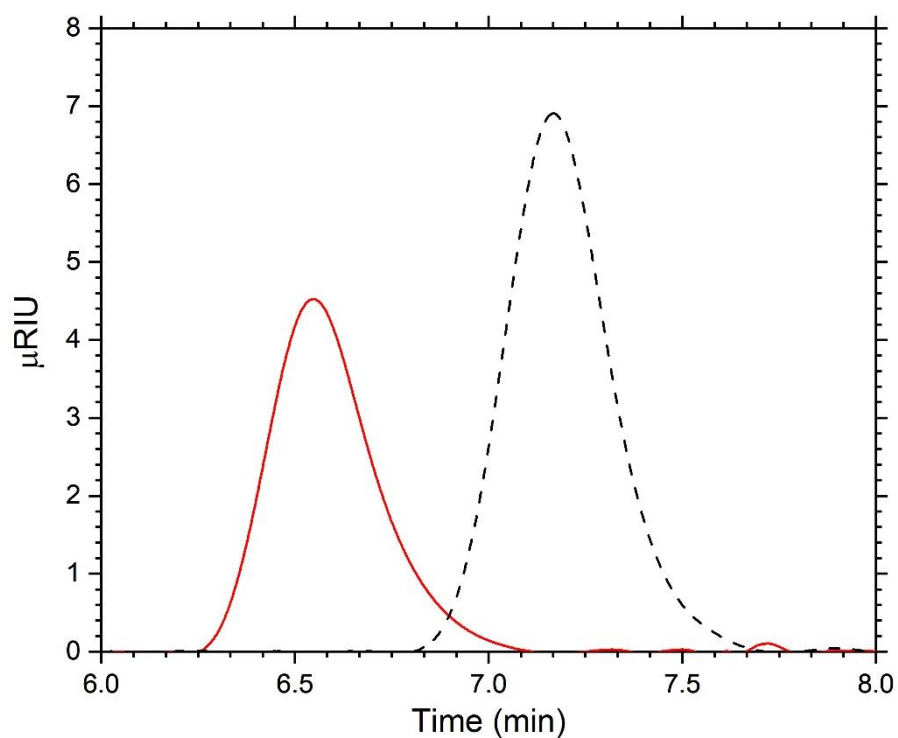


Figure 5.6. – APC chromatogram of  $\text{PEG}_{5000}\text{-OH}$  (black, dashed) and polymer 6,  $\text{PEG}_{5000}\text{-}b\text{-PPhe}_{25}$  (red).

The results obtained show that DKP polymerisation is a viable method to create poly(amino acids) blocks from an alcohol-bearing macroinitiator. The versatility of the polymerisation enables the creation of amphiphilic block copolymers, in this instance PEG methyl ether was used as the macro-initiator for DKP polymerisation. Such polymers have great potential to form nanoparticles due to amphiphilicity owing to the hydrophilic PEG block and hydrophobic poly(amino acid) block. Such nanoparticles may have the capacity to encapsulate hydrophobic therapeutics and, due to the ester linkage between the two blocks, may be sensitive to acidic conditions and therefore capable of acid-triggered payload release.

### **5.3.3. Formation of PEG-*b*-Poly(amino acid) Nanoparticles**

In order to function as a drug delivery vehicle, the nanoparticles formed by the self-assembly of the produced PEG-*b*-poly(amino acids) must demonstrate stability in aqueous solution. As such, the capability of the block copolymers to self-assemble upon nanoprecipitation in aqueous medium was assessed using dynamic light scattering (DLS) and scanning electron microscopy (SEM). The nanoparticles were produced via the dropping-in method<sup>27</sup>; this involved dissolving the polymer in a volatile organic solvent (chloroform) and adding dropwise to a rapidly stirring aqueous medium (PBS buffer solution). The subsequent evaporation of the organic solvent yields a nanoparticle dispersion via a reliable and straightforward method. All six block copolymers were capable of self-assembly to form nanoparticles in aqueous solution at 1 mg mL<sup>-1</sup> polymer concentration (Table 5.3.).

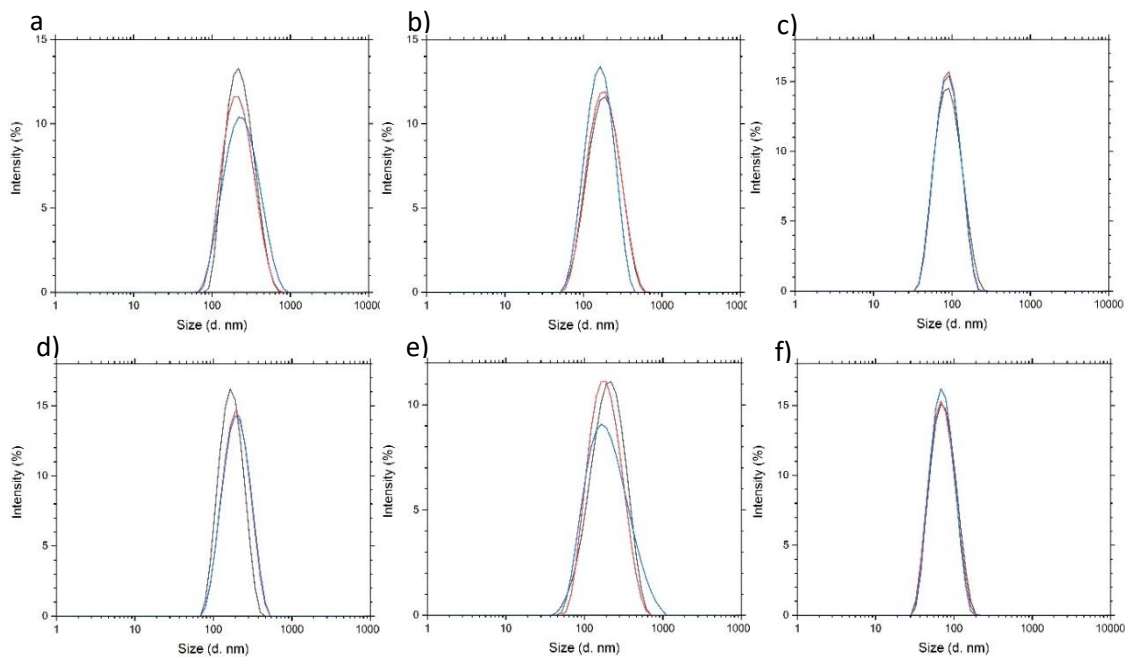


Figure 5.7. - DLS traces, taken in triplicate, of nanoparticle dispersions of a) polymer 1, PEG-*b*-PGly<sub>31</sub>, b) polymer 2, PEG-*b*-PGly<sub>14</sub>, c) polymer 3, PEG-*b*-PGly<sub>20</sub>, d) polymer 4, PEG-*b*-PAla<sub>6</sub>, e) polymer 5, PEG-*b*-PAla<sub>14</sub> and f) polymer 6, PEG-*b*-PPhe<sub>25</sub>.

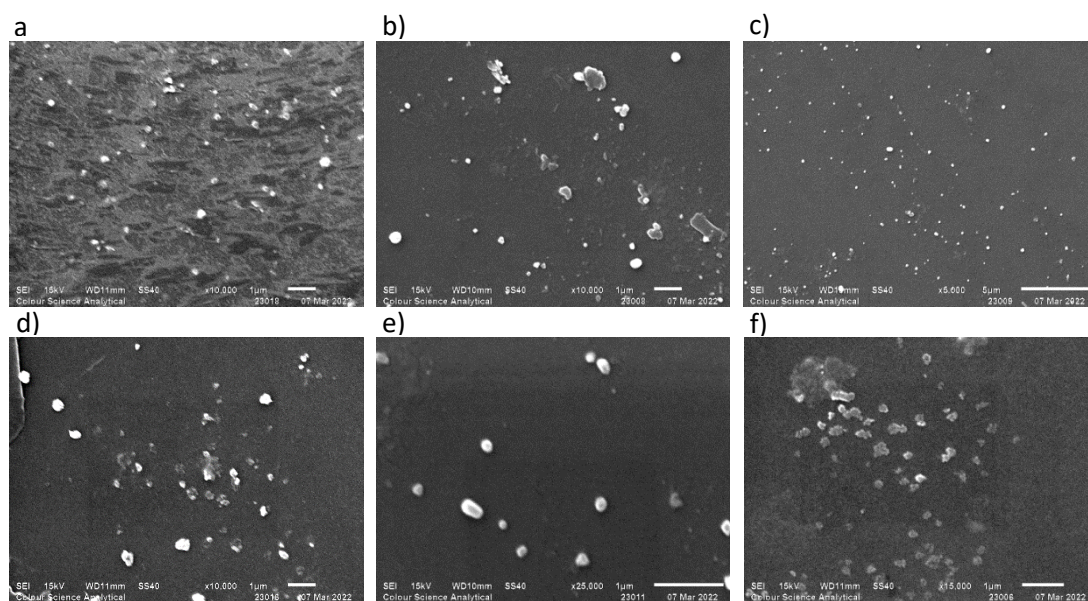


Figure 5.8. - SEM images representative of nanoparticle dispersions of a) polymer 1, PEG-*b*-PGly<sub>31</sub> with 1  $\mu\text{m}$  scale bar, b) polymer 2, PEG-*b*-PGly<sub>14</sub> with 1  $\mu\text{m}$  scale bar, c) polymer 3, PEG-*b*-PGly<sub>20</sub> with 5  $\mu\text{m}$  scale bar, d) polymer 4, PEG-*b*-PAla<sub>6</sub> with 1  $\mu\text{m}$  scale bar, e) polymer 5, PEG-*b*-PAla<sub>14</sub> with 1  $\mu\text{m}$  scale bar and f) polymer 6, PEG-*b*-PPhe<sub>25</sub> with 1  $\mu\text{m}$  scale bar.

The diameters of the nanoparticles shown in the SEM images were measured using ImageJ to obtain an average particle size and polydispersity of each nanoparticle dispersion. For each

sample, a minimum of 100 diameter values were measured. Where there were fewer than 100 nanoparticles in a single image, a minimum of 35 measurements were taken. The polydispersity values from the SEM measurements were calculated as follows:

$$\text{polydispersity} = \frac{\sigma^2}{d_{av}^2}$$

Where  $\sigma$  = standard deviation of nanoparticle diameter and  $d_{av}$  = average nanoparticle diameter. The results of these calculations, along with those obtained using DLS, are shown in Table 5.3.

*Table 5.3.* - Mean particle size and polydispersity values of polymers 4-9. Values obtained by DLS and SEM analyses.

	Formula	DLS measurements		SEM measurements	
		Particle Size (d.nm)	Polydispersity	Particle Size (d.nm)	Polydispersity
1	PEG <sub>112</sub> - <i>b</i> -PGly <sub>31</sub>	210	0.22	176	0.24
2	PEG <sub>112</sub> - <i>b</i> -PGly <sub>14</sub>	181	0.20	185	0.19
3	PEG <sub>112</sub> - <i>b</i> -PGly <sub>20</sub>	91	0.17	97	0.22
4	PEG <sub>112</sub> - <i>b</i> -PAla <sub>6</sub>	189	0.19	206	0.23
5	PEG <sub>112</sub> - <i>b</i> -PAla <sub>14</sub>	182	0.24	188	0.17
6	PEG <sub>112</sub> - <i>b</i> -PPhe <sub>25</sub>	69	0.13	83	0.18

For all nanoparticles, DLS and SEM analyses showed reasonable agreement for respective nanoparticle dispersions. Critically, nanoparticles had polydispersity values below the threshold of 0.3 for a monodisperse sample, indicating nanoparticle stability in aqueous solution and suggesting the possibility of long-term storage. Based on their dimensions, nanoparticles of polymer 1 may be applicable for intravenous/intramuscular administration, whilst nanoparticles of polymers 1, 2, 4 and 5 have the potential for ocular application (Table 1.2.)<sup>13</sup>. Crucially, nanoparticles of all the amphiphilic block copolymers, except for polymer 1, are applicable as long-circulating carriers to tumour site<sup>13</sup>. Due to an average particle size of less than 100 nm, nanoparticles of polymers 3 and 6 may have the capacity to cross the blood-brain barrier and consequently applicable as a therapeutic for brain tumours<sup>28</sup>. These results illustrate the controlled nature of this novel polymerisation route and its capability to produce amphiphilic polymers with narrow  $\Delta$  that are able to self-assemble to form discrete nanoparticles.

#### 5.3.4. Drug Release Studies from PEG-*b*-Poly(amino acid) Nanoparticle Dispersions

In preparation of dox-loaded PEG-*b*-poly(amino acid) nanoparticle dispersions, dox hydrochloride was converted to dox free-base by stirring with trimethylamine. Dox hydrochloride is water-soluble whereas dox free-base is not soluble in water or any aqueous solution<sup>29</sup>. As such, dox free-base requires encapsulation to dissolve or even suspend in aqueous conditions and is readily encapsulated during nanoprecipitation.

Nanoparticles formed from polymers 2, 3, 4 and 5 were assessed for their capacity to encapsulate doxorubicin free-base, and subsequently release the chemotherapeutic doxorubicin under acidic conditions that are associated with the endosomes of cells. After nanoprecipitation and one week of dialysis of the four nanoparticle dispersions, the dialysates of each dispersion were analysed using UV-vis spectrophotometry and the absorption at 500 nm (corresponding to doxorubicin content) was converted using a calibration curve to produce a concentration of doxorubicin in solution and subsequently a mass of dox that was not encapsulated. For the dox-loaded nanoparticle dispersions of polymers 2, 3, 4 and 5, the amount of dox that was not encapsulated was 0.16 mg, 0.1 mg, 0.26 mg and 0.16 mg respectively. Consequently, the nanoparticles of polymers 2, 3, 4 and 5 had a drug encapsulation efficiency of 92±3wt%, 95±1wt%, 87±6wt% and 92±5wt% respectively and a drug loading content of 15.5±0.5wt%, 16.0±0.1wt%, 14.8±0.9wt% and 26.9±1.1wt% respectively. This encapsulation efficiency compares very favourably with current poly(amino acid)-based nanoparticles<sup>12,15</sup>.

When compared to extracellular pH of healthy tissues and blood at pH 7.4, the extracellular pH of most solid tumours is lower, ranging from pH 6.5 to 7.2. The drop in pH is exaggerated within cancerous cells, where endosomal pH ranges from 5.0 to 6.0 and lysosomal pH 4.0 to 5.0. Nanoparticles may enter these environments via endocytosis. The pH gradient within cancerous cells is caused by hypoxia which increases the rate of glycolysis. This results in an increase in production of lactate and protons in extracellular microenvironments.<sup>14</sup> Each polymer synthesised in this research contains an ester linkage between the PEG block and the poly(amino acid) block which may be cleavable by acid-catalysed hydrolysis. Therefore, acidic conditions serve as an appropriate and plausible trigger for the evaluation of these nanoparticle dispersions as drug delivery vehicles for anti-cancer therapy. As such, the dox-loaded nanoparticle dispersions were each split into two equal portions by volume, where one portion of each was incubated in a pH 5 acetate buffer solution to closely mimic cancerous endosomal pH and the other incubated in a pH 7.4 phosphate-buffered saline solution as a control to mimic physiological fluid.

The release of doxorubicin from the loaded nanoparticles was then assessed against aqueous solutions of pH 5.0 and pH 7.4, with the latter used to simulate physiological fluid. A temperature of 37.0°C was maintained to further simulate physiological conditions.

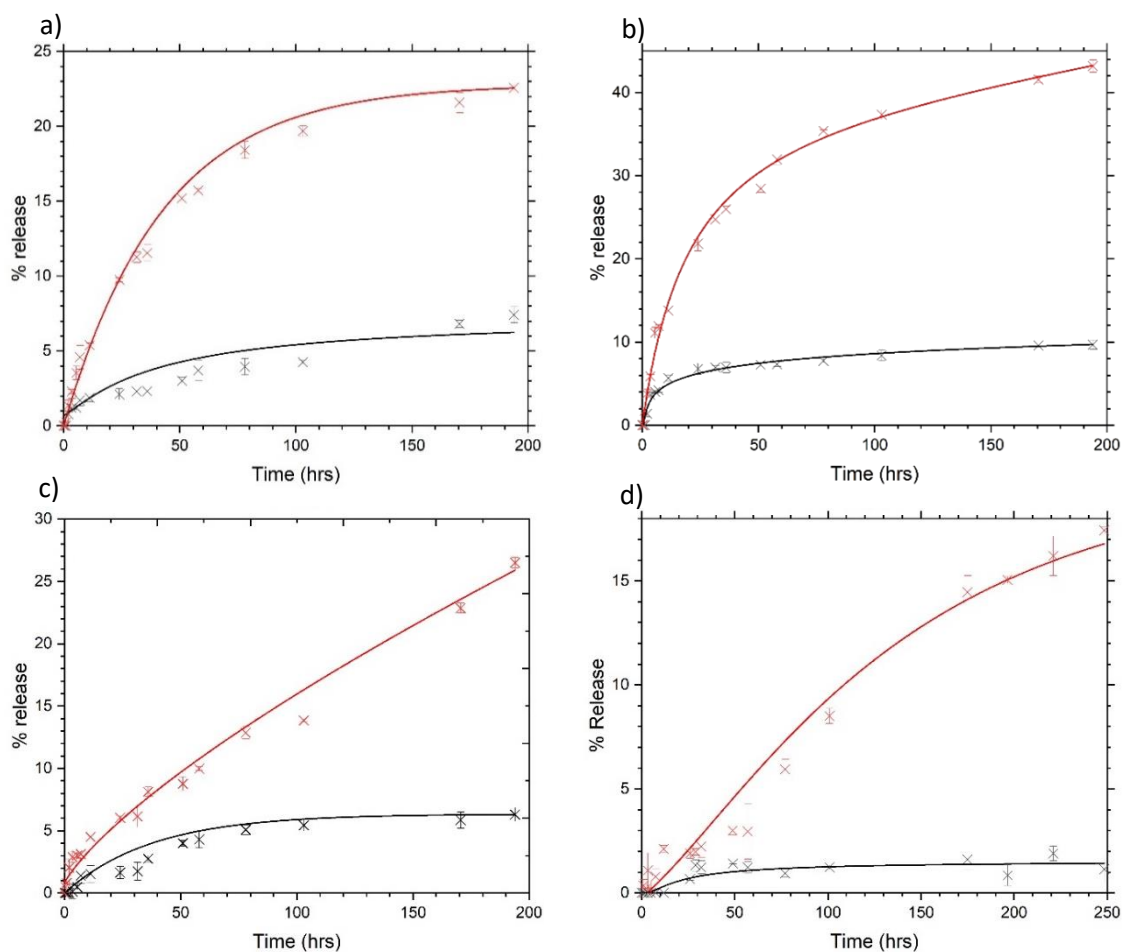


Figure 5.9. - Release of doxorubicin from nanoparticles of a) polymer 2, PEG<sub>112</sub>-*b*-PGly<sub>14</sub>, b) polymer 3, PEG<sub>112</sub>-*b*-PGly<sub>20</sub>, c) polymer 4, PEG<sub>112</sub>-*b*-PALa<sub>6</sub> and d) polymer 5, PEG<sub>112</sub>-*b*-PALa<sub>14</sub>, in response to incubation in acetate buffer at pH 5.0 (red) and PBS buffer at pH 7.4 (black).

There was a profound difference in the extent of Dox release to pH 5.0 solution compared to release to pH 7.4 solution (Figure 5.9.). As a consequence of a retention of dox within the dialysis membranes, the obtained values and traces can be taken as a minimum release value for each time point. In all cases a rapid “burst” release of doxorubicin was avoided and crucially, Dox release to pH 7.4 solution was negligible in all cases. The final release of doxorubicin was 3.5, 4.6, 4.2 and 12.4 times more in pH 5.0 than pH 7.4 for nanoparticles of polymers 2, 3, 4 and 5 respectively, demonstrating the sensitivity of the nanoparticles to acidic conditions. For all nanoparticle dispersions, when incubated at pH 7.4, the release did not exceed 10%, demonstrating the lack of leakage and stability of the nanoparticles.



#### 5.4. Conclusions

Poly(amino acid) synthesis by ROP of DKPs has been successfully utilised as an original and straightforward route to PEG-*b*-poly(amino acid) block copolymers. PEG-*b*-poly(amino acid) block copolymers of glycine, alanine and phenylalanine were successfully synthesised to a variety of poly(amino acid) polymer lengths. The observed monomer conversion was variable, with some of the polymerisations achieving high monomer conversions of 100% and others as low as 17.5%. Despite this, all polymerisations resulted in polymers with very narrow  $\bar{M}_w/\bar{M}_n$  and as such compared favourably to similar NCA polymerisations. Furthermore, all polymers produced were capable of self-assembly in aqueous solution to form nanoparticles with average particle sizes and polydispersity that suggest suitability for use as delivery agents in a biomedical setting. The selected nanoparticle dispersions were capable of Dox encapsulation and demonstrated excellent encapsulation efficiency. The nanoparticles showed minimal leakage at pH 7.4 and, crucially, the nanoparticles proved susceptible to acid-mediated release at pH 5, resulting in the acid-triggered release of encapsulated dox free-base from the nanoparticles. The syntheses outlined could serve as a template for controlled poly(amino acid) block copolymer synthesis and nanoparticle production at an industrial scale. With optimisation of the polymerisation to improve % monomer conversion, such as a more potent catalyst system, and maximising the drug loading content of the nanoparticles, the nanoparticles produced pose as a genuine option for effective chemotherapeutic encapsulation and stimulus-targeted release.

## 5.5. References

---

- 1) Ammala, A. Biodegradable polymers as encapsulation materials for cosmetics and personal care products. *International Journal of Cosmetic Science*. 2012, **35**(2), 113-124.
- 2) Lee, B. K., Yun, Y. and Park, K. PLA micro- and nano-particles. *Advanced Drug Delivery Reviews*. 2016, **107**, 176-191.
- 3) Guido, C., Testini, M., D'Amone, S., Cortese, B., Grano, M., Gigli, G. and Palamà, I. E. Capsid-like biodegradable poly-glycolic acid nanoparticles for a long-time release of nucleic acid molecules. *Materials Advances*. 2021, **2**(1), 310-321.
- 4) Witt, S., Scheper, T. and Walter, J-G. Production of polycaprolactone nanoparticles with hydrodynamic diameters below 100 nm. *Engineering in Life Sciences*. 2019, **19**(10), 658-665.
- 5) Boddu, S. H. S., Bhagav, P., Karla, P. K., Jacob, S., Adatiya, M. D., Dhameliya, T. M., Ranch, K. M. and Tiwari, A. K. Polyamide/Poly(Amino Acid) Polymers for Drug Delivery. *Journal of Functional Biomaterials*. 2021, **12**(4), 58-82.
- 6) Adhikari, C. Polymer nanoparticles-preparations, applications and future insights: a concise review. *Polymer-Plastics Technology and Materials*. 2021, **60**(18), 1996-2024.
- 7) Patra, J. K., Das, G., Fraceto, L. F., Campos, E. V. R., Rodriguez-Torres, M. d. P., Acosta-Torres, L. S., Diaz-Torres, L. A., Grillo, R., Swamy, M. K., Sharma, S., Habtemariam, S. and Shin, H-S. Nano based drug delivery systems: recent developments and future prospects. *Journal of Nanobiotechnology*. 2018, **16**, 71-104.
- 8) Li, Q., Li, X. and Zhao, C. Strategies to Obtain Encapsulation and Controlled Release of Small Hydrophilic Molecules. *Frontiers in Bioengineering and Biotechnology*. 2020, **8**, 437-442.
- 9) Khuphe, M, Ingram, N and Thornton, P, D. Exploiting poly( $\alpha$ -hydroxy acids) for the acid-mediated release of doxorubicin and reversible inside-out nanoparticle self-assembly. *Nanoscale*. 2018, **10**(29), 14201-14206.
- 10) Yu, H, Ingram, N, Rowley, J, V, Parkinson, S, Green, D, C, Warren, N, J and Thornton, P, D. Thermoresponsive polysarcosine-based nanoparticles. *Journal of Materials Chemistry B*. 2019, **7**(26), 4217-4223.
- 11) de la Rica, R, Aili, D and Stevens, M, M. Enzyme-responsive nanoparticles for drug release and diagnostics. *Advanced Drug Delivery Reviews*. 2012, **64**(11), 967-978.

- 
- 12) Price, D. J., Khuphe, M., Davies, R. P. W., McLaughlan, J. R., Ingram, N. and Thornton, P. D. Poly(amino acid)-polyester graft copolymer nanoparticles for the acid-mediated release of doxorubicin. *Chemical Communications*. 2017, **53**, 8687-8690.
- 13) Danaei, M., Dehghankhold, M., Ataei, S., Davarani, F. H., Javanmard, R., Dokhani, A., Khorasani, S. and Mozafari, M. R. Impact of Particle Size and Polydispersity Index on the Clinical Applications of Lipidic Nanocarrier Systems. *Pharmaceutics*. 2018, **10**, 57-73.
- 14) Liu, Y., Wang, W., Yang, J., Zhou, C. and Sun, J. pH-sensitive polymeric micelles triggered drug release for extracellular and intracellular drug targeting deliver. *Asian Journal of Pharmaceutical Sciences*. 2013, **8**(3), 159-167.
- 15) Kataoka, K., Matsumoto, T., Yokoyama, M., Okano, T., Sakurai, Y., Fukushima, S., Okamoto, K. and Kwon, G. S. Doxorubicin-loaded poly(ethylene glycol)-poly( $\beta$ -benzyl-L-aspartate) copolymer micelles: their pharmaceutical characteristics and biological significance. *Journal of Controlled Release*. 2000, **64**(1-3), 143-153.
- 16) Pokorna, A., Bobal, P., Oravec, M., Rarova, L., Bobalova, J. and Jampilek, J. Investigation of Permeation of Theophylline through Skin Using Selected Piperazine-2,5-Diones. *Molecules*. 2019, **24**(3), 566-579.
- 17) Manchineella, S., Voshavar, C. and Govindaraju, T. Radical-Scavenging Antioxidant Cyclic Dipeptides and Silk Fibroin Biomaterials. *European Journal of Organic Chemistry*. 2017, **30**, 4363-4369.
- 18) Basiuk, V. A., Gromovoy, T. Y., Chuiko, A. A., Soloshonok, V. A. and Kukhar, V. P. A Novel Approach to the Synthesis of Symmetric Optically Active 2,5-Dioxopiperazines. *Synthesis*. 1992, **5**, 449-451.
- 19) D'Souza, A. A. and Shegokar, R. Polyethylene glycol (PEG): a versatile polymer for pharmaceutical applications. Expert opinion on drug delivery. 2016, **13**(9). 1257-1275.
- 20) Baumann, A., Tuerck, D., Prabhu, S., Dickmann, L. and Sims, J. Pharmacokinetics, metabolism and distribution of PEGs and PEGylated proteins: quo vadis? *Drug Discovery Today*. 2014, **19**(10), 1623-1631.
- 21) Kutikov, A. B. and Song, J. Biodegradable PEG-Based Amphiphilic Block Copolymers for Tissue Engineering Applications. *ACS biomaterials science & engineering*. 2015, **1**(7), 463-480.

- 
- 22) U.S. Food and Drug Administration. CFR – Code of Federal Regulations Title 21. [Online]. 2020. [25/02/21]. Available from: <https://www.accessdata.fda.gov/scripts/cdrh/cfdocs/cfCFR/CFRSearch.cfm?fr=175.300>
- 23) Ryner, M., Stridsberg, K. and Albertsson, A-C. Mechanism of Ring-Opening Polymerisation of 1,5-Dioxepan-2-one and L-Lactide with Stannous 2-Ethylhexanoate. A Theoretical Study. *Macromolecules*. 2001, **34**, 3877-3881.
- 24) Wiradharma, N., Khan, M., Tong, Y. W., Wang, S. and Yang, Y-Y. Self-assembled Cationic Peptide Nanoparticles Capable of Inducing Efficient Gene Expression In Vitro. *Advanced Functional Materials*. 2008, **18**(6), 943-951.
- 25) Ma, J., Zhang, J., Chi, L., Liu, C., Li, Y. and Tian, H. Preparation of poly(glutamic acid) shielding micelles self-assembled from polylysine-*b*-polyphenylalanine for gene and drug codelivery. *Chinese Chemical Letters*. 2020, **31**(6), 1427-1431.
- 26) Buckinx, A-L., Rubens, M., Cameron, N. R., Bakkali-Hassani, C., Sokolova, A. and Junkers, T. The effects of molecular weight dispersity on block copolymer self-assembly. *Polymer Chemistry*. 2022, **13**(23), 3444-3450.
- 27) Schubert, S., Delaney, J. T. and Schubert, U. S. Nanoprecipitation and nanoformulation of polymers: from history to powerful possibilities beyond poly(lactic acid). *Soft Matter*. 2011, **7**(5), 1581-1588.
- 28) Senapati, S., Mahanta, A. K., Kumar, S. and Maiti, P. Controlled drug delivery vehicles for cancer treatment and their performance. *Signal Transduction and Targeted Therapy*. 2018, **3**, article no: 7 [no pagination].
- 29) Yuan, Y., Choi, K., Choi, S-O. and Kim, J. Early stage release control of an anticancer drug by drug-polymer miscibility in a hydrophobic fiber-based drug delivery system. *RSC Advances*. 2018, **8**, 19791-19803.

## Chapter 6 – Ring-Opening Polymerisation of Sarcosine-DKP as a Route to Polysarcosine-Based Enzyme-Sensitive Vehicles and Polysarcolation

### Abstract

Polymers that are water-soluble and charge-neutral are vital within applications involving surfactants and self-assembly. The most prevalent and commercially available is poly(ethylene glycol) which is widely used in consumer goods, as well as bespoke healthcare products. However, its common, and arguably excessive, usage within commercial and biomedical applications has resulted in deleterious side-effects that have compromised its efficacy, increasing the demand for an alternative. Polysarcosine shows promise as an alternative due to water solubility and biocompatibility. Currently, polysarcosine is produced most commonly via the ROP of sarcosine NCA, the synthesis of which typically requires the use of extremely toxic reagents, limiting industrial applicability. Although less hazardous synthetic routes to sarcosine NCA have been proposed, they are compromised by the requirement of more meticulous purification and several reaction steps. Reported in this chapter is the synthesis and novel ROP of sarcosine DKP as a safer, greener and more efficient route to polysarcosine and polysarcosine-based materials. Such materials may be applicable in a wide range of consumer and biomedical applications, including use as enzyme-responsive materials for the controlled release of therapeutic molecules.

### 6.1. Introduction

There are a limited number of polymers known that are water-soluble but charge-neutral; the most prominent and commonly used of these is poly(ethylene glycol) (PEG)<sup>1</sup>. PEG is a popular polymer within commercial and biomedical markets, for use in nanoparticle formation<sup>2</sup> and drug conjugation<sup>3</sup> to enhance therapeutic solubility and pharmacokinetics<sup>2,3</sup>. PEG is also used in cleansing agents<sup>4</sup>, emulsifiers<sup>5</sup>, skin care<sup>6</sup> and humectants<sup>7</sup>. However, there is a significant emergence in the literature of an “anti-PEG” immune response, resulting in accelerated clearance of PEGylated therapeutics<sup>8</sup>. Additionally, PEG has been shown to trigger complement activation, leading to hypersensitivity reactions, also known as complement activation-related pseudo-allergy (CARPA)<sup>9</sup>. Moreover, larger PEG chains, 10,000 g mol<sup>-1</sup> and greater, are poorly metabolised within the body and, consequently, accumulate in the kidneys and can result in kidney damage<sup>10</sup>. As such, an alternative to PEG that boasts enhanced biodegradability and biocompatibility is in demand.

A polymer that shows promise as an alternative to PEG is polysarcosine<sup>11</sup> (PSar); a peptoid comprised of a repeating glycine structure with a methyl group attached to the nitrogen atom. PSar has excellent biocompatibility and biodegradation via oxidative degradation<sup>12</sup>, as well as the capacity to form random coils in aqueous solution<sup>13</sup>. As a consequence of the methyl group attached to the nitrogen, polysarcosine has no H-donor site for hydrogen bonding, which impedes interactions between polymer chains. However, due to the H-acceptor oxygen, interaction with water is favourable, resulting in water solubility<sup>14</sup>. Therefore, polysarcosine shows applicability as part of an amphiphilic block copolymer to form nanoparticles for controlled release<sup>15</sup>, or as the polymeric component of a prodrug to improve the pharmacokinetic profile of a drug<sup>16</sup>.

PSar can be produced via solid state peptide synthesis<sup>17</sup>, which has its own limitations and drawbacks<sup>18</sup>, or more commonly by the ROP of sarcosine NCA<sup>19</sup>, which is typically synthesised using phosgene or its liquid or crystalline derivatives<sup>20</sup>. However, phosgene is a highly toxic, gaseous reagent, with an incredibly low lethal concentration<sup>21</sup>. As such, the industrial use of polysarcosine is limited due to the cost and hazardous nature of its production.

Whilst the phosgene-free syntheses of NCAs have been attempted, they are compromised by requiring several reaction steps as well as meticulous purification<sup>22,23</sup>. Specifically, Endo and Sudo<sup>24</sup> avoid the use of phosgene by converting the respective amino acid into its urethane derivative using diphenyl carbonate, a much less hazardous analogue of phosgene. The urethane is then cyclised into the N-carboxyanhydride which can then be ring-opening polymerised. Despite the phosgene-free nature, the increase in number of synthetic steps, as well as the resultant purification required, increases the cost of production via this route<sup>24</sup>. Furthermore, whilst this method may be suitable for the creation of sarcosine NCA, it has not been demonstrated as of yet.

A recently proposed route to NCA synthesis that could be utilised for sarcosine NCA production, in the absence of phosgene, is by the conversion of a Boc-protected amino acid using T3P. The reaction is activated by the opening of T3P using heat or basic conditions. The linear T3P esterifies the exposed carboxylic acid of the amino acid, providing an excellent leaving group. After cleavage of the Boc and T3P groups, the exposed amino acid can cyclise, yielding the desired NCA and a collection of side products. This route promises to be a reasonable method to produce NCAs on small or large scales. However, it is in early stages of development and currently requires substantial purification to remove the side products.<sup>25</sup> Whilst T3P is cheaper

and less hazardous than phosgene, its required involvement in this synthetic route increases the cost of production.

The ROP of DKPs offers an alternative route to poly(amino acid) synthesis that avoids the use of coupling agents or cyclising agents such as triphosgene. Specifically, DKP ROP may be exploited for the creation of polysarcosine in a highly safe and cost-effective manner for the first time. Sarcosine DKP is a cyclic dipeptoid formed via the direct bis-condensation of two sarcosine molecules. It can be synthesised by heating at 175 °C in glycerol, which is both simple and environmentally benign.

Whilst sarcosine DKP has not been ring-opening polymerised, glycine DKP, alanine DKP, phenylalanine DKP and lysine(Cbz) DKP have been successfully polymerised, both from a small molecule (Chapter 4) and PEG (Chapter 5) using tin(II) 2-ethylhexanoate as a Lewis acid catalyst. However, in the case of sarcosine DKP, a more potent catalyst system may be required to open the stable tertiary lactam bond.

PSar may be used as the hydrophilic component of an amphiphilic block copolymer that is susceptible to hydrolysis by a target enzyme. Such enzyme-sensitive materials may be used in various biomedical applications due to their response to a specific, target enzyme<sup>26</sup>. Enzyme specificity may be exploited for the highly-controlled release of therapeutic molecules from amphiphilic block copolymer carriers such as drug delivery vehicles<sup>27</sup>. DKP ROP enables the insertion of dipeptides within polymer chains ensuring that the desired amino acids flank the peptide bonds that the enzyme has the capability to cleave. For instance, the ROP of alanine DKP ensures that the resultant chains possess di-alanine segments that are susceptible to hydrolysis by elastase. This feature may be exploited to produce any poly(amino acid) copolymer that possesses elastase sensitivity. The inverse may also be accessed via asymmetric DKP synthesis and subsequent ROP. In theory, asymmetric DKPs can be produced via the combination of two different amino acids and heating in glycerol, the ROP of which may produce a polymer with alternating repeat units. This structure should lack any adjacent repeat units of the same amino acid and consequently, should not degrade in the presence of enzymes that possess specificity to cleave the peptide bond that links identical amino acids.

The green and facile synthesis of sarcosine DKP, and controlled polymerisation to form PSar is reported for the first time. Amphiphilic PSar-*b*-PAla block copolymers were created from polysarcosine macro-initiators, whilst polysarcosine-*ran*-polyalanine random copolymers were created via the random DKP co-ROP of Sar-DKP and Ala-DKP. The latter uniquely presents enzyme sensitivity due to the di-alanine segments that DKP ROP guarantees. Formation of

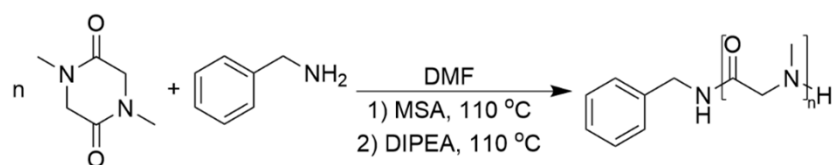
nanoparticles and hydrogels from the PSar-PAla block and random copolymers were achieved, the capability of such materials to encapsulate or absorb a therapeutic respectively and release in the presence of elastase was assessed. A pro-drug system of camptothecin-PSar was also produced and its water solubility quantified, demonstrating polysarculation. Additionally, sarcosine-phenylalanine DKP synthesis and polymerisation was also achieved for the first time, producing an alternating poly(amino acid) structure that shows resistance to enzyme degradation.

## 6.2. Experimental Section

### 6.2.1. Synthesis of 2,5-Diketopiperazines

The DKPs of alanine, sarcosine and sarcosine-phenylalanine were synthesised based upon previously established methods<sup>28,29,30</sup>, the descriptions of their syntheses can be found in Chapter 3.

### 6.2.2. Synthesis of Polysarcosine



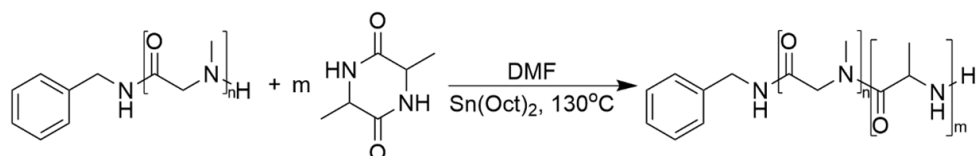
*Scheme 6.1.* - ROP of sarcosine DKP, initiated by benzylamine and catalysed initially by methanesulfonic acid (MSA) and followed by DIPEA catalysis, at 110 °C.

Sarcosine DKP (Table 6.1.) was added to an oven-dried vessel, flushed with  $N_{2(g)}$  and dissolved in anhydrous DMF (5 mL). Benzylamine (Table 6.1.) and methanesulfonic acid (Table 6.1.) were added to separate oven-dried vessels, flushed with  $N_{2(g)}$  and dissolved in anhydrous DMF (2 x 2mL). The benzylamine and methanesulfonic acid solutions were simultaneously added to the sarcosine-DKP solution. The mixture was stirred at 110 °C under constant flow of  $N_{2(g)}$  for up to five days (Table 6.1.), after which the mixture was allowed to cool and a prepared solution of DIPEA (Table 6.1.) in DMF (2 mL) was added. The reaction was restored to 110 °C and stirred under constant flow of  $N_{2(g)}$  for a minimum of two additional days (Table 6.1.). The reaction solution was allowed to cool and PSar precipitated in ice-cold diethyl ether (90 mL). The PSar produced were washed with additional ice-cold diethyl ether (90 mL) to thoroughly remove any



remaining reaction solvent and collected by centrifuge (4500 rpm, 30 s, 0 °C). The solids were then dried in a vacuum oven (50 °C) overnight.

#### 6.2.4. Synthesis of Polysarcosine-*b*-Polyalanine Copolymers



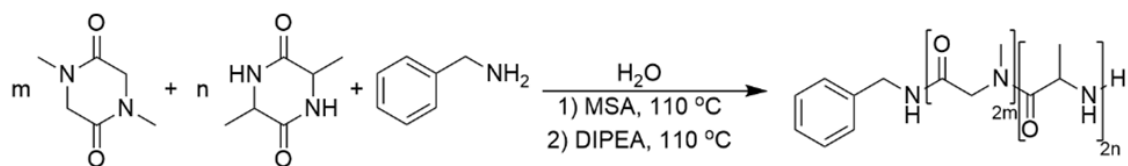
*Scheme 6.2.* - ROP of alanine DKP, initiated by polysarcosine and catalysed using tin(II) 2-ethylhexanoate ( $\text{Sn}(\text{Oct})_2$ ).

Polysarcosine (Table 6.1.) was added to an oven-dried vessel, flushed with  $\text{N}_{2(g)}$  and dissolved in anhydrous DMF (5 mL). In a separate vessel, alanine DKP (Table 6.1.) and tin(II) 2-ethylhexanoate (Table 6.1.) were flushed with  $\text{N}_{2(g)}$  and dissolved in anhydrous DMF (Table 6.1.). This solution was added to the polysarcosine solution and the mixture stirred at 130 °C under constant flow of  $\text{N}_{2(g)}$  for an allotted period of time (Table 6.1.). The mixture was allowed to cool to room temperature and added to ice-cold diethyl ether (90 mL). The precipitate was collected by centrifugation (4500 rpm, 30 s, 0 °C) and washed with additional diethyl ether (90 mL). The solids were then dried in a vacuum oven (50 °C) overnight.

*Table 6.1.* - Reagents, conditions, amounts and results of polymerisations of sarcosine DKP and block co-polymerisations of alanine DKP from polysarcosine.

Polymer	Monomer amount (mmol)	Initiator		Catalyst				Solvent		Temp. (°C)	Reaction time
		Name	Amount (mmol)	Name	Amount (mmol)	Name	Amount (mmol)	Name	Volume (mL)		
1	10.56	Benzylamine	0.264	MSA	0.66	DIPEA	1.32	DMF	10	110	117+142
2	22.02	Benzylamine	0.44	MSA	1.10	DIPEA	2.20	DMF	20	110	93 + 93
3	7.034	Benzylamine	0.141	-	-	DIPEA	0.281	Water	10	80	288
4	5.8	PSar 3	0.0425	-	-	DIPEA	0.281	Water	10	80	528
5	10.55	Benzylamine	0.106	MSA	0.26	DIPEA	0.528	$\text{CHCl}_3$	5	65	91 + 337
6	2.81	Polymer 1	0.0717	$\text{Sn}(\text{Oct})_2$	0.04	-	-	DMF	10	130	115
7	2.12	Polymer 2	0.0708	$\text{Sn}(\text{Oct})_2$	0.07	-	-	DMF	10	130	360
8	0.38	Polymer 5	0.379	$\text{Sn}(\text{Oct})_2$	0.04	-	-	DMF	10	130	142
9	0.76	Polymer 5	0.379	$\text{Sn}(\text{Oct})_2$	0.04	-	-	DMF	10	130	142

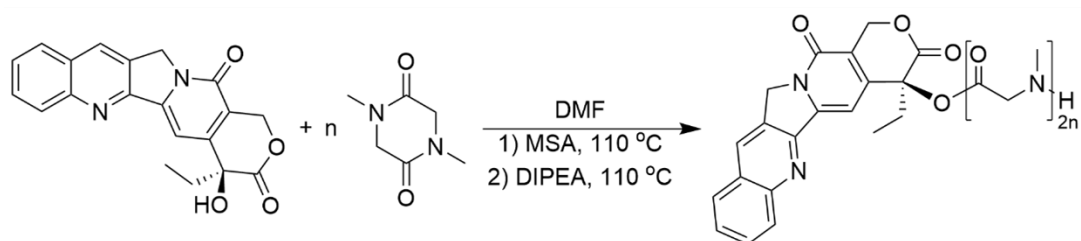
### 6.2.5. Synthesis of Polysarcosine-*ran*-Polyalanine Copolymer



*Scheme 6.3.* - One-pot ROP of a sarcosine DKP and alanine DKP, initiated by benzylamine to produce polysarcosine-*ran*-polyalanine. The polymerisation is initially catalysed using MSA, followed by DIPEA, all of which at 110 °C.

Sarcosine DKP (450 mg, 3.16 mmol) and alanine DKP (50 mg, 0.35 mmol) were added to an oven-dried vessel, flushed with  $\text{N}_{2(\text{g})}$  and dissolved in deionised water (8 mL). Benzylamine (7.6  $\mu\text{L}$ , 0.070 mmol) and methanesulfonic acid (9.1  $\mu\text{L}$ , 0.14 mmol) were added and the mixture was stirred at 80 °C under constant flow of  $\text{N}_{2(\text{g})}$  for 48 hours, after which the mixture was allowed to cool to room temperature and DIPEA (60.8  $\mu\text{L}$ , 0.35 mmol) was added. The reaction was returned to 80 °C and stirred under constant flow of  $\text{N}_{2(\text{g})}$  for a further 120 hours. The reaction solution was allowed to cool to room temperature, frozen using liquid nitrogen and lyophilised, obtaining a solid polymer 10. This polymerisation, targeted 90 repeat of sarcosine and 10 repeat units of alanine within the polymer.

### 6.2.6. Synthesis of Camptothecin-Polysarcosine



*Scheme 6.4.* - ROP of sarcosine DKP from camptothecin, catalysed initially by MSA, followed by DIPEA, all of which at 110 °C.

Sarcosine DKP (400 mg, 2.81 mmol) and MSA (24.4  $\mu\text{L}$ , 0.375 mmol) were added to an oven-dried vessel, sealed, flushed with  $\text{N}_{2(\text{g})}$  and dissolved in anhydrous DMF (5 mL). Separately, camptothecin (65.4 mg, 0.187 mmol) was added to an oven-dried vessel, sealed, flushed with  $\text{N}_{2(\text{g})}$  and dissolved in anhydrous DMF (5 mL). The camptothecin solution was added to the original mixture via needle and syringe. The mixture was stirred at 110 °C under  $\text{N}_{2(\text{g})}$  flow for 44

hours, after which time the reaction was allowed to cool to room temperature. Separately, DIPEA (130.6  $\mu\text{L}$  0.750 mmol) was added to an oven-dried vessel, sealed, flushed with  $\text{N}_{2(\text{g})}$  and dissolved in anhydrous DMF (2 mL). The DIPEA solution added to the reaction mixture via needle and syringe, returned to 110  $^{\circ}\text{C}$  and stirred under  $\text{N}_{2(\text{g})}$  flow for 24 hours. The reaction mixture was allowed to cool and the reaction solution was added dropwise to ice-cold diethyl ether (90 mL). The precipitate was collected by centrifugation (4500 rpm, 0  $^{\circ}\text{C}$ , 30 seconds) and washed with additional ice-cold diethyl ether (50 mL). The solid product was then dried *in vacuo*.

### 6.2.7. Synthesis of Polysarcosine-*alt*-Polyphenylalanine



*Scheme 6.5.* - ROP of sarcosine-L-phenylalanine DKP, initiated by benzylamine and catalysed initially by MSA and followed by the catalysis of DIPEA, at 110  $^{\circ}\text{C}$ .

Sar-Phe DKP (500 mg, 2.29 mmol) and MSA (8.84 mg, 0.092 mmol) were added to an oven-dried vessel and flushed with  $\text{N}_{2(\text{g})}$ . Separately, benzylamine (4.91 mg, 0.046 mmol) was dissolved in anhydrous DMF (10 mL) and added via syringe to the reaction mixture. The solution was stirred at 110  $^{\circ}\text{C}$  under constant flow of  $\text{N}_{2(\text{g})}$  for 47 hours, after which the reaction was allowed to cool to room temperature. DIPEA (23.78 mg, 0.184 mmol) was dissolved in anhydrous DMF (2 mL) and added to the reaction mixture via syringe. The reaction was returned to 110  $^{\circ}\text{C}$  and stirred for a further 122 hours, after which it was cooled to room temperature and precipitated in ice-cold diethyl ether (90 mL). The solids were collected via centrifugation (4500 rpm, 0  $^{\circ}\text{C}$ , 3 min) and washed further with ice-cold diethyl ether (90 mL). The obtained solid was dried *in vacuo* (40  $^{\circ}\text{C}$ ) overnight.

### 6.2.8. Enzyme Degradation of Polysarcosine-*alt*-Polyphenylalanine

Polysarcosine<sub>35</sub>-*alt*-polyphenylalanine<sub>35</sub> was weighed out into two equal portions (75 mg) and suspended in deionised water (10 mL). To one portion, neutrophil elastase (8 units) was added. To the second portion, thermolysin from *Geobacillus Stearothermophilus* (8 units) was added. The two samples were incubated at 37  $^{\circ}\text{C}$  with continuous stirring for one week, after which the samples were frozen using liquid nitrogen and lyophilised.

### 6.2.9. Preparation of PSar-*ran*-PAla Copolymer Gels

To PSar-*ran*-PAla (32 mg), deionised water (20  $\mu$ L) was added and the suspension was sonicated to ensure thorough mixing. Further deionised water was added in 20  $\mu$ L portions to take the mixture to and beyond the point of gelation, which was recorded.

### 6.2.10. Preparation of PSar-*b*-PAla Copolymer Nanoparticles

Nanoparticles of the polysarcosine-*b*-polyalanine copolymers were prepared based upon a previously established nanoprecipitation method<sup>31</sup>. Each polymer (10 mg) was dissolved in chloroform (1 mL) and the solution added dropwise to deionised water (10 mL) under vigorous stirring. The dispersions were left stirring overnight at room temperature, after which there was no apparent organic phase. All nanoparticle dispersions were made at a concentration of 1 mgmL<sup>-1</sup>.

### 6.2.11. Preparation of Dox-loaded Nanoparticles

Doxorubicin hydrochloride (10 mg, 18.4  $\mu$ mol) was dissolved in anhydrous chloroform (4 mL) in a foil-wrapped vessel. Triethylamine (100  $\mu$ L, 0.72  $\mu$ mol) was added and the solution stirred at room temperature for 5 hours.

Polymer 6 (20 mg) was dissolved in chloroform (1 mL) and added dropwise, along with the prepared dox solution, to PBS buffer solution (pH 7.4, 20 mL) under vigorous stirring. The mixture was allowed to stir in a foil-wrapped vessel until the chloroform had evaporated. The nanoparticle solution was split into four equal portions and dialysed (2000 Da M.W.C.O.) for four days against PBS buffer solution (200 mL) to remove excess, free doxorubicin.

### 6.2.12. Enzyme-Mediated Release of Doxorubicin from Dox-Loaded Nanoparticles

The four portions of dox-loaded nanoparticle solutions were retrieved from the PBS solution, a 1 mL aliquot of which was analysed by UV-vis spectrophotometry. A small amount of elastase (8 units) was added to one of the dox-loaded nanoparticle solutions, within the dialysis tubing. To another, a larger amount of elastase (20 units), to the third, a large amount of chymotrypsin (20 units) was added and nothing was added to the final portion. Each batch was then dialysed (M.W.C.O. 2000 Da) against fresh PBS buffer solution (100 mL). The vessels were incubated in the dark under constant agitation at 37°C. At predetermined intervals, 1 mL aliquots were removed from the dialysate and analysed by UV-vis spectrophotometry.

The amount of dox released at each time point was quantified by UV-vis spectrophotometry using a prepared standard calibration curve (appendix VI). The release from the nanoparticles was studied over the course of 100 hours.

### **6.3. Results and Discussion**

#### **6.3.1. Synthesis of 2,5-Diketopiperazines**

The DKPs of sarcosine, L-alanine and sarcosine-L-phenylalanine were synthesised as reported in Chapter 3. Sar-Phe-DKP was synthesised using this method for the first time. Whilst sarcosine DKP and phenylalanine DKP also form during the reaction, the DKPs were separable by exploitation of their differences in solubility. Phenylalanine DKP precipitated from the glycerol solution on cooling to room temperature and was obtainable by vacuum filtration. Impurities such as unreacted amino acid and glycerol were removed from the phenylalanine DKP sample by washing at the filter with ice-cold deionised water. The remaining products, sarcosine DKP and Sar-Phe DKP were extracted by chloroform and evaporated to dryness. On addition of ice-cold methanol, sarcosine DKP dissolved whilst Sar-Phe DKP was insoluble and could be collected by vacuum filtration and purified by washing at the filter with ice-cold methanol. What remained in solution was sarcosine DKP and was purified as reported in section 3.2.11. The successful syntheses of the DKPs were confirmed by FTIR spectroscopy (appendix I), <sup>1</sup>H NMR spectroscopy (appendix II) and LC-MS (appendix III). The expansion of accessible DKPs from this method demonstrates its facility to produce materials with a wide-range of functionality and, crucially, in the absence of additional, toxic reagents.

#### **6.3.2. Synthesis of Polysarcosine**

To determine if polysarcosine, a hydrophilic and charge-neutral polymer, can be produced from Sar DKP, the ROP of Sar DKP was attempted from benzylamine using tin(II) 2-ethylhexanoate (Sn(Oct)<sub>2</sub>) as the catalyst. However, these attempts were unsuccessful in opening the stable tertiary lactam. Sn(Oct)<sub>2</sub> was replaced with an acid/base catalyst system of MSA and DIPEA. MSA was utilised to protonate the oxygen of the amide, weakening the amide bond and allowing the initial ring to open. DIPEA was used to deprotonate the secondary amine of the active chain end and facilitate propagation.

The polymerisations of polymers 1 and 2 were conducted in anhydrous DMF at 110 °C. After confirmation of a successful polymerisation, more mild conditions were explored such as refluxing in anhydrous chloroform for polymer 5 and 80 °C in water for polymers 3 and 4.

Polymers 1 to 5 were characterised and the extent of polymerisation quantified using FTIR spectroscopy (appendix I),  $^1\text{H}$  NMR spectroscopy (Figure 6.1. and appendix II) and MALDI-TOF mass spectrometry (Figure 6.2. and appendix VII). All polymerisations were initiated using benzylamine, the five protons of which come to resonance between 7.14-7.26 ppm in the  $^1\text{H}$  NMR spectrum. Therefore, integrals of the peaks corresponding to the polymer repeat unit were normalised to these peaks. PSar shows two peaks in the  $^1\text{H}$  NMR spectrum; one at 4.10 ppm corresponding to the protons of the  $\text{CH}_2$  group and one at 2.96 ppm corresponding to the protons of the  $\text{CH}_3$ . By normalising the integrals as described, the integrals for the peaks in the  $^1\text{H}$  NMR spectrum (Figure 6.1.) for polymer 1 were 154 for the  $\text{CH}_2$  peak and 231 for the  $\text{CH}_3$  peak. This signifies 77 repeat units of the polymer and therefore a 96% monomer conversion. Analysis by MALDI-TOF (Figure 6.2.) produced a distribution with a number averaged molecular weight ( $M_n$ ) = 5486  $\text{g mol}^{-1}$  and a weight averaged molecular weight ( $M_w$ ) = 5582  $\text{g mol}^{-1}$ . This corresponds to 76 repeat units and a  $\text{Đ}$  of 1.018. Whilst the  $\text{Đ}$  value was obtained using MALDI-TOF, which generally produces lower values than SEC, it is a very narrow  $\text{Đ}$  which indicates that the polymerisation boasts significant control and compares favourably to NCA ROP. Additionally, the distance between peaks within the distribution is equal to the repeat unit of polysarcosine (71  $\text{g mol}^{-1}$ ), further confirming the successful polymerisation.

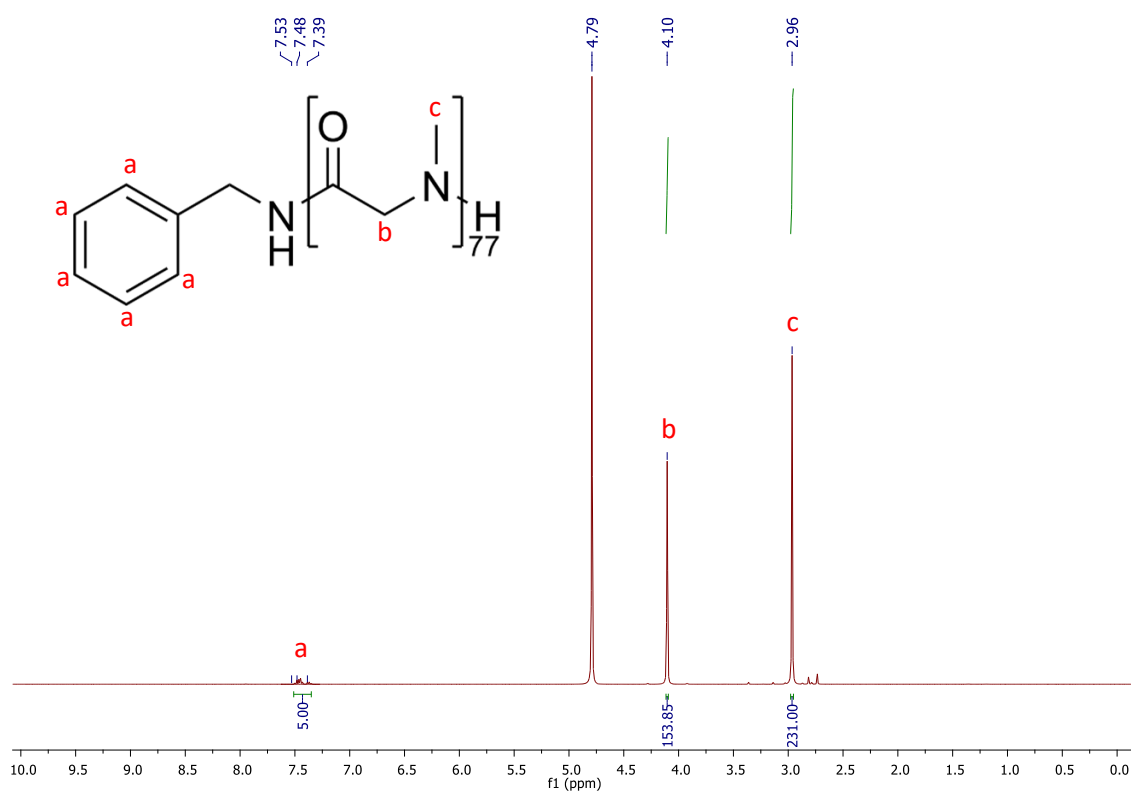


Figure 6.1. –  $^1\text{H}$  NMR spectrum ( $\text{D}_2\text{O}$ , 500 MHz) of polymer 1, polysarcosine<sub>77</sub>.

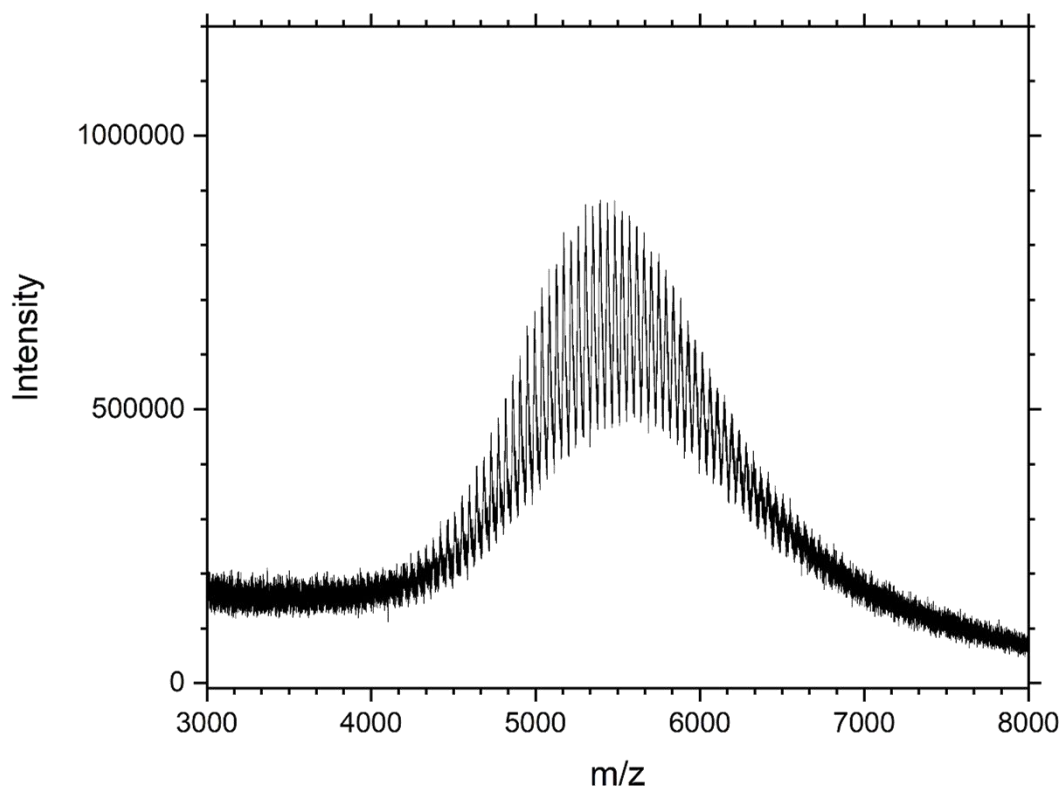


Figure 6.2. – MALDI-TOF spectrum of polymer 1, polysarcosine<sub>77</sub>.

The spectra of polymers 2 to 5 were analysed as detailed above for polymer 1, the results of which are highlighted in Table 6.2. Obtaining polysarcosine with a number of repeat units greater than 150 seemed to be restricted. Perhaps this can be overcome with a stronger catalyst such as aluminium trichloride to increase the rate of polymerisation.  $\bar{M}_n$  values were obtained by MALDI-TOF analysis. As such, they are perhaps lower than what may be obtained using size exclusion chromatography. Despite this, it is clear the polymers obtained have a very narrow  $\bar{M}_w/\bar{M}_n$ , suggesting the likelihood of self-assembly as part of a block copolymer and further emphasising the value of DKP ROP.

Table 6.2. – Targeted number of repeat units and observed number of repeat units of homo polysarcosine (polymers 1-5), by NMR and MALDI analyses.

Polymer	Target N <sup>o</sup> repeat units	NMR	MALDI	$\bar{M}_w/\bar{M}_n$
1	80	76	77	1.02
2	100	80	79	1.05
3	100	82	76	1.06
4	300	104	100	1.09
5	200	140	139	1.11

### 6.3.3. Synthesis of Polysarcosine-*b*-Polyalanine

To produce an amphiphilic block copolymer that is solely comprised of amino acid repeat units, alanine DKP was polymerised from polysarcosine using Sn(Oct)<sub>2</sub> catalyst. The ROP was conducted in DMF at 130 °C, a method that has shown success when polymerising DKPs from PEG methyl ether (Chapter 5). The resultant materials should be capable of self-assembly in aqueous solution and show sensitivity to hydrolysis via cleavage of the peptide bond that Ala repeat units when incubated with elastase<sup>32</sup>.

Polymers 6 to 9 were characterised using FTIR spectroscopy (appendix I), <sup>1</sup>H NMR spectroscopy and MALDI-TOF. The CH<sub>3</sub> of polyalanine comes to resonance in a <sup>1</sup>H NMR spectrum at 1.43-1.45 ppm, whereas the CH of polyalanine comes to resonance at 4.00-4.06 ppm. By normalising the integrals as described above, the integrals for the peaks in the <sup>1</sup>H NMR spectrum (Figure 6.3.) for polymer 6 were 9 for the protons of the CH group and 27 for the protons of the CH<sub>3</sub> of the alanine block, the integrals for the polysarcosine peaks were as described for polymer 1. Therefore, the polymer is PSar<sub>77</sub>-*b*-PAla<sub>9</sub>. Analysis by MALDI-TOF (Figure 6.4.) produced a distribution with a number averaged molecular weight ( $M_n$ ) = 6074 g mol<sup>-1</sup> and a weight averaged molecular weight ( $M_w$ ) = 6239 g mol<sup>-1</sup> and a Đ of 1.027. As for the PSar homopolymers, the Đ is very low, increasing the probability of the formation of uniform nanoparticles upon self-assembly. When subtracting the molecular weight values obtained from the MALDI-TOF spectrum of polymer 1, the number averaged molecular weight ( $M_n$ ) = 588 g mol<sup>-1</sup> and weight averaged molecular weight ( $M_w$ ) = 657 g mol<sup>-1</sup> for the polyalanine block. This corresponds to 9 alanine repeat units. This shows good agreement between the <sup>1</sup>H NMR spectrum and MALDI-TOF. The spectra of polymers 7, 8 and 9 were analysed as detailed above for polymer 6, the results of which are highlighted in Table 6.3.



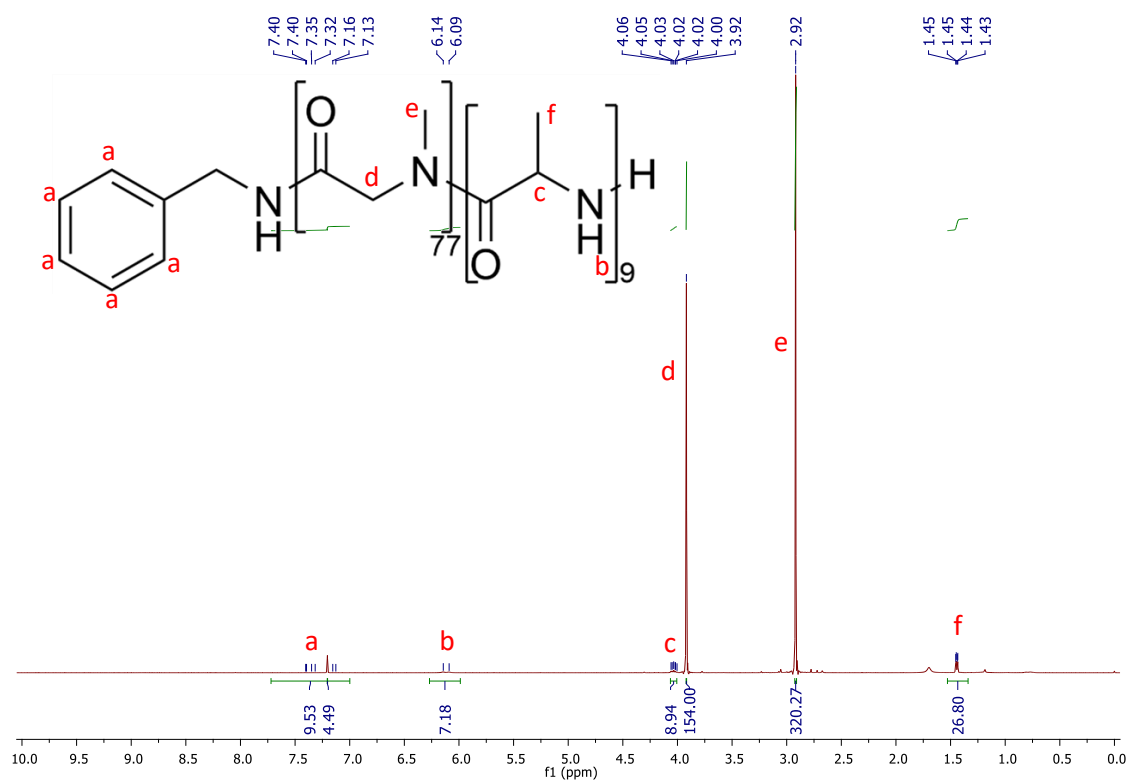


Figure 6.3. –  $^1\text{H}$  NMR spectrum ( $\text{CDCl}_3$ , 500 MHz) of polymer 6,  $\text{PSar}_{77}\text{-}b\text{-PAla}_9$ .

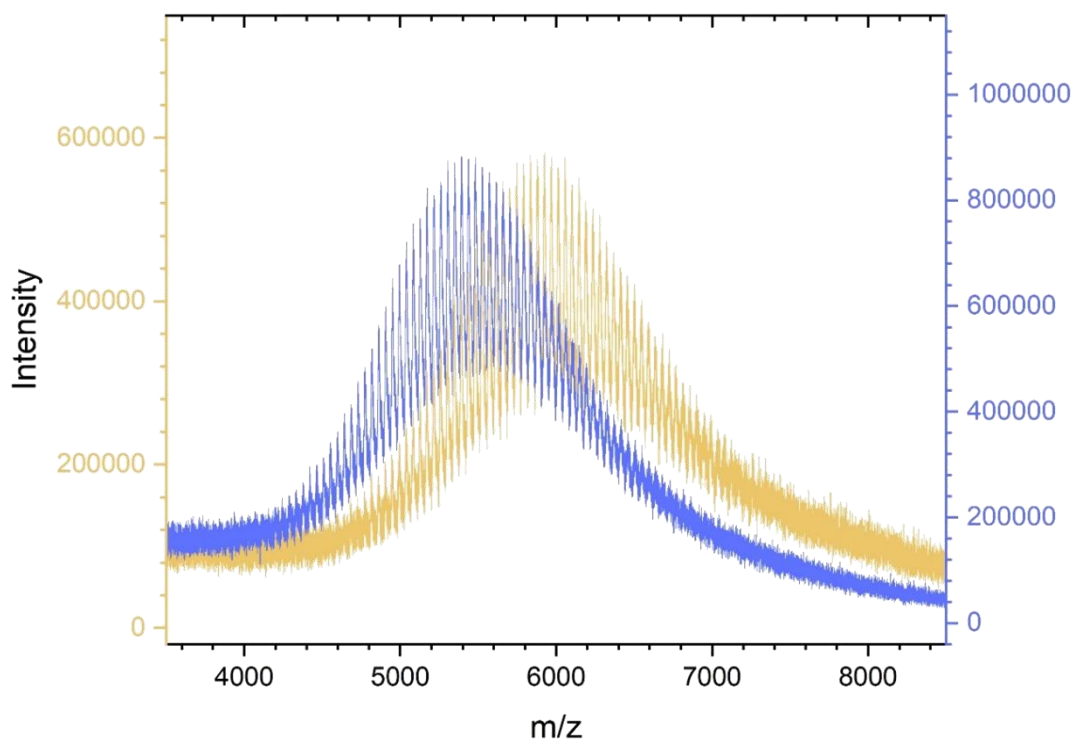


Figure 6.4. – MALDI-TOF spectra of polymer 1, polysarcosine<sub>77</sub> (blue) and polymer 6, polysarcosine<sub>77</sub>-*b*-polyalanine<sub>9</sub> (yellow).

Table 6.3. - Targeted number of repeat units and observed number of repeat units of polysarcosine-block-polyalanine (polymers 6-9), by NMR and MALDI analyses.

Polymer	Target N <sup>o</sup> repeat units	NMR	MALDI	Đ
6	78	9	9	1.03
7	60	11	9	1.06
8	20	14	13	1.14
9	40	12	11	1.15

As is the case for ROP of alanine DKP from PEG, % monomer conversions from polysarcosine is variable and the length of observed polyalanine blocks is limited. However, even short polyalanine blocks have sufficient hydrogen bonding to induce self-assembly<sup>33</sup>. Additionally, all of the resultant polymers had low Đ and as such, their consistent self-assembly is more probable.

#### 6.3.4. Synthesis of Polysarcosine-*ran*-Polyalanine

Polymers that possess both hydrophobic and hydrophilic sites alternating within the chain produced from DKPs are original and may have the capacity to gelate in aqueous solution. Gelation is proposed to result due to H-bond interactions between PAla sections, physically maintaining the hydrophilic PSar sections of the copolymer. As such, sarcosine DKP and alanine DKP were random copolymerised in a one-pot reaction from benzylamine. The polymerisation was catalysed initially with methanesulfonic acid and subsequently with DIPEA in deionised water. Polymer 10 was characterised using FTIR spectroscopy (appendix I), <sup>1</sup>H NMR spectroscopy (Figure 6.5.) and MALDI-TOF (Figure 6.6.). The spectra were analysed as described for polymers 6-9, resulting in an observed number of repeat units as PSar<sub>70</sub>-*ran*-PAla<sub>8</sub> from the <sup>1</sup>H NMR spectrum. Analysis by MALDI-TOF shows good agreement with that of the <sup>1</sup>H NMR spectrum, with M<sub>n</sub> = 5129 g mol<sup>-1</sup> and M<sub>w</sub> = 5595 g mol<sup>-1</sup> and a low Đ of 1.092. The obtained MALDI-TOF distribution of the polymer had low intensity; this is due to the stability of the polymer and poorly ionisable groups within the polymer.

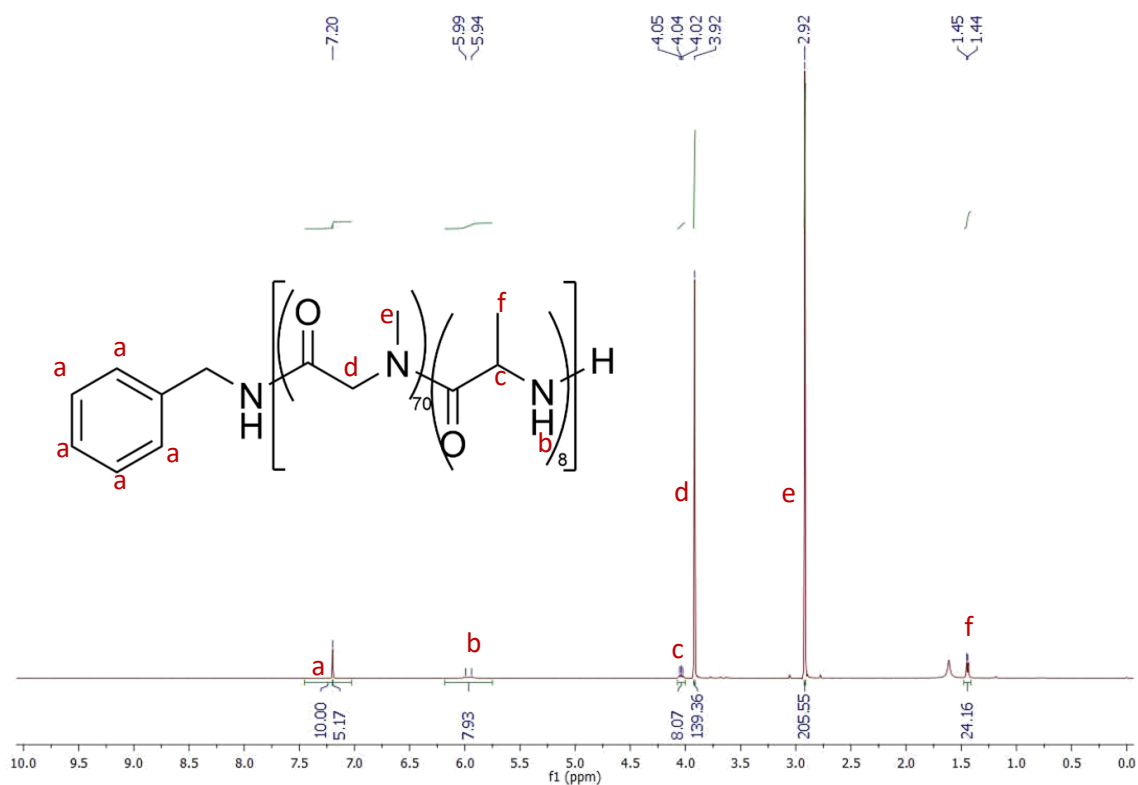


Figure 6.5. –  $^1\text{H}$  NMR spectrum ( $\text{CDCl}_3$ , 500 MHz) of polymer 10, polysarcosine<sub>70</sub>-ran-polyalanine<sub>8</sub>.

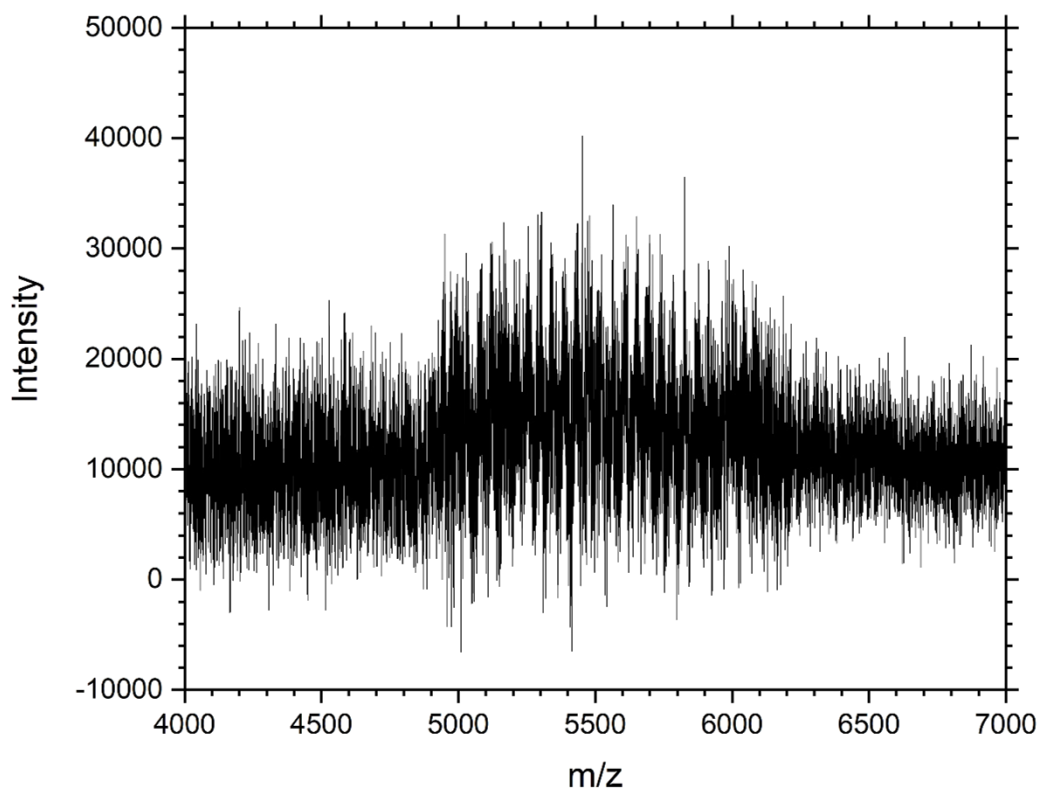


Figure 6.6. – MALDI-TOF spectrum of polymer 10, polysarcosine<sub>70</sub>-ran-polyalanine<sub>8</sub>.

Polymer 10 was then assessed for its water uptake and capacity to gelate in aqueous conditions. After the addition of 300  $\mu$ L of deionised water, polymer 10 had formed a physical gel structure and had retained its structural integrity. Therefore, the minimum weight percentage of PSar<sub>70</sub>-*ran*-PAla<sub>8</sub> required to form a physical hydrogel was 9.6%. This is a reasonable value for a physical gel. However, perhaps it could be improved upon by producing higher molecular weight random copolymers bearing greater hydrogen bonding. This rudimentary study provides an insight into using random copolymers from DKPs to produce physical hydrogels. More extensive research that involves the application of the materials, for the controlled release of proteins for instance, is plausible future work.

### 6.3.5. Synthesis of Polysarcosine-*alt*-Polyphenylalanine

Polypeptides and polypeptoids bearing an alternating structure that is highly ordered may possess unique physicochemical properties that are absent in both random copolymers and their respective homopolymers. Although solid-phase peptide synthesis possesses the control required to produce such a structure, its exponential loss in yield as higher molecular weight polymers are targeted compromises its yield. However, ROP of an asymmetric DKP may provide a facile and straightforward route to an alternating polymer. An asymmetric DKP may ring-open exclusively at one of the amide bonds or at a mixture of both, depending on the relative bond strength of the two amide links. As such, the polymer may be composed of repeat units in a perfectly alternating structure (ABABABAB), or partial alternation (ABABBAABBA).

To produce a polymer with a structure that regularly alternates from one amino acid to another along the chain, sarcosine-phenylalanine DKP was ring-opening polymerised from benzylamine in DMF. The polymerisation was again catalysed initially by MSA, followed by DIPEA. The polymer obtained may show resistance to breakdown by selective enzymes such as elastase. The polymer was characterised using FTIR spectroscopy (appendix I), <sup>1</sup>H NMR spectroscopy (Figure 6.7.) and MALDI-TOF (Figure 6.8.). Polysarcosine-*alt*-polyphenylalanine shows several peaks in the <sup>1</sup>H NMR spectrum. The protons of the CH<sub>3</sub> peak of the sarcosine repeat unit is observed as described previously. However, in this polymer, the protons of the CH<sub>2</sub> peak of the phenylalanine group has been split into two doublet of doublets at 3.13-3.10 ppm and 2.87-2.83 ppm; this is due to the diastereotopic relationship of these protons. The peaks corresponding to the phenylalanine repeat unit were as follows: the NH peak at 8.25 ppm, the CH's of the phenyl group between 7.26-7.30 ppm and 7.08-7.10 ppm, the CH peak at 4.13-4.15 ppm and the CH<sub>2</sub> peak at 2.83-3.13 ppm.

By integrating these peaks and normalising the integrals to those of the benzylamine initiator, the resultant number of repeat units were 35 each of sarcosine and phenylalanine. Analysis by MALDI-TOF produced a distribution with a number averaged molecular weight ( $M_n$ ) = 7295 g mol<sup>-1</sup> and a weight averaged molecular weight ( $M_w$ ) = 7635 g mol<sup>-1</sup> and a narrow  $\bar{D}$  of 1.047. This corresponds to a number of repeat units of 35 of each amino acid and shows excellent agreement with the values obtained from the <sup>1</sup>H NMR spectrum. Given the observed number of repeat units, and the targeted number of repeat units as 50 of each of sarcosine and phenylalanine, the percentage monomer conversion of this polymerisation is 70%. This could be improved upon by using a stronger catalyst system.

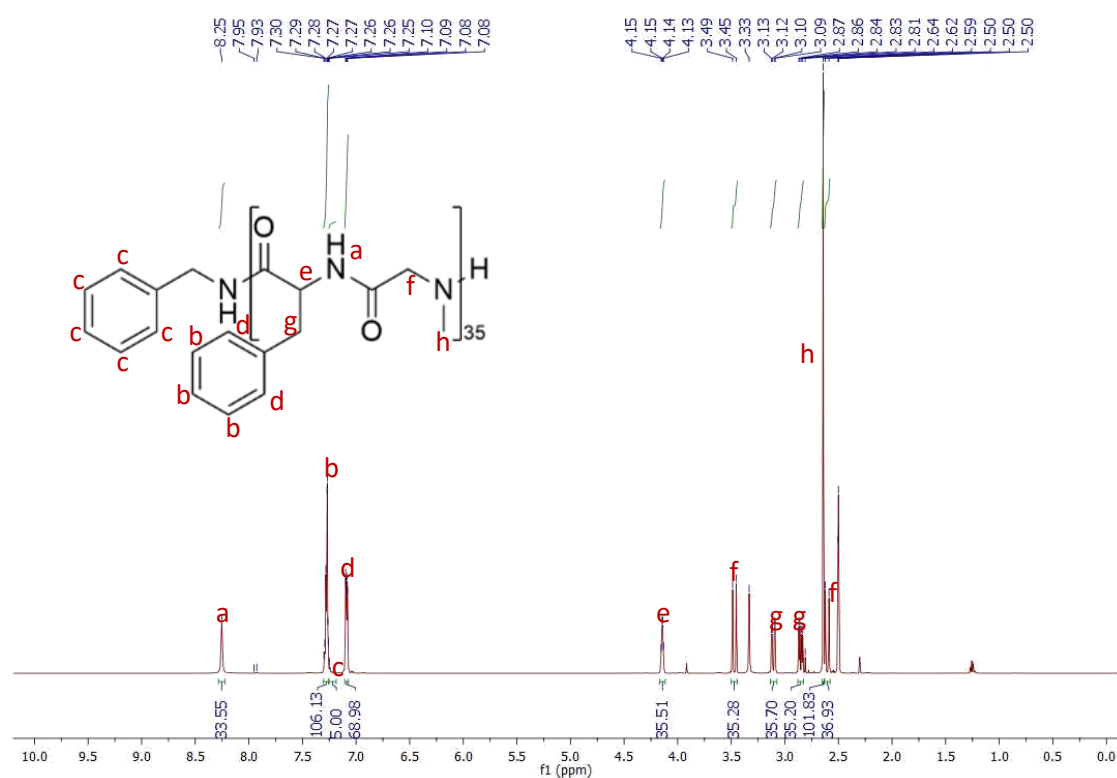


Figure 6.7. – <sup>1</sup>H NMR spectrum (DMSO-d<sub>6</sub>, 500 MHz) of polymer 11, polysarcosine<sub>35</sub>-alt-polyphenylalanine<sub>35</sub>.

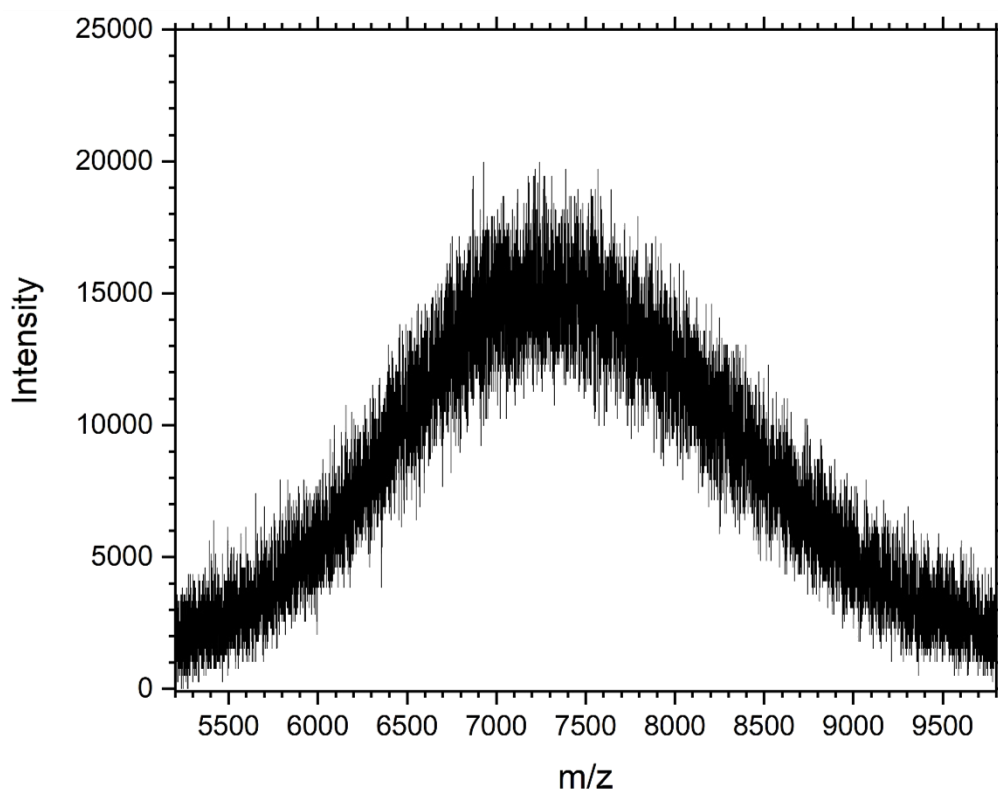


Figure 6.8. – MALDI-TOF spectrum of polymer 11, polysarcosine<sub>35</sub>-*alt*-polyphenylalanine<sub>35</sub>.

To determine the extent to which polysarcosine-*alt*-polyphenylalanine is resistant to enzymatic degradation, polymer 11 was separately incubated with 8 units of neutrophil elastase and thermolysin from *Geobacillus Stearothermophilus* at 37 °C for one week. Elastase was selected as a selective enzyme that targets dipeptide groups bearing small R groups (alanine, glycine, sarcosine). A lack of degradation of the polymer on incubation with elastase may indicate a lack of adjacent sarcosine repeat units, informing how perfectly alternating the repeat units of the polymer are and therefore whether one amide bond of Sar-Phe DKP opens more readily. Thermolysin is a non-selective enzyme and was utilised to determine what level of resistance PSar-*alt*-PPhe shows to enzymatic degradation. The extent of degradation was determined using MALDI-TOF. Incubation with elastase had no effect on polymer 11, MALDI-TOF spectra of the resultant material showed very similar distributions to that of the starting polymer. However, incubation with thermolysin showed substantial degradation of the polymer. Analysis by MALDI-TOF (Figure 6.9.) showed a range of distributions between 500 and 2500 g mol<sup>-1</sup>. Additionally, there were no apparent distributions remaining between 5000 and 10000 g mol<sup>-1</sup>. This indicates that polymer 11 shows resistance to selective enzymes that can cleave dipeptides with small R groups (elastase). Despite this, the polymer is degradable via incubation with thermolysin.

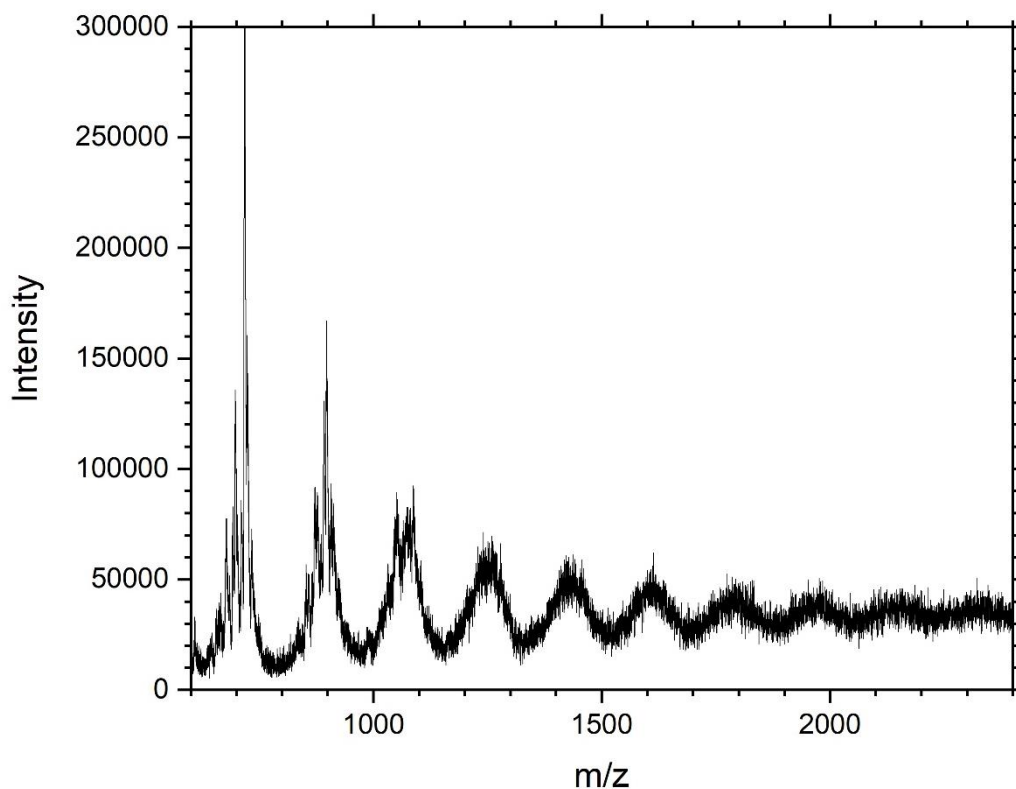


Figure 6.9. – MALDI-TOF spectrum of the degradation products of polymer 11 after incubation with thermolysin at 37 °C for one week.

### 6.3.6. Polysarcolation of Camptothecin

Drug molecules that suffer from poor water solubility are commonly conjugated to PEG as part of a pro-drug system to boost their bioavailability and pharmacokinetic profile<sup>34</sup>, camptothecin is such a therapeutic. To determine the capacity to which polysarcosine, produced via ROP of sarcosine-DKP, can enhance the water solubility of a hydrophobic therapeutic, sarcosine DKP was polymerised using camptothecin as an initiator. The polymerisation was carried out in DMF and catalysed initially with MSA and subsequently with DIPEA. The resultant pro-drug was analysed by <sup>1</sup>H NMR spectroscopy (Figure 6.10.), FTIR spectroscopy (appendix I) and MALDI-TOF (Figure 6.11.) which confirmed the successful ROP of sarcosine DKP from the tertiary alcohol group of camptothecin. Analysis by <sup>1</sup>H NMR spectroscopy showed an average of 14 repeat units of polysarcosine, which showed reasonable agreement with that of MALDI-TOF which produced a distribution with a number averaged molecular weight ( $M_n$ ) = 1566 g mol<sup>-1</sup>, a weight averaged molecular weight ( $M_w$ ) = 1706 g mol<sup>-1</sup> and a narrow  $\mathcal{D}$  of 1.089.

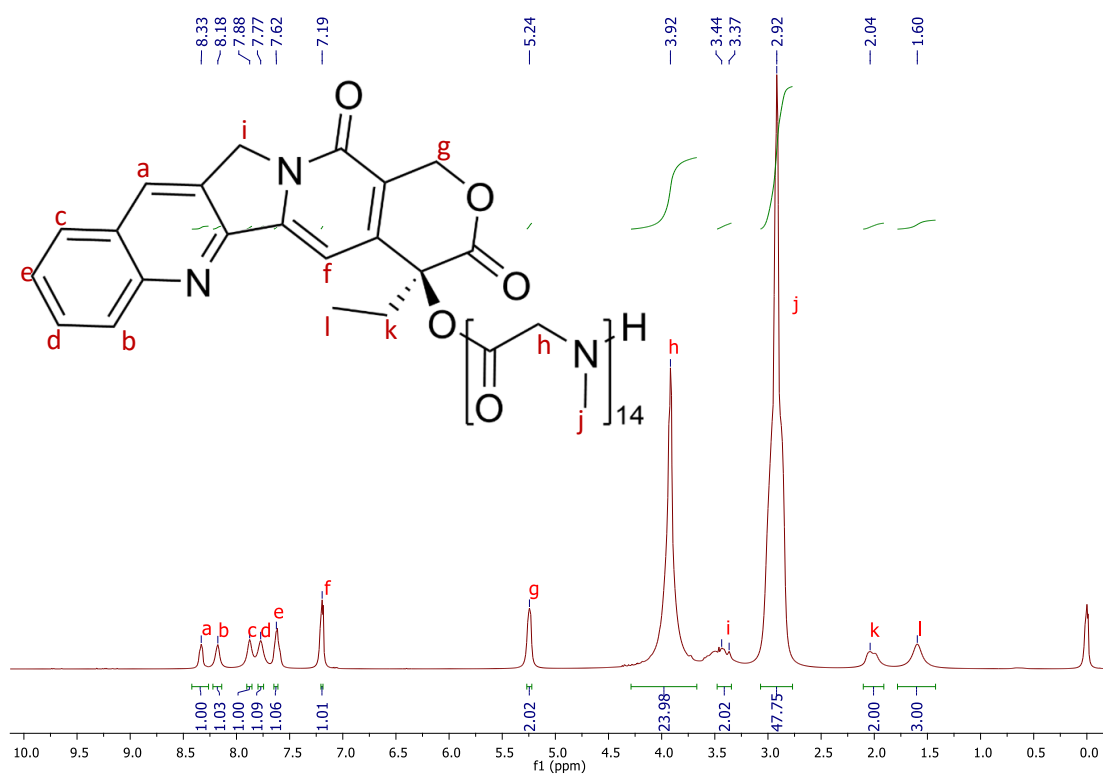


Figure 6.10. – <sup>1</sup>H NMR spectrum (CDCl<sub>3</sub>, 500 MHz) of camptothecin-polysarcosine<sub>14</sub>.

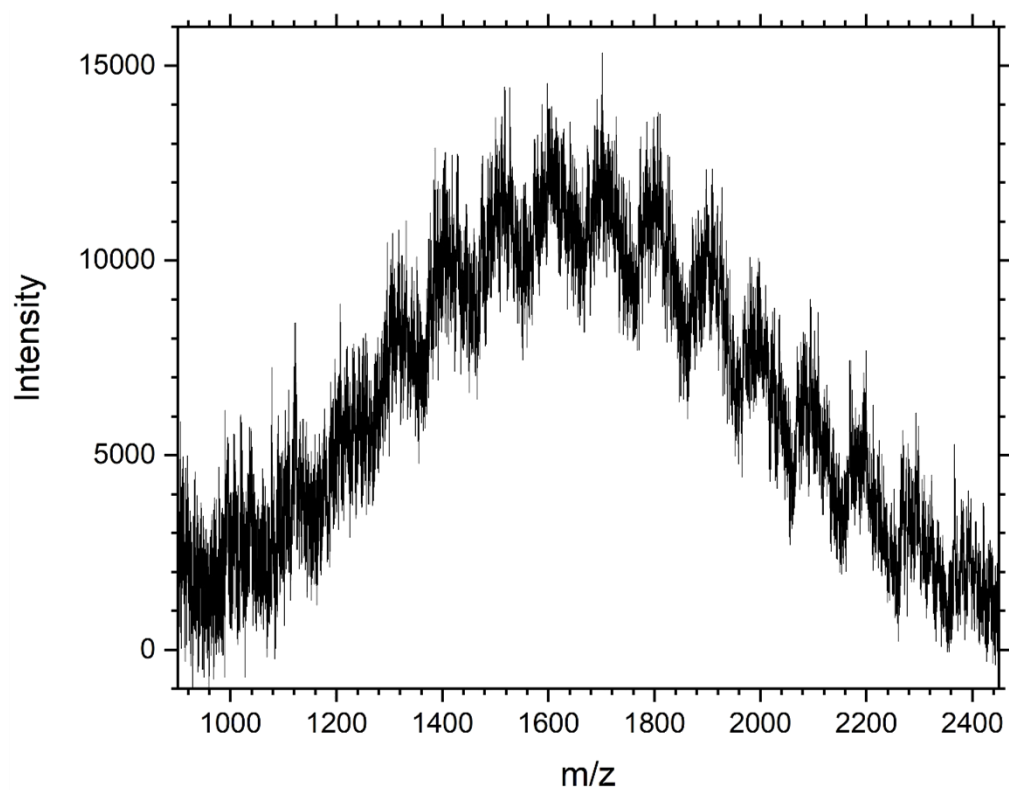


Figure 6.11. – MALDI-TOF spectrum of camptothecin-polysarcosine<sub>14</sub>.



To quantify the extent to which grafting polysarcosine to camptothecin had improved the water solubility of the later, camptothecin and camptothecin-polysarcosine<sub>14</sub> were each added to deionised water at an equimolar amount. Both samples were vigorously stirred and sonicated for at least 10 minutes to ensure thorough mixing. The mixtures were analysed using UV-vis spectrophotometry.

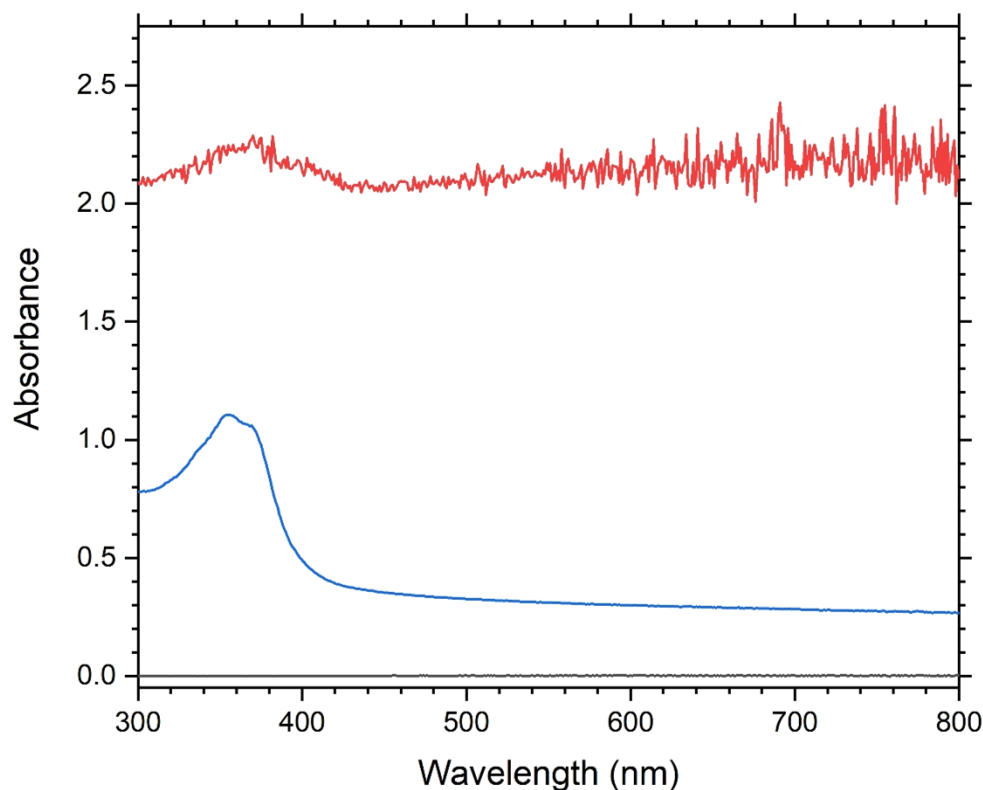


Figure 6.12. - UV-vis spectrum of camptothecin suspended in deionised water ( $1 \text{ mg mL}^{-1}$ ) (red) and camptothecin-polysarcosine<sub>14</sub> dissolved in deionised water ( $7 \text{ mg mL}^{-1}$ ) (blue).

Despite the very low concentration, free camptothecin was unable to dissolve in deionised water at  $1 \text{ mg mL}^{-1}$  and formed a cloudy suspension. This is observable in the UV-vis spectrum (Figure 6.12.); the red trace corresponding to camptothecin has a much higher baseline absorbance, as well as substantial noise between 600 and 800 nm. However, camptothecin-polysarcosine<sub>14</sub> fully dissolved at  $7 \text{ mg mL}^{-1}$ , this is illustrated in the UV-vis spectrum with a low absorbance and little noise.

### 6.3.7. Polysarcosine-*b*-Polyalanine Nanoparticles

In order to function as a drug delivery vehicle, the nanoparticles formed by the self-assembly of the produced polysarcosine-*b*-polyalanine must demonstrate stability in aqueous solution. As such, the capability of the block copolymers to self-assemble upon nanoprecipitation in aqueous medium was assessed using dynamic light scattering (DLS) and scanning electron microscopy (SEM). The nanoparticles were produced via the dropping-in method<sup>35</sup>; this involved dissolving the polymer in a volatile organic solvent (chloroform) and adding dropwise to a rapidly stirring aqueous medium (phosphate-buffered saline (PBS) buffer solution). The subsequent evaporation of the organic solvent yields a nanoparticle dispersion via a reliable and straightforward method. All four block copolymers were capable of self-assembly to form nanoparticles in aqueous solution at 1 mg mL<sup>-1</sup> polymer concentration (Table 6.4.).

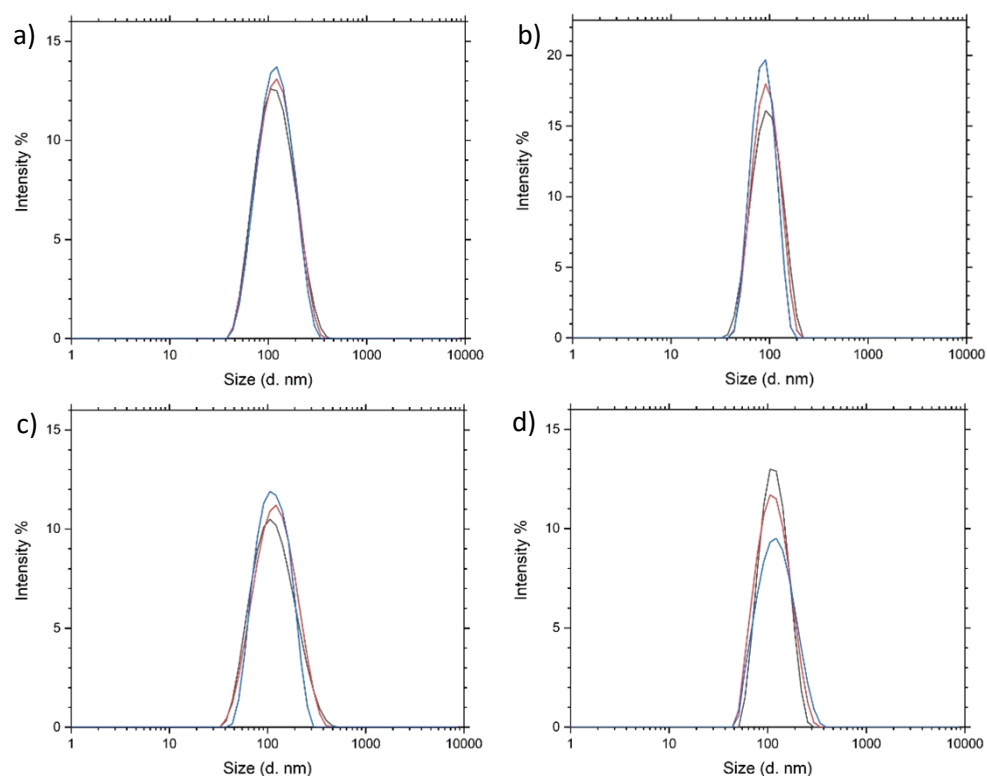


Figure 6.13. – DLS traces of nanoparticle dispersions of: a) polymer 6, b) polymer 7, c) polymer 8 and d) polymer 9.

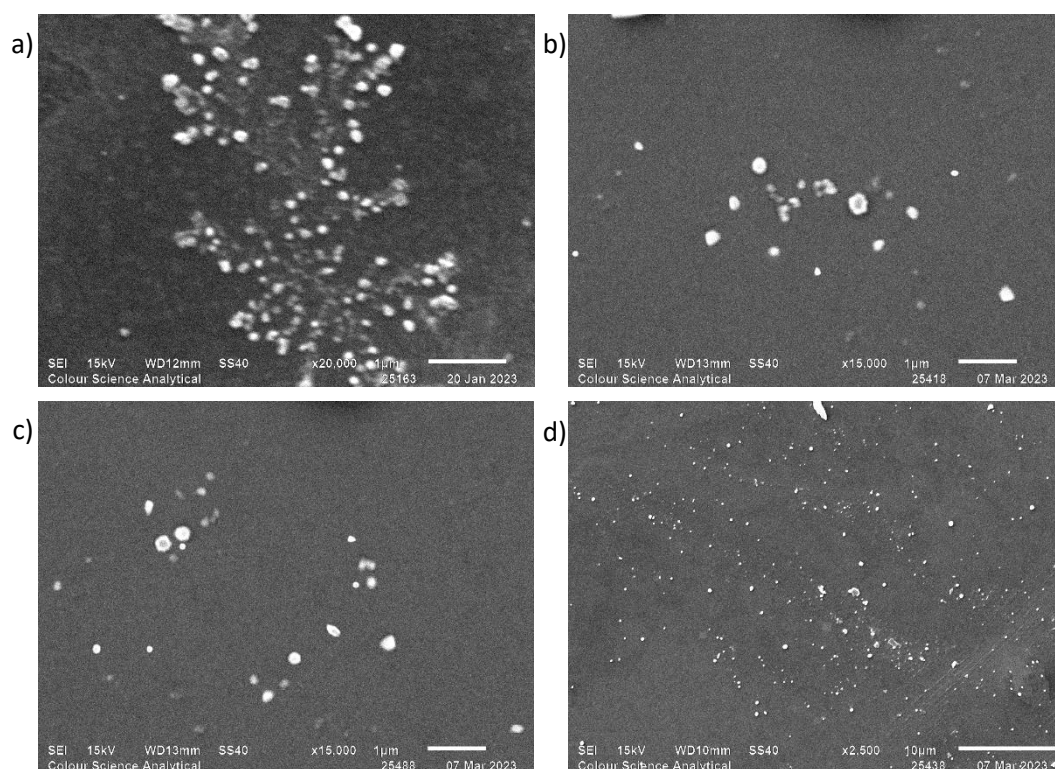


Figure 6.14. – SEM images of nanoparticles of: a) polymer 6 (1 μm scale bar), b) polymer 7 (1 μm scale bar), c) polymer 8 (1 μm scale bar) and d) polymer 9 (10 μm scale bar).

The diameters of the nanoparticles shown in the SEM images were measured using ImageJ to obtain an average particle size and polydispersity of each nanoparticle dispersion. For each sample, a minimum of 100 diameter values were measured. Where there were fewer than 100 nanoparticles in a single image, at least 35 measurements were taken. The dispersity values from the SEM measurements were calculated as follows:

$$\text{Polydispersity} = \frac{\sigma^2}{d_{av}^2}$$

Where  $\sigma$  = standard deviation of nanoparticle diameter and  $d_{av}$  = average nanoparticle diameter. The results of these calculations, along with those obtained using DLS, are shown in Table 6.4.

The nanoparticles of each dispersion have an average diameter that is less than 200 nm, making them suitable for intravenous application, as well as applicable as long-circulating carriers to a target site<sup>36</sup>. Additionally, nanoparticles of polymer 7 have an average particle size that is less than 100 nm, which may allow for diffusion across the blood-brain barrier<sup>37</sup>. All nanoparticle

dispersions, aside from nanoparticles of polymer 8, have a polydispersity lower than 0.2, which is the minimum industrial standard for a monodisperse sample, further supporting their applicability for medicinal use<sup>36</sup>.

*Table 6.4.* – Average particle diameter and polydispersity of nanoparticle solutions of polymers 6-9, determined by DLS and SEM analyses.

Polymer	Formula	DLS measurements		SEM measurements	
		Particle Size (d.nm)	Polydispersity	Particle Size (d.nm)	Polydispersity
6	PSar <sub>77</sub> - <i>b</i> -PAla <sub>9</sub>	128	0.17	135	0.13
7	PSar <sub>79</sub> - <i>b</i> -PAla <sub>9</sub>	94	0.11	103	0.15
8	PSar <sub>139</sub> - <i>b</i> -PAla <sub>13</sub>	125	0.20	117	0.24
9	PSar <sub>139</sub> - <i>b</i> -PAla <sub>11</sub>	123	0.14	118	0.15

### 6.3.8. Enzyme-Mediated Release of Doxorubicin from Dox-Loaded Nanoparticles

Doxorubicin is a commonly used chemotherapeutic, however, its interaction with healthy tissue results in devastating side effects due to its extreme toxicity. Encapsulation and subsequent targeted release of doxorubicin can result in more effective chemotherapy treatment with greatly reduced side effects. Recent studies have shown that in cancerous settings, myeloid cell production is accelerated<sup>38</sup>. This leads to an increased production of neutrophil elastase at the cancerous site<sup>38</sup> and as such, provides scope for use of elastase as a trigger for a drug delivery vehicle bearing an anti-cancer therapeutic.

Nanoparticles produced from the self-assembly of polymer 6, PSar<sub>77</sub>-*b*-PAla<sub>9</sub>, were assessed for their capacity to encapsulate doxorubicin free-base in aqueous conditions. Of the 10 mg of Dox added, 8.1 mg was encapsulated within 20 mg of polymeric nanoparticles, resulting in 81±3% encapsulation efficiency and 29±1% drug loading content. Over the course of the drug release study, samples were taken of the dialysate of each of the nanoparticle dispersions at regular intervals. These samples were studied via UV-vis spectrophotometry. The chromophore within the doxorubicin structure produces a strong red colour which results in a peak at 480 nm in the UV-vis spectrum<sup>39</sup>. For each sample, the absorbance value of the peak at 480 nm was converted to a concentration value of doxorubicin using a calibration curve. This concentration was divided by the total volume of dialysate to produce a weight value of doxorubicin and compared to the

original encapsulated amount of doxorubicin to produce a drug release percentage. These values were plotted on graph of drug release percentage against time which is shown below.

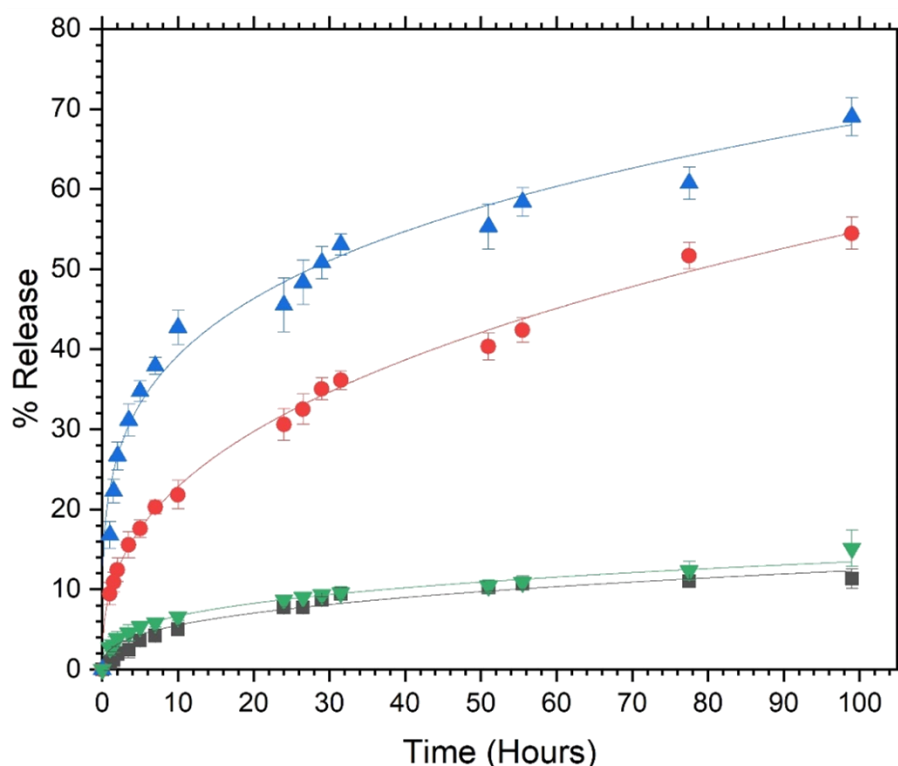


Figure 6.15. – Percentage drug release over time from nanoparticles of polymer 6 when incubated with: ■) No enzyme, ▼) 20U chymotrypsin, ●) 8U elastase and ▲) 20U elastase.

There was minimal release, or leakage, from the nanoparticles that were incubated without an enzyme, showing a maximum release of  $11\pm 1\%$ . This demonstrates that the nanoparticles are robust enough to prevent significant burst release and resultant systemic exposure to doxorubicin under these conditions. Similarly, the nanoparticles incubated with 20 units of chymotrypsin, an enzyme capable of hydrolysing peptides bearing amino acids with larger R groups such as phenylalanine, showed a maximum release of  $15\pm 2\%$ . This demonstrates the selectivity of enzymes and the specificity that can be imparted upon the resultant polymer. Incubation with eight units of elastase and 20 units of elastase resulted in a maximum percentage release of  $54\pm 2\%$  and  $69\pm 2\%$ , respectively, demonstrating the sensitivity of the polymer to elastase degradation and confirming its suitability as a trigger for targeted release. Crucially, burst release has been avoided and a prolonged, steady release achieved. The results highlight the potential that the system has for enabling the controlled and prolonged release of a chemotherapeutic in response to a target protease enzyme.

#### 6.4. Conclusion

The repeatable ring-opening polymerisation of sarcosine DKP is reported for the first time, providing a cheaper, safer and more environmentally friendly route to polysarcosine compared to conventional NCA ROP. This provides greater scope for industrial use of polysarcosine, providing competition for the well-established PEG. Additionally, various polysarcosine-based materials were also produced via the novel ROP, including amphiphilic block copolymers, random copolymers and alternating copolymers. Whilst polysarcosine-*alt*-polyphenylalanine showed little degradation to neutrophil elastase, polysarcosine-*block*-polyalanine degraded upon incubation with neutrophil elastase, demonstrating the control of the ROP and the tuneable properties of the resultant polymers. Furthermore, polysarcosine-*block*-polyalanine nanoparticles displayed sensitivity to neutrophil elastase, resulting in a prolonged release of doxorubicin upon incubation with neutrophil elastase, demonstrating its applicability as a therapeutic delivery vehicle to sites characterised by an overexpression of elastase.

## 6.5. References

---

- 1) D'souza, A.A. and Shegokar, R. Polyethylene glycol (PEG): a versatile polymer for pharmaceutical applications. *Expert Opinion on Drug Delivery*. 2016, **13**(9), 1257-1275.
- 2) Suk, J.S., Xu, Q., Kim, N., Hanes, J. and Ensign, L.M. PEGylation as a strategy for improving nanoparticle-based drug and gene delivery. *Advanced Drug Delivery Reviews*. 2016, **99**, 28-51.
- 3) Kang, J.S., Deluca, P.P. and Lee, K.C. Emerging PEGylated drugs. *Expert Opinion on Emerging Drugs*. 2009, **14**(2), 363-380.
- 4) Moon, W. Optimal and Safe Bowel Preparation for Colonoscopy. *Clinical Endoscopy*. 2013, **46**(3), 219-223.
- 5) Wang, Z., Song, J., Zhang, S., Xu, X-Q. and Wang, Y. Formulating Polyethylene Glycol as Supramolecular Emulsifiers for One-Step Double Emulsions. *Langmuir*. 2017, **33**(36), 9160-9169.
- 6) Jang, H-J., Shin, C. Y. and Kim, K-B. Safety Evaluation of Polyethylene Glycol (PEG) Compounds for Cosmetic Use. *Toxicological Research*. 2015, **31**(2), 105-136.
- 7) Ermawati, D. E., Surya, A. P., Setyawati, R. and Niswah, S. U. The effect of glycerine and polyethylene glycol 400 as humectant on stability and antibacterial activity of nanosilver biosynthetic peel-off mask. *Journal of Applied Pharmaceutical Science*. 2022, **12**(4), 80-89.
- 8) Yang, Q. and Lai, S. K. Anti-PEG immunity: emergence, characteristics, and unaddressed questions. *Wiley interdisciplinary reviews. Nanomedicine and nonbiotechnology*. 2015, **7**(5), 655-677.
- 9) Nogueira, S. S., Schlegel, A., Maxeiner, K., Weber, B., Barz, M., Schroer, M. A., Blanchet, C. E., Svergun, D. I., Ramishetti, S., Peer, D., Langguth, P., Sahin, U. and Haas, H. Polysarcosine-Functionalized Lipid Nanoparticles for Therapeutic mRNA Delivery. *ACS Applied Nano Materials*. 2020, **3**, 10634-10645.
- 10) Baumann, A., Tuerck, D., Prabhu, S., Dickmann, L. and Sims, J. Pharmacokinetics, metabolism and distribution of PEGs and PEGylated proteins: quo vadis? *Drug Discovery Today*. 2014, **19**(10), 1623-1631.
- 11) Hu, Y., Hou, Y., Wang, H. and Lu, H. Polysarcosine as an Alternative to PEG for Therapeutic Conjugation. *Bioconjugate Chemistry*. 2018, **29**, 2232-2238.
- 12) Secker, C., Brosnan, S. M., Luxenhofer, R. and Schlaad, H. Poly( $\alpha$ -Peptoid)s Revisited: Synthesis, Properties, and Use as Biomaterial. *Macromolecular Bioscience*. 2015, **15**, 881-891.

- 
- 13) Kirshebaum, K., Barron, A. E., Goldsmith, R. A., Armand, P., Bradley, E. K., Truong, K. T. V., Dill, K. A., Cohen, F. E. and Zuckermann, R. N. Sequence-specific polypeptoids: A diverse family of heteropolymers with stable secondary structure. *Proceedings of the National Academy of Sciences*. 1998, **95**(8), 4303-4308.
- 14) Fetsch, C., Grossmann, A., Holz, L., Nawroth, J. F. and Luxenhofer, R. Polypeptoids from N-Substituted Glycine N-Carboxyanhydrides: Hydrophilic, Hydrophobic, and Amphiphilic Polymers with Poisson Distribution. *Macromolecules*. 2011, **44**, 6746-6758.
- 15) Yu, H., Ingram, N., Rowley, J. V., Parkinson, S., Green, D. C., Warren, N. J. and Thornton, P. D. Thermoresponsive polysarcosine-based nanoparticles. *Journal of Materials Chemistry B*. 2019, **7**, 4217-4223.
- 16) Conilh, L., Fournet, G., Fourmaux, E., Murcia, A., Martera, E-L., Joseph, B., Dumontet, C. and Viricel, W. Exatecan Antibody Drug Conjugates Based on a Hydrophilic Polysarcosine Drug-Linker Platform. *Pharmaceuticals*. 2021, **14**(3), 247-263.
- 17) Zuckermann, R. N. Peptoid Origins. *Biopolymers*. 2011, **96**(5), 545-555.
- 18) Secker, C., Brosnan, S. M., Luxenhofer, R. and Schlaad, H. Poly( $\alpha$ -Peptoid)s Revisited: Synthesis, Properties, and Use as Biomaterial. *Macromolecular Bioscience*. 2015, **15**, 881-891.
- 19) Birke, A., Ling, J. and Barz, Matthias. Polysarcosine-containing copolymers: Synthesis, characterization, self-assembly, and applications. *Progress in Polymer Science*. 2018, **81**, 163-208.
- 20) Mazo, A. R., Allison-Logan, S., Karimi, F., Chan, N. J-A., Qiu, W., Duan, W., O'Brien-Simpson, N. M. and Qiao, G. G. Ring opening polymerisation of  $\alpha$ -amino acids: advances in synthesis, architecture and applications of polypeptides and their hybrids. *Chemical Society Reviews*. 2020, **49**, 4737-4834.
- 21) The National Institute for Occupational Safety and Health (NIOSH). *Phosgene*. 2014. [25/02/2023]. Available from: <https://www.cdc.gov/niosh/idlh/75445.html>
- 22) Fujita, Y., Koga, K., Kim, H-K., Wang, X-S., Sudo, A., Nishida, H. and Endo, T. Phosgene-free synthesis of N-carboxyanhydrides of  $\alpha$ -amino acids based on bisarylcarbonates as starting compounds. *Journal of Polymer Science Part A: Polymer Chemistry*. 2007, **45**(22), 5365-5370.
- 23) Koga, K., Sudo, A. and Endo, T. Revolutionary phosgene-free synthesis of  $\alpha$ -amino acid N-carboxyanhydrides using diphenyl carbonate based on activation of  $\alpha$ -amino acids by converting



---

into imidazolium salts. *Journal of Polymer Science Part A: Polymer Chemistry*. 2010, **48**(19), 4351-4355.

24) Endo, T. and Sudo, A. Well-Defined Construction of Functional Macromolecular Architectures Based on Polymerization of Amino Acid Urethanes. *Biomedicines*. 2020, **8**(9), 317-335.

25) Laconde, G., Amblard, M. and Martinez, J. Synthesis of  $\alpha$ -Amino Acid N-Carboxyanhydrides. *Organic Letters*. 2021, **23**, 6412-6416.

26) Brouns, J. E. P. and Dankers, P. Y. W. Introduction of Enzyme-Responsivity in Biomaterials to Achieve Dynamic Reciprocity in Cell-Material Interactions. *Biomacromolecules*. 2021, **22**(1), 4-23.

27) Hu, Q., Katti, P. S. and Gu, Z. Enzyme-Responsive Nanomaterials for Controlled Drug Delivery. *Nanoscale*. 2014, **6**(21), 12273-12286.

28) Pokorna, A., Bobal, P., Oravec, M., Rarova, L., Bobalova, J. and Jampilek, J. Investigation of Permeation of Theophylline through Skin Using Selected Piperazine-2,5-Diones. *Molecules*. 2019, **24**(3), 566-579.

29) Manchineella, S., Voshavar, C. and Govindaraju, T. Radical-Scavenging Antioxidant Cyclic Dipeptides and Silk Fibroin Biomaterials. *European Journal of Organic Chemistry*. 2017, **30**, 4363-4369.

30) Basiuk, V. A., Gromovoy, T. Y., Chuiko, A. A., Soloshonok, V. A. and Kukhar, V. P. A Novel Approach to the Synthesis of Symmetric Optically Active 2,5-Dioxopiperazines. *Synthesis*. 1992, **5**, 449-451.

31) Khuphe, M. and Thornton, P.D. Poly(hydroxy acid) Nanoparticles for the Encapsulation and Controlled Release of Doxorubicin. *Macromolecular Chemistry and Physics*. **219**(23), 1800352-1800356.

32) Oh, H. J., Joo, M. K., Sohn, Y. S. and Jeong, B. Secondary Structure Effect of Polypeptide on Reverse Thermal Gelation and Degradation of l/dl-Poly(alanine)-Polyoxamer-l/dl-Poly(alanine) Copolymers. *Macromolecules*. 2008, **41**(21), 8204-8209.

33) Buckinx, A-L., Rubens, M., Cameron, N. R., Bakkali-Hassani, C., Sokolova, A. and Junkers, T. The effects of molecular weight dispersity on block copolymer self-assembly. *Polymer Chemistry*. 2022, **13**(23), 3444-3450.

- 
- 34) Veronesse, F. M. and Mero, A. The impact of PEGylation on biological therapies. *BioDrugs*. 2008, **22**(5), 315-329.
- 35) Schubert, S., Delaney, J. T. and Schubert, U. S. Nanoprecipitation and nanoformulation of polymers: from history to powerful possibilities beyond poly(lactic acid). *Soft Matter*. 2011, **7**(5), 1581-1588.
- 36) Danaei, M., Dehghankhold, M., Ataei, S., Davarani, F.H., Javanmard, R., Dokhani, A., Khorasani, S. and Mozafari, M.R. Impact of Particle Size and Polydispersity Index on the Clinical Applications of Lipidic Nanocarrier Systems. *Pharmaceutics*. 2018, **10**, 57-73.
- 37) Senapati, S., Mahanta, A.K., Kumar, S. and Maiti, P. Controlled drug delivery vehicles for cancer treatment and their performance. *Signal Transduction and Targeted Therapy*. 2018, **3**, article no: 7 [no pagination].
- 38) Lerman, I. and Hammes, S. R. Neutrophil elastase in the tumor microenvironment. *Steroids*. 2018, **133**, 96-101.
- 39) Huang, J., Zong, C., Shen, H., Cao, Y., Ren, B. and Zhang, Z. Tracking the intracellular drug release of graphene oxide using surface-enhanced Raman spectroscopy. *Nanoscale*. 2013, **5**, 10591-10598.

## **Chapter 7 – Electrospinning of Polyalanine-based, Elastase-Responsive Nanofibres as Potential Materials for the Treatment of Chronic Wounds**

### **Abstract**

Porous polymeric materials are structures used in a wide variety of applications. Whilst there are several methods of porous polymeric material production, electrospinning is most useful for the production of materials to be applied within the biomedical sector. An area of increasing interest is the development of new materials for the treatment of chronic wounds, which are exposed injuries that cannot heal without additional treatment. This can be the result of a combination of infection, increased inflammation and the overexpression of neutrophil proteases such as elastase. This enzyme overexpression is detrimental to the production and maintenance of elastin, an important factor in skin health and healing. An emerging treatment for chronic wounds are electrospun nanofibres of biocompatible polymers which aid in the maintenance of moisture, prevent infection and facilitate cell growth and tissue regeneration at the wound site. Such materials are porous in nature and are widely applied as scaffolds or dressings for cell growth. Their efficacy can be optimised via the inclusion of highly biocompatible poly(amino acids) such as polyalanine, a poly(amino acid) that can be selectively degraded enzymatically by elastase. Such an addition could result in a material that boasts greater hydrophilicity, tensile strength and crucially, elastase responsivity which may result in the capacity to steadily release a payload of therapeutic(s) and bioactive agents. As such, the electrospinning of elastase-responsive polyalanine and hydrophilic polysarcosine each with a polycaprolactone carrier is reported for the first time. The resultant electrospun nanofiber materials were assessed for their water uptake capacity, tensile strength and capacity to respond to elastase incubation in order to provide scope for their potential applicability as dressings for chronic wound treatments.

### **7.1. Introduction**

Porous polymeric materials are three-dimensional (3D) structures that contain pores throughout their structure. The versatility to produce polymeric scaffolds of different chemical functionalities and mechanical properties through simple changes to the polymer synthesis and/or processing ensures their wide-ranging applicability. Successful material uses include matrices of controlled delivery<sup>1</sup>, scaffolds for 3D cell culture and tissue engineering<sup>2</sup>, catalytic supports<sup>3</sup>, chemical and biological sensors<sup>4</sup>, and implants<sup>5</sup> have been reported. Although

polymer scaffolds designed for use in catalysis and filtration are commonly produced from persistent, non-biodegradable polymers, applications that involve *in vivo* placement of a porous material, such as scaffolds for tissue engineering and chronic wound healing devices, require material degradability<sup>6</sup>. There is therefore a strong need for the creation of highly functional and tuneable biodegradable polymers that can be processed to form porous polymeric materials, particularly for new healthcare technologies such as the creation of effective devices for chronic wound healing.

Wound healing has four defined stages – the accumulation of platelets and fibrin to form a clot at the wound site (haemostasis), the recruitment of neutrophils and monocytes to remove foreign bodies, bacteria and damaged intrinsic tissues (inflammation), the growth of new blood vessels at the wound site, resulting in the production of enhanced collagen factor and granulation tissue (proliferation), and the conversion of granulation tissue to a more stable extracellular matrix (remodelling)<sup>7,8,9</sup>.

The complete healing of acute wounds is typically achieved within 12 weeks<sup>10</sup>. Chronic wounds are defined as wounds that fail to proceed through the normal phases of wound healing in an orderly and timely manner<sup>9</sup>. Commonly, chronic wounds stall in the inflammation phase of healing<sup>9</sup>. In acute wounds that proceed through the stages of healing as expected, proteases are tightly regulated by their inhibitors, whereas in chronic wounds, protease levels exceed that of their respective inhibitors, leading to destruction of extracellular matrix (ECM) and degradation of growth factors and their receptors<sup>9</sup>. The proteolytic destruction of ECM not only prevents the wound from moving forward into the proliferative phase but also attracts more inflammatory cells, thus amplifying the inflammation cycle<sup>11</sup>. The use of polymeric materials to produce a dressing may result in an optimum treatment method for chronic wounds. Polymers, particularly poly(amino acids), are versatile materials that can be fine-tuned to suit an application. In the case of chronic wound treatment, a polymeric material can be tuned to be non-antigenic, biocompatible, biodegradable, semi-permeable, flexible, cost effective, non-adhering to the wound bed, protective from infection and impact, able to maintain moisture, and able to load therapeutics<sup>12,13,14</sup>.

Whilst there are numerous methods to create porous polymeric materials, such as emulsion templating<sup>15</sup>, particle leaching<sup>16</sup>, gas foaming<sup>17</sup>, and 3D printing<sup>18</sup>, electrospinning may be used to produce materials that are designed to maintain moisture at the wound site<sup>19,20</sup> and can be tailor-made to the size and shape of a given wound<sup>21</sup>, enhancing their capacity to protect a wound from physical damage as well as infection. Such materials are soft and mechanically

flexible and, as an effective mimic for human ECM structure<sup>10</sup>, electrospun fibres can modulate skin cell proliferation and allow for growth and repair of human tissue throughout their structure or at the surface of the structure depending on pore size<sup>22,23</sup>. Additionally, electrospun materials have a large specific surface area<sup>10</sup>, which is effective in absorbing wound exudate as well as promoting nutrient transfer and gas exchange<sup>19,20</sup>. Furthermore, high porosity allows for loading of therapeutics such as anaesthetics, antimicrobial agents and bioactive molecules<sup>24,25</sup>. Not only can the command position of the fibres be altered, but the morphology, arrangement and therefore the physicochemical properties can be fine-tuned simply by altering the parameters of the electrospinning process in order to produce nanofibre structures optimised for any wound in question<sup>10</sup>.

Currently, SurgiClot, a dextran-based nanofibre dressing, is the only commercially available nanofibre wound dressing on the market<sup>26</sup>. As well as providing a physical barrier, it contains human thrombin and fibrinogen to induce and then facilitate wound clotting and is successfully implemented as a haemostatic dressing for cancellous bone bleeding<sup>27</sup>. However, due to the clotting factors used, SurgiClot cannot be used intravascularly as it may result in a life-threatening thromboembolic event<sup>27</sup>. Additionally, it cannot be used in the presence of an active infection or a contaminated wound as it may propagate the infection<sup>27</sup>. Furthermore, SurgiClot cannot be used in conjunction with antiseptics such as alcohol, iodine or heavy metal ions as these can denature the proteins present in the dressing<sup>27</sup>. Therefore, SurgiClot would not be a suitable treatment for chronic wounds, and the development of more appropriate materials is paramount.

In 2012, Yuan *et al.*<sup>28</sup> produced electrospun nanofibre mats of a blend of poly(hydroxybutylate-co-hydroxyvalerate) (PHBV) and m-keratin, which were successful in enhancing cell proliferation and accelerated wound recovery when compared to the PHBV control<sup>28</sup>. As such, the resultant mats showed promise as a candidate for acute wound dressings and tissue repair. However, as with SurgiClot, this system does not have the capacity to reduce the excessive overexpression of neutrophils and proteases present in chronic wounds in order to reduce inflammation and facilitate healing.

Polycaprolactone (PCL) is a synthetic polyester that is actively used in research to produce nanofibres via electrospinning either alone or as a carrier for a copolymer or therapeutics that are suitable as dressings or as tissue engineering scaffolds<sup>29</sup>. PCL is biocompatible and, most notably, it can be electrospun with relative ease<sup>29</sup>. It has excellent solubility in high vapour pressure organic solvents<sup>30</sup> and the parameters used to electrospin PCL into nanofibres with

diameter, pore size and morphology most similar to the physical structure of human ECM have been determined<sup>30</sup>. However, despite their excellent physical properties, PCL nanofibres are hydrophobic and consequently suffer from poor water uptake capacity. Additionally, PCL nanofibres alone do not have the capacity to resolve the excessive presence of elastase and other neutrophils present in chronic wounds and therefore would not be effective in facilitating healing. However, by including a combination of antiseptics, bioactive agents, neutrophil inhibitors and a copolymer that is capable of breakdown at a chronic wound site in order to trigger release of the encapsulated therapeutics, the resultant material may be effective in facilitating healing in chronic wounds.

Polyalanine (PAla), a poly(amino acid) with a methyl R group, is a biomimetic and as such, it has excellent biocompatibility and biodegradability. Its use as part of an electrospun biomaterial is somewhat unexplored thus far, however, it has excellent physical properties such as high toughness and durability<sup>31</sup> owing to the considerable H-bonding between polymer chains and may therefore enhance the tensile strength of a nanofibre material. Critically, polyalanine is sensitive to enzymatic degradation by elastase<sup>32</sup> and therefore, electrospun PCL/PAla copolymer nanofibre materials may be uniquely suited to facilitate healing in chronic wounds as a human extracellular matrix replicate that may be capable of releasing a payload upon exposure to elastase.

As reported in Chapters 4 and 6, polyalanine and polysarcosine can be produced by the ROP of their respective DKPs, rendering the process as straightforward and mild. The novel electrospinning of polycaprolactone with polyalanine or polysarcosine, to form PCL, PCL/PAla and PCL/PSar copolymer nanofibre mats, is reported as a means to produce fibrous networks with enhanced mechanical properties (PCL/PAla) or hydrophilicity (PCL/PSar) compared to networks created from PCL only. The optimum parameters and conditions of electrospinning each polymer mixture in order to produce nanofibres of a morphology comparable to the physical structure of human ECM were identified. The resultant nanofibre mats were assessed for their average nanofibre diameter, water uptake capacity, tensile strength and sensitivity to elastase. The results included may provide scope for further investigation into the materials produced for their capacity to facilitate healing in chronic wounds.

## **7.2. Experimental Details**

### **7.2.1. Synthesis of Diketopiperazines**

The DKPs of alanine and sarcosine were synthesised according to previously established synthetic route<sup>33, 34, 35</sup> as described in Chapter 3, sections 3.2.1., 3.2.3. and 3.2.11.

### **7.2.2. ROP of Diketopiperazines**

The synthesis of the polyalanine that was utilised in this chapter is reported in Chapter 4 as polymer 2 (Table 4.1.). The synthesis of the polysarcosine that was utilised in this chapter is reported in Chapter 5 as polymer 5 (Table 6.1.).

### **7.2.3. Preparation of Polymer Solutions**

Polycaprolactone (Average  $M_w$  70 kDa, 0.7 g) was added to a 1:1 mix of hexafluoroisopropanol (HFIP) and chloroform ( $\text{CHCl}_3$ ) (10 mL), polyalanine (Average  $M_w$  5280 Da, 0.4 g) was added to a 1:1 mix of HFIP/ $\text{CHCl}_3$  (8 mL) and polysarcosine (Average  $M_w$  10 kDa, 0.4 g) was added to a 1:1 mix of HFIP/ $\text{CHCl}_3$  (8 mL). For all, full solvation was ensured by sonication and stirring using a vortex genie.

### **7.2.4. Electrospinning of Polymer Solutions**

Within a ventilated cupboard, the respective polymer solution/combination of solutions (Table 7.1.) was added to a syringe with a blunted 21-gauge needle and a conductive target was prepared using aluminium foil and fixed in place. The syringe was loaded into a syringe pump such that the needle was directed toward the aluminium target with a working distance of 10 cm. A charged clip was clamped to the needle of the syringe and a grounding clip was clamped to the aluminium target. The syringe pump was set to a flow rate (Table 7.1.) and turned on. The electrospinning equipment was isolated and a DC voltage (Table 7.1.) was applied. After an allotted period of time (Table 7.1.), the current was turned off, the syringe pump turned off and the fibre mat and target collected.

*Table 7.1.* – Parameters of electrospinning PCL, PCL/PAla and PCL/PSar nanofibres including solvent selection, weight percentage of polymer in solution, ratio of polymer solutions, potential difference applied during electrospinning, flow rate of solution, and time of electrospinning.

Spin	Polymer 1	Solvent (wt.% of polymer)	Polymer 2	Solvent (wt.% of polymer)	Ratio of Polymer Solutions	Potential difference (kV)	Flow rate (mL/hour)	Time (hours)
1	PCL	HFIP (7%)	-	-	-	11	1	1
2	PCL	HFIP/CHCl <sub>3</sub> (7%)	-	-	-	20	1.5	1
3	PCL	HFIP/CHCl <sub>3</sub> (7%)	PAla	DMF/ACN (5%)	01:01	19	2	0.5
4	PCL	HFIP/CHCl <sub>3</sub> (7%)	PAla	DMF/ACN (5%)	04:01	19	2	0.5
5	PCL	HFIP (7%)	PAla	HFIP/CHCl <sub>3</sub> (5%)	01:01	11	2	0.75
6	PCL	HFIP (7%)	PAla	HFIP/CHCl <sub>3</sub> (5%)	01:01	11	1	1
7	PCL	HFIP (7%)	PAla	HFIP/CHCl <sub>3</sub> (5%)	01:01	20	2	1
8	PCL	HFIP (7%)	PSar	CHCl <sub>3</sub> (5%)	01:01	14	2	1.5

*Table 7.2.* - Percentage beading by area, average nanofibre diameter with standard deviation and average pore diameter with standard deviation of the 8 electrospun samples.

Spin	% beading	Av. Nanofibre Diameter (nm)	$\sigma$	Av. Pore Diameter (nm)	$\sigma$
1	10.5	71	24	850	236
2	0	315	187	1964	917
3	19.6	75	25	614	235
4	15.3	67	15	285	105
5	4.3	60	17	293	109
6	0.6	62	15	201	61
7	0.9	120	41	249	83
8	0	167	58	376	136



### **7.2.5. Water Uptake Testing of Nanofibre Samples**

A sample of PCL, PCL/PAla and PCL/PSar nanofibres, produced in spins 2, 7 and 8 respectively were immersed in deionised water for 24 hours at room temperature. After which, the nanofibre samples were removed from the water and patted dry with absorbent material to remove excess water until they were no longer visibly wet. The samples were weighed before and after immersion in water and their water uptake calculated.

### **7.2.6. Tensile Testing of Nanofibre Samples**

The nanofibres from spin 2 (PCL), spin 7 (PCL/PAla) and spin 8 (PCL/PSar) were tested for their tensile strength. Samples measuring at least 1 cm by 4 cm were taken from each nanofibre mat and their width and thickness measured using callipers and recorded. The sample was clamped in a tensile testing rig and the gauge length measured and recorded. A separation rate of 5 mm min<sup>-1</sup> was set and the samples tested until failure.

### **7.2.7. Enzyme Degradation Study of PCL/PAla Nanofibre Samples**

Samples measuring 1 cm by 5 cm were taken from the nanofibre mat produced in spin 7, weighed and incubated in a solution of neutrophil elastase (8 units) in deionised water (10 mL). At each of the following time points, 0.5, 1, 1.5 and 2 hours, a sample was collected from the elastase solution and washed thoroughly with deionised water. The sample was then allowed to thoroughly dry under gentle air flow and weighed again. Degradation was monitored by weight loss, SEM, FTIR spectroscopy (appendix I) and tensile testing.

## **7.3. Results and Discussion**

### **7.3.1. Synthesis of Diketopiperazines**

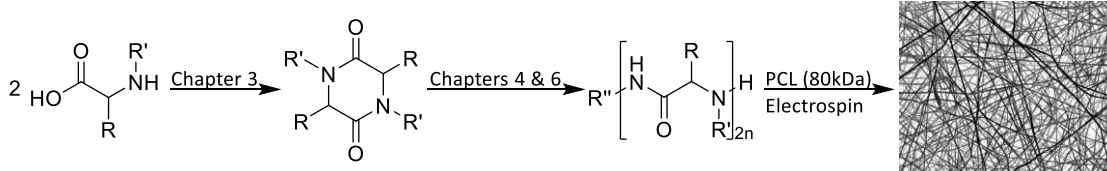
Alanine DKP and sarcosine DKP were synthesised as reported in Chapter 3. Polyalanine boasts extensive hydrogen bonding, resulting in excellent physical properties such as high mechanical strength<sup>31,36</sup> and consequently, its inclusion may enhance the tensile strength of PCL-based electrospun material. Critically, polyalanine is sensitive to enzymatic breakdown by elastase<sup>37</sup>; an enzyme that is overexpressed in chronic wounds, resulting in a detrimental effect on wound healing. The inclusion of polyalanine within an electrospun nanofibre mat may result in an elastase-responsive material that has the capacity to encapsulate a therapeutic and release it in the presence of elastase. Polysarcosine was selected primarily for its hydrophilicity and

biocompatibility<sup>38</sup>. As part of an electrospun material, polysarcosine may enhance water uptake capacity of the material, augmenting its capacity to absorb wound exudate and maintain an optimally moist wound environment.

### 7.3.2. ROP of Diketopiperazines

The ROP of alanine DKP and sarcosine DKP are reported in Chapters 4 and 6 respectively. The molecular weights of the polymers utilised in this chapter were determined using <sup>1</sup>H NMR spectroscopy, as well as MALDI-TOF mass spectrometry. Analysis of the yielded polyalanine using <sup>1</sup>H NMR spectroscopy showed 65 repeat units, whereas analysis by MALDI-TOF spectrometry produced a distribution with number-averaged molecular weight ( $M_n$ ) = 4900 g mol<sup>-1</sup> and weight-averaged molecular weight ( $M_w$ ) = 5280 g mol<sup>-1</sup> with a Đ of 1.07. Analysis of the synthesised polysarcosine showed 140 repeat units according to <sup>1</sup>H NMR spectroscopy, whilst analysis by MALDI-TOF spectrometry produced a distribution with  $M_n$  = 9223 g mol<sup>-1</sup> and  $M_w$  = 10043 g mol<sup>-1</sup> and Đ of 1.09. These two polymers were selected for having the highest molecular weights of the polyalanine and polysarcosine samples produced. The electrospinning process can be significantly influenced by the molecular weight of the polymer(s) used, in that the diameter of electrospun fibres increases with polymer molecular weight<sup>39</sup>. However, the electrospinning process can fail as a consequence of polymer molecular weights that are too low or too high. Whilst the molecular weights of the polyalanine and polysarcosine selected are at the lower end of the acceptable range for electrospinning (9000-155,000 g mol<sup>-1</sup>)<sup>40</sup>, the inclusion of a polycaprolactone carrier that has a molecular weight of 80,000 g mol<sup>-1</sup> should increase the probability of the successful production of nanofibres.

### 7.3.3. Electrospinning of PCL, PCL/PAIa and PCL/PSar Nanofibres



*Scheme 7.1.* – Amino acid to nanofibres; via DKP synthesis, DKP ROP and electrospinning with PCL.

The determination of suitable and optimum parameters for electrospinning polyalanine and polysarcosine each with a polycaprolactone carrier in order to produce nanofibres that had an average fibre diameter between 50 - 500 nm was a central objective. A structure comprised of such nanofibres most optimally serves as a replicate of human ECM and allows for gas and solution exchange whilst preventing bacterial infiltration and cell ingrowth<sup>41,42</sup>. As such, a variety of parameters were trialled and the resultant nanofibres were assessed (Table 7.1.). All nanofibre mats were analysed by SEM (Figures 7.1. to 7.5.) to obtain a population distribution of nanofibre and pore diameters (Table 7.1.), as well FTIR spectroscopy (appendix I) to confirm polymer content within the nanofibre mats.

Initially, PCL was dissolved in hexafluoroisopropanol (HFIP) at a concentration of 7wt% and electrospun with a potential difference of 11 kV and a flow rate of 1 mL/hour. Analysis by SEM (Figure 7.1., Image A) showed a distribution of nanofibre diameter with an average of 71 (SD = 24 nm) and 10.5% of beading/electrospray by area. Despite the successful fibre formation, this sample contained a substantial amount of beading and electrospay, as well as an average fibre diameter at the lower end of the acceptable range to mimic human ECM. The occurrence of electrospay indicates low viscosity and low potential difference. Whilst beading within nanofibres may result in drug delivery material that more successfully prevents burst release of a therapeutic<sup>43</sup>, it also compromises the physical properties of the network and detrimentally affects the applicability of the material as a wound healing dressing. As such, the subsequent attempt at producing PCL nanofibres (Table 7.1., Spin 2) utilised a solution of PCL dissolved in 1:1 HFIP/chloroform at 7wt% and the electrospinning was carried out with a higher flow rate of 1.5 mL/hour to increase average nanofibre diameter and a higher potential difference of 20 kV to reduce beading and electrospay. Analysis of spin 2 by SEM (Figure 7.1., Image B) showed a larger average nanofibre diameter of 315 nm (SD = 187 nm) and no beading/electrospray. As such, these parameters were taken as an improvement upon spin 1.

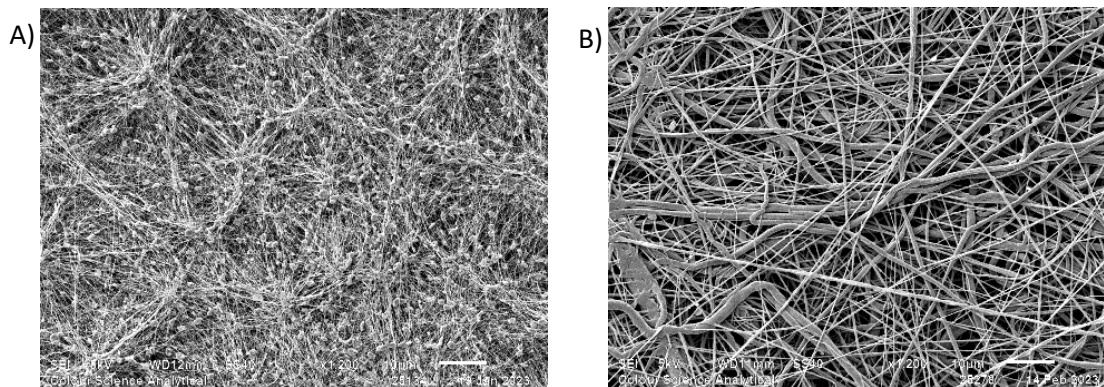


Figure 7.1. – Representative SEM images of PCL fibres produced in A) spin 1, and B) spin 2 with scale bars of 10 µm.

To electrospin PCL/PAla nanofibres, PCL was dissolved as described above for spin 2 and PAla was dissolved in a 1:1 ratio of DMF/ACN at 5wt%. The two solutions were combined in a 1:1 ratio and electrospun with a flow rate of 2 mL/hour and a potential difference of 20 kV (Table 7.1., Spin 3). Analysis by SEM (Figure 7.2., Image A) showed nanofibres of 75 nm (SD = 25 nm) with more beading and electrospray than fibre content. This may be due to slow evaporation rate of the DMF/ACN solvent system, as well as higher viscosity. A repeat of spin 3 with a higher ratio of PCL solution to PAla solution (4:1) (Table 7.1., Spin 4) showed similar amounts of electrospray and beading (Figure 7.2., Image B). As such, an alternative solvent system for PAla was considered.

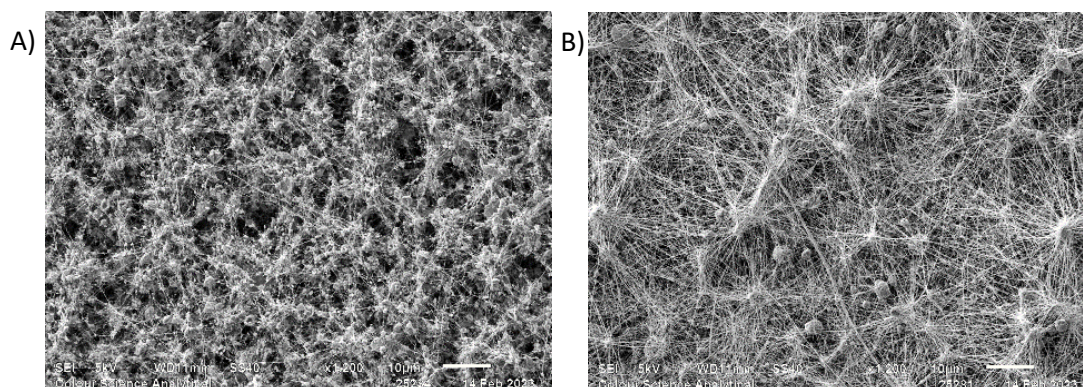
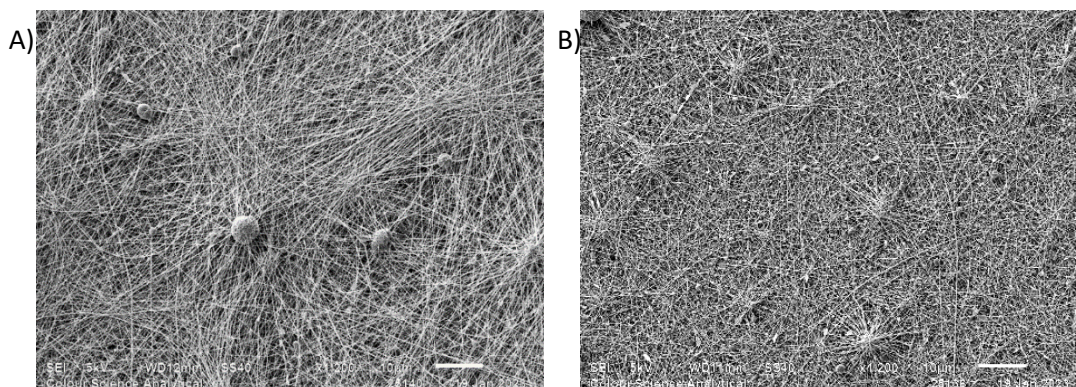


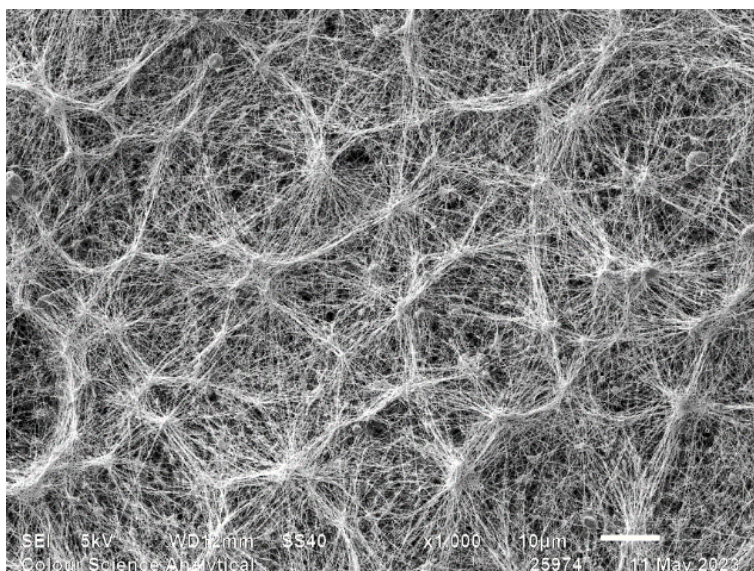
Figure 7.2. – Representative SEM images of PCL/PAla nanofibres produced in A) spin 3, and B) spin 4 with scale bars of 10 µm.

For spin 5, PCL was dissolved in HFIP at a concentration of 7wt%, as for spin 1, and PALa was dissolved in a 1:1 ratio of HFIP/chloroform at a concentration of 5wt%. The two solutions were combined in a 1:1 ratio and electrospun with a potential difference of 11 kV and a flow rate of 2 mL/hour. Analysis by SEM (Figure 7.3., Image A) showed a marked reduction in electrospay and beading, with an average nanofibre diameter of 60 nm (SD = 17 nm). Spin 5 was repeated (Table 7.1., Spin 6) with half the flow rate (1 mL/hour) and showed even less electrospay and beading (Figure 7.3., Image B), with a similar average nanofibre diameter of 62 nm (SD = 15 nm). To increase the average nanofibre diameter, spin 5 was repeated again (Table 7.1., Spin 7) with an increased potential difference of 20 kV. Analysis of the resultant nanofibre mat by SEM (Figure 7.4.) showed very little electrospay or beading, with an average nanofibre diameter of 120 nm (SD = 41 nm). The conditions used in spin 7 were taken as most optimum due to the morphology of the resultant nanofibre mat.



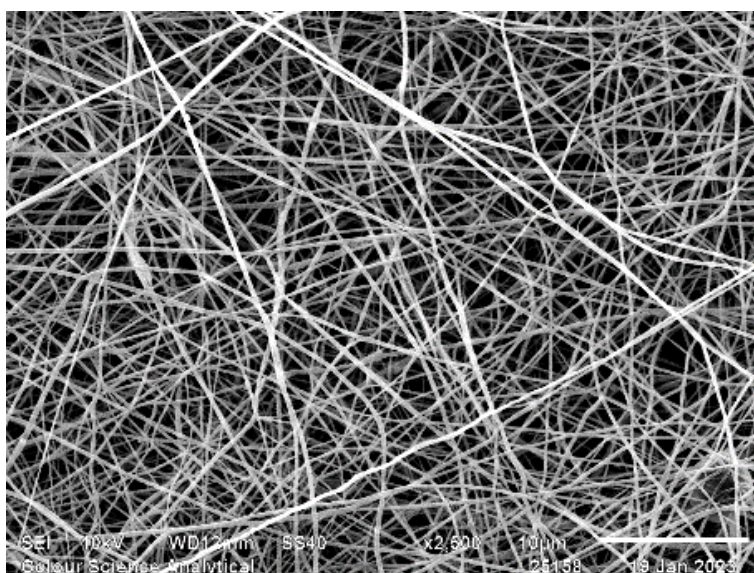
*Figure 7.3.* – Representative SEM images of PCL/PALa nanofibres produced in A) spin 5, and B) spin 6 with scale bars of 10  $\mu\text{m}$ .





*Figure 7.4.* - Representative SEM image of PCL/PAla nanofibres produced in spin 7, with a scale bar of 10  $\mu\text{m}$ .

For the electrospinning of PCL with PSar, PCL was dissolved as for spin 1 (7wt% in HFIP) and PSar was dissolved in chloroform at a concentration of 5wt%. The two solutions were combined at a 1:1 ratio and electrospun with a flow rate of 2 mL/hr and a potential difference of 14 kV (Table 7.1., Spin 8). The resultant nanofibre mat was assessed using SEM (Figure 7.5.) and found to have no electrospray or beading. The average nanofibre diameter was 167 nm (SD = 58 nm) and the average pore diameter was 376 nm (SD = 136 nm).



*Figure 7.5.* - Representative SEM image of PCL/PSar nanofibres produced in spin 8, with a scale bar of 10  $\mu\text{m}$ .

All the PCL/PAla nanofibre mats and the PCL/PSar nanofibre mat had average nanofibre diameters within the range of fibre diameter that is most prevalent within natural ECM (50-500 nm) and were therefore suitable as a mimic of the physical structure of natural ECM. The average pore sizes of all PCL/PAla mats were greater than 200 nm and less than 1  $\mu\text{m}$ . As such, all the mats had sufficient porosity for gas permeation<sup>44</sup>, but narrow enough pores that they may prevent microbial infiltration and cell ingrowth which may prevent infection and allow for removal of the material from a wound site without causing secondary wound damage<sup>41,45</sup>.

#### **7.3.4. Water Uptake Testing of Nanofibre Mats**

Effective wound dressings require the capacity to both maintain moisture levels and absorb exudate at a wound site<sup>44</sup>. As such, assessment of water uptake capacity (Table 7.2.) by the nanofibre mats was conducted as a rudimentary but representative way to determine their capacity to uptake and maintain water, providing evidence for their potential efficacy as wound dressings. The nanofibre mats from spin 2, spin 7 and spin 8 were selected for water uptake assessment as they had the most consistent nanofibres of diameters between 50-500 nm out of the PCL, PCL/PAla and PCL/PSar nanofibre mats respectively. A portion of each was taken, weighed and immersed in deionised water for 24 hours. After which, the excess water was removed from the surface of the samples by patting dry using filter paper and the samples weighed again. Whilst this drying method is rudimentary and subject to error, it ensured that water taken up into the samples was not driven out using heat or air flow. The water uptake percentage results are reported in Table 7.2. and calculated as follows:

$$\text{Water uptake \%} = \frac{\text{Mass after} - \text{Mass before}}{\text{Mass before}} \times 100$$

*Table 7.3. – Weights of nanofibre samples before and after immersion in deionised water and their % water uptake and results from tensile testing including maximum stress and strain, elastic moduli and toughness of PCL, PCL/PAla and PCL/PSar nanofibre samples taken from spin 2, spin 7 and spin 8 respectively.*

Sample	Weight (mg)		% Water Uptake	Maximum strain %		Maximum stress (kPa)		Young's moduli (kPa)			Toughness (MPa)
	Before	After		Error	Error	Initial, E	Tangent, E <sub>t</sub>	Secant, E <sub>s</sub>			
PCL	0.5	1.7	240	93.1	12.3	2458	450	3130	2010	2640	2.14
PCL/PAla	2.8	19.5	596	59.1	5.2	12300	1600	36580	26000	20780	3.59
PCL/PSar	0.5	10.8	2060	69.4	7.7	5740	1100	4240	10470	8270	2.42

Despite the hydrophobicity of PCL, the PCL nanofibre mat produced from spin 2 had a water uptake percentage of 240%. This may be as a result of the capacity of PCL to act as a hydrogen bond acceptor. Whilst polyalanine is also a hydrophobic polymer, it is less hydrophobic than polycaprolactone as a consequence of its capacity to accept and donate in hydrogen bonding. The PCL/PAla nanofibre mat produced in spin 7 had a water uptake percentage of 596%; a substantially higher percentage than that of PCL nanofibres alone. Polysarcosine is a hydrophilic polymer and the PCL/PSar nanofibre mat produced in spin 8 had a water uptake percentage of 2060%, over an eight-fold increase upon that of PCL nanofibres alone. As such, the inclusion of polyalanine and polysarcosine in polycaprolactone nanofibres can dramatically improve water uptake, enhancing the materials applicability as dressings for high exuding wounds, as well as those requiring a moist environment to be maintained.

### **7.3.5. Tensile Testing of Nanofibre Mats**

In order to perform most optimally as a wound dressing, a material should have similar mechanical properties to healthy human skin<sup>44</sup>. More specifically, the material should be flexible and, at a minimum, have similar tensile stress and toughness to human skin. Samples of the PCL, PCL/PAla and PCL/PSar nanofibre mats produced in spins 2, 7 and 8 respectively were assessed for their tensile properties (Figure 7.6., Table 7.2.). Each sample was clamped in place and subjected to a separation rate of 5 mm min<sup>-1</sup>. The resultant force against displacement curves were used to produce stress against strain curves by dividing the force data by the cross-sectional area of the mat to produce stress (kPa) and by dividing the displacement by the gauge length to produce strain percentage.



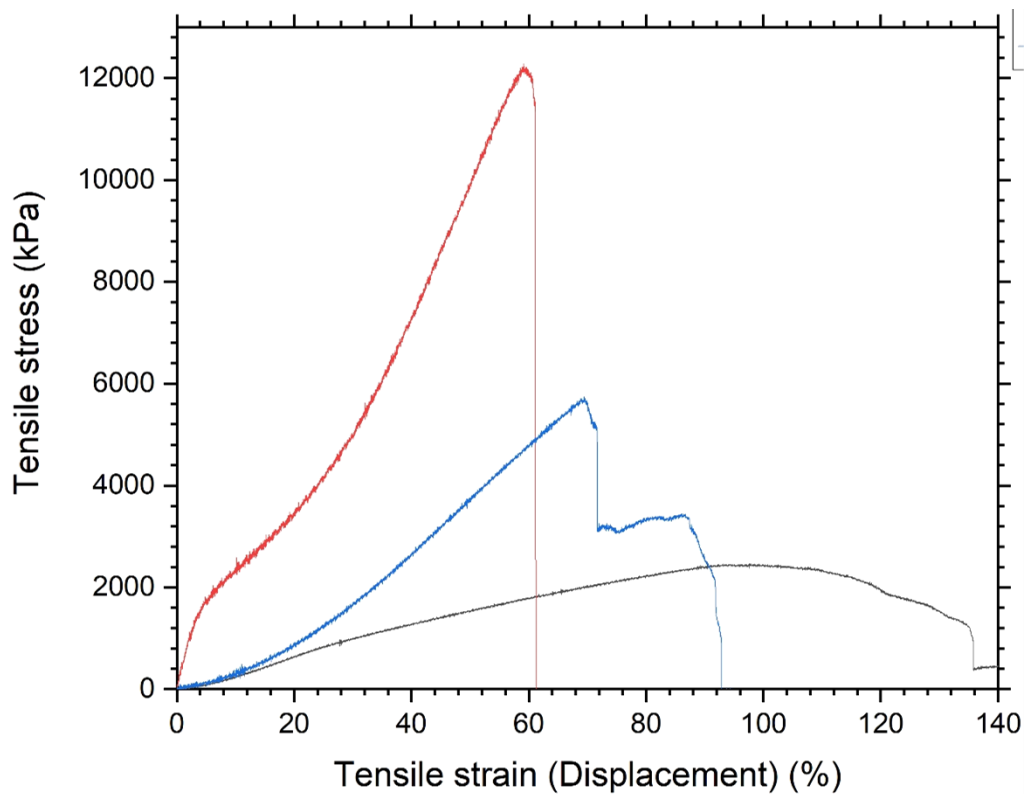


Figure 7.6. – Stress-strain curves of PCL nanofibres produced in spin 2 (black), PCL/PAla nanofibres produced in spin 7 (red) and PCL/PSar nanofibres produced in spin 8 (blue).

The PCL nanofibres produced in spin 2 endured a maximum tensile stress of  $2,458 \pm 450$  kPa. The PCL/PSar nanofibre mat produced in spin 8 endured a maximum tensile stress of  $5740 \pm 1100$  kPa showing a much greater capacity to bear tension when compared to PCL nanofibres. Furthermore, the PCL/PAla nanofibre mat endured a maximum tensile stress of  $12300 \pm 1600$  kPa, nearly five times greater than that of PCL nanofibres. Whilst there is substantial error between samples of the same mat (caused by fibre alignment and deformations within the fibre structure), there is no overlap between samples from different mats, signifying an augmentation of the physical properties due to the inclusion of PAla or PSar within the nanofibre network. Both nanofibre samples that included a poly(amino acid) had a lower maximum strain percentage, where the PCL, PCL/PAla and PCL/PSar nanofibre samples endured a maximum strain percentage of 93.1%, 59.1% and 69.4% respectively. Despite this, the PCL/PAla and PCL/PSar nanofibre samples had greater elastic moduli and toughness than the PCL nanofibre sample (Table 7.2.), with PCL/PAla having the highest tensile strength. According to a study published in 2019 on the tensile strength of full-thickness skin<sup>46</sup>, maximum tensile stress of healthy human skin can be between 7130-69770 kPa depending on where on the body the skin originated and the age of the donor<sup>46</sup>. The PCL/PSar nanofibre mat had a tensile strength

comparable to the bottom end of the range of healthy human skin, whereas the PCL/PAla nanofibre mat boasted a tensile strength well within the range of healthy human skin. As such, the PCL/PSar and PCL/PAla nanofibres possess tensile strengths suitable for use as a wound healing dressing.

### 7.3.6. Enzyme Degradation Study of PCL/PAla Nanofibre Samples

Wounds that fail to heal and become chronic wounds most commonly stall in the inflammation stage due to an overexpression of neutrophil proteases such as elastase<sup>10</sup>. A plausible treatment for this may be the application of a nanofibre dressing that can encapsulate therapeutics including bioactive agents and elastase inhibitors and subsequently release its therapeutic payload upon contact with elastase. As such, the PCL/PAla nanofibre mat produced in spin 7 was assessed for its sensitivity to elastase degradation, which would allow an entrapped therapeutic to be released from the fibrous network. The PCL/PAla nanofibre samples were incubated with 8U of neutrophil elastase in deionised water at room temperature for 2 hours. Samples were taken every half an hour of the study and assessed by weight loss, FTIR spectroscopy (appendix I), SEM and tensile testing. The results of these analyses are summarised in Table 7.4. and Table 7.5.

*Table 7.4.* – % mass loss, % beading, average fibre diameter, average pore diameter, and carbonyl intensities in FTIR spectra of PCL/PAla nanofibre samples that had been incubated with neutrophil elastase for 0, 0.5, 1, 1.5 and 2 hours.

Time (hrs)	% mass loss	% beading	Av. Fibre Diameter (nm)	$\sigma$	Av. Pore Diameter (nm)	$\sigma$	FTIR Carbonyl Intensity		
							PAla	PCL	Ratio
0	0	0	120	41	249	83	61.2	24.2	2.5
0.5	5.8	2.2	76	18	393	143	54.8	39.5	1.4
1	15.9	1.5	61	13	393	167	52.7	47.5	1.1
1.5	24.6	4.4	52	14	597	338	38	58.9	0.6
2	35.5	3.6	49	13	1353	838	21.6	64.6	0.3

Table 7.5. - Maximum strain, maximum stress, elastic moduli and toughness of PCL/PAla nanofibre samples that had been incubated with neutrophil elastase for 0, 0.5, 1, 1.5 and 2 hours.

Time (hrs)	Maximum strain %	Maximum stress (kPa)	Elastic Moduli (kPa)			Toughness (MPa)
			Initial, E	Tangent, E <sub>T</sub>	Secant, E <sub>S</sub>	
0	59.1	12281	36580	26000	20780	3.59
0.5	62.6	11545	10960	26720	18440	2.91
1	65.1	9783	15960	14280	15030	3.32
1.5	67.6	7207	16770	14640	10660	2.11
2	69	6549	9470	9660	9490	1.14

Samples of the PCL/PAla nanofibre mat incubated with neutrophil elastase were taken after 0, 30, 60, 90 and 120 minutes of incubation and showed a percentage mass loss of 0%, 5.8%, 15.9%, 24.6% and 35.5% respectively. A control sample of PCL/PAla nanofibres was incubated in deionised water only for 120 minutes and showed 0% loss in mass, indicating that mass loss of PCL/PAla nanofibres is due to neutrophil elastase activity.

FTIR spectroscopy (appendix I) of the PCL/PAla nanofibre samples illustrated that increased exposure to elastase resulted in a decreased ratio of intensity of the polyalanine carbonyl peak at 1674 cm<sup>-1</sup> to intensity of the polycaprolactone carbonyl peak at 1725 cm<sup>-1</sup> from 2.5 to 0.3 (Figure 7.7.). This signifies a selective decrease in polyalanine present in the sample ascribed to degradation of the polyalanine present in the nanofibre mats by elastase.

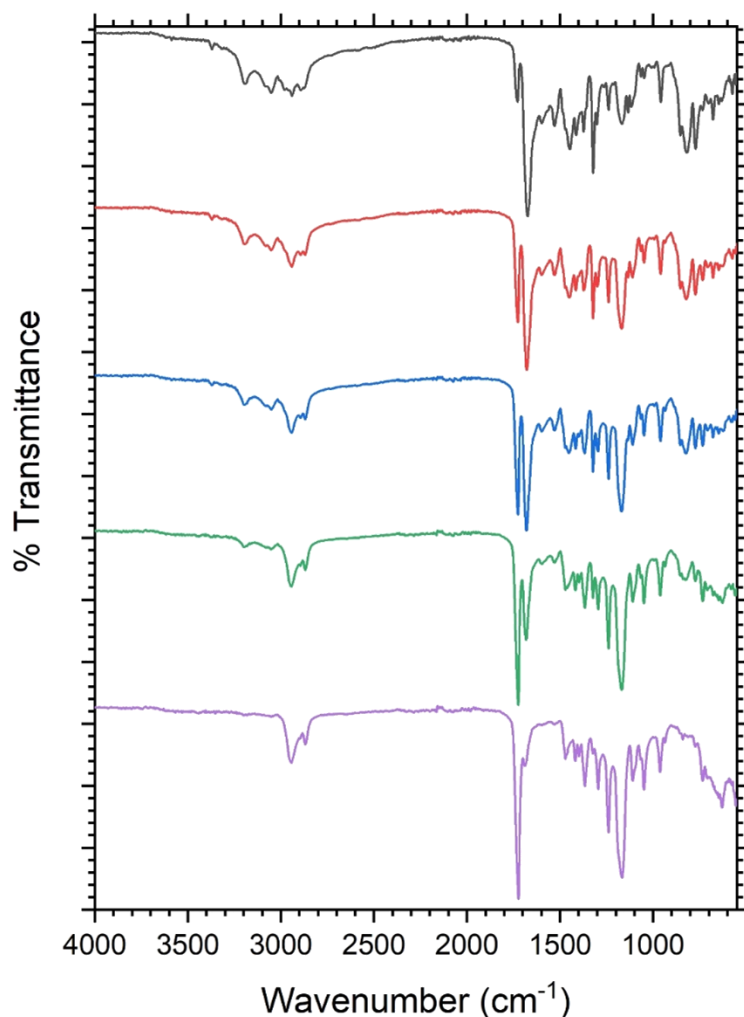


Figure 7.7. – FTIR spectra of PCL/PAla nanofibre samples produced in spin 7 before (black) and after incubation with neutrophil elastase for 30 minutes (red), one hour (blue), 1.5 hours (green) and 2 hours (purple).

The incubated PCL/PAla samples were assessed using SEM (Figure 7.8.), the images of which were utilised to produce a distribution of fibre diameter and pore diameter. Analysis of the incubated PCL/PAla nanofibre samples by SEM showed that with increased incubation with elastase, average fibre diameter decreased from 120 nm to 49 nm (Table 7.3.). Additionally, increased incubation with elastase showed an increase in average pore diameter from 249 nm to 1353 nm. Despite this, the nanofibre mat remained intact and its nanofibre matrix maintained after two hours of exposure to elastase. As such, this indicates the degradation of polyalanine sections of nanofibre and the retention of polycaprolactone fibres with increased porosity. This may indicate the capacity for increased gas and nutrient/therapeutic transfer between the dressing and the wound.

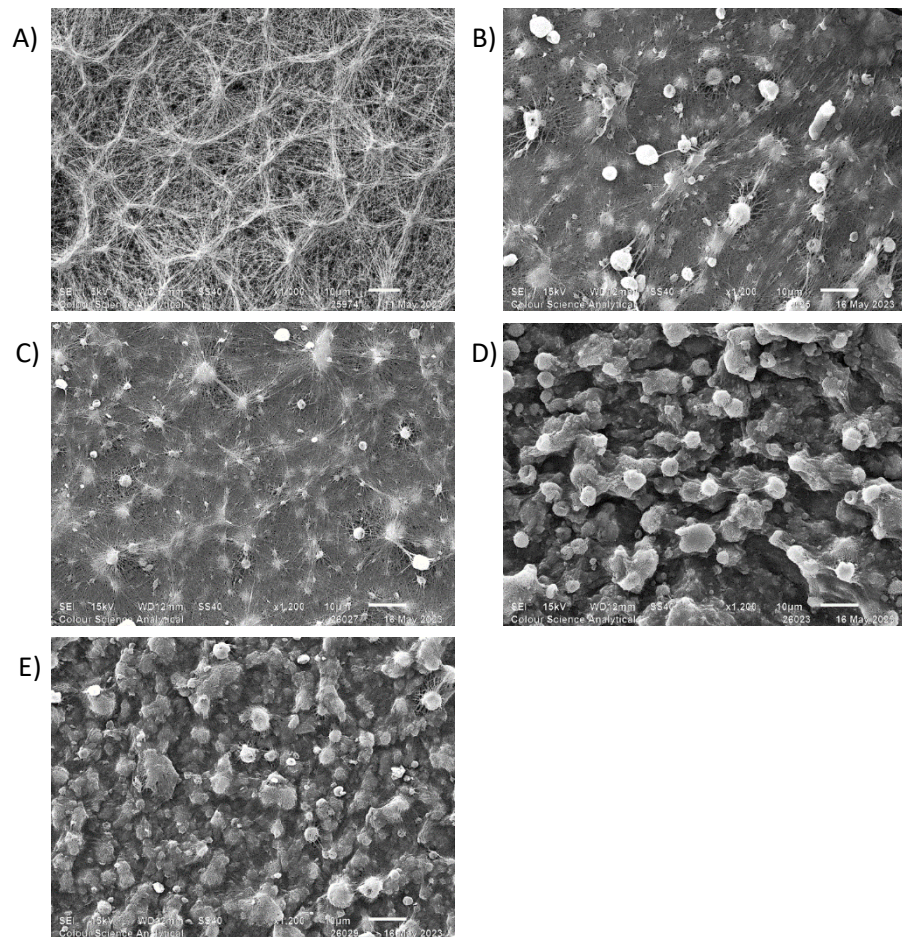


Figure 7.8. – SEM image of PCL/PAla nanofibres produced in spin 7 A) 0 minutes, B) 30 minutes, C) 60 minutes, D) 90 minutes and E) 120 minutes of incubation with 8U elastase.

Samples of the PCL/PAla nanofibre mat that had been incubated in elastase were also assessed for their tensile properties as described above for PCL, PCL/PSar and PCL/PAla nanofibres (Figure 7.9.).

Increased incubation time of PCL/PAla nanofibre samples with elastase resulted in a decrease in maximum stress from 12281 kPa to 6549 kPa and an increase in maximum strain percentage from 59.1% to 69%. This is demonstrative that the degradation of the component present within the nanofibres that is enhancing maximum stress capacity increases with increased time of elastase incubation. As illustrated in the stress against strain curve shown in Figure 7.9., the PCL/PAla nanofibre sample can tolerate a greater maximum stress than that of PCL alone. Therefore, elastase is selectively degrading polyalanine nanofibres within the mat. Despite this, the most degraded nanofibre sample, after 2 hours of incubation, had a greater maximum stress than the PCL nanofibre mat produced in spin 2 and retained structural integrity.

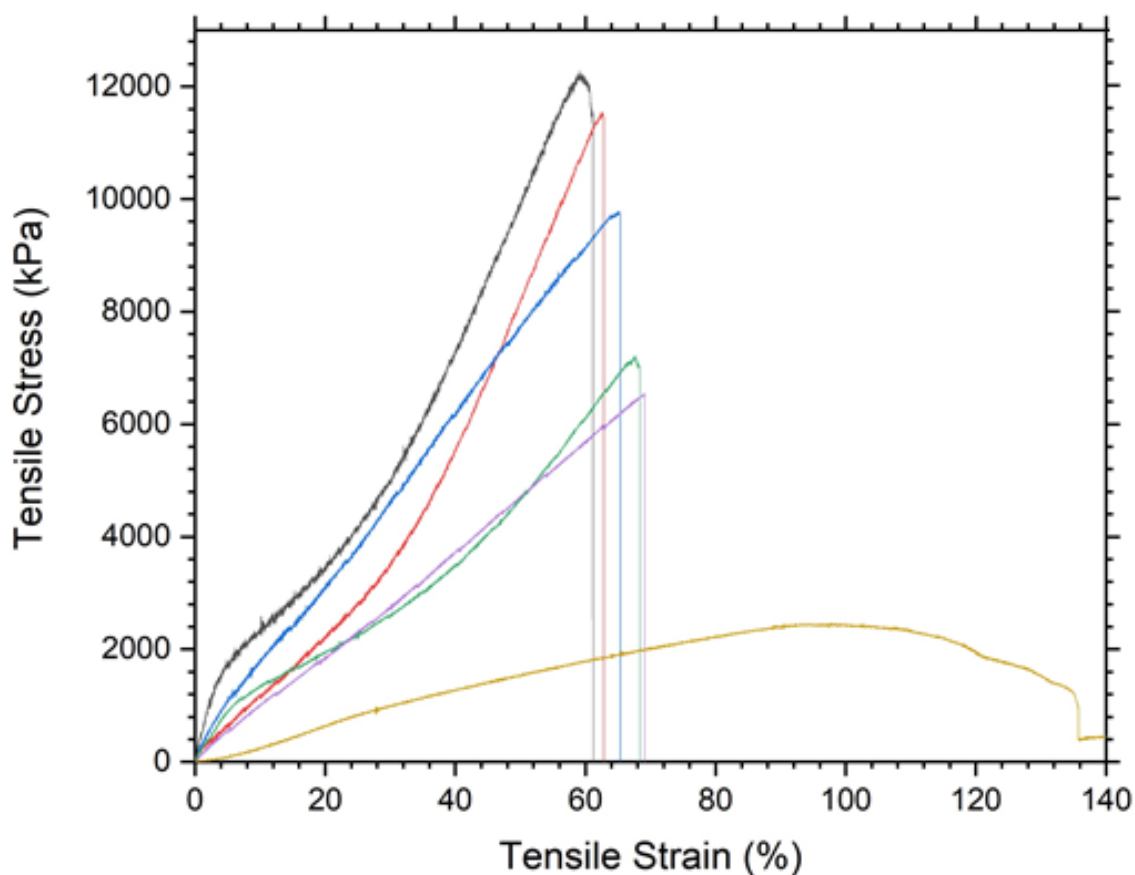


Figure 7.9. – Stress-strain curves of PCL nanofibres (brown), PCL/PAla nanofibres before (black) and after incubation with elastase for 30 minutes (red), 1 hour (blue), 1.5 hours (green) and 2 hours (purple).

#### 7.4. Conclusion

The electrospinning of polycaprolactone with polysarcosine and polyalanine has been reported for the first time, along with the parameters required to produce nanofibre structures that can replicate the physical structure of human ECM from these combinations of polymers. The resultant PCL/PAla and PCL/PSar nanofibre mats compared well with that of PCL, bearing enhanced physicochemical properties that are well suited for use as a chronic wound dressing. The PCL/PAla and the PCL/PSar nanofibre mats displayed excellent water uptake capacity indicating the capability to maintain moisture and absorb exudate at a wound site. The PCL/PSar and PCL/PAla nanofibre mats displayed excellent tensile strength, boasting a maximum tensile stress greater than that of PCL alone and that were within the range of healthy human skin. Furthermore, upon increased elastase exposure, the resultant effect on the samples of the PCL/PAla nanofibre mat were: an increase in percentage mass loss, a decrease in ratio of polyalanine:polycaprolactone content, a decrease in nanofibre diameter, an increase in pore

diameter, a decrease in maximum stress capacity and a small increase in maximum strain percentage. These effects are demonstrative of the selective degradation of polyalanine present in the PCL/PAla nanofibre mat by elastase and, notably, indicates a potential capacity to release an encapsulated payload that can inhibit elastase, following material exposure to elastase. Overall, the resultant PCL/PAla and PCL/PSar nanofibre materials displayed physicochemical properties that were superior to that of un-augmented PCL nanofibres and indicate a greater suitability to facilitate healing in chronic wounds as a dressing.

## 7.5. References

---

- 1) Tang, Y., Varyambath, A., Ding, Y., Chen, B., Huang, X., Zhang, Y., Yu, D-G., Kim, I. and Song, W. Porous organic polymers for drug delivery: hierarchical pore structures, variable morphologies, and biological properties. *Biomaterials Science*. 2022, **10**(19), 5369-5390.
- 2) Maksoud, F. J., Velázquez de la Paz, M. F., Hann, A. J., Thanarak, J., Reilly, G. C., Claeysens, F., Green, N. H. and Zhang, Y. Z. Porous biomaterials for tissue engineering: a review. *Journal of Materials Chemistry B*. 2022, **22**(40), 8111-8165.
- 3) Poupat, R., Grande, D., Carbonnier, B. and Le Droumaguet, B. Porous polymers and metallic nanoparticles: A hybrid wedding as a robust method toward efficient supported catalytic systems. *Progress in Polymer Science*. 2019, **96**, 21-42.
- 4) Wang, S., Li, H., Hunag, H., Cao, X., Chen, X. and Cao, D. Porous organic polymers as a platform for sensing applications. *Chemical Society Reviews*. 2022, **51**(6), 2031-2080.
- 5) Kovylin, R. S., Aleynik, D. Ya. And Fedushkin, I. L. Modern Porous Polymer Implants: Synthesis, Properties, and Application. *Polymer Science Series C*. 2021, **63**, 29-46.
- 6) Deng, S., Chen, A., Chen, W., Lai, J., Pei, Y., Wen, J., Yang, C., Luo, J., Zhang, J., Lei, C., Varma, S. N. and Liu, C. Fabrication of Biodegradable and Biocompatible Functional Polymers for Anti-Infection and Augmenting Wound Repair. *Polymers (Basel)*. 2023, **15**(1), 120-140.
- 7) Eming, S. A., Martin, P. and Tomic-Canic, M. Wound repair and regeneration: mechanisms, signalling, and translation. *Science translational medicine*. 2014, **6**, 265sr6.
- 8) Sun, B. K., Sibrashvili, Z. and Khavari, P. A. Advances in skin grafting and treatment of cutaneous wounds. *Science*. 2014, **346**, 941-945.
- 9) Frykberg, R. G. and Banks, J. Challenges in the Treatment of Chronic Wounds. *Advances in Wound Care (New Rochelle)*. 2015, **4**(9), 560-582.
- 10) Ji, Y., Song, W., Xu, L., Yu, D-G. and Bligh, S. W. A. A Review on Electrospun Poly(amino acid) Nanofibers and Their Applications of Hemostasis and Wound Healing. *Biomolecules*. 2022, **12**, 794-820.
- 11) McCarty, S. M. and Percival, S. L. Proteases and delayed healing. *Advanced Wound Care*. 2013, **2**, 438-447.



- 
- 12) Yuan, Z., Sheng, D., Jiang, L., Shafiq, M., Khan, A.R., Hashim, R., Chen, Y., Li, B., Xie, X., Chen, J., Morsi, Y., Mo, X. and Chen, S. Vascular endothelial growth factor-capturing aligned electrospun polycaprolactone/gelatin nanofibers promote patellar ligament regeneration. *Acta Biomaterialia*. 2022, **140**, 233–246.
- 13) Kant, V., Kumari, P., Jitendra, D.K., Ahuja, M. and Kumar, V. Nanomaterials of Natural Bioactive Compounds for Wound Healing: Novel Drug Delivery Approach. *Current Drug Delivery*. 2021, **18**, 1406–1425.
- 14) Li, J., Guan, S., Su, J., Liang, J., Cui, L. and Zhang, K. The Development of Hyaluronic Acids Used for Skin Tissue Regeneration. *Current Drug Delivery*. 2021, **18**, 836–846.
- 15) Zhang, T., Sanguramath, R. A., Israel, S. and Silverstein, M. S. Emulsion Templating: Porous Polymers and Beyond. *Macromolecules*. 2019, **52**(15), 5445-5479.
- 16) Prasad, A., Sankar, M. R. and Katiyar, V. State of Art on Solvent Casting Particulate Leaching Method for Orthopedic Scaffolds Fabrication. *Materials today: Proceedings*. 2017, **4**(2A), 898-907.
- 17) Costantini, M. and Barbetta A. 6 – Gas foaming technologies for 3D scaffold engineering. In: Deng, Y. and Kuiper, J. Woodhead Publishing, 2018, 127-149.
- 18) Wang, C., Huang, W., Zhou, Y., He, L., He, Z., Chen, Z., He, X., Tian, S., Liao, J., Lu, B., Wei, Y. and Wang, M. 3D printing of bone tissue engineering scaffolds. *Bioactive Materials*. 2020, **5**(1), 82-91.
- 19) Luraghi, A., Peri, F. and Moroni, L. Electrospinning for drug delivery applications: A review. *Journal of Controlled Release*. 2021, **334**, 463-484.
- 20) Liu, R., Hou, L., Yue, G., Li, H., Zhang, J., Liu, J., Miao, B., Wang, N., Bai, J., Cui, Z., Liu, T. and Zhao, Y. Progress of Fabrication and Applications of Electrospun Hierarchically Porous Nanofibers. *Advanced Fiber Materials*. 2022, **4**, 604-630.
- 21) Svinterikos, E. and Zuburtikudis, I. Tailor-Made Electrospun Nanofibers of Biowaste Lignin/Recycled Poly(Ethylene Terephthalate). *Journal of Polymers and the Environment*. 2017, **25**, 465-478.
- 22) Safonova, L., Bobrova, M., Efimov, A., Davydova, L., Tenchurin, T., Bogush, V., Agapova, O. and Agapov, I. Silk Fibroin/Spidroin Electrospun Scaffolds for Full-Thickness Skin Wound Healing in Rats. *Pharmaceutics*. 2021, **13**(10), 1704-1716.

- 
- 23) Wang, M., Tan, Y., Li, D., Xu, G., Yin, D., Xiao, Y., Chen, X., Zhu, X. and Shi, X. Negative Isolation of Circulating Tumor Cells Using a Microfluidic Platform Integrated with Streptavidin-Functionalized PLGA Nanofibers. *Advanced Fiber Materials*. 2021, **3**, 192–202.
- 24) Varshosaz, J., Choopannejad, Z., Minaiyan, M. and Kharazi, A.Z. Rapid hemostasis by nanofibers of polyhydroxyethyl methacrylate/polyglycerol sebacic acid: An in vitro/in vivo study. *Journal of Applied Polymer Science*. 2021, **138**(5), 49785-49800.
- 25) Adeli, H., Khorasani, M.T. and Parvazinia, M. Wound dressing based on electrospun PVA/chitosan/starch nanofibrous mats: Fabrication, antibacterial and cytocompatibility evaluation and in vitro healing assay. *International Journal of Biological Macromolecules*. 2019, **122**, 238–254.
- 26) Azimi, B., Maleki, H., Zavagna, L., De la Ossa, J. G., Linari, S., Lazzeri, A. and Danti, S. Bio-Based Electrospun Fibers for Wound Healing. *Journal of Functional Biomaterials*. 2020, **11**, 67-102.
- 27) URL St. Teresa Medical INC. *SurgiClot Hemostatic Dressing – Instructions for Use*. [70000NZ IFU]. [Online]. 2915 Waters Road, Suite 108, Eagan, Minnesota 55121, USA: St. Teresa Medical, Inc., 2023. [10/08/2023]. Available from: <https://stteresamedical.com/support/instructions-for-use>
- 28) Yuan, J., Geng, J., Xing, Z., Shim, K-J., Han, I., Kim, J-C., Kang, I-K. and Shen, J. Novel wound dressing based on nanofibrous PHBV-keratin mats. *Journal of Tissue Engineering and Regenerative Medicine*. 2012, **9**(9), 1027-1035.
- 29) Dwivedi, R., Kumar, S., Pandey, R., Mahajan, A., Nandana, D., Katti, D. S. and Mehrotra, D. Polycaprolactone as biomaterial for bone scaffolds: Review of literature. *Journal of Oral Biology and Craniofacial Research*. 2020, **10**(1), 381-388.
- 30) Azari, A., Golchin, A., Maymand, M. M., Mansouri, F. and Ardeshtyrlajimi, A. Electrospun Polycaprolactone Nanofibers: Current Research and Applications in Biomedical Application. *Advanced Pharmaceutical Bulletin*. 2022, **12**(4), 658-672.
- 31) Tsuchiya, K., Masunaga, H. and Numata, K. Tensile Reinforcement of Silk Films by the Addition of Telechelic-Type Polyalanine. *Biomacromolecules*. 2017, **18**(3), 1002-1009.
- 32) Oh, H. J., Joo, M. K., Sohn, Y. S. and Jeong, B. Secondary Structure Effect of Polypeptide on Reverse Thermal Gelation and Degradation of l/dl-Poly(alanine)-Polyoxamer-l/dl-Poly(alanine) Copolymers. *Macromolecules*. 2008, **41**(21), 8204-8209.

- 
- 33) Pokorna, A., Bobal, P., Oravec, M., Rarova, L., Bobalova, J. and Jampilek, J. Investigation of Permeation of Theophylline through Skin Using Selected Piperazine-2,5-Diones. *Molecules*. 2019, **24**(3), 566-579.
- 34) Manchineella, S., Voshavar, C. and Govindaraju, T. Radical-Scavenging Antioxidant Cyclic Dipeptides and Silk Fibroin Biomaterials. *European Journal of Organic Chemistry*. 2017, **30**, 4363-4369.
- 35) Basiuk, V. A., Gromovoy, T. Y., Chuiko, A. A., Soloshonok, V. A. and Kukhar, V. P. A Novel Approach to the Synthesis of Symmetric Optically Active 2,5-Dioxopiperazines. *Synthesis*. 1992, **5**, 449-451.
- 36) Zhao, S., Ye, X., Wu, M., Ruan, J., Wang, X., Tang, X. and Zhong, B. Recombinant Silk Proteins with Additional Polyalanine Have Excellent Mechanical Properties. *International Journal of Molecular Sciences*. 2021, **22**(4), 1513-1526.
- 37) Oh, H. J., Joo, M. K., Sohn, Y. S. and Jeong, B. Secondary Structure Effect of Polypeptide on Reverse Thermal Gelation and Degradation of l/dl-Poly(alanine)-Polyoxamer-l/dl-Poly(alanine) Copolymers. *Macromolecules*. 2008, **41**(21), 8204-8209.
- 38) Birke, A., Ling, J. and Barz, M. Polysarcosine-containing copolymers: Synthesis, characterization, self-assembly, and applications. *Progress in Polymer Science*. 2018, **81**, 163-208.
- 39) Koski, A., Yim, K. and Shivkumar, S. Effect of molecular weight on fibrous PVA produced by electrospinning. *Materials Letters*. 2004, **58**, 493-497.
- 40) Tao, J. and Shivkumar, S. Molecular weight dependent structural regimes during the electrospinning of PVA. *Materials Letters*. 2007, **61**(11-12), 2325-2328.
- 41) Kanani, A. G. and Bahrami, S. H. Review on Electrospun Nanofibers Scaffold and Biomedical Applications. *Trends in Biomaterials & Artificial Organs*. 2010, **24**(2), 93-115.
- 42) Bhattarai, N., Edmondson, D., Veiseh, O., Matsen, F. A. and Zhang, M. Electrospun chitosan-based nanofibers and their cellular compatibility. *Biomaterials*. 2005, **26**(31), 176-184.
- 43) Somvipart, S., Kanokpanont, S., Rangkupan, R., Ratanavaraporn, J. and Damrongsakkul, S. Development of electrospun beaded fibers from Thai silk fibroin and gelatin for controlled release application. *International Journal of Biological Macromolecules*. 2013, **55**, 176-184.

---

44) Abrigo, M., McArthur, S. L. and Kingshott, P. Electrospun Nanofibers as Dressings for Chronic Wound Care: Advances, Challenges and Future Prospects. *Macromolecular Bioscience*. 2014, **14**, 772-792.

45) Zhang, Y., Lim, C. T., Ramakrishna, S. and Huang, Z-M. Recent Development of Polymer Nanofibers for Biomedical and Biotechnological Applications. *Journal of Materials Science: Materials in Medicine*. 2005, **16**, 933-946.

46) Holmdahl, V., Backman, O., Gunnarsson, U. and Strigård, K. The Tensile Strength of Full-Thickness Skin: A Laboratory Study Prior to Its Use as Reinforcement in Parastomal Hernia Repair. *Frontiers in Surgery*. 2019, **6**, [no pagination].

## Chapter 8 – Expansion of Poly(amino acid) Library and ROP Conditions

### Abstract

DKP ROP as a route to poly(amino acids) is a new and relatively unexplored methodology. When compared to well-established NCA ROP and solid-state peptide-synthesis (SSPS), the range of accessible poly(amino acids) from DKP ROP is much narrower and requires expansion. Additionally, NCA ROP and SSPS have benefited from years of optimisation since their inception, rendering them as relatively efficient processes. As a consequence of its novelty, DKP ROP lacks such essential optimisation which may compromise its efficacy. Reported in this chapter is the expansion of accessible poly(amino acids) from DKP ROP. In addition, attempts to optimise DKP ROP as a process in order to produce polymers with higher molecular weight, greater % monomer conversion, enhanced environment credentials, and faster reaction rates are described. Poly(amino acids) that are challenging to produce by NCA ROP, most notably polyproline, are included to further emphasise the usefulness of DKP ROP.

### 8.1. Introduction

This thesis marks the introduction of DKP ROP as a route to poly(amino acids). Whilst the poly(amino acids) reported so far have boasted impressive  $\mathcal{D}$  values ( $<1.15$ ), and the synthetic procedure is relatively green and inexpensive, the variety of poly(amino acids) produced from DKP ROP thus far is narrow and requires expansion in order to broaden the use case of DKP ROP for poly(amino acid) synthesis. Additionally, some of the polymerisations, such as those of alanine DKP, have suffered from relatively low monomer conversions and, when compared with NCA ROP, long reaction times. It is anticipated that this is due to the stability of DKPs when compared to NCAs, but attempts must be made to ensure that DKP ROP is optimised to be as efficient as possible. It is plausible that DKP ROP can also be optimised with respect to the reagents and conditions utilised in order to reach higher molecular weight polymers, higher % monomer conversion and faster reaction rates.

NCA ROP can be used to access a relatively wide range of homopolymers and a variety of copolymers, as can solid-state peptide-synthesis<sup>1</sup>. Whilst each of these methods have their own collections of strengths and flaws, which are highlighted previously, they have been used to make polymers of nearly every canonical amino acid as well as polymers of non-canonical amino acids<sup>2</sup>. Within NCA synthesis and NCA ROP, there are well-defined optimisation pathways in order to minimise NCA degradation and facilitate the efficient production of polymers with narrow dispersity<sup>3</sup>. NCA synthesis via the Fuchs-Farthing<sup>3</sup> method has been optimised by

selection of cyclisation agent, selection of acid scavenger system, when to apply heat to the reaction mixture in order to generate phosgene *in situ* and how long to heat for, and the selection of methods of product purification<sup>4</sup>. Additionally, the parameters of NCA ROP that have been optimised include the selection of initiator, temperature of the reaction, selection of catalyst or lack thereof, and the direction of the reaction via the normal amine mechanism or the activated monomer mechanism<sup>4</sup>. These procedural changes have been utilised in concert or alone in order to improve the efficiency of the process and, ultimately, to improve the quality and range of poly(amino acids) obtainable by NCAs.

However, there are poly(amino acids) that, thus far, appear to be inaccessible via NCA ROP, such as polyproline, a polymer of growing interest within bio-based cryopreservation. Graham *et al.*<sup>5</sup> recently reported the polycondensation of proline using 1-ethyl-3-(3-dimethylaminopropyl) carbodiimide (EDC) as a coupling reagent<sup>5</sup>. A collection of lower molecular weight polyproline samples were produced with, for the majority, low  $\bar{M}_w$  values ( $<1.03$ )<sup>5</sup>. The capacity of polyproline to act as an ice-recrystallisation inhibitor was confirmed using cryo-confocal microcapillary microscopy and an A549 cryopreservation assay, highlighting the value of polyproline within a cryopreservation setting<sup>5</sup>. Whilst polyproline was afforded after a single step process at low temperature, the requirement of EDC and use of dichloromethane (DCM) compromises the affordability and green credentials of this route, rendering the potential scalability to industrial level as uncertain.

Although the synthesis and polymerisation of arginine NCA has been reported previously<sup>6</sup>, polyarginine is a polymer of considerable value owing to its enhanced capacity for cell penetration<sup>7</sup>. Additionally, synthesis of polyarginine via NCA ROP is not commonly reported due to the inconsistent nature of the synthesis in terms of purity and yield of the product. Similarly, methionine NCA synthesis and polymerisation have also been reported<sup>8</sup>. The use of polymethionine has been reported across a wide variety of applications, including as the hydrophobic block of a PEG-*b*-PMet copolymer capable of producing oxidation-sensitive micelles and vesicles via ROPISA of methionine NCA<sup>8</sup>.

Within lactone ROP, a well-established alternative to Lewis acid catalysis is the use of enzymes; an enzyme that is most commonly used is *Candida Antarctica* Lipase B (CALB)<sup>9</sup>. The active site of CALB contains a serine unit which bears a primary alcohol group as its side chain; the alcohol group both initiates and catalyses the ROP of lactones by nucleophilically attacking the carbonyl carbon of the lactone<sup>10</sup>. Although enzyme-catalysed ROP (eROP) is not widely reported, Schwab *et al.*<sup>11</sup> present the eROP of 2-azetidinone catalysed by CALB, producing low molecular weight

poly( $\beta$ -alanine)<sup>11</sup>. Whilst ring-strain present in 2-azetidinone most likely contributed to its ring-opening, there is scope for application to DKP eROP. Additionally, given appropriate reaction conditions, it is plausible that the primary alcohol present in the active site of CALB may be capable of nucleophilic attack of the carbonyl carbon of a lactam, such as a DKP.

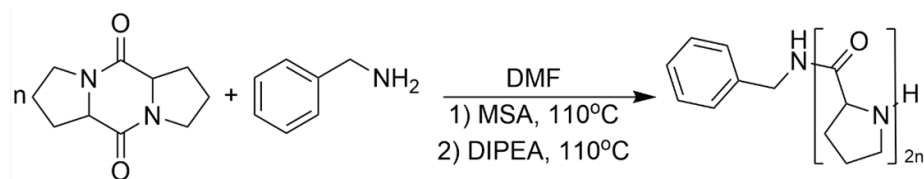
The ROP of proline DKP, as well as the ROP of other DKPs such as methionine DKP and a 2,2,4,6,7-pentamethyldihydrobenzofuran-5-sulfonyl-arginine (arginine(Pbf)) DKP, are reported. Syntheses involving the use of alternative catalysts are also reported, as well as the use of alternative, less environmentally impactful solvents.

## 8.2. Experimental Details

### 8.2.1. Synthesis of DKPs

The DKPs of proline, methionine, tryptophan and arginine(Pbf), were synthesised as reported in Chapter 3.

### 8.2.2. Synthesis of Polyproline



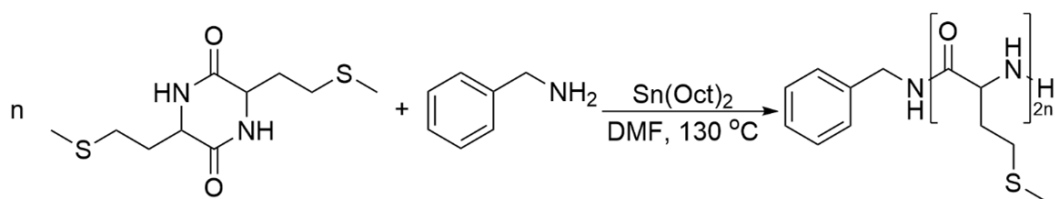
*Scheme 8.1.* - Reaction scheme of ROP of proline DKP, initiated with benzylamine and catalysed using MSA initially, followed by neutralisation and base catalysis with DIPEA, at 110 °C.

Proline DKP (1.568 g, 8.07 mmol) was added to an oven-dried vessel and flushed with  $N_{2(g)}$ . Benzylamine (24.7 mg, 0.231 mmol) and methanesulfonic acid (55.4 mg, 0.577 mmol) were separately dissolved in anhydrous DMF (2 mL) in a sealed vessel and flushed with  $N_{2(g)}$ . Anhydrous DMF (6 mL) was added to the proline DKP and the MSA and benzylamine solutions were also added simultaneously. The reaction mixture was heated to 110 °C with constant flow of  $N_{2(g)}$  for 44 hours, after which the reaction mixture was allowed to cool to room temperature. DIPEA (149.1 mg, 1.153 mmol) was dissolved in anhydrous DMF (2 mL) in a sealed vessel and flushed with  $N_{2(g)}$ . The DIPEA solution was added to the reaction mixture, which was then heated to 110 °C and stirred under constant flow of  $N_{2(g)}$  for a further 116 hours. The reaction mixture was then cooled to room temperature, unsealed and a steady flow of  $N_{2(g)}$  blown over it,

removing the DMF. The solids were redissolved in deionised water (6 mL) and dialysed (2000 Da molecular weight cut-off) against deionised water for two days with frequent water changes to remove unreacted monomer. The solution was frozen and lyophilised to obtain an off-white solid.

This procedure was repeated with a higher ration of proline DKP:benzylamine, as well as using chloroform instead of DMF as the solvent as follows: Proline DKP (0.5 g, 2.57 mmol) was added to an oven-dried vessel and flushed with  $N_{2(g)}$ . Benzylamine (1.10 mg, 0.010 mmol) and methanesulfonic acid (10.4 mg, 0.108 mmol) were separately dissolved in anhydrous chloroform (4 mL) in a sealed vessel and flushed with  $N_{2(g)}$ . Anhydrous chloroform (6 mL) was added to the proline DKP and the MSA and benzylamine solutions were also added simultaneously. The reaction mixture was heated to 110 °C with constant flow of  $N_{2(g)}$  for 24 hours, after which the reaction mixture was allowed to cool to room temperature. DIPEA (27.92 mg, 0.216 mmol) was dissolved in anhydrous chloroform (2 mL) in a sealed vessel and flushed with  $N_{2(g)}$ . The DIPEA solution was added to the reaction mixture, which was then heated to 60 °C and stirred under constant flow of  $N_{2(g)}$  for a further 96 hours. The reaction mixture was then cooled to room temperature, unsealed and evaporated to dryness. The solids were redissolved in deionised water (6 mL) and dialysed (M.W.C.O. 2000 Da) against deionised water for two days with frequent water changes to remove unreacted monomer. The solution was frozen and lyophilised to obtain an off-white solid.

### 8.2.3. Synthesis of Polymethionine



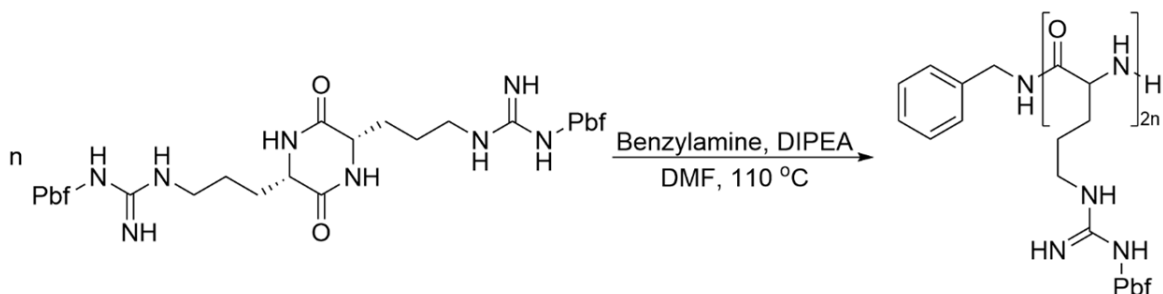
*Scheme 8.2.* – Ring-opening polymerisation of methionine DKP at 130 °C in anhydrous DMF, initiated from benzylamine and catalysed by tin(II) 2-ethylhexanoate.

Methionine DKP (400 mg, 1.52 mmol) was added to an oven-dried vessel, sealed and flushed with  $N_{2(g)}$ . Separately, tin(II) 2-ethylhexanoate (33  $\mu$ L, 0.102 mmol) and benzylamine (6  $\mu$ L, 0.051 mmol) were dissolved in anhydrous DMF (8 mL) and the solution added to the reaction vessel.



The mixture was stirred at 130 °C for two days, after which it was cooled to room temperature and added to ice-cold diethyl ether (90 mL). The precipitate was washed with additional ice-cold diethyl ether (90 mL) and dried *in vacuo*.

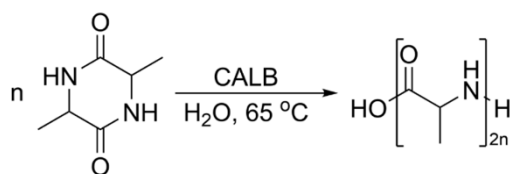
#### 8.2.4. Synthesis of Polyarginine(Pbf)



*Scheme 8.3.* – ROP of arginine(Pbf) DKP from benzylamine in DMF at 110 °C, catalysed by N,N-diisopropylethylamine.

Arginine(Pbf) DKP (400 mg, 0.49 mmol) was added to an oven-dried vessel and flushed with  $N_{2(g)}$ . Separately, Benzylamine (2  $\mu$ L, 0.016 mmol) and N,N-diisopropylethylamine (9.54  $\mu$ L, 0.066 mmol) were dissolved in anhydrous DMF (8 mL) and added to the reaction vessel. The mixture was stirred at 110 °C for two days, after which it was cooled to room temperature. The reaction mixture was added to ice-cold diethyl ether (90 mL), causing the product to precipitate. The solid was washed with additional ice-cold diethyl ether (90 mL) and dried *in vacuo*.

#### 8.2.5. eROP of Alanine DKP



*Scheme 8.4.* – Enzyme-catalysed ring-opening polymerisation of alanine DKP in deionised water at 65 °C, catalysed by *Candida Antarctica Lipase B*.

Alanine DKP (400 mg, 2.11 mmol) and CALB (106 mg, 211 U) were added to an oven-dried vessel, sealed and flushed with  $N_{2(g)}$ . The mixture was dissolved in deionised water (5 mL) and heated

to 65 °C and stirred for 20 hours. The immobilised enzyme was removed by hot filtration, the reaction mixture frozen in liquid nitrogen and lyophilised.

### **8.3. Results and Discussion**

#### **8.3.1. ROP of DKPs**

The DKPs of alanine, proline, arginine(Pbf) and methionine were synthesised as described in Chapter 3, the % yields of each synthesis are 76%, 69%, 63% and 59% respectively. All of these DKPs, aside from alanine DKP, were synthesised by this method for the first time, demonstrating the broad applicability of the direct amino acid bis-condensation as a reaction platform for creating cyclic monomers for poly(amino acid) synthesis. As a consequence of its helical structure, and alternating sites of hydrophilicity and hydrophobicity, polyproline boasts impressive ice-recrystallisation inhibition (IRI) activity<sup>5</sup>. As such, it is a polymer of significant interest within cell-monolayer cryopreservation and perhaps more broadly in food preservation and donor organ preservation.

Polyarginine is a polymer of widespread and increasing demand. Owing to its unique R group, the guanidinium group, polyarginine is able to act as a nucleophile. Additionally, homopolymers that are comprised of a high percentage of cationic amino acids are uniquely suited to cross cellular membranes, rendering them excellent vehicles that facilitate the cellular uptake of bioactive agents<sup>12</sup>. When compared to alternative cationic homopolypeptides, such as polylysine, polyarginine interacts more strongly with phospholipid bilayers<sup>13</sup>, emphasising the value in polyarginine and, therefore, the value in the development of a cost-effective route to its production. Furthermore, commercially available polyarginine, that has a broad dispersity, is for sale at £320+VAT for 100 mg<sup>14</sup>, which is extremely expensive. However, within DKP synthesis and polymerisation, the exposed guanidinium group of arginine (amino acid, DKP or polymer) may result in side reactions, such as competing with the  $\alpha$ -amine group for nucleophilic attack of the carbonyl, that are detrimental to the production of the DKP and, subsequently the polymer. As such, a Pbf protecting group, which is tolerant to higher temperatures and basic conditions, was used to minimise the occurrence of side reactions caused by the guanidinium group.

Whilst polymethionine is not a widely used polymer, there is a recent emergence in the literature of its use as a polymeric component within a collection of sensors, such as gold nanoparticle (NP)-polymethionine sensor for the electrochemical detection of paroxetine<sup>15</sup>, as well as a polymethionine/graphene oxide composite film electrode for the individual and

simultaneous determination of 5-hydroxyindole acetic acid and tyrosine<sup>16</sup>. As such, a method of polymethionine production that is cheap, green and facile is of value.

### 8.3.2. Synthesis of Polyproline

To determine the feasibility of producing polyproline from proline DKP, the ROP of proline DKP was attempted from benzylamine in DMF using a combined catalyst system of MSA and DIPEA. As described for sarcosine DKP, proline DKP is a bis-tertiary lactam. A second ROP attempt was conducted in chloroform in order to determine whether any solvent effects caused by DMF hinder or facilitate polymerisation. Factors, such as the rate of polymerisation, degree of polymerisation, and % monomer conversion may be impacted by the solvent used for the polymerisation. It is plausible that, due to greater interactions between DMF and the monomers and propagating polymer chains, DMF may inhibit the rate of polymerisation relative to that of chloroform. The two polyproline samples produced were assessed using FTIR spectroscopy (appendix I), <sup>1</sup>H NMR spectroscopy (Figure 8.1. and Figure 8.3.), and MALDI-TOF mass spectrometry (Figure 8.2. and Figure 8.4.).

Both polymerisations (PPro-1 (DMF) and PPro-2 (chloroform)) were initiated using benzylamine, the five protons of which come to resonance between 7.14-7.26 ppm in the <sup>1</sup>H NMR spectrum. Therefore, integrals of the peaks corresponding to the polymer repeat unit were normalised to these peaks. Polyproline shows four peaks in the <sup>1</sup>H NMR spectrum; the methine CH at 4.34 ppm, methylene CH<sub>2</sub> adjacent to the nitrogen at 3.36-3.47 ppm, and the two other methylene CH<sub>2</sub> groups between 2.21-2.23 ppm and 1.88-1.99 ppm respectively. By normalising the integrals as described, the integrals for the peaks in the <sup>1</sup>H NMR spectrum (Figure 8.1.) for PPro-1 signified 59 repeat units and therefore an 84% monomer conversion. Analysis by MALDI-TOF was difficult; the polyproline ionised poorly and, as such, a higher power laser was required to ionise the sample whilst the instrument detection was set to linear mode in order to produce a distribution. This resulted in distributions with poorer resolution compared to other poly(amino acid) samples, where polymers of separate lengths were not distinguishable. Despite this, PPro-1 had a distribution where  $M_n = 5393 \text{ g mol}^{-1}$  and  $M_w = 5604 \text{ g mol}^{-1}$  and therefore  $\mathcal{D} = 1.06$ .

PPro-2, produced by the ROP of proline DKP in chloroform, was assessed as described for PPro-1; the <sup>1</sup>H NMR spectrum (Figure 8.3.) showed peak integrals signifying 104 repeat units and therefore a 41% monomer conversion. Analysis by MALDI-TOF (Figure 8.4. produced a distribution of PPro-2 where  $M_n = 9295 \text{ g mol}^{-1}$  and  $M_w = 10098 \text{ g mol}^{-1}$  and therefore  $\mathcal{D} = 1.09$ .

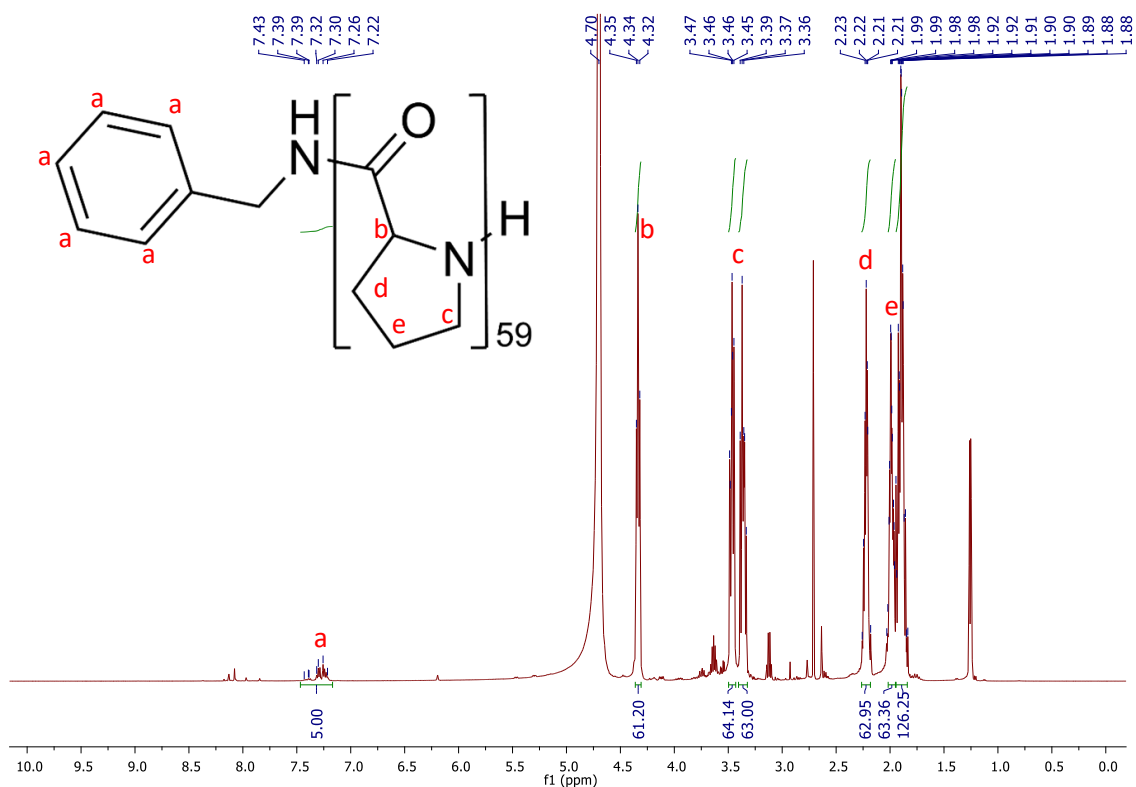


Figure 8.1. – <sup>1</sup>H NMR (D<sub>2</sub>O, 500 MHz) spectrum of polymer 13, PPro<sub>59</sub>.

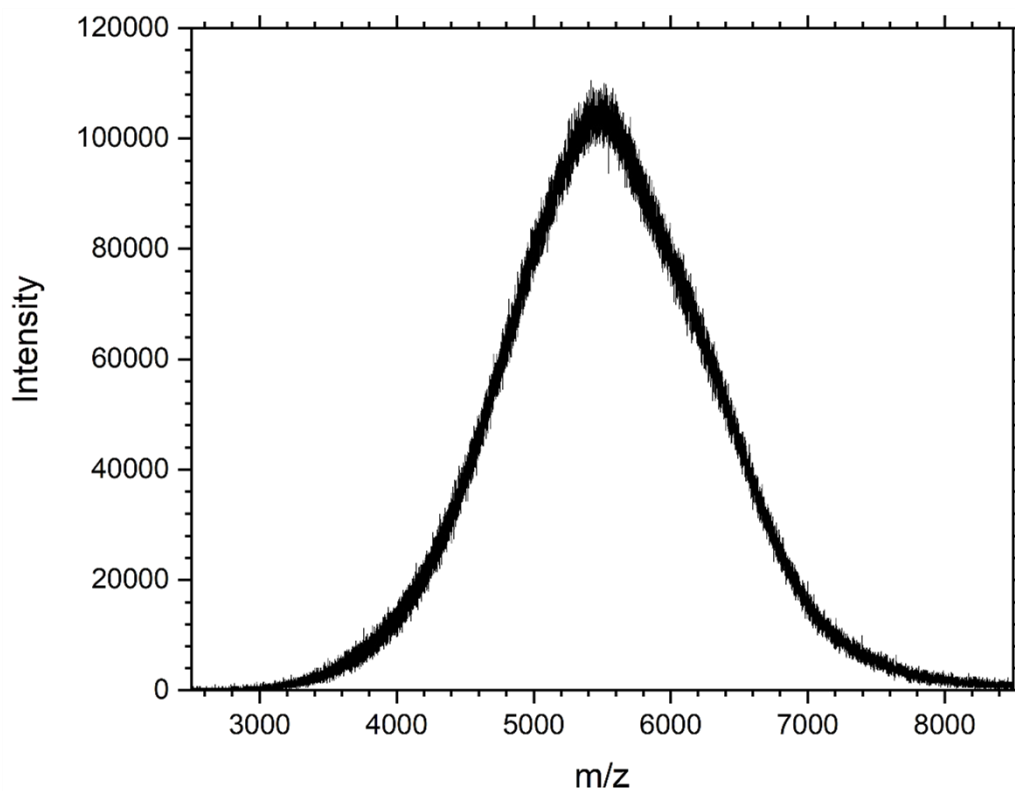


Figure 8.2. – MALDI-TOF spectrum of polymer 13, PPro<sub>59</sub>.

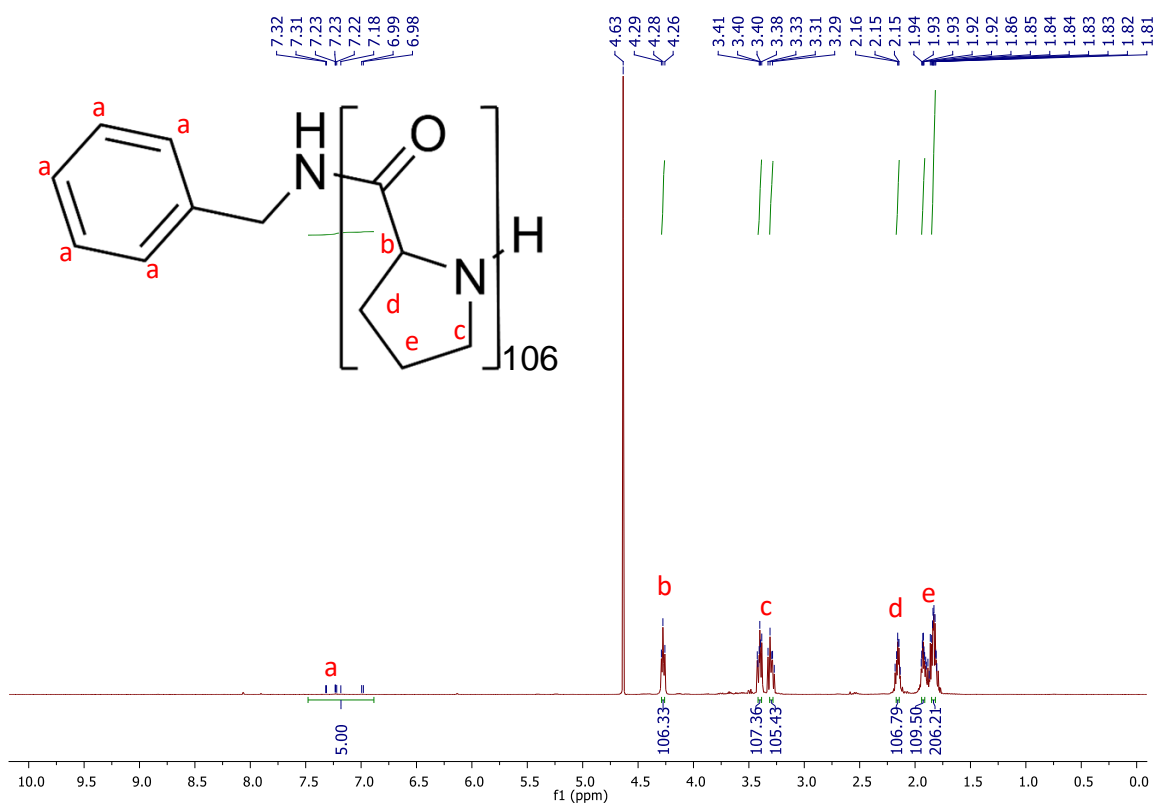


Figure 8.3. –  $^1\text{H}$  NMR ( $\text{D}_2\text{O}$ , 500 MHz) spectrum of PPro<sub>106</sub>.

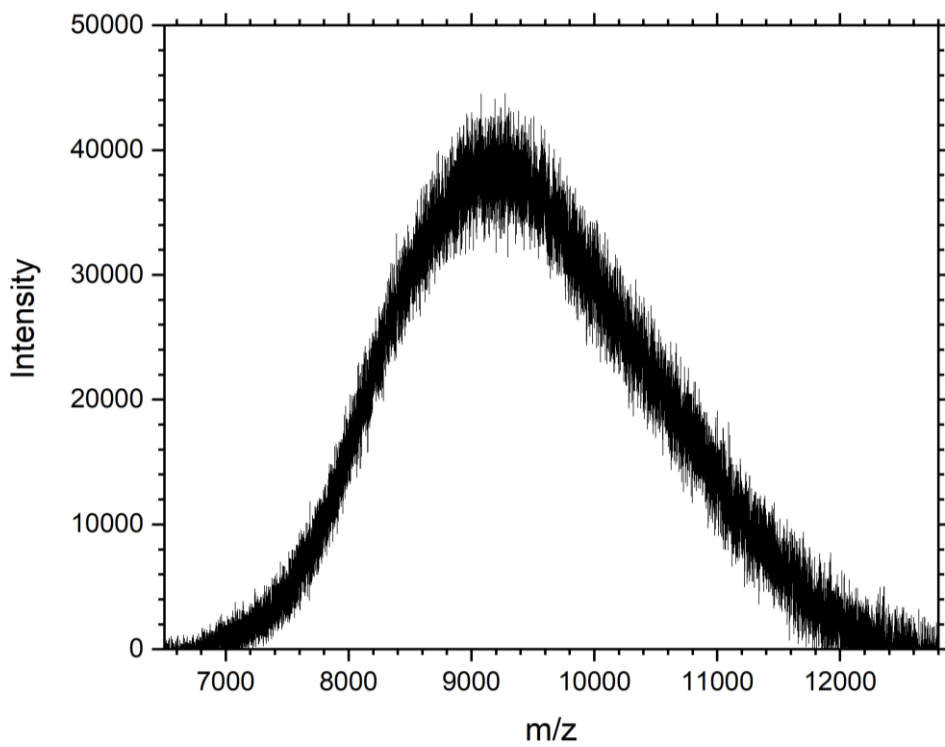


Figure 8.4. – MALDI-TOF spectrum of PPro<sub>103</sub>.

Whilst a lower % monomer conversion was observed in chloroform, the obtained polyproline had nearly double the number of repeat units observed for PPro-1 after a much shorter reaction time (160 hours (PPro-1) and 120 hours (PPro-2)) and a lower reaction temperature (110 °C (PPro-1) and 60 °C (PPro-2)). This suggests that chloroform facilitates a faster rate of polymerisation than DMF, perhaps as a consequence of greater interactions between DMF, the propagating chain and monomers within the reaction than that of chloroform. However, the poor environmental credentials and hazardous nature of chloroform ensure that it remains an undesirable reaction solvent. Greener solvents, such as Cyrene<sup>17</sup> or dimethyl isosorbide<sup>18</sup>, may be more suitable in this respect.

### 8.3.3. Synthesis of Polymethionine

To determine the capacity to which methionine DKP could be utilised as a precursor to polymethionine, the ROP of methionine DKP was attempted from benzylamine using tin(II) 2-ethylhexaoate as a Lewis acid and coordination catalyst. As a consequence of limited access to MALDI-TOF mass spectrometry and size-exclusion chromatography (SEC), mass data for polymethionine was not collected. However, the product was analysed using <sup>1</sup>H NMR spectroscopy (Figure 8.5.).

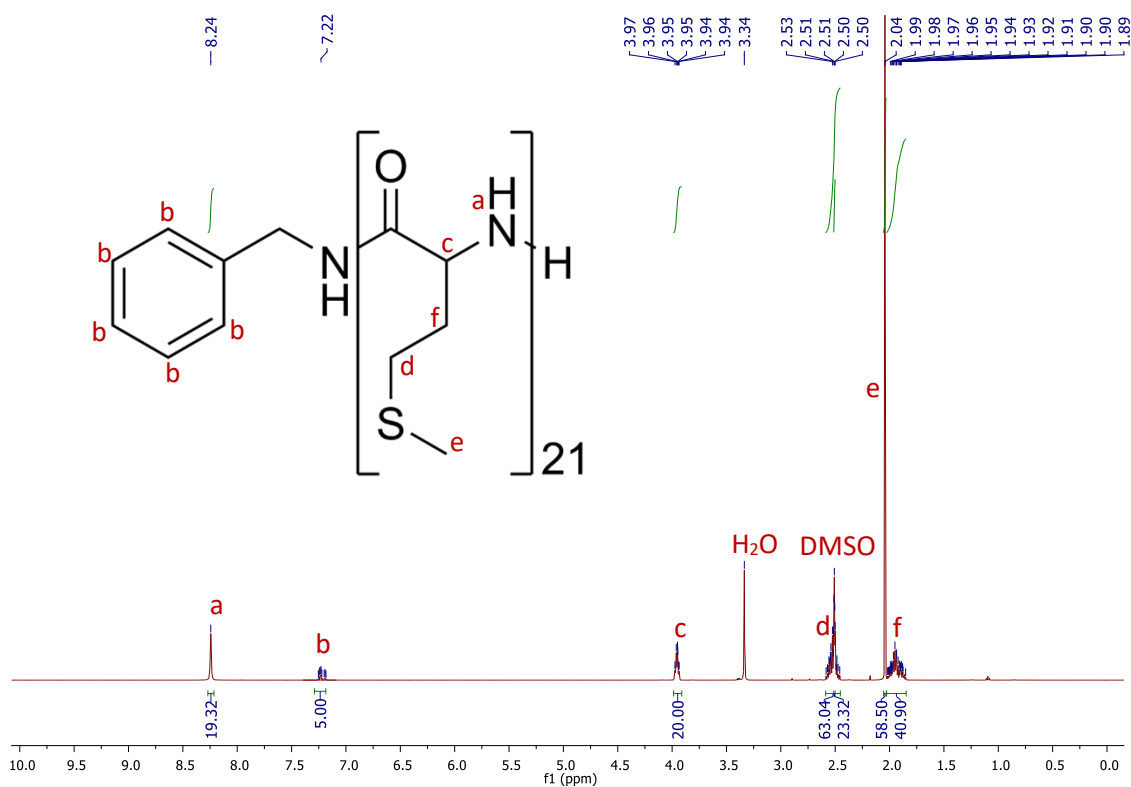


Figure 8.5. – <sup>1</sup>H NMR (DMSO-d<sub>6</sub>, 500 MHz) spectrum of polymethionine<sub>21</sub>.

As described for previous polymers that were initiated using benzylamine, the integrals of repeat unit peaks were normalised to the benzylamine peaks. Polymethionine has five proton environments that shift as follows: N-H group at 8.24 ppm, C-H group at the  $\alpha$ -carbon at 3.94-3.97 ppm, CH<sub>2</sub> peak adjacent to the sulphur atom at 2.50-2.53 ppm, CH<sub>3</sub> group at 2.04 ppm and the remaining CH<sub>2</sub> group at 1.89-1.99 ppm. Once normalised to the integration of the peaks corresponding to the protons of the benzylamine initiator, the integrals corresponding to the methionine repeat unit indicate an average of 21 repeat units, signifying a 35% monomer conversion. Whilst the <sup>1</sup>H NMR spectrum is indicative that polymerisation was successful, it is difficult to state conclusively that the polymer has formed without mass data from techniques such as SEC or MALDI-TOF mass spectrometry. Additionally, FTIR spectroscopy (appendix I) cannot be used to monitor monomer conversion as spectra of the DKP and the respective polymer are near identical.

#### **8.3.4. Synthesis of Polyarginine(Pbf)**

To determine whether polyarginine can be synthesised from arginine DKPs, the ROP of arginine(Pbf) DKP was initiated from benzylamine in DMF with DIPEA as a base catalyst. As described for polymethionine in section 8.3.3., access to MALDI-TOF mass spectrometry and SEC was limited. As such, mass data for polyarginine(Pbf) was not collected. However, the product was analysed using <sup>1</sup>H NMR spectroscopy (Figure 8.7.). The peaks in the <sup>1</sup>H NMR spectrum were normalised to the integrals of the peaks corresponding to the benzylamine proton environments as described above. The polyarginine(Pbf) repeat unit has 14 proton environments and they correspond to the peaks in the <sup>1</sup>H NMR spectrum as shown in Figure 8.7. Following the aforementioned integration normalisation, the observed average number of repeat units of polyarginine(Pbf) is 24, signifying a 39% monomer conversion. As described for polymethionine, although the <sup>1</sup>H NMR spectrum indicates successful polymerisation of arginine(Pbf) DKP, it is difficult to state as such conclusively without mass data.

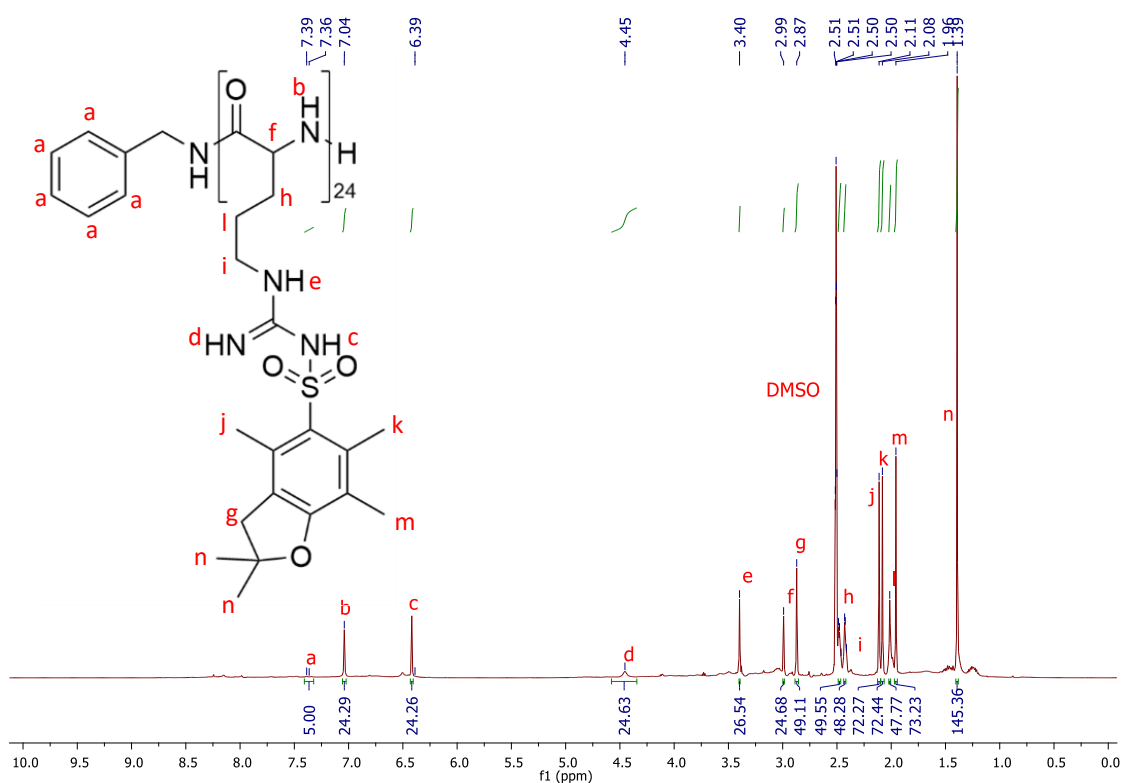


Figure 8.6. – <sup>1</sup>H NMR (DMSO-d<sub>6</sub>, 500 MHz) spectrum of polyarginine(Pbf)<sub>24</sub>.

### 8.3.5. eROP of Alanine DKP from CALB

Thus far, the reported ROPs of a variety of DKPs have relied upon transition metal catalysts or Lewis acid or base organic catalysts in concert with high polymerisation temperatures. Whilst the process as a whole (from amino acid to poly(amino acid) via DKP ROP) is relatively green when compared to the common NCA ROP pathway, the DKP ROP process could be further optimised in order to reduce its environmental impact and potential hazards. For this reason, the enzyme-catalysed ROP of alanine DKP was attempted in deionised water at 65 °C for 24 hours using (CALB) as an enzymatic catalyst. Whilst CALB is more commonly known for the enzyme-catalysed ROP of lactones<sup>19</sup>, its use as a catalyst for lactam ROP has also been reported<sup>11,20</sup>. As for polymethionine and polyarginine(Pbf) above, access to MALDI-TOF was limited. As such, mass data for the product of the attempted eROP was not collected. However, in contrast to alanine DKP, the product was insoluble in DMF, suggesting polyalanine formation but preventing GPC analysis.



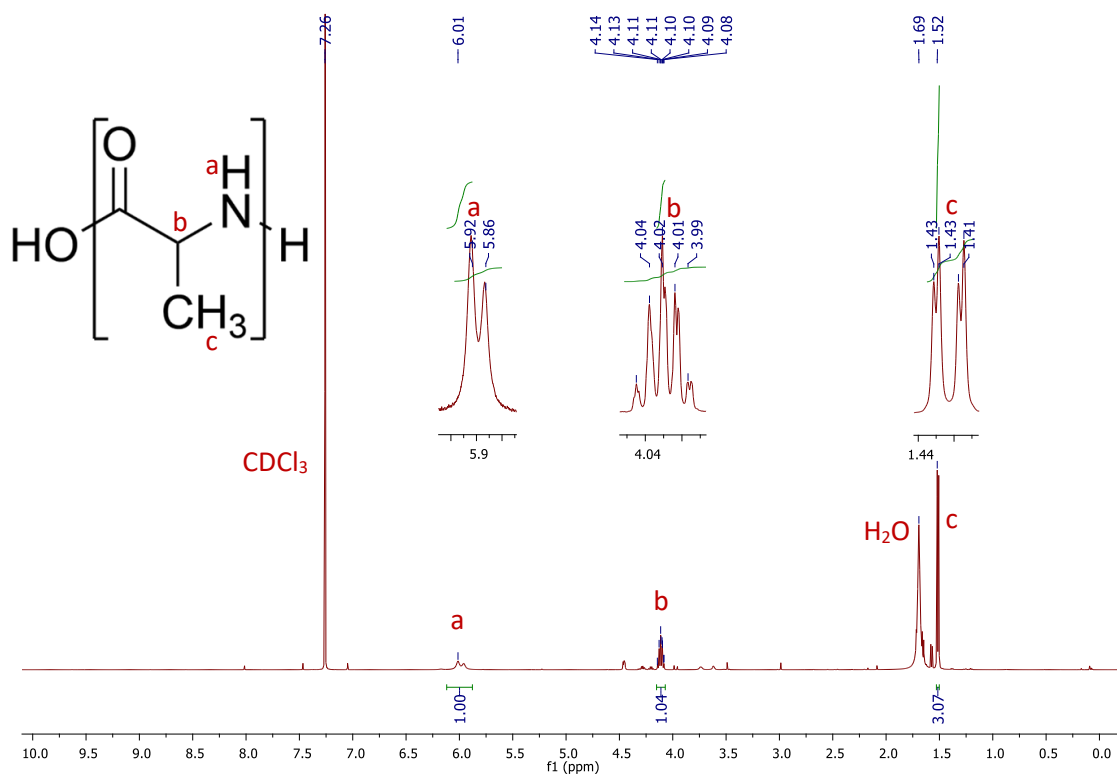


Figure 8.7. – $^1\text{H}$  NMR (CDCl<sub>3</sub>, 500 MHz) spectrum of polyalanine produced via enzyme-catalysed ROP of alanine DKP.

As a consequence of the lack of an initiator in the reaction, as well as the lack of mass data, it is difficult to determine whether ROP has occurred. A feature that indicated, at a minimum, ring-opening was the solubility of the reaction product in water and how it compared to the solubility of alanine DKP in water. Alanine DKP (10 mg) was dissolved in the minimum amount of deionised water (2 mL). The product (10 mg) was also added to 2 mL of deionised water and was insoluble. Further deionised water (2 mL) was added and the product remained insoluble. The two solutions were analysed using UV-vis spectrophotometry (Figure 8.9.). The much higher absorbance and noise of the product trace indicates a cloudy mixture and therefore lack of solubility. This indicates that, at least, ring-opening of alanine DKP has occurred.

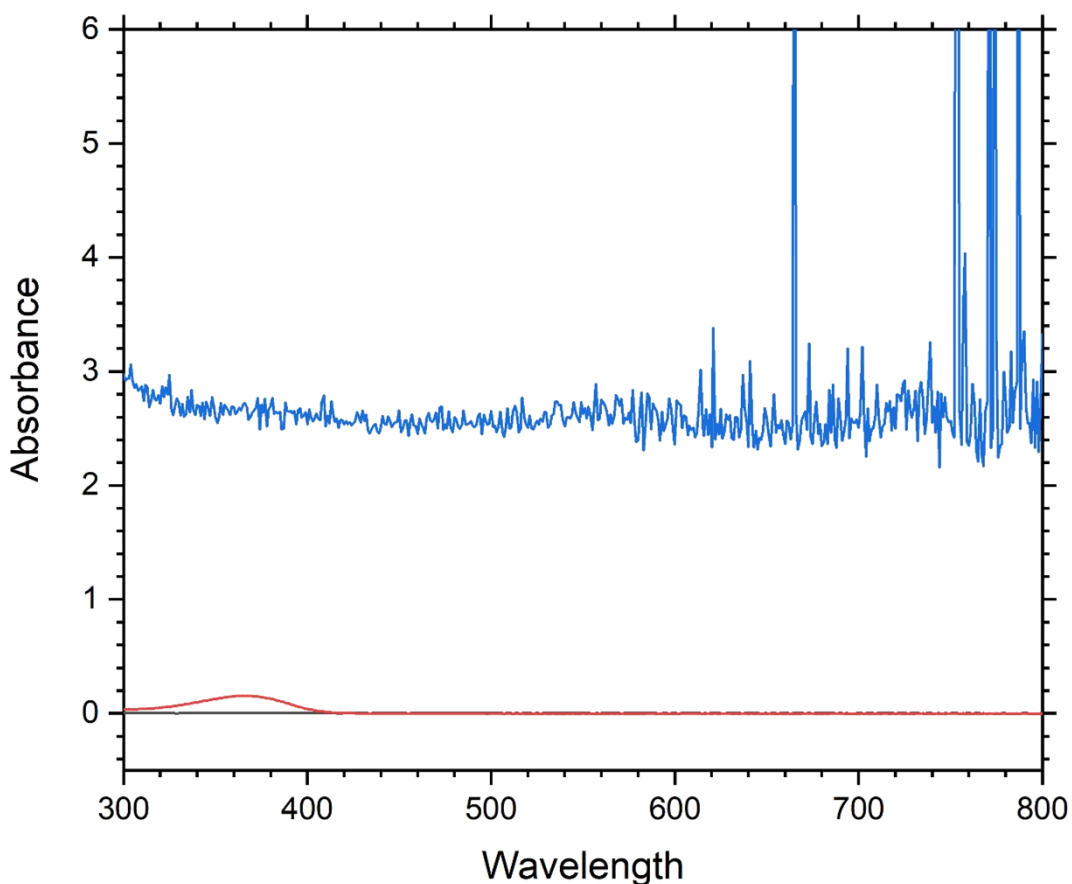


Figure 8.8. – UV-vis spectrum of alanine DKP (red) dissolved in deionised water ( $5 \text{ mg mL}^{-1}$ ) and polyalanine (blue) suspended in deionised water ( $2.5 \text{ mg mL}^{-1}$ ).

#### 8.4. Conclusions

The syntheses of polyproline, polymethionine and polyarginine(Pbf) have been reported for the first time. Whilst lower percentage monomer conversions were observed compared to previously described poly(amino acids), these polymers were achieved following shorter reaction times. Unfortunately, as a consequence of limited access to MALDI-TOF and SEC, mass data was not obtained for several of the polymers reported in this chapter. Despite this, the data obtained, primarily  $^1\text{H}$  NMR spectroscopy, was indicative of successful polymerisation. Additionally, alternative solvents such as deionised water and chloroform were utilised and found to be suitable solvents for DKP ROP. The novel eROP of alanine DKP was also explored using CALB as the catalyst, resulting in, at a minimum, DKP ring-opening. Whilst this exploration into accessible poly(amino acids) from DKP ROP has only scratched the surface, the contents reported in this chapter are demonstrative that DKP ROP may be expanded to access a plethora of poly(amino acids) and provides scope for the use of a variety of solvents and catalysts.

## 8.5. References

---

- 1) Mazo, A. R., Allison-Logan, S., Karimi, F., Chan, N. J-A., Qiu, W., Duan, W., O'Brien-Simpson, N. and Qaio, G. G. Ring opening polymerization of  $\alpha$ -amino acids: advances in synthesis, architecture and their applications of polypeptides and their hybrids. 2020, **49**(14), 4595-5102.
- 2) Song, Z., Tan, Z. and Cheng, J. Recent Advances and Future Perspectives of Synthetic Polypeptides from N-Carboxyanhydrides. *Macromolecules*. 2019, **52**, 8521-8539.
- 3) Eom, K. H., Baek, S. and Kim, I. N-Heterocyclic Carbene-Catalyzed Random Copolymerization of N-Carboxyanhydrides of  $\alpha$ -Amino Acids. *Polymers (Basel)*. 2021, **13**(21), 3674-3683.
- 4) González-Henriquez, C. M., Sarabia-Vallejos, M. A. and Rodrigues-Hernández, J. Strategies to Fabricate Polypeptide-Based Structures via Ring-Opening Polymerization of N-Carboxyanhydrides. *Polymers*. 2017, **9**(11), 551-602.
- 5) Graham, B., Bailey, T. L., Healey, J. R. J., Marcellini, M., Deville, S. and Gibson, M. I. Polyproline as a Minimal Antifreeze Protein Mimic That Enhances the Cryopreservation of Cell Monolayers. *Angewandte Chemie International Edition*. 2017, **56**(50), 15941-15944.
- 6) Lu, D., Zhang, Y., Li, T., Li, Y., Wang, H., Shen, Z., Wei, Q. and Lei, Z. Synthesis and tissue adhesiveness of temperature-sensitive hyperbranched poly(amino acid)s with functional side groups. *Polymer Chemistry*. 2016, **7**(10), 1963-1970.
- 7) Oh, D., Shirazi, A. N., Northup, K., Sullivan, B., Tiwari, R. K., Bisoffi, M. and Parang, K. Enhanced Cellular Uptake of Short Polyarginine Peptides through Fatty Acylation and Cyclization. *Molecular Pharmaceutics*. 2014, **11**(8), 2845-2854.
- 8) Duro-Castano, A., Rodriguez-Arco, L., Ruiz-Perez, L., De Pace, C., Marchello, G., Noble-Jesus, C. and Battaglia, G. One-pot synthesis of oxidation-sensitive supramolecular gels and vesicles. *Biomacromolecules*. 2021, **22**(12), 5052-5064.
- 9) Rowley, J. V., Wall, P., Yu, H., Tronci, G., Devine, D. A., Vernon, J. J. and Thornton, P. D. Antimicrobial Dye-Conjugated Polyglobalide-Based Organogels. *ACS Applied Polymer Materials*. 2020, **2**(7), 2927-2933.
- 10) Engel, J., Cordellier, A., Huang, L. and Kara, S. Enzymatic Ring-Opening Polymerization of Lactones: Traditional Approaches and Alternative Strategies. 2019, **11**(20), 4983-4997.

- 
- 11) Schwab, L. W., Kroon, R., Schouten, A. J. and Loos, K. Enzyme-Catalyzed Ring-Opening Polymerization of Unsubstituted  $\beta$ -Lactam. *Macromolecular Rapid Communications*. 2008, **29**(10), 794-797.
- 12) Mitchel, D. J., Kim, D. T., Steinman, L., Fathman, C. G. and Rothbard, J. B. Polyarginine enters cells more efficiently than other polycationic homopolymers. *Journal of Peptide Research*. 2000, **56**(5), 318-315.
- 13) Robison, A. D., Sun, S., Poyton, M. F., Johnson G. A., Pellois, J-P., Jungwirth, P., Vazdar, M. and Cremer, P. S. Polyarginine Interacts More Strongly and Cooperatively than Polylysine with Phospholipid Bilayers. *Journal of Physical Chemistry B*. 2016, **120**(35), 9287-9296.
- 14) MERCK-Millipore-Sigma-Aldrich. *Poly-L-arginine hydrochloride*. [Online]. 2023. [Accessed 27/10/23]. Available from: <https://www.sigmaaldrich.com/GB/en/product/sigma/p4663>
- 15) Al-Mhyawi, S. R., Ahmed, R. K. and El Nashar, R. M. Application of a Conducting Poly-Methionine/Gold Nanoparticles-Modified Sensor for the Electrochemical Detection of Paroxetine. *Polymers (Basel)*. 2021, **13**(22), 3981-3995.
- 16) Swathy, S., Matthew, M. R. and Kumar, K. G. Poly L- methionine/Electrochemically Reduced Graphene Oxide Composite Film Modified Glassy Carbon Electrode for the Simultaneous Determination of 5-hydroxyindole Acetic Acid and Tyrosine. *Journal of the Electrochemical Society*. 2022, **169**(8), 087519.
- 17) Brouwer, T. and Schuur, B. Dihydrolevoglucosenone (Cyrene), a Biobased Solvent for Liquid-Liquid Extraction Applications. *ACS Sustainable Chemistry & Engineering*. 2020, **8**(39), 14807-14817.
- 18) Dimethyl Isosorbide as a Green Solvent for Sustainable Ultrafiltration and Microfiltration Membrane Preparation. *ACS Sustainable Chemistry & Engineering*. 2020, **8**(1), 659-668.
- 19) Engel, S., Höck, H., Bocola, M., Keul, H., Schwaneberg, U. and Möller, M. CaLB Catalyzed Conversion of  $\epsilon$ -Caprolactone in Aqueous Medium. Part 1: Immobilization of CaLB to Microgels. *Polymers*. 2016, **8**(10), 372-387.
- 20) Varghese, M. and Grinstaff, M. W. Beyond nylon 6: polyamides *via* ring opening polymerization of designer lactam monomers for biomedical applications. *Chemical Society Reviews*. 2022, **51**(19), 8258-8275.

## Conclusions and Future Work

Reported in this thesis are the invention and development of the ROP of a host of DKPs to form a wide range of poly(amino acids) that boast a variety of physicochemical properties and very narrow dispersities. To the knowledge of the author, the ROP of DKPs has not been previously reported, making this thesis the first account of poly(amino acid) synthesis via DKP ROP. This polymerisation may be the most applicable route to narrow dispersity poly(amino acids) for industrial scale, owing to its straightforward nature, minimal requirement for hazardous reagents and costly reagents, and relatively green credentials. This thesis may ultimately serve as an introduction to DKP ROP, as there is scope for extensive future work in order to develop DKP ROP as a new and promising reaction platform for poly(amino acid) synthesis.

Initially, a collection of DKPs were successfully synthesised via the direct bis-condensation of the respective amino acid(s) by heating in glycerol or ethylene glycol between 175-190 °C. For some DKPs, the obtained yields were low, perhaps as a consequence of competitive oligomerisation and side reactions with the solvent. However, the syntheses were achieved via a single, straightforward step requiring minimal purification. Several DKPs were synthesised numerous times with consistent yields, validating the repeatability of DKP creation in this manner. No additional reagents were required and the solvent, glycerol, has no known hazards, verifying the safety and low environmental impact of the procedure. Furthermore, this synthesis was used to produce a wide variety of DKPs, including asymmetric DKPs, demonstrating its broad utility. DKP synthesis could be improved from both a process perspective and in terms of expansion of attainable DKPs. Future work could focus on DKPs that have not yet been synthesised via this route, and are of value, including serine DKP, glutamic acid DKP, cysteine DKP, non-canonical DKPs such as vinylglycine DKP, and additional asymmetric DKPs such as lysine-glutamic acid DKP. The polymer formed from lysine-glutamic acid DKP may be capable of straightforward covalent and/or physical cross-linking post-polymerisation, yielding useful materials including nanoparticles, porous scaffolds, and hydrogels.

Chapter 4 reports were the ROP of glycine DKP, alanine DKP, phenylalanine DKP and lysine(Cbz) DKP. The polymerisations were controlled and environmentally benign, resulting in poly(amino acids) of each DKP with narrow dispersity. The versatility of the process of creating poly(amino acids) from DKPs was demonstrated in the reporting of four different poly(amino acids); the circularity of polymer synthesis owing to the biodegradability of poly(amino acids) was shown by the enzymatic degradation of polyalanine by elastase and subsequent ROP using the alanine recovered. Polymer synthesis was also achieved using deionised water as the solvent, as well as

via Lewis acid/coordination catalysis and base catalysis. Successful deprotection of polylysine(Cbz) was also achieved, yielding a polymer bearing free, primary amines. Future work may include the optimisation of the polymerisation procedure, including the increase in % monomer conversion by using more active catalysts, such as zinc chloride, as well as other transition metal catalysts. Additionally, a kinetic study of the ROP of each DKP could be carried out to more fully understand the polymerisation process, possibly facilitating shortened reaction time.

Chapter 5 reports the use of DKP ROP to produce PEG-*b*-poly(amino acid) block copolymers of glycine, alanine and phenylalanine with a variety of poly(amino acid) lengths. The observed monomer conversion % was variable, with some of the polymerisations reaching high monomer conversions of 100% and others as low as 17.5%. Despite this, all polymerisations resulted in polymers with very narrow  $\bar{M}_w/\bar{M}_n$  and as such compared favourably to similar NCA polymerisations. Furthermore, self-assembly of the amphiphilic PEG-*b*-poly(amino acids) in aqueous solution to form nanoparticles was successful, with average particle sizes and polydispersity that suggest suitability for use as delivery agents in a biomedical setting. Dox encapsulation within selected nanoparticle dispersions was successful and a high encapsulation efficiency of >87% was achieved. The nanoparticles showed minimal leakage at pH 7.4 and, crucially, the nanoparticles proved susceptible to acid-mediated release at pH 5, resulting in the acid-triggered release of encapsulated dox free-base between 3.5 and 12.4 times greater than the respective release in PBS buffer (pH 7.4). Whilst pH 5 serves as a relevant trigger for release (matches cancerous lysosomal pH), future work could involve the drug release in buffers with more moderate pH, such as 6.5 which matches extracellular pH at tumour sites. Furthermore, extensive *in vitro* studies of the dox-loaded nanoparticles to indicate their real world efficacy and potential applicability as part of anti-cancer therapeutics should be performed.

Included in Chapter 6 is the novel and repeatable synthesis of polysarcosine by Sar DKP ROP, as well as the synthesis of PSar-*b*-PAla, PSar-*ran*-PAla, PSar-*alt*-PPhe and Camp-PSar via DKP ROP. The polymerisations reported provide greater scope for industrial use of polysarcosine, providing competition for the well-established PEG. Polysarcosine-*block*-polyalanine nanoparticles displayed sensitivity to neutrophil elastase, resulting in a prolonged release of doxorubicin upon incubation with neutrophil elastase, demonstrating its applicability as a therapeutic delivery vehicle to sites characterised by an overexpression of elastase. Future work may focus on the refinement of the polymerisation of sarcosine DKP by utilising a more active catalyst as aluminium trichloride to facilitate a high monomer conversion with shorter reaction

times. Additionally, *in vitro* dox release studies from nanoparticles of PSar-*b*-PAla may inform how effective they are as an enzyme sensitive drug delivery vehicles.

Reported in Chapter 7 is the electrospinning of polysarcosine and polyalanine with polycaprolactone, along with the parameters required to produce nanofibre structures comparable to the physical structure of human ECM from these combinations of polymers. The resultant PCL/PAla and PCL/PSar nanofibre mats compared favourably to PCL fibres, bearing enhanced physicochemical properties that are well suited for use as a chronic wound dressing. The PCL/PAla and the PCL/PSar nanofibre mats displayed excellent water uptake capacity indicating the capability to maintain moisture and absorb exudate at a wound site. The PCL/PSar and PCL/PAla nanofibre mats displayed excellent tensile strength, boasting a maximum tensile stress greater than that of PCL alone and that were within the range of healthy human skin. Notably, the PCL/PAla nanofibres degraded upon elastase exposure, demonstrating that these materials may be able to release a therapeutic payload at the chronic wound site in response to over-expressed elastase. Future work could focus on further tensile testing of nanofibres when wet, as well as more quantitative studies of the porosity of the fibres. Other future work may include the encapsulation of a therapeutic within a PCL/PAla nanofibre network and subsequent incubation with elastase to investigate release properties. Subsequent investigations may include *in vitro* release studies, as well as the electrospinning of alternative nanofibre mats such as PCL/PAla-*ran*-PSar.

Finally, Chapter 8 reports the expansion of accessible poly(amino acids) created by DKP ROP to polyproline, polymethionine and polyarginine(Pbf). Despite the lower percentage monomer conversions, these polymerisations were typically accomplished with shorter reaction times, improving the efficiency of DKP ROP as a process. Additionally, alternative solvents such as deionised water and chloroform were utilised and found to be suitable solvents for DKP ROP. The novel eROP of alanine DKP was also explored using CALB as the catalyst, resulting in, at a minimum, DKP ring-opening. Future work could include assessing the synthesised polymers using SEC or MALDI-TOF to compliment the results obtained by <sup>1</sup>H NMR spectroscopy. Also, the synthesis of poly(amino acids) from other natural and non-natural amino acid DKPs, and the use of alternative catalysts, solvents and initiators, would be a worthwhile endeavour. This will further expand the scope of materials produced by this new and exciting form of polymerisation.

**List of Publications**

Upon the date of submission of this thesis, there are no formally published journal articles based upon the work contained in this thesis. However, a patent application, titled “Synthesis of poly(amino acids)” and numbered “GB2219045.8”, has been filled and published. This application contains work from all six results-based chapters of the thesis, chapters 3-8. Additionally, a manuscript, based upon the work reported in Chapter 4, has been submitted for publication and is under review.



## Appendices

### Appendix I – FTIR Spectroscopy

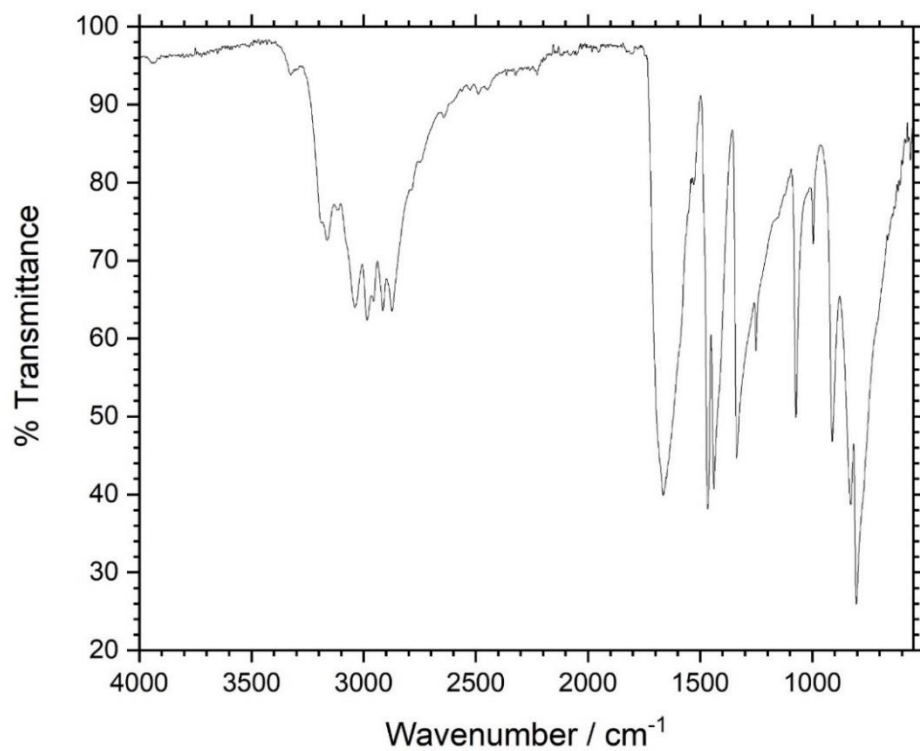


Figure A1.1. – FTIR spectrum of glycine DKP.

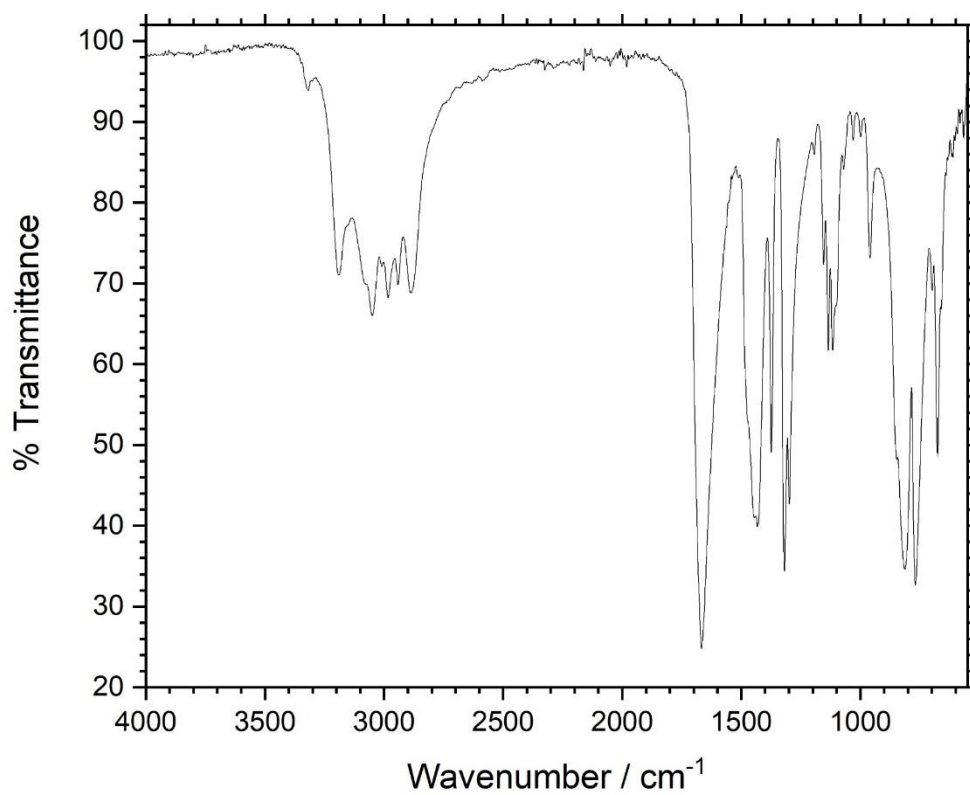


Figure A1.2. - FTIR spectrum of alanine DKP.

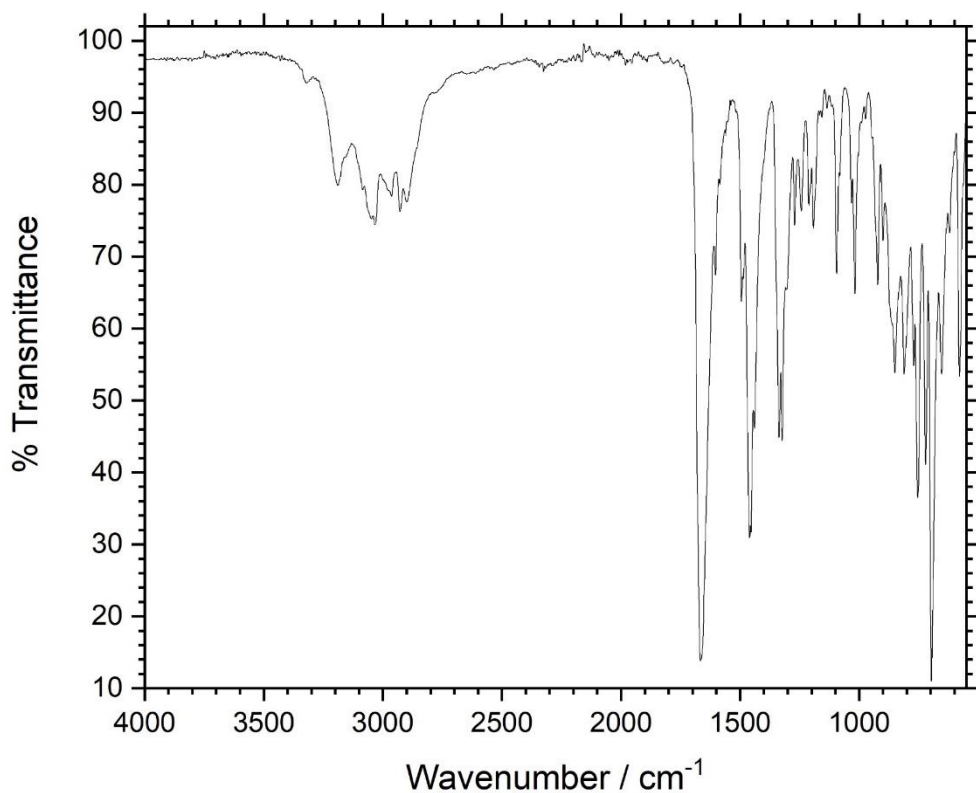


Figure A1.3. - FTIR spectrum of phenylalanine DKP.

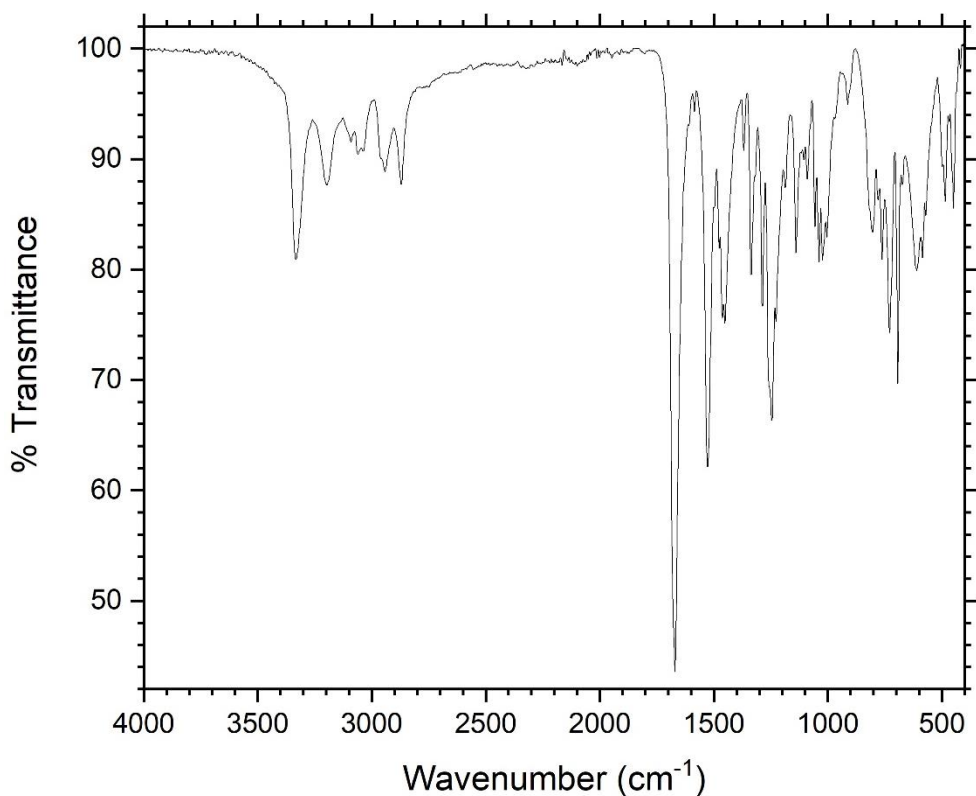


Figure A1.4. - FTIR spectrum of Lysine(Cbz) DKP.

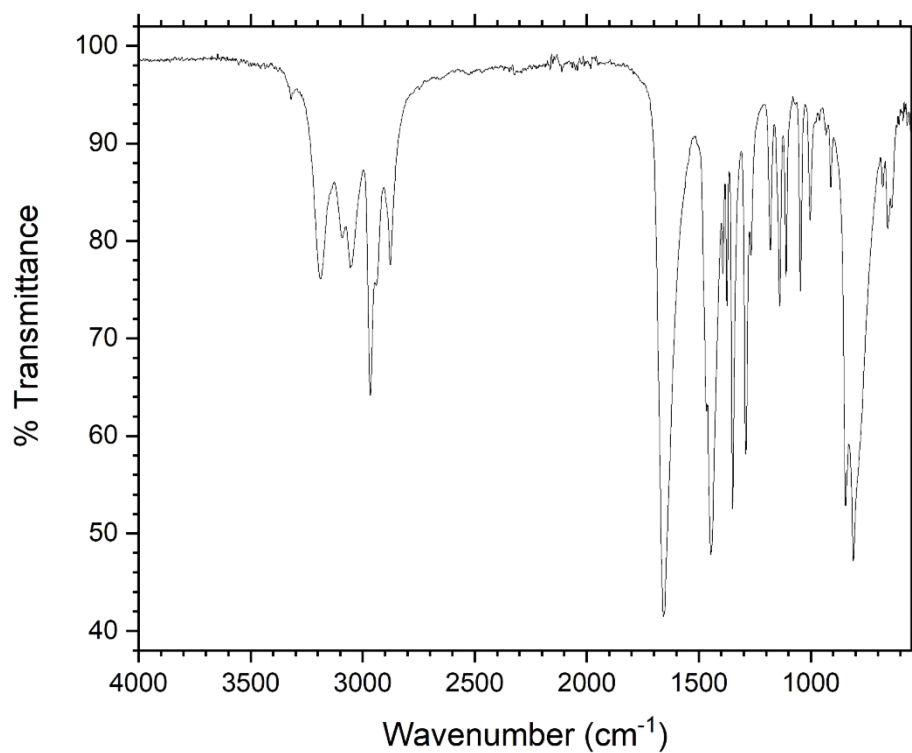


Figure AI.5.11 - FTIR spectrum of valine DKP.

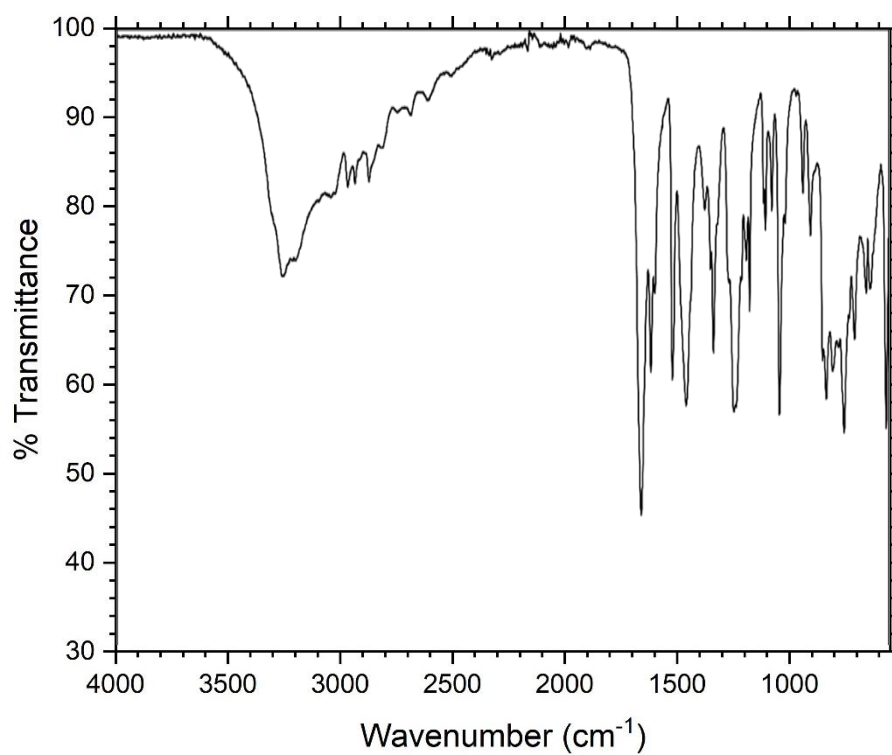


Figure AI.6. – FTIR spectrum of tyrosine DKP

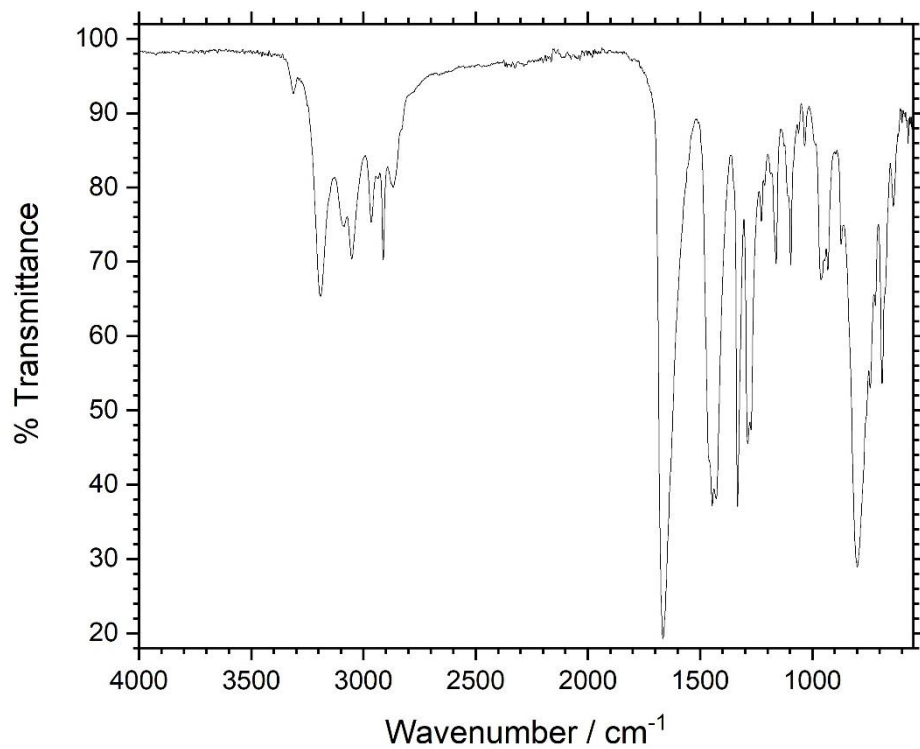


Figure A1.7 – FTIR spectrum of methionine DKP.

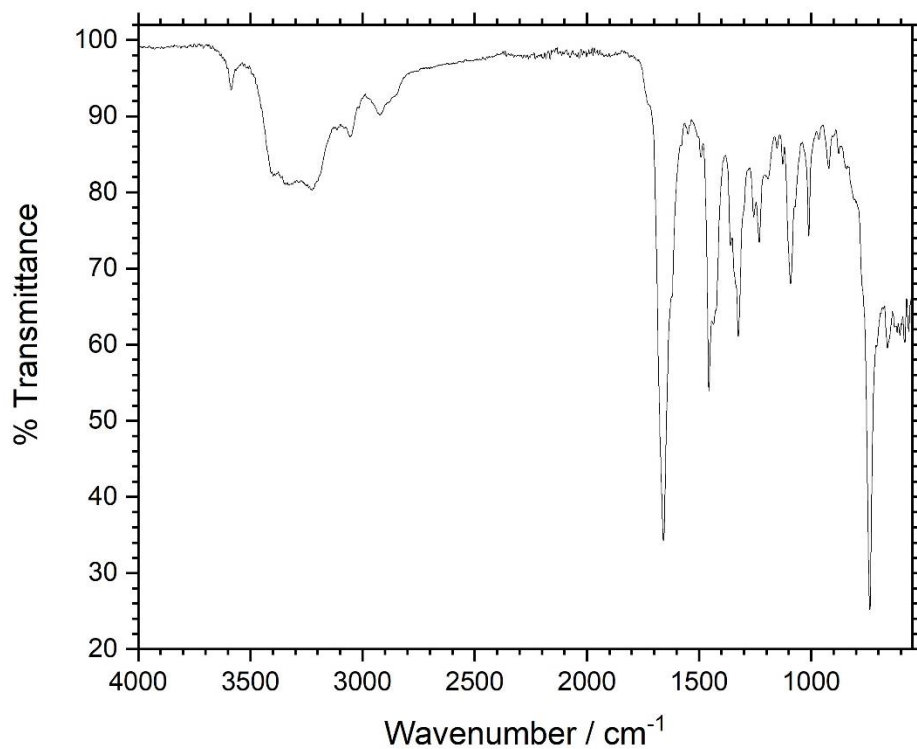


Figure A1.8. – FTIR spectrum of tryptophan DKP.

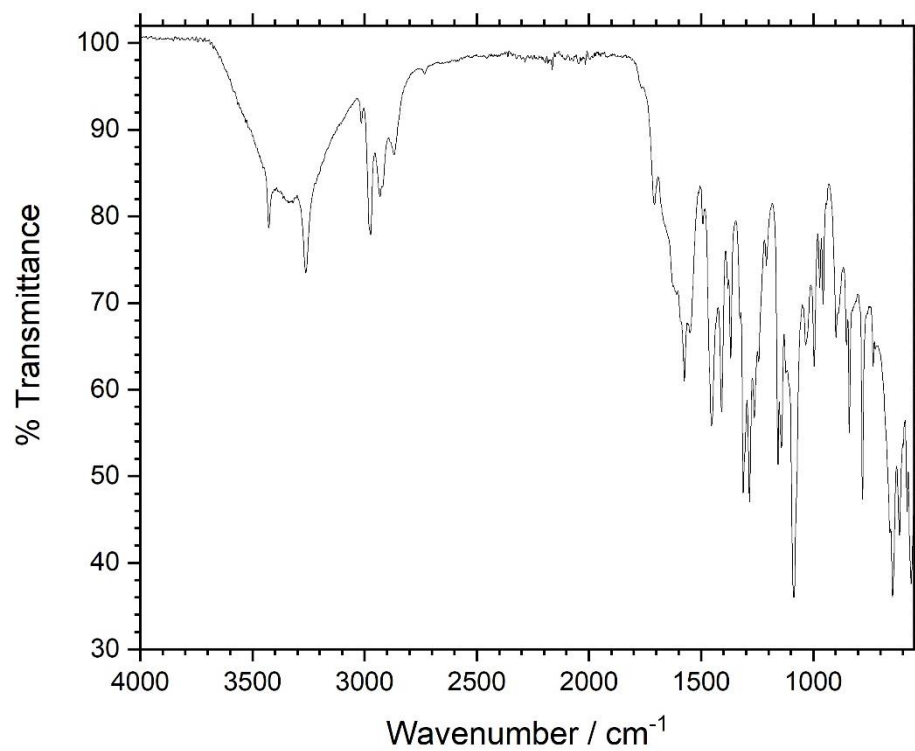


Figure A1.9. – FTIR spectrum of arginine(Pbf) DKP.

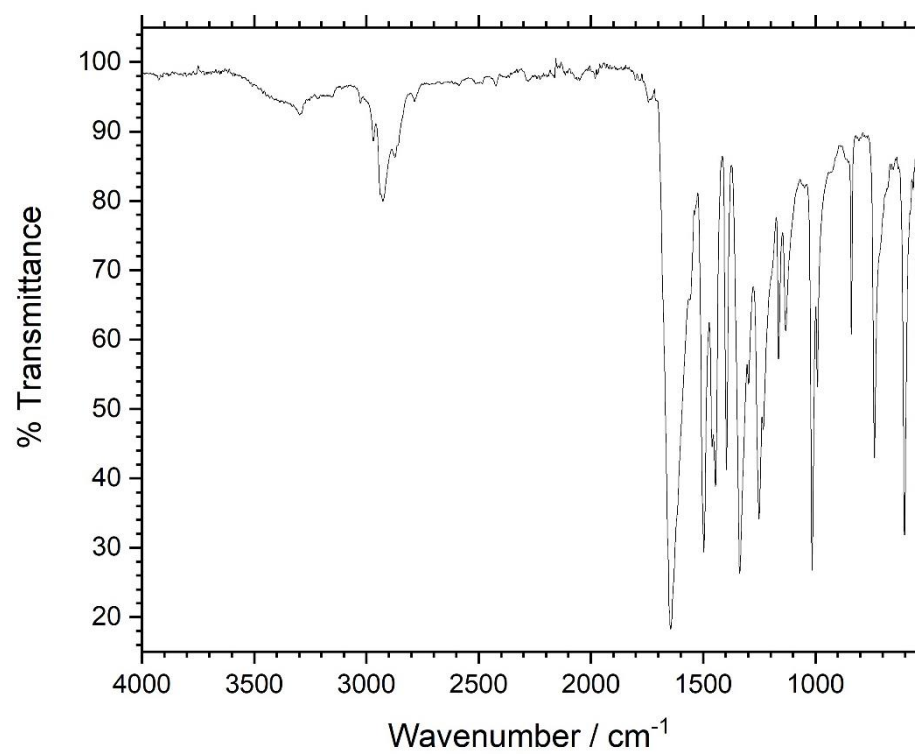


Figure A1.10. – FTIR spectrum of sarcosine DKP.

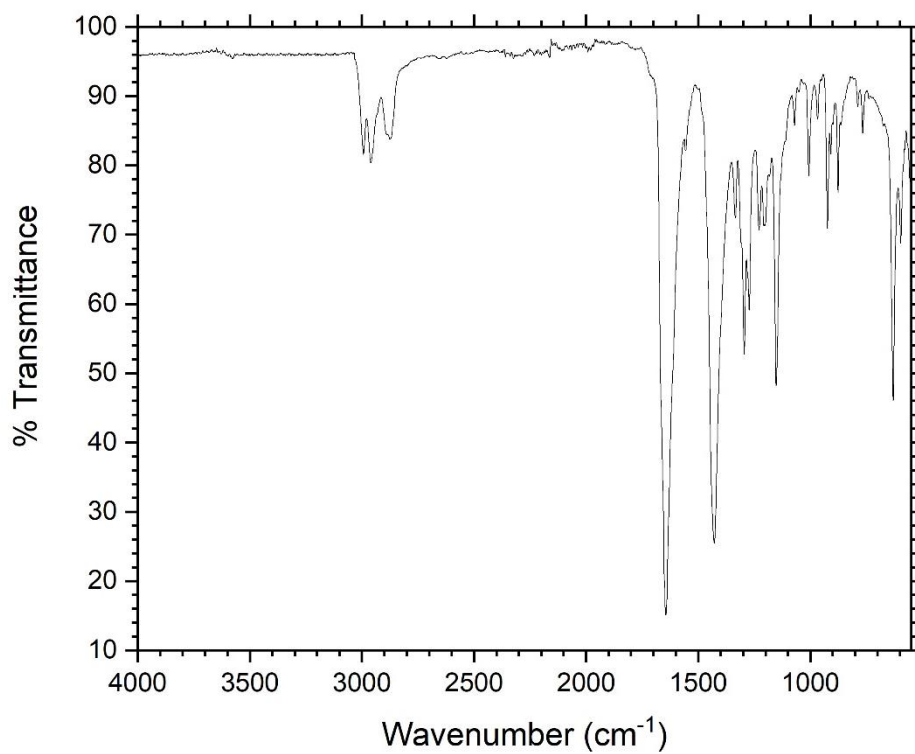


Figure A1.11. – FTIR spectrum of proline DKP.

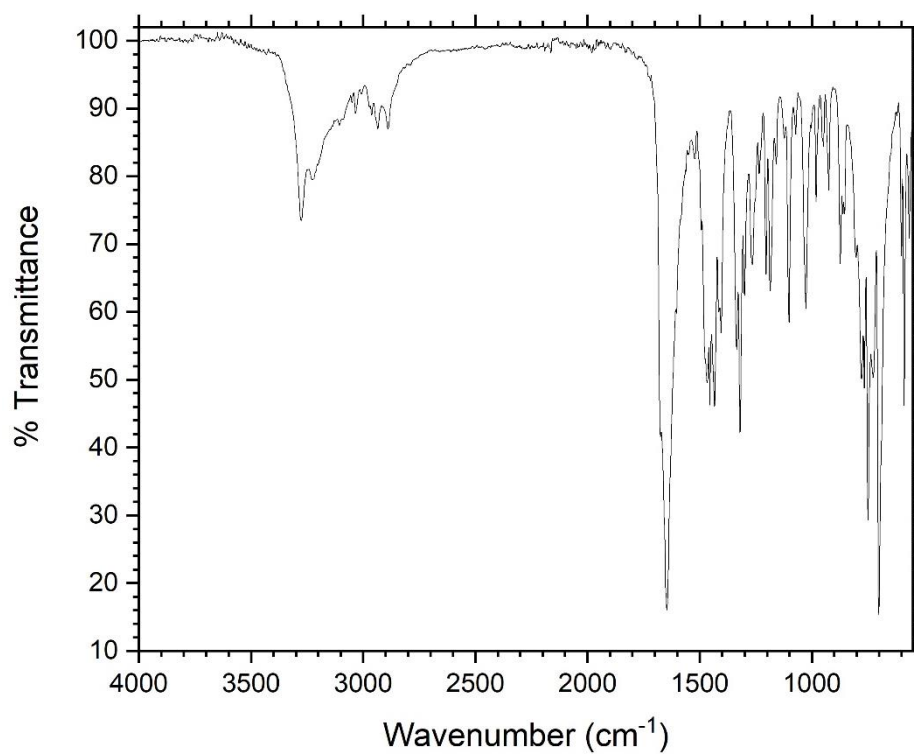


Figure A1.12. – FTIR spectrum of sarcosine-phenylalanine DKP.

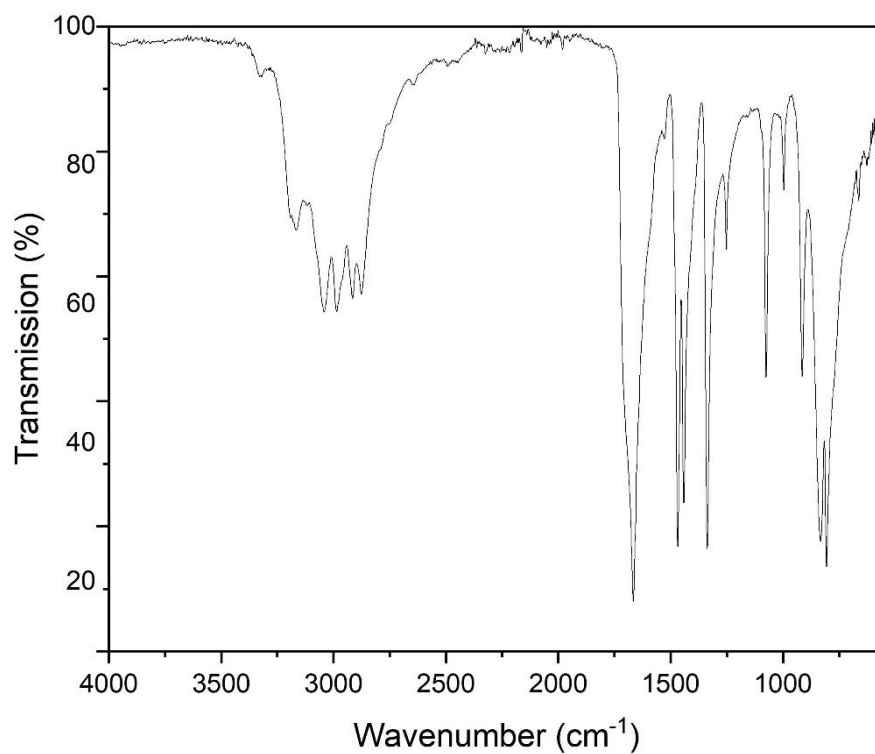


Figure A1.13. – FTIR spectrum of PGLy<sub>54</sub> (labelled polymer 1 in Chapter 4, Table 4.1. and Table 4.2.).

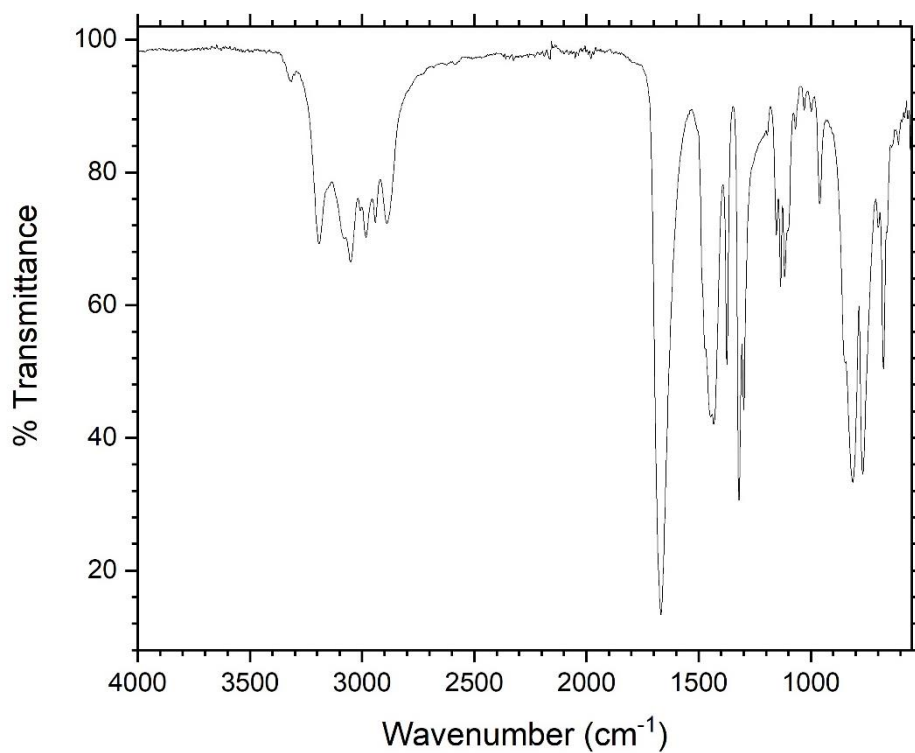


Figure A1.14. – FTIR spectrum of PAla<sub>68</sub> (labelled polymer 2 in Chapter 4, Table 4.1. and Table 4.2.).

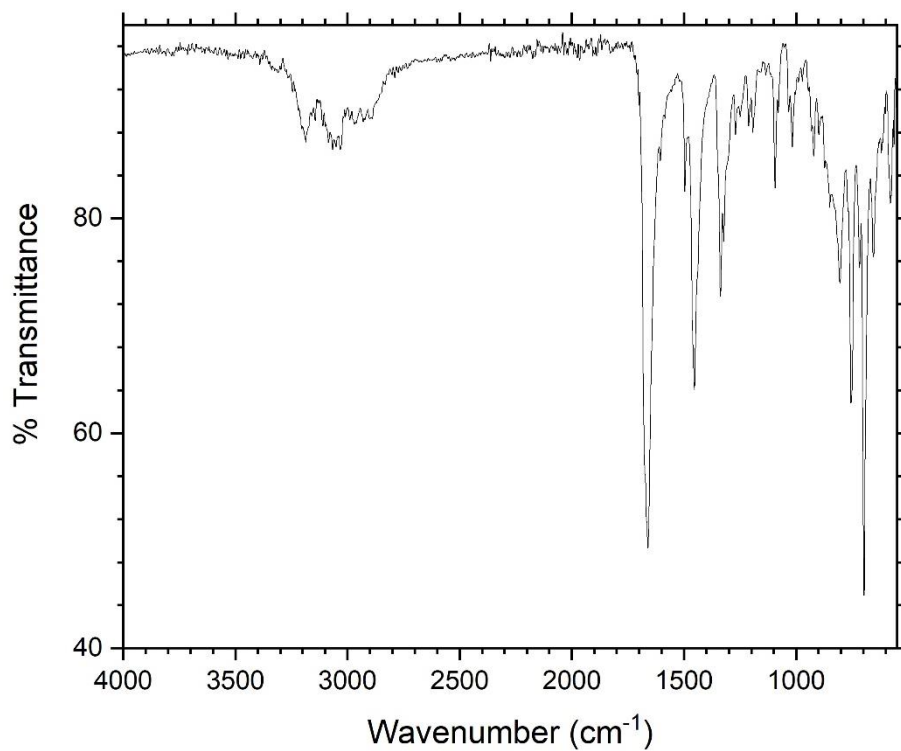


Figure A1.15. – FTIR spectrum of PPhe<sub>37</sub> (labelled polymer 3 in Chapter 4, Table 4.1. and Table 4.2.).

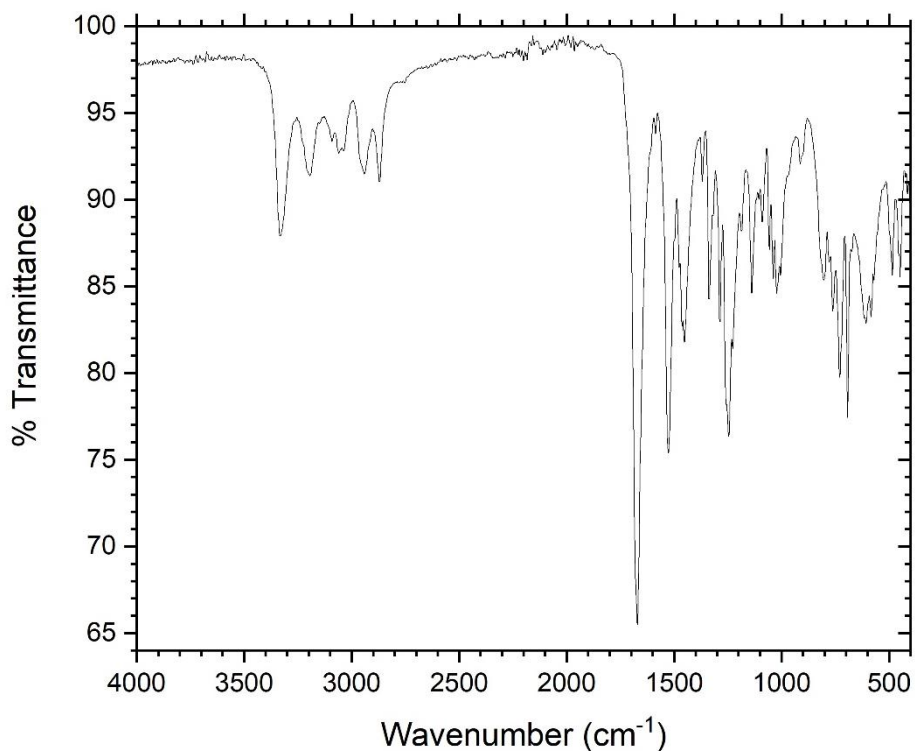


Figure A1.16. – FTIR spectrum of PLys(Cbz)<sub>47</sub> (labelled polymer 4 in Chapter 4, Table 4.1. and Table 4.2.).



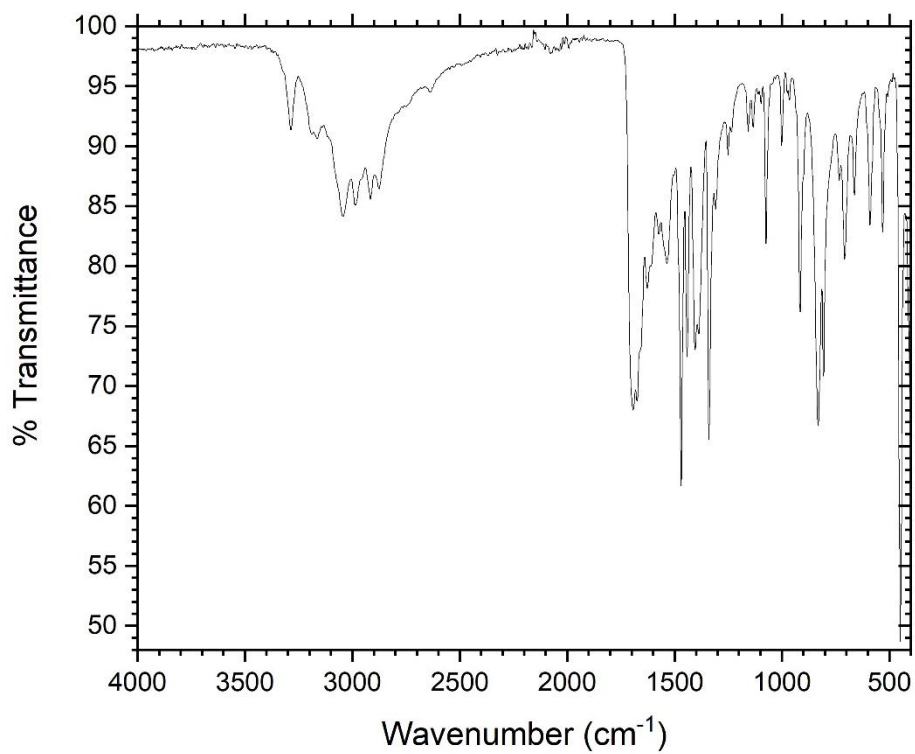


Figure A1.17. – FTIR spectrum of PGly<sub>48</sub> (labelled polymer 5 in Chapter 4, Table 4.1. and Table 4.2.).

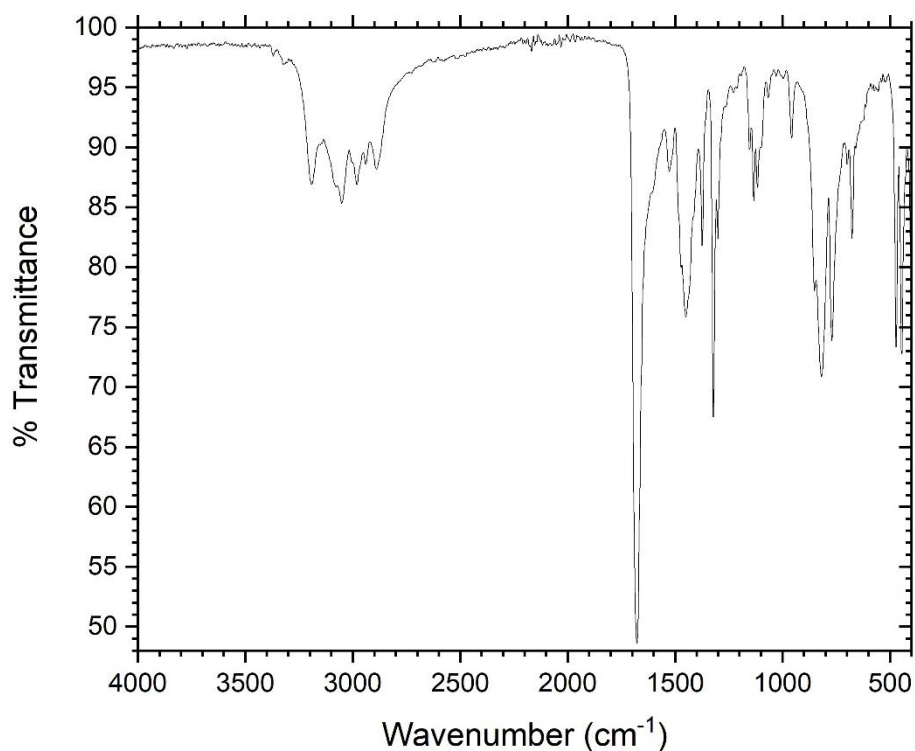


Figure A1.18. – FTIR spectrum of PAla<sub>45</sub> (labelled polymer 6 in Chapter 4, Table 4.1. and Table 4.2.).

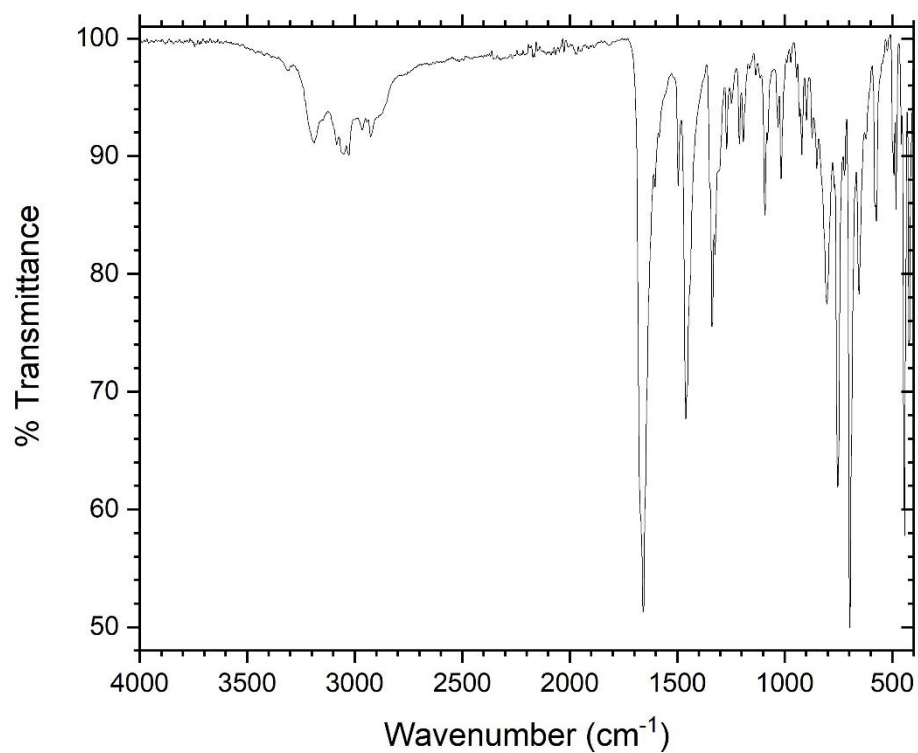


Figure A1.19. – FTIR spectrum of PPhe<sub>18</sub> (labelled polymer 7 in Chapter 4, Table 4.1. and Table 4.2.).

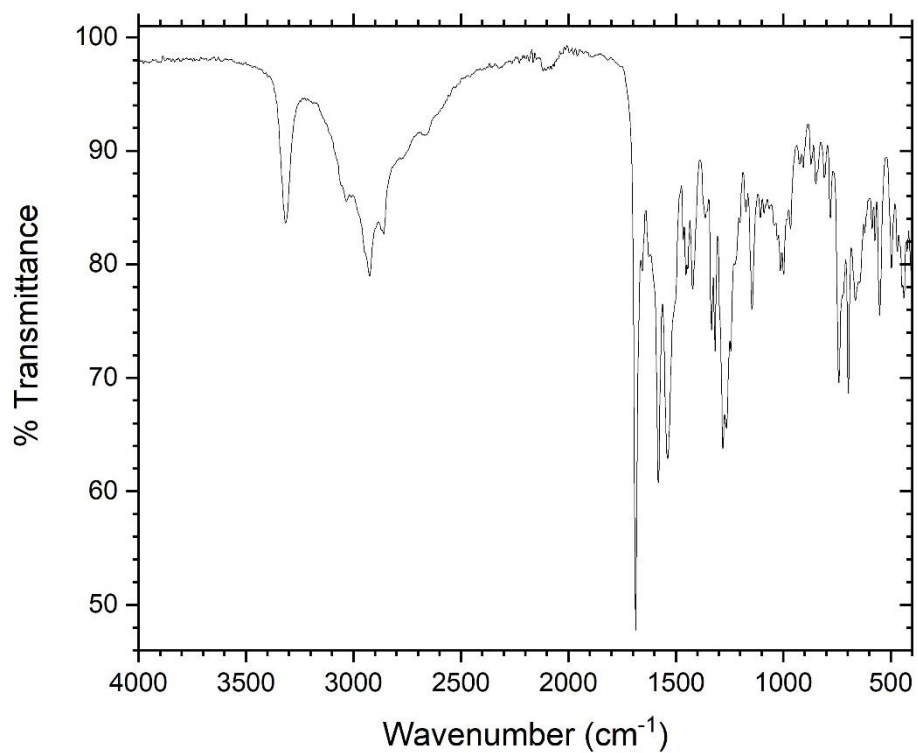


Figure A1.20. – FTIR spectrum of PLys(Cbz)<sub>15</sub> (labelled polymer 8 in Chapter 4, Table 4.1. and Table 4.2.).

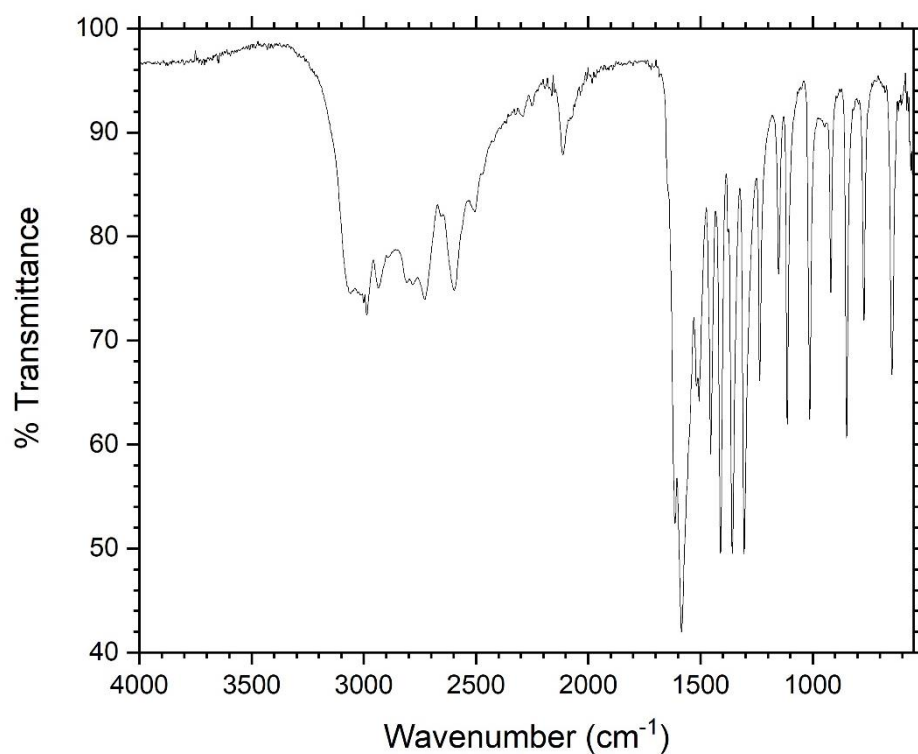


Figure A1.21. - FTIR spectrum of the products of the enzymatic degradation of PALa<sub>68</sub> (labelled polymer 2 in Chapter 4, Table 4.1. and Table 4.2.).

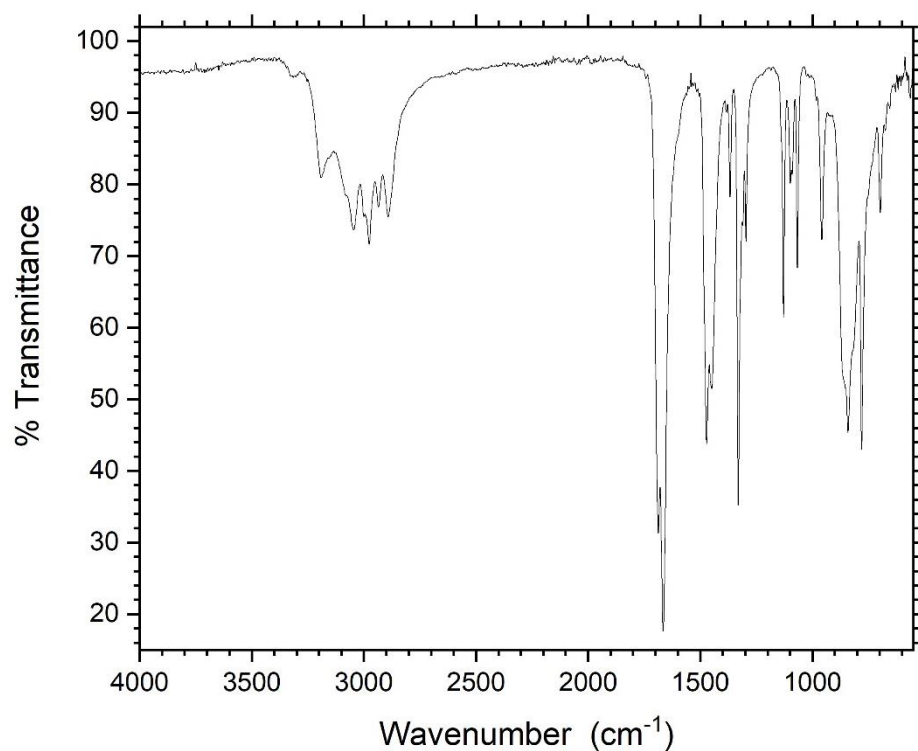


Figure A1.22. - FTIR spectrum of alanine DKP produced from the products of the enzymatic degradation of PALa<sub>68</sub> (labelled polymer 2 in Chapter 4, Table 4.1. and Table 4.2.).

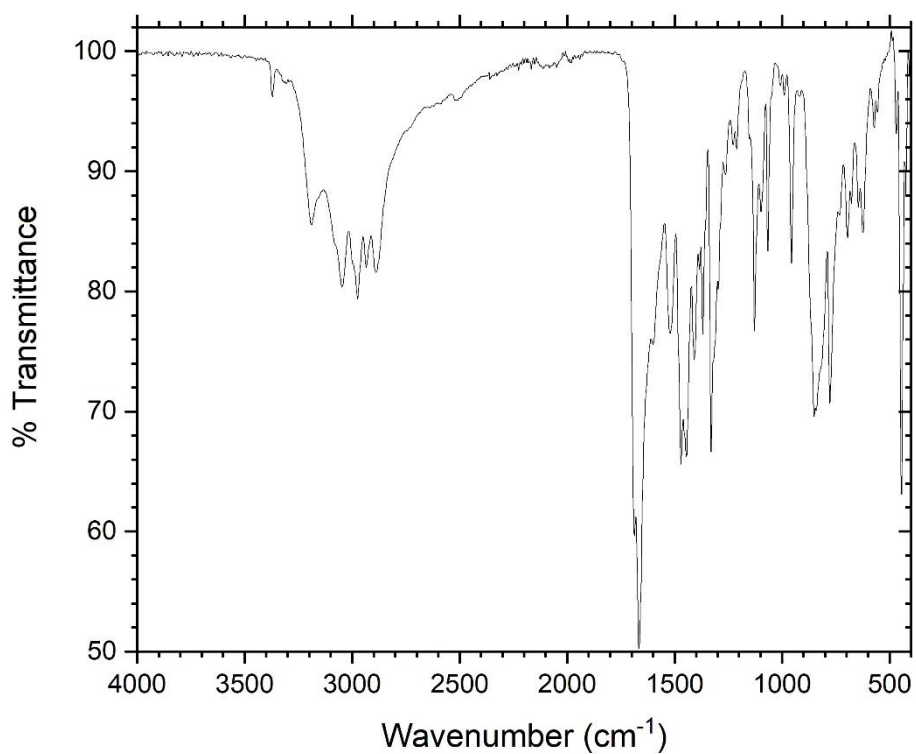


Figure A1.23. – FTIR spectrum of PGly<sub>39</sub> (labelled polymer 9 in Chapter 4, Table 4.1. and Table 4.2.).

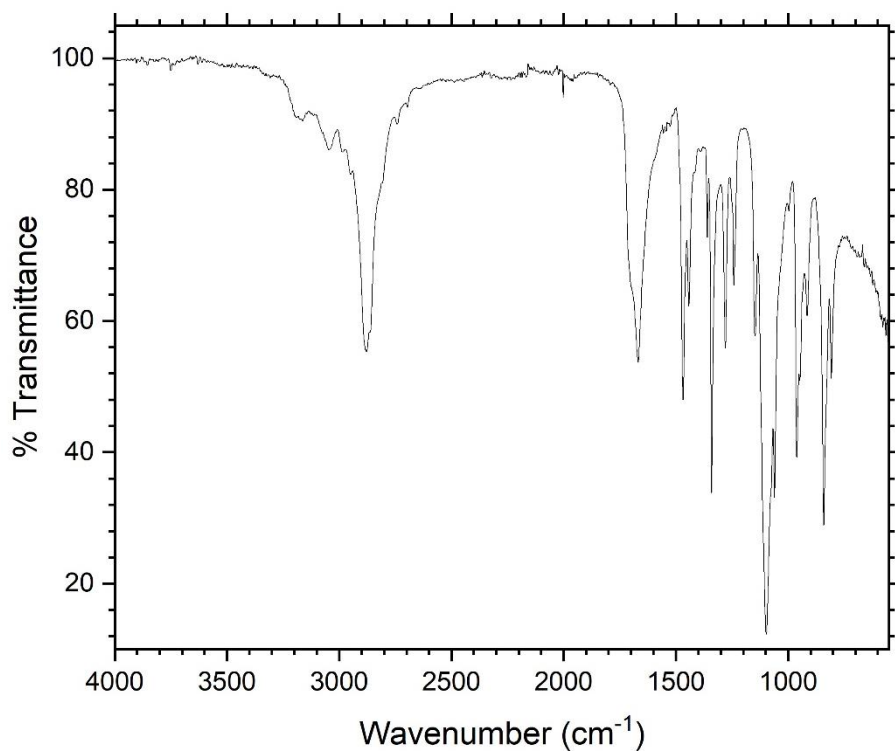


Figure A1.24. – FTIR spectrum of PEG-*b*-PGly<sub>30</sub> (labelled polymer 1 in Chapter 5, Table 5.1. and Table 5.2.).

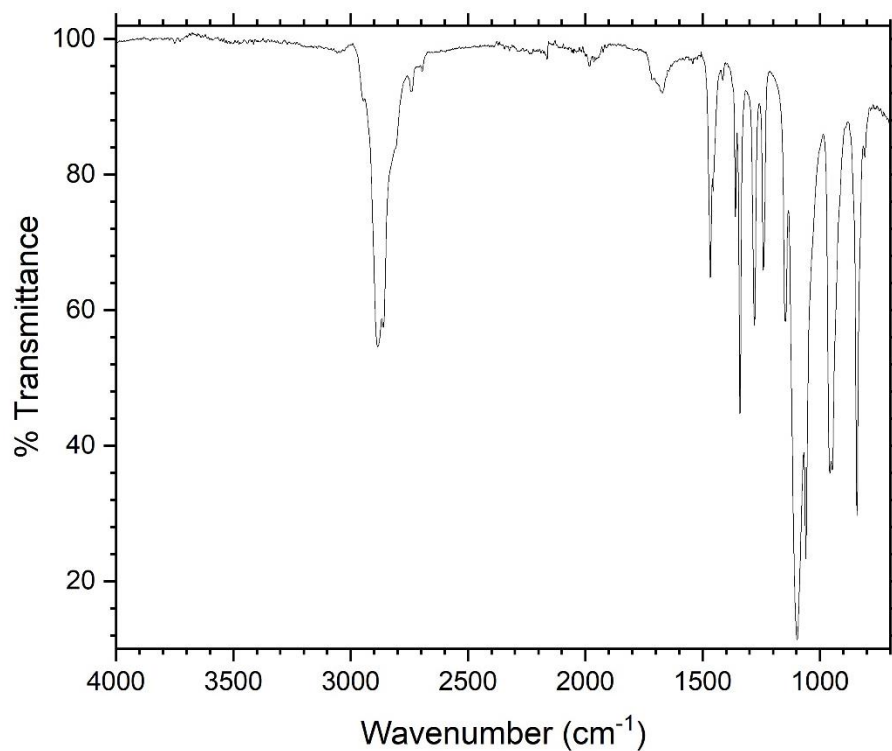


Figure A1.25. – FTIR spectrum of PEG-*b*-PGly<sub>14</sub> (labelled polymer 2 in Chapter 5, Table 5.1. and Table 5.2.).

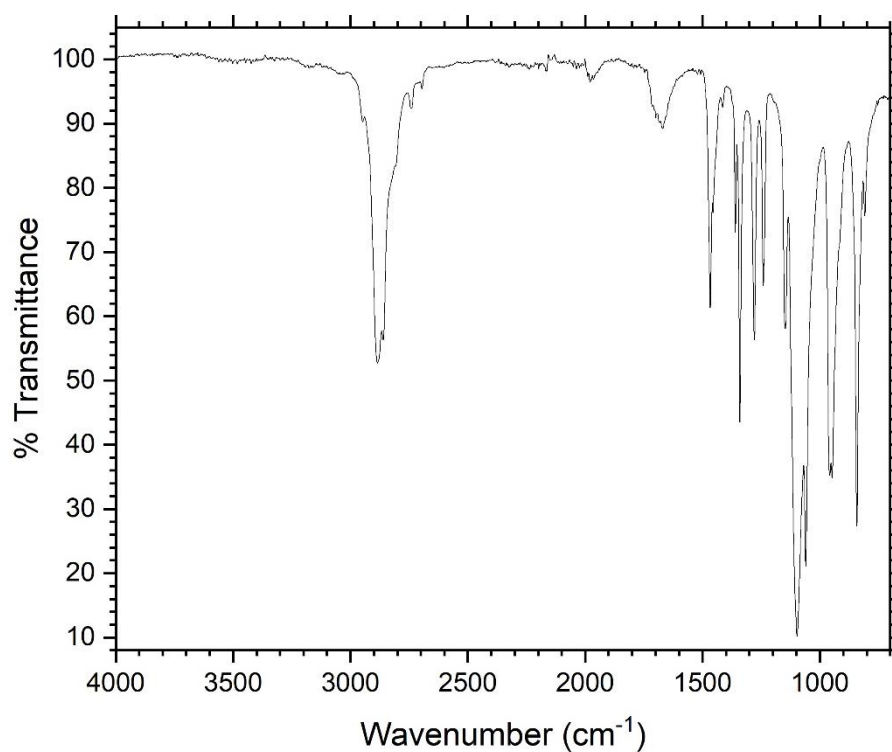


Figure A1.26. – FTIR spectrum of PEG-*b*-PGly<sub>20</sub> (labelled polymer 3 in Chapter 5, Table 5.1. and Table 5.2.).

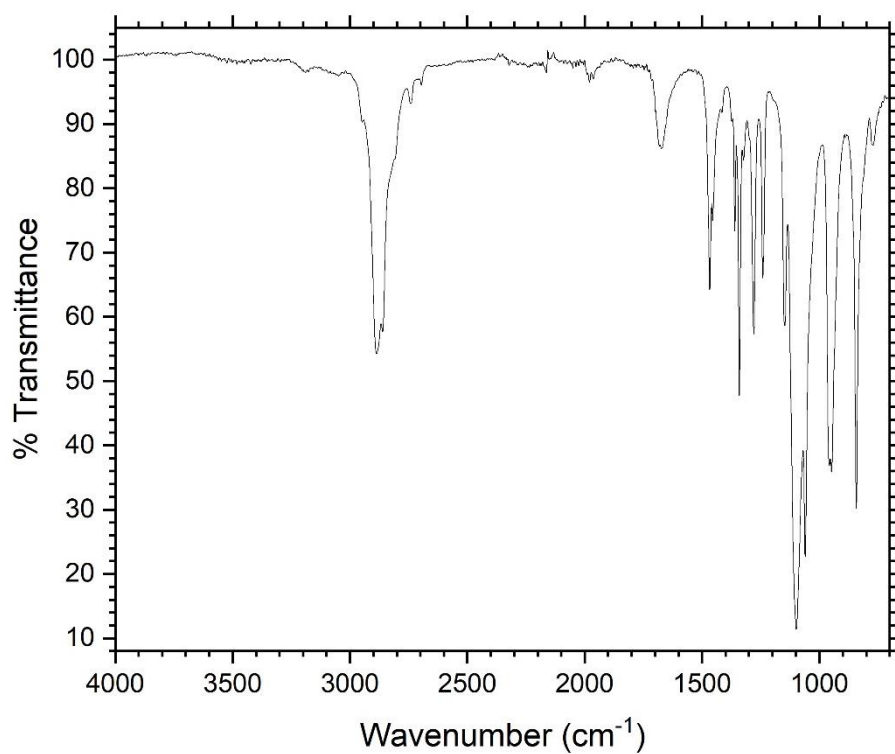


Figure A1.27. – FTIR spectrum of PEG-*b*-PALa<sub>6</sub> (labelled polymer 4 in Chapter 5, Table 5.1. and Table 5.2.).

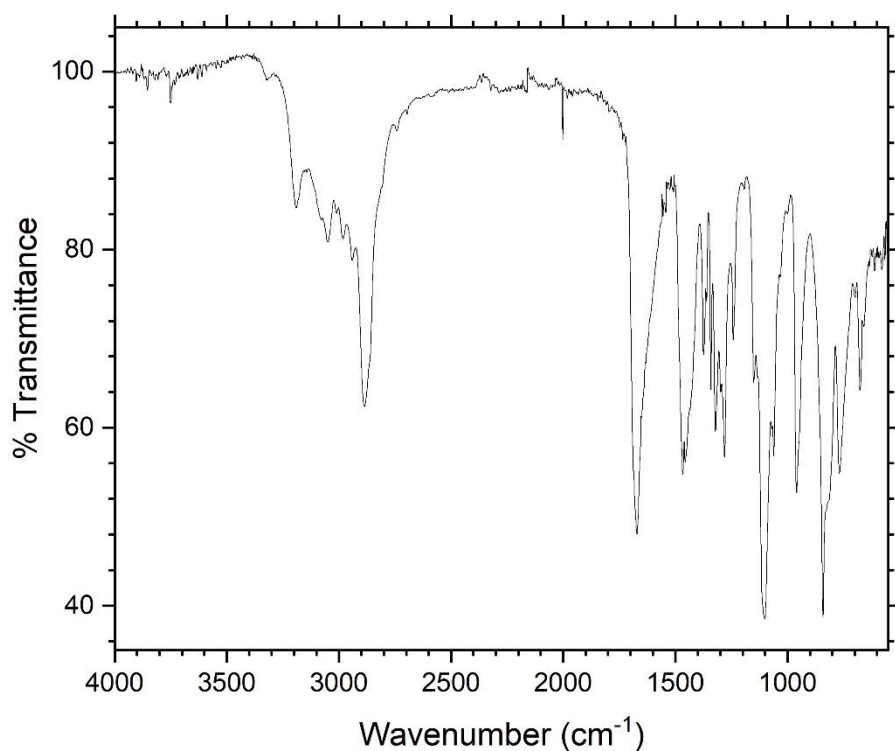


Figure A1.28. – FTIR spectrum of PEG-*b*-PALa<sub>12</sub> (labelled polymer 5 in Chapter 5, Table 5.1. and Table 5.2.).

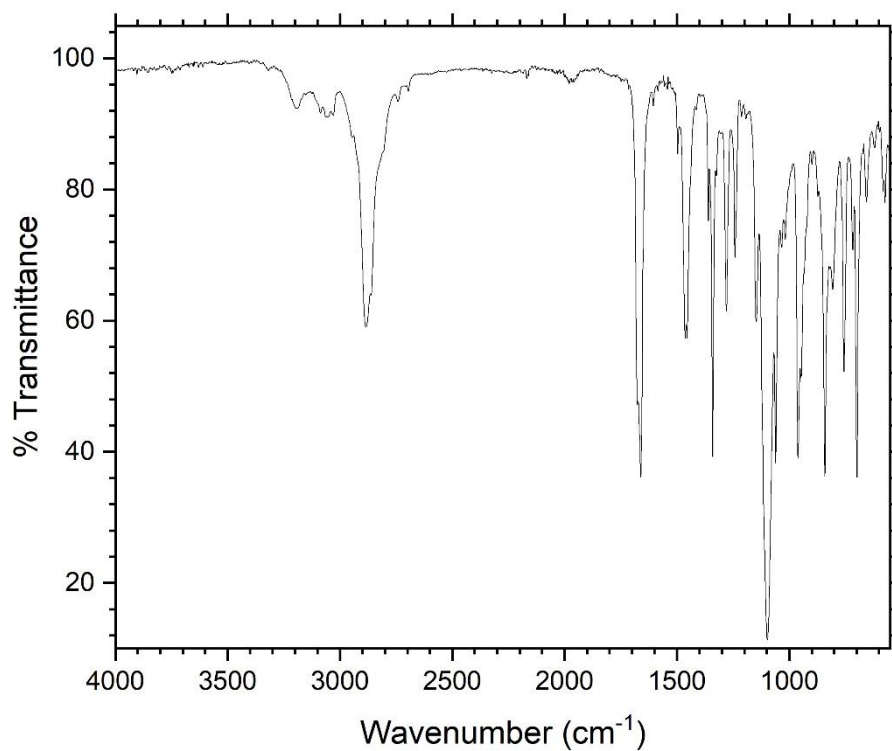


Figure AI.29. – FTIR spectrum of PEG-*b*-PAIa<sub>25</sub> (labelled polymer 6 in Chapter 5, Table 5.1. and Table 5.2.).

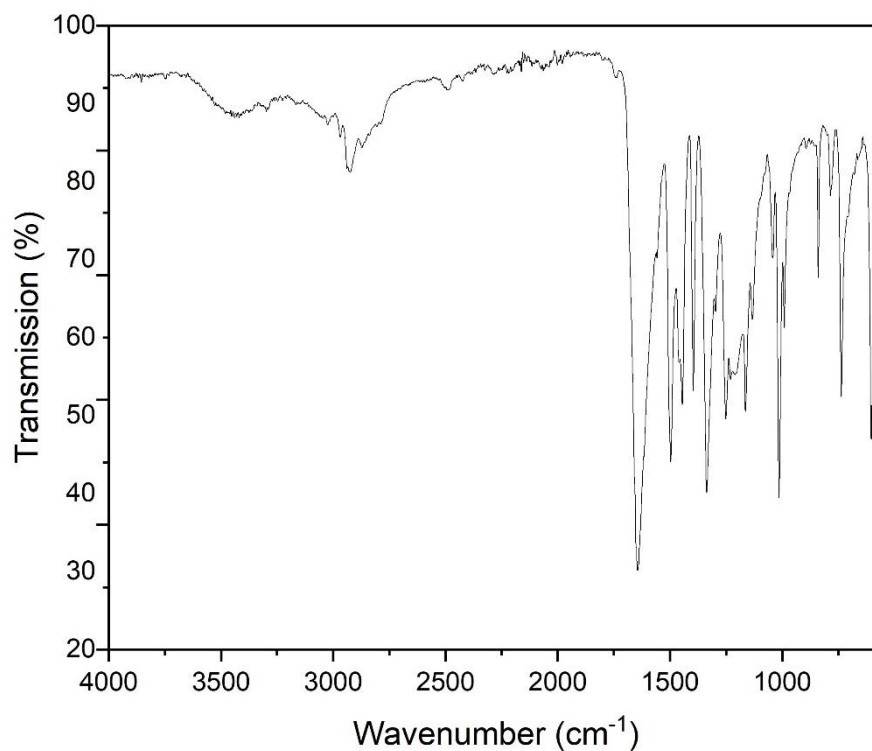


Figure AI.30. – FTIR spectrum of PSar<sub>77</sub> (labelled polymer 1 in Chapter 6, Table 6.1. and Table 6.2.).

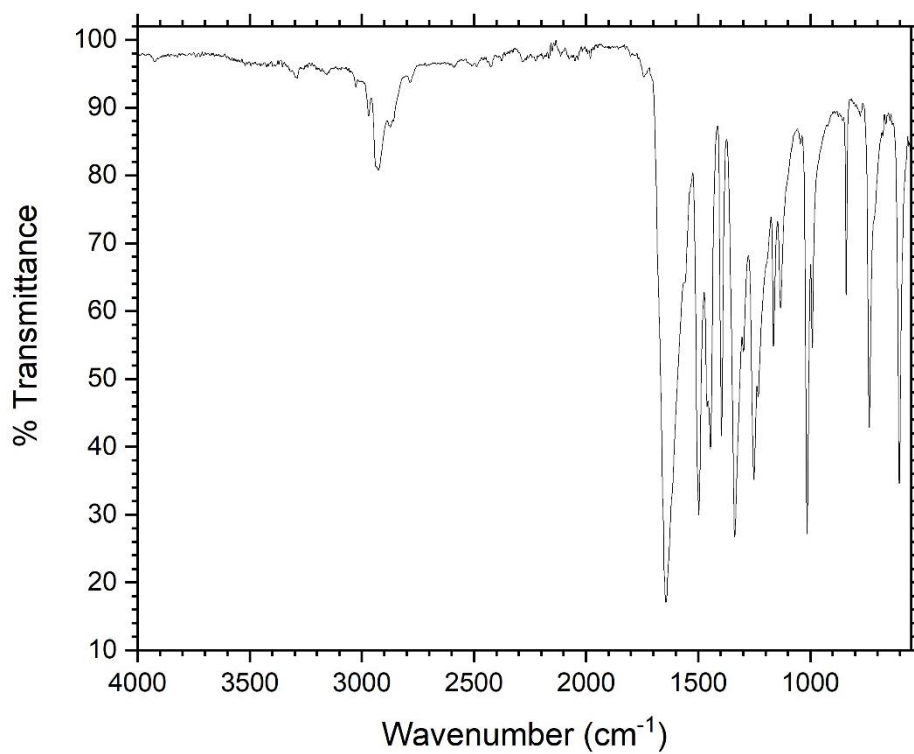


Figure A1.31. – FTIR spectrum of PSar<sub>79</sub> (labelled polymer 2 in Chapter 6, Table 6.1. and Table 6.2.).

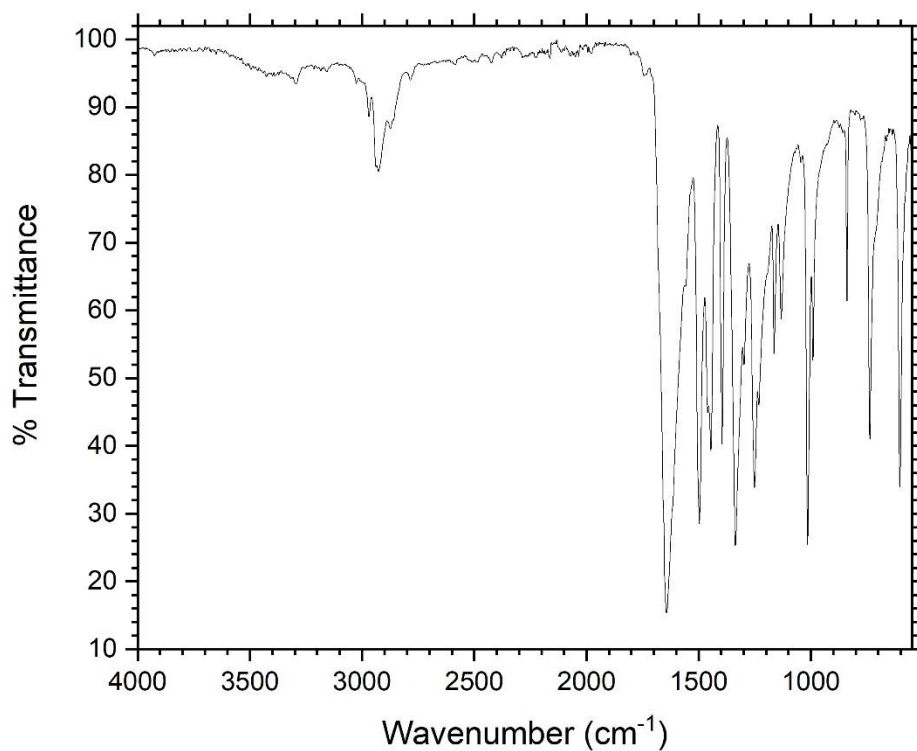


Figure A1.32. – FTIR spectrum of PSar<sub>76</sub> (labelled polymer 3 in Chapter 6, Table 6.1. and Table 6.2.).



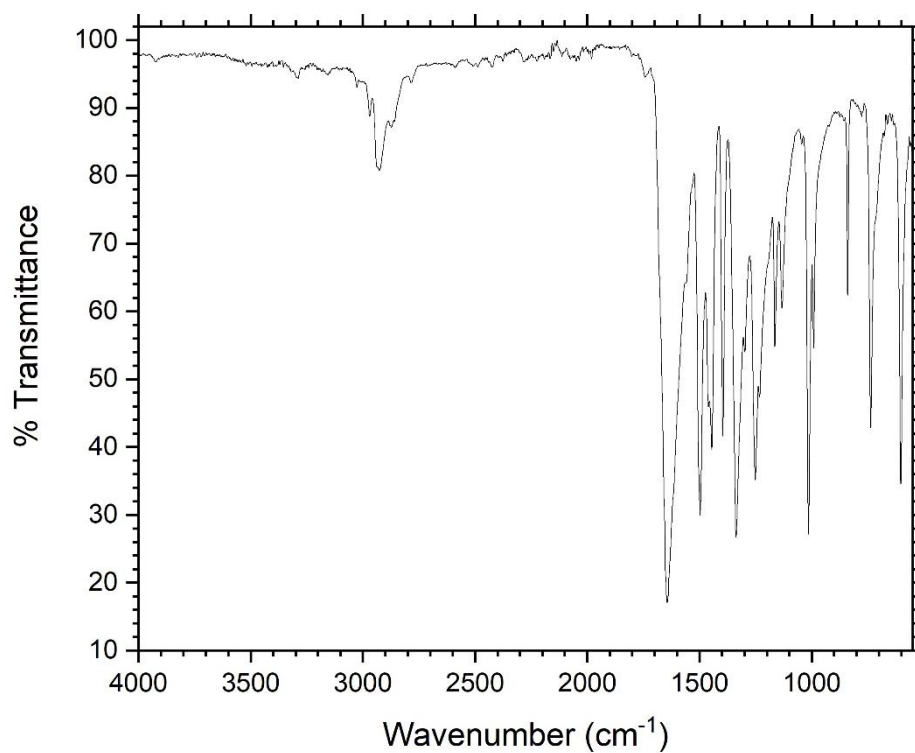


Figure A1.33. – FTIR spectrum of PSar<sub>100</sub> (labelled polymer 4 in Chapter 6, Table 6.1. and Table 6.2.).

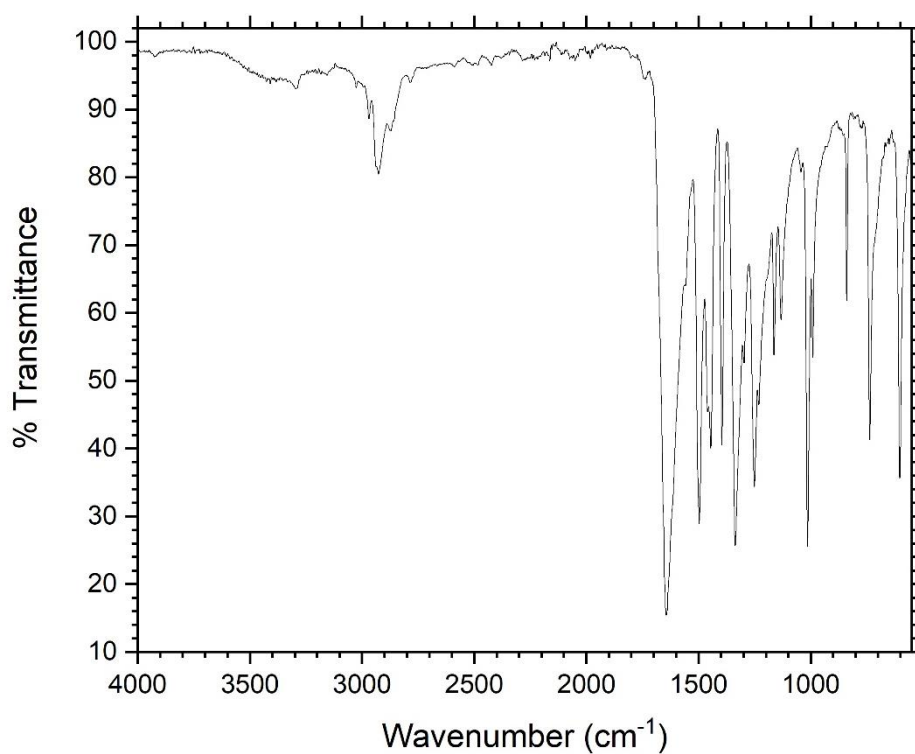


Figure A1.34. – FTIR spectrum of PSar<sub>139</sub> (labelled polymer 5 in Chapter 6, Table 6.1. and Table 6.2.).

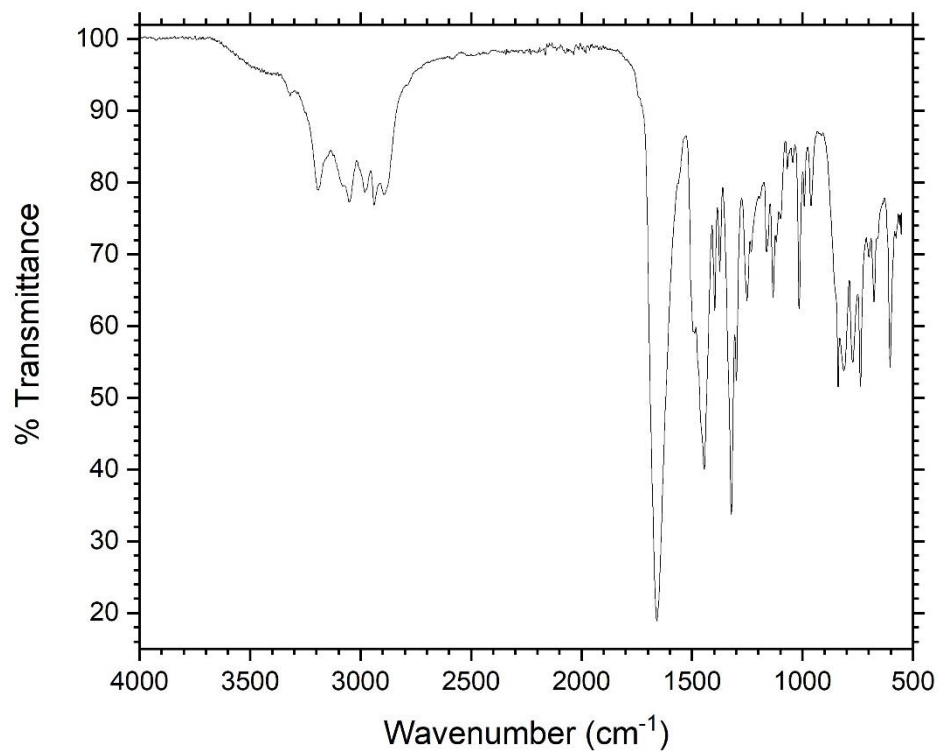


Figure A1.35. – FTIR spectrum of PSar<sub>77</sub>-b-PAla<sub>9</sub> (labelled polymer 6 in Chapter 6, Table 6.1. and Table 6.3.).

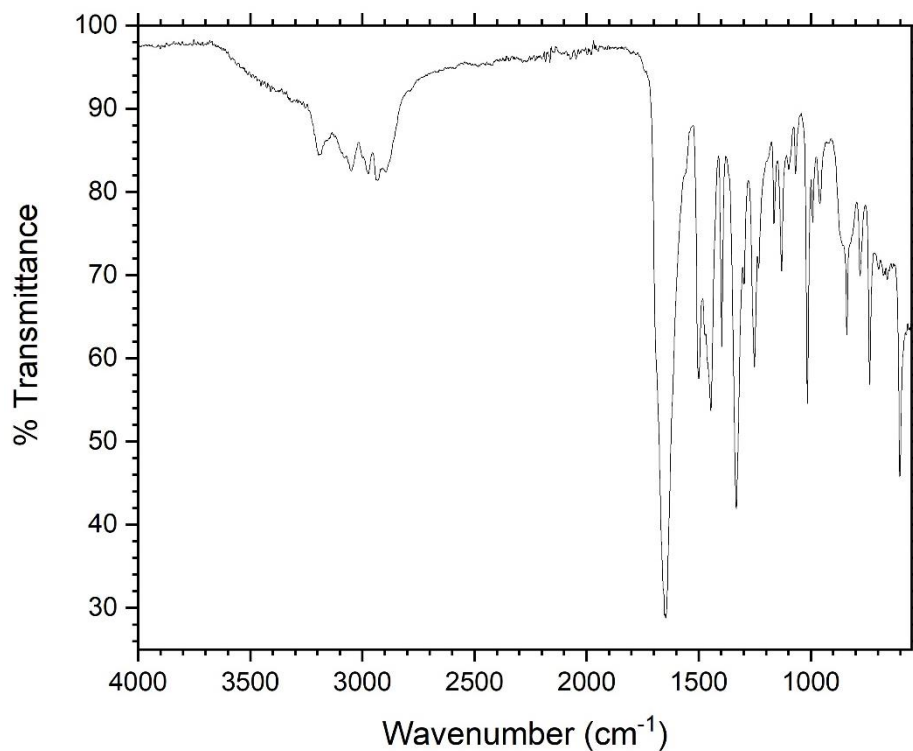


Figure A1.36. – FTIR spectrum of PSar<sub>79</sub>-b-PAla<sub>9</sub> (labelled polymer 7 in Chapter 6, Table 6.1. and Table 6.3.).

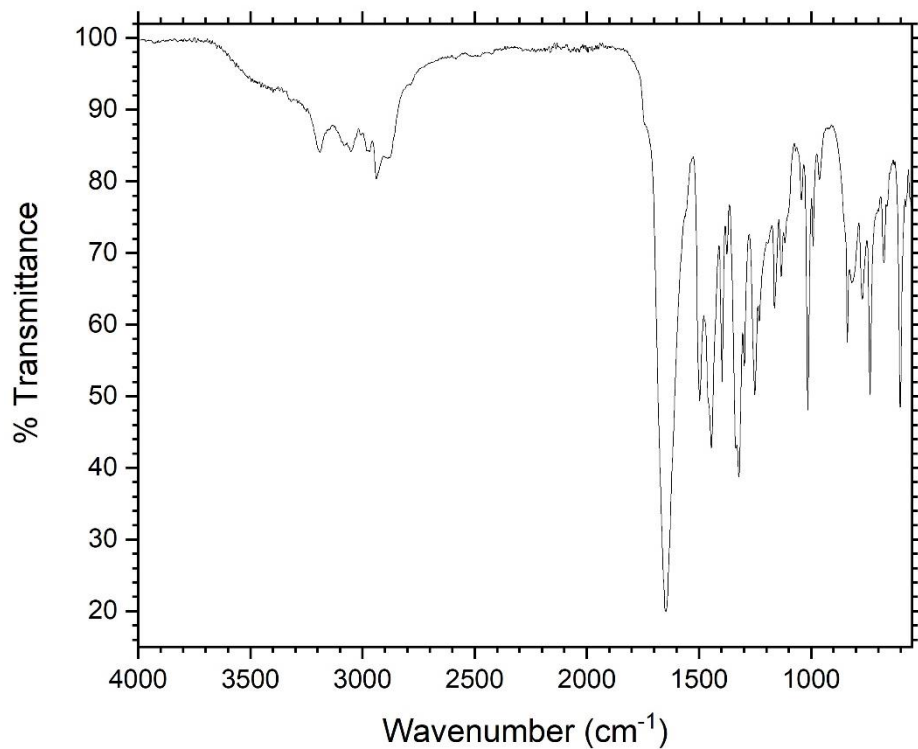


Figure AI.37. – FTIR spectrum of PSar<sub>139</sub>-*b*-PAla<sub>13</sub> (labelled polymer 8 in Chapter 6, Table 6.1. and Table 6.3.).

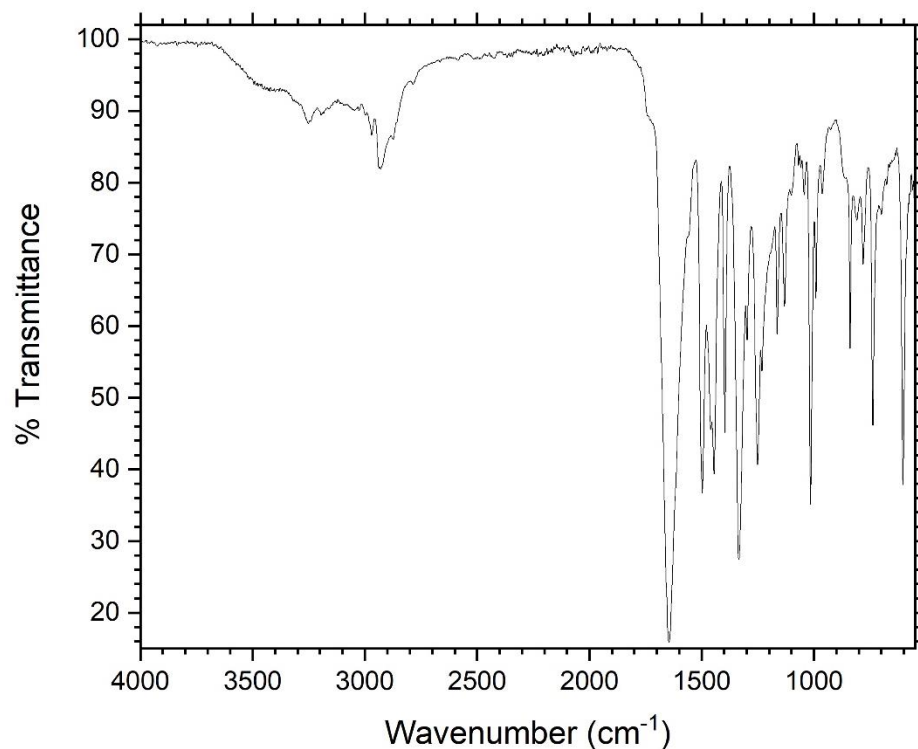


Figure AI.38. – FTIR spectrum of PSar<sub>139</sub>-*b*-PAla<sub>12</sub> (labelled polymer 9 in Chapter 6, Table 6.1. and Table 6.3.).

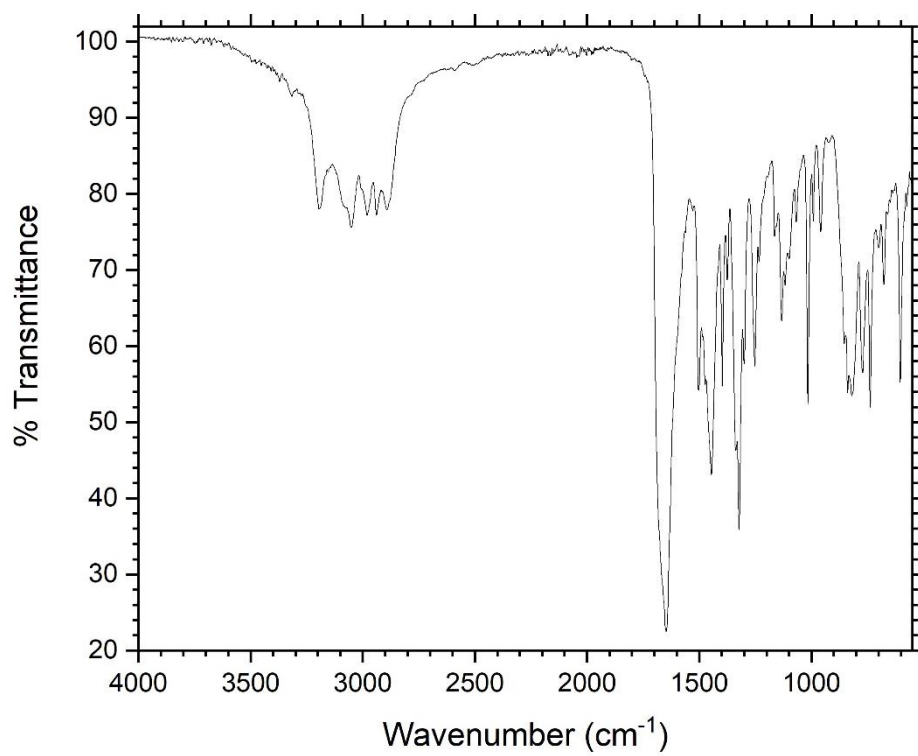


Figure A1.39. – FTIR spectrum of PSar<sub>70</sub>-ran-PAla<sub>8</sub> (labelled polymer 10 in Chapter 6).

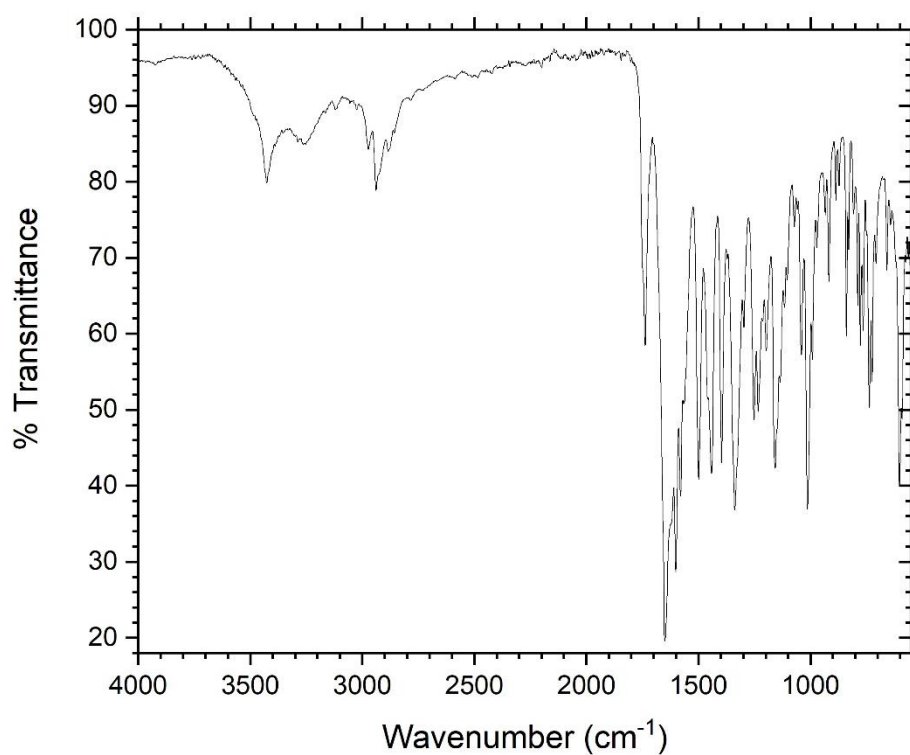


Figure A1.40. – FTIR spectrum of Camptothecin-PSar<sub>14</sub> (Chapter 6).

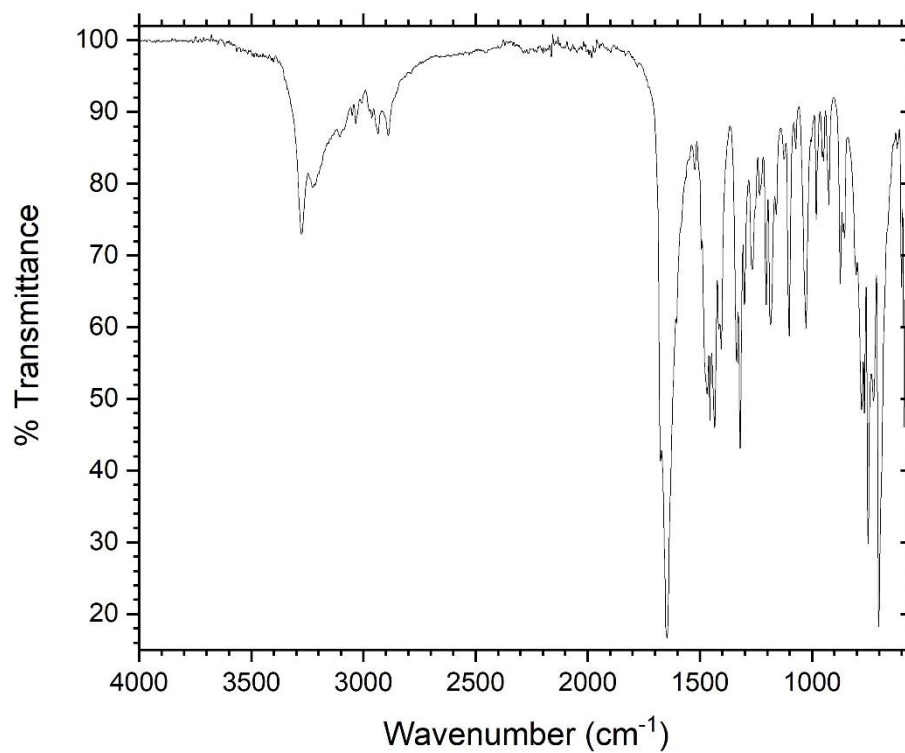


Figure A1.41. – FTIR spectrum of Poly(Sar-Phe)<sub>35</sub> (Chapter 6).

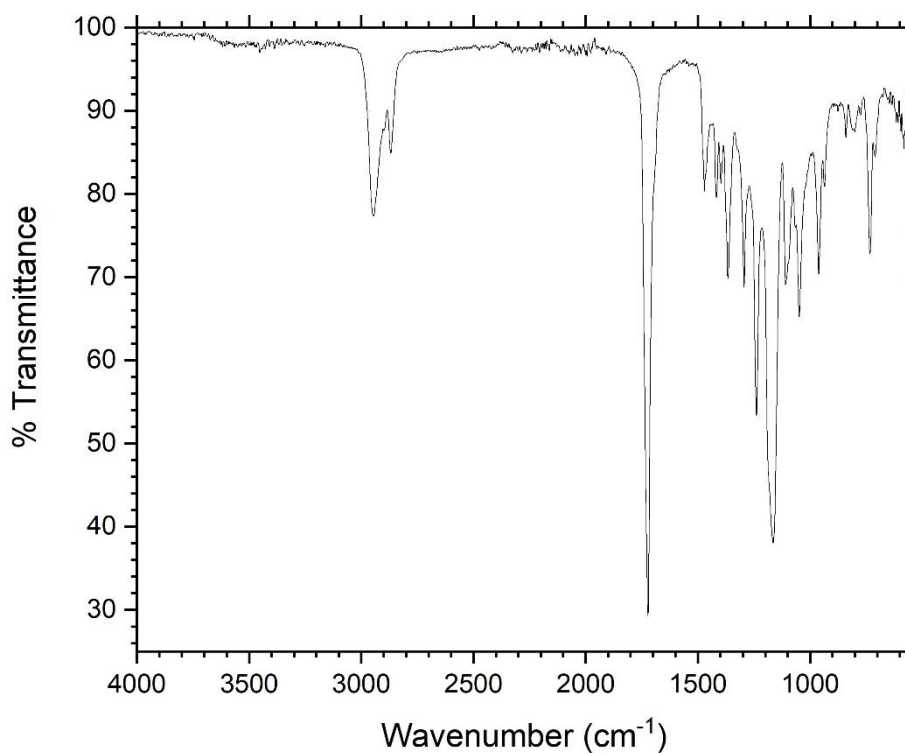


Figure A1.42. – FTIR spectrum of PCL nanofibres produced in spin 1 (Chapter 7, Table 7.1. and Table 7.2.).

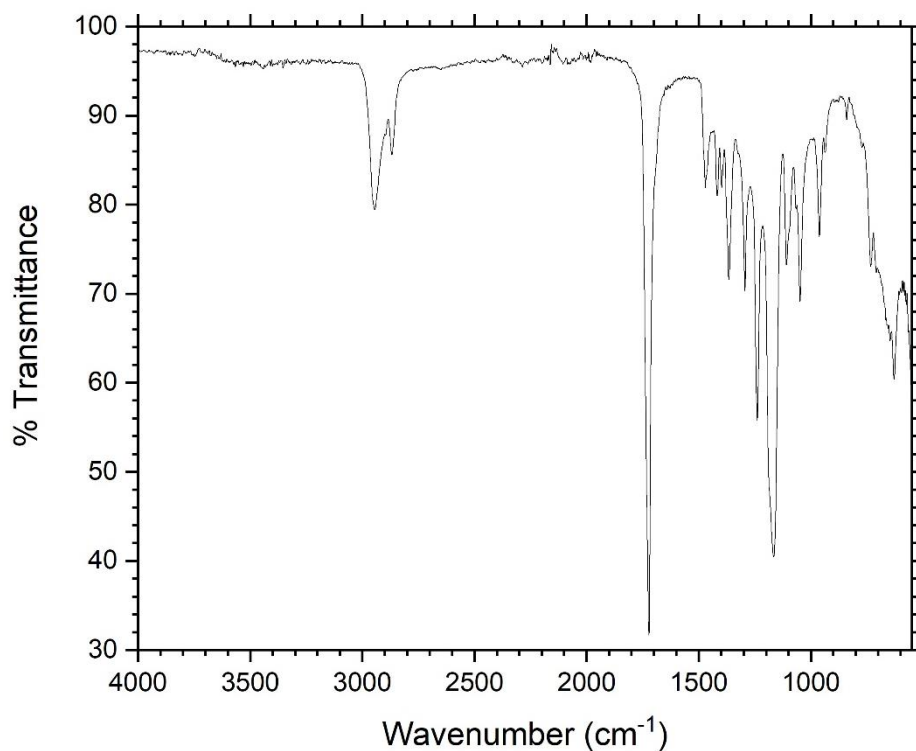


Figure A1.43. – FTIR spectrum of PCL nanofibres produced in spin 2 (Chapter 7, Table 7.1. and Table 7.2.).

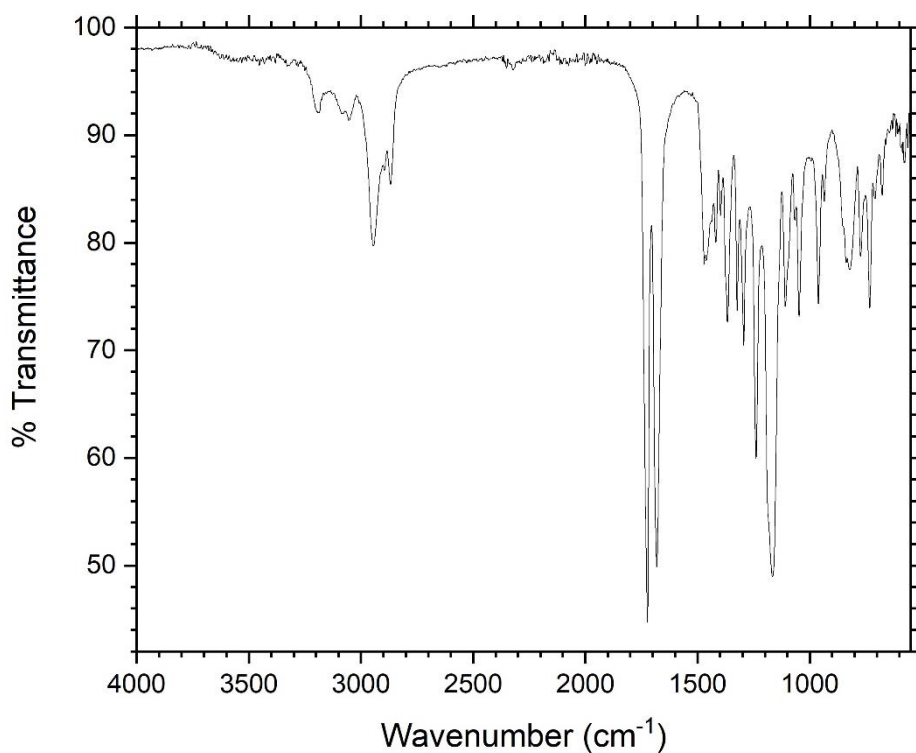


Figure A1.44. – FTIR spectrum of PCL/PAla nanofibres produced in spin 3 (Chapter 7, Table 7.1. and Table 7.2.).

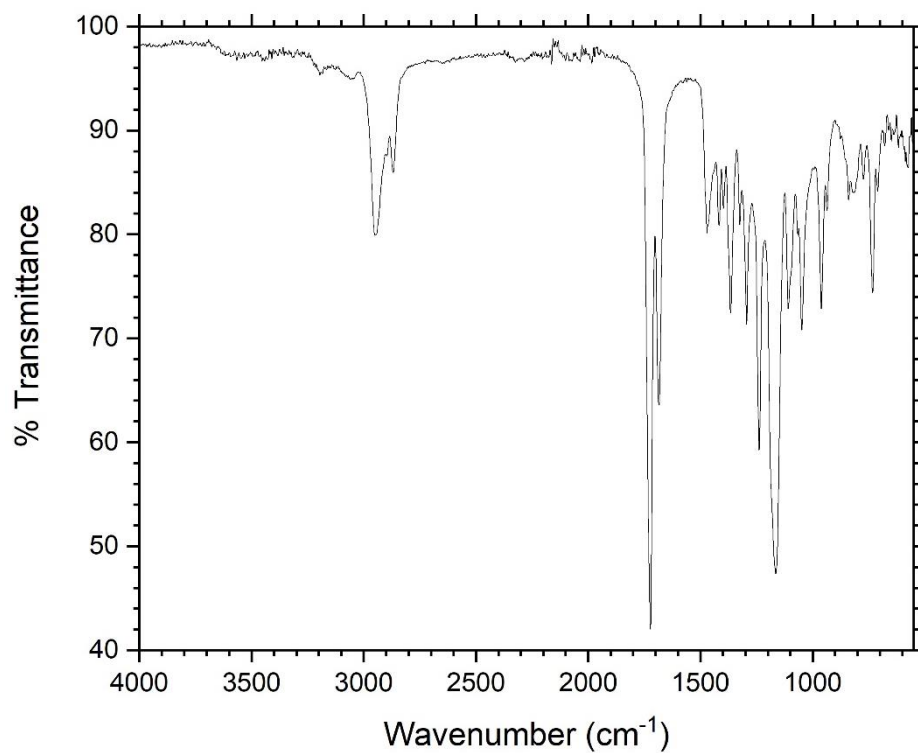


Figure A1.45. – FTIR spectrum of PCL/PAla nanofibres produced in spin 4 (Chapter 7, Table 7.1. and Table 7.2.).

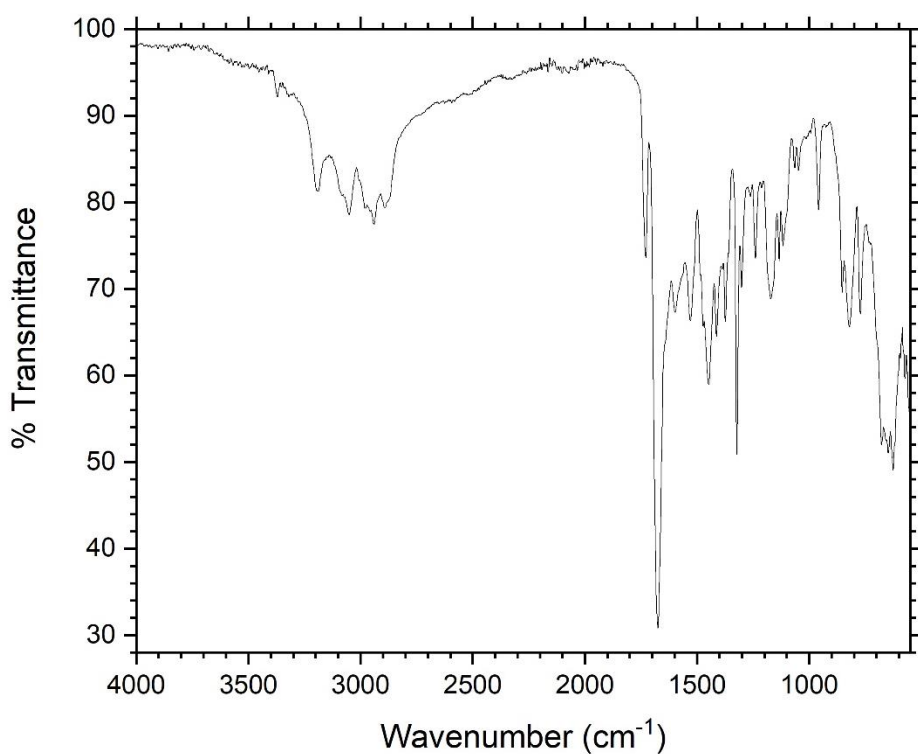


Figure A1.46. – FTIR spectrum of PCL/PAla nanofibres produced in spin 5 (Chapter 7, Table 7.1. and Table 7.2.).

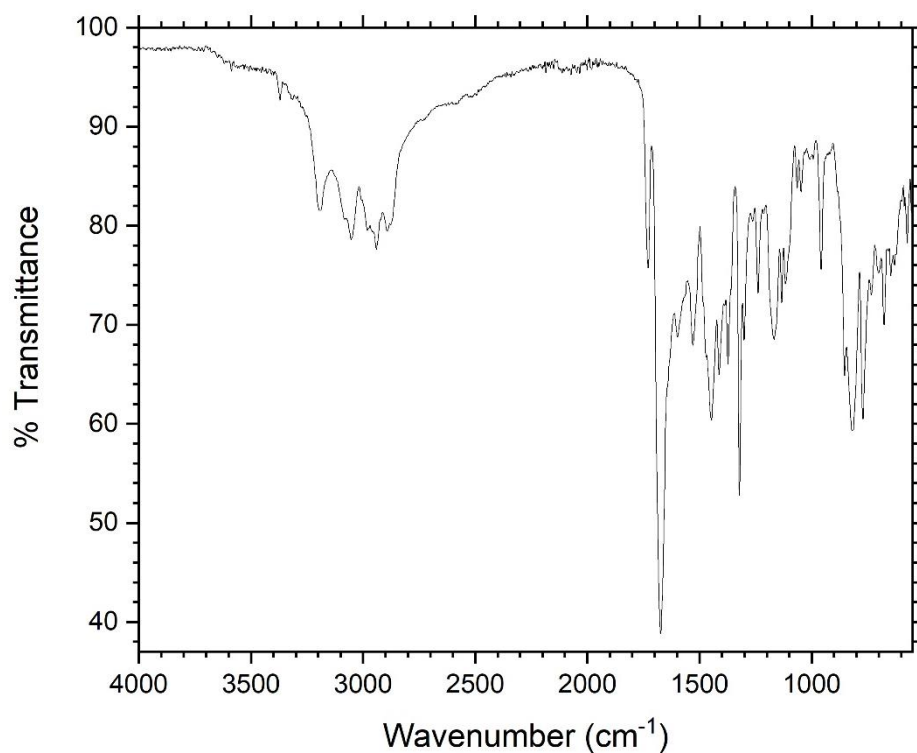


Figure A1.47. – FTIR spectrum of PCL/PAla nanofibres produced in spin 6 (Chapter 7, Table 7.1. and Table 7.2.).

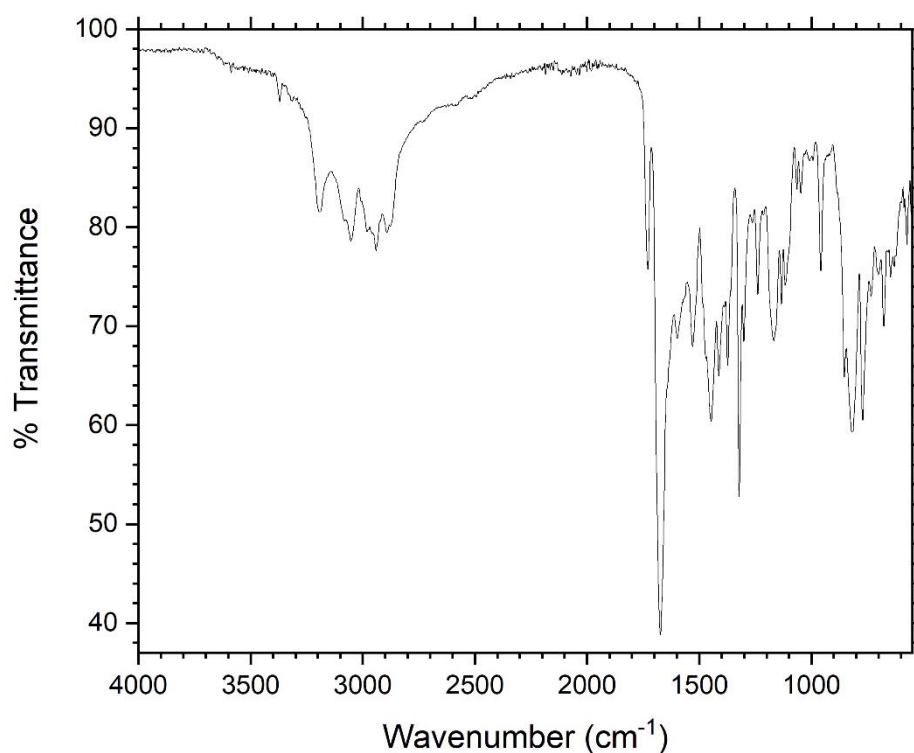


Figure A1.48. – FTIR spectrum of PCL/PAla nanofibres produced in spin 7 (Chapter 7, Table 7.1. and Table 7.2.).



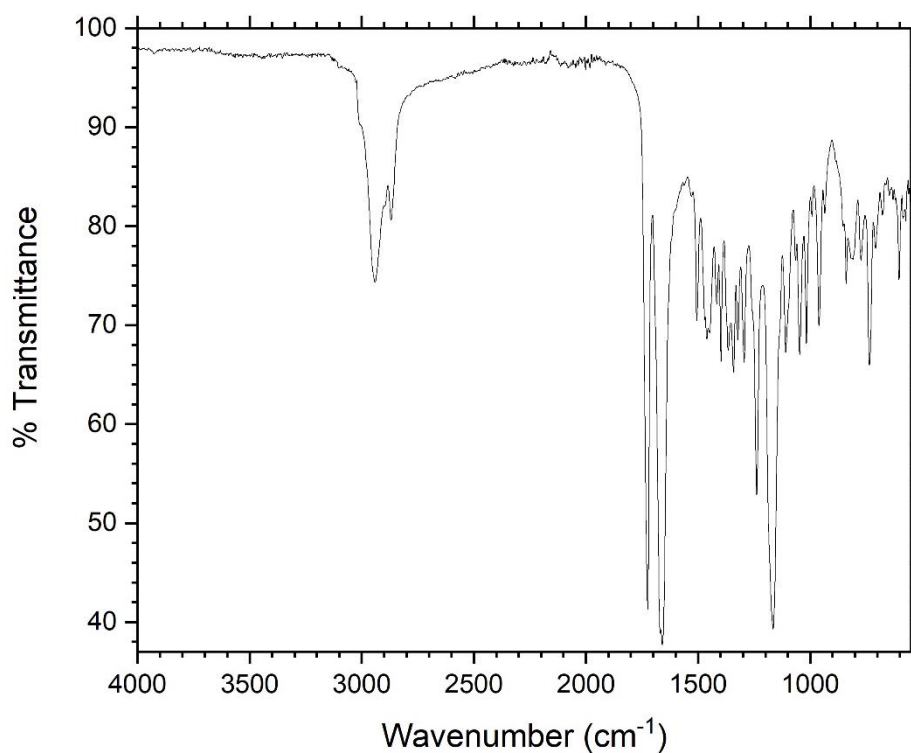


Figure A1.49. – FTIR spectrum of PCL/PSar nanofibres produced in spin 8 (Chapter 7, Table 7.1. and Table 7.2.).

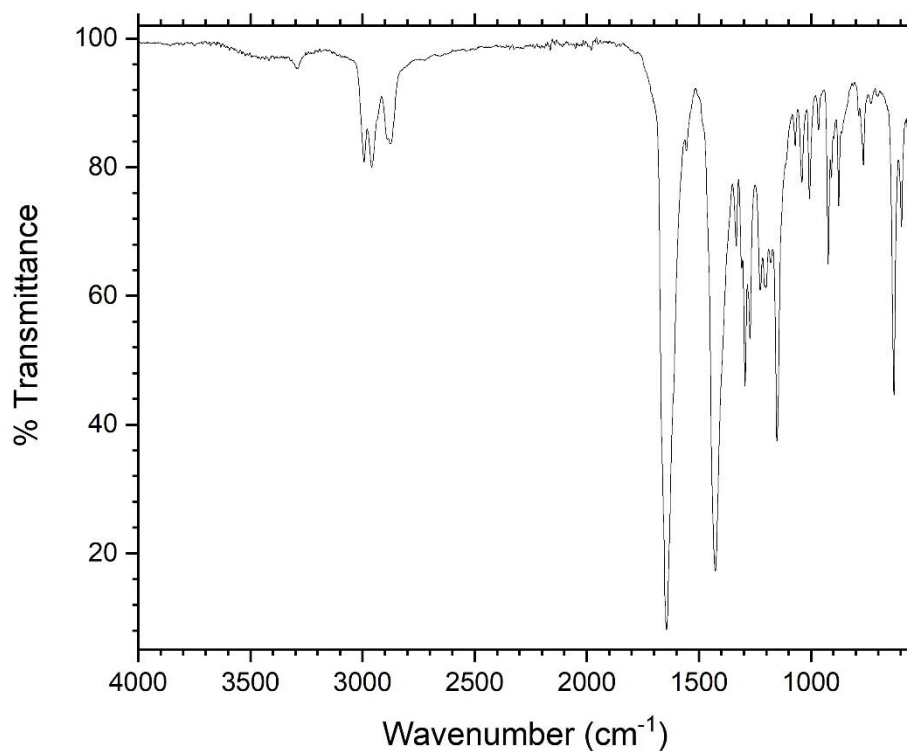


Figure A1.50. – FTIR spectrum of PPro<sub>59</sub> (PPro-1 in Chapter 8).

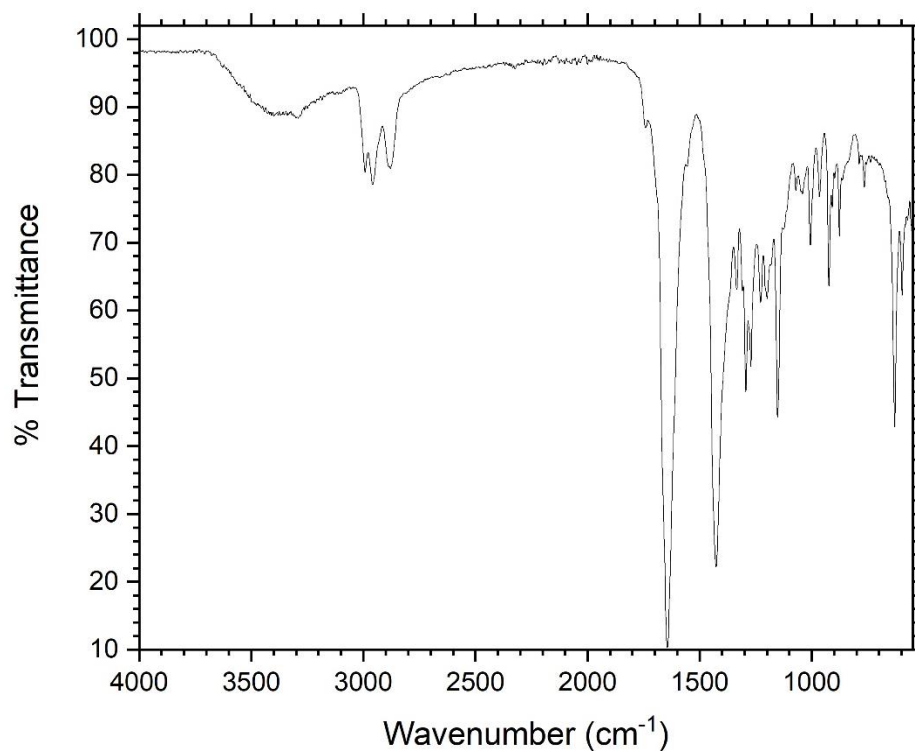


Figure AI.51. – FTIR spectrum of PPro<sub>103</sub> (PPro-2 in Chapter 8).

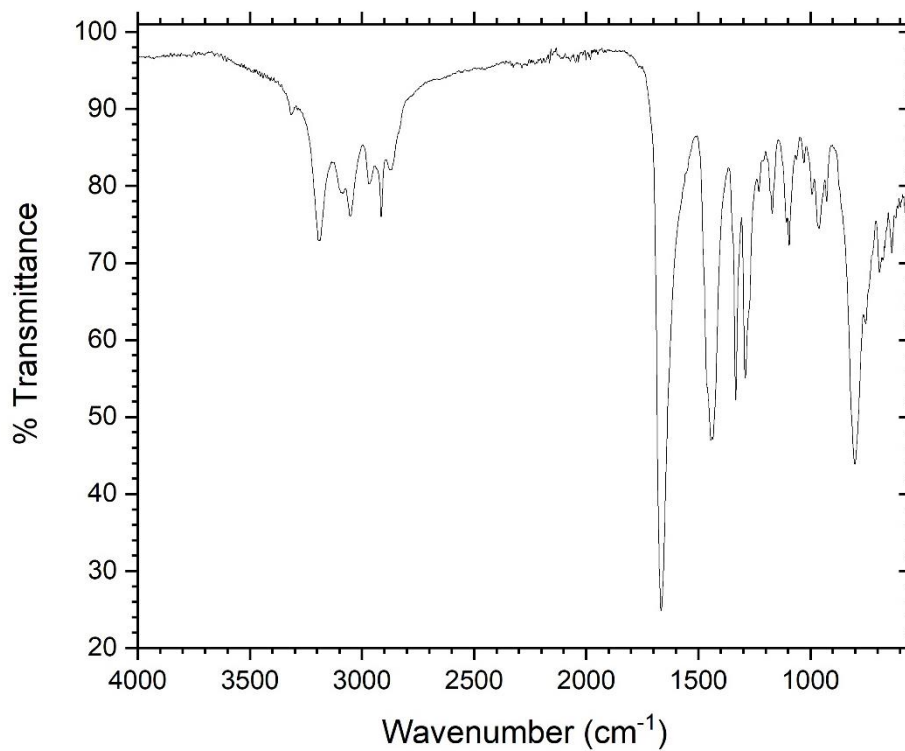


Figure AI.52. – FTIR spectrum of PMet<sub>21</sub> (Chapter 8).

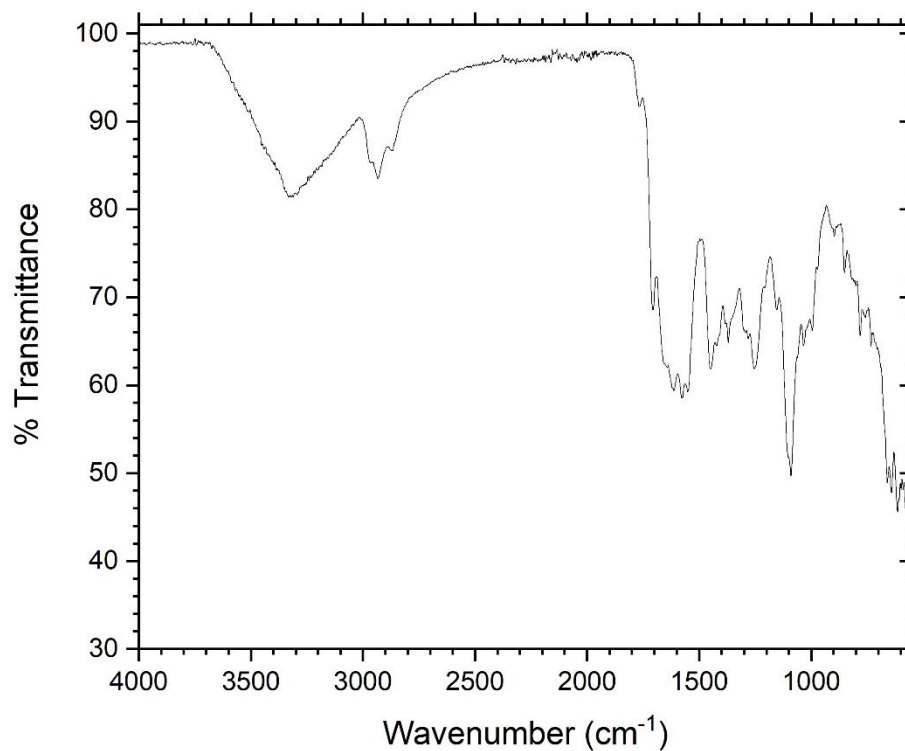


Figure A1.53. – FTIR spectrum of PArg(Pbf)<sub>24</sub> (Chapter 8).

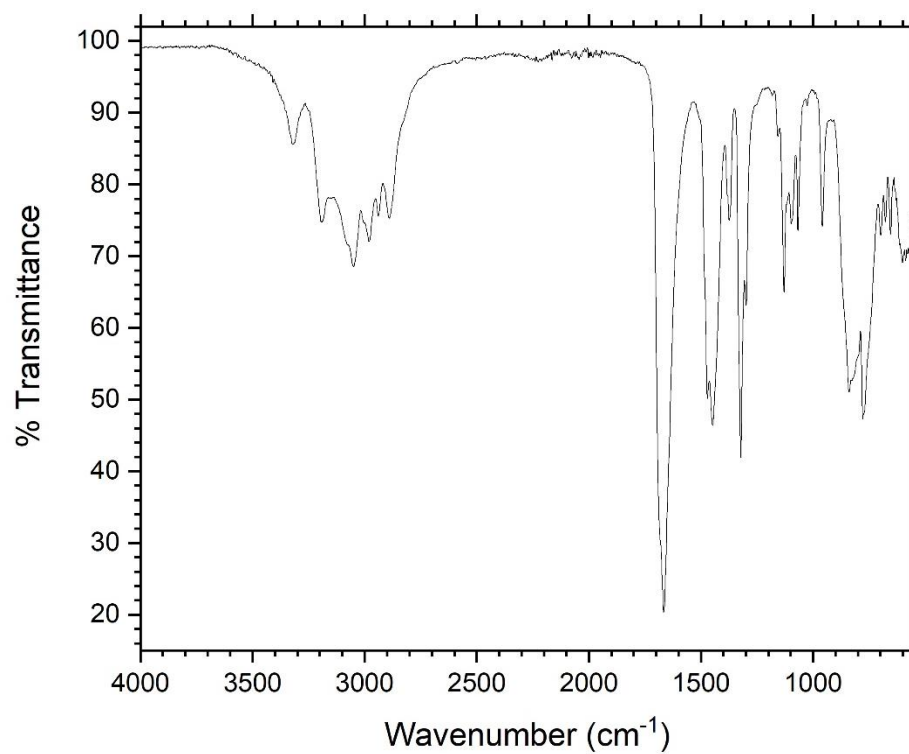


Figure A1.54. – FTIR spectrum of the products of eROP of alanine DKP (Chapter 8).

## Appendix II – $^1\text{H}$ NMR Spectroscopy

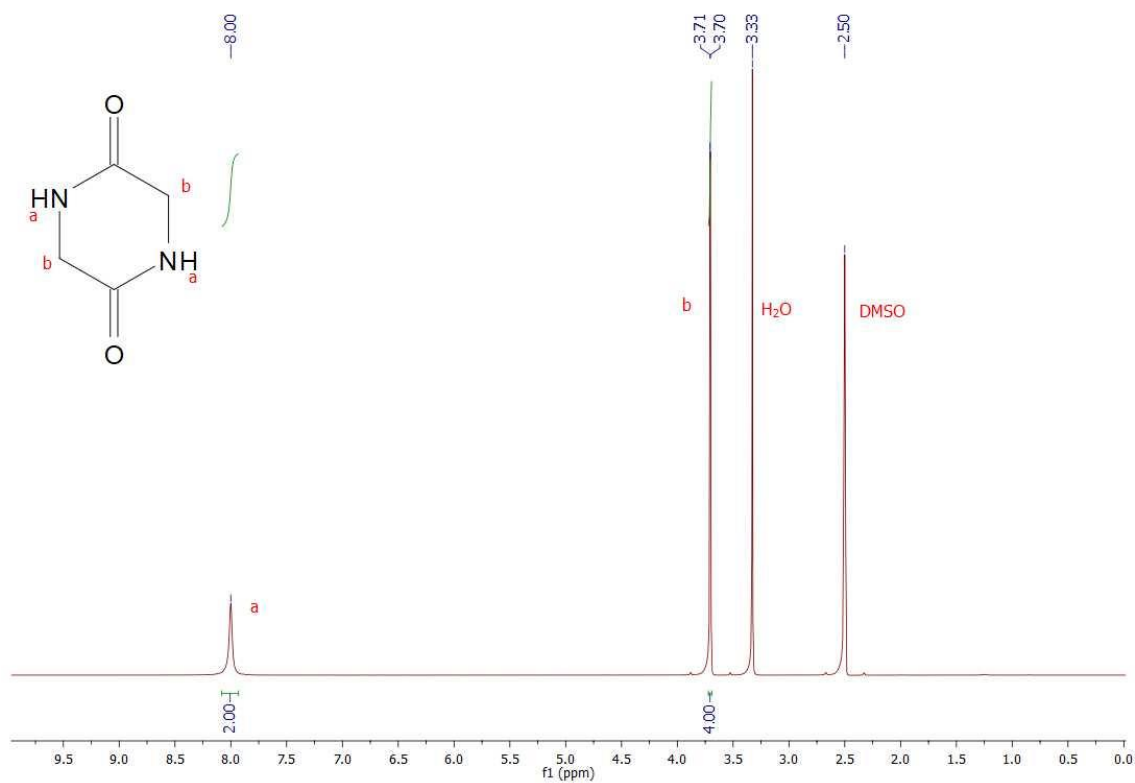


Figure AII.1. –  $^1\text{H}$  NMR spectrum (DMSO- $d_6$ , 400 MHz) of glycine DKP.

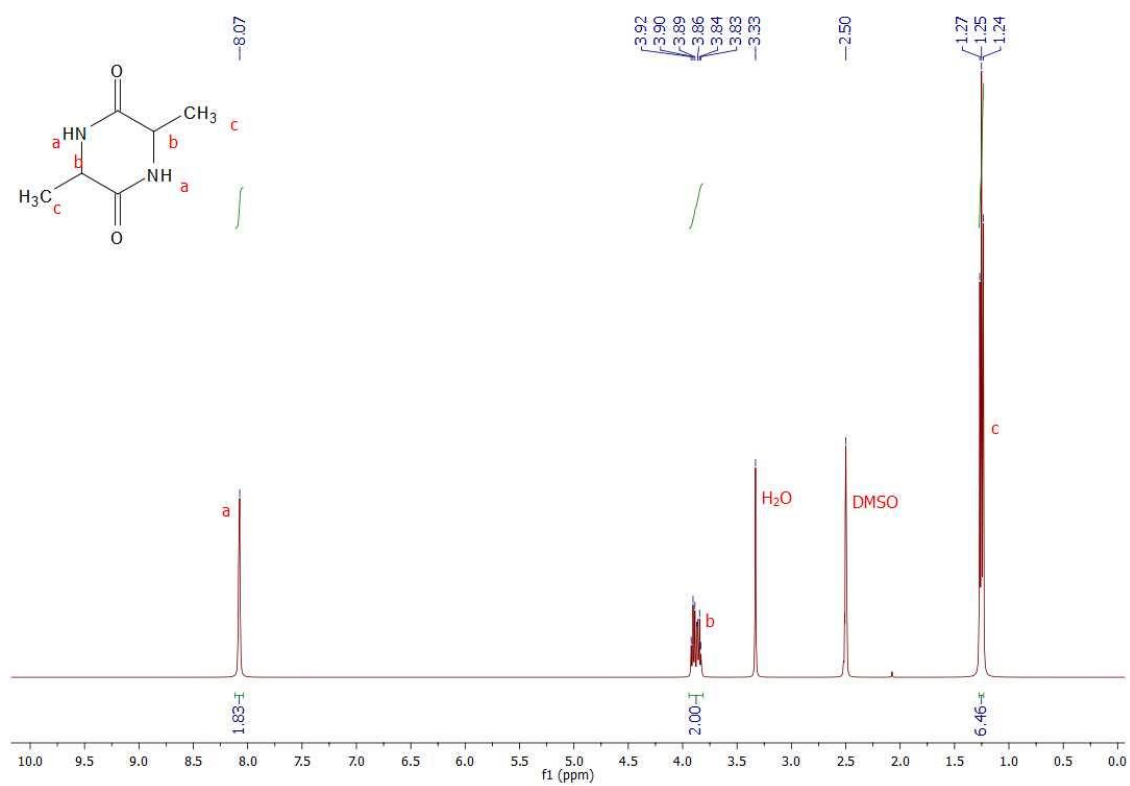


Figure AII.2. –  $^1\text{H}$  NMR spectrum (DMSO- $d_6$ , 400 MHz) of alanine DKP.

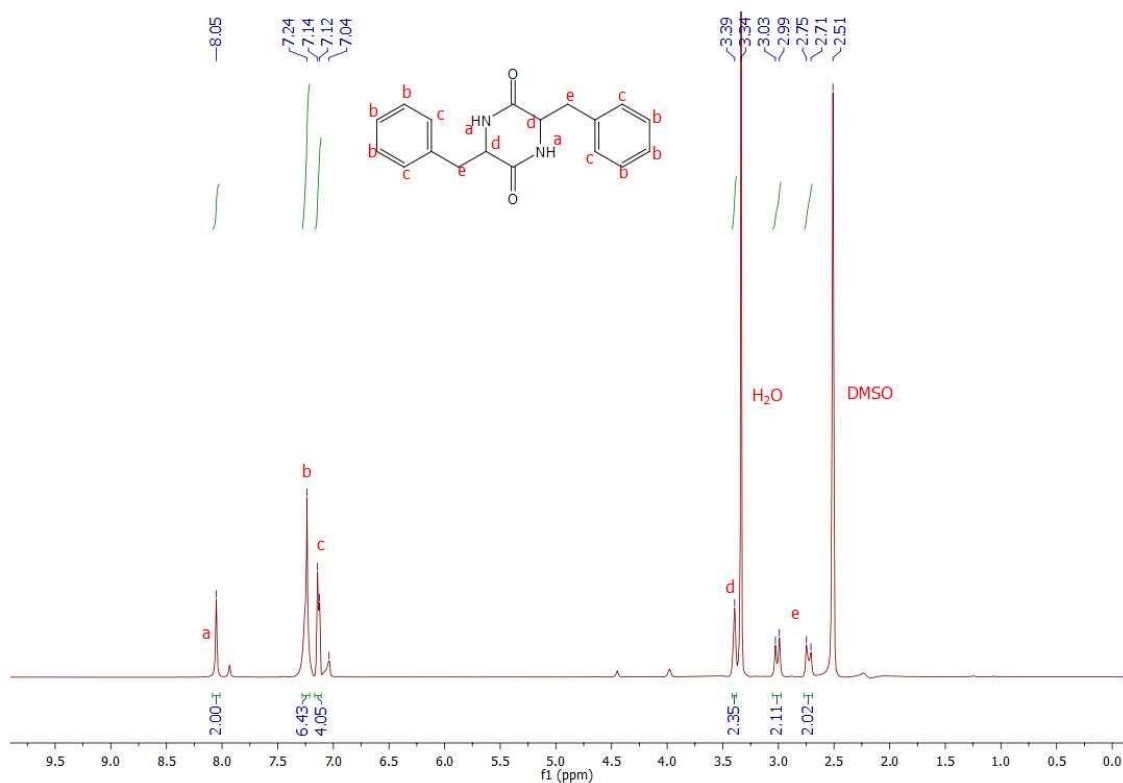


Figure All.3. – <sup>1</sup>H NMR spectrum (DMSO-d<sub>6</sub>, 400 MHz) of phenylalanine DKP.

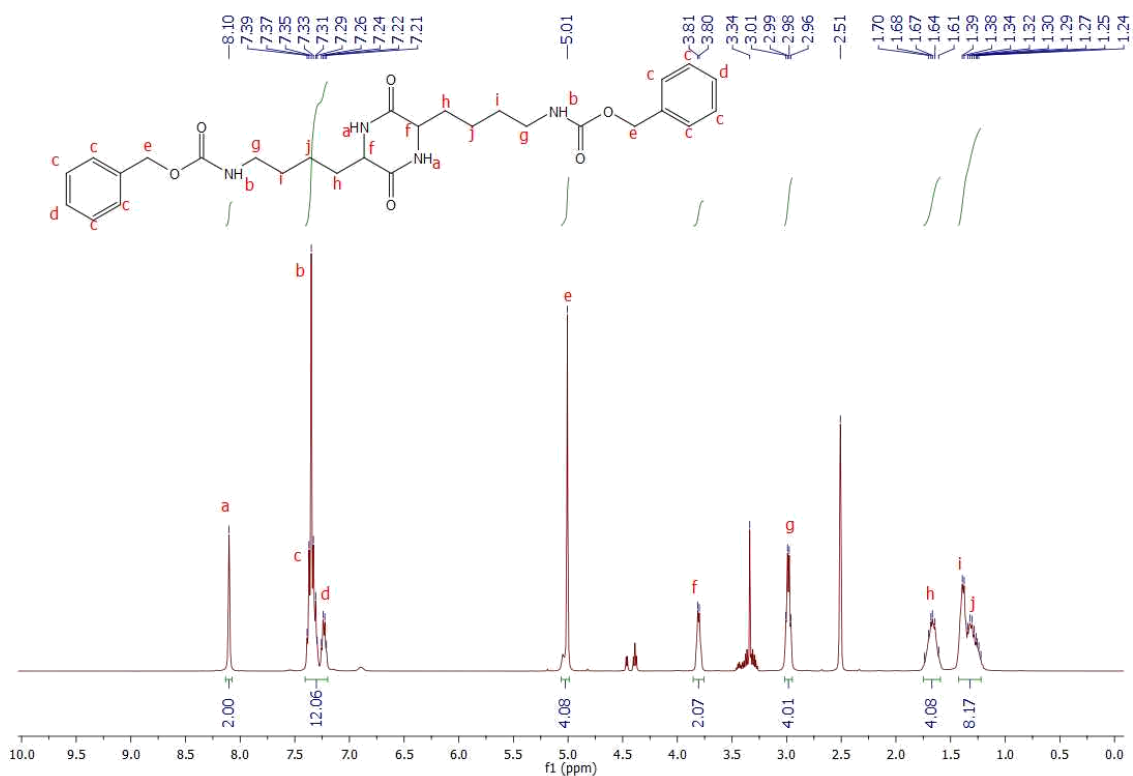


Figure All.4. – <sup>1</sup>H NMR spectrum (DMSO-d<sub>6</sub>, 400 MHz) of lysine(Cbz) DKP.

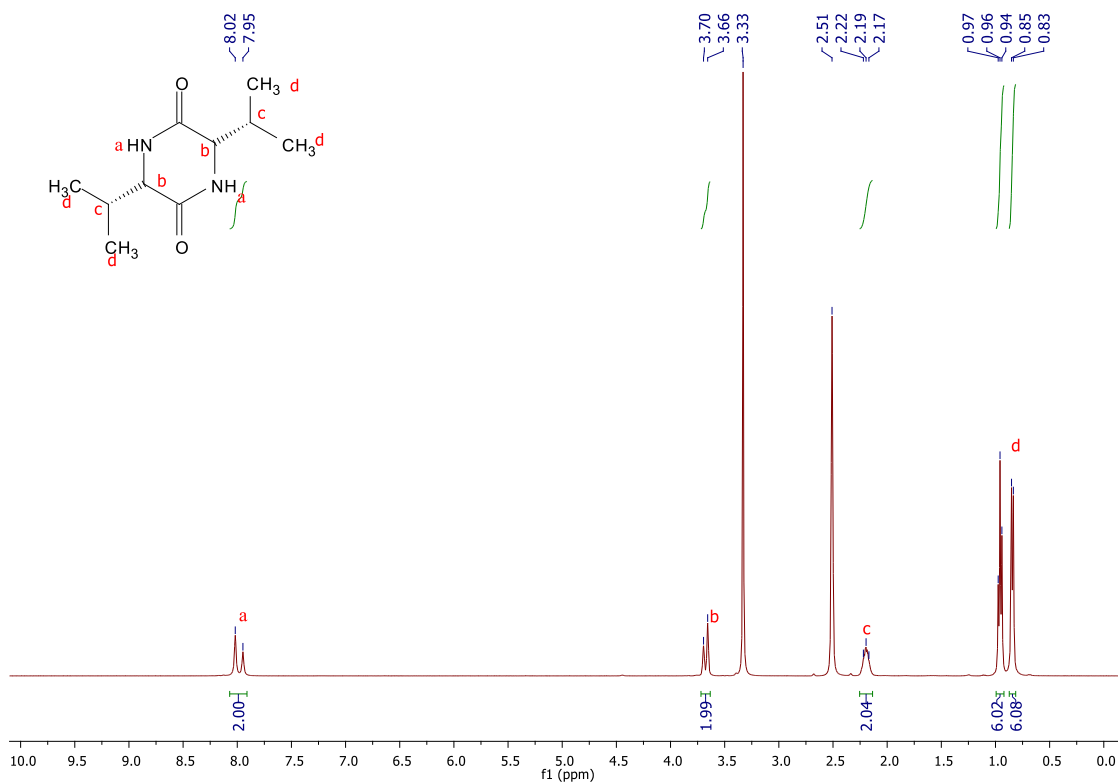


Figure AII.5. – <sup>1</sup>H NMR spectrum (DMSO-d<sub>6</sub>, 400 MHz) of valine DKP.

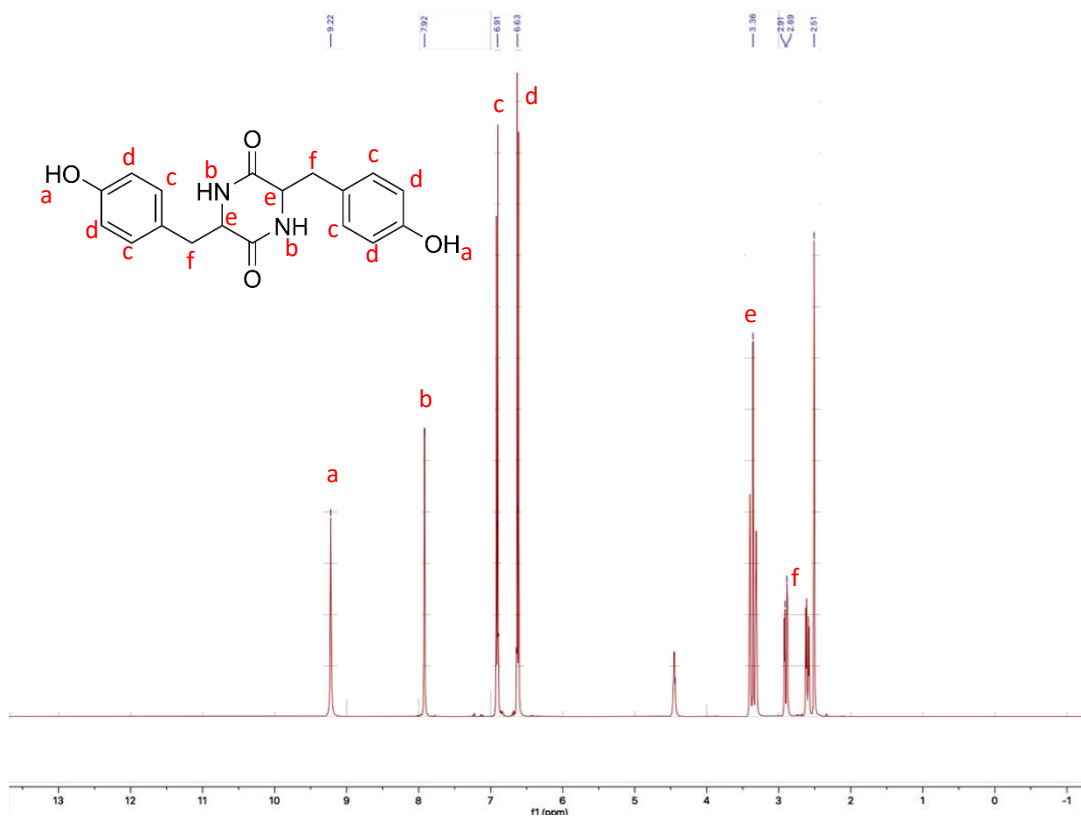


Figure AII.6. – <sup>1</sup>H NMR spectrum (DMSO-d<sub>6</sub>, 400 MHz) of tyrosine DKP.

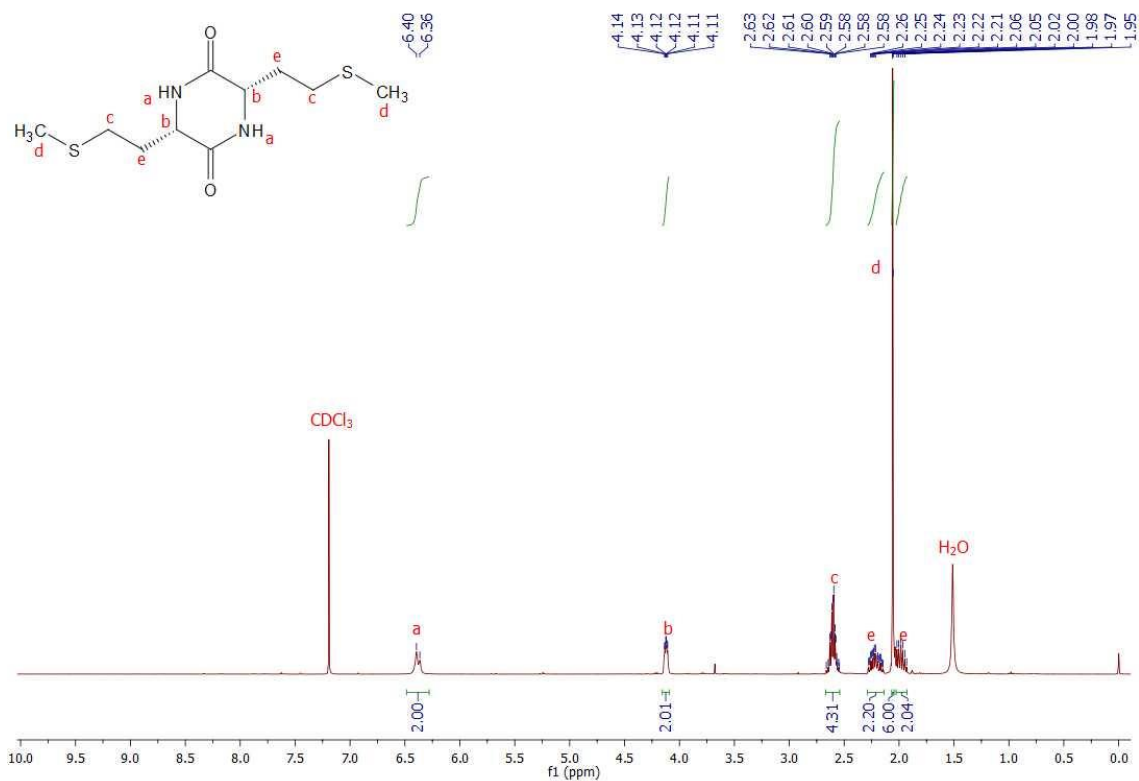


Figure AII.7. –  $^1\text{H}$  NMR spectrum (CDCl<sub>3</sub>, 400 MHz) of methionine DKP.

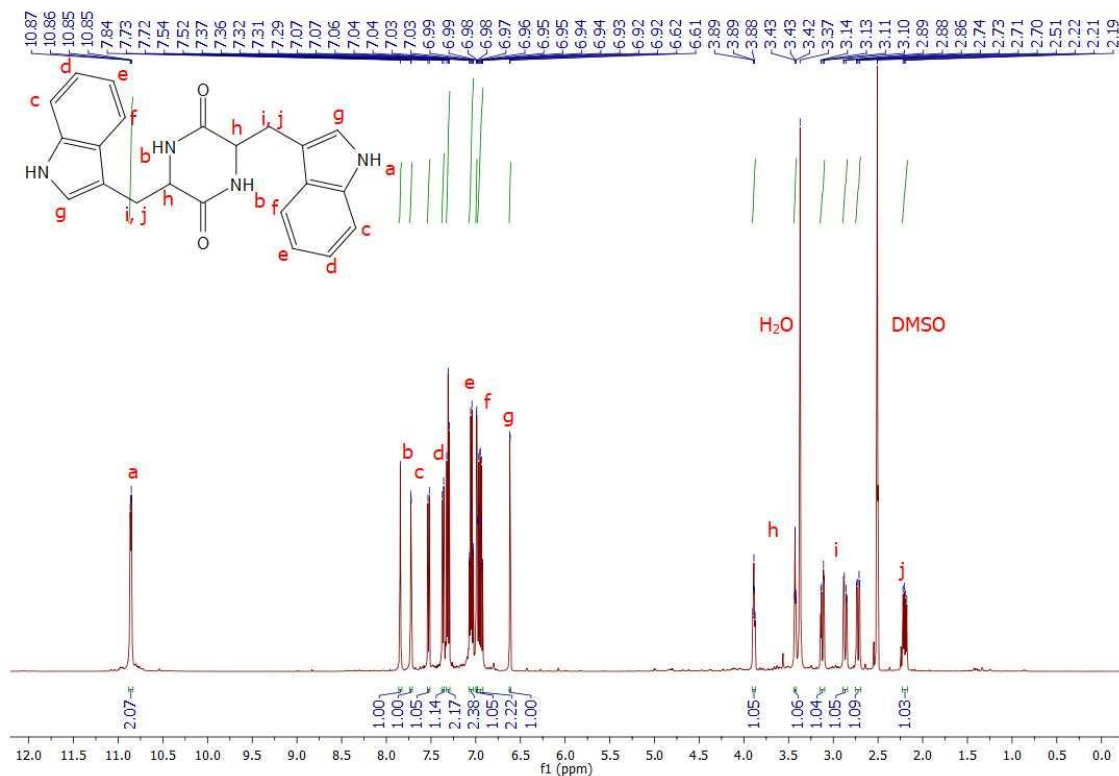


Figure AII.8. –  $^1\text{H}$  NMR spectrum (DMSO-d<sub>6</sub>, 400 MHz) of tryptophan DKP.

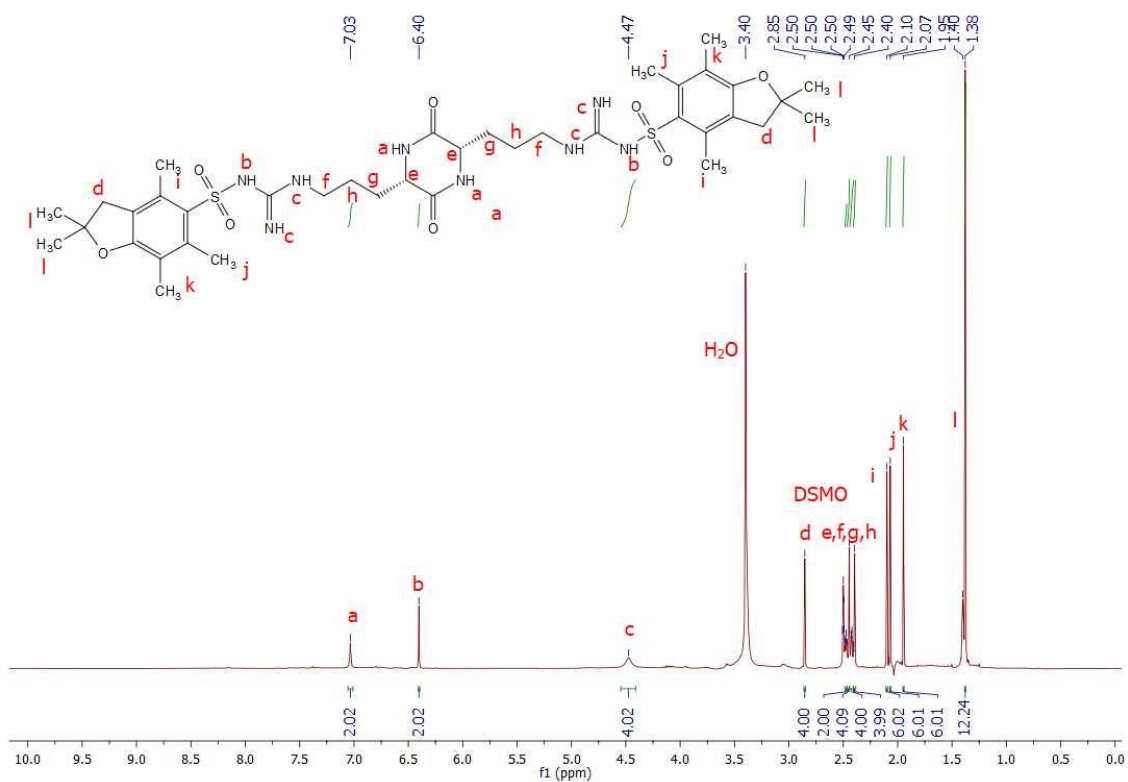


Figure A11.9. –  $^1\text{H}$  NMR spectrum (DMSO- $d_6$ , 400 MHz) of arginine(Pbf) DKP.

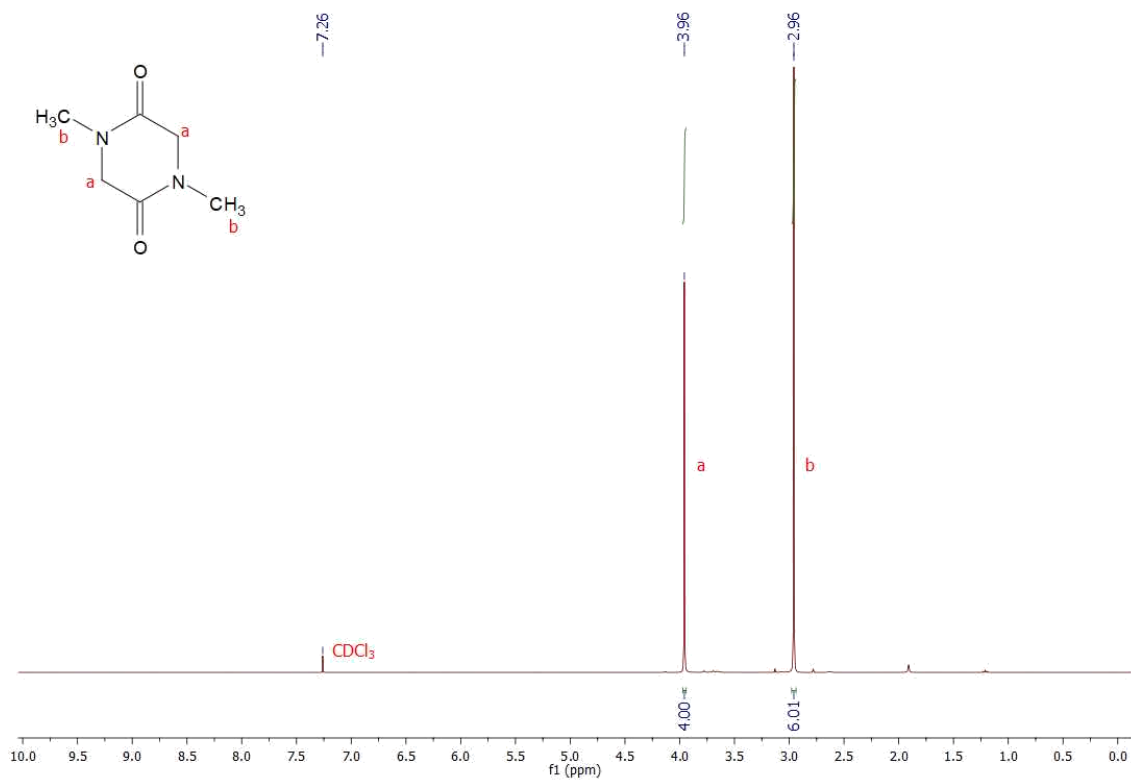


Figure A11.10. –  $^1\text{H}$  NMR spectrum (CDCl<sub>3</sub>, 400 MHz) of sarcosine DKP.



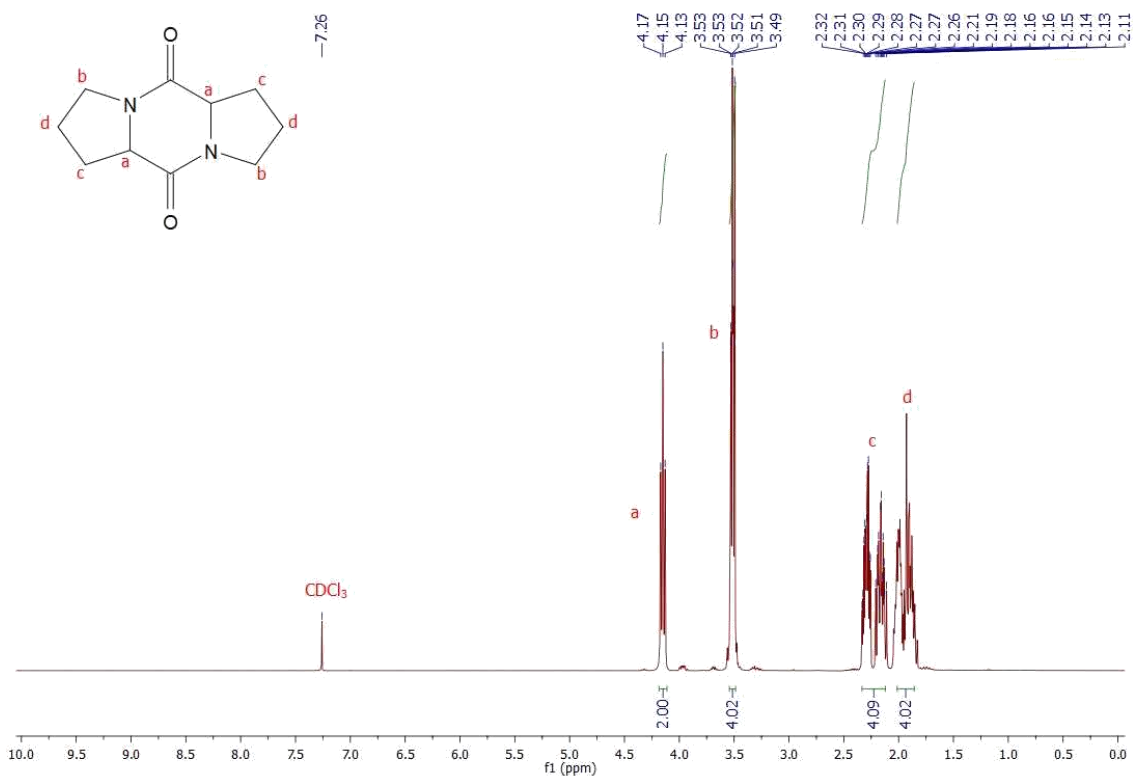


Figure AII.11. – <sup>1</sup>H NMR spectrum (CDCl<sub>3</sub>, 400 MHz) of proline DKP.

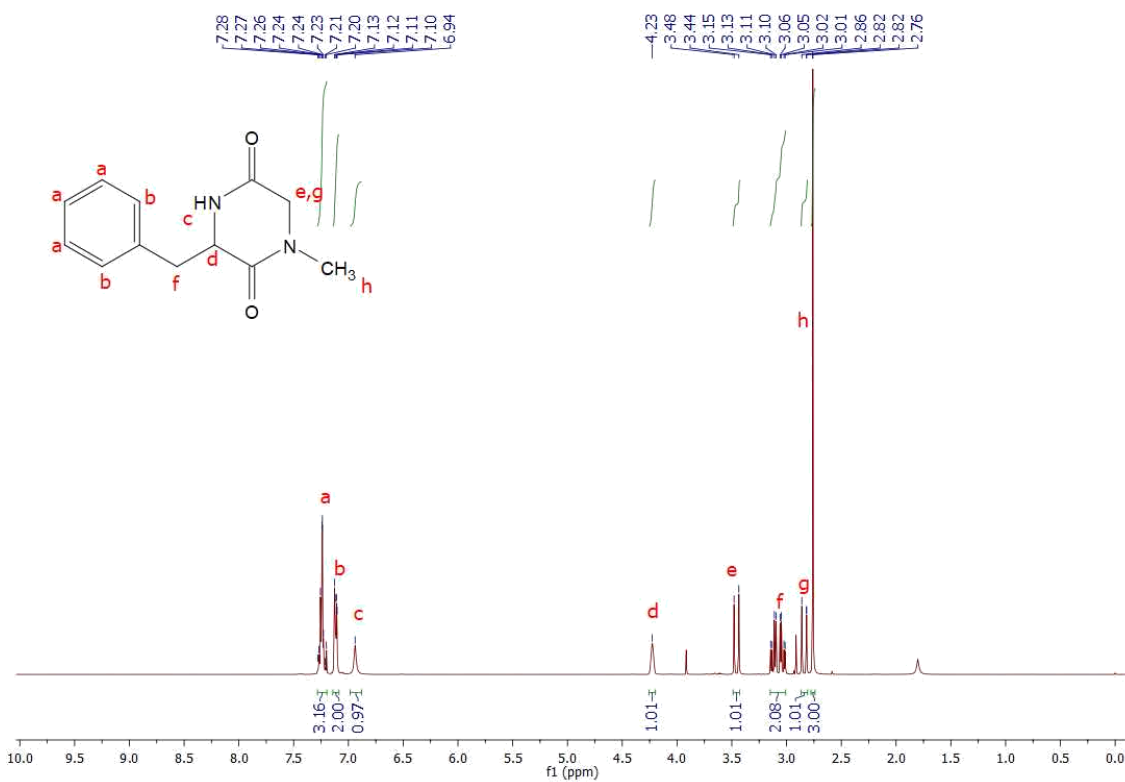


Figure AII.12. – <sup>1</sup>H NMR spectrum (CDCl<sub>3</sub>, 400 MHz) of sarcosine-phenylalanine DKP.

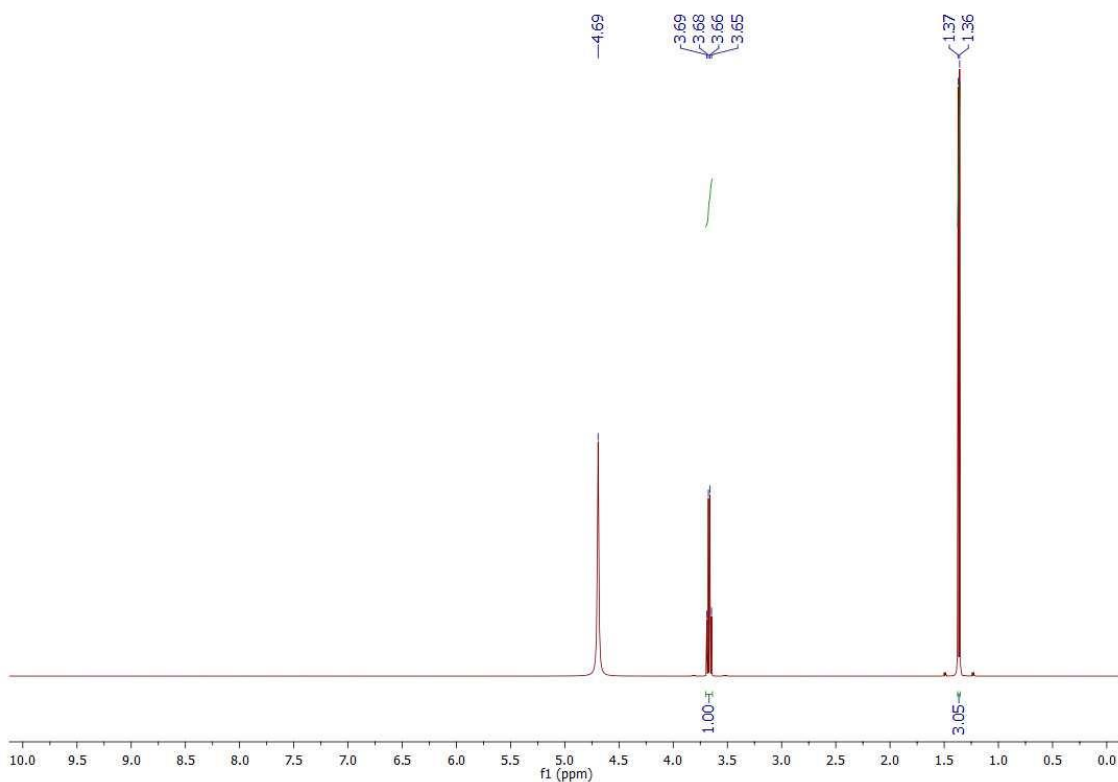


Figure AII.13. –  $^1\text{H}$  NMR spectrum ( $\text{D}_2\text{O}$ , 500 MHz) of the enzymatic degradation products of  $\text{PALa}_{65}$  (chapter 4, Table 4.1., polymer 2), alanine.

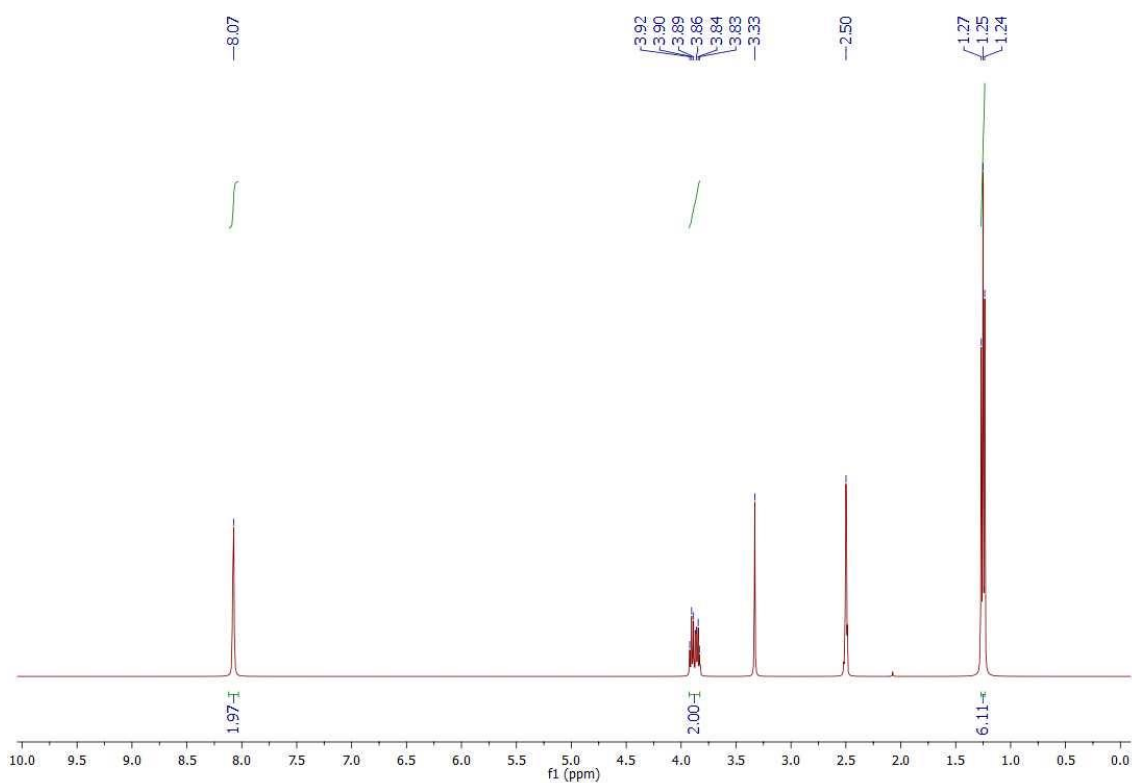


Figure AII.14. –  $^1\text{H}$  NMR spectrum ( $\text{DMSO-d}_6$ , 400 MHz) of alanine DKP, synthesised from the degradation products of  $\text{PALa}_{65}$  (chapter 4, Table 4.1., polymer 2).

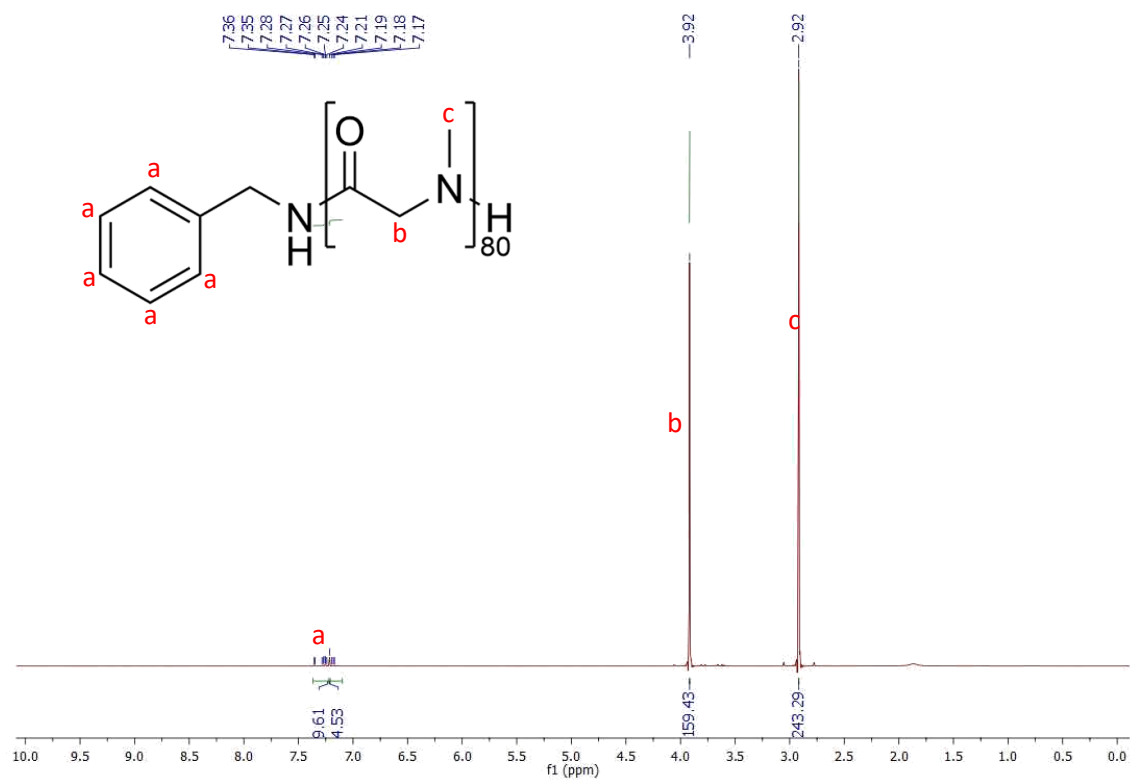


Figure AII.15. – <sup>1</sup>H NMR spectrum (CDCl<sub>3</sub>, 500 MHz) of polymer 2, polysarcosine<sub>80</sub>.

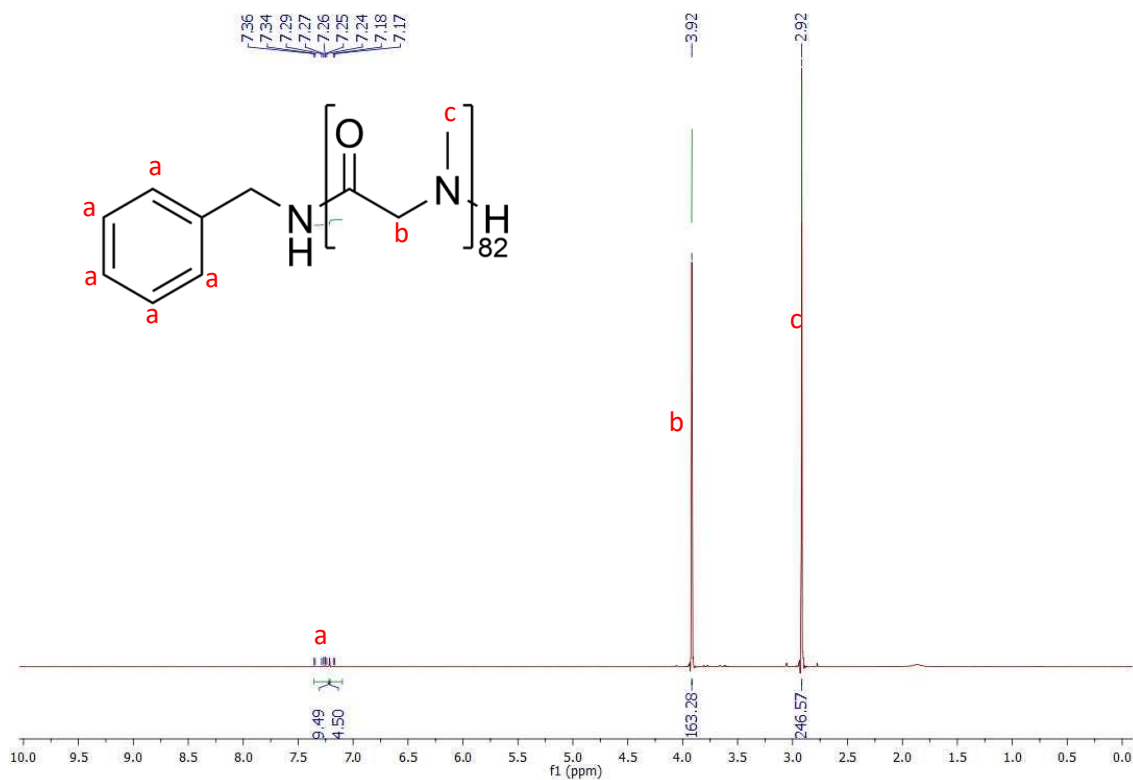


Figure AII.16. – <sup>1</sup>H NMR spectrum (CDCl<sub>3</sub>, 500 MHz) of polymer 3, polysarcosine<sub>82</sub>.

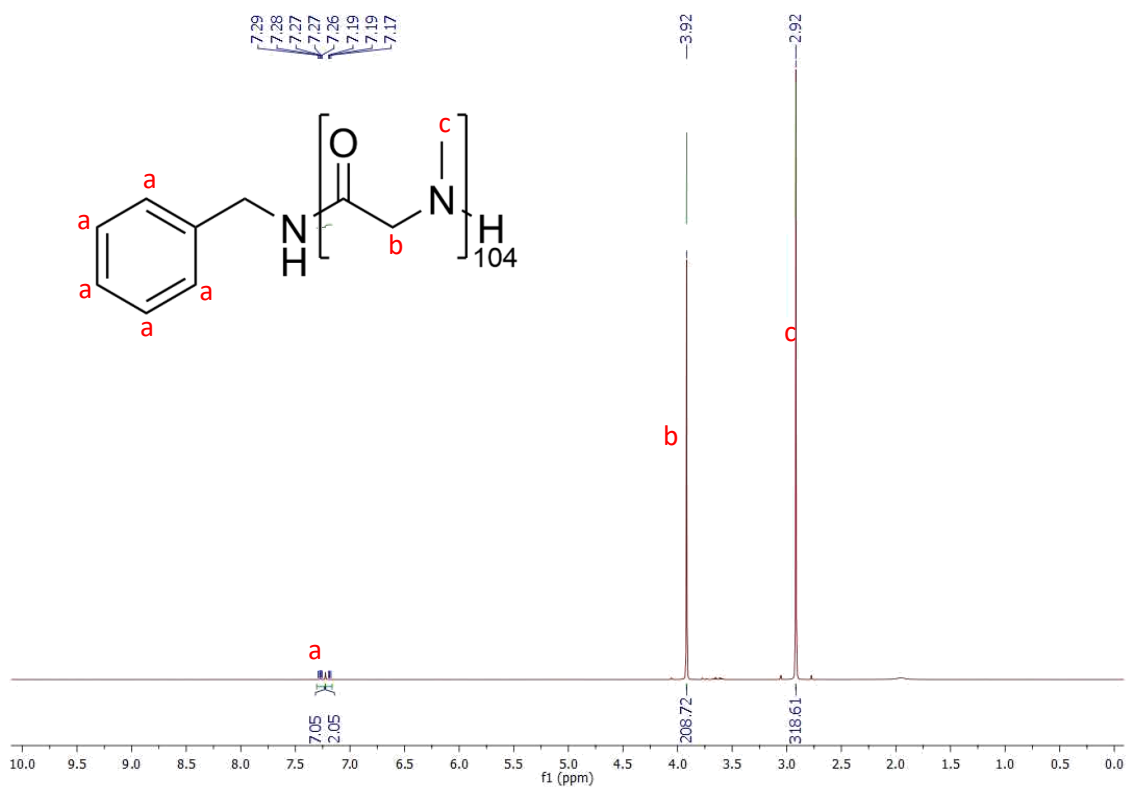


Figure AII.17. <sup>1</sup>H NMR spectrum (CDCl<sub>3</sub>, 500 MHz) of polymer 4, polysarcosine<sub>104</sub>.

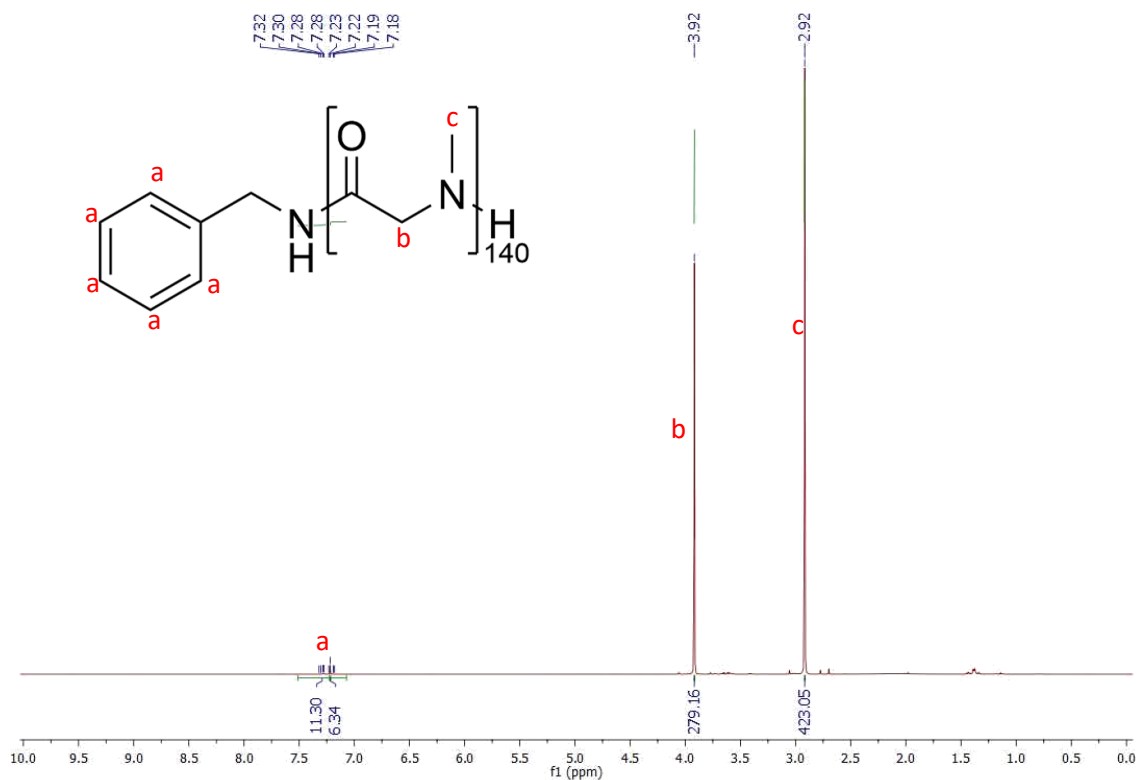


Figure AII.18. <sup>1</sup>H NMR spectrum (CDCl<sub>3</sub>, 500 MHz) of polymer 5, polysarcosine<sub>140</sub>.

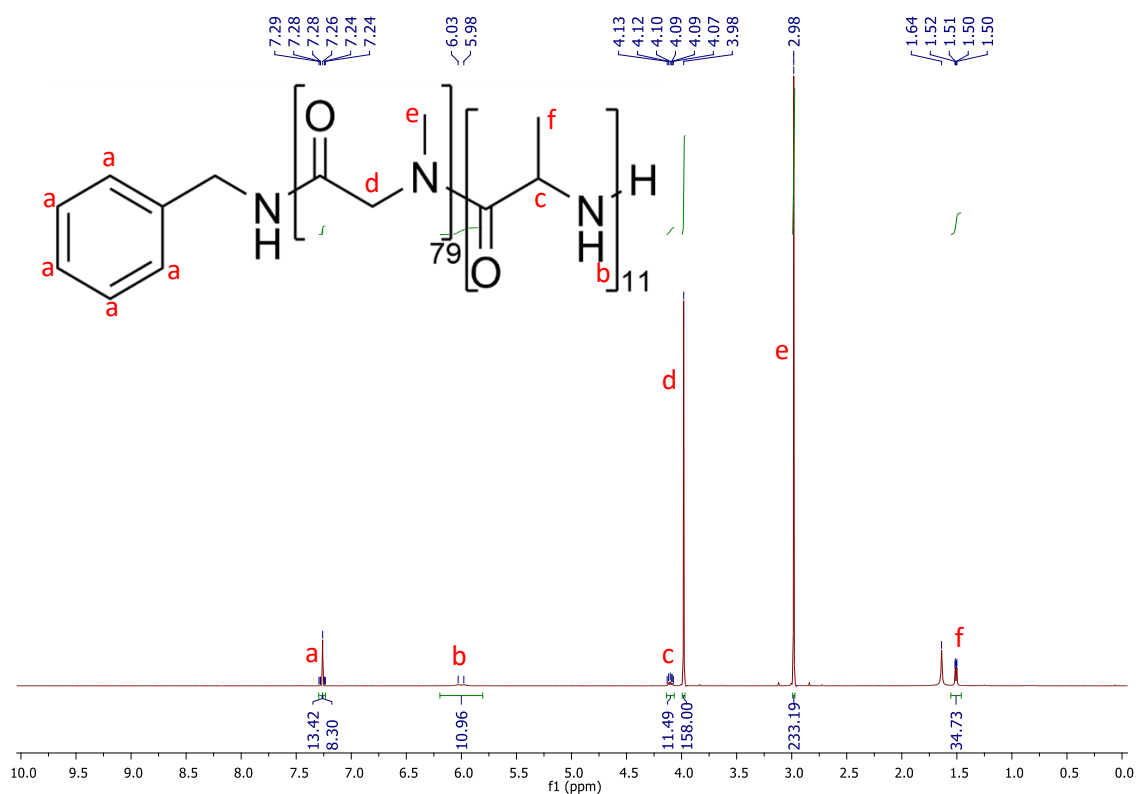


Figure All.19. – <sup>1</sup>H NMR spectrum (CDCl<sub>3</sub>, 500 MHz) of polymer 7, polysarcosine<sub>79</sub>-*b*-polyalanine<sub>11</sub>.

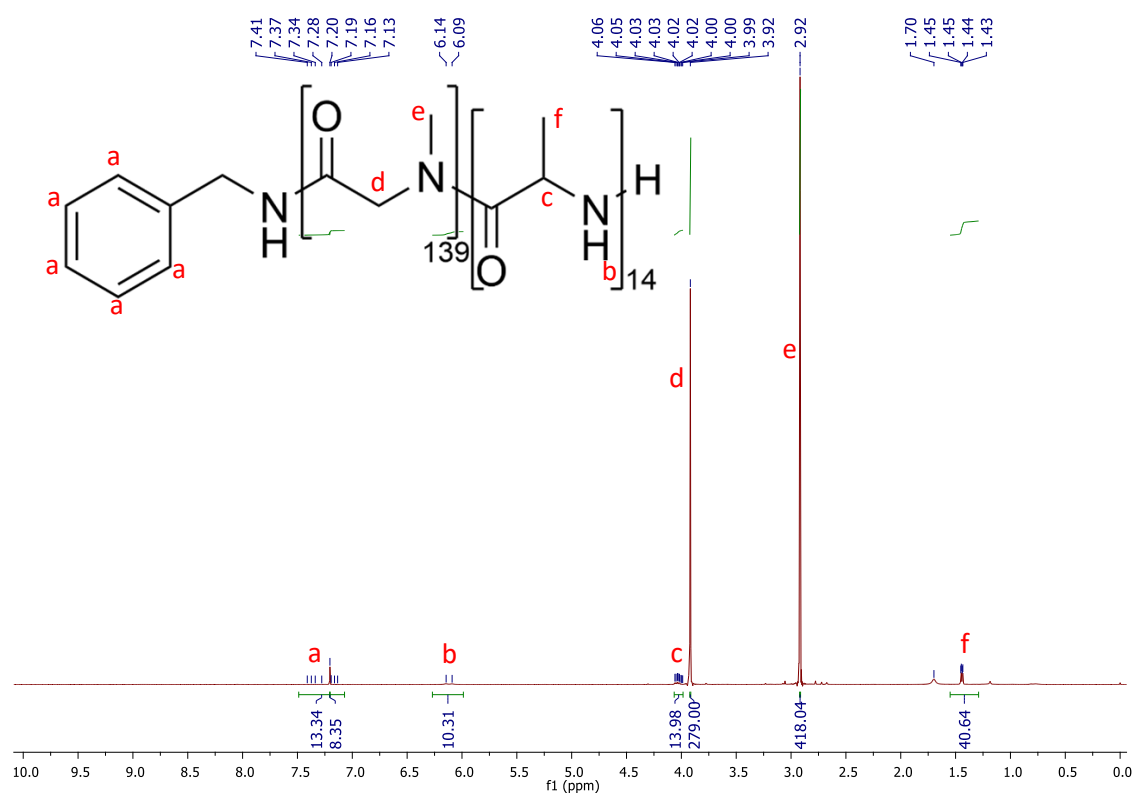


Figure All.20. – <sup>1</sup>H NMR spectrum (CDCl<sub>3</sub>, 500 MHz) of polymer 8, polysarcosine<sub>139</sub>-*b*-polyalanine<sub>14</sub>.

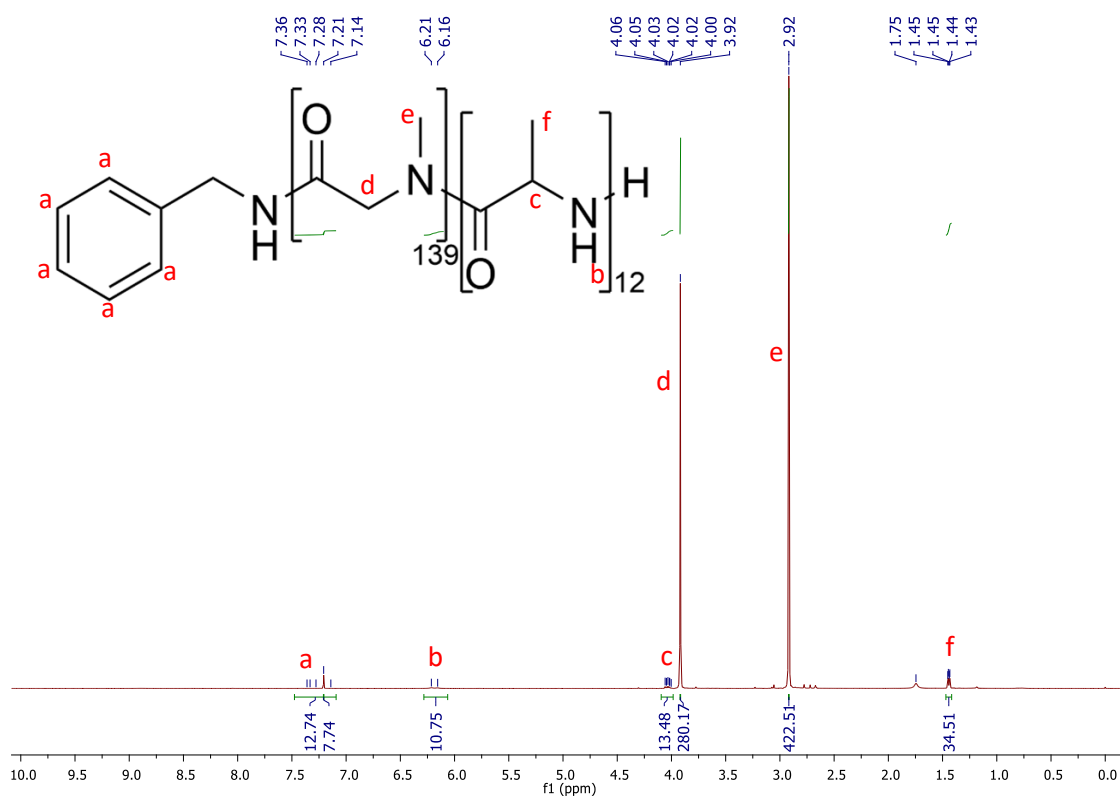


Figure AII.20. – <sup>1</sup>H NMR spectrum (CDCl<sub>3</sub>, 500 MHz) of polymer 9, polysarcosine<sub>139</sub>-b-polyalanine<sub>12</sub>.

Appendix III – Liquid Chromatography-Mass Spectrometry (LC-MS)

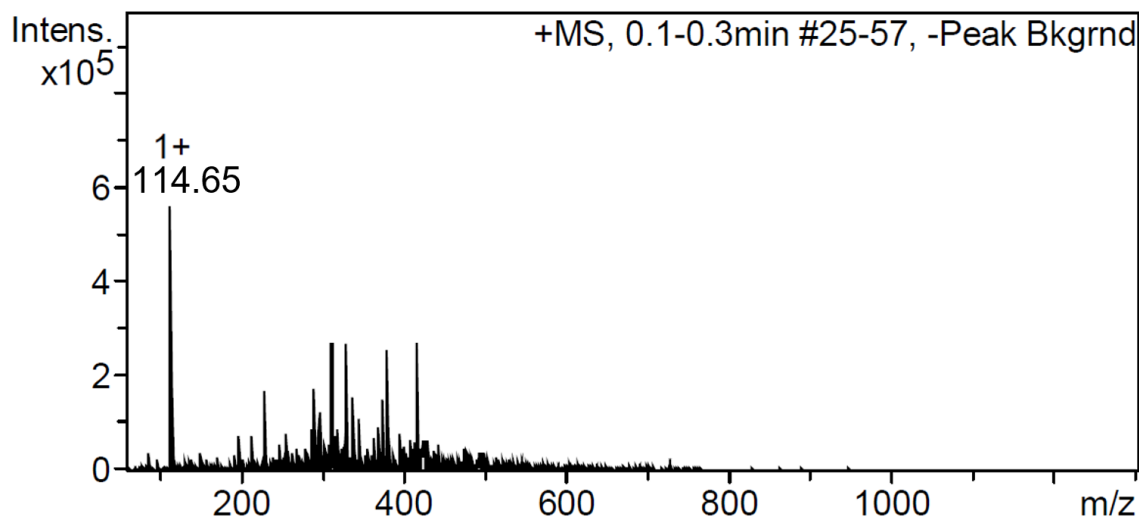


Figure AIII.1. – LC-MS chromatogram of glycine DKP.

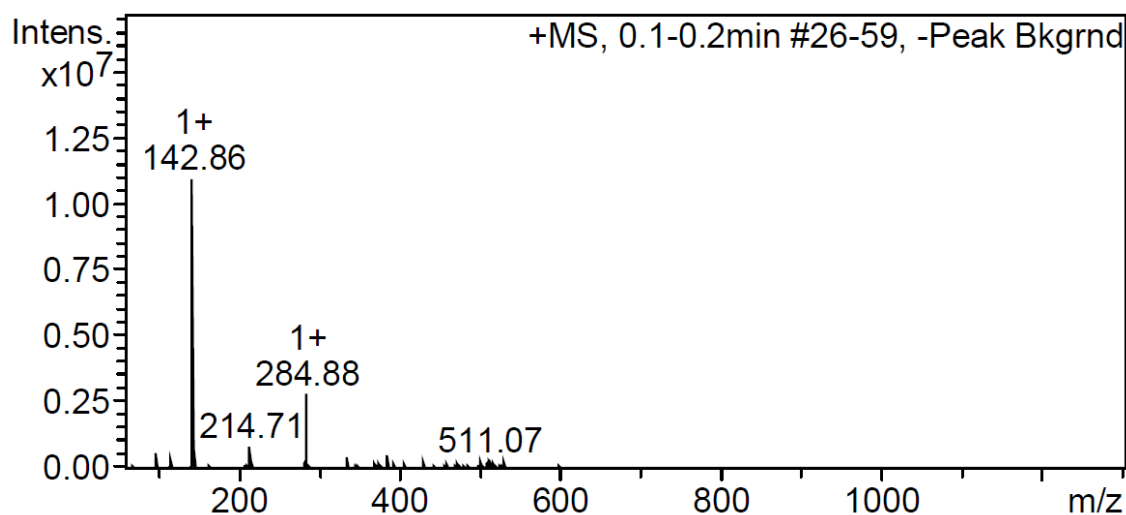


Figure AIII.2. – LC-MS chromatogram of alanine DKP.

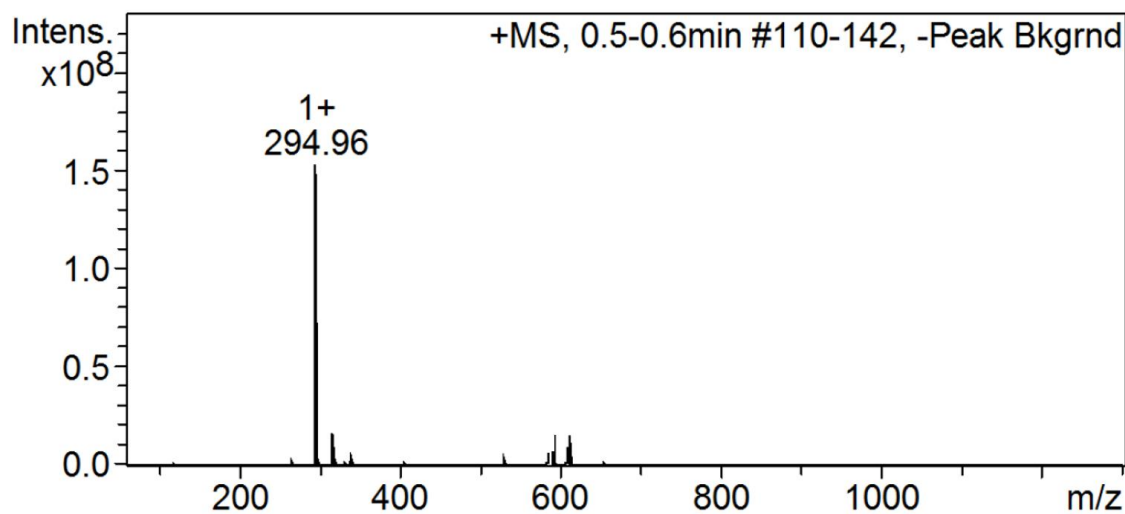


Figure AIII.3. – LC-MS chromatogram of phenylalanine DKP.

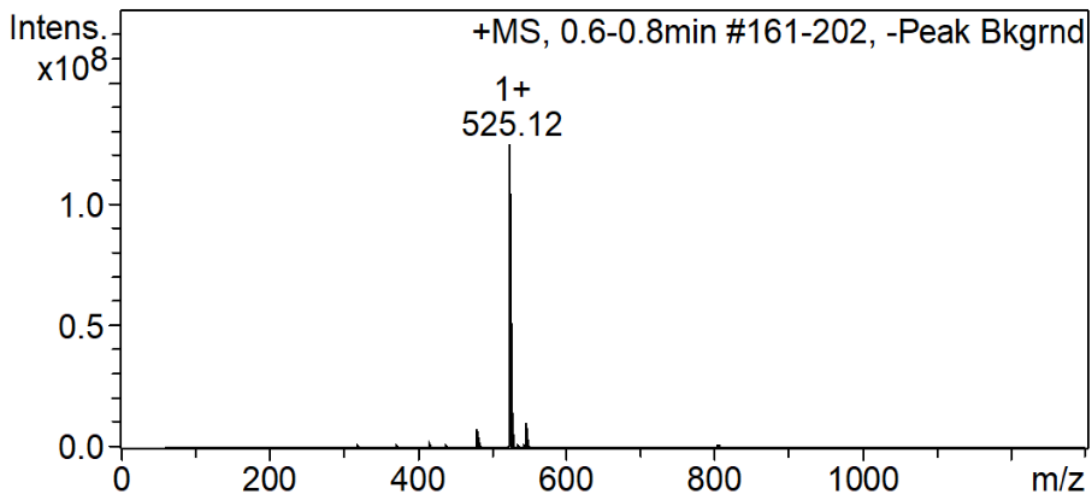


Figure AIII.4. - LC-MS of lysine(Cbz) DKP.

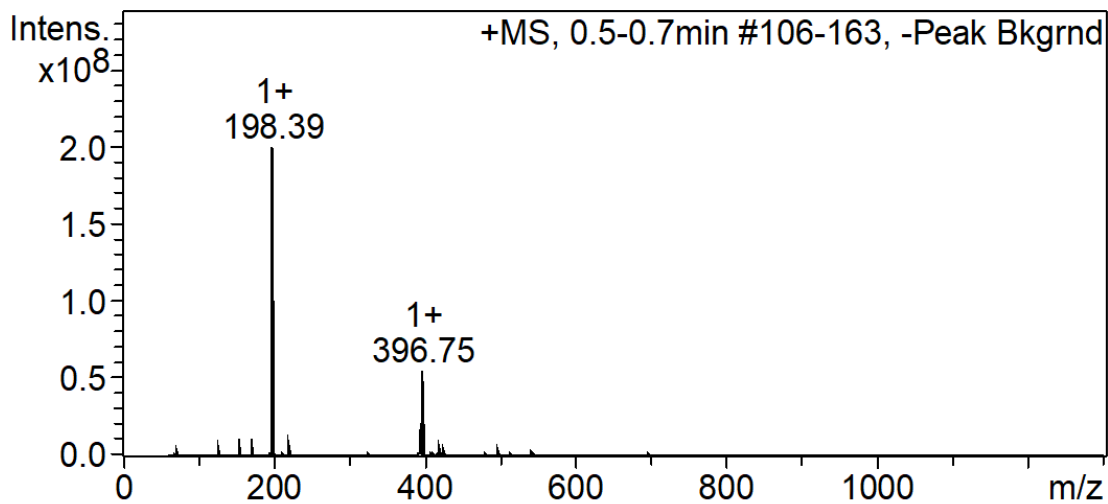


Figure AIII.5. - LC-MS of valine DKP.

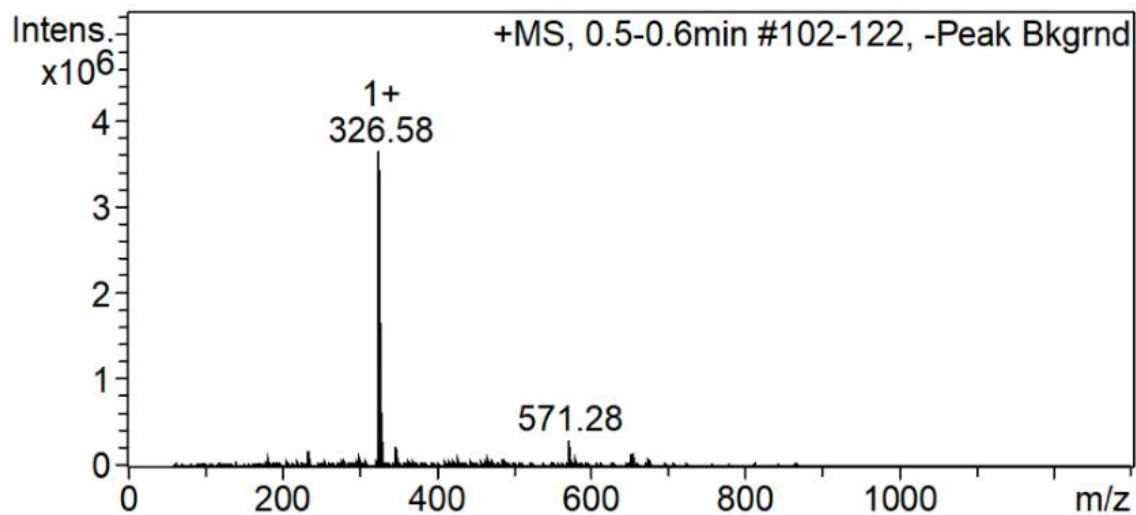


Figure AIII.6. - LC-MS of tyrosine DKP.



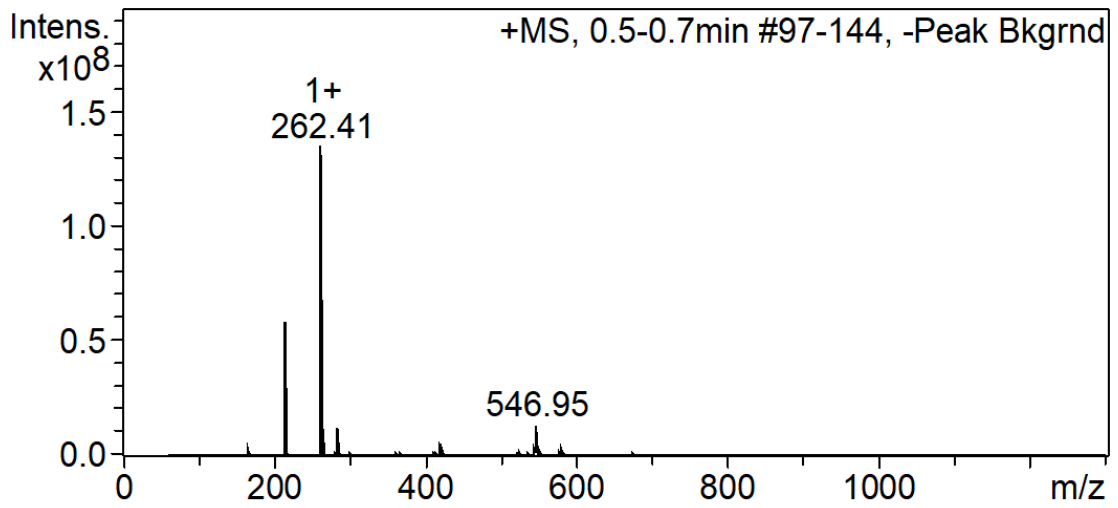


Figure AIII.7. - LC-MS of methionine DKP.

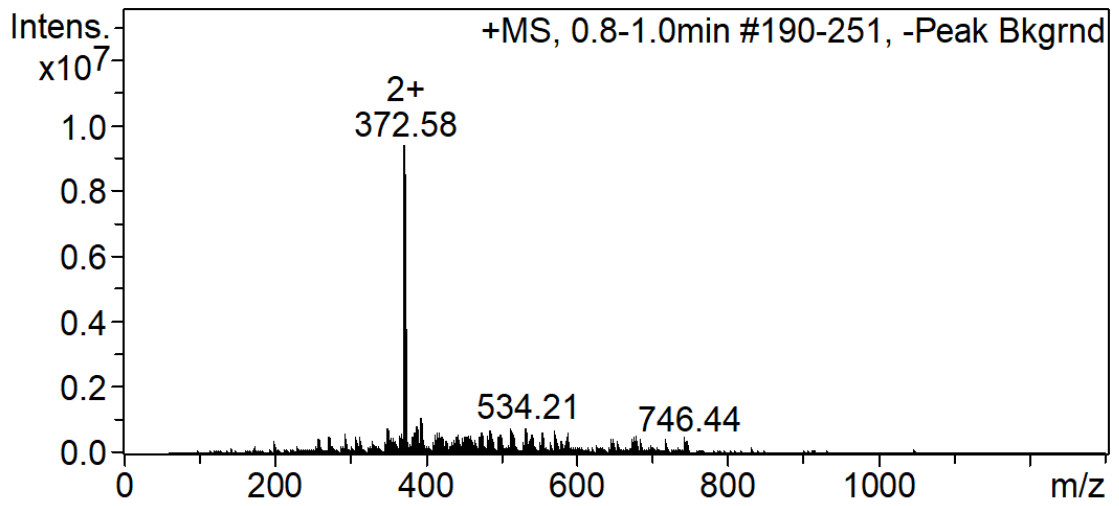


Figure AIII.8. - LC-MS of tryptophan DKP.

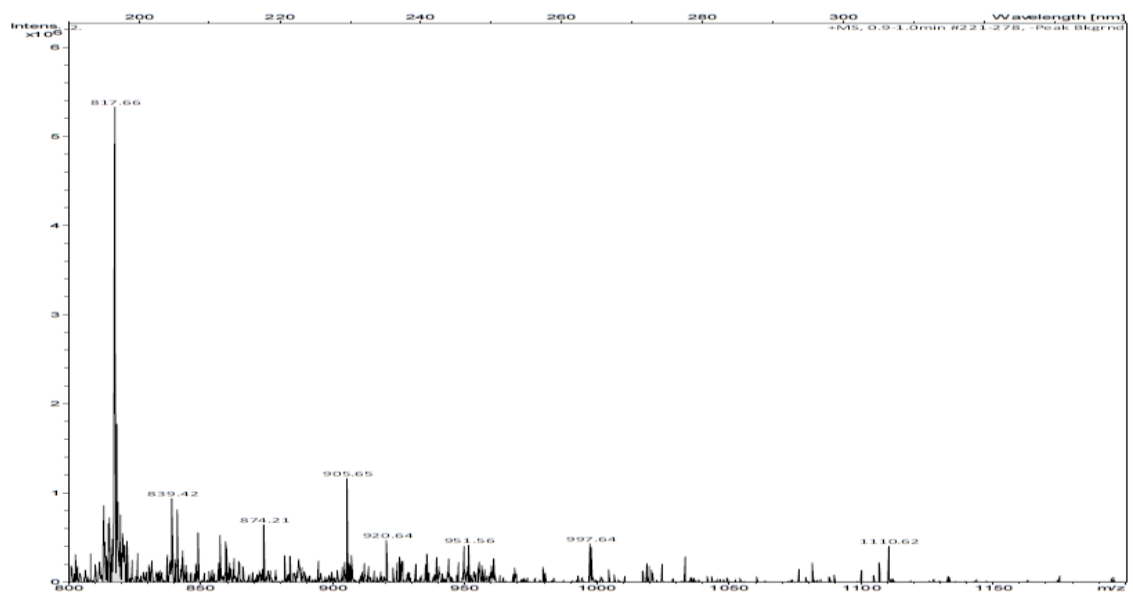


Figure AIII.9. - LC-MS of arginine(Pbf) DKP.

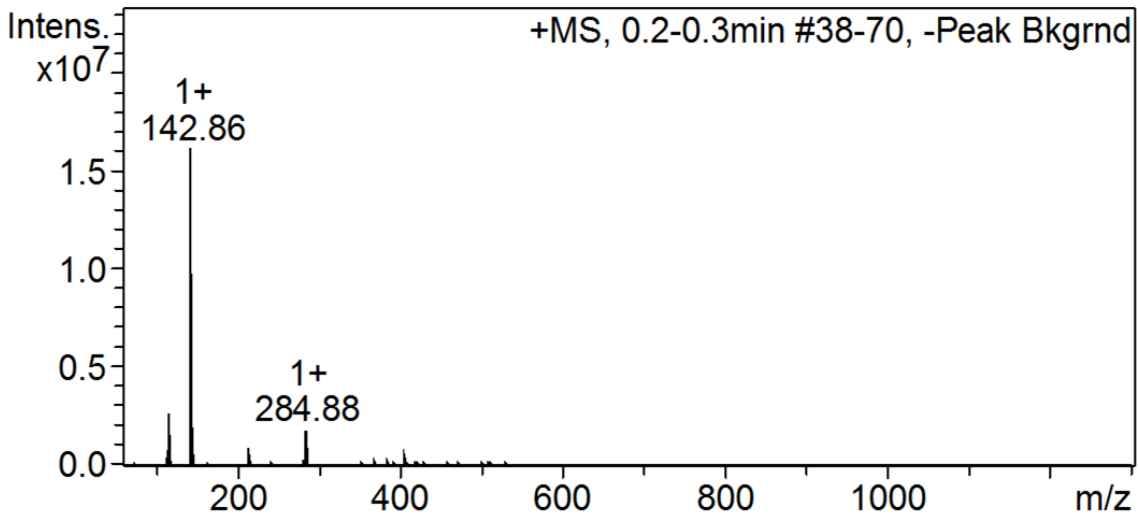


Figure AIII.10. - LC-MS of sarcosine DKP.

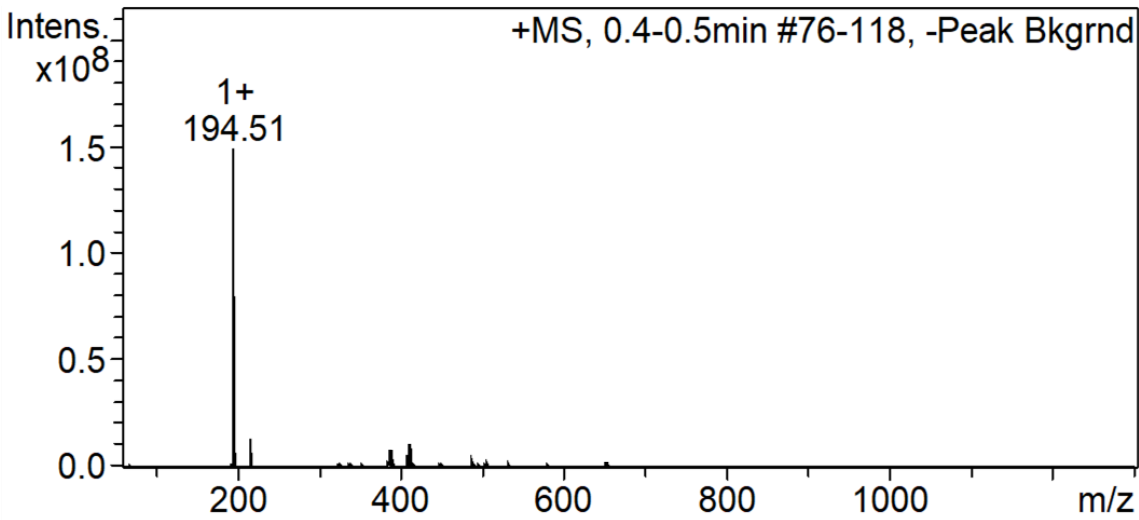


Figure AIII.11. - LC-MS of proline DKP.

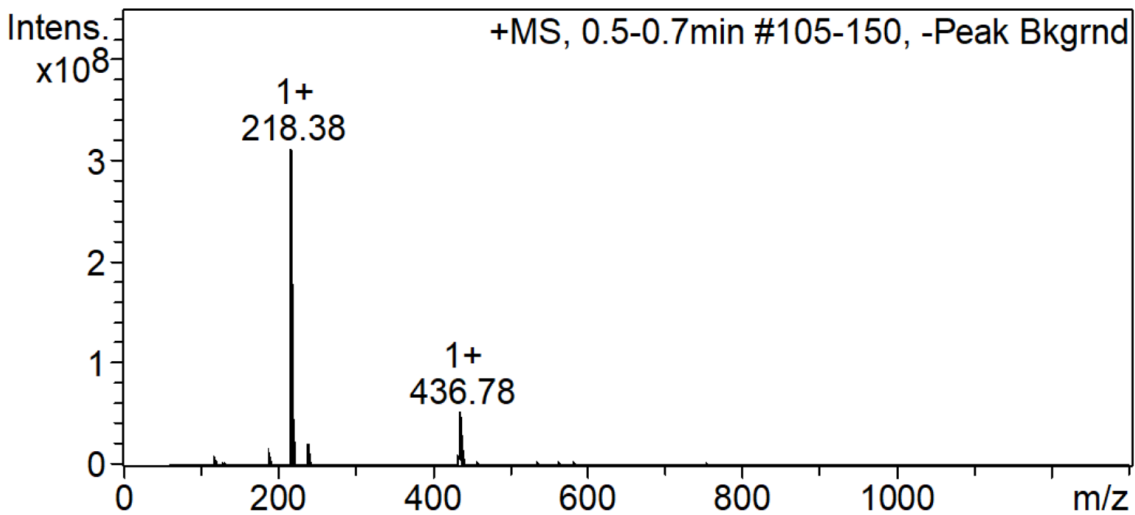


Figure AIII.12. - LC-MS of sarcosine-phenylalanine DKP.

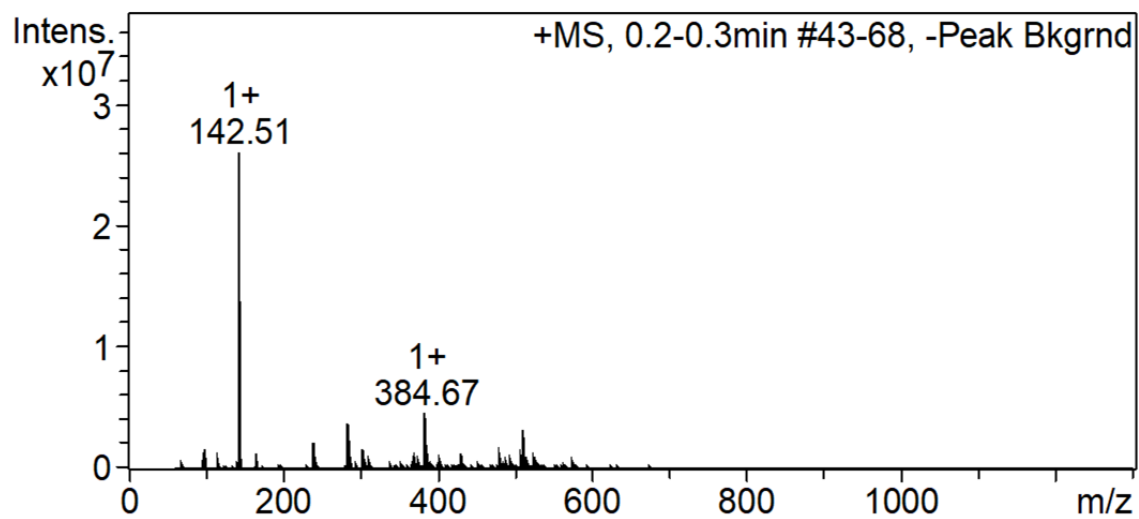


Figure AIII.13. – LC-MS of alanine DKP, synthesised from the degradation products of PAla<sub>65</sub> (chapter 4, Table 4.1., polymer 2).

## Appendix IV – High-Performance Liquid Chromatography (HPLC)

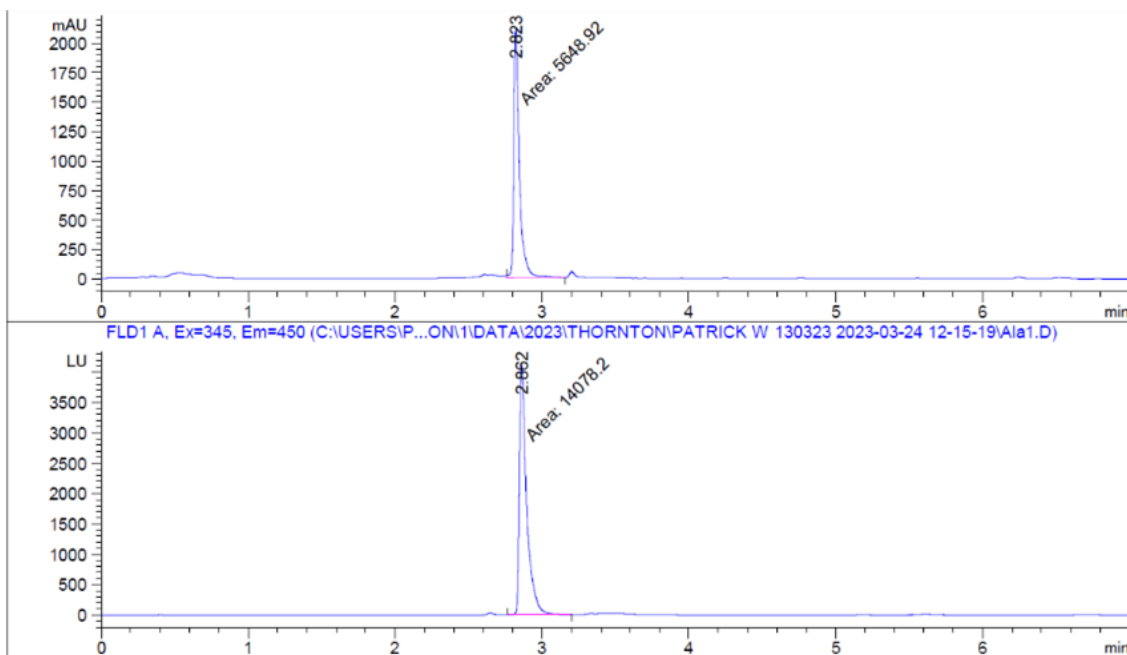


Figure AIV.1. – HPLC chromatogram of bought L-alanine.

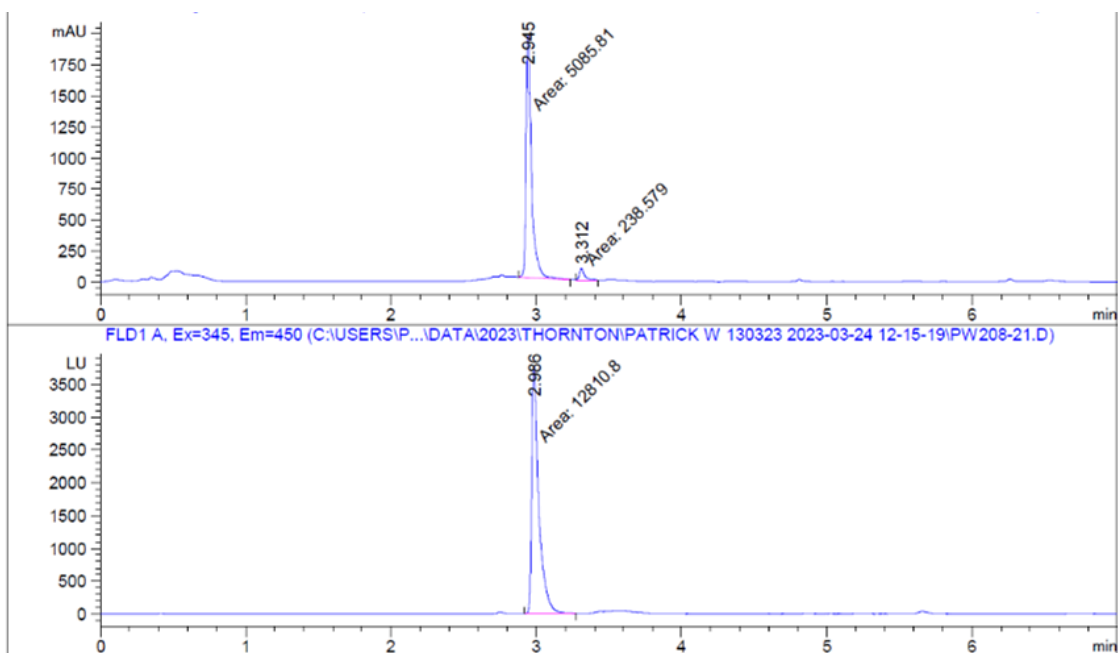


Figure AIV.2. – HPLC chromatogram of the enzymatic degradation products of PALa<sub>65</sub> (chapter 4, Table 4.1., polymer 2).

## Appendix V – UV-visible (UV-vis) Spectrophotometry

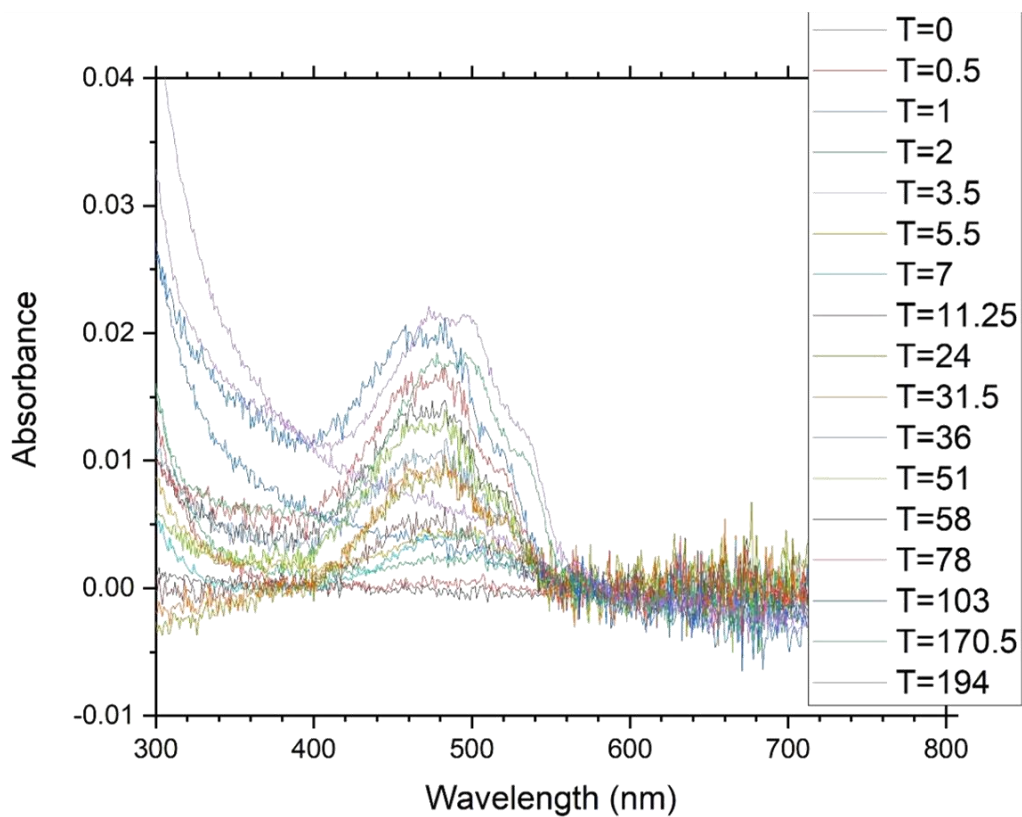


Figure AV.1. – UV-visible spectrum of acetate buffer solution (pH 5.0) containing doxorubicin released from nanoparticles of PEG<sub>112</sub>-b-PGLy<sub>14</sub> (Chapter 5, Table 5.1., polymer 2).

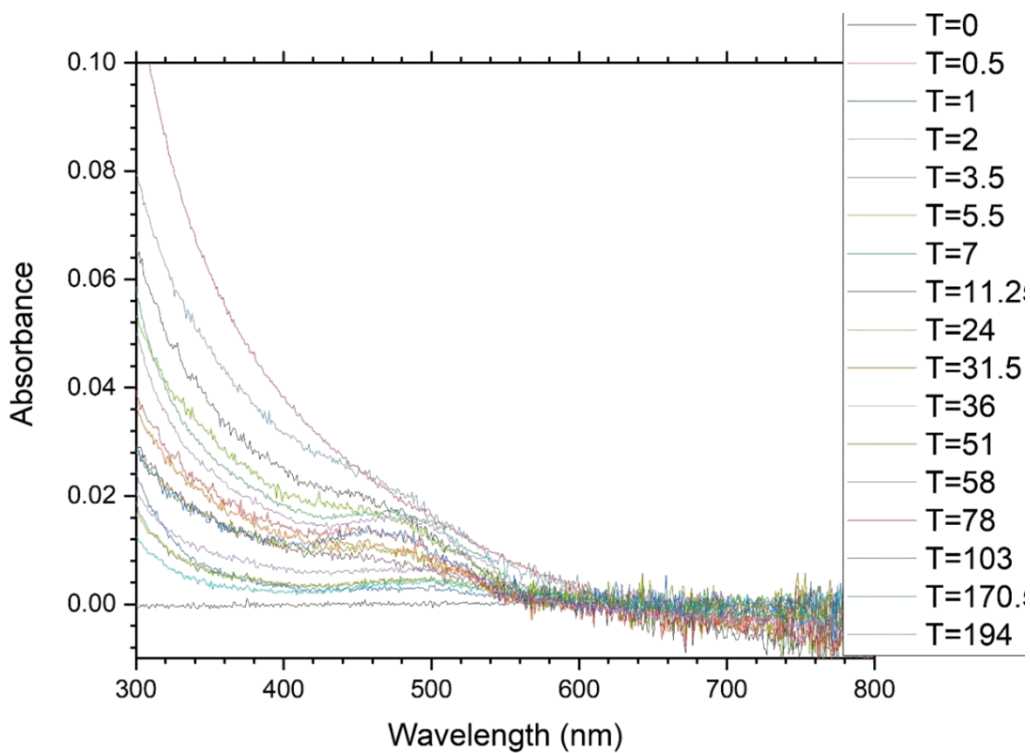


Figure AV.2. – UV-visible spectrum of PBS solution (pH 7.4) containing doxorubicin released from nanoparticles of PEG<sub>112</sub>-b-PGLy<sub>14</sub> (Chapter 5, Table 5.1., polymer 2).

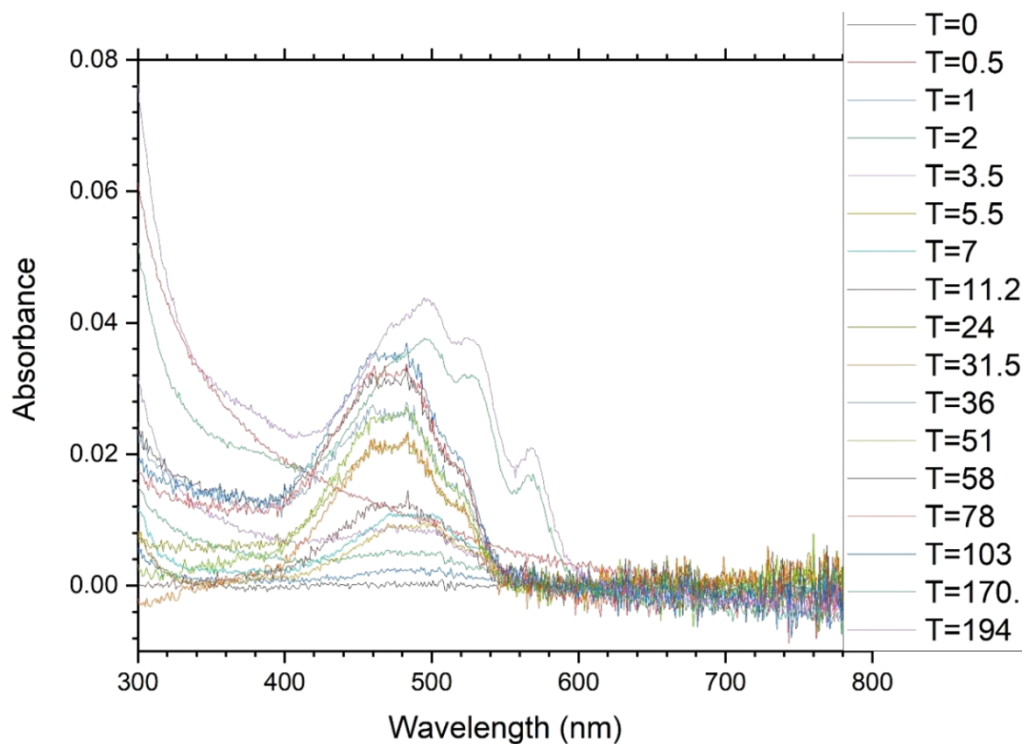


Figure AV.3. – UV-visible spectrum of acetate buffer solution (pH 5.0) containing doxorubicin released from nanoparticles of PEG<sub>112</sub>-b-PGly<sub>20</sub> (Chapter 5, Table 5.1., polymer 3).

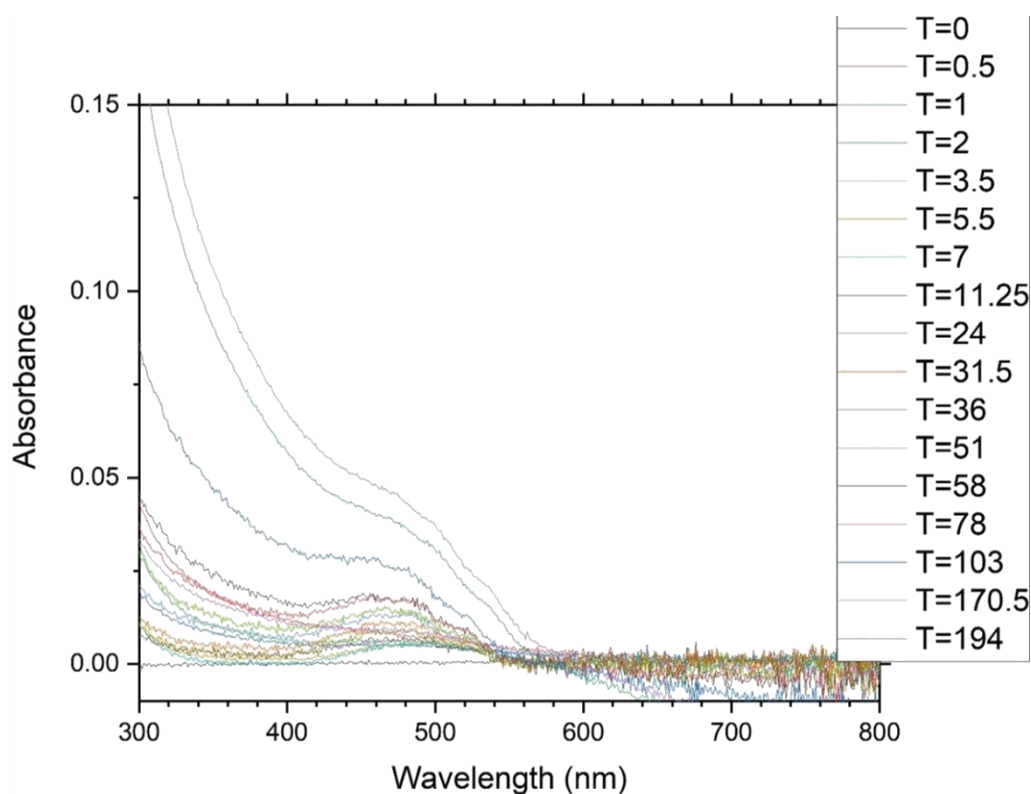


Figure AV.4. – UV-visible spectrum of PBS solution (pH 7.4) containing doxorubicin released from nanoparticles of PEG<sub>112</sub>-b-PGly<sub>20</sub> (Chapter 5, Table 5.1., polymer 3).

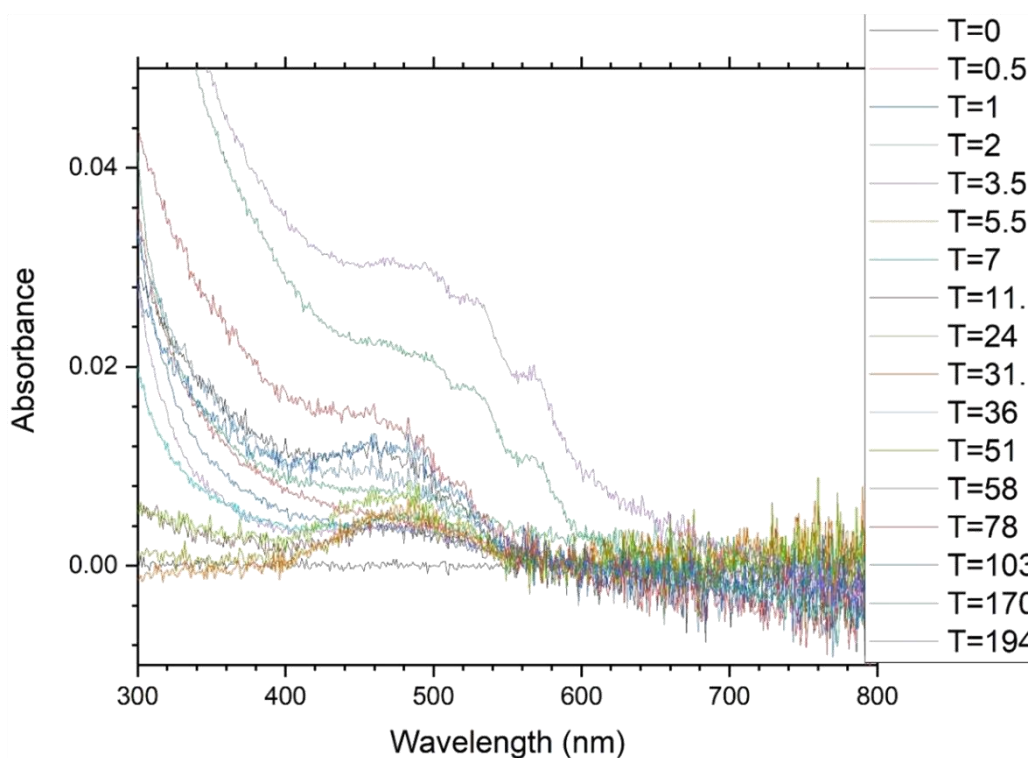


Figure AV.5. – UV-visible spectrum of acetate buffer solution (pH 5.0) containing doxorubicin released from nanoparticles of PEG<sub>112</sub>-b-PALa<sub>6</sub> (Chapter 5, Table 5.1., polymer 4).

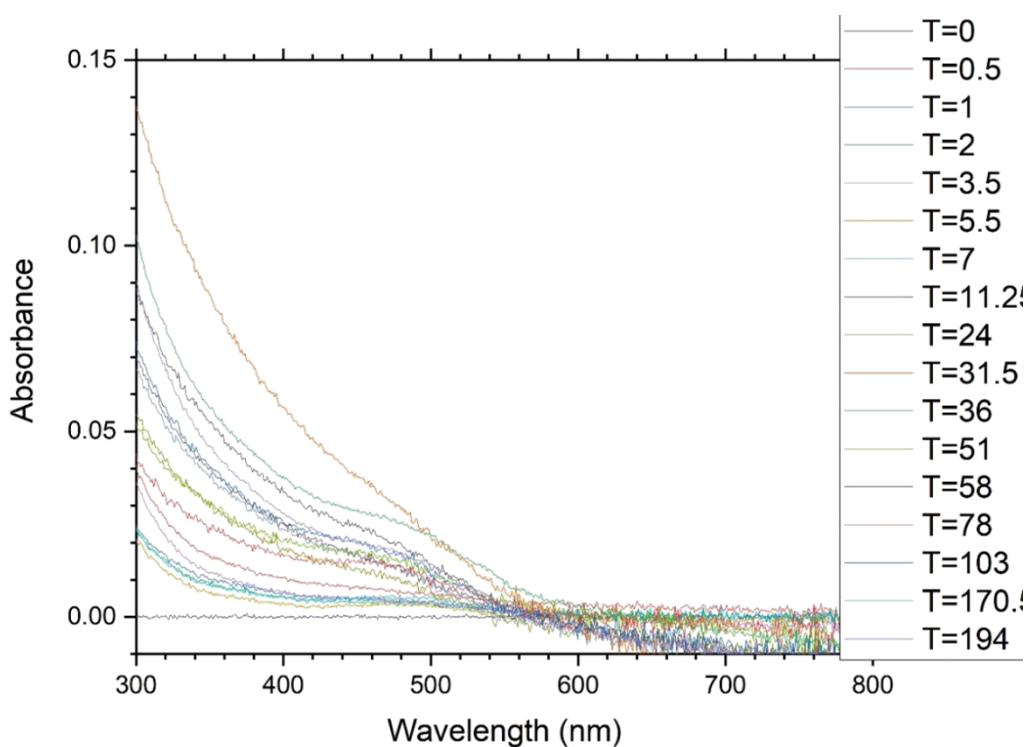


Figure AV.6. – UV-visible spectrum of PBS solution (pH 7.4) containing doxorubicin released from nanoparticles of PEG<sub>112</sub>-b-PALa<sub>6</sub> (Chapter 5, Table 5.1., polymer 4).

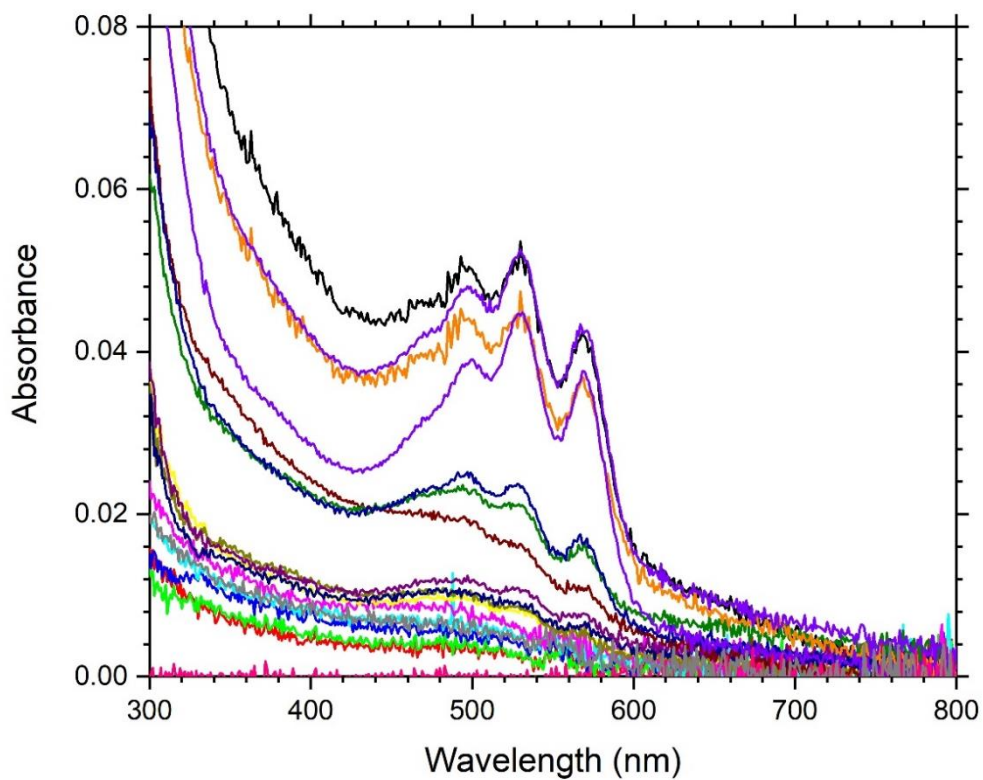


Figure AV.7. – UV-visible spectrum of acetate buffer solution (pH 5.0) containing doxorubicin released from nanoparticles of PEG<sub>112</sub>-*b*-PAla<sub>11</sub> (Chapter 5, Table 5.1., polymer 5).

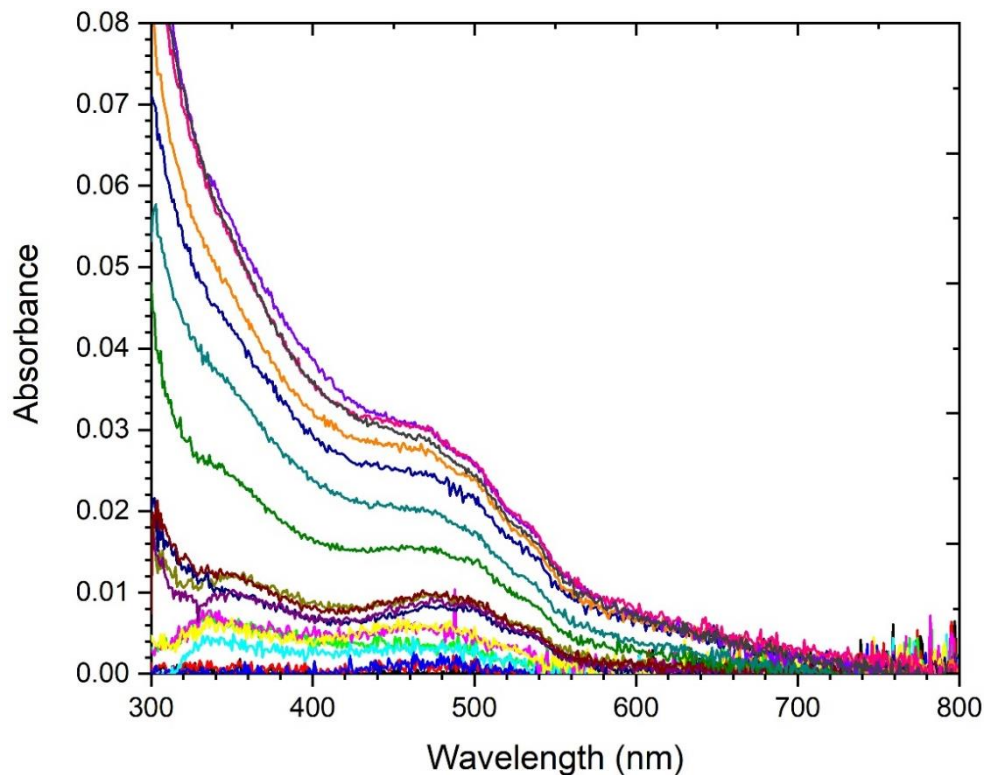


Figure AV.8. – UV-visible spectrum of PBS solution (pH 7.4) containing doxorubicin released from nanoparticles of PEG<sub>112</sub>-*b*-PAla<sub>11</sub> (Chapter 5, Table 5.1., polymer 5).



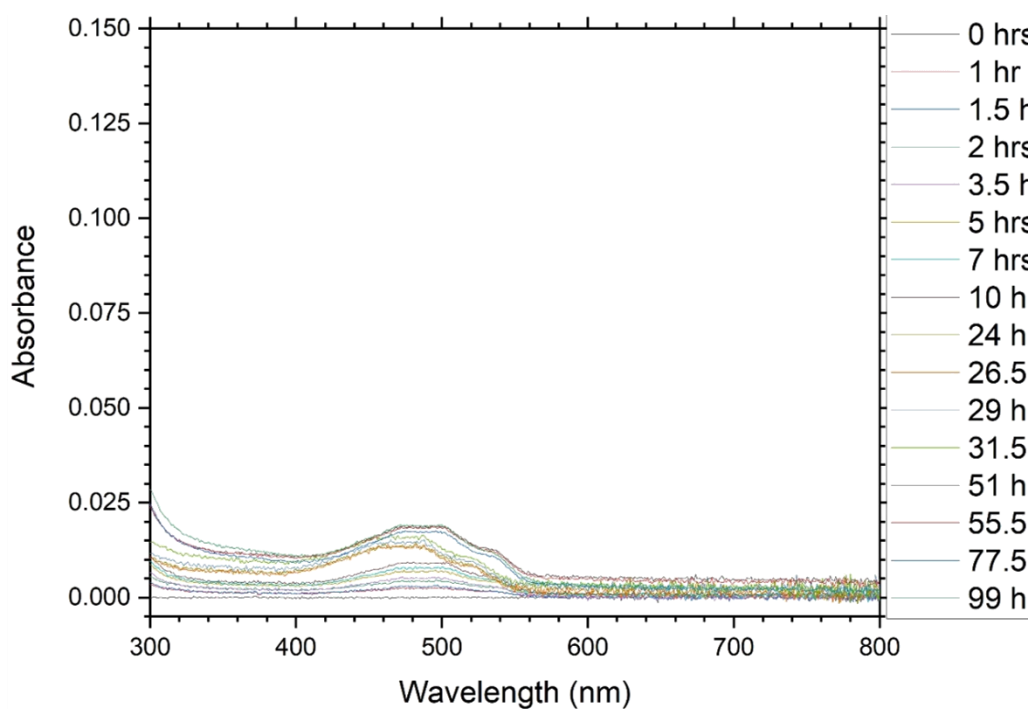


Figure AV.9. - UV-visible spectra of PBS buffer solution containing the dialysate from dox-loaded nanoparticles of PSAr<sub>77</sub>-b-PAla<sub>9</sub> (Chapter 6, Table 6.1., polymer 6), incubated at 37 °C with no enzyme, sampled at time points listed.

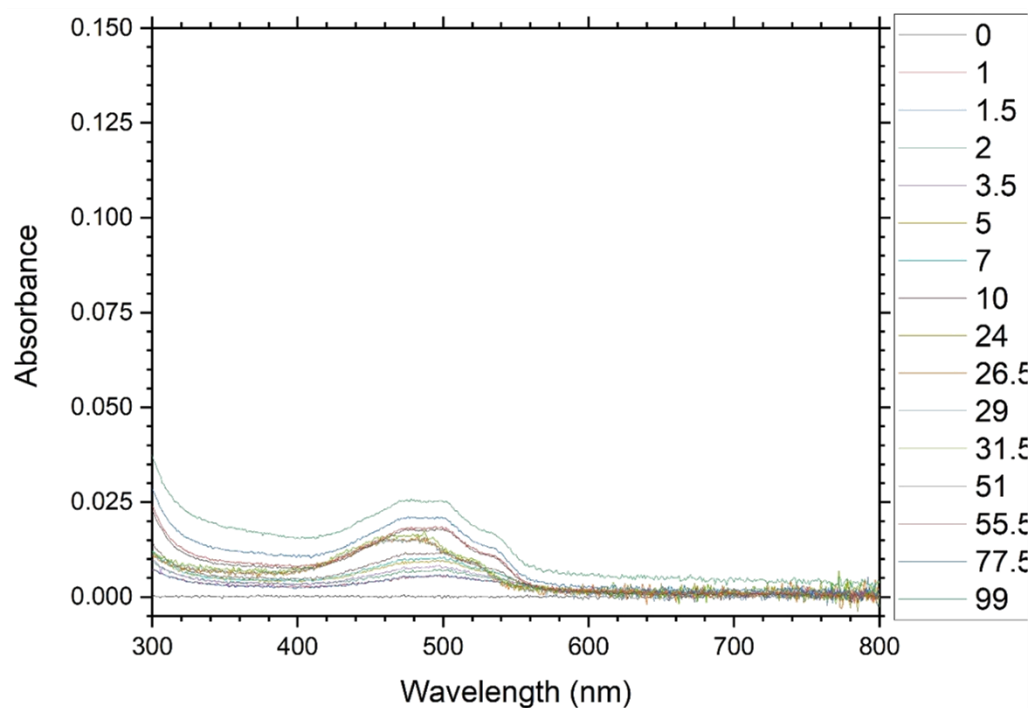


Figure AV.10. - UV-visible spectra of PBS buffer solution containing the dialysate from dox-loaded nanoparticles of PSAr<sub>77</sub>-b-PAla<sub>9</sub> (Chapter 6, Table 6.1., polymer 6), incubated at 37 °C with 20 units of chymotrypsin, sampled at time points listed.

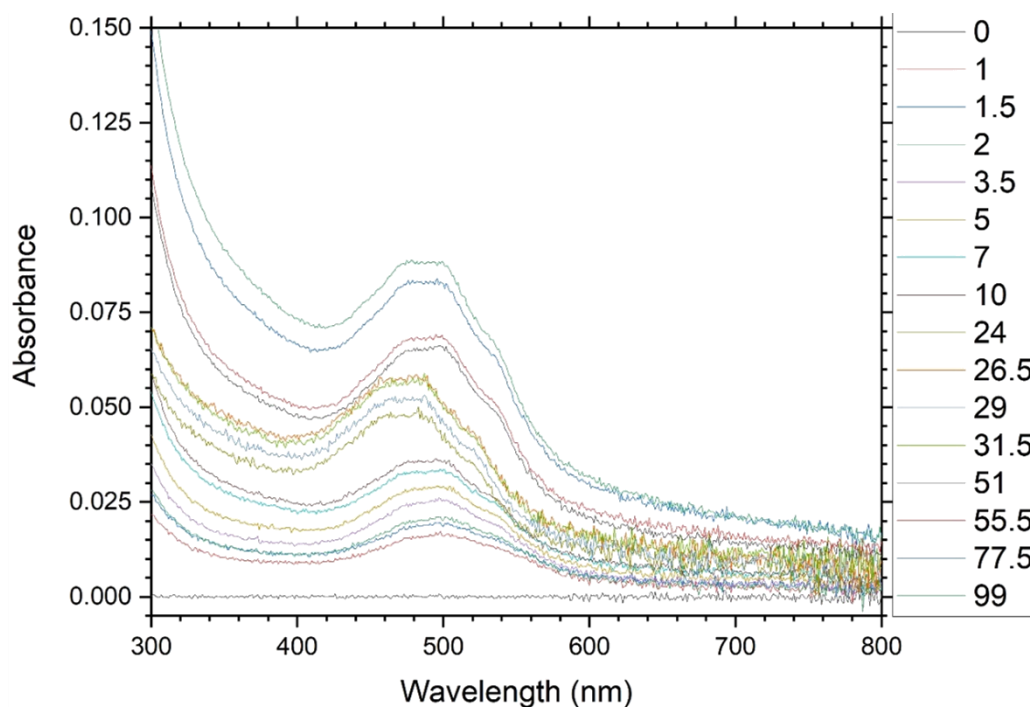


Figure AV.11. - UV-visible spectra of PBS buffer solution containing the dialysate from dox-loaded nanoparticles of PSar<sub>77</sub>-b-PAla<sub>9</sub> (Chapter 6, Table 6.1., polymer 6), incubated at 37 °C with 8 units of neutrophil elastase, sampled at time points listed.

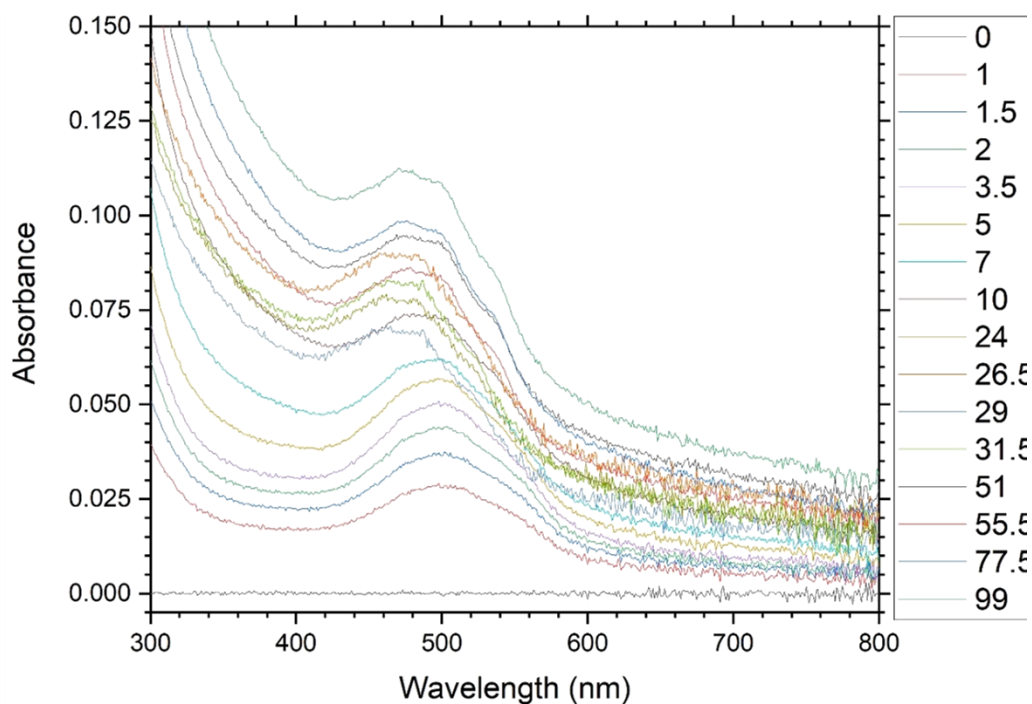


Figure AV.12. - UV-visible spectra of PBS buffer solution containing the dialysate from dox-loaded nanoparticles of PSar<sub>77</sub>-b-PAla<sub>9</sub> (Chapter 6, Table 6.1., polymer 6), incubated at 37 °C with 20 units of neutrophil elastase, sampled at time points listed.

Appendix VI – Calibration Curves

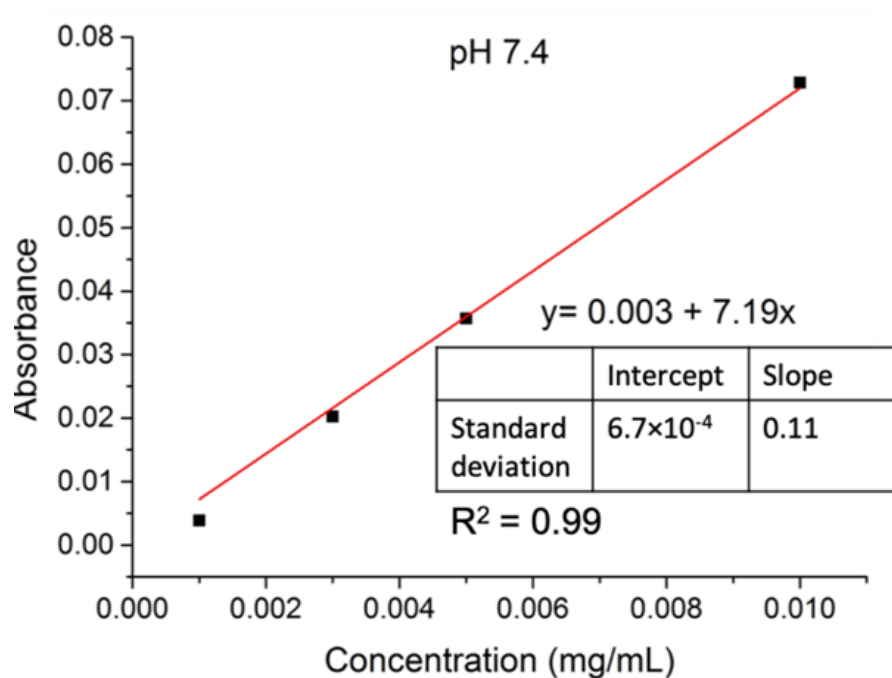


Figure AVI.1. - Calibration curve and best fit line of Doxorubicin in PBS buffer solution (pH 7.4) with different concentrations.

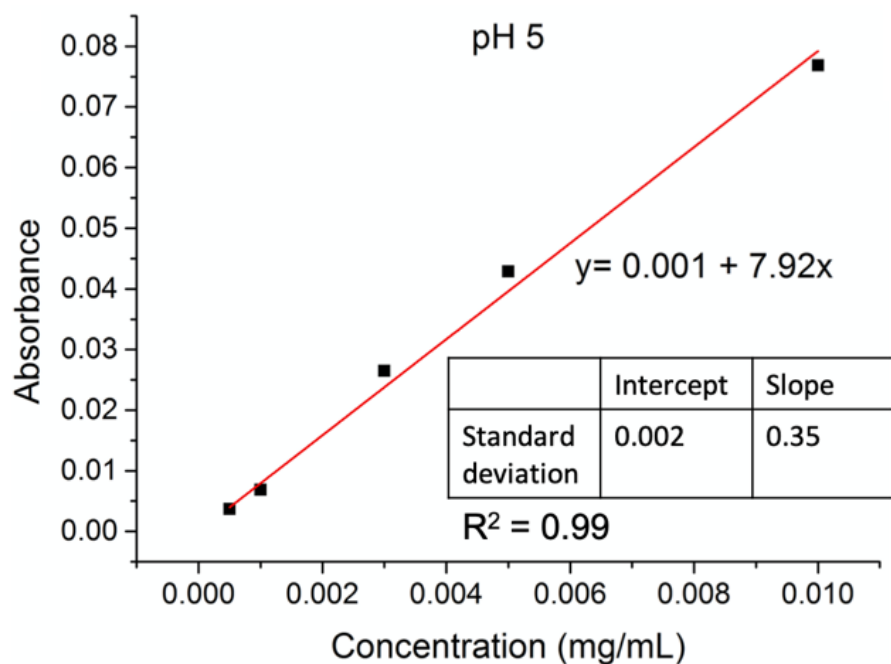


Figure AVI.2. - Calibration curves and best fit lines of Doxorubicin in pH 5 acetate buffer solution at various concentrations.

## Appendix VII – MALDI-TOF Mass Spectrometry

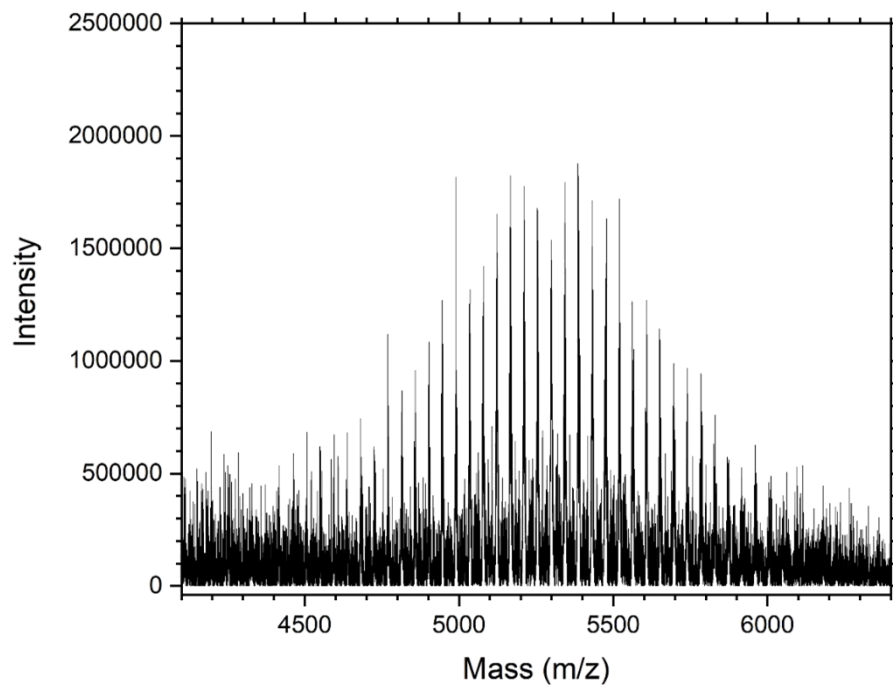


Figure AVII.1. – MALDI-TOF spectrum of polymer 2, polysarcosine<sub>79</sub>.

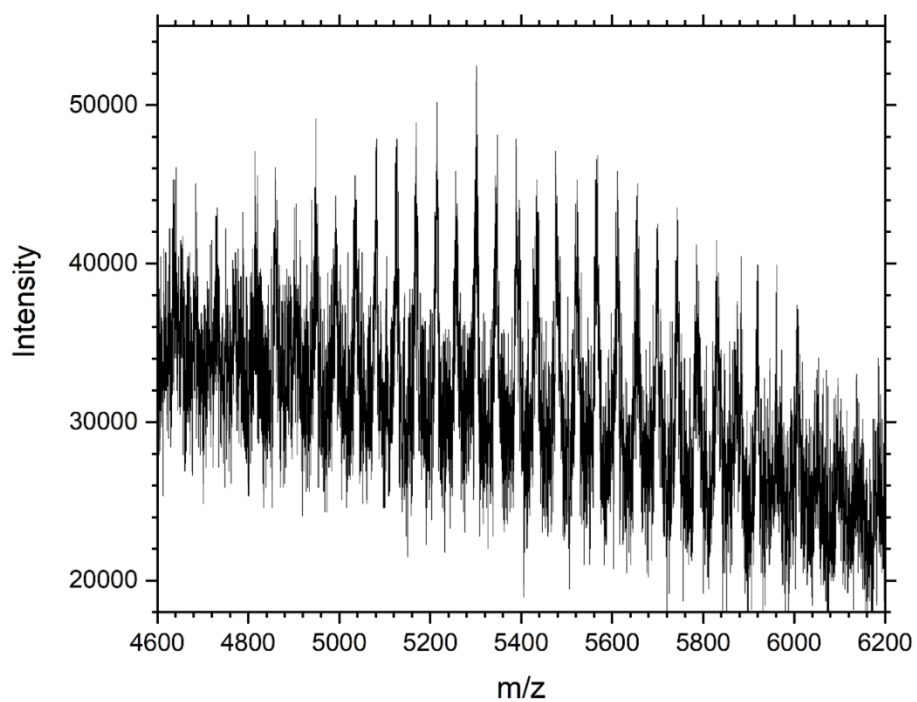


Figure AVII.2. – MALDI-TOF spectrum of polymer 3, polysarcosine<sub>76</sub>.

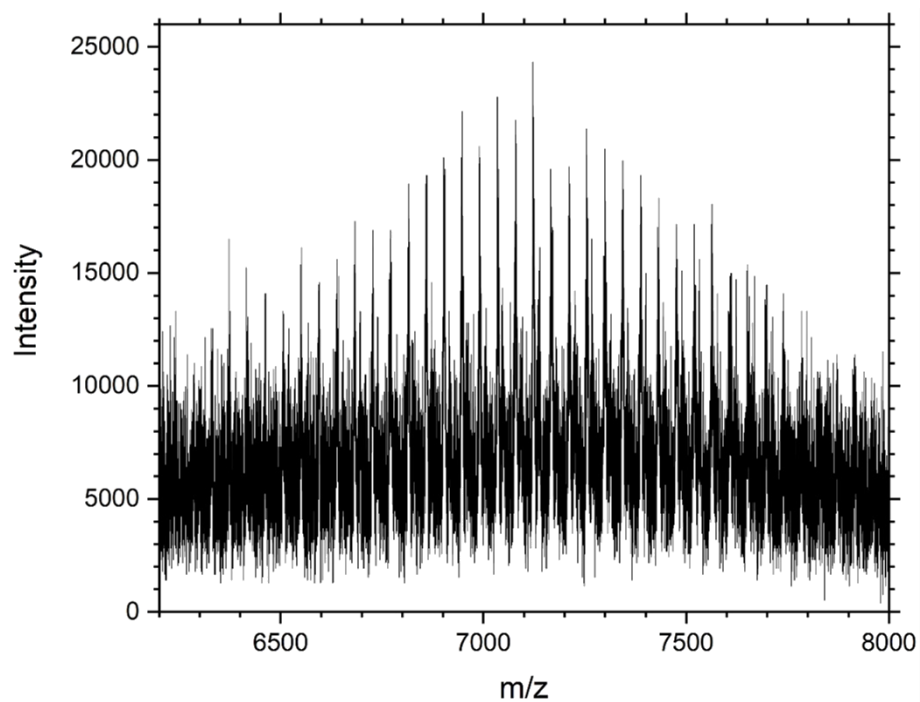


Figure AVII.3. – MALDI-TOF spectrum of polymer 4, polysarcosine<sub>100</sub>.

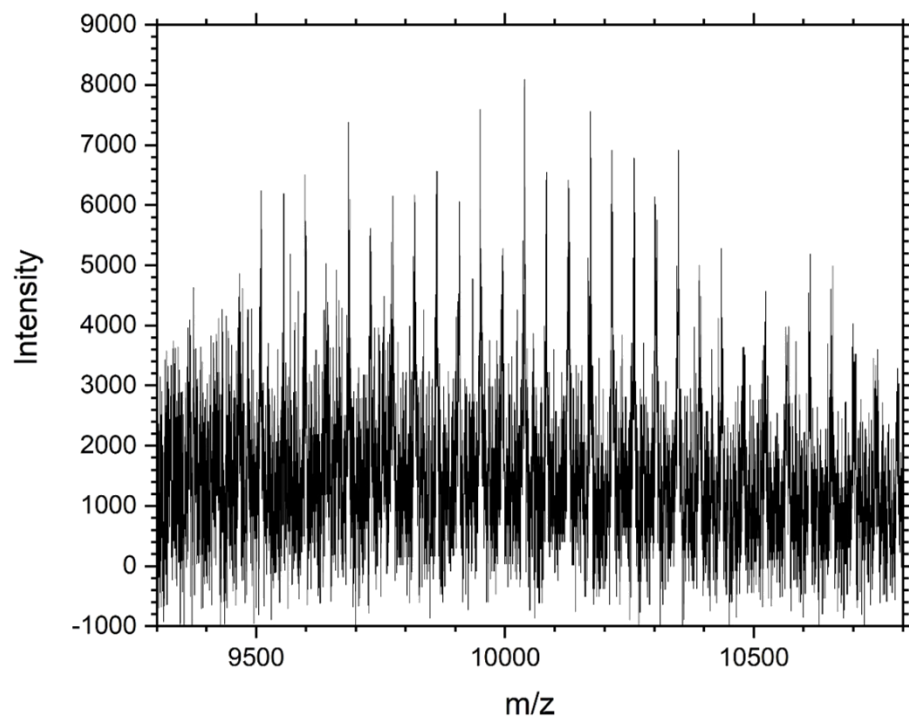


Figure AVII.4. – MALDI-TOF spectrum of polymer 5, polysarcosine<sub>139</sub>.

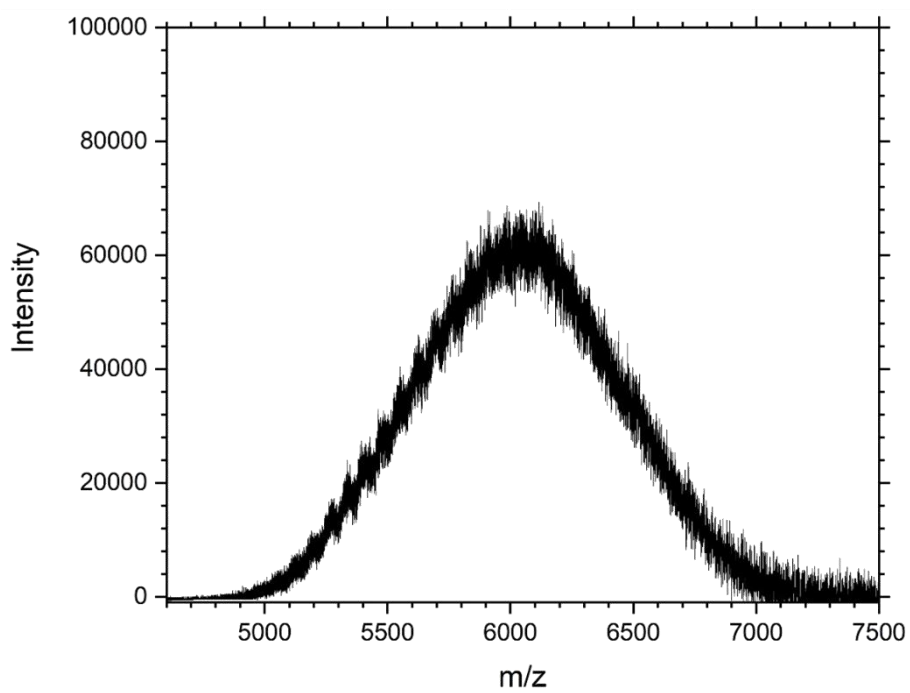


Figure AVII.5. – MALDI-TOF spectrum of polymer 7, polysarcosine<sub>79</sub>-*b*-polyalanine<sub>11</sub>.

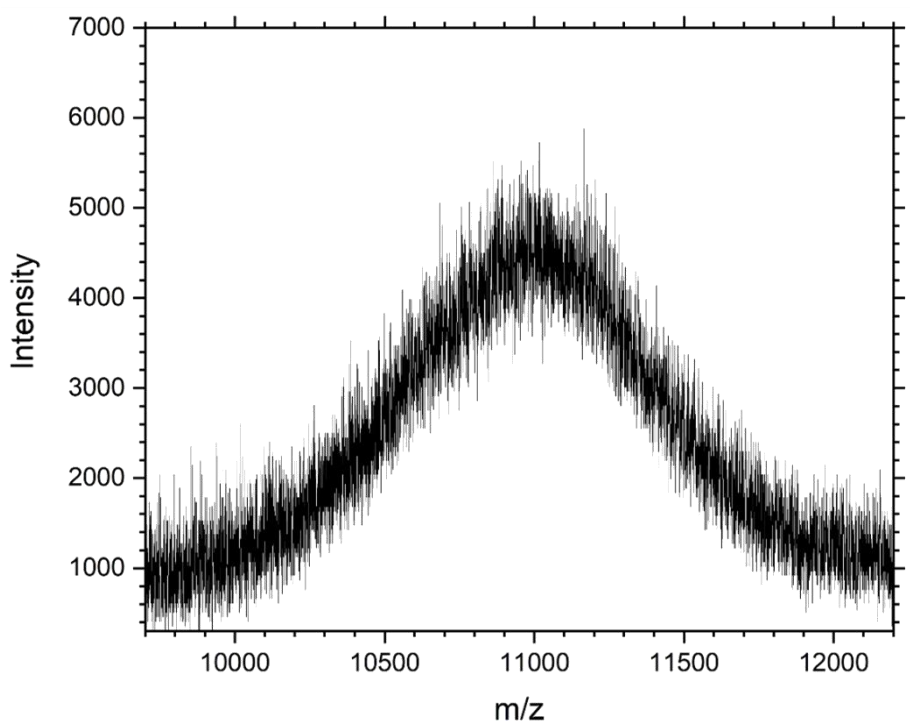


Figure AVII.6. – MALDI-TOF spectrum of polymer 8, polysarcosine<sub>139</sub>-*b*-polyalanine<sub>13</sub>.

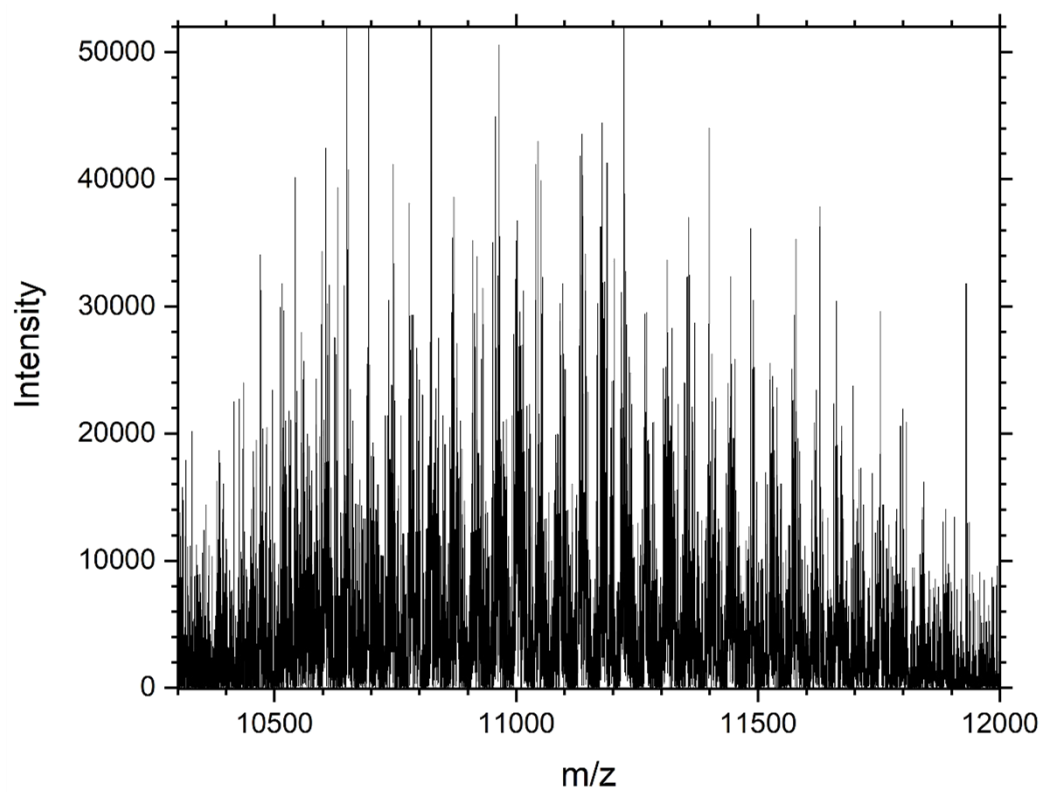


Figure AVII.7. – MALDI-TOF spectrum of polymer 9, polysarcosine<sub>139</sub>-*b*-polyalanine<sub>11</sub>.